

# DEVELOPMENTAL MODELS 2.0

EDITED BY: Mo Li, Keiichiro Suzuki, Alessandra Giorgetti and Ying Gu  
PUBLISHED IN: Frontiers in Cell and Developmental Biology



# frontiers

## Frontiers eBook Copyright Statement

The copyright in the text of individual articles in this eBook is the property of their respective authors or their respective institutions or funders. The copyright in graphics and images within each article may be subject to copyright of other parties. In both cases this is subject to a license granted to Frontiers.

The compilation of articles constituting this eBook is the property of Frontiers.

Each article within this eBook, and the eBook itself, are published under the most recent version of the Creative Commons CC-BY licence.

The version current at the date of publication of this eBook is CC-BY 4.0. If the CC-BY licence is updated, the licence granted by Frontiers is automatically updated to the new version.

When exercising any right under the CC-BY licence, Frontiers must be attributed as the original publisher of the article or eBook, as applicable.

Authors have the responsibility of ensuring that any graphics or other materials which are the property of others may be included in the CC-BY licence, but this should be checked before relying on the CC-BY licence to reproduce those materials. Any copyright notices relating to those materials must be complied with.

Copyright and source acknowledgement notices may not be removed and must be displayed in any copy, derivative work or partial copy which includes the elements in question.

All copyright, and all rights therein, are protected by national and international copyright laws. The above represents a summary only. For further information please read Frontiers' Conditions for Website Use and Copyright Statement, and the applicable CC-BY licence.

ISSN 1664-8714

ISBN 978-2-83250-597-7

DOI 10.3389/978-2-83250-597-7

## About Frontiers

Frontiers is more than just an open-access publisher of scholarly articles: it is a pioneering approach to the world of academia, radically improving the way scholarly research is managed. The grand vision of Frontiers is a world where all people have an equal opportunity to seek, share and generate knowledge. Frontiers provides immediate and permanent online open access to all its publications, but this alone is not enough to realize our grand goals.

## Frontiers Journal Series

The Frontiers Journal Series is a multi-tier and interdisciplinary set of open-access, online journals, promising a paradigm shift from the current review, selection and dissemination processes in academic publishing. All Frontiers journals are driven by researchers for researchers; therefore, they constitute a service to the scholarly community. At the same time, the Frontiers Journal Series operates on a revolutionary invention, the tiered publishing system, initially addressing specific communities of scholars, and gradually climbing up to broader public understanding, thus serving the interests of the lay society, too.

## Dedication to Quality

Each Frontiers article is a landmark of the highest quality, thanks to genuinely collaborative interactions between authors and review editors, who include some of the world's best academicians. Research must be certified by peers before entering a stream of knowledge that may eventually reach the public - and shape society; therefore, Frontiers only applies the most rigorous and unbiased reviews. Frontiers revolutionizes research publishing by freely delivering the most outstanding research, evaluated with no bias from both the academic and social point of view. By applying the most advanced information technologies, Frontiers is catapulting scholarly publishing into a new generation.

## What are Frontiers Research Topics?

Frontiers Research Topics are very popular trademarks of the Frontiers Journals Series: they are collections of at least ten articles, all centered on a particular subject. With their unique mix of varied contributions from Original Research to Review Articles, Frontiers Research Topics unify the most influential researchers, the latest key findings and historical advances in a hot research area! Find out more on how to host your own Frontiers Research Topic or contribute to one as an author by contacting the Frontiers Editorial Office: [frontiersin.org/about/contact](https://frontiersin.org/about/contact)



# DEVELOPMENTAL MODELS 2.0

Topic Editors:

**Mo Li**, King Abdullah University of Science and Technology, Saudi Arabia

**Keiichiro Suzuki**, Osaka University, Japan

**Alessandra Giorgetti**, Institut d'Investigacio Biomedica de Bellvitge (IDIBELL),

Spain

**Ying Gu**, Beijing Genomics Institute (BGI), China

*Dr. Ying Gu is employed by BGI-Research, all other Topic Editors declare no conflicts of interest.*

**Citation:** Li, M., Suzuki, K., Giorgetti, A., Gu, Y., eds. (2022). Developmental Models 2.0. Lausanne: Frontiers Media SA. doi: 10.3389/978-2-83250-597-7

# Table of Contents

<b>05</b>	<b><i>Editorial: Developmental Models 2.0</i></b>
	Alessandra Giorgetti, Ying Gu, Keiichiro Suzuki and Mo Li
<b>08</b>	<b><i>Protein Expression Landscape Defines the Formation Potential of Mouse Blastoids From EPSCs</i></b>
	Zheyang Min, Ke Zhong, Yuxin Luo, Yong Fan and Yang Yu
<b>15</b>	<b><i>Heart in a Dish: From Traditional 2D Differentiation Protocols to Cardiac Organoids</i></b>
	Gustavo Ramirez-Calderon, Giovanni Colombo, Carlos A. Hernandez-Bautista, Veronica Astro and Antonio Adamo
<b>23</b>	<b><i>Toward Best Practices for Controlling Mammalian Cell Culture Environments</i></b>
	Shannon G. Klein, Alexandra Steckbauer, Samhan M. Alsolami, Silvia Arossa, Anieka J. Parry, Mo Li and Carlos M. Duarte
<b>33</b>	<b><i>Studying Kidney Diseases Using Organoid Models</i></b>
	Meng Liu, Angelysia Cardilla, Joanne Ngeow, Ximing Gong and Yun Xia
<b>45</b>	<b><i>Human Intestinal Organoids: Promise and Challenge</i></b>
	Jasin Taelman, Mònica Diaz and Jordi Guiu
<b>54</b>	<b><i>From Mice to Men: Generation of Human Blastocyst-Like Structures In Vitro</i></b>
	Dorian Luijckx, Vinidhra Shankar, Clemens van Blitterswijk, Stefan Giselbrecht and Erik Vrij
<b>75</b>	<b><i>Integrative Single-Cell RNA-Seq and ATAC-Seq Analysis of Mesenchymal Stem/Stromal Cells Derived from Human Placenta</i></b>
	Jinlu Li, Quanlei Wang, Yanru An, Xiaoyan Chen, Yanan Xing, Qiuting Deng, Zelong Li, Shengpeng Wang, Xi Dai, Ning Liang, Yong Hou, Huanming Yang and Zhouchun Shang
<b>92</b>	<b><i>Transcriptomic Profile of the Mouse Postnatal Liver Development by Single-Nucleus RNA Sequencing</i></b>
	Jiangshan Xu, Shijie Hao, Quan Shi, Qiuting Deng, Yujia Jiang, Pengcheng Guo, Yue Yuan, Xuyang Shi, Shuncheng Shangguan, Huiwen Zheng, Guangyao Lai, Yaling Huang, Yang Wang, Yumo Song, Yang Liu, Liang Wu, Zhifeng Wang, Jiehui Cheng, Xiaoyu Wei, Mengnan Cheng, Yiwei Lai, Giacomo Volpe, Miguel A. Esteban, Yong Hou, Chuanyu Liu and Longqi Liu
<b>103</b>	<b><i>Adapting Physiology in Functional Human Islet Organogenesis</i></b>
	Eiji Yoshihara
<b>117</b>	<b><i>Archetypal Architecture Construction, Patterning, and Scaling Invariance in a 3D Embryoid Body Differentiation Model</i></b>
	Olga Gordeeva, Andrey Gordeev and Pavel Erokhov
<b>141</b>	<b><i>Pancreatic Organoids for Regenerative Medicine and Cancer Research</i></b>
	Joan Casamitjana, Elisa Espinet and Meritxell Rovira

- 154** *A Cellular Resolution Spatial Transcriptomic Landscape of the Medial Structures in Postnatal Mouse Brain*  
Mengnan Cheng, Liang Wu, Lei Han, Xin Huang, Yiwei Lai, Jiangshan Xu, Shuai Wang, Mei Li, Huiwen Zheng, Weimin Feng, Zirui Huang, Yujia Jiang, Shijie Hao, Zhao Li, Xi Chen, Jian Peng, Pengcheng Guo, Xiao Zhang, Guangyao Lai, Qiuting Deng, Yue Yuan, Fangming Yang, Xiaoyu Wei, Sha Liao, Ao Chen, Giacomo Volpe, Miguel A. Esteban, Yong Hou, Chuanyu Liu and Longqi Liu
- 164** *Calreticulin Identified as One of the Androgen Response Genes That Trigger Full Regeneration of the Only Capable Mammalian Organ, the Deer Antler*  
Qianqian Guo, Junjun Zheng, Hengxing Ba, Hongmei Sun, Jingjie Zhai, Wenying Wang and Chunyi Li
- 181** *Approaches to Kidney Replacement Therapies—Opportunities and Challenges*  
Biao Huang, Zipeng Zeng, Chennan C. Zhang, Megan E. Schreiber and Zhongwei Li
- 192** *The Chemokine Receptor CXCR4 Regulates Satellite Cell Activation, Early Expansion, and Self-Renewal, in Response to Skeletal Muscle Injury*  
Ahmed S. Shams, Robert W. Arpke, Micah D. Gearhart, Johannes Weiblen, Ben Mai, David Oyler, Darko Bosnakovski, Omayma M. Mahmoud, Gamal M. Hassan and Michael Kyba

# Editorial: Developmental models 2.0

Alessandra Giorgetti<sup>1\*</sup>, Ying Gu<sup>2\*</sup>, Keiichiro Suzuki<sup>3,4,5\*</sup> and Mo Li<sup>6\*</sup>



## OPEN ACCESS

### EDITED AND REVIEWED BY

Valerie Kouskoff,  
The University of Manchester,  
United Kingdom

### \*CORRESPONDENCE

Alessandra Giorgetti,  
agiorgetti@idibell.cat  
Ying Gu,  
guying@genomics.cn  
Keiichiro Suzuki,  
ksuzuki@chem.es.osaka-u.ac.jp  
Mo Li,  
mo.li@kaust.edu.sa

### SPECIALTY SECTION

This article was submitted to Stem Cell Research, a section of the journal Frontiers in Cell and Developmental Biology

RECEIVED 27 September 2022

ACCEPTED 29 September 2022

PUBLISHED 12 October 2022

### CITATION

Giorgetti A, Gu Y, Suzuki K and Li M (2022), Editorial: Developmental models 2.0.  
*Front. Cell Dev. Biol.* 10:1055139.  
doi: 10.3389/fcell.2022.1055139

### COPYRIGHT

© 2022 Giorgetti, Gu, Suzuki and Li. This is an open-access article distributed under the terms of the [Creative Commons Attribution License \(CC BY\)](#). The use, distribution or reproduction in other forums is permitted, provided the original author(s) and the copyright owner(s) are credited and that the original publication in this journal is cited, in accordance with accepted academic practice. No use, distribution or reproduction is permitted which does not comply with these terms.

<sup>1</sup>Regenerative Medicine Program, Institut d'Investigació Biomèdica de Bellvitge (IDIBELL), Department of Pathology and Experimental Therapeutics, Faculty of Medicine and Health Sciences, Barcelona University, Barcelona, Spain, <sup>2</sup>BGI-Shenzhen, Shenzhen, China, <sup>3</sup>Institute for Advanced Co-Creation Studies, Osaka University, Suita, Japan, <sup>4</sup>Graduate School of Engineering Science, Osaka University, Toyonaka, Japan, <sup>5</sup>Graduate School of Frontier Bioscience, Osaka University, Suita, Japan, <sup>6</sup>Bioscience Program, Biological and Environmental Science and Engineering Division (BESE), King Abdullah University of Science and Technology, Thuwal, Saudi Arabia

### KEYWORDS

pluripotent stem cell, blastoid, organoid, regenerative medicine, 3D cell culture, single-cell "omics"

## Editorial on the Research Topic Developmental models 2.0

Human pluripotent stem cells (PSCs), including embryonic stem cells (ESCs) and induced pluripotent stem cells (iPSCs), have enabled the modeling of human development and helped to illuminate mechanisms of monogenic disease, complex disease, and cancer. Lately, the striking ability of PSCs to self-organize has engendered three-dimension (3D) models of human development. The 3D embryonic cell models partially reconstruct the complex architecture of mammalian early embryonic structures and therefore hold great potential for stem cell and developmental studies. In this Research Topic, [Gordeeva et al.](#) described a 3D embryoid body differentiation model and compared the spatiotemporal growth and patterning dynamics of embryoid bodies formed from different stem cell origins and culture conditions. [Min et al.](#) profiled the proteome and the protein phosphorylation of blastoids—blastocyst-like 3D structures derived from extended pluripotent stem cells (EPSC). By comparing the protein expression profiles of EPSC blastoids with mouse blastocysts, they indicated that glucose metabolism is key to blastoid formation and brought new insights into the similarities and differences between blastoid and blastocyst at the proteome level. In addition, [Luijckx et al.](#) provided a comprehensive comparison of current protocols for mouse ([Rivron et al., 2018; Kime et al., 2019; Li R et al., 2019; Sozen et al., 2019; Vrij et al., 2019](#)) and human ([Fan et al., 2021; Liu et al., 2021; Sozen et al., 2021; Yanagida et al., 2021; Yu et al., 2021; Kagawa et al., 2022](#)) blastoid formation, including the sources of stem cells, the key signaling molecules used in culture medium, and the experimental timelines, and further discussed to which extent these blastoids recapitulate the blastocyst in mouse and human, offering an informative resource to facilitate researchers to study early embryonic developments using blastoids.

Beyond stem cell based early embryonic models, the development of *ex vivo* organoid cultures has gained substantial attention as a model to study regenerative medicine and

diseases in several tissues since the seminal work in 2009 (Li M et al., 2019). While human intestinal organoids were among the first human organoid types that were successfully established *in vitro*, many protocols have since been optimized for organoids of many other tissue types, including the pancreas, liver, kidney, stomach, and lung among others. As organoid technology has improved, we have seen a dramatic expansion in its application, providing insights on a range of tissues—both healthy and diseased—as well as in drug development, and organ transplantation. Indeed, organoids can be used to study healthy or diseased tissue and can be generated from embryonic progenitors, adult-derived stem/progenitor cells, tumor samples or differentiated from iPSCs or ESCs. For instance, human intestinal organoids can represent a sufficiently complex *in vitro* model of intestinal tissue from fetal to adult human stages of development, which are otherwise difficult to access. Taelman et al. summarized the differences, advantages, and disadvantages of these intestinal organoid models and discussed the applications of human intestinal organoids. However, current intestinal organoid culture strategies still lack the complex interaction with *in vivo* growth factors, extracellular matrix composition and multi-organ physiology.

Pancreatic organoids were first described in 2013 to model two major devastating diseases: diabetes and pancreatic ductal adenocarcinoma. Casamitjana et al. performed an in-depth review of the characteristics of pancreatic organoids derived from different cell types. They emphasized the potential of pancreatic organoids in future tissue transplantation and personalized medicine and highlighted the limitations of pancreatic organoids to recapitulate tissue differentiation and architecture. Human PSCs offer an unlimited supply of source materials for the generation of 3D human islet-like clusters that are transplantable and ameliorate diabetes in animal models. Yoshihara highlighted the recent progress of generation of stem cell-derived 3D-structured human islets. The author also discussed multiple missing factors in the generation of fully functional human islets, including pancreatic exocrine and immune cell interaction, peripheral neuro-vasculature system, paracrine regulation, organ-organ interaction, and physiological environmental cues.

Chronic kidney disease (CKD) is a general term for heterogeneous disorders affecting kidney structure and function. When kidney function continues to decline, CKD patients may develop end-stage renal disease (ESRD, or kidney failure). Organ transplantation and dialysis continue to represent the only therapeutic options available. However, in the last two decades major advances in stem cell biology, gene editing, and bioengineering are now delivering options in regenerative medicine to treat CKD. Li et al. comprehensively summarized the most prevailing and innovative progress of the current approaches to solving the shortage of donor kidneys and how these approaches can complement each other, with stem cell

technologies at the center of these interconnections (Huang et al.). A clear example is the development of stem cell derived kidney progenitors and organoids that may be utilized to provide a reliable source of proximal tubule cells that are needed in commercializing the bioartificial kidney device. Liu et al. reviewed kidney disease model studies using *in vitro* tools including kidney organoids derived from normal human fetal/adult tissues, human PSCs and primary tissues of kidney cancer. They covered many topics including polycystic kidney disease and other genetic kidney diseases, and non-genetic kidney diseases. Both papers also discussed the remaining challenges of translating advances in kidney organoid research into new therapies.

Human cardiac lineages can be differentiated in traditional two-dimensional monolayer culture or by adopting 3D culture methods. Ramirez-Calderon et al. summarized the most advanced 3D methods for deriving human cardiac organoids from human PSCs and discussed the potential applications of cardiac organoids in the pharmaceutical and bioengineering fields, including the emerging question of Severe Acute Respiratory Syndrome CoronaVirus 2 (SARS-CoV-2) infection in the heart.

These primary research and reviews highlight the fact that organoids are heterogeneous in shape and size; moreover, the absence of blood supply and interactions with non-parenchymal cell types limit their potential. For these reasons, future works are needed to standardize organoid cultures, including co-cultures with other cells (mesenchymal, endothelial, neuronal, and immune cells), and to improve cell maturation to generate more faithful models. To this end, improvements in culture methodology could make 3D stem cell models more robust and reproducible. Klein et al. argue that paying due attention to culture environments is critical to improve the reproducibility and translation of preclinical research. They outline the main sources of cell culture environmental instability and deliver best practice recommendations, thus making an important step towards enhancing the physiological relevance of *in vitro* cellular models. Additionally, a higher resolution understanding of the molecular events unfolding during development or tissue homeostasis could guide better 3D differentiation protocols. Single-cell OMICs analysis promise to deliver unprecedented insights into human development and disease pathogenesis. In this Research Topic, Xu et al. applied single-nucleus RNA sequencing (snRNA-seq), which could resolve multiple cell types better than single-cell RNA sequencing (scRNA-seq), to profile cell types, dynamics of cellular composition, and hepatocyte differentiation trajectories during postnatal murine liver development. A complete understanding of the development of complex organs such as the brain requires not only cell type taxonomy (which scRNA-seq excels at) but also spatial information of cells or genes at the organ level. Cheng et al. applied Stereo-seq, a DNA nanoball patterned array-based high-resolution spatial transcriptomic technology, to medial structures in postnatal

mouse brain. Their data provided subcellular distribution of 27,330 genes, region-specific gene regulatory networks, 41 cell types localized in different regions. This rich resource for developmental study is accessible as an open and interactive database (<https://db.cngb.org/stomics/datasets/STDS0000139?tab=explore>). Li et al. performed integrative scRNA-seq and single cell assay for transposase-accessible chromatin sequencing (scATAC-seq) analysis in mesenchymal stem/stromal cells derived from placenta (PMSCs). Their data revealed subsets of PMSCs and nominated potential cis and trans regulatory factors in the subtypes.

Besides high-through profiling of mRNA and chromatin accessibility, mechanistic dissection of regulatory pathways during tissue regeneration pays dividends for improving stem cell differentiation and developing novel therapies. In this regard, Shams et al. showed that signaling through the chemokine receptor CXCR4 is essential to normal early activation, proliferation and self-renewal of muscle stem cells (or satellite cells), which are responsible for regenerating muscle fibers following acute skeletal muscle injury. Among mammals, deer has the unique ability to fully regenerate a lost organ, the antler. Guo et al. explored the gene expression changes during the activation of the pedicle periosteum (harboring stem-like cells) that triggers the initiation of antler regeneration. Their findings suggest that calreticulin (CALR), an androgen response gene, is likely a downstream mediator of androgen hormones for initiating antler regeneration.

The topic editors hope the readers enjoy reading these new papers centered around stem cell models as much as we do. The exciting research advances summarized in this volume will

undoubtedly have a positive impact on the translational values of stem cell models.

## Author contributions

All authors listed have made a substantial, direct, and intellectual contribution to the work and approved it for publication.

## Conflict of interest

Author YG was employed by company BGI-Shenzhen.

The remaining authors declare that the research was conducted in the absence of any commercial or financial relationships that could be construed as a potential conflict of interest.

## Publisher's note

All claims expressed in this article are solely those of the authors and do not necessarily represent those of their affiliated organizations, or those of the publisher, the editors and the reviewers. Any product that may be evaluated in this article, or claim that may be made by its manufacturer, is not guaranteed or endorsed by the publisher.

## References

- Fan, Y., Min, Z., Alsolami, S., Ma, Z., Zhang, E., Chen, W., et al. (2021). Generation of human blastocyst-like structures from pluripotent stem cells. *Cell Discov.* 7, 81. doi:10.1038/s41421-021-00316-8
- Kagawa, H., Javali, A., Khoei, H. H., Sommer, T. M., Sestini, G., Novatchkova, M., et al. (2022). Human blastoids model blastocyst development and implantation. *Nature* 601, 600–605. doi:10.1038/s41586-021-04267-8
- Kime, C., Kiyonari, H., Ohtsuka, S., Kohbayashi, E., Asahi, M., Yamanaka, S., et al. (2019). Induced 2C expression and implantation-competent blastocyst-like cysts from primed pluripotent stem cells. *Stem Cell Rep.* 13, 485–498. doi:10.1016/j.stemcr.2019.07.011
- Li, M., Izpisua Belmonte, J. C., Boyer, C. J., and Alexander, J. S. (2019). Organoids-preclinical models of human disease. *N. Engl. J. Med.* 380, 1981–1982. doi:10.1056/NEJMc1903253
- Li, R., Zhong, C., Yu, Y., Liu, H., Sakurai, M., Yu, L., et al. (2019). Generation of blastocyst-like structures from mouse embryonic and adult cell cultures. *Cell* 179, 687–702. doi:10.1016/j.cell.2019.09.029
- Liu, X., Tan, J. P., Schroder, J., Aberkane, A., Ouyang, J. F., Mohenska, M., et al. (2021). Modelling human blastocysts by reprogramming fibroblasts into iBlastoids. *Nature* 591, 627–632. doi:10.1038/s41586-021-03372-y
- Rivron, N. C., Frias-Aldeguer, J., Vrij, E. J., Boisset, J. C., Korving, J., Vivie, J., et al. (2018). Blastocyst-like structures generated solely from stem cells. *Nature* 557, 106–111. doi:10.1038/s41586-018-0051-0
- Sozen, B., Cox, A. L., De Jonghe, J., Bao, M., Hollfelder, F., Glover, D. M., et al. (2019). Self-organization of mouse stem cells into an extended potential blastoid. *Dev. Cell* 51, 698–712. doi:10.1016/j.devcel.2019.11.014
- Sozen, B., Jorgensen, V., Weatherbee, B. A. T., Chen, S., Zhu, M., and Zernicka-Goetz, M. (2021). Reconstructing aspects of human embryogenesis with pluripotent stem cells. *Nat. Commun.* 12, 5550. doi:10.1038/s41467-021-25853-4
- Vrij, E. J., Scholte op Reimer, Y. S., Frias Aldeguer, J., Misteli Guerreiro, I., Kind, J., Koo, B.-K., et al. (2019). Chemically-defined induction of a primitive endoderm and epiblast-like niche supports post-implantation progression from blastoids. bioRxiv, 510396.
- Yanagida, A., Spindlow, D., Nichols, J., Dattani, A., Smith, A., and Guo, G. (2021). Naive stem cell blastocyst model captures human embryo lineage segregation. *Cell Stem Cell* 28, 1016–1022.e4. e1014. doi:10.1016/j.stem.2021.04.031
- Yu, L., Wei, Y., Duan, J., Schmitz, D. A., Sakurai, M., Wang, L., et al. (2021). Blastocyst-like structures generated from human pluripotent stem cells. *Nature* 591, 620–626. doi:10.1038/s41586-021-03356-y





# Protein Expression Landscape Defines the Formation Potential of Mouse Blastoids From EPSCs

Zheyang Min<sup>1,2†</sup>, Ke Zhong<sup>1†</sup>, Yuxin Luo<sup>3</sup>, Yong Fan<sup>1</sup> and Yang Yu<sup>2,3\*</sup>

<sup>1</sup>Department of Obstetrics and Gynecology, Key Laboratory for Major Obstetric Diseases of Guangdong Province, Key Laboratory of Reproduction and Genetics of Guangdong Higher Education Institutes, The Third Affiliated Hospital of Guangzhou Medical University, Guangzhou, China, <sup>2</sup>Beijing Key Laboratory of Reproductive Endocrinology and Assisted Reproductive Technology and Key Laboratory of Assisted Reproduction, Ministry of Education, Center of Reproductive Medicine, Department of Obstetrics and Gynecology, Peking University Third Hospital, Beijing, China, <sup>3</sup>Stem Cell Research Center, Peking University Third Hospital, Beijing, China

## OPEN ACCESS

### Edited by:

Ying Gu,  
Beijing Genomics Institute (BGI), China

### Reviewed by:

Ling Shuai,  
Nankai University, China  
Ronghui Li,  
Salk Institute for Biological Studies,  
United States

### \*Correspondence:

Yang Yu  
yuyang5012@hotmail.com

<sup>†</sup>These authors have contributed  
equally to this work

### Specialty section:

This article was submitted to  
Stem Cell Research,  
a section of the journal  
Frontiers in Cell and Developmental  
Biology

**Received:** 21 December 2021

**Accepted:** 17 January 2022

**Published:** 08 February 2022

### Citation:

Min Z, Zhong K, Luo Y, Fan Y and Yu Y  
(2022) Protein Expression Landscape  
Defines the Formation Potential of  
Mouse Blastoids From EPSCs.  
Front. Cell Dev. Biol. 10:840492.  
doi: 10.3389/fcell.2022.840492

Preimplantation embryo development is a precisely regulated process organized by maternally inherited and newly synthesized proteins. Recently, some studies have reported that blastocyst-like structures, named blastoids, can be generated from mouse ESCs (embryonic stem cells) or EPSCs (extended pluripotent stem cells). In this study, to explore the dynamic expression characteristics of proteins and their PTMs in mouse EPS blastoids, we revealed the protein expression profile of EPS blastoids and metabolite characteristics by TMT-based quantitative mass spectrometry (MS) strategy. Furthermore, the protein phosphorylation sites were identified to show the phosphoproteomic analysis in blastoids compared with mouse early embryos. Above all, our study revealed the protein expression profile of EPS blastoids compared with mouse embryos during preimplantation development and indicated that glucose metabolism is key to blastoid formation.

**Keywords:** blastoids, mEPSCs, proteome, glucose metabolism, phosphorylation, post translation modifications

## INTRODUCTION

Preimplantation embryo development is a precisely regulated process organized by maternally inherited and newly synthesized proteins. After fertilization, the embryo is controlled by maternal RNAs and proteins before ZGA (zygotic gene activation) (Xue et al., 2013). The blastomeres then compact, polarize and generate the first two lineage segregations of the inner cell mass (ICM) and the trophectoderm (TE). There are many questions to be answered regarding this process. Recently, some studies have reported that blastocyst-like structures, named blastoids, can be generated from mouse ESCs (embryonic stem cells) or EPSCs (extended pluripotent stem cells), which can partially mimic early mouse embryo development *in vitro* (Rivron et al., 2018; Li et al., 2019; Sozen et al., 2019). This new model of early embryo development needs to be better understood because of differences in developmental efficiency, gene expression and biofunction. Proteins mediate most biological processes, and the biological function of a protein requires posttranslational modifications (PTMs) (Schwanhaussner et al., 2013; Snider and Omary, 2014). The proteome landscape can provide direct access to the molecular details of early embryos. Understanding the dynamic changes in the mouse EPS blastoid proteome and PTMs provides insight into the mechanism of blastocyst-like structure generation and natural mouse embryogenesis.

## MATERIALS AND METHODS

### EPS Blastoids Generation

EPSCs were cultured on fresh mitomycin C-treated MEFs in N2B27 basal medium supplemented with 10 ng/ml LIF (R&D Systems, 7,734), 3 mM CHIR99021 (Tocris, 4,423), 2 mM (S)-(+)-dimethylene maleate (Tocris, 1,425), and 2 mM minocycline hydrochloride (Selleckchem, S4226) (hereinafter referred to as N2B27-LCDM). The N2B27-LCDM medium was changed every day. N2B27 basal medium was prepared as follows: 240 ml DMEM/F12 (Thermo Fisher Scientific, 11330-032), 240 ml neurobasal (Thermo Fisher Scientific, 21103-049), 2.5 ml N2 supplement (Thermo Fisher Scientific, 17502-048), 5 ml B27 supplement (Thermo Fisher Scientific, 12587-010), 1% nonessential amino acids (Thermo Fisher Scientific, 11140-050), 1% L-glutamax (Thermo Fisher Scientific, 35050-061), 0.1 mM  $\beta$ -mercaptoethanol (Thermo Fisher Scientific, 21985-023), 1% penicillin/streptomycin (Thermo Fisher Scientific, 15140-122), and 5% knockout serum replacement (KSR, Thermo Fisher Scientific, A3181502). EPS colonies were dissociated into single cells by TrypLE Express Enzyme (Thermo Fisher Scientific, 12604021), and the MEFs were transferred to a 0.2% gelatin-coated plate at 37°C for 30 min. AggreWell 400 (STEMCELL Technologies, 34415) was prepared following the manufacturer's instructions. EPS blastoid basal medium was composed of 25% TSC basal medium (see above), 25% N2B27 basal medium (see above), and 50% KSOM (see above). Approximately 6,000 cells (5 cells per microwell for 1,200 microwells) were resuspended in EPS blastoids basal medium supplemented with 2 mM ROCK inhibitor Y-27632 (Selleckchem, S1049), 12.5 ng/ml rhFGF4 (R&D, 235-F4), 0.5 mg/ml heparin (Sigma, H3149), 3 mM CHIR99021 (Tocris, 4,423), and 0.5 mM A83-01 (Selleckchem, S7692) and seeded into one well of a 24-well AggreWell plate. The blastoid culturing conditions were as follows: 37°C, 20% O<sub>2</sub>, 5% CO<sub>2</sub> and saturated humidity. The day of cell seeding was counted as Day 0 of the process. The medium was removed 24 h later (Day 1) and replaced with fresh medium supplemented with 5 ng/ml BMP4 (R&D Systems, 314-BP-010) and without Y-27632. EPS aggregates and blastoids were manually picked up using a mouth pipette (homemade) or analysis or downstream experiments. To test the effect of 2-DG on EPS blastoid induction, chemicals were added to the medium at Day 1 for 72 h.

### Immunofluorescence Staining

The samples were fixed with 4% paraformaldehyde in phosphate buffered saline (PBS) for 20 min at room temperature, washed three times with PBS, and permeabilized with 0.2% Triton X-100 in PBS for 15–30 min. After blocking with 5% BSA in PBS for 1 h at room temperature, samples were then incubated with primary antibody diluted in blocking buffer overnight at 4°C. After primary antibody incubation, the samples were washed three times with PBS containing 0.1% Tween 20. Samples were washed three times with PBS containing 0.1% Tween 20 and incubated with fluorescence-conjugated secondary antibodies diluted in blocking buffer at temperature for 2 h. Nuclei were stained with Hoechst 33342 (Sigma, 94403) at 1  $\mu$ g/ml. Zeiss LSM 710

was used for imaging. Images were processed by ZEN (Zeiss) and Fiji (ImageJ, V2.0.0) software. The primary antibodies and dilutions were as follows: mouse anti-OCT4 (Santa Cruz, sc5279, polyclonal, 1:200), anti-CDX2 (Abcam, ab76541, 1:200), and rabbit anti-YAP (Cell Signaling Technology, 14074, monoclonal, 1:200). The secondary antibodies were Alexa Fluor 488 goat anti-rabbit IgG (H + L) (Thermo Fisher Scientific, A-11008), Alexa Fluor 555 goat anti-mouse IgG (H + L) (Cell Signaling Technology, 4409S), and Alexa Fluor 647 goat anti-rabbit IgG (H + L) (Abcam, ab150083, GR3269213).

### Protein Extraction, Trypsin Digestion and TMT Labeling

The EPS blastoids were collected at Day 3 and Day 5. The samples of the two groups were mixed separately, and quantitative phosphorylated proteomics analysis was performed. There were three technical replicates. The sample was sonicated three times on ice using a high-intensity ultrasonic processor (Scientz) in lysis buffer (8 M urea, 1% protease Inhibitor Cocktail). The remaining debris was removed by centrifugation at 12,000 g at 4°C for 10 min. Finally, the supernatant was collected, and the protein concentration was determined with a BCA kit according to the manufacturer's instructions.

For digestion, the protein solution was reduced with 5 mM dithiothreitol for 30 min at 56°C and alkylated with 11 mM iodoacetamide for 15 min at room temperature in darkness. The protein sample was then diluted by adding 100 mM NH<sub>4</sub>HCO<sub>3</sub> to a urea concentration less than 2 M. Finally, trypsin was added at a 1:50 trypsin-to-protein mass ratio for the first digestion overnight and a 1:100 trypsin-to-protein mass ratio for a second 4 h digestion.

After trypsin digestion, the peptide was desalted by a Strata X C18 SPE column (Phenomenex) and vacuum-dried. Peptide was reconstituted in 0.5 M TEAB and processed according to the manufacturer's protocol for the TMT kit. Briefly, one unit of TMT reagent was thawed and reconstituted in acetonitrile. The peptide mixtures were then incubated for 2 h at room temperature and pooled, desalted and dried by vacuum centrifugation. The digested peptides from EPS blastoids at Day 3 and Day 5 with three biological replicates were labeled with TMT<sup>6</sup>-126, TMT<sup>6</sup>-127, TMT<sup>6</sup>-128, TMT<sup>6</sup>-129, TMT<sup>6</sup>-130, and TMT<sup>6</sup>-131 Labeling Reagent (Thermo Fisher Scientific), respectively, following the manufacturer's protocol.

### Phosphorylated Peptide Enrichment

To enrich phosphorylation-modified peptides, most of labeled peptide was dissolved in the enrichment buffer solution (50% acetonitrile/0.5% acetic acid), and the supernatant was transferred to the pre-washed IMAC material, which was placed on a rotating shaker and gently shaken for incubation. After incubation, the material was washed three times with the buffer solution (50% acetonitrile/0.5% acetic acid and 30% acetonitrile/0.1% trifluoroacetic acid) successively. Finally, the phosphopeptides were eluted from the materials with 10% ammonia water, and the eluted fractions were combined and vacuum-dried (Riley and Coon, 2016).

## Reversed-Phase-High Performance Liquid Chromatography Fraction

The tryptic peptides were fractionated into fractions by high pH reverse-phase HPLC using Thermo Betasil C18 column (5  $\mu$ m particles, 10 mm ID, 250 mm length). Briefly, peptides were first separated with a gradient of 8–32% acetonitrile (pH 9.0) over 60 min into 60 fractions. Then, the peptides were combined into six fractions and dried by vacuum centrifuging.

## Liquid Chromatography With Tandem Mass Spectrometry Analysis

For LC-MS/MS analysis, the resulting peptides were desalted with C18 ZipTips (Millipore) according to the manufacturer's instructions. To ensure the high confidence identification of the results, the identification data was filtered with the criterion of localization probability >0.75.

These peptides were dissolved in 0.1% formic acid (solvent A) and directly loaded onto a homemade reversed-phase analytical column (15 cm length, 75  $\mu$ m i. d.). The gradient was comprised of a solvent B (0.1% formic acid in 98% acetonitrile) with an increase from 6% to 23% over 26 min, then an increase from 23% to 35% over 8 min, a climb to 80% over 3 min, and a hold at 80% for the last 3 min, all at a constant flow rate of 400 nL/min on an EASY-nLC 1000 UPLC system.

The peptides were subjected to an NSI source followed by tandem mass spectrometry (MS/MS) in Q Exactive<sup>TM</sup> Plus (Thermo) coupled online to UPLC. The electrospray voltage applied was 2.0 kV. The m/z scan range was 350–1800 for a full scan, and intact peptides were detected in the Orbitrap at a resolution of 70,000. Peptides were then selected for MS/MS using the NCE setting of 28, and the fragments were detected in the Orbitrap at a resolution of 17,500. A data-dependent procedure that alternated between one MS scan followed by 20 MS/MS scans with a 15.0 s dynamic exclusion was used. The automatic gain control (AGC) was set at 5E4. Fixed first mass was set as 100 m/z.

## Mass Spectrometry-Based Global Analysis of Phosphorylation

To identify protein phosphorylation, we used the SEQUEST algorithm in the Proteome Discoverer software suite (Thermo Fisher Scientific). The search parameters included a differential modification on serine, threonine, and tyrosine residues of 79.9663 amu, indicating the addition of phosphorous group(s). Proteome Discoverer further calculated the quantitative information of the TMT-tagged reporter ions at the modified peptide level. And the TMT quantified significance difference threshold was 1.3 times. For phosphorylation, quantitative information and localized phosphorylation sites were assembled to derive quantified phosphorylation sites.

## Metabolomics

To detect as many metabolites as possible, untargeted metabolomics profiling was performed on the XploreMET platform (Metabo-Profile, Shanghai, China). The sample preparation procedures were performed according to previously published methods with modifications (Zhen et al., 2019).

## Statistical Analysis

Data are presented as the mean values  $\pm$ SEM. Comparisons between the two groups were determined by two-tailed Student's *t* test. Statistical analyses were performed with GraphPad Prism software for individual analysis, and statistical significance is shown as not significant (NS), \**p* < .05, \*\**p* < .01.

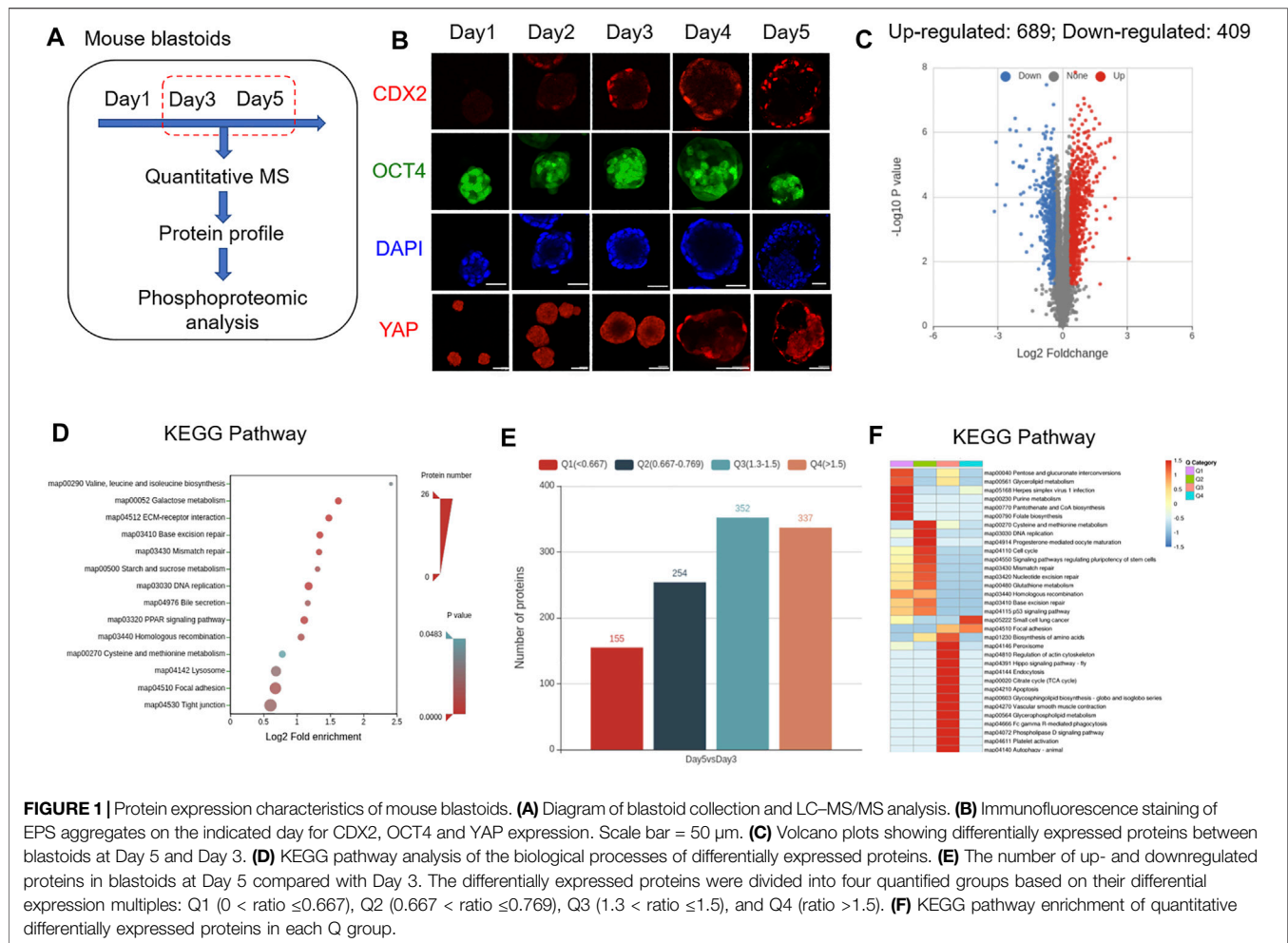
## Motif Analysis of Phosphorylation Sites

Software MoMo and Motif-X algorithms were used to analyze the motif characteristics of the phosphorylation sites. Peptide sequences composed of six amino acids in the upstream and downstream of all identified phosphorylation sites were analyzed. Analysis and comparison background were peptide sequences of six amino acids upstream and downstream of all potential phosphorylation sites in species. When the number of peptides in a characteristic sequence form was greater than 20 and the statistical test *p* value was less than .000001, the characteristic sequence form was considered as a motif of the phosphorylation peptide.

## RESULTS

### Dynamic Expression Characteristics of Proteins and PTMs in Mouse EPS Blastoids

To explore the dynamic expression characteristics of proteins and their PTMs in mouse EPS blastoids, a tandem mass tag TMT-based quantitative mass spectrometry (MS) strategy was used. Based on TMT-based quantitative MS, we analyzed the protein expression profiles of blastoids at Day 3 and Day 5, which are the key stages for embryo polarization and lineage specification (Figure 1A). For each stage, 30,000 blastoids were selected, and the experiment was performed in three biological replicates. During 5 days of blastoid development, dynamic changes in the TE marker CDX2 and EPI marker OCT4 were observed (Figure 1B). We identified approximately 6,324 proteins from 30,000 EPS blastoids each ( $\sim 5 \times 10^6$  cells) at Day 3 and Day 5. All peptides identified were of high mass accuracy and had good repeatability (Supplementary Figures S1A,B). The distribution of protein sequence coverage was very similar among the three replicates (Supplementary Figure S1C). When comparing blastoids between Day 5 and Day 3, the upregulated proteins were 689, and the downregulated proteins were 409 (Figure 1C). KEGG pathway analysis of differentially expressed proteins in blastoids revealed that these proteins were enriched in amino biosynthesis and galactose/sucrose metabolism (Figure 1D). These differentially expressed proteins were divided into four quantified groups based on their differential expression multiples: Q1 (0 < ratio  $\leq$  0.667), Q2 (0.667 < ratio  $\leq$  0.769), Q3 (1.3 < ratio  $\leq$  1.5), and Q4 (ratio > 1.5) (Figure 1E). For the four quantified



**FIGURE 1 |** Protein expression characteristics of mouse blastoids. **(A)** Diagram of blastoid collection and LC-MS/MS analysis. **(B)** Immunofluorescence staining of EPS aggregates on the indicated day for CDX2, OCT4 and YAP expression. Scale bar = 50  $\mu$ m. **(C)** Volcano plots showing differentially expressed proteins between blastoids at Day 5 and Day 3. **(D)** KEGG pathway analysis of the biological processes of differentially expressed proteins. **(E)** The number of up- and downregulated proteins in blastoids at Day 5 compared with Day 3. The differentially expressed proteins were divided into four quantified groups based on their differential expression multiples: Q1 (0 < ratio  $\leq$  0.667), Q2 (0.667 < ratio  $\leq$  0.769), Q3 (1.3 < ratio  $\leq$  1.5), and Q4 (ratio > 1.5). **(F)** KEGG pathway enrichment of quantitative differentially expressed proteins in each Q group.

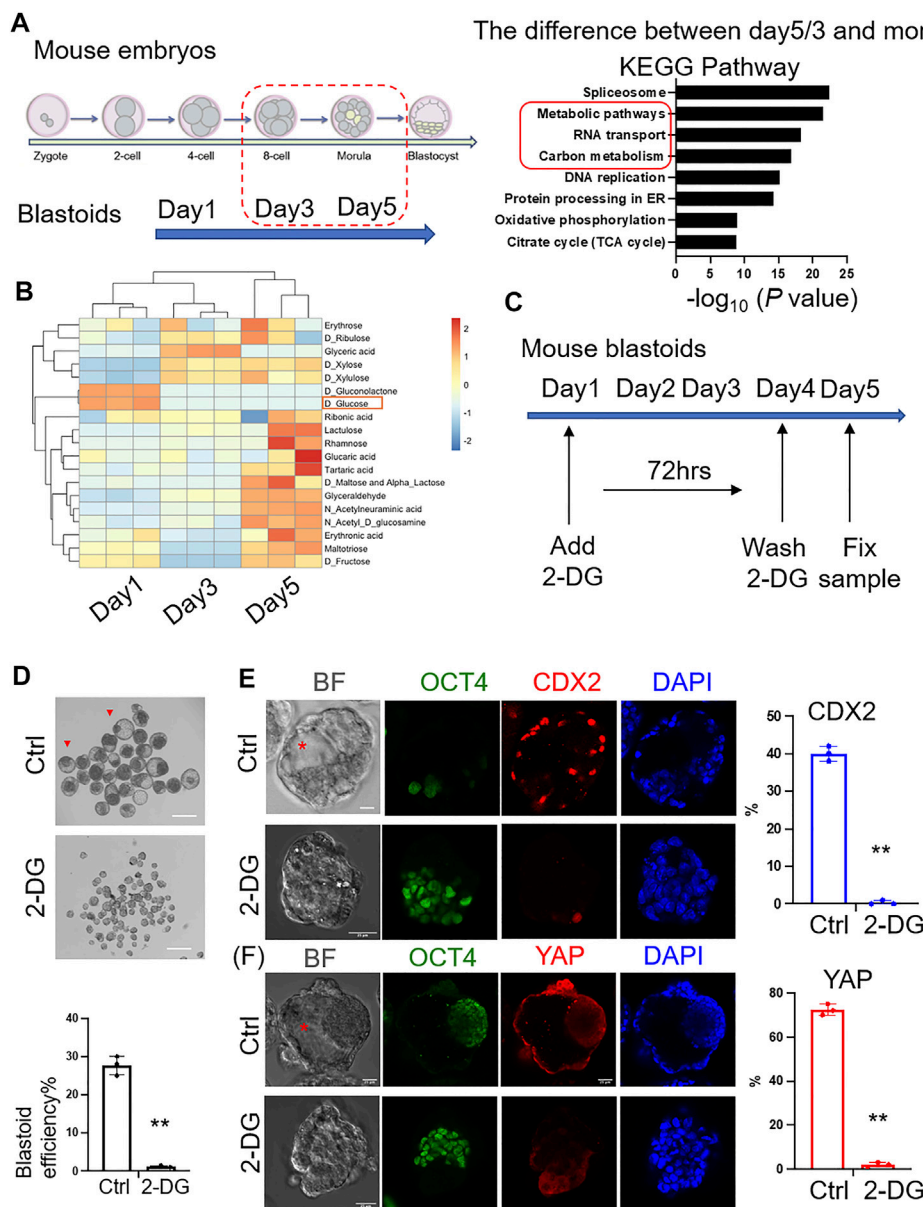
groups, Q1 and Q2 downregulated proteins were enriched in glycerolipid, purine and amino acid metabolism. Q3 and Q4 upregulated proteins were enriched in the Hippo signaling pathway, TCA cycle and apoptosis (Figure 1F).

## Glucose Metabolism Influenced the Formation of Mouse Blastoids and Embryogenesis

To compare the similarities of protein expression between mouse EPS blastoids and preimplantation mouse embryos (Gao et al., 2017), unsupervised hierarchical clustering was analyzed and indicated that the protein expression profiles of blastoids at Days 3 and 5 were similar to the 8-cell to morula stage mouse embryos (Supplementary Figures S2A,B). The overlapping number of differentially expressed proteins between Day 5/Day 3 blastoids and morula/8-cell stage embryos was 437 (Supplementary Figure S2C). We next found that the differentially expressed proteins between blastoids and mouse embryos were enriched in metabolic pathways and carbon metabolism (Figure 2A). Then, the metabolite analysis of blastoids at Day 1 to Day 5 showed that the content of glucose was decreased during blastoid culture (Figure 2B). Some research reported that glucose signaling

controls TE cell fate and is necessary for TE marker activation and specification in mouse early embryos. Glucose is transported to the cytoplasm of embryos from the external environment and controls the nuclear translocation of YAP through the hexosamine biosynthetic pathway (HBP). Then, it mediates mTOR pathway activation to control TFAP2C translation through pentose phosphate pathway (PPP). The complex formed by nuclear-localized YAP and TFAP2C activates CDX2 expression for TE specification (Chi et al., 2020; Zhu and Zernicka-Goetz, 2020). Therefore, based on the decreased glucose and the above information, we hypothesized that the absorption of glucose was necessary for blastoid formation. To explore the importance of glucose metabolism in mouse embryo development, we sought to test the role of glucose in early blastoid formation. Then, 2-DG (2-deoxy-D-glucose), an analog of glucose, was added to the culture medium to inhibit glucose utilization (Figure 2C). As expected, the efficiency of cavity formation was decreased significantly in the 2-DG-treated group compared with the control group (Figure 2D). The expression percentage of the TE marker CDX2 and TE nuclear localized marker YAP was decreased significantly compared with that of the control group (Figures 2E,F). Our data therefore provide clues on the key role of glucose metabolism in blastoid formation as well as mouse embryogenesis.





**FIGURE 2 |** Importance of glucose metabolism to the formation of mouse blastoids. **(A)** KEGG analysis of differentially expressed proteins between blastoids and mouse embryos at the indicated stages. **(B)** Metabolites of blastoids and cultured medium of blastoids at Days 1, 3 and 5. **(C)** EPS aggregates cultured in control and 2-DG medium. 2-DG was added to the medium on Day 1 and washed off on Day 4 (~72 h). **(D)** Phase-contrast images of EPS aggregates after 5 days of blastoid culture medium supplemented with vehicle (top) and 2-DG (down). The quantification of blastoid formation efficiency with the indicated treatment was performed. Scale bar = 150  $\mu\text{m}$  \*\*,  $p < .01$ . **(E)** Immunofluorescence staining of EPS aggregates of the control and 2-DG-treated groups at Day 5 for CDX2 expression. Scale bar = 25  $\mu\text{m}$  \*\*,  $p < .01$ . Red asterisk indicates cavity. **(F)** Immunofluorescence staining of EPS aggregates of the control and 2-DG-treated groups at Day 5 for YAP expression. Scale bar = 25  $\mu\text{m}$  \*\*,  $p < .01$ . Red asterisk indicates cavity.

## Characteristics and Regulation of Protein Phosphorylation in Mouse Blastoids and Blastocysts

Signal transduction through protein phosphorylation may play an important role during early embryo development; therefore, we combined high-accuracy and high-resolution liquid chromatography-tandem mass spectrometry (LC-MS/MS) to profile the phosphorylation events for serine, threonine, and

tyrosine phosphorylation of enriched modified peptides. This analysis identified 7,852 phosphopeptides from 2,935 proteins, indicating widespread activation of phosphorylation in early embryos. When statistically significant difference existed ( $p$  value was below .05), the change of differential modification quantity over 1.3 was regarded as significant up-regulation, and that less than 1/1.3 was regarded as significant down-regulation. Therefore, the number of hyperphosphorylated sites was 1,054, and the number of

hypophosphorylated sites was 883 (**Supplementary Figure S3A**). All phosphopeptides identified were of high mass accuracy and had good repeatability (**Supplementary Figures S1D,E**). The overlapping number of differentially phosphorylated proteins between Day 5/Day 3 blastoids and morula/8-cell stage embryos was 447 (**Supplementary Figure S2D**). KEGG pathway and Gene ontology (GO) analysis of differentially phosphorylated proteins in blastoids at Day 3 and Day 5 revealed that these differential proteins were enriched in RNA splicing and mRNA metabolic processes (**Supplementary Figures S3B,C**). The distribution of serine, threonine, and tyrosine phosphorylation sites were shown in the **Supplementary Figure S3D**, serine phosphorylation sites accounted for more than 90%, while tyrosine phosphorylation sites were less than 1%. For four of the quantified phosphorylated protein groups, Q1 and Q2 hypophosphorylated proteins were enriched in the spliceosome, Hippo signaling pathway and amino acid metabolism. Q3 and Q4 hyperphosphorylated proteins were enriched in glycolysis/gluconeogenesis and apoptosis (**Supplementary Figure S3E,F**). These results were similar to differentially expressed proteins. Furthermore, Hippo Signaling Pathway plays an essential role in the specification of ICM and TE in the early embryo development (Yagi et al., 2007; Nishioka et al., 2009; Kaneko and DePamphilis, 2013; Rayon et al., 2014; Posfai et al., 2017). In the outer cells, the Hippo pathway is quiescent, and the unphosphorylated YAP enters the nucleus and binds to Tead4 to form a complex that activates the expression of TE-specific genes, promoting TE differentiation. In the inner cells, the Hippo pathway is activated and YAP is phosphorylated. Phosphorylated YAP is retained in the cytoplasm and subsequently degraded, preventing the expression of TE-specific genes. Instead, abundant expression of pluripotent transcription factors promotes ICM differentiation. The formation of TE and ICM analogs is also a key event for the successful generation of mouse blastoids. We therefore explored the phosphorylation and cellular localization of YAP in mouse blastoids. Immunofluorescence staining of EPS aggregates showed that YAP was predominantly localized in the cytoplasm of blastoids before Day 3. Nuclear YAP localization was evident in most outside cells in the blastoids at Day 5 (**Figure 1B**). Similarly, phosphorylated YAP was decreased (i.e., increased nonphosphorylated YAP in TE nuclear localization) at Day 5 compared with Day 3 in blastoids (**Supplementary Figures S4A,B**), which was consistent with the change in phosphorylated YAP during mouse early embryo development (**Supplementary Figure S4C**) (Rayon et al., 2014; Posfai et al., 2017). Previous studies found phosphorylation changes in multiple enzymes participating in glycogenesis downstream of insulin signaling (Gao et al., 2017). At the protein level, glycogen synthase 1 (GYS1) was rapidly decreased in the morula stage (**Supplementary Figure S4E**). Key enzymes in glycogenesis are gradually degraded, and those in glycogenolysis are increased during embryo development. However, in the blastoids, these key enzymes were all increased except for GYS1, which was stable in blastoids from Day 3 to Day 5 (**Supplementary Figure S4D**). Furthermore, the detected phosphorylated sites of

GYS1 in blastoids were different from those in mouse embryos (**Supplementary Figures S4F,G**). In early preimplantation embryos *in vivo*, the glycogen content is high from MII to the morula stage but degrades during the blastocyst stage (Thomson and Brinster, 1966). These results indicated that abnormal glycogen metabolism may lead to differences between blastoids and mouse embryos and provide clues to improve the generation of mouse blastoids.

## DISCUSSION

In this study, we revealed the protein expression profile of blastoids and metabolite characteristics. Furthermore, the protein phosphorylation sites were identified to show the phosphoproteomic analysis in blastoids compared with mouse early embryos. Clustering analysis revealed that the protein profile of blastoids at Days 3 and 5 was more similar to that of 8-cell to morula stage embryos. As the protein expression profile underwent a major shift in the blastocyst stage, the protein expression in blastoids at Day 5 was distinct from that at the blastocyst stage and more similar to that at the morula stage. This may be a result of blastoid implantation failure and further development to birth, although the RNA profile is more similar to blastocysts for blastoids at Day 5 (Gao et al., 2017). Furthermore, phosphorylation protein analysis revealed abnormal glycogen and glucose metabolism, indicating the contribution to the difference between blastoids and natural mouse embryos. Glucose is necessary for TE marker activation and specification in mouse early embryos. Glucose is transported to the cytoplasm of embryos from the external environment, supporting development through multiple pathways. It controls the nuclear translocation of YAP through the hexosamine biosynthetic pathway (HBP). Then, it mediates mTOR pathway activation to control TFAP2C translation. Nuclear-localized YAP and TFAP2C form a complex to activate CDX2 expression for TE specification (Chi et al., 2020; Zhu and Zernicka-Goetz, 2020). In EPS blastoids, the requirement of glucose for TE-like cell specification and blastoid cavity formation was also shown in the 2-DG treatment experiment (**Figure 2F**). In recent years, haploid TSCs (haiTSCs) from the trophoblast layer has been established and become a platform to explore the mechanisms of extraembryonic lineage specification and placental development (Peng et al., 2019; Xu et al., 2021). For further exploring the function of glucose for TE-like cell specification, haiTSCs will be a powerful tool. Moreover, haiTSCs could provide cues on how to form normal TE-like cells owing to their single genome and advantages of genetic screening. Above all, our study revealed the protein expression profile of EPS blastoids compared with mouse embryos during preimplantation development and indicated that glucose metabolism is key to blastoid formation.

## DATA AVAILABILITY STATEMENT

The datasets presented in this study can be found in online repositories. The names of the repository/repositories and accession number(s) can be found below: ProteomeXchange Consortium via the PRIDE partner repository with the dataset identifier PXD031002.



## AUTHOR CONTRIBUTIONS

ZM and KZ performed the bioinformatics analyses and molecular and cellular experiments. ZM wrote the manuscript. YY and YF designed the study and revised the manuscript. YY conceived the idea and ZM and YL revised the manuscript. All authors contributed to the article and approved the submitted version.

## FUNDING

This work was supported by the National Key Research and Development Program of China (2021YFC2700303), the Strategic

Priority Research Program of the Chinese Academy of Sciences (XDA16020703), the National Natural Science Funds (82192873, 81925013, 81971831, 82071612), and Outstanding Overseas Returnees Fund of the Peking University Third Hospital (No. BYSYLXHG2019002). This study was approved by the Institutional Review Board of the Peking University Third Hospital (S2020022).

## SUPPLEMENTARY MATERIAL

The Supplementary Material for this article can be found online at: <https://www.frontiersin.org/articles/10.3389/fcell.2022.840492/full#supplementary-material>

## REFERENCES

- Chi, F., Sharpley, M. S., Nagaraj, R., Roy, S. S., and Banerjee, U. (2020). Glycolysis-Independent Glucose Metabolism Distinguishes TE from ICM Fate during Mammalian Embryogenesis. *Dev. Cell* 53, 9–26. doi:10.1016/j.devcel.2020.02.015
- Gao, Y., Liu, X., Tang, B., Li, C., Kou, Z., Li, L., et al. (2017). Protein Expression Landscape of Mouse Embryos during Pre-implantation Development. *Cel Rep.* 21, 3957–3969. doi:10.1016/j.celrep.2017.11.111
- Kaneko, K. J., and Depamphilis, M. L. (2013). TEAD4 Establishes the Energy Homeostasis Essential for Blastocoel Formation. *Development* 140, 3680–3690. doi:10.1242/dev.093799
- Li, R., Zhong, C., Yu, Y., Liu, H., Sakurai, M., Yu, L., et al. (2019). Generation of Blastocyst-like Structures from Mouse Embryonic and Adult Cell Cultures. *Cell* 179, 687–702. doi:10.1016/j.cell.2019.09.029
- Nishioka, N., Inoue, K.-i., Adachi, K., Kiyonari, H., Ota, M., Ralston, A., et al. (2009). The Hippo Signaling Pathway Components Lats and Yap Pattern Tead4 Activity to Distinguish Mouse Trophoblast from Inner Cell Mass. *Dev. Cell* 16, 398–410. doi:10.1016/j.devcel.2009.02.003
- Peng, K., Li, X., Wu, C., Wang, Y., Yu, J., Zhang, J., et al. (2019). Derivation of Haploid Trophoblast Stem Cells via Conversion *In Vitro*. *iScience* 11, 508–518. doi:10.1016/j.isci.2018.12.014
- Posfai, E., Petropoulos, S., De Barros, F. R. O., Schell, J. P., Jurisica, I., Sandberg, R., et al. (2017). Position- and Hippo Signaling-dependent Plasticity during Lineage Segregation in the Early Mouse Embryo. *Elife* 6, e22906. doi:10.7554/eLife.22906
- Rayon, T., Menchero, S., Nieto, A., Xenopoulos, P., Crespo, M., Cockburn, K., et al. (2014). Notch and Hippo Converge on Cdx2 to Specify the Trophoblast Lineage in the Mouse Blastocyst. *Dev. Cell* 30, 410–422. doi:10.1016/j.devcel.2014.06.019
- Riley, N. M., and Coon, J. J. (2016). Phosphoproteomics in the Age of Rapid and Deep Proteome Profiling. *Anal. Chem.* 88, 74–94. doi:10.1021/acs.analchem.5b04123
- Rivron, N. C., Frias-Aldeguer, J., Vrij, E. J., Boisset, J.-C., Korving, J., Vivié, J., et al. (2018). Blastocyst-like Structures Generated Solely from Stem Cells. *Nature* 557, 106–111. doi:10.1038/s41586-018-0051-0
- Schwanhäusser, B., Busse, D., Li, N., Dittmar, G., Schuchhardt, J., Wolf, J., et al. (2013). Correction: Corrigendum: Global Quantification of Mammalian Gene Expression Control. *Nature* 495, 126–127. doi:10.1038/nature11848
- Snider, N. T., and Omary, M. B. (2014). Post-translational Modifications of Intermediate Filament Proteins: Mechanisms and Functions. *Nat. Rev. Mol. Cell Biol* 15, 163–177. doi:10.1038/nrm3753
- Sozen, B., Cox, A. L., De Jonghe, J., Bao, M., Hollfelder, F., Glover, D. M., et al. (2019). Self-Organization of Mouse Stem Cells into an Extended Potential Blastoid. *Dev. Cell* 51, 698–712. doi:10.1016/j.devcel.2019.11.014
- Thomson, J. L., and Brinster, R. L. (1966). Glycogen Content of Preimplantation Mouse Embryos. *Anat. Rec.* 155, 97–102. doi:10.1002/ar.1091550111
- Xu, M., Zhang, W., Geng, M., Zhao, Y., Sun, S., Gao, Q., et al. (2021). Rapid Generation of Murine Haploid-Induced Trophoblast Stem Cells via a Tet-On System. *STAR Protoc.* 2, 100881. doi:10.1016/j.xpro.2021.100881
- Xue, Z., Huang, K., Cai, C., Cai, L., Jiang, C.-y., Feng, Y., et al. (2013). Genetic Programs in Human and Mouse Early Embryos Revealed by Single-Cell RNA Sequencing. *Nature* 500, 593–597. doi:10.1038/nature12364
- Yagi, R., Kohn, M. J., Karavanova, I., Kaneko, K. J., Vullhorst, D., Depamphilis, M. L., et al. (2007). Transcription Factor TEAD4 Specifies the Trophoblast Lineage at the Beginning of Mammalian Development. *Development* 134, 3827–3836. doi:10.1242/dev.010223
- Zhen, N., Gu, S., Ma, J., Zhu, J., Yin, M., Xu, M., et al. (2019). CircHMGCS1 Promotes Hepatoblastoma Cell Proliferation by Regulating the IGF Signaling Pathway and Glutaminolysis. *Theranostics* 9, 900–919. doi:10.7150/thno.29515
- Zhu, M., and Zernicka-Goetz, M. (2020). Living a Sweet Life: Glucose Instructs Cell Fate in the Mouse Embryo. *Dev. Cell* 53, 1–2. doi:10.1016/j.devcel.2020.03.012

**Conflict of Interest:** The authors declare that the research was conducted in the absence of any commercial or financial relationships that could be construed as a potential conflict of interest.

**Publisher's Note:** All claims expressed in this article are solely those of the authors and do not necessarily represent those of their affiliated organizations, or those of the publisher, the editors and the reviewers. Any product that may be evaluated in this article, or claim that may be made by its manufacturer, is not guaranteed or endorsed by the publisher.

Copyright © 2022 Min, Zhong, Luo, Fan and Yu. This is an open-access article distributed under the terms of the Creative Commons Attribution License (CC BY). The use, distribution or reproduction in other forums is permitted, provided the original author(s) and the copyright owner(s) are credited and that the original publication in this journal is cited, in accordance with accepted academic practice. No use, distribution or reproduction is permitted which does not comply with these terms.



# Heart in a Dish: From Traditional 2D Differentiation Protocols to Cardiac Organoids

Gustavo Ramirez-Calderon<sup>†</sup>, Giovanni Colombo<sup>†</sup>, Carlos A. Hernandez-Bautista, Veronica Astro and Antonio Adamo\*

Biological and Environmental Science and Engineering Division, King Abdullah University of Science and Technology, Thuwal, Saudi Arabia

## OPEN ACCESS

### Edited by:

Keiichiro Suzuki,  
Osaka University, Japan

### Reviewed by:

Aitor Aguirre,  
Michigan State University,  
United States

### \*Correspondence:

Antonio Adamo  
antonio.adamo@kaust.edu.sa

<sup>†</sup>These authors have contributed  
equally to this work and share first  
authorship

### Specialty section:

This article was submitted to  
Stem Cell Research,  
a section of the journal  
Frontiers in Cell and Developmental  
Biology

**Received:** 16 January 2022

**Accepted:** 26 January 2022

**Published:** 17 February 2022

### Citation:

Ramirez-Calderon G, Colombo G,  
Hernandez-Bautista CA, Astro V and  
Adamo A (2022) Heart in a Dish: From  
Traditional 2D Differentiation Protocols  
to Cardiac Organoids.  
Front. Cell Dev. Biol. 10:855966.  
doi: 10.3389/fcell.2022.855966

Human pluripotent stem cells (hPSCs) constitute a valuable model to study the complexity of early human cardiac development and investigate the molecular mechanisms involved in heart diseases. The differentiation of hPSCs into cardiac lineages *in vitro* can be achieved by traditional two-dimensional (2D) monolayer approaches or by adopting innovative three-dimensional (3D) cardiac organoid protocols. Human cardiac organoids (hCOs) are complex multicellular aggregates that faithfully recapitulate the cardiac tissue's transcriptional, functional, and morphological features. In recent years, significant advances in the field have dramatically improved the robustness and efficiency of hCOs derivation and have promoted the application of hCOs for drug screening and heart disease modeling. This review surveys the current differentiation protocols, focusing on the most advanced 3D methods for deriving hCOs from hPSCs. Furthermore, we describe the potential applications of hCOs in the pharmaceutical and tissue bioengineering fields, including their usage to investigate the consequences of Severe Acute Respiratory Syndrome CoronaVirus 2 (SARS-CoV2) infection in the heart.

**Keywords:** organoids, cardiac differentiation, disease modeling, cardiogenesis, pluripotent stem cell (PSC), cardiac development, cardiac maturation

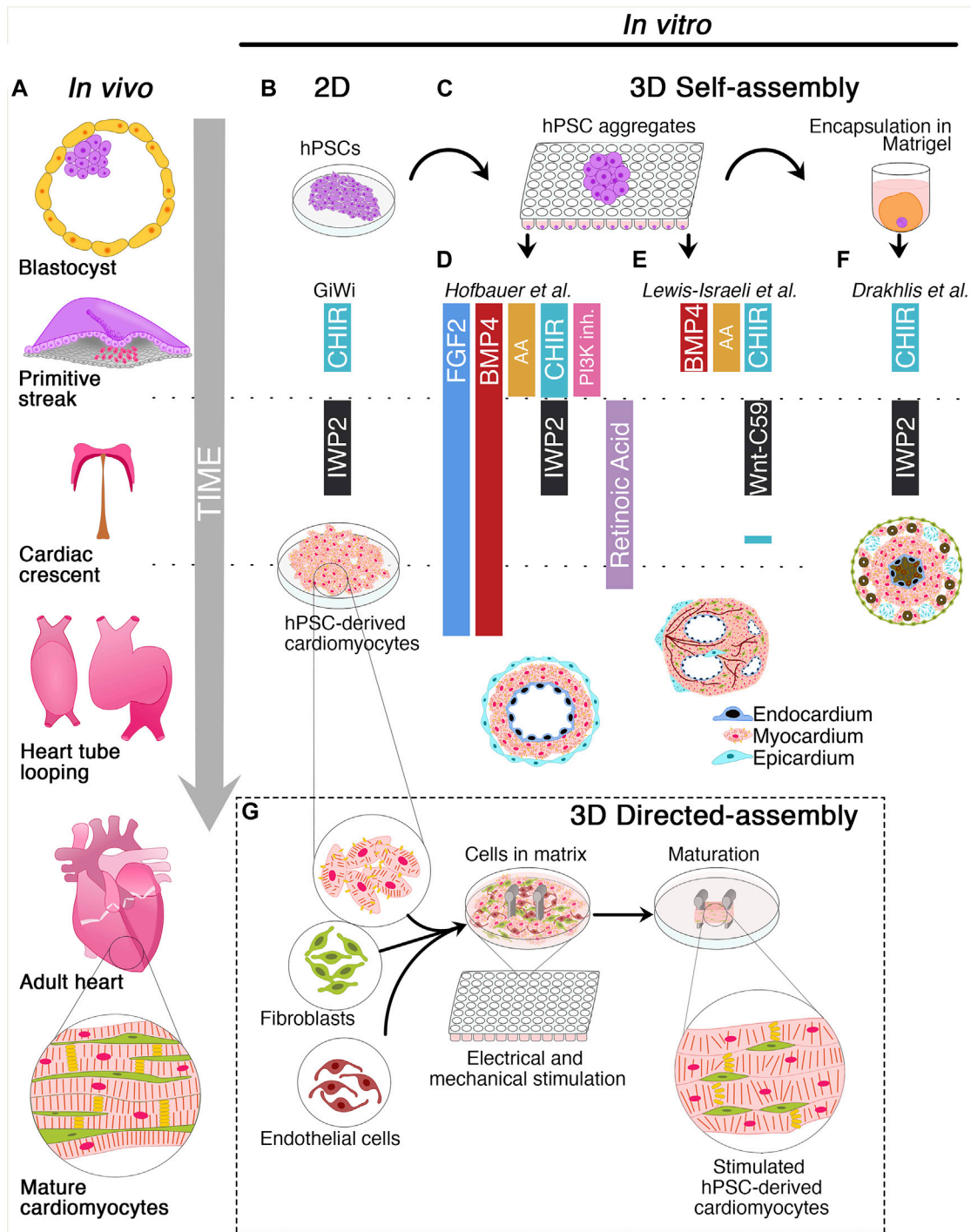
## INTRODUCTION

The knowledge on human cardiogenesis has been chiefly based on either post-mortem studies or animal models for a long time. Consequently, the use of human pluripotent stem cells (hPSCs) as an *in vitro* model to study cardiac development has flourished over the last two decades. hPSCs are suitable for regenerative medicine, tissue engineering, and drug screening applications owing to their unique proliferative capacity and potential to differentiate into virtually all somatic cell types.

Here, we emphasize the latest breakthroughs in the fields of cell biology and tissue bioengineering that open the road for the generation of 3D human cardiac organoids (hCOs).

## CARDIAC DEVELOPMENT AT A GLANCE

The heart is the first organ to be formed during embryonic development to pump nutrients, hormones, proteins, and waste once the embryo's size limits diffusion (Vincent and Buckingham, 2010). Heart development begins shortly after embryo gastrulation (Buckingham et al., 2005). During mesodermal commitment, the anterior primitive streak cells start expressing the master



**FIGURE 1** | Schematic of cardiac development and 2D/3D culture methods for the derivation of human cardiac organoids. **(A)** Timeline of cardiac development *in vivo*. The blastocyst originates the primitive streak from which the mesodermal layer emerges. Cardiovascular progenitors migrate through the primitive streak to form the cardiac crescent at the embryo's midline and generate the heart tube. Subsequently, heart tube looping and remodeling produce the final heart architecture. **(B)** Description of 2D GiWi differentiation protocol. hPSCs are treated with CHIR99021 (GSK3 inhibitor/Wnt activator) to induce primitive streak and mesoderm, followed by IWP2 (Wnt-inhibitor) treatment to trigger the cardiac commitment. The GiWi 2D protocol generates immature fetal-like hPSC-derived cardiomyocytes. **(C)** 3D self-assembly of human cardiac organoids begins with hPSCs aggregation in ultra-low attachment plates. However, only Drakhlis et al. used an additional hPSC aggregate encapsulation in Matrigel. **(D)** Hofbauer et al. implemented FGF2 and BMP4 throughout the mesoderm induction, cardiac mesoderm, and cardiomyocyte specification. Additionally, this method relies on Activin A (AA), CHIR99021, and LY294002 (PI3K-inhibitor) for mesoderm induction, IWP2, and retinoic acid for cardiac mesoderm induction. Additional co-culture with epicardial aggregates generates hCOs with chamber-like structures and three layers composed of epicardium, (Continued)

**FIGURE 1** | myocardium, and endocardium. **(E)** Lewis-Israeli et al. adopted a modified GiWi protocol by adding BMP4, AA, and CHIR99021 for mesodermal induction and Wnt-C59 (Wnt-inhibitor) for cardiac mesoderm formation. A subsequent CHIR99021 treatment triggers epicardial induction. These organoids develop chambers and vessel-like structures. **(F)** Drakhlis et al. described a GiWi protocol to generate hCOs with an inner and outer layer resembling the anterior and posterior foregut endoderm (brown color). These hCOs have a mid-myocardial layer without chamber-like structures and some epicardial-like cells (septum-transversum-like anlagen) in the outer layer. **(G)** Directed assembly of hCOs combines hPSC-derived cardiomyocytes with fibroblasts and endothelial cells in a hydrogel matrix surrounding two elastomeric poles. After hydrogel condensation, hCOs are mechanically or electrically stimulated or both to induce a mature-like phenotype.

regulator of cardiac progenitor specification Mesoderm Posterior BHLH Transcription Factor 1 (*MESP-1*), together with the surface markers Kinase Insert Domain Receptor (*KDR*) and Platelet-Derived Growth Factor Receptor (*PDGFR*) and migrate bilaterally forming the cardiac crescent at the midline, the future heart's site (Saga et al., 1996; Saga et al., 2000; Bondue et al., 2011; Lescroart et al., 2014; BurrIDGE et al., 2015; Lescroart et al., 2018). As the embryo grows, the cardiac crescent fuses at the midline and forms the heart tube, which contains an inner layer of endocardial cells and an outer layer of myocardial cells and begins to pump blood almost immediately (Vincent and Buckingham, 2010; BurrIDGE et al., 2015; Sahara et al., 2015). Independent of the crescent, a subset of cells from the proepicardial organ invades the developing heart tube to form the epicardium, the outermost layer of the heart. A further extension, looping, and remodeling of the cardiac tube, together with the contribution of the cardiac neural crest cells originating from the dorsal neural tube, leads to the valve and septum formation and the generation of ventricular and atrial chambers (Vincent and Buckingham, 2010; BurrIDGE et al., 2015; Sahara et al., 2015) (**Figure 1A**). The developed heart consists of multiple cell types including cardiomyocytes (CMs), vascular smooth muscle cells, endothelial cells, fibroblasts, and conductive system cells. The spatiotemporal assembly of these cells generates the three-layer structure of the heart, composed of endocardium, myocardium, epicardium, and the interconnected four chambers of the organ. Intriguingly, CM maturation continues until adulthood (Yang et al., 2014). CMs undergo dynamic changes during cardiac development to reach the mature contractile force and electrophysiological phenotype, including variations in cell size, sarcomere ultrastructure, metabolic substrate, mitochondrial content, nuclei number, gap junction distribution, and proliferation rate (Yang et al., 2014).

## MOLECULAR CUES DRIVING HUMAN PLURIPOTENT STEM CELLS DIFFERENTIATION INTO CARDIOMYOCYTES

Protocols for hPSC differentiation into CMs rely on three steps mimicking the sequential modulation of pathways driving cardiogenesis *in vivo* (Laflamme et al., 2007; Yang et al., 2008; Kattman et al., 2011). The first stage is based on the use of Activin A (AA), Bone Morphogenetic Protein 4 (BMP4), and basic Fibroblast Growth Factor (bFGF) to induce primitive streak and mesoderm specification. AA is a potent inducer of mesoderm and endoderm in *Xenopus* embryonic explants (Marvin et al., 2001). Additionally, the secretion of AA,

Transforming Growth Factor-Beta (TGF- $\beta$ ), and BMP4 from hypoblast and anterior endoderm drives the cardiac induction in chick embryos (Smith and Eichele, 1991; Ladd et al., 1998; Nakajima et al., 2002; Laflamme et al., 2007). Since Wnt inhibition promotes heart formation in *Xenopus* (Marvin et al., 2001), chicks, and mouse embryonic stem cells (Ueno et al., 2007), the second stage relies on Wnt inhibitors, such as DKK-1, IWP2, IWP4, or Wnt-C59 to promote cardiac mesoderm differentiation. The third stage aims at developing cardiovascular lineages and promoting the specification of a non-homogenous population of CMs, smooth muscle, and endothelial cells (Yang et al., 2008; Kattman et al., 2011). The most employed chemically-defined protocol known as GiWi (GSK-inhibition/Wnt-inhibition) allows the generation of about 80% of CMs from several hPSC lines. This method drives the specification into mesoderm precursors by treating the cells with CHIR99021, a glycogen synthase kinase-3 $\beta$  (GSK-3 $\beta$ ) inhibitor that activates the canonical Wnt/ $\beta$ -catenin pathway. Mesodermal precursors are then differentiated into cardiac mesodermal progenitors by Wnt inhibition (Lian et al., 2012; Lian et al., 2013; BurrIDGE et al., 2014; Lian et al., 2015). Unfortunately, the planar architecture and the high heterogeneity of the hPSC-derived CMs hinder the application of 2D protocols for regenerative medicine purposes.

## 3D CULTURE METHODS FOR THE DERIVATION OF HUMAN CARDIAC ORGANIDS

Human organoids can be obtained through the self-assembly of hPSCs induced by morphogens or by the directed assembly from previously differentiated stem cells (Li and Izpisua Belmonte, 2019; Schutgens and Clevers, 2020; Zhao et al., 2021; Lewis-Israeli et al., 2021a) (**Figures 1B–G**). Although the derivation of human organoids of the intestine (Sato et al., 2011), brain (Lancaster et al., 2013), and lung (Miller et al., 2019) was reported several years ago, hCOs have been only recently generated, likely due to the developmental and structural complexity of the heart (Lewis-Israeli et al., 2021a; Zhao et al., 2021). hCOs resemble key embryo developmental features, such as primitive streak induction, cardiac specification, chamber formation by cavitation, epicardium formation, and vascularization. Moreover, hCOs are composed of diverse cell subtypes, such as CMs, endothelial, smooth muscle, and epicardial cells, including endodermal derivatives (Drakhlis et al., 2021a; Drakhlis et al., 2021b; Hofbauer et al., 2021; Lewis-Israeli et al., 2021b).

In the following sections, we will discuss the two most recent approaches to generate hCOs from hPSCs (**Table 1**). The first section will navigate through the “self-assembly” method that



**TABLE 1 |** Generation of hCOs by the self-assembly and the directed assembly methods.

References	Cell source	Method	Platform	Applications	hCO features
Drakhlis et al. (2021a)	hESCs and hiPSCs	Self-assembly	Round bottom ultra-low attachment 96-well plate, Matrigel-embedded	Modeling early cardiomyogenesis and genetic heart defects <i>in vitro</i> (NKX2.5-KO HFOs recapitulate <i>in vivo</i> phenotype)	HFOs including inner (anterior foregut endoderm-like), myocardial, and outer (posterior foregut endoderm-like) layers
Hofbauer et al. (2021)	hESCs and hiPSCs	Self-assembly	Round bottom ultra-low attachment 96-well plate, later co-culture with hPSC-derived epicardial clusters	Modeling early cardiomyogenesis (HAND1-KO hCOs) and developmental injury <i>in vitro</i> (cryoinjury of hCOs)	Cavity-containing hCOs, including endocardial and myocardial layer. Outer epicardial layer obtained by co-culture with hPSC-derived epicardial clusters
Lewis-Israeli et al. (2021a)	hESCs and hiPSCs	Self-assembly	Round bottom ultra-low attachment 96-well plate	Modeling early cardiomyogenesis and disease condition <i>in vitro</i> (pregestational diabetes-induced congenital heart defects)	Cavity-containing hCOs, including endocardial, myocardial and epicardial layers
Ma et al. (2015); Hoang et al. (2018); Hoang et al. (2021)	hESCs and hiPSCs	Self-assembly	Micropatterned 6-well plate	Developmental drug toxicity assays (pregnancy risk drugs)	hCOs include a central area of CMs with a perimeter of myofibroblasts
Tiburcy et al. (2017)	(hESCs and hiPSCs) hPSC derived-CMs and human foreskin fibroblasts	Directed assembly	Casting in medical-grade type I collagen hydrogels, later mechanical stimulation by dynamic stretching between two elastomeric pillars	Advance CMs maturation and modeling heart failure <i>in vitro</i> (chronic catecholamine overstimulation)	EHTs with fetal-like CMs
Ronaldson-Bouchard et al. (2018)	hiPSCs	Directed assembly	Casting in fibrin hydrogels, later mechanical stimulation by dynamic stretching between two elastomeric pillars and electrical stimulation	Improving hPSC-derived CM maturation and modeling pathological cardiac hypertrophy (via endothelin-1 treatment)	EHT with extensive T-tubule network and mature calcium handling
Mills et al. (2017); Mills et al. (2019); Mills et al. (2021)	hESCs and hiPSCs	Directed assembly	Heart-dyno: casting in collagen I and Matrigel hydrogels in a well insert containing two elastomeric pillars	Screening for cardiac maturation, cardiomyocyte proliferation, and drugs to treat SARS-CoV-2-induced cardiac dysfunction	hCOs with fatty acid oxidation metabolism, DNA damage response, and cell cycle arrest

exploits the intrinsic property of hPSC aggregates to drive a spatiotemporal organized differentiation mediated by exogenous morphogens. The second part of the review will present “directed assembly” protocols that rely on the co-culture of hPSC-derived CMs, endothelial, or mural cells on different supports, such as extra cellular matrix (ECM), scaffolds, or bioengineering devices.

## SELF-ASSEMBLY METHOD

### Human Cardiac Organoids Generation in Ultra-Low Attachment Platforms

In recent years, the round bottom ULA plates have been used as a high-throughput platform to screen favorable conditions for hCO generation (Drakhlis et al., 2021a; Drakhlis et al., 2021b; Hofbauer et al., 2021; Lewis-Israeli et al., 2021b). Indeed, it has been shown that self-assembling hPSC-3D aggregates can give rise to hCOs, even in Matrigel-free protocols (Hofbauer et al., 2021; Lewis-Israeli et al., 2021b) (**Figure 1C**). Before inducing the differentiation, a defined number of hPSCs is seeded in each well, and the round bottom ULA plate is centrifuged to promote hPSC aggregate formation. From these aggregates, employing a modified GiWi protocol, it is possible to generate hCOs resembling crucial stages of early cardiomyogenesis, such as mesoderm specification, cardiac mesoderm induction, and

cardiac cavity formation (Drakhlis et al., 2021a; Drakhlis et al., 2021b; Hofbauer et al., 2021; Lewis-Israeli et al., 2021b).

Hofbauer and others developed an ECM-free protocol to produce hPSC-derived hCOs forming beating chamber-like architectures with an inner endocardial and an outer myocardial layer (**Figure 1D**) (Hofbauer et al., 2021). This method exploits an optimized WNT and AA treatment during mesoderm induction and a reduced retinoic acid stimulation during the cardiac mesoderm stage to direct the differentiation towards a ventricular-like fate (Zhang et al., 2011). Interestingly, this model demonstrated that a WNT-BMP-HAND1 axis controls the generation of the chamber-like structures and that the cavitation process is independent of CM differentiation. Indeed, the disruption of the HAND1 signaling suppresses the chamber formation process but does not affect CM differentiation, indicating that cell-type specification and organ morphogenesis are independently regulated processes. Notably, when hPSC-derived epicardial aggregates are co-cultured with these hCOs, they recapitulate the canonical three-layer architecture composed of epicardium, myocardium, and endocardium. Moreover, the authors elegantly proved that the three-lineage-model of hCOs responds to a cardiac injury similarly to the human heart tissue by triggering the migration of fibroblast-like cells toward the injured site and promoting the local accumulation of ECM (Hofbauer et al., 2021).

A pioneering study by Lewis-Israeli and others increased the structural complexity of hCOs by applying a three-step Wnt signaling modulation protocol (activation/inhibition/activation) (Lewis-Israeli et al., 2021b). Indeed, the second exogenous induction of the Wnt pathway promotes the clustering of epicardial cells in the external layer of the hCOs, ultimately surrounding the myocardial tissue (**Figure 1E**). Interestingly, the authors showed that it is possible to model pregestational diabetes-induced congenital heart disease “in a dish” by finely tuning hCO exposure to glucose and insulin concentrations mimicking the pathological diabetic values. Strikingly, this treatment led to the formation of hCOs carrying structural defects and altered metabolism (Lewis-Israeli et al., 2021b).

Drakhlis et al. generated hCOs by encapsulating hPSC aggregates in Matrigel droplets that are subsequently differentiated using a modified GiWi protocol (Drakhlis et al., 2021a). The authors referred to these organoids as “Heart-Forming Organoids” (HFOs). HFOs have a complex organization characterized by an inner and outer layer, patterning anterior and posterior foregut endoderm, respectively. These structures are separated by a ring-shaped mid-layer which resembles the primitive streak specification and the subsequent cardiac *primordium* (Drakhlis et al., 2021a; Drakhlis et al., 2021b) (**Figure 1F**). Furthermore, the potential of the HFOs as an *in vitro* model of early cardiogenesis was tested by generating NKX2.5-KO HFOs. Surprisingly, NKX2.5-KO HFOs displayed loosely arranged CMs in the mid-layer and larger diameter than *wild-type* HFOs (Drakhlis et al., 2021a). Notably, the phenotype of NKX2.5-KO HFOs is reminiscent of the lack of tissue compactness observed in NKX2.5-KO transgenic mice (Lyons et al., 1995).

### 3D-Derived Cardiac Microchambers

The controlled biophysical features of micropatterning allow studying differentiation more in detail than traditional methods based on the formation of heterogeneous embryoid bodies (Warmflash et al., 2014). Therefore, scientists developed strategies for generating hCOs in geometric-confined microchambers (Ma et al., 2015). To evaluate the influence of the geometric confinement on cardiac differentiation, scientists fabricated microchambers of circular, triangular, and squared cell culture areas at the micron scale using standard lithography techniques and oxygen plasma etching of tissue culture plates (Ma et al., 2015; Hoang et al., 2018). hPSCs were seeded in Matrigel-coated microchambers and differentiated employing the GiWi protocol. These geometric confinements produced a beating CM area at the center and an increased myofibroblast density at the perimeter of the microchamber (Ma et al., 2015). This model was used to evaluate the developmental toxicity of nine drugs with different reported toxicity grades during pregnancy. Interestingly, most of the tested drugs resulted in abnormal CM contraction and impaired hCO formation. Hoang and others tested the same nine drugs *in vivo* on Zebrafish whole embryos and confirmed a developmental toxicity comparable to the *in vitro* hCO model (Hoang et al., 2021).

## DIRECTED-ASSEMBLY METHOD

### Engineered Heart Tissues

The directed-assembly method produces a type of hCOs acquiring heart tissue-like structures, also known as Engineered Heart Tissues (EHTs). Overall, this methodology combines hPSC derived-cardiac cells and ECM substrates in casting molds to generate hydrogels (**Figure 1G**). These cell-laden bioengineered hydrogels require a few days to condensate and acquire their final scaffold properties (Zimmerman et al., 2000; Mills et al., 2017; Tiburcy et al., 2017; Vogues et al., 2017; Ronaldson-Bouchard et al., 2018; Mills et al., 2019; Zhao et al., 2019; Mills et al., 2021). Nowadays, scientists have developed various methodologies for deriving shape-controlled EHTs that differ for differentiation stimuli, cell subtypes, and ECM composition.

Tiburcy and others recently improved CM maturation in EHTs and defined the cellular and chemical components to fulfill the good manufacturing practice required for clinical translation (Tiburcy et al., 2017). hPSC derived-CMs and human foreskin fibroblasts were cast in medical-grade type I collagen hydrogels to form ring-shaped EHTs that were mechanically stimulated by dynamic stretching. CMs isolated from these EHTs showed rod-shaped and a remarkable degree of sarcomere organization, besides the postnatally developed M-bands (Kamakura et al., 2013). Additionally, mature EHTs showed enhanced contractile force in response to increased pacing frequencies (Tiburcy et al., 2017), a human heart trait developed along the first year after birth (Wiegerinck et al., 2009). Moreover, EHTs responded inotropically (by enhancing the force) and lusitropically (by increasing relaxation) to  $\beta$ -adrenergic stimulation. Furthermore, chronic catecholamine-treated EHTs resemble a heart failure model, including contractile dysfunction, CM hypertrophy, and Natriuretic Peptide release (Yang and Murry, 2017). Although Tiburcy's EHTs improved several CM maturation features compared to previous methods, their clinical application is hindered by substantial differences with the adult human heart. These EHTs have a lower force of contraction and lower CM volume than the adult heart, and their transcriptome recapitulates the expression profile of the human fetal heart (Tiburcy et al., 2017; Yang and Murry, 2017).

Another approach to promote CM maturation employs electromechanical stimulation (Ronaldson-Bouchard et al., 2018). This method combines hPSC-derived CMs at the early stage of differentiation and human dermal fibroblast in a 3:1 ratio. The cell mixture is encapsulated in a fibrin hydrogel cast around two elastomeric pillars designed to mimic the mechanical load of the native human myocardium. After several days in culture, hCOs were subjected to intensive training by modulating the electrical stimulation. The intensive training enhanced the maturation of CMs that displayed highly organized sarcomeres, gap junctions at CM poles, and a remarkable transverse (T)-tubule network. Despite the maturation hallmarks attained by intensively trained CMs, the native human myocardium is characterized by higher magnitudes of contraction, action potential upstroke, and conduction velocity (Hasenfuss et al., 1991).

Both Tiburcy's and Ronaldson-Bouchard's approaches harbored a degree of complexity and required expertise that



have potentially limited their usage and throughput. On the contrary, the Heart dynamometer (Heart-dyno), developed by Mills et al. in light of the minimal required tissue handling, has been constantly used in recent years. This method relies on a 96-well plate screening platform to identify favorable conditions for hCO growth, maturation, and functions (Mills et al., 2017; Mills et al., 2019; Mills et al., 2021). This approach generates an hPSC-derived cardiac cell population composed of 70% CMs and 30% mural cells, subsequently mixed with collagen I and Matrigel to cast a hydrogel in a cell culture insert-well containing two elastomeric poles. Like previous approaches, the hydrogel condensates around the poles during 5 days forming the hCOs, which are exposed to mechanical load by the elasticity of the poles for ten additional days. Using the Heart-dyno, the authors identified a chemically defined maturation media supplemented with palmitate, reduced glucose, and no insulin. These conditions improved contraction forces and expression of ventricular Myosin regulatory Light Chain 2 (*MLC2v*), decreased cell cycle activity, and induced a metabolic switch from glycolysis to fatty acid oxidation, which increased CMs oxygen consumption rate and mitochondrial content (Mills et al., 2017).

## APPLICATION OF HUMAN CARDIAC ORGANOID AS A DRUG SCREENING PLATFORM

The directed assembly method promotes the maturation of CMs by mechanical load and electrical stimulation. The enhanced maturation of CMs made this approach suitable for drug screening studies, testing CM pro-proliferative compounds, and modeling SARS-CoV-2-induced cardiac complications *in vitro* (Mills et al., 2017; Voges et al., 2017; Mills et al., 2019; Mills et al., 2021).

The Heart-dyno system has been recently used to investigate the bilateral ventricular diastolic dysfunctions developed in SARS-CoV-2 patients (Mills et al., 2021). To identify the pro-inflammatory cytokines driving the cardiac dysfunction, also known as cardiac cytokine storm, Mills and others screened several pro-inflammatory cytokines elevated in SARS-CoV-2 patients on hCOs. The combination of IFN- $\gamma$ , IL-1 $\beta$ , and poly(I:C) caused a robust diastolic dysfunction together with bromodomain-containing protein 4 (BRD4) activation. Significantly, treatment with bromodomain 2 (BD2)-selective BET inhibitors reduced the cytokine storm-induced diastolic dysfunction in hCOs and SARS-CoV-2 infected mice, and has the potential to reduce SARS-CoV-2 infection of cardiac cells (Mills et al., 2021).

## LIMITATION AND FUTURE PERSPECTIVE

Here, we reviewed some advanced techniques for the production of cardiac 3D organoids starting from hPSCs. The approaches described above generate morphological and functional models that partially resemble the *in vivo* heart development. Importantly, each model displays unique characteristics that suit specific purposes, but all show some limitations.

ULA-derived self-assembled hCOs represent helpful *in vitro* models to recapitulate the early stages of heart development and the dynamic cell-to-cell interactions occurring during cardiomyogenesis. This method relies on the intrinsic capacity of hPSCs to self-organize, implying a stochastic arrangement in the three-dimensional space. Thus, this variability hampers the reproducibility of the studies (Jabaudon and Lancaster, 2018). On the other hand, the micropatterning platform represents a valuable alternative to develop spatially organized multicellular structures. However, the contribution of batch-to-batch variable components of Matrigel along the differentiation should be carefully evaluated (Pagliarosi et al., 2020) and substituted with well-defined synthetic molecules whenever possible (Gjorevski et al., 2016). Unfortunately, the structural complexity of *in vivo* organs, such as the four cardiac chambers, valves, and inflow/outflow tract, cannot be faithfully recreated with these models. Furthermore, self-assembly-derived hCOs resemble the characteristics of fetal-like organs and cannot be employed to model heart diseases occurring in later stages of development. In this regard, the directed assembly approach offers a promising alternative based on casting platforms, such as the EHTs, that provide an excellent cellular system to optimize CM maturation while more closely mimicking the *in vivo* physiology. However, EHT-derived CMs fail to fully recapitulate the adult heart tissue anatomy. Interestingly, the recent application of the Heart-dyno model in SARS-CoV-2 research showed its tremendous potential. Innovative approaches could be based on the formation of multicellular “assembloids,” as recently reported for the brain tissue (Paşca, 2018). Assembloids were first reported by Paşca’s group that fused cortical and subpallium spheroids, reproducing an unprecedented neural circuit (Birey et al., 2017). This approach gave rise to interregional interactions that had never been investigated before. Thus, we foresee a possible application of this technique to generate heart assembloids that include cardiac-related cell lineages.

In conclusion, we reviewed the latest 3D methodologies to derive hCOs from hPSCs, which promise to further advance translational medicine applications of hPSCs. The use of these models could provide novel insights into understanding human cardiogenesis, injury processes, and developmental drug toxicities.

## AUTHOR CONTRIBUTIONS

GR-C, GC, CAH-B, VA, and AA collected bibliographic information and wrote the manuscript. GR-C. and GC equally contributed to this work.

## FUNDING

This work was supported by KAUST baseline research funding (BAS 1077-01-01) to AA.

## ACKNOWLEDGMENTS

The authors would like to thank Carol Buitrago-López for her support in the figure drawing.

## REFERENCES

- Birey, F., Andersen, J., Makinson, C. D., Islam, S., Wei, W., Huber, N., et al. (2017). Assembly of Functionally Integrated Human Forebrain Spheroids. *Nature* 545 (7652), 54–59. doi:10.1038/nature22330
- Bondue, A., Tännler, S., Chiapparo, G., Chabab, S., Ramialison, M., Paulissen, C., et al. (2011). Defining the Earliest Step of Cardiovascular Progenitor Specification during Embryonic Stem Cell Differentiation. *J. Cel Biol.* 192 (5), 751–765. doi:10.1083/jcb.201007063
- Buckingham, M., Meilhac, S., and Zaffran, S. (2005). Building the Mammalian Heart from Two Sources of Myocardial Cells. *Nat. Rev. Genet.* 6 (11), 826–835. doi:10.1038/nrg1710
- Burridge, P. W., Matsa, E., Shukla, P., Lin, Z. C., Churko, J. M., Ebert, A. D., et al. (2014). Chemically Defined Generation of Human Cardiomyocytes. *Nat. Methods* 11 (8), 855–860. doi:10.1038/nmeth.2999
- Burridge, P. W., Sharma, A., and Wu, J. C. (2015). Genetic and Epigenetic Regulation of Human Cardiac Reprogramming and Differentiation in Regenerative Medicine. *Annu. Rev. Genet.* 49, 461–484. doi:10.1146/annurev-genet-112414-054911
- Drakhlis, L., Biswanath, S., Farr, C.-M., Lupanow, V., Teske, J., Ritzenhoff, K., et al. (2021a). Human Heart-Forming Organoids Recapitulate Early Heart and Foregut Development. *Nat. Biotechnol.* 39, 737–746. doi:10.1038/s41587-021-00815-9
- Drakhlis, L., Devadas, S. B., and Zweigerdt, R. (2021b). Generation of Heart-Forming Organoids from Human Pluripotent Stem Cells. *Nat. Protoc.* 16, 5652–5672. doi:10.1038/s41596-021-00629-8
- Gjorevski, N., Sachs, N., Manfrin, A., Giger, S., Bragina, M. E., Ordóñez-Morán, P., et al. (2016). Designer Matrices for Intestinal Stem Cell and Organoid Culture. *Nature* 539 (7630), 560–564. doi:10.1038/nature20168
- Hoang, P., Kowalczewski, A., Sun, S., Winston, T. S., Archilla, A. M., Lemus, S. M., et al. (2021). Engineering Spatial-Organized Cardiac Organoids for Developmental Toxicity Testing. *Stem Cel. Rep.* 16 (5), 1228–1244. doi:10.1016/j.stemcr.2021.03.013
- Hoang, P., Wang, J., Conklin, B. R., Healy, K. E., and Ma, Z. (2018). Generation of Spatial-Patterned Early-Developing Cardiac Organoids Using Human Pluripotent Stem Cells. *Nat. Protoc.* 13 (4), 723–737. doi:10.1038/nprot.2018.006
- Hofbauer, P., Jahnel, S. M., Papai, N., Giesshammer, M., Deyett, A., Schmidt, C., et al. (2021). Cardioids Reveal Self-Organizing Principles of Human Cardiogenesis. *Cell* 184, 3299–3317. doi:10.1016/j.cell.2021.04.034
- Jabaudon, D., and Lancaster, M. (2018). Exploring Landscapes of Brain Morphogenesis with Organoids. *Development* 145 (22), dev172049. doi:10.1242/dev.172049
- Kamakura, T., Makiyama, T., Sasaki, K., Yoshida, Y., Wuriyanghai, Y., Chen, J., et al. (2013). Ultrastructural Maturation of Human-Induced Pluripotent Stem Cell-Derived Cardiomyocytes in a Long-Term Culture. *Circ. J.* 77 (5), 1307–1314. doi:10.1253/circj.CJ-12-0987
- Kattman, S. J., Witty, A. D., Gagliardi, M., Dubois, N. C., Niapour, M., Hotta, A., et al. (2011). Stage-specific Optimization of Activin/nodal and BMP Signaling Promotes Cardiac Differentiation of Mouse and Human Pluripotent Stem Cell Lines. *Cell stem cell* 8 (2), 228–240. doi:10.1016/j.stem.2010.12.008
- Ladd, A. N., Yatskevych, T. A., and Antin, P. B. (1998). Regulation of Avian Cardiac Myogenesis by Activin/TGF $\beta$  and Bone Morphogenetic Proteins. *Dev. Biol.* 204 (2), 407–419. doi:10.1006/dbio.1998.9094
- Laflamme, M. A., Chen, K. Y., Naumova, A. V., Muskheli, V., Fugate, J. A., Dupras, S. K., et al. (2007). Cardiomyocytes Derived from Human Embryonic Stem Cells in Pro-survival Factors Enhance Function of Infarcted Rat Hearts. *Nat. Biotechnol.* 25 (9), 1015–1024. doi:10.1038/nbt1327
- Lancaster, M. A., Renner, M., Martin, C.-A., Wenzel, D., Bicknell, L. S., Hurles, M. E., et al. (2013). Cerebral Organoids Model Human Brain Development and Microcephaly. *Nature* 501 (7467), 373–379. doi:10.1038/nature12517
- Lescroart, F., Chabab, S., Lin, X., Rulands, S., Paulissen, C., Rodolosse, A., et al. (2014). Early Lineage Restriction in Temporally Distinct Populations of Mesp1 Progenitors during Mammalian Heart Development. *Nat. Cel Biol* 16 (9), 829–840. doi:10.1038/ncb3024
- Lescroart, F., Wang, X., Lin, X., Swedlund, B., Gargouri, S., Sánchez-Dànes, A., et al. (2018). Defining the Earliest Step of Cardiovascular Lineage Segregation by Single-Cell RNA-Seq. *Science* 359 (6380), 1177–1181. doi:10.1126/science.aao4174
- Lewis-Israeli, Y. R., Wasserman, A. H., and Aguirre, A. (2021a). Heart Organoids and Engineered Heart Tissues: Novel Tools for Modeling Human Cardiac Biology and Disease. *Biomolecules* 11 (9), 1277. doi:10.3390/biom11091277
- Lewis-Israeli, Y. R., Wasserman, A. H., Gabalski, M. A., Volmert, B. D., Ming, Y., Ball, K. A., et al. (2021b). Self-assembling Human Heart Organoids for the Modeling of Cardiac Development and Congenital Heart Disease. *Nat. Commun.* 12 (1), 1–16. doi:10.1038/s41467-021-25329-5
- Li, M., and Izpisua Belmonte, J. C. (2019). Organoids - Preclinical Models of Human Disease. *N. Engl. J. Med.* 380 (6), 569–579. doi:10.1056/NEJMra1806175
- Lian, X., Bao, X., Zilberter, M., Westman, M., Fisahn, A., Hsiao, C., et al. (2015). Chemically Defined, Albumin-free Human Cardiomyocyte Generation. *Nat. Methods* 12 (7), 595–596. doi:10.1038/nmeth.3448
- Lian, X., Hsiao, C., Wilson, G., Zhu, K., Hazeltine, L. B., Azarin, S. M., et al. (2012). Cozzarelli Prize Winner: Robust Cardiomyocyte Differentiation from Human Pluripotent Stem Cells via Temporal Modulation of Canonical Wnt Signaling. *Proc. Natl. Acad. Sci.* 109 (27), E1848–E1857. doi:10.1073/pnas.1200250109
- Lian, X., Zhang, J., Azarin, S. M., Zhu, K., Hazeltine, L. B., Bao, X., et al. (2013). Directed Cardiomyocyte Differentiation from Human Pluripotent Stem Cells by Modulating Wnt/ $\beta$ -Catenin Signaling under Fully Defined Conditions. *Nat. Protoc.* 8 (1), 162–175. doi:10.1038/nprot.2012.150
- Lyons, I., Parsons, L. M., Hartley, L., Li, R., Andrews, J. E., Robb, L., et al. (1995). Myogenic and Morphogenetic Defects in the Heart Tubes of Murine Embryos Lacking the Homeo Box Gene Nkx2-5. *Genes Dev.* 9 (13), 1654–1666. doi:10.1101/gad.9.13.1654
- Ma, Z., Wang, J., Loskill, P., Huebsch, N., Koo, S., Svedlund, F. L., et al. (2015). Self-organizing Human Cardiac Microchambers Mediated by Geometric Confinement. *Nat. Commun.* 6 (1), 1–10. doi:10.1038/ncomms8413
- Marvin, M. J., Di Rocco, G., Gardiner, A., Bush, S. M., and Lassar, A. B. (2001). Inhibition of Wnt Activity Induces Heart Formation from Posterior Mesoderm. *Genes Dev.* 15 (3), 316–327. doi:10.1101/gad.855501
- Miller, A. J., Dye, B. R., Ferrer-Torres, D., Hill, D. R., Overeem, A. W., Shea, L. D., et al. (2019). Generation of Lung Organoids from Human Pluripotent Stem Cells *In Vitro*. *Nat. Protoc.* 14 (2), 518–540. doi:10.1038/s41596-018-0104-8
- Mills, R. J., Humphrey, S. J., Fortuna, P. R. J., Lor, M., Foster, S. R., Quaife-Ryan, G. A., et al. (2021). BET Inhibition Blocks Inflammation-Induced Cardiac Dysfunction and SARS-CoV-2 Infection. *Cell* 184 (8), 2167–2182. doi:10.1016/j.cell.2021.03.026
- Mills, R. J., Parker, B. L., Quaife-Ryan, G. A., Voges, H. K., Needham, E. J., Bornot, A., et al. (2019). Drug Screening in Human PSC-Cardiac Organoids Identifies Pro-proliferative Compounds Acting via the Mevalonate Pathway. *Cell stem cell* 24 (6), 895–907. doi:10.1016/j.stem.2019.03.009
- Mills, R. J., Titmarsh, D. M., Koenig, X., Parker, B. L., Ryall, J. G., Quaife-Ryan, G. A., et al. (2017). Functional Screening in Human Cardiac Organoids Reveals a Metabolic Mechanism for Cardiomyocyte Cell Cycle Arrest. *Proc. Natl. Acad. Sci. USA* 114 (40), E8372–E8381. doi:10.1073/pnas.1707316114
- Nakajima, Y., Yamagishi, T., Ando, K., and Nakamura, H. (2002). Significance of Bone Morphogenetic Protein-4 Function in the Initial Myofibrillogenesis of Chick Cardiogenesis. *Dev. Biol.* 245 (2), 291–303. doi:10.1006/dbio.2002.0637
- Pagliarini, O., Picchio, V., Chimentì, I., Messina, E., and Gaetani, R. (2020). Building an Artificial Cardiac Microenvironment: A Focus on the Extracellular Matrix. *Front. Cel Dev. Biol.* 8, 919. doi:10.3389/fcell.2020.559032
- Paşca, S. P. (2018). The Rise of Three-Dimensional Human Brain Cultures. *Nature* 553 (7689), 437–445. doi:10.1038/nature25032
- Ronaldson-Bouchard, K., Ma, S. P., Yeager, K., Chen, T., Song, L., Sirabella, D., et al. (2018). Advanced Maturation of Human Cardiac Tissue Grown from Pluripotent Stem Cells. *Nature* 556 (7700), 239–243. doi:10.1038/s41586-018-0016-3
- Saga, Y., Hata, N., Kobayashi, S., Magnuson, T., Seldin, M. F., and Taketo, M. M. (1996). MesP1: a Novel Basic helix-loop-helix Protein Expressed in the Nascent Mesodermal Cells during Mouse Gastrulation. *Development* 122 (9), 2769–2778. doi:10.1242/dev.122.9.2769
- Saga, Y., Kitajima, S., and Miyagawa-Tomita, S. (2000). Mesp1 Expression Is the Earliest Sign of Cardiovascular Development. *Trends Cardiovascular Medicine* 10 (8), 345–352. doi:10.1016/S1050-1738(01)00069-X

- Sahara, M., Santoro, F., and Chien, K. R. (2015). Programming and Reprogramming a Human Heart Cell. *Embo J.* 34 (6), 710–738. doi:10.15252/embj.201490563
- Sato, T., Stange, D. E., Ferrante, M., Vries, R. G. J., Van Es, J. H., Van Den Brink, S., et al. (2011). Long-term Expansion of Epithelial Organoids from Human colon, Adenoma, Adenocarcinoma, and Barrett's Epithelium. *Gastroenterology* 141 (5), 1762–1772. doi:10.1053/j.gastro.2011.07.050
- Schutgens, F., and Clevers, H. (2020). Human Organoids: Tools for Understanding Biology and Treating Diseases. *Annu. Rev. Pathol. Mech. Dis.* 15, 211–234. doi:10.1146/annurev-pathmechdis-012419-032611
- Smith, S. M., and Eichele, G. (1991). Temporal and Regional Differences in the Expression Pattern of Distinct Retinoic Acid Receptor-Beta Transcripts in the Chick Embryo. *Development* 111 (1), 245–252. doi:10.1242/dev.111.1.245
- Tiburcy, M., Hudson, J. E., Balfanz, P., Schlick, S., Meyer, T., Chang Liao, M.-L., et al. (2017). Defined Engineered Human Myocardium with Advanced Maturation for Applications in Heart Failure Modeling and Repair. *Circulation* 135 (19), 1832–1847. doi:10.1161/CIRCULATIONAHA.116.024145
- Ueno, S., Weidinger, G., Osugi, T., Kohn, A. D., Golob, J. L., Pabon, L., et al. (2007). Biphasic Role for Wnt/beta-Catenin Signaling in Cardiac Specification in Zebrafish and Embryonic Stem Cells. *Proc. Natl. Acad. Sci.* 104 (23), 9685–9690. doi:10.1073/pnas.0702859104
- Vincent, S. D., and Buckingham, M. E. (2010). How to Make a Heart. *Curr. Top. Dev. Biol.* 90, 1–41. doi:10.1016/S0070-2153(10)90001-X
- Voges, H. K., Mills, R. J., Elliott, D. A., Parton, R. G., Porrello, E. R., and Hudson, J. E. (2017). Development of a Human Cardiac Organoid Injury Model Reveals Innate Regenerative Potential. *Development* 144 (6), 1118–1127. doi:10.1242/dev.143966
- Warmflash, A., Sorre, B., Etoc, F., Siggia, E. D., and Brivanlou, A. H. (2014). A Method to Recapitulate Early Embryonic Spatial Patterning in Human Embryonic Stem Cells. *Nat. Methods* 11 (8), 847–854. doi:10.1038/nmeth.3016
- Wiegerinck, R. F., Cojoc, A., Zeidenweber, C. M., Ding, G., Shen, M., Joyner, R. W., et al. (2009). Force Frequency Relationship of the Human Ventricle Increases during Early Postnatal Development. *Pediatr. Res.* 65 (4), 414–419. doi:10.1203/PDR.0b013e318199093c
- Yang, L., Soonpaa, M. H., Adler, E. D., Roepke, T. K., Kattman, S. J., Kennedy, M., et al. (2008). Human Cardiovascular Progenitor Cells Develop from a KDR+ Embryonic-Stem-Cell-Derived Population. *Nature* 453 (7194), 524–528. doi:10.1038/nature06894
- Yang, X., Pabon, L., and Murry, C. E. (2014). Engineering Adolescence. *Circ. Res.* 114 (3), 511–523. doi:10.1161/CIRCRESAHA.114.300558
- Yang, X., and Murry, C. E. (2017). One Stride Forward: Maturation and Scalable Production of Engineered Human Myocardium. *Circulation* 135 (19), 1848–1850. doi:10.1161/CIRCULATIONAHA.117.024751
- Zhang, Q., Jiang, J., Han, P., Yuan, Q., Zhang, J., Zhang, X., et al. (2011). Direct Differentiation of Atrial and Ventricular Myocytes from Human Embryonic Stem Cells by Alternating Retinoid Signals. *Cell Res* 21 (4), 579–587. doi:10.1038/cr.2010.163
- Zhao, D., Lei, W., and Hu, S. (2021). Cardiac Organoid - a Promising Perspective of Preclinical Model. *Stem Cel Res Ther* 12 (1), 1–10. doi:10.1186/s13287-021-02340-7
- Zhao, Y., Rafatian, N., Feric, N. T., Cox, B. J., Aschar-Sobbi, R., Wang, E. Y., et al. (2019). A Platform for Generation of Chamber-specific Cardiac Tissues and Disease Modeling. *Cell* 176 (4), 913–927. doi:10.1016/j.cell.2018.11.042
- Zimmermann, W. H., Fink, C., Kralisch, D., Remmers, U., Weil, J., and Eschenhagen, T. (2000). Three-dimensional Engineered Heart Tissue from Neonatal Rat Cardiac Myocytes. *Biotechnol. Bioeng.* 68 (1), 106–114. doi:10.1002/(sici)1097-0290(20000405)68:1<106:aid-bit13>3.0.co;2-3

**Conflict of Interest:** The authors declare that the research was conducted in the absence of any commercial or financial relationships that could be construed as a potential conflict of interest.

**Publisher's Note:** All claims expressed in this article are solely those of the authors and do not necessarily represent those of their affiliated organizations, or those of the publisher, the editors and the reviewers. Any product that may be evaluated in this article, or claim that may be made by its manufacturer, is not guaranteed or endorsed by the publisher.

Copyright © 2022 Ramirez-Calderon, Colombo, Hernandez-Bautista, Astro and Adamo. This is an open-access article distributed under the terms of the Creative Commons Attribution License (CC BY). The use, distribution or reproduction in other forums is permitted, provided the original author(s) and the copyright owner(s) are credited and that the original publication in this journal is cited, in accordance with accepted academic practice. No use, distribution or reproduction is permitted which does not comply with these terms.



# Toward Best Practices for Controlling Mammalian Cell Culture Environments

Shannon G. Klein<sup>1</sup>, Alexandra Steckbauer<sup>1</sup>, Samhan M. Alsolami<sup>2</sup>, Silvia Arossa<sup>1</sup>,  
Anieka J. Parry<sup>1</sup>, Mo Li<sup>2\*</sup> and Carlos M. Duarte<sup>1\*</sup>

<sup>1</sup>Red Sea Research Center (RSRC) and Computational Bioscience Research Center (CBRC), King Abdullah University of Science and Technology, Thuwal, Saudi Arabia, <sup>2</sup>Biological and Environmental Science and Engineering Division (BESE), King Abdullah University of Science and Technology, Thuwal, Saudi Arabia

## OPEN ACCESS

### Edited by:

Jangho Kim,  
Chonnam National University, South  
Korea

### Reviewed by:

Ignacio Gimenez,  
University of Zaragoza, Spain  
Elisa Cimetta,  
University of Padua, Italy

### \*Correspondence:

Mo Li  
mo.li@kaust.edu.sa  
Carlos M. Duarte  
carlos.duarte@kaust.edu.sa

### Specialty section:

This article was submitted to  
Stem Cell Research,  
a section of the journal  
Frontiers in Cell and Developmental  
Biology

**Received:** 03 October 2021

**Accepted:** 26 January 2022

**Published:** 21 February 2022

### Citation:

Klein SG, Steckbauer A, Alsolami SM,  
Arossa S, Parry AJ, Li M and  
Duarte CM (2022) Toward Best  
Practices for Controlling Mammalian  
Cell Culture Environments.  
Front. Cell Dev. Biol. 10:788808.  
doi: 10.3389/fcell.2022.788808

The characterization, control, and reporting of environmental conditions in mammalian cell cultures is fundamental to ensure physiological relevance and reproducibility in basic and preclinical biomedical research. The potential issue of environment instability in routine cell cultures in affecting biomedical experiments was identified many decades ago. Despite existing evidence showing variable environmental conditions can affect a suite of cellular responses and key experimental readouts, the underreporting of critical parameters affecting cell culture environments in published experiments remains a serious problem. Here, we outline the main sources of potential problems, improved guidelines for reporting, and deliver recommendations to facilitate improved culture-system based research. Addressing the lack of attention paid to culture environments is critical to improve the reproducibility and translation of preclinical research, but constitutes only an initial step towards enhancing the relevance of *in vitro* cell cultures towards *in vivo* physiology.

**Keywords:** batch culture, reproducibility, pH, oxygen, carbon dioxide, stem cells, cancer cells

## INTRODUCTION

Mammalian cell cultures have been a foundational resource in almost every biomedical research program since the 1990s (Petricciani, 1995; Hu and Aunins, 1997; Merten, 2006). The use of mammalian cell cultures as preclinical models ranges from the characterization of *in vivo* physiological mechanisms and manipulation of disease-related pathways to the maintenance of stem cells for therapeutic purposes. Culture systems are used to maintain cells in a state that mimics *in vivo* physiological conditions (Papkovsky, 2004; Michl et al., 2019), ensuring the clinical compatibility of experimental findings. Physiological conditions in mammalian cell cultures typically aim to mimic conditions in extracellular fluids, including temperature, typically adjusted to 37°C, O<sub>2</sub> to 18.6%–20.9%, CO<sub>2</sub> to 5%, and pH adjusted to 7.4 units (Wenger et al., 2015). Maintaining relevant physiological conditions in cell cultures is of paramount importance to ensure the reproducibility of published findings and the translational relevance of experimental data to clinical applications. Yet, inadequate reproducibility of experimental findings in biomedical research is an increasingly well-recognized problem (Begley, 2013; Collins and Tabak, 2014), contributing to delays in drug discovery and therapies (Freedman et al., 2015).

Best-practice guidelines are used to ensure standards in biomedical research, encompassing multiple aspects of the research practice (Baust et al., 2017), but have not yet included comprehensive standards for the reporting or control of environmental conditions in cell-culture systems. The most common approach to *in vitro* cell culture is when cells are grown either in suspension or as adherent monolayers in standard media within tissue culture flasks (defined here as “standard batch culture”). This approach is most popular since it reliably induces the proliferation of cells, is affordable, and



scalable in terms of the possible number of biological replicates and treatments. Although the standard batch culture of cells meets the critical need for continuous sources of biological material, most biomedical researchers using standard culture systems acknowledge that they are limited in their capacity to maintain cell homeostasis within the physiological limits experienced *in vivo* (Place et al., 2017; Al-Ani et al., 2018; Hirsch and Schildknecht, 2019). Despite this awareness and the scope for substantial environmental variability during the standard batch culture of cells (Michl et al., 2019), recent assessments show that the majority of research papers rely on nominal set points and fail to directly verify and report environmental parameters (Al-Ani et al., 2018; Michl et al., 2019; Klein et al., 2021b). Standard batch culture systems undergo substantial environmental changes owing to cell metabolic activity (Balin et al., 1976; Naciri et al., 2008; Vallejos et al., 2010; Pradhan et al., 2012; Al-Ani et al., 2018; Michl et al., 2019), with pH declines reaching 0.9 units, O<sub>2</sub> levels declining down to 0.95%, and CO<sub>2</sub> values reaching up to 10.45% (Klein et al., 2021b). In light of these reported changes, the apparent reliance on nominal set points to ensure physiological relevance and reproducibility in biomedical research requires urgent reconsideration. Although Eagle (1971) first highlighted environmental drift in standard batch cultures almost 50 years ago, we are aware of only three papers that collectively measured and reported O<sub>2</sub> or CO<sub>2</sub> regimes in *in vitro* cultures of mammalian cells (Balin et al., 1976; Naciri et al., 2008; Vallejos et al., 2010). Inadequate control and reporting of environmental conditions in cell cultures is, therefore, a candidate contributor to irreproducibility in basic and preclinical biomedical research.

Here, we provide guidelines for the reporting and control of environmental conditions in cell culture systems, with a focus on metabolic gases (O<sub>2</sub> and CO<sub>2</sub>) and the associated acid-base balance driving pH. We (i) raise awareness of the imperative to control and monitor cell culture environments in biomedical research, (ii) propose short- and long-term standards for control, monitoring, and reporting with consideration of resource availability, and (iii) highlight the steps needed for these recommendations to be achieved. We outline the most common problems resulting in uncontrolled environmental conditions and associated confounding factors, and then provide a range of solutions. We also supply a reporting workflow that ensures improved standards for the reporting and control of culture environments to enhance reproducibility and progress in biomedical research.

## THE PROBLEMS

### Environmental Instability in Cell Culture Media

Documented reports of deoxygenation and disruptions to acid-base stability in culture media caused by cellular metabolism equate to a median pH shift of 0.425 units and a median O<sub>2</sub> shift of 10.6% from target (nominal) values (see, Klein et al., 2021b). Cells are capable of buffering against extracellular reductions in

pH to maintain alkaline pH of the cytoplasm (Johnson et al., 1976; L'allemain et al., 1984; Lindström and Sehlin, 1984; Pouyssegur et al., 1985; McBrien et al., 2013). However, such mechanisms (e.g., Na<sup>+</sup>/H<sup>+</sup> antiporters or histone deacetylation) consume cellular energy and can alter gene transcription and reduce cellular growth through changes in the acetylation state of chromatin (Boron and Russell, 1983; Bowen and Levinson, 1984; Boron, 2004). Changes in dissolved gases are also well known to substantially affect cellular physiology. Besides the role of O<sub>2</sub> in affecting the most fundamental characteristics of *in vitro* cell cultures (Packer and Fuehr, 1977), including the dependence of cellular metabolism on O<sub>2</sub> (Ast and Mootha, 2019), deoxygenation can also activate the hypoxia-inducible factor (HIF) transcription system, which triggers the expression of most genes responsible for cellular adaptation to varying O<sub>2</sub> levels (Semenza et al., 1991; Wang et al., 1995; Semenza, 2012). Minor deviations in dCO<sub>2</sub> can also induce a wide range of cellular responses (Bumke et al., 2003; Kikuchi et al., 2017; Kikuchi et al., 2019), affecting the function of biomolecules and the proteome (Duarte et al., 2020).

The impacts of compromised acid-base stability and O<sub>2</sub> delivery on cellular responses during *in vitro* cell culture are not confined to theory (see syntheses by; Ast and Mootha, 2019; Keeley and Mann, 2019; Klein et al., 2021b). Briefly, for instance, Michl and others (2019) showed that cellular growth of three colorectal cell-lines (NCI-H747, DLD1, Caco2) was optimal at pH 7.4, but when medium pH deviated from 7.4 by > 0.3 units all three cell lines exhibited reduced rates of proliferation. Medium acidification during *in vitro* cell culture can also initiate pro-inflammatory signaling responses in human aortic smooth muscle cells (Tomura et al., 2005) and cells of the human nucleus pulposus (Gilbert et al., 2016). A transcriptomic study, focusing on human fibroblasts, revealed that reductions in medium pH (to pH 6.7) modulated the expression of 2,068 genes (out of 12,565) by more than two-fold after only 24 h of culture (Bumke et al., 2003). Constraining O<sub>2</sub> availability during *in vitro* cell culture appears to be similarly crucial. For example, HepG2 cultures at confluence rapidly depleted O<sub>2</sub> levels to <1% to self-inflict a switch from oxidative phosphorylation to glycolysis, despite being cultured in incubator conditions providing ambient atmospheric O<sub>2</sub> levels (18.6%–20.9%) (Wolff et al., 1993). These findings are highly consistent with observations of other cell types, including human hepatocytes (Ng et al., 2014) and rat renal mesangial cells (Metzen et al., 1995), where perturbed O<sub>2</sub> levels correlated with anomalous cellular responses (Keeley and Mann, 2019). Although limited, some evidence suggests that variable culture environments can also affect the reproducibility of cell culture experiments. Indeed, barcoding experiments showed that cancer cell-line evolution occurred from positive clonal selection that was highly sensitive to culture conditions (Ben-David et al., 2018). Further experiments testing the cell-line strains against anti-cancer compounds uncovered disparate drug responses, although the exact sources of instabilities in culture environments that promoted cell-line heterogeneity were not resolved (Ben-David et al., 2018).

## Factors Contributing to Environmental Instability in Cell Culture Media

Most commercial media contain buffering systems that act only to regulate pH, whereas levels of dissolved O<sub>2</sub> and CO<sub>2</sub> are regulated by atmosphere re-equilibration. The initial stability of medium pH is typically achieved by mimicking the physiologically relevant CO<sub>2</sub>/HCO<sub>3</sub><sup>−</sup> buffering system (Michl et al., 2019). Most media formulations contain a known concentration of HCO<sub>3</sub><sup>−</sup>, which upon exposure to an incubator that nominally maintains a CO<sub>2</sub>-rich atmosphere (typically 5% CO<sub>2</sub> in air), equilibrates to spontaneously produce H<sup>+</sup> ions and stabilize pH (**Supplementary Box S1**). Although the CO<sub>2</sub>/HCO<sub>3</sub><sup>−</sup> buffer system is indeed the primary physiological buffering system in mammalian fluids (Boron, 2004; Michl et al., 2019), standard cell cultures lack the regulatory systems (e.g., changes in respiratory rate, vascular remodeling, renal control of HCO<sub>3</sub><sup>−</sup> and H<sup>+</sup>) present in the mammalian body. Such systems regulate for the changes in dissolved gases, waste products (e.g., lactic acid), and H<sup>+</sup> ions involved in cellular metabolism, thereby achieving conditions that maintain homeostasis (**Supplementary Box S1**). Although consistent observations of pH instability in standard cell cultures prompted the use of additional exogenous buffers in media formulations to enhance medium buffering capacity (Eagle, 1971), such approaches can, in some cases, promote unpredictable changes in pH and introduce confounding artifacts (Michl et al., 2019, see below).

In the case of O<sub>2</sub>, medium deoxygenation is caused by the disparity between rates of O<sub>2</sub> consumption via cellular metabolism and the replenishment of O<sub>2</sub> at the air-medium interface (Place et al., 2017; Al-Ani et al., 2018). Specifically, O<sub>2</sub> first dissolves at the air-medium interface and then diffuses through the liquid (at least several millimeters) to reach and oxygenate cell microenvironments (Place et al., 2017) even as cells undergo exponential growth. This is contrary to *in vivo* physiology, where most cells exist within 100 μm to the nearest capillaries that replenish O<sub>2</sub> and act to remove excess CO<sub>2</sub>. Besides the role of CO<sub>2</sub> in affecting medium acid-base chemistry, levels of CO<sub>2</sub>/HCO<sub>3</sub><sup>−</sup> readily diffuse across cell membranes to moderate intracellular pH (Gutknecht et al., 1977), act as metabolic inhibitors, and may induce complex transcriptional responses (Cottier et al., 2012; Follonier et al., 2013), and signal other critical reactions (see, Blombach and Takors, 2015). In concert, these processes interact to create a changing environmental gradient from the surface of the medium down to the microenvironment of the cells (Place et al., 2017). The effect of unstirred medium layers also presumably determines the delivery of nutrients/growth factors and the removal of other metabolic waste products (e.g., lactic acid), which can also act to directly and indirectly moderate environmental variation (Michl et al., 2019).

Changes in the culture environment may also initiate complex feedback mechanisms, where cellular responses to variations in the culture environment could, in turn, inflict greater intrusions of environmental stability and promote unpredictable outcomes. For instance, perturbations to dissolved O<sub>2</sub> levels in culture

medium can induce cells to switch away from oxidative phosphorylation towards anaerobic glycolysis (Wolff et al., 1993), leading to large accumulations of lactic acid that force medium acidification (Michl et al., 2019). Another example lies in the role of carbonic anhydrases (CA), which catalyze the hydration of CO<sub>2</sub>. Švastová and others showed that medium deoxygenation in cell cultures of human cancer cell lines induced the expression and activity of carbonic anhydrases, which resulted in enhanced acidification of the culture medium (Švastová et al., 2004).

## Lack of Detailed Methodological Reporting

The lack of monitoring and reporting of environmental conditions in cell culture-systems is a pervasive, but under-recognized problem (Hunter, 2017; Al-Ani et al., 2018; Michl et al., 2019; Klein et al., 2021a; Klein et al., 2021b). A recent synthesis examining this problem sub-sampled 688 papers published between 2014 and 2019 and found that most papers reported the medium manufacturer, but only one third reported the type of culture system utilized and 42% reported temperature and CO<sub>2</sub> incubator settings (Klein et al., 2021b). Another post-publication analysis reported that less than half of studies published in *Cancer Research* and *Nature* in the third quarter of 2017 described the brand of medium, and only one-tenth declared the medium-buffering regime (Michl et al., 2019). Even when protocols are declared, there is an unfortunate prevalence of papers stating, “as previously described by ref. (x),” which often leads to a chain of citations that generate confusion as to the specific procedures, reagents, and materials involved (Freedman et al., 2015). In cases where environmental parameters are measured, these are often not reported. The apparent under appreciation of reporting measured environmental parameters is exemplified by published bioreactor experiments that report only the target levels of environmental parameters (e.g., Karst et al., 2016; Abecasis et al., 2017). Indeed, these systems, by design, typically require consistent monitoring of the controlled parameters via a feedback loop to achieve the desired control.

## Failure to Monitor Mammalian Cell Culture Environments

A recent synthesis revealed that despite differences in cell type, medium formulation, and buffering components, all investigated standard batch cultures exhibited environmental drift after only a few days of culture (Klein et al., 2021b). Despite this, less than 0.05% of studies monitored pH, CO<sub>2</sub>, or O<sub>2</sub> levels in cell cultures. Klein et al. (2021a) reported median declines in dissolved O<sub>2</sub> down to 7.3%, and increases in dissolved CO<sub>2</sub> to values ranging from 7.5% to 9.5%, compared to the nominal O<sub>2</sub> and CO<sub>2</sub> targets of 21% and 5%, respectively. The reported median decline in pH was 0.43 units, but in some particularly extreme cases, cell metabolic activity promoted pH reductions that approached one pH unit (Eagle, 1971) and dissolved O<sub>2</sub> decreased down to 0.95% (Vallejos et al., 2010). In such extreme cases, variations in culture conditions may resemble levels consistent with hypercapnia and hypoxia rather than conditions typical of *in vivo* extracellular fluids, although *in vivo* environments vary



considerably among selected tissues (Ast and Mootha, 2019). It is implicitly assumed that culture temperature is controlled at 37°C and thus, incubator temperatures were only reported in 42% of papers between 2014 and 2019 (Klein et al., 2021b). However, a number of studies used different culture temperatures (Brinkhof et al., 2015; Xu et al., 2017), which highlights the need to declare and monitor the incubation temperature.

## Artefacts Introduced by Forcing of Non-Physiological Controls

Numerous approaches are used to control culture conditions, either to maintain physiological conditions or to test the effects of departures from those conditions (e.g., hypoxia; Grayson et al., 2006; acidosis; Kikuchi et al., 2017). However, some approaches misrepresent *in vivo* physiology and in doing so, inadvertently introduce artefacts and biases that could compromise reproducibility and relevance of the study to cellular function in the living organism. For instance, NVBs (e.g., HEPES, PIPES, or MES) are used to enhance acid-base stability of medium because the physiological  $\text{HCO}_3^-/\text{CO}_2$  buffering system can exhibit high volatility and a weak buffering capacity (**Supplementary Box S1**). However, it is vital to consider how NVBs introduce active molecules and acid-base reactions absent from mammalian fluids and existing evidence, although limited, indicates that NVBs could induce toxicity and anomalous cellular responses in particular cell types (Good et al., 1966; Lepe-Zuniga et al., 1987; Hanrahan and Tabcharani, 1990; Stea and Nurse, 1991). In particular, HEPES is commonly included in commercial media formulations, yet emerging reports demonstrate a range of possible side-effects. Briefly, HEPES activated lysosomal transcription factors in macrophages (Tol et al., 2018), inhibited the prion protein conversion in neural stem cells and affected their viability and differentiation (Delmouly et al., 2011). Another study showed cellular uptake of HEPES in human cell lines (MCF-7, U2OS, HeLa) that persisted for 48 h after cells were returned to HEPES-free media (Depping and Seeger, 2019).

Recent assessments also shows that NVB addition may not fully prevent pH declines in standard batch cultures and may lead to unexpected pH changes when interacting with the  $\text{HCO}_3^-/\text{CO}_2$  buffering system, although predictable pH levels can be obtained when appropriate protocols are used (see, Michl et al., 2019). Researchers often manipulate medium pH by titrating acids and bases to achieve a desired level. The titration of acids and bases (including HCl, NaOH, and NVBs) introduces osmolytes ( $\text{Na}^+$ ,  $\text{Cl}^-$ ) to cell medium and can result in substantial changes to medium osmolality by > 10% (Michl et al., 2019). Supra-physiological osmolality can directly affect cell membrane tension and volume (Pedersen et al., 2013), but can also moderate how cells respond to other environmental parameters (Dezengotita et al., 1998). For instance, hybridoma cells exposed to elevated  $\text{CO}_2$  conditions exhibited reduced growth rates when osmolality was held constant at 361 mOsm  $\text{kg}^{-1}$ , but cell growth rates further declined by 30% when medium osmolality was 415 mOsm  $\text{kg}^{-1}$  (Dezengotita et al., 1998).

## THE SOLUTIONS

### Measure Environmental Parameters

Key environmental parameters (temperature,  $\text{O}_2$ ,  $\text{CO}_2$ , and pH) should be accurately measured and reported. Researchers should also consider measurements of osmolality and hydrostatic pressure (if experiments are not conducted at atmospheric pressure) because these variables are required for unit conversions of dissolved gases (Christmas and Bassingthwaite, 2017), thereby facilitating accurate replication and comparisons of conditions among studies. Ideally, measurements of key parameters ( $\text{O}_2$ ,  $\text{CO}_2$ , and pH) should be conducted to capture the variability that cell cultures experience, either continuously where logging systems can be used or via non-autonomous, regular measurements. A basic understanding of the expected variability for each of these parameters in specific experimental setups can be used to help guide the frequency of measurements required to capture the variability. As a minimum requirement in routine cell cultures, initial and final values are required for cases of linear drift characteristic of many batch culture experiments (Michl et al., 2019), whereas frequent recording (e.g., 1-min intervals) are likely required for advanced bioreactor systems involving gas and/or acid and base additions. Measuring these parameters at concurrent time points is critical to understand the interdependencies among parameters, and guide the explanation of their possible forcing on cellular responses (e.g., proliferation, metabolism, changes in gene transcription, epigenetic regulation). For instance, the solubility of dissolved gases, and thus the influence of  $\text{CO}_2$  on acid-base chemistry, is strongly dependent on temperature, osmolality, humidity, and pressure (Christmas and Bassingthwaite, 2017). Although thermal regimes of cell cultures may be reliably inferred from calibrated incubators, levels of dissolved  $\text{O}_2$  and  $\text{CO}_2$ , as well as pH must be measured directly in the culture medium because cellular metabolism directly affects these parameters (**Supplementary Table S1**). Measuring systems capable of delivering the required precision and accuracy are available for all key environmental parameters. Such systems range in cost, from moderately priced sensors for temperature, pH,  $\text{O}_2$ , and salinity to the more expensive sensing equipment required for monitoring dissolved  $\text{CO}_2$ , which often require complex calibration protocols (**Supplementary Table S1**).

Levels of relative humidity and media evaporation are equally important considerations for the control of cell culture environments. Since variations in both factors result in changes to osmolality as well as solute and gas concentrations, that in turn, affect diffusion. Unfortunately, variations in relative humidity even in sophisticated incubators are common (Triaud et al., 2003), but they should be recognized and remedied. Low-cost sensors are available to monitor relative humidity levels inside incubators (**Supplementary Table S1**, Rajan et al., 2017) and should also be reported alongside key environmental variables. For relative humidity and the minimization of medium evaporation, water baths or pans placed inside incubators provide a simple and cost-effective solution to maintaining adequate levels, although this approach is limited in its capacity for precise control and can elevate the risk of condensation and contamination. Watertight joints in culture

# PRINCE GUIDELINES

[Preferred Reporting Items for describing the Nature of Culturing Environments]



## ID & HISTORY

- Describe origin and history of cultured cells
- Protocols of cell extraction, isolation, authentication



## CULTURE SET-UP

- Describe system
- Include: culture vessel, growth area, header space, volume ratio, working volume



## EQUIPMENT

- Sensors/meters used to measure environmental conditions
- Include consumables (e.g. pH-sensitive dyes)



## SET POINTS

- Declare environmental parameters
- Include: temperature, initial media pH, oxygen, carbon dioxide levels



## PARAMETER CONTROL

- Explain how conditions were adjusted to achieve each set point



## CALIBRATIONS

- Report any calibration methods for dyes, meters, sensors



## FORMULATION

- Report the media recipe, and its buffering system
- Include any additives (e.g. serum, antibiotics)



## MAINTENANCE

- How the culture is established, replenished
- Include: media exchanges, passaging, cell detachment



## MEASUREMENTS

- Measuring the monitoring of parameters
- Include: frequency, timing, equipment



## DATA & AVAILABILITY

- Report descriptive statistics for culture environment data
- Archive protocols, data online - for free



## OTHER RESOURCES

- Include additional data, cited protocols as supplementary
- Avoid "as described by ref [x]" statements



See the full guide for PRINCE in cell-based research

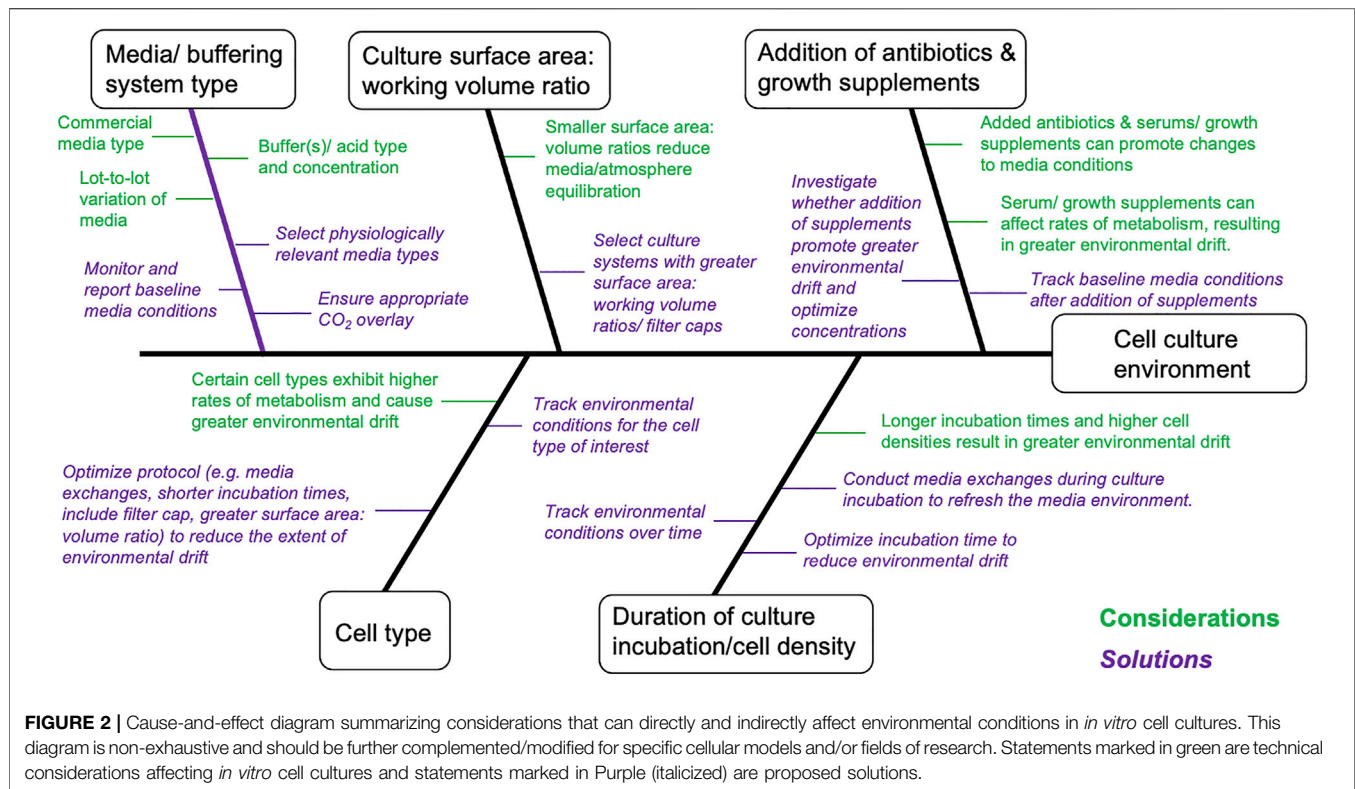
**FIGURE 1** | An overview of the PRINCE (Preferred Reporting Items for describing the Nature of Culturing Environments) guidelines. The QR provides access to the full PRINCE reporting checklist (also in **Supplementary Extended Materials S1**) containing an exhaustive list of reporting items.

incubators may also require frequent maintenance and replacement, where needed (Rajan et al., 2017). More sophisticated and costly options are available for the control of relative humidity (and minimization of medium desiccation), including direct steam humidification systems and incubators capable of two-sided controls (**Supplementary Table S1**).

Accordingly, we provide reporting guidelines (**Figure 1**, **Supplementary Extended Materials S1**) along with sample method descriptions (**Supplementary Extended Materials S2**), to guide practitioners into conducting and reporting characterizations of environmental regimes and promote a greater understanding of the factors that may affect precision and accuracy of experiments. Indeed, researchers could consider conducting pilot experiments to understand if variability in environmental factors significantly affects key experimental readouts.

## Control Environmental Parameters

A reasonable degree of control over environmental conditions is achievable in routine culture systems, but requires consideration of workflow factors that can, directly and indirectly, promote environmental drift (**Figure 2**). Interpretation and reproducibility of biomedical experiments involving mammalian cell cultures mandate that environmental parameters (temperature, O<sub>2</sub>, CO<sub>2</sub>, and pH) be at least monitored and reported, and where possible environmental variation minimized and controlled. Environmental stability is most easily achieved in advanced bioreactor culture systems, whereas achieving stability in routine batch culture systems is most challenging, with perfusion systems (and chemostats) providing intermediate solutions (**Table 1**). Batch cultures are typically maintained in incubators that maintain temperature (typically 37°C) and guarantee a CO<sub>2</sub> level (typically



5%) in the atmosphere. In batch culture set-ups, researchers often select culture medium that contains a pH indicator dye [e.g., Phenol Red (PhR)] to guide the renewal of cell medium, but medium color changes assessed “by eye” can lead to undetected pH declines (Michl et al., 2019). Indeed, batch cell cultures are the most popular, inexpensive and scalable culture system, in terms of the possible number of replicates and treatments, with <1% of the published literature utilizing cybernetic bioreactor or chemostat culture systems (2014–2019, Klein et al., 2021b). Chemostat and perfusion systems were first described in 1950 for use in bacterial cultures (Novick and Szilard, 1950a; b) and later adopted for mammalian cells in 1961 (Cohen and Eagle, 1961). Such systems can maintain environmental conditions and cell growth rates via a continuous dilution of the culture with fresh medium (Cohen and Eagle, 1961). More

sophisticated bioreactor culture systems were first introduced in the 1970s to culture mammalian cells (Knazek et al., 1972; Fouron, 1987) and typically involve the automated control of temperature, gas addition (O<sub>2</sub>, CO<sub>2</sub>), and/or acids and bases to maintain set targets for temperature, dissolved gases and pH. Bioreactors provide the best capacity to control environmental conditions, but are most costly in the context of capital investment, maintenance, and operations. Importantly, many bioreactor systems lack flexibility in the number of biological replicates and the volume of culture media (often larger than that of batch culture) that can be manipulated, which translates into greater time and monetary costs. While traditional bioreactor systems are ideal for cells culture in suspension, attached cell monolayers require different solutions. For these cell types, advanced bench top culture systems providing

**TABLE 1 |** Constraints, advantages, and solutions for improved environmental control and reproducibility for three major types of culture systems.

Culture system	Constraints	Advantages	Solutions
Monitored Batch	Limited control of environmental conditions; limited reproducibility	Effective temperature control; affordability; low maintenance; high replication possible; sterilization and autoclaving of vessels not required	Monitor environmental conditions (optimize protocol to reduce environmental drift; report environmental conditions and detailed protocols
Chemo stat/ Perfusion set-ups/ Micro-fluidics	Time investment in optimizing set-up; moderate maintenance required; moderate cost for equipment; high consumption of consumables	Affordability; effective control of conditions; control of growth rates of suspended cells; small - moderate scale replication possible	Monitor environmental conditions; optimize flow/perfusion rates; report environmental conditions and detailed protocols
Bioreactor	High-cost; high consumption of consumables / typically require larger volumes of media	Precise control of environmental conditions; control growth rate of suspended cells; high-frequency environmental monitoring. Scalable in the number of culture vessels	Randomize and repeat experiments on small-scale bioreactor set-ups; report environmental regimes and detailed protocols



convection of culture media (**Supplementary Table S1**), which are also expandable in terms of replication, will likely provide the best capacity for adherent cell types (see, Kreß et al., 2021). We provide considerations as well as suggestions for improved environmental control for culture systems ranging in complexity from batch cultures to bioreactors (**Table 1** and **Supplementary Table S2**).

## Report Procedures to Monitor and Control Environmental Data

Precise control and monitoring of environmental conditions for mammalian cell cultures need be accompanied by reporting of the procedures used—a requirement, that is, not yet sufficiently emphasized nor enforced by the majority of scientific journals. A survey assessing the reporting requirements of leading biomedical journals for publications involving mammalian cells (Cell, Nature, Science, etc.; cf. **Supplementary Extended Materials S3**) revealed that only *Nature Research*, *Science*, *Cell*, and *EMBO press* journals require a standardized declaration of reporting practices to be published as a form attached to the electronic version of the published papers (see Nature Reporting Standards and MDAR Reporting Standards). However, none of the information required in this form addresses the monitoring and control of critical environmental conditions for research conducted using mammalian cell cultures (hereafter referred to as “cell-based experiments”). Strengthening reporting requirements and standards will likely place greater emphasis on cell culturing environments and, in turn, likely enhance the reproducibility of cell-based experiments as well as their relevance to the *in vivo* environment. We address this gap by offering the PRINCE (Preferred Reporting Information on the Nature of Cell-culturing Environments) guidelines (**Supplementary Extended Materials S1**) as a checklist for the parsimonious reporting of the monitoring and control of critical environmental conditions in the experiments reported in the papers. The PRINCE reporting checklist is designed to be adopted by journals publishing cell-based experiments and be included as a required declaration at the time of submission, thereby available to be assessed by peer reviewers, to then become available as an appendix to the electronic version of the published papers (**Supplementary Extended Materials S1**). This will ensure much needed standardized reporting of cell culture conditions.

## Report Resulting Environmental Data

Monitoring and controlling environmental conditions for cell-based experiments must be accompanied by reporting the data obtained as an essential step to identify possible environmental artifacts affecting the reproducibility of the findings and their comparisons among studies. The lack of detailed methodological and data reporting prevalent in studies published to date has been attributed to strict word and page limits enforced by publishers (Freedman et al., 2015). However, while many journals, dictate strict restrictions on the main body of the published text, most journals encourage providing all relevant details in extended materials, thereby extending the space available to accurately describe the procedures used and report additional data helping interpret the results presented. Online repositories are also available for more detailed reporting of protocols (e.g., Nature’s Protocol Exchange, Dryad) and datasets (e.g., Dryad,

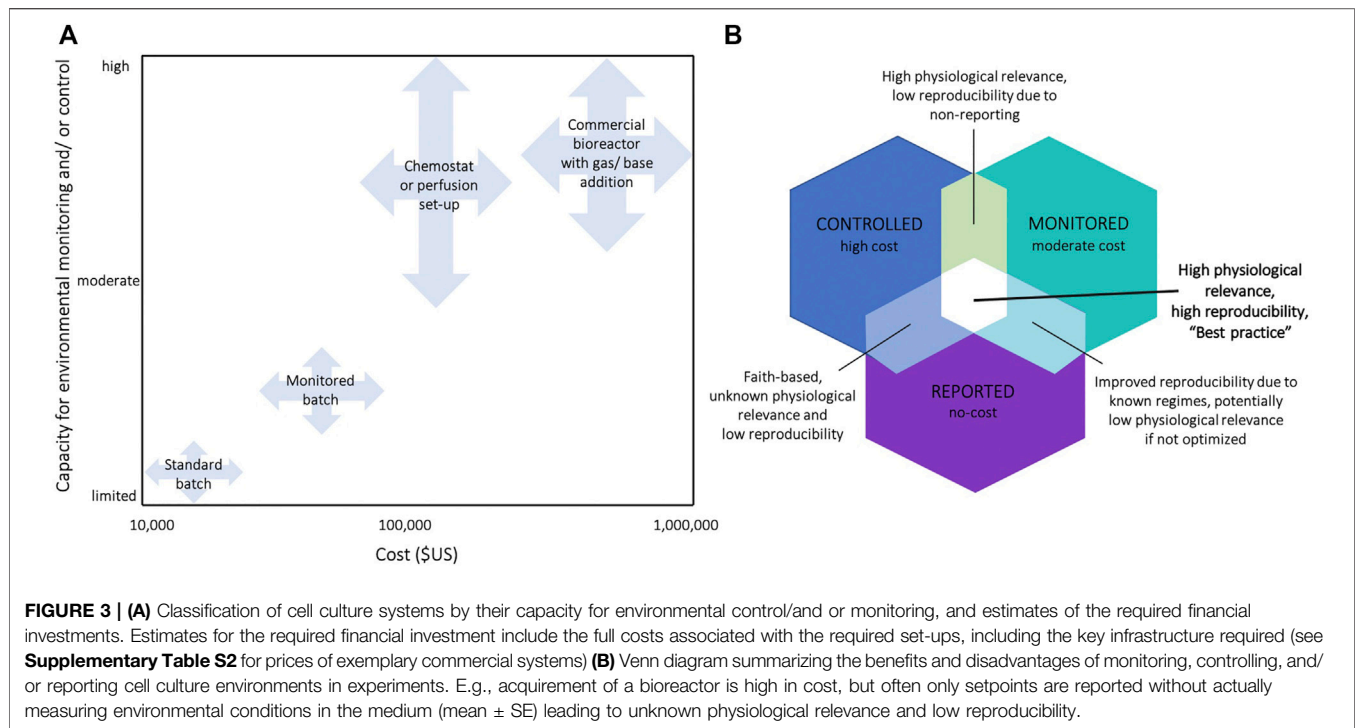
figshare and Zenodo). These data repositories were designed to meet journal and funder requirements for data availability and most of these offer data curation services that streamline the uploading process and ensure sustained access to the data.

Minimum reporting requirements should include the mean and a metric of dispersion (e.g., SD, SEM or range) for each of the monitored environmental parameters. In cases where environmental parameters display a monotonous trend over time, the slope, a metric of dispersion, as well as the probability of the slope being equal to zero may be reported to describe the change over time and can be fitted using simple linear regression analysis. Ideally, researchers would accompany such summary statistics with a supplementary figure displaying environmental regimes over time (Michl et al., 2019), so that the published findings can be interpreted alongside the nature of cell-culture conditions.

## Recommendations

The task of enhancing standards for environmental control, monitoring, and reporting in biomedical research may initially seem overwhelming provided the current absence of a culture to this end (Collins and Tabak, 2014; Baker, 2016; Hunter, 2017). Enhancing standards is also hindered by the limited availability of affordable culture systems capable of advanced environmental monitoring and control for a broad range of cell types. The lack of appropriate tools in turn contributes to the lack of awareness of the true extent of environmental instability. However, reporting only nominal set-points used in cell culture systems without verification cannot be a sustainable solution.

Resolving the issue without a systematic approach may risk putting more burden on researchers’ time, resources, and expertise. As an immediate requirement, initial and final values of key parameters should be measured and reported in the batch cultures of cell lines used in experiments. This requirement should capture existing environmental variation affecting published findings, ensuring accurate interpretation of the reported results and improved reproducibility. The provided PRINCE reporting checklist is designed to apply to a range of culture systems, from routine batch cultures to advanced culture systems (e.g., perfusion set-ups and bioreactors). Next, existing protocols must be optimized to minimize environmental variation in routine cultures (**Supplementary Table S1**). The third step is to build the capacity and infrastructure, supported by a sufficient understanding of the causes and consequences of variability in these conditions. Where needed, postgraduate biomedical programs may be revised to strengthen these competences. The next step, which requires significant investment over longer time frames (years to decades), involves the routine use of advanced cell culture technologies that allow precise and accurate control and monitoring of environmental conditions (**Figure 3**, **Supplementary Table S1**). Pending these advancements, reporting requirements should then extend to include proliferative, maintenance culture vessels, not only those dedicated to experimental assessments. Researchers should then consider the relevance *in vitro* culture environments to the levels under which particular cell types exist *in vivo*. For instance, O<sub>2</sub> levels vary across human tissues and range from 13% O<sub>2</sub> in the lung-pulmonary vein to 1–3% O<sub>2</sub> in the uterus (Ast and Mootha, 2019). By considering how niche *in vivo* environments affect experimental



outcomes, researchers could further increase the robustness of their experiments and increase the likelihood that findings have relevance to focal *in vivo* compartments (Ast and Mootha, 2019). Particular fields within biomedical science (e.g., 3D cultures and stem cell research) are already making great strides in this arena (Ryall et al., 2015; Shyh-Chang and Ng, 2017), although reliable reports of environmental parameters within selected human tissues are presently limited (Al-Ani et al., 2018; Ast and Mootha, 2019) and this research area warrants further attention.

Ultimately, improved characterization and control over environmental conditions in cell cultures will enhance the reliability of experimental findings and the confidence in their translation to clinical applications, which should provide sufficient rationale for funding bodies and institutions to invest in the necessary infrastructure. Indeed, funding agencies could consider supporting research initiatives aiming to further investigate the effects on environmental factors on commonly studied biological responses (i.e., gene expression, histone modification, metabolic pathways) in model cell lines (e.g., Bumke et al., 2003; Ben-David et al., 2018; Muelas et al., 2018). This will provide a systematic understanding of the impacts of environmental control on cell culture experiments. Transitioning towards advanced culture systems capable of mimicking *in vivo* conditions not only requires consideration of environmental parameters, but also necessitates attention to other chemical and physical factors known to program cell fate. Such factors include, but are not limited to, the common usage non-physiological concentrations of growth factors (Rubin, 2007; Holohan et al., 2013; Langhans, 2018), and antibiotics (Ryu et al., 2017), as well as the physical structure of cell microenvironments, which can alter cell morphology and function (Darnell et al., 2018). For many of these factors, existing recommendations that aim to increase the relevance

of *in vitro* cultures to *in vivo* physiology are available (Baker, 2016; Muelas et al., 2018; Hirsch and Schildknecht, 2019).

## AUTHOR CONTRIBUTIONS

CD, ML, and SK conceptualized the study. SK, AS and CD designed and wrote the first draft of the manuscript. SK, AS, AP, SMA and SA prepared the display figures and extended materials. All authors contributed to, and approved, the final version of the manuscript.

## FUNDING

King Abdullah University of Science and Technology (KAUST) funded this research through baseline funding to CD and ML. (BAS/1/1080-01-01).

## ACKNOWLEDGMENTS

We thank J. E. Thomson for assistance with design of the display figures.

## SUPPLEMENTARY MATERIAL

The Supplementary Material for this article can be found online at: <https://www.frontiersin.org/articles/10.3389/fcell.2022.788808/full#supplementary-material>



## REFERENCE

- Abecasis, B., Aguiar, T., Arnault, É., Costa, R., Gomes-Alves, P., Aspegren, A., et al. (2017). Expansion of 3D Human Induced Pluripotent Stem Cell Aggregates in Bioreactors: Bioprocess Intensification and Scaling-Up Approaches. *J. Biotechnol.* 246, 81–93. doi:10.1016/j.jbiotec.2017.01.004
- Al-Ani, A., Toms, D., Kondro, D., Thundathil, J., Yu, Y., and Ungrin, M. (2018). Oxygenation in Cell Culture: Critical Parameters for Reproducibility Are Routinely Not Reported. *PLOS ONE* 13, e0204269. doi:10.1371/journal.pone.0204269
- Ast, T., and Mootha, V. K. (2019). Oxygen and Mammalian Cell Culture: Are We Repeating the experiment of Dr. Ox? *Nat. Metab.* 1, 858–860. doi:10.1038/s42255-019-0105-0
- Baker, M. (2016). Reproducibility: Respect Your Cells!. *Nature* 537, 433–435. doi:10.1038/537433a
- Balin, A. K., Goodman, D. B. P., Rasmussen, H., and Cristofalo, V. J. (1976). Atmospheric Stability in Cell Culture Vessels. *In Vitro Cell.Dev.Biol.-Plant* 12, 687–692. doi:10.1007/bf02797472
- Baust, J. M., Buehring, G. C., Campbell, L., Elmore, E., Harbell, J. W., Nims, R. W., et al. (2017). Best Practices in Cell Culture: an Overview. *In Vitro Cell.Dev.Biol.-Animal* 53, 669–672. doi:10.1007/s11626-017-0177-7
- Begley, C. G. (2013). Six Red Flags for Suspect Work. *Nature* 497, 433–434. doi:10.1038/497433a
- Ben-David, U., Siranosian, B., Ha, G., Tang, H., Oren, Y., Hinohara, K., et al. (2018). Genetic and Transcriptional Evolution Alters Cancer Cell Line Drug Response. *Nature* 560, 325–330. doi:10.1038/s41586-018-0409-3
- Blombach, B., and Takors, R. (2015). CO<sub>2</sub>-Intrinsicproduct ,essential Substrate ,and Regulatory Trigger of Microbial and Mammalian Production Processes. *Front. Bioeng. Biotechnol.* 3, a108. doi:10.3389/fbioe.2015.00108
- Boron, W. F. (2004). Regulation of Intracellular pH. *Adv. Physiol. Edu.* 28, 160–179. doi:10.1152/advan.00045.2004
- Boron, W. F., and Russell, J. M. (1983). Stoichiometry and Ion Dependencies of the Intracellular-pH-Regulating Mechanism in Squid Giant Axons. *J. Gen. Physiol.* 81, 373–399. doi:10.1085/jgp.81.3.373
- Bowen, J. W., and Levinson, C. (1984). H<sup>+</sup> Transport and the Regulation of Intracellular pH in Ehrlich Ascites Tumor Cells. *J. Membran Biol.* 79, 7–18. doi:10.1007/bf01868522
- Brinkhof, B., Van Tol, H. T., Groot Koerkamp, M. J., Riemers, F. M., Ijzer, S. G., Mashayekhi, K., et al. (2015). A mRNA Landscape of Bovine Embryos after Standard and MAPK-Inhibited Culture Conditions: a Comparative Analysis. *BMC Genomics* 16, 277. doi:10.1186/s12864-015-1448-x
- Bumke, M. A., Neri, D., and Elia, G. (2003). Modulation of Gene Expression by Extracellular pH Variations in Human Fibroblasts: a Transcriptomic and Proteomic Study. *Proteomics* 3, 675–688. doi:10.1002/pmic.200300395
- Christmas, K. M., and Bassingthwaite, J. B. (2017). Equations for O<sub>2</sub> and CO<sub>2</sub> Solubilities in saline and Plasma: Combining Temperature and Density Dependencies. *J. Appl. Physiol.* 122, 1313–1320. doi:10.1152/jappphysiol.01124.2016
- Cohen, E. P., and Eagle, H. (1961). A Simplified Chemostat for the Growth of Mammalian Cells: Characteristics of Cell Growth in Continuous Culture. *J. Exp. Med.* 113, 467–474. doi:10.1084/jem.113.2.467
- Collins, F. S., and Tabak, L. A. (2014). Policy: NIH Plans to Enhance Reproducibility. *Nature* 505, 612–613. doi:10.1038/505612a
- Cottier, F., Raymond, M., Kurzai, O., Bolstad, M., Leewattanapasuk, W., Jiménez-López, C., et al. (2012). The bZIP Transcription Factor Rca1p Is a Central Regulator of a Novel CO<sub>2</sub> Sensing Pathway in Yeast. *Plos Pathog.* 8, e1002485. doi:10.1371/journal.ppat.1002485
- Darnell, M., O'Neil, A., Mao, A., Gu, L., Rubin, L. L., and Mooney, D. J. (2018). Material Microenvironmental Properties Couple to Induce Distinct Transcriptional Programs in Mammalian Stem Cells. *Proc. Natl. Acad. Sci. USA* 115, E8368–E8377. doi:10.1073/pnas.1802568115
- Delmouly, K., Belondrade, M., Casanova, D., Milharet, O., and Lehmann, S. (2011). HEPES Inhibits the Conversion of Prion Protein in Cell Culture. *J. Gen. Virol.* 92, 1244–1250. doi:10.1099/vir.0.027334-0
- Depping, R., and Seeger, K. (2019). 1H-NMR Spectroscopy Shows Cellular Uptake of HEPES Buffer by Human Cell Lines-An Effect to Be Considered in Cell Culture Experiments. *Anal. Bioanal. Chem.* 411, 797–802. doi:10.1007/s00216-018-1518-4
- Dezengotita, V. M., Kimura, R., and Miller, W. M. (1998). Effects of CO<sub>2</sub> and Osmolality on Hybridoma Cells: Growth, Metabolism and Monoclonal Antibody Production. *Cytotechnology* 28, 213–227. doi:10.1007/978-94-011-4786-6\_22
- Duarte, C. M., Jaremko, L., and Jaremko, M. (2020). Hypothesis: Potentially Systemic Impacts of Elevated CO<sub>2</sub> on the Human Proteome and Health. *Front. Public Health* 8, 543322. doi:10.3389/fpubh.2020.543322
- Eagle, H. (1971). Buffer Combinations for Mammalian Cell Culture. *Science* 174, 500–503. doi:10.1126/science.174.4008.500
- Follonier, S., Escapa, I. F., Fonseca, P. M., Henes, B., Panke, S., Zinn, M., et al. (2013). New Insights on the Reorganization of Gene Transcription in *Pseudomonas Putida* KT2440 at Elevated Pressure. *Microb. Cell Fact* 12, 30–19. doi:10.1186/1475-2859-12-30
- Fouron, Y. (1987). Growing Cultures in Perfusion Bioreactors. *Nature* 327, 537–538. doi:10.1038/327537a0
- Freedman, L. P., Gibson, M. C., Ethier, S. P., Soule, H. R., Neve, R. M., and Reid, Y. A. (2015). Reproducibility: Changing the Policies and Culture of Cell Line Authentication. *Nat. Methods* 12, 493–497. doi:10.1038/nmeth.3403
- Gilbert, H. T. J., Hodson, N., Baird, P., Richardson, S. M., and Hoyland, J. A. (2016). Acidic pH Promotes Intervertebral Disc Degeneration: Acid-Sensing Ion Channel -3 as a Potential Therapeutic Target. *Sci. Rep.* 6, 37360. doi:10.1038/srep37360
- Good, N. E., Winget, G. D., Winter, W., Connolly, T. N., Izawa, S., and Singh, R. M. M. (1966). Hydrogen Ion Buffers for Biological Research\*. *Biochemistry* 5, 467–477. doi:10.1021/bi00866a011
- Grayson, W. L., Zhao, F., Izadpanah, R., Bunnell, B., and Ma, T. (2006). Effects of Hypoxia on Human Mesenchymal Stem Cell Expansion and Plasticity in 3D Constructs. *J. Cel. Physiol.* 207, 331–339. doi:10.1002/jcp.20571
- Gutknecht, J., Bisson, M. A., and Testeson, F. C. (1977). Diffusion of Carbon Dioxide through Lipid Bilayer Membranes: Effects of Carbonic Anhydrase, Bicarbonate, and Unstirred Layers. *J. Gen. Physiol.* 69, 779–794. doi:10.1085/jgp.69.6.779
- Hanrahan, J. W., and Tabcharani, J. A. (1990). Inhibition of an Outwardly Rectifying Anion Channel by HEPES and Related Buffers. *J. Membran Biol.* 116, 65–77. doi:10.1007/bf01871673
- Hirsch, C., and Schildknecht, S. (2019). *In Vitro* research Reproducibility: Keeping up High Standards. *Front. Pharmacol.* 10, 1484. doi:10.3389/fphar.2019.01484
- Holohan, C., van Schaeybroeck, S., Longley, D. B., and Johnston, P. G. (2013). Cancer Drug Resistance: an Evolving Paradigm. *Nat. Rev. Cancer* 13, 714–726. doi:10.1038/nrc3599
- Hu, W.-S., and Aunins, J. G. (1997). Large-scale Mammalian Cell Culture. *Curr. Opin. Biotechnol.* 8, 148–153. doi:10.1016/s0958-1669(97)80093-6
- Hunter, P. (2017). The Reproducibility "crisis". *EMBO Rep.* 18, 1493–1496. doi:10.15252/embr.201744876
- Johnson, J. D., Epel, D., and Paul, M. (1976). Intracellular pH and Activation of Sea Urchin Eggs after Fertilisation. *Nature* 262, 661–664. doi:10.1038/262661a0
- Karst, D. J., Serra, E., Villiger, T. K., Soos, M., and Morbidelli, M. (2016). Characterization and Comparison of ATF and TFF in Stirred Bioreactors for Continuous Mammalian Cell Culture Processes. *Biochem. Eng. J.* 110, 17–26. doi:10.1016/j.bej.2016.02.003
- Keeley, T. P., and Mann, G. E. (2019). Defining Physiological Normoxia for Improved Translation of Cell Physiology to Animal Models and Humans. *Physiol. Rev.* 99, 161–234. doi:10.1152/physrev.00041.2017
- Kikuchi, R., Iwai, Y., Tsuji, T., Watanabe, Y., Koyama, N., Yamaguchi, K., et al. (2019). Hypercapnic Tumor Microenvironment Confers Chemoresistance to Lung Cancer Cells by Reprogramming Mitochondrial Metabolism *In Vitro*. *Free Radic. Biol. Med.* 134, 200–214. doi:10.1016/j.freeradbiomed.2019.01.014
- Kikuchi, R., Tsuji, T., Watanabe, O., Yamaguchi, K., Furukawa, K., Nakamura, H., et al. (2017). Hypercapnia Accelerates Adipogenesis: A Novel Role of High CO<sub>2</sub> in Exacerbating Obesity. *Am. J. Respir. Cel Mol Biol* 57, 570–580. doi:10.1165/rcmb.2016-0278oc
- Klein, S. G., Alsolami, S. M., Arossa, S., Ramos Mandujano, G., Parry, A. J., Steckbauer, A., et al. (2021a). *In Situ* monitoring Reveals Cellular Environmental Instabilities in Human Pluripotent Stem Cell Culture. *Commun. Biol.* (in press). doi:10.1038/s42003-022-03065-w
- Klein, S. G., Alsolami, S. M., Steckbauer, A., Arossa, S., Parry, A. J., Ramos Mandujano, G., et al. (2021b). A Prevalent Neglect of Environmental Control in Mammalian Cell Culture Calls for Best Practices. *Nat. Biomed. Eng.* 5, 787–792. doi:10.1038/s41551-021-00775-0

- Knazek, R. A., Gullino, P. M., Kohler, P. O., and Dedrick, R. L. (1972). Cell Culture on Artificial Capillaries: an Approach to Tissue Growth *In Vitro*. *Science* 178, 65–67. doi:10.1126/science.178.4056.65
- Kreß, S., Almeria, C., and Kasper, C. (2021). “Lab Equipment for 3D Cell Culture,” in *Basic Concepts on 3D Cell Culture*. Editors C. Kasper, D. Egger, and A. Lavrentieva (Cham: Springer International Publishing), 27–67.
- L'allemain, G., Paris, S., and Pouyssegur, J. (1984). Growth Factor Action and Intracellular pH Regulation in Fibroblasts. Evidence for a Major Role of the Na<sup>+</sup>/H<sup>+</sup> Antiport. *J. Biol. Chem.* 259, 5809–5815. doi:10.1016/s0021-9258(18)91086-0
- Langhans, S. A. (2018). Three-Dimensional *In Vitro* Cell Culture Models in Drug Discovery and Drug Repositioning. *Front. Pharmacol.* 9, 6. doi:10.3389/fphar.2018.00006
- Lepe-Zuniga, J. L., Zigler, J. S., Jr, and Gery, I. (1987). Toxicity of Light-Exposed HEPES media. *J. Immunological Methods* 103, 145. doi:10.1016/0022-1759(87)90253-5
- Lindström, P., and Sehlin, J. (1984). Effect of Glucose on the Intracellular pH of Pancreatic Islet Cells. *Biochem. J.* 218, 887–892.
- Mcbrian, M. A., Behbahan, I. S., Ferrari, R., Su, T., Huang, T.-W., Li, K., et al. (2013). Histone Acetylation Regulates Intracellular pH. *Mol. Cell* 49, 310–321. doi:10.1016/j.molcel.2012.10.025
- Merten, O.-W. (2006). Introduction to Animal Cell Culture Technology—Past, Present and Future. *Cytotechnology* 50, 1–7. doi:10.1007/s10616-006-9009-4
- Metzen, E., Wolff, M., Fandrey, J., and Jelkmann, W. (1995). Pericellular PO<sub>2</sub> and O<sub>2</sub> Consumption in Monolayer Cell Cultures. *Respiration Physiol.* 100, 101–106. doi:10.1016/0034-5687(94)00125-j
- Michl, J., Park, K. C., and Swietach, P. (2019). Evidence-based Guidelines for Controlling pH in Mammalian Live-Cell Culture Systems. *Commun. Biol.* 2, 144. doi:10.1038/s42003-019-0393-7
- Naciri, M., Kuystermans, D., and Al-Rubeai, M. (2008). Monitoring pH and Dissolved Oxygen in Mammalian Cell Culture Using Optical Sensors. *Cytotechnology* 57, 245–250. doi:10.1007/s10616-008-9160-1
- Ng, S., March, S., Galstian, A., Hanson, K., Carvalho, T., Mota, M. M., et al. (2014). Hypoxia Promotes Liver-Stage Malaria Infection in Primary Human Hepatocytes *In Vitro*. *Dis. Model. Mech.* 7, 215–224. doi:10.1242/dmm.013490
- Novick, A., and Szilard, L. (1950a). Description of the Chemostat. *Science* 112, 715–716. doi:10.1126/science.112.2920.715
- Novick, A., and Szilard, L. (1950b). Experiments with the Chemostat on Spontaneous Mutations of Bacteria. *Proc. Natl. Acad. Sci.* 36, 708–719. doi:10.1073/pnas.36.12.708
- Packer, L., and Fuehr, K. (1977). Low Oxygen Concentration Extends the Lifespan of Cultured Human Diploid Cells. *Nature* 267, 423–425. doi:10.1038/267423a0
- Papkovsky, D. B. (2004). Methods in Optical Oxygen Sensing: Protocols and Critical Analyses. *Methods Enzymol.* 381, 715–735. doi:10.1016/s0076-6879(04)81046-2
- Pedersen, S. F., Hoffmann, E. K., and Novak, I. (2013). Cell Volume Regulation in Epithelial Physiology and Cancer. *Front. Physiol.* 4, 233. doi:10.3389/fphys.2013.00233
- Petricciani, J. C. (1995). The Acceptability of Continuous Cell Lines: A Personal & Historical Perspective. *Cytotechnology* 18, 9–13. doi:10.1007/bf00744314
- Place, T. L., Domann, F. E., and Case, A. J. (2017). Limitations of Oxygen Delivery to Cells in Culture: An Underappreciated Problem in Basic and Translational Research. *Free Radic. Biol. Med.* 113, 311–322. doi:10.1016/j.freeradbiomed.2017.10.003
- Pouyssegur, J., Franchi, A., L'allemain, G., and Paris, S. (1985). Cytoplasmic pH, a Key Determinant of Growth Factor-Induced DNA Synthesis in Quiescent Fibroblasts. *FEBS Lett.* 190, 115–119. doi:10.1016/0014-5793(85)80439-7
- Pradhan, K., Pant, T., and Gadgil, M. (2012). *In Situ* pH Maintenance for Mammalian Cell Cultures in Shake Flasks and Tissue Culture Flasks. *Biotechnol. Prog.* 28, 1605–1610. doi:10.1002/btpr.1614
- Rajan, D. K., Verho, J., Kreutzer, J., Välimäki, H., Ihala, H., Lekkala, J., et al. (2017). “Monitoring pH, Temperature and Humidity in Long-Term Stem Cell Culture in CO<sub>2</sub> Incubator,” in 2017 IEEE International Symposium on Medical Measurements and Applications (MeMeA) (IEEE), 470–474.
- Rubin, H. (2007). The Logic of the Membrane, Magnesium, Mitosis (MMM) Model for the Regulation of Animal Cell Proliferation. *Arch. Biochem. Biophys.* 458, 16–23. doi:10.1016/j.abb.2006.03.026
- Ryall, J. G., Cliff, T., Dalton, S., and Sartorelli, V. (2015). Metabolic Reprogramming of Stem Cell Epigenetics. *Cell stem cell* 17, 651–662. doi:10.1016/j.stem.2015.11.012
- Ryu, A. H., Eckalbar, W. L., Kreimer, A., Yosef, N., and Ahituv, N. (2017). Use Antibiotics in Cell Culture with Caution: Genome-wide Identification of Antibiotic-Induced Changes in Gene Expression and Regulation. *Sci. Rep.* 7, 7533. doi:10.1038/s41598-017-07757-w
- Semenza, G. L. (2012). Hypoxia-inducible Factors in Physiology and Medicine. *Cell* 148, 399–408. doi:10.1016/j.cell.2012.01.021
- Semenza, G. L., Neufeldt, M. K., Chi, S. M., and Antonarakis, S. E. (1991). Hypoxia-inducible Nuclear Factors Bind to an Enhancer Element Located 3' to the Human Erythropoietin Gene. *Proc. Natl. Acad. Sci.* 88, 5680–5684. doi:10.1073/pnas.88.13.5680
- Shyh-Chang, N., and Ng, H.-H. (2017). The Metabolic Programming of Stem Cells. *Genes Dev.* 31, 336–346. doi:10.1101/gad.293167.116
- Stea, A., and Nurse, C. A. (1991). Contrasting Effects of HEPES vs HCO<sub>3</sub><sup>-</sup> Buffered media on Whole-Cell Currents in Cultured Chemoreceptors of the Rat Carotid Body. *Neurosci. Lett.* 132, 239–242. doi:10.1016/0304-3940(91)90310-p
- Švastová, E., Hulíř, K., Rafajová, M., Zatoňová, M., Gibadulinová, A., Casini, A., et al. (2004). Hypoxia Activates the Capacity of Tumor-Associated Carbonic Anhydrase IX to Acidify Extracellular pH. *FEBS Lett.* 577, 439–445.
- Tol, M. J., Van Der Lienden, M. J. C., Gabriel, T. L., Hagen, J. J., Scheij, S., Veenendaal, T., et al. (2018). HEPES Activates a Mit/TFE-dependent Lysosomal-Autophagic Gene Network in Cultured Cells: A Call for Caution. *Autophagy* 14, 437–449. doi:10.1080/15548627.2017.1419118
- Tomura, H., Wang, J.-Q., Komachi, M., Damirin, A., Mogi, C., Tobo, M., et al. (2005). Prostaglandin I<sub>2</sub> Production and cAMP Accumulation in Response to Acidic Extracellular pH through OGR1 in Human Aortic Smooth Muscle Cells. *J. Biol. Chem.* 280, 34458–34464. doi:10.1074/jbc.m505287200
- Triaud, F., Clenet, D.-H., Cariou, Y., Le Neel, T., Morin, D., and Truchaud, A. (2003). Evaluation of Automated Cell Culture Incubators. *JALA: J. Assoc. Lab. Automation* 8, 82–86. doi:10.1016/s1535-5535(03)00018-2
- Vallejos, J. R., Brorson, K. A., Moreira, A. R., and Rao, G. (2010). Dissolved Oxygen and pH Profile Evolution after Cryovial Thaw and Repeated Cell Passing in a T-75 Flask. *Biotechnol. Bioeng.* 105, 1040–1047. doi:10.1002/bit.22649
- Wang, G. L., Jiang, B. H., Rue, E. A., and Semenza, G. L. (1995). Hypoxia-inducible Factor 1 Is a basic-helix-loop-helix-PAS Heterodimer Regulated by Cellular O<sub>2</sub> Tension. *Proc. Natl. Acad. Sci.* 92, 5510–5514. doi:10.1073/pnas.92.12.5510
- Wenger, R., Kurtcuoglu, V., Scholz, C., Marti, H., and Hoogewijs, D. (2015). Frequently Asked Questions in Hypoxia Research. *Hp* 3, 35–43. doi:10.2147/HP.S92198
- Wolff, M., Fandrey, J., and Jelkmann, W. (1993). Microelectrode Measurements of Pericellular PO<sub>2</sub> in Erythropoietin-Producing Human Hepatoma Cell Cultures. *Am. J. Physiology-Cell Physiol.* 265, C1266–C1270. doi:10.1152/ajpcell.1993.265.5.c1266
- Muelas, M. W., Ortega, F., Breitling, R., Bendtsen, C., and Westerhoff, H. V. (2018). Rational Cell Culture Optimization Enhances Experimental Reproducibility in Cancer Cells. *Sci. Rep.* 8, 3029. doi:10.1038/s41598-018-21050-4
- Xu, S., Gavin, J., Jiang, R., and Chen, H. (2017). Bioreactor Productivity and media Cost Comparison for Different Intensified Cell Culture Processes. *Biotechnol. Prog.* 33, 867–878. doi:10.1002/btpr.2415

**Conflict of Interest:** The authors declare that the research was conducted in the absence of any commercial or financial relationships that could be construed as a potential conflict of interest.

**Publisher's Note:** All claims expressed in this article are solely those of the authors and do not necessarily represent those of their affiliated organizations, or those of the publisher, the editors, and the reviewers. Any product that may be evaluated in this article, or claim that may be made by its manufacturer, is not guaranteed or endorsed by the publisher.

Copyright © 2022 Klein, Steckbauer, Alsolami, Arossa, Parry, Li and Duarte. This is an open-access article distributed under the terms of the Creative Commons Attribution License (CC BY). The use, distribution or reproduction in other forums is permitted, provided the original author(s) and the copyright owner(s) are credited and that the original publication in this journal is cited, in accordance with accepted academic practice. No use, distribution or reproduction is permitted which does not comply with these terms.



# Studying Kidney Diseases Using Organoid Models

Meng Liu<sup>1†</sup>, Angelysia Cardilla<sup>1†</sup>, Joanne Ngeow<sup>1,2</sup>, Ximing Gong<sup>1\*</sup> and Yun Xia<sup>1\*</sup>

<sup>1</sup>Lee Kong Chian School of Medicine, Nanyang Technological University Singapore, Singapore, Singapore, <sup>2</sup>Cancer Genetics Service, National Cancer Centre Singapore, Singapore, Singapore

## OPEN ACCESS

### Edited by:

Keiichi Suzuki,  
Osaka University, Japan

### Reviewed by:

Ryuji Morizane,  
Massachusetts General Hospital,  
United States  
Zhongwei Li,  
University of Southern California,  
United States

### \*Correspondence:

Ximing Gong  
ximing.gong@ntu.edu.sg  
Yun Xia  
yunxia@ntu.edu.sg

<sup>†</sup>These authors share first authorship

### Specialty section:

This article was submitted to  
Stem Cell Research,  
a section of the journal  
Frontiers in Cell and Developmental  
Biology

**Received:** 29 December 2021

**Accepted:** 14 February 2022

**Published:** 03 March 2022

### Citation:

Liu M, Cardilla A, Ngeow J, Gong X  
and Xia Y (2022) Studying Kidney  
Diseases Using Organoid Models.  
Front. Cell Dev. Biol. 10:845401.  
doi: 10.3389/fcell.2022.845401

The prevalence of chronic kidney disease (CKD) is rapidly increasing over the last few decades, owing to the global increase in diabetes, and cardiovascular diseases. Dialysis greatly compromises the life quality of patients, while demand for transplantable kidney cannot be met, underscoring the need to develop novel therapeutic approaches to stop or reverse CKD progression. Our understanding of kidney disease is primarily derived from studies using animal models and cell culture. While cross-species differences made it challenging to fully translate findings from animal models into clinical practice, primary patient cells quickly lose the original phenotypes during *in vitro* culture. Over the last decade, remarkable achievements have been made for generating 3-dimensional (3D) miniature organs (organoids) by exposing stem cells to culture conditions that mimic the signaling cues required for the development of a particular organ or tissue. 3D kidney organoids have been successfully generated from different types of source cells, including human pluripotent stem cells (hPSCs), adult/fetal renal tissues, and kidney cancer biopsy. Alongside gene editing tools, hPSC-derived kidney organoids are being harnessed to model genetic kidney diseases. In comparison, adult kidney-derived tubuloids and kidney cancer-derived tumoroids are still in their infancy. Herein, we first summarize the currently available kidney organoid models. Next, we discuss recent advances in kidney disease modelling using organoid models. Finally, we consider the major challenges that have hindered the application of kidney organoids in disease modelling and drug evaluation and propose prospective solutions.

**Keywords:** kidney organoid, kidney disease, iPSC, disease modelling, differentiation, tubuloid, tumoroid, PKD

## INTRODUCTION

The global prevalence of Chronic Kidney Disease (CKD) and End Stage Renal Disease (ESRD) is increasing with an alarming rate (Go et al., 2004; Bikbov et al., 2020). The clinical presentation of CKD and ESRD is often associated with cardiovascular diseases, diabetes, and hypertension (Gansevoort et al., 2013; Matsushita et al., 2015; Webster et al., 2017). Currently, hemodialysis and transplantation remain to be the primary treatment options for ESRD. Dialysis substantially reduces patients' life quality, while the availability of transplantable kidney is consistently insufficient (Tonelli et al., 2011). These limitations strongly suggest that there is an urgency to develop new therapeutic approaches to fight the global burden of kidney diseases.

A better understanding of the mechanistic underpinning of CKD will help develop novel treatments and preventive methods. The underlying causes of CKD can be broadly classified into genetic and non-genetic. Genetic kidney diseases are caused by mutations of single or multiple genes, being those germline inherited or somatically acquired. Examples of genetic

kidney diseases include polycystic kidney disease (PKD), glomerular nephropathy, and renal cancer (Hildebrandt, 2010). Non-genetic kidney diseases can lead to acute kidney injury (AKI), which may be caused by infection, toxic chemicals, or systemic vascular complication such as diabetes and hypertension, although these could be associated with genetic factors as well (Thomas et al., 2015; Makris and Spanou, 2016).

Traditionally, animal models, and monolayer cell culture have been employed to understand kidney development and disease. Undoubtedly, these models have a profound impact on the way we approach disease modelling and drug discovery. Nevertheless, knowledge derived from traditional model systems cannot always be extrapolated to human due to interspecies differences. Organoids are a cluster of cells that self-organize into three-dimensional (3D) structures and could recapitulate critical features of the cognate organ. Organoids can be derived from human pluripotent stem cells (hPSCs) and adult/fetal tissues. The last decade has witnessed the explosion of disease modelling studies employing organoids as the model system, including kidney organoids. Despite numerous limitations of kidney organoids, including the fetal-like state and existence of off-target cells, they are by far the most physiologically relevant model of human kidney. Here, we first revisit the “conventional” models for kidney diseases, followed by discussion of the most prevailing approaches for generating different types of kidney organoids. Then, we consider the current utility and limitation of kidney organoids for disease modelling, as well as contemplate future prospects in generating kidney organoids of higher physiological relevance for faithfully recapitulating kidney diseases.

## “CONVENTIONAL” MODELS FOR STUDYING KIDNEY DISEASES

Mouse models have been extensively used to recapitulate kidney diseases due to the evolutionarily conserved developmental program, involving reciprocal interaction between metanephric mesenchyme (MM) and ureteric bud (UB), as well as the similarity in organ architecture and physiological function (Kim & Dressler, 2005; Taguchi et al., 2014; Takasato & Little, 2015; McMahon, 2016). Indeed, mutations in genes that are crucial for mouse kidney development are associated with congenital anomalies of the kidney and urinary tract (CAKUT) syndromes in human (Hwang et al., 2014; Nicolaou et al., 2015). The recent development of CRISPR/Cas9 genome editing tools greatly facilitated the investigation of human kidney diseases with complex genetic traits (Li et al., 2013; Sander & Joung, 2014).

Polycystic kidney disease (PKD) represents one of the most common monogenic kidney diseases, constituting approximately 3% of CKD cases. PKD can be mainly categorised into autosomal dominant (ADPKD) and autosomal recessive (ARPKD) (Wilson, 2004), typically induced by germline mutation of *PKD1* or *PKD2*, and *PKHD1*, respectively (Qian et al., 1996; Pei et al., 1999). Because homozygous germline deletion of *Pkd1* or *Pkd2* in mice

lead to embryonic lethality, conditional/kidney-specific knockout, and hypomorphic models are more suitable to investigate ADPKD pathogenesis (Herron et al., 2002; Leeuwen et al., 2004; Piontek et al., 2004; Piontek et al., 2007; Yu et al., 2007; Takakura et al., 2008). PCK rats harbouring *Pck* mutation progressively develop cysts in distal tubule and collecting duct, hence are often used for ARPKD studies (Lager et al., 2001). Although genetic PKD mouse models recapitulate key pathological features of PKD, they cannot emulate many complex mechanisms such as the “second-hit” action in ADPKD and the highly variable disease severity caused by different mutations (Happé and Peters, 2014). Moreover, mTOR inhibitors sirolimus and everolimus failed the clinical trial despite the beneficial effects observed in PKD mouse models, highlighting interspecies differences in disease mechanism (Serra et al., 2010; Walz et al., 2010). Whole exome sequencing has identified a list of novel genes associated with PKD, such as *GANAB* and *DNAJB11* in ADPKD and *DZIP1L* in ARPKD (Lu et al., 2017), requiring new models for interrogating the roles of these new genes in PKD pathogenesis.

Glomerular nephropathy is characterized by disruption of glomerular filtration, such as focal segmental glomerulosclerosis (FSGS) and IgA nephropathy (Meyrier, 2005; Roberts, 2014). FSGS mouse models have been established by introducing orthologous genetic aberrations identified in patients (Kaplan et al., 2000; Mele et al., 2011; Plageman et al., 2011). While genetic mouse models (knockouts of *Actn4* or *Myo1e*) that recapitulate the secondary forms of FSGS are available, primary FSGS models with unknown cause are lacking (Henderson et al., 2008; Krendel et al., 2009). Spontaneous ddY mouse and CD89 transgenic mouse have been widely used for modelling IgA nephropathy. However, they couldn’t mirror complex real-life scenarios in different patients (Launay et al., 2000; Coppo et al., 2002; Moura et al., 2008). Spontaneous lupus mouse strain NZB/NZWFI (BW) develops glomerulonephritis and vasculitis, thus has been widely used for lupus study (Eilat et al., 1976; Satoh et al., 1995; Neubert et al., 2008; Mukundan et al., 2009; Li et al., 2011). Nevertheless, differences between mouse and human in immune system activation and response to challenge, in both the innate and adaptive arms, suggest us to exercise extra caution when we translate paradigms in mouse to human.

Both genetic and non-genetic mouse models are available for studying diabetic nephropathy (DN). While type I diabetes is most commonly induced by streptozotocin-mediated pancreatic  $\beta$ -cells ablation (Rossini et al., 1978; Toniolo et al., 1980; Leiter, 1982), type II diabetes mouse model is usually developed by genetic modification of leptin receptor (Maffei et al., 1995; Lee et al., 1996). Unfortunately, the correlation between genetic background and phenotype severity in different mouse strains remains an obstacle for DN studies (Brosius et al., 2009; Brosius and Alpers, 2013; Betz and Conway, 2016). Acute kidney injury (AKI) can be induced by ischemia-reperfusion injury (IRI), drug toxicity or sepsis (Andres et al., 1962; Zwacka et al., 1998; Piliponsky et al., 2008). The most commonly used IRI mouse models are unstable, due to variable surgery proficiency. It is



important to establish reproducible AKI models that are independent of human errors.

Renal cancer studies have employed either mouse models with genetic modification of oncogenes and/or tumour suppressors (Kapitsinou & Haase, 2008; Wang et al., 2014; Gu et al., 2017; Harlander et al., 2017; Nargund et al., 2017), or xenograft models with tumour biopsies derived from patients (Prochazka et al., 1992; Lee & Motzer, 2017). Nevertheless, these models are far from being able to recapitulate human renal tumour microenvironment.

In addition to mouse models, conventional 2-dimensional (2D) monolayer cell culture has contributed substantially to our understanding of kidney diseases. Patient-derived primary kidney cells provide the opportunity to study donor-specific phenotypes. However, limited expansion capability and complicated tissue isolation process have prompted the generation of immortalized cell lines, wherein cells are genetically modified to acquire indefinite proliferation capability, such as HK2 human proximal tubular epithelial cells (Ryan et al., 1994). To study podocytes, a major breakthrough came with the establishment of immortalized temperature-sensitive podocytes where cell growth and differentiation could be regulated under specific condition (Mundel et al., 1997; Saleem et al., 2002). Despite its simplicity, accessibility and low cost, monolayer cell culture has numerous limitations. Among these, deprivation of 3D tissue architecture prohibited the recapitulation of disease phenotypes that involve cell-cell or cell-extracellular matrix (ECM) interaction. To this point, collagen I matrix embedding has enabled MDCK cells to form 3D polarized tubular structure with lumen formation, mimicking renal epithelial cysts in PKD (Mangoo-Karim et al., 1989; Yamaguchi et al., 1995; Boletta et al., 2000; O'Brien et al., 2002). Although these conventional models of kidney diseases will continue to contribute to our knowledge, the limitations of these models have raised the urgent need for developing new models that could faithfully emulate human kidney diseases, being those genetic or non-genetic.

## ESTABLISHMENT OF KIDNEY ORGANIDS

The last decade has borne witness to a large body of studies that aim to differentiate hPSCs into kidney organoids that present both the cellular repertoire and 3D structure of human kidney. Earlier study using mouse embryonic stem cells (ESCs) provided valuable insights into the specific biochemical signals required for renal lineage commitment (Kim & Dressler, 2005). In 2013, three studies demonstrated successful differentiation of hPSCs into MM or UB lineages that are capable of self-organizing into 3D tubular structures upon either aggregation with mouse embryonic kidney cells or co-culture with mouse embryonic spinal cord (Mae et al., 2013; Xia et al., 2013; Taguchi et al., 2014). Moving forward, Takasato et al reported simultaneous derivation of both MM and UB from hPSCs, followed by self-organization into 3D kidney tubular structures in the absence of embryonic mouse tissues (Takasato et al., 2014). At the end of 2015, two seminal

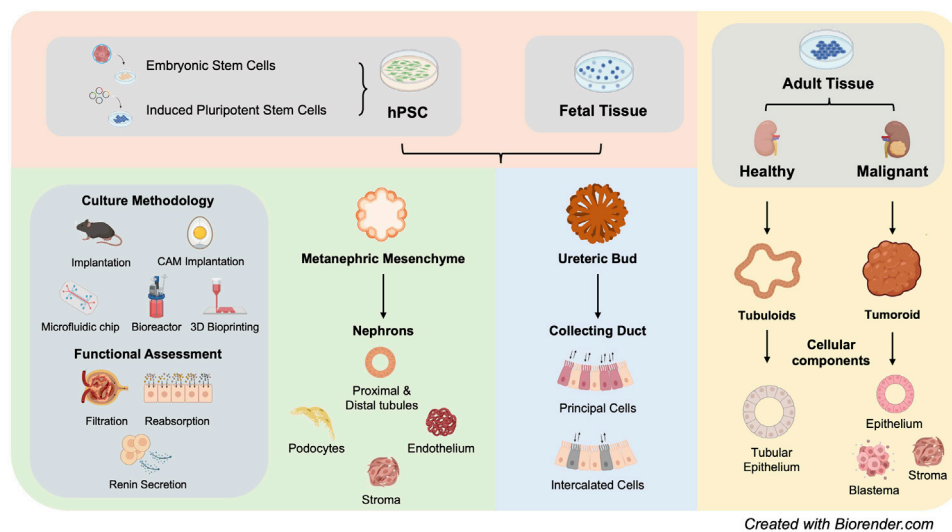
studies demonstrated for the first time that hPSCs can be efficiently differentiated into self-assembled 3D kidney organoids (Morizane et al., 2015; Takasato et al., 2015).

### Figure 1

Substantial structural and functional characterization of hPSC-derived kidney organoids have been performed. Overall, these organoids are comprised of segmentally patterned nephron-like structures, stromal cells and endothelial cells, showing high congruence with human fetal kidney. Nevertheless, these kidney organoids presented rudimentary function, such as tubular reabsorption represented by proximal tubule epithelium-mediated dextran uptake (Freedman et al., 2015; Takasato et al., 2015; Przepiorski et al., 2018; Low et al., 2019) and secretion of functional renin (Shankar et al., 2021). Within kidney organoids, glomerular podocytes adopt the structural conformation reminiscent of glomerulus, facilitating selective isolation, and enrichment of glomerulus-like structures for studying nephrotic syndrome (Hale et al., 2018; Yoshimura et al., 2019). Due to the highly complex cell composition, kidney organoids, alongside single-cell RNA-sequencing (scRNAseq), enabled characterization of inter-cellular cross-talk and disease relevance, pointing out new directions for future exploration (Wu et al., 2018; Low et al., 2019; Ungricht et al., 2021).

Kidney is a filtration organ, the functionality of which is indispensable of a patterned vascular network. Although endothelial cells could be generated alongside nephron epithelium using these differentiation protocols (Freedman et al., 2015; Takasato et al., 2015), they are under-represented. Various approaches have been developed to vascularize hPSC-derived kidney organoids. VEGF-A, being those exogenously administered into differentiation culture (Czerniecki et al., 2018) or those autologously generated by podocytes (Low et al., 2019), greatly facilitated kidney organoid vascularization. Despite the existence of a rich vascular network within kidney organoids, most glomeruli remained avascular (Low et al., 2019). Engraftment of kidney organoids into immune-compromised mouse (Bantounas et al., 2018; van den Berg et al., 2018; Low et al., 2019) or chick chorioallantoic membrane (CAM) (Garreta et al., 2019) facilitated glomerular vascularization. The grafted kidney organoids not only got anastomosed with the host circulation system, but also established putative glomerular filtration barrier. Most importantly, the grafted kidney organoids were capable of handling systemically injected dextran in a size-selective manner, indicating functional maturation. However, engraftment of kidney organoids into model organisms largely limited their downstream utility. To this point, Homan et al developed a microfluidic chip culture that employed fluid flow to enhance vascularization and maturation of kidney organoids, circumventing the necessity of a host circulation system (Homan et al., 2019). Despite successful vascular invasion into glomerulus, kidney organoids did not display a similar level of vascularization in comparison with the transplanted organoids.





**FIGURE 1 |** Summary of current kidney organoid models (hPSC: human pluripotent stem cells).

There has been a long-standing debate about whether UB lineage exists within hPSC-derived kidney organoids, despite the existence of  $GATA3^+$  tubule population. UB is originated from anterior intermediate mesoderm, different from MM which is originated from posterior intermediate mesoderm. In 2017, a landmark study demonstrated successful generation of UB organoids with a single collecting duct tree, forming properly patterned renal macro-anatomy upon aggregation with mouse PSC-derived MM and embryonic mouse kidney stromal progenitor cells (Taguchi and Nishinakamura, 2017). Recently, a number of UB differentiation protocols have been developed with improvements considering long-term culture maintenance, stable formation of expandable branching epithelium, as well as maturation into collecting duct-like structures (Mae et al., 2020; Uchimura et al., 2020; Zeng et al., 2021). Recent single cell transcriptomic analyses of both mouse and human embryonic kidneys revealed that many UB lineage markers, including  $GATA3$  and  $AQP2$ , are expressed in distal connecting tubules that are supposed to be descendants of MM (Combes et al., 2019a). Based on a widely-used protocol for kidney organoid generation, a recent study developed an alternative approach to induce ureteric epithelium identity, via harnessing the cellular plasticity of distal nephrons that were derived from MM kidney organoids (Howden et al., 2021). Whether the observed cellular plasticity of distal nephron reproduces normal development or homeostasis of human kidney warrants further investigation.

Apart from hPSC-derived kidney organoids, both fetal and adult renal tissues can give rise to organoids, when provided with a suitable culture condition. Mouse and human embryonic kidney derived UB and MM cells can be captured for long-term *in vitro* culture within a synthetic niche. MM cells of different origins, including mouse/human embryonic kidneys and hPSCs, could be kept in non-differentiated progenitor state while remain competent

to differentiate into segmentally patterned nephron structures (Brown et al., 2015; Li et al., 2016). Likewise, synthetic niche has been recently developed for UB cells from mouse embryonic origin or hPSCs (Yuri et al., 2017; Zeng et al., 2021). In 2019, Clevers team developed the first protocol to generate kidney organoids, termed tubuloids, from adult human kidney tubular epithelial cells and urine-derived tubular epithelial cells. Tubuloids, grown in semi-solid ECM, are comprised of a mixed population of kidney epithelium, adopting distinctive apical-basal polarity (Schutgens et al., 2019). Alternatively, tubular epithelial cells could be generated from fibroblasts via transcription factor-directed reprogramming alongside the action of defined growth factors (Kaminski et al., 2016). Both approaches allow long-term maintenance and stable expansion of healthy adult kidney epithelium *ex vivo*, providing opportunities to study kidney tissue regeneration.

Tumoroids have been generated from many different types of malignant tissues, such as colorectal tumour (Fujii et al., 2016), liver tumour (Broutier et al., 2017), and ovarian tumour (Kopper et al., 2019). Recently, the establishment of tumoroids from renal tumour biopsy has been reported by several groups, demonstrating long-term propagation of tumoroids with defined culture cocktail (Grassi et al., 2019; Schutgens et al., 2019; Fendler et al., 2020). Kidney tumoroids recapitulate the heterogeneity of the parental tumour tissue, displaying tri-phasic histology of epithelial, stromal, and blastema components. Different culture condition results in distinctive *in vitro* characteristics of tumoroids, such as expansion capacity and tissue morphology (Fendler et al., 2020). The technical feasibility for tumoroid generation has enabled biobanking of kidney tumoroids (Calandrini et al., 2020).

The availability of various kidney organoid models has opened a new avenue for modelling human kidney diseases,

including genetic diseases, infection and nephrotoxicity, within a 3D tissue microenvironment (**Figure 1**).

## ORGANOID MODELS OF KIDNEY DISEASES

### Polycystic Kidney Disease

Human PSCs are highly amenable for genetic manipulation, making it feasible to introduce genetic aberrations that are associated with genetic kidney diseases. Among these, PKD has been most frequently studied using hPSC-derived kidney organoids. In ADPKD patients, cysts are primarily located in the proximal tubules, while ARPKD patients have more collecting duct cysts. Nevertheless, fetal stage cysts of ARPKD patients are often observed in proximal tubules. Towards the late stage of PKD, cysts are observed along the entire length of nephrons (Bergmann et al., 2018). Freedman et al introduced truncating mutations of *PKD1* or *PKD2* into hPSCs and differentiated them into kidney organoids (Freedman et al., 2015). Although spontaneous cyst formation was observed in PKD knockout organoids after long term culture (~Day 58), cystogenesis was not efficient under adhesion culture condition (~6%) presumably due to different tissue microenvironment between *in vivo* and *in vitro* systems. To improve cystogenesis, Freedman group applied suspension culture, leading to a 10-fold increase in the efficiency of cystogenesis (Cruz et al., 2017). The cystic kidney organoids presented cellular phenotypes of ADPKD, including fluid accumulation and proliferation of cyst-lining epithelial cells. This study also demonstrated a previously unregistered role of adhesive microenvironment in restraining cyst dilation during the early stage of PKD.

The question remains as to what extent patient iPSC- or gene-edited PSC-derived cystic kidney organoids recapitulate PKD pathology. It is quite common that stress paradigm is required for patient iPSC derivatives to present disease phenotypes that typically manifest during adulthood. Decades of studies using animal models and monolayer cell culture have clearly demonstrated aberrant intracellular levels of cAMP and  $\text{Ca}^{2+}$  in PKD (Torres and Harris, 2014). Hence, forskolin, a potent activator of adenylyl cyclase (AC), is frequently used to induce cyst formation in kidney organoids that are derived from patient iPSCs or gene-edited hPSCs. Shimizu et al generated kidney organoids from ADPKD patient iPSCs, and cysts were predominantly observed in proximal tubules following exposure to forskolin (Shimizu et al., 2020). On the contrary, Cruz et al observed no striking difference between PKD and non-PKD PSC-derived kidney organoids upon cAMP induction using forskolin or 8-Br-cAMP (Cruz et al., 2017). Kuraoka et al generated UB organoids from both ADPKD patient iPSCs and gene-edited *PKD1* mutant iPSCs. Cyst formation was observed in UB stalk region after forskolin treatment, recapitulating the initial stage of ADPKD cystogenesis (Koptides and Deltas, 2000; Kuraoka et al., 2020).

Comparing with ADPKD, ARPKD has a lower incidence and typically manifests at fetal or neonatal stage. Low et al generated kidney organoids from ARPKD patient iPSCs and gene-corrected isogenic iPSCs. Cyst dilation was specifically observed in patient iPSC-derived kidney organoids, first in the proximal region and then extended to the distal region after

forskolin or 8-Br-cAMP stimulation, recapitulating gestational cyst formation of ARPKD (Nakanishi et al., 2000; Gunay-Aygun et al., 2006; Woollard et al., 2007; Low et al., 2019). In a recent study, Howden et al obtained ureteric epithelium culture via a detour from *PKHD1*<sup>null</sup> iPSC-derived MM organoids and observed spontaneous cyst formation under ureteric stalk culture condition, mimicking ureteric epithelium-originated cyst in ARPKD (Howden et al., 2021). Collecting duct cyst formation is usually attributed to vasopressin-mediated activation of AVPR2, which preferentially couples with Gs to activate AC, leading to cAMP production (Boertien et al., 2013). Kuraoka et al observed cyst formation in UB organoids after vasopressin treatment, due to expression of *AVPR1A* instead of *AVPR2*, further implying the immaturity of UB organoids (Boertien et al., 2013; Kuraoka et al., 2020). The proliferation phenotype of cystic epithelium is also associated with activation of mitogen-activated protein kinase/extracellular regulated kinase (MAPK/ERK) signalling. To this point, Shimizu et al employed epidermal growth factor (EGF) to activate the MAPK/ERK pathway to initiate cyst formation by boosting cell proliferation (Shimizu et al., 2020). However, only a slight increase of organoid size was detected instead of obvious cyst formation, indicating a minor contribution of MAPK/ERK signalling to cyst initiation.

PKD organoid models offer great prospects to evaluate the therapeutic effects of candidate drugs. Cystic fibrosis transmembrane conductance regulator (CFTR) mediates fluid accumulation during cystogenesis (Davidow et al., 1996). CFTR inhibitor successfully blocked cyst formation in ADPKD and ARPKD patient iPSC-derived kidney organoids (Low et al., 2019; Shimizu et al., 2020). Thapsigargin, which inhibits sarco/endoplasmic reticulum  $\text{Ca}^{2+}$  ATPase, also repressed forskolin-induced cyst formation in ARPKD organoids (Low et al., 2019). In another study, everolimus, which showed encouraging results in mouse model, albeit failed to retard disease progression in ADPKD patients, significantly suppressed forskolin-induced cyst formation in ADPKD organoids (Shimizu et al., 2020). In addition to validating compounds with known effects on cystogenesis, cystic kidney organoids also enabled screening of compounds that have unknown effects on cyst formation. Blebbistatin, a non-muscle myosin II inhibitor, can significantly induce cyst formation in PKD organoids (Czerniecki et al., 2018). These studies highlight the capability of kidney organoids in recapitulating critical PKD machinery, enabling exploration of novel PKD pathways and screening for new drugs.

### Other Genetic Kidney Diseases

Genetic lesions that lead to defective glomerular structure, such as defects in glomerular basement membrane (GBM) and loss of slit diaphragms (SD), can cause proteinuria and/or haematuria (Boute et al., 2000; Daehn and Duffield, 2021). Understanding of glomerular nephropathy is hampered by complex 3D structure of glomerulus and limited proliferation capacity of podocytes. hPSC-derived kidney organoids provide the possibility to overcome these limitations. In a proof-of-concept study, *PODXL*<sup>-/-</sup> hPSCs were generated by gene editing for studying human glomerular

development. The results showed Podocalyxin plays critical roles in microvillus formation and cell spacing in hPSC-derived podocytes (Doyonnas et al., 2001; Kim et al., 2017). Genetic mouse model study further corroborated these results (Kim et al., 2017). *NPHS1* encodes NEPHRIN protein, which is a major component of SD. Mutations in *NPHS1* were initially identified in patients with Finnish-type congenital nephrotic syndrome (CNS) (Patrakka et al., 2000). Tanigawa et al used iPSCs from patients with *NPHS1* mutation to study SD formation. Podocytes derived from *NPHS1* mutant patient iPSCs exhibited reduced cell surface localization of NEPHRIN. Upon implantation beneath mouse renal capsule, *NPHS1* was also absent at cell junction, despite the formation of well-organized foot processes. Genetic correction of *NPHS1* mutation successfully restored SD formation (Tanigawa et al., 2018). In a separate study, Hale et al isolated and enriched glomerular-like structures from hPSC-derived kidney organoids to study CNS, and observed hypertrophied podocytes in *NPHS1* mutant patient-derived organoids (Hale et al., 2018).

Mucin 1 kidney disease (MKD) is a toxic proteinopathy caused by *MUC1* frameshift (*MUC1*-fs) mutation (Kirby et al., 2013). Dvela-Levitt et al showed that *MUC1*-fs accumulated in TMED9 vesicles between *cis*-Golgi and ER in MKD patient iPSC-derived kidney organoids. The effect of BRD4780 on *MUC1*-fs protein levels was tested in MKD patient iPSC-derived kidney organoids. Similar with the observation in mouse disease model, BRD4780 managed to clear the mutant protein from intracellular compartments in patient-derived organoids. (Dvela-Levitt et al., 2019).

Cystinosis is a rare lysosomal-storage disease associated with accumulation of cystine in renal proximal tubule, mainly caused by mutations in cystine transporter *CTNS* (*CTNS*). *CTNS*<sup>-/-</sup> patient iPSC-derived kidney organoids exhibited enlarged lysosome, elevated cystine accumulation, increased apoptosis, and perturbed basal autophagy flux. Dual treatment of cysteamine/everolimus is more effective in slowing down disease progression than single treatment, providing potential therapeutic strategy (Hollywood et al., 2020).

## Renal Cancer

Recent development and characterization of renal cancer-derived tumoroids demonstrated successful preservation of critical genetic and phenotypic features of parental tumour tissues. Clear cell renal cell carcinoma-derived tumoroids contained epithelial and mesenchymal cells with renal cancer specific marker expression such as HIF1 $\alpha$ . The tumoroids remain propagative after xenotransplantation (Grassi et al., 2019). Calandrini et al established a biobank from various childhood kidney cancers including Wilms tumours, renal cell carcinomas (RCC), malignant rhabdoid tumours of the kidney (MRTK), etc. These tumoroids displayed tri-phasic histology of epithelial, stromal and blastema components. In addition, MRTK tumoroids represent the first cancer organoid that can sustain long-term *in vitro* expansion of tumours of non-epithelial origin (Calandrini et al., 2020). Research using renal cancer-derived tumoroids is still in its infancy, requiring further improvement of the methodology for downstream applications.

## Non-Genetic Kidney Diseases

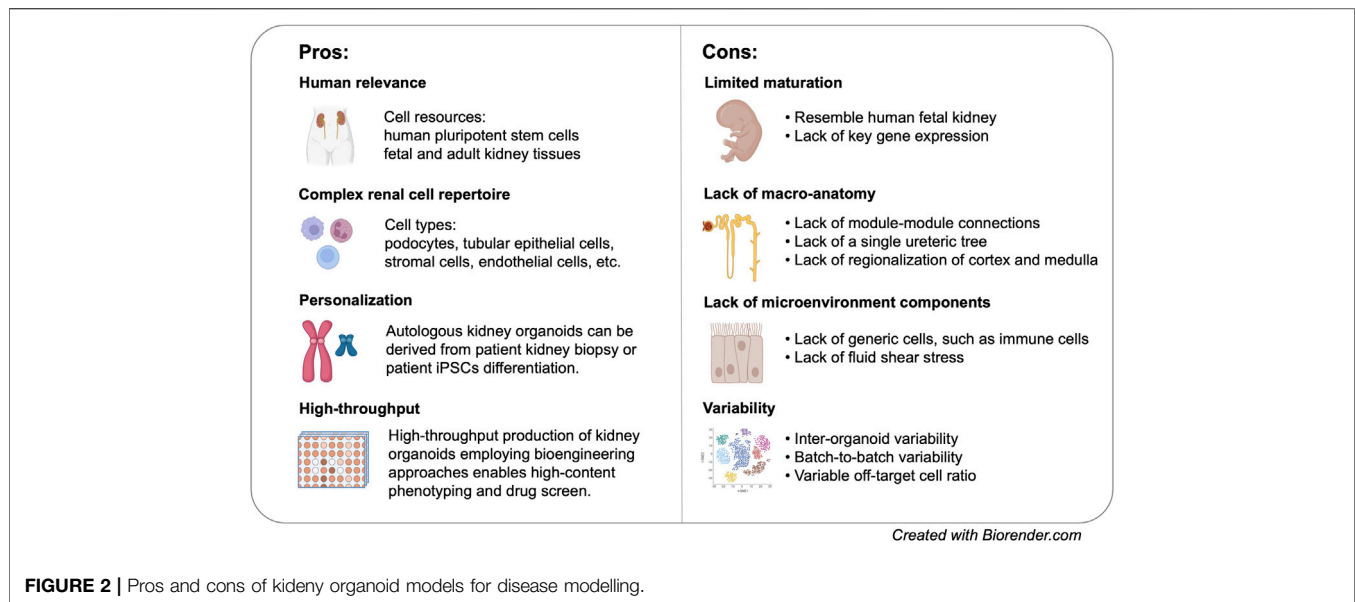
Human PSC-derived kidney organoids have been less often used for modelling non-genetic diseases, possibly due to immaturity, the lack of blood perfusion and fluid flow, and the absence of immune components. Nonetheless, several studies successfully employed kidney organoids for investigating pathogen-renal interaction. BK virus infection is a common cause of kidney transplant failure (Hirsch et al., 2005). Schutgens et al infected adult renal epithelium-derived tubuloids with BK virus. The infected tubuloids presented enlarged nuclei and detectable DNA fragment, reminiscent of BK nephropathy. Furthermore, a clinically used DNA polymerase inhibitor cidofovir significantly decreased BK copy number in infected tubuloids (Schutgens et al., 2019).

Severe acute respiratory syndrome coronavirus 2 (SARS-CoV-2) is responsible for the ongoing global pandemic. Patients with hypertension and diabetes have a higher risk of severe symptoms (Fang et al., 2020), though the underlying mechanism remains unclear. Angiotensin converting enzyme 2 (ACE2), the principle target of SARS-CoV-2, is also expressed in kidney (Vaduganathan et al., 2020). Human recombinant ACE2 effectively reduced the number of infected cells in kidney organoids (Monteil et al., 2020). Human kidney organoids have also been employed to test a novel soluble human ACE2 protein, 1-618-ABD. The results suggested potent neutralization of SARS-CoV-2 by soluble ACE2 1-618-ABD (Wysocki et al., 2021). Furthermore, a recent study revealed SARS-CoV-2 infection drives fibrosis in kidney organoids, corroborating the association between COVID-19 and kidney fibrosis in some patients (Jansen et al., 2021).

Drug-induced nephrotoxicity represents a significant contributor to acute kidney injury (AKI) and CKD. Kidney organoids can respond to different drugs or environmental stresses by expressing tissue specific injury markers. While gentamycin and cisplatin induced kidney injury marker 1 (KIM1) expression and tubular epithelium apoptosis in hPSCs-derived kidney organoid (Freedman et al., 2015; Morizane et al., 2015; Takasato et al., 2015), adriamycin treatment caused podocyte damage and loss (Kumar et al., 2019; Lawlor et al., 2021). These studies revealed previously unappreciated features of kidney organoids, further expanding their utility for modelling a wider spectrum of kidney diseases, as well as for drug screening and toxicological studies.

## LIMITATIONS OF KIDNEY ORGANIDS FOR DISEASE MODELLING

Global transcriptomic analysis of hPSC-derived kidney organoids indicated that these organoids resemble first/second trimester human fetal kidney, making it an ideal model to study kidney development (Takasato et al., 2015; Garreta et al., 2019). Nevertheless, *in vitro* differentiation of kidney organoids does not necessarily follow the same trajectory as *in vivo* development. As a simple matter of fact, glomerulus-like structures from hPSCs can be formed in 3 weeks of time, while the first layers of human metanephric glomeruli are detected around 7 weeks after fertilization. The recently discovered cellular plasticity of distal



nephron segments may or may not reflect *in vivo* lineage relationship. scRNA-seq further revealed the absence of key functional proteins in specific cells associated with kidney-related disorders (Park et al., 2018; Wu et al., 2018). Tolvaptan, the only FDA-approved drug for inhibiting cyst dilation, targets AVPR2 in the collecting duct (Torres et al., 2017). However, modulation of vasopressin receptor in kidney organoid is mostly through AVPR1A due to the lack of AVPR2 expression in current kidney organoid models (Freedman et al., 2015; Kuraoka et al., 2020). Likewise, scRNA-seq revealed minimal detection of OCT2 transporter in proximal tubule that mediates the uptake of numerous chemical compounds and drugs, such as metformin and cisplatin (Wu et al., 2018; Combes et al., 2019b). Although cisplatin induces proximal tubule damage in hPSC-derived kidney organoids, there is no clear evidence whether the uptake was mediated via the “cognate” transporter (Freedman et al., 2015; Morizane et al., 2015). (Figure 2).

Single cell analysis greatly facilitated the revelation of cellular diversity of kidney organoids. Indeed, kidney organoids contain podocytes, proximal tubule, loop of Henle (LoH), distal tubule, and stromal populations (Czerniecki et al., 2018; Wu et al., 2018; Combes et al., 2019b). Although nephron segment-specific cells are present in MM kidney organoid, there is lack of specification within each of the segments, such as proximal tubular segmentation or the establishment of descending, and ascending LoH (Kanai et al., 1994; Cristofori et al., 2007). Unbiased single cell analysis showed that organoid variability can be attributed to the presence of off-target cells and variations in temporal maturation (Czerniecki et al., 2018; Wu et al., 2018; Combes et al., 2019b). The relative abundance of renal and non-renal cells may also be highly variable (Wu et al., 2018; Phipson et al., 2019). When modelling genetic diseases, inter-organoid variability and batch-to-batch variability may lead to confounding observation when we compare disease phenotypes between patient-derived and isogenic control

organoids. In one of the studies, day 18 patient derived organoid with *IFT140* mutation was unexpectedly most similar to day 25 control organoid (Phipson et al., 2019).

Most importantly, generic cell populations are severely under-represented in hPSC-derived kidney organoids, including different types of vascular endothelial cells, renal stroma (England et al., 2020), immune components, etc. Many adult-onset kidney diseases are intimately associated with these “non-renal” cells. For example, kidney fibrosis is characterized by phenotypic change in renal stroma and an excessive production of ECM, ultimately leading to renal failure. In a recent study, transcriptomic analysis of day 35 wild-type kidney organoids suggested that kidney fibrosis is on the way (Ungrecht et al., 2021). This characteristic requires us to exercise extra caution in evaluating the fibrotic status using organoid models. The absence of immune components within organoid represents a major limitation for modelling infectious diseases as it precludes the possibility to study renal-immune interaction and autoimmune kidney diseases. Although many studies demonstrated that kidney organoids are “infectable”, the presented phenotypes may be over-simplified comparing with *in vivo* scenarios.

Another major limitation of kidney organoids is the lack of close-to-native macro-anatomy. The 3D arrangement of current kidney organoids makes it impossible to access renal function that requires higher-order organ architecture, such as renal filtration, tubular reabsorption, and urine concentration. Most UB organoids, except those derived from mouse ESCs using protocol developed by Nishinakamura group (Taguchi and Nishinakamura, 2017), do not harbour a single trunk ureteric tree. Furthermore, none of the UB protocols has realized bifurcation of more than two branching events (Taguchi and Nishinakamura, 2017; Uchimura et al., 2020; Zeng et al., 2021). Very recently, Nishinakamura group succeeded in generating high-order kidney organoids via differentiating mouse ESCs separately into nephron progenitors, UB progenitors, and



stromal progenitors followed by aggregating all progenitors together (Tanigawa et al., 2022). Although it remains a distant goal to generate kidney organoids with regionalized cortex and medulla, the current achievements may bring us towards the ultimate goal in a few years.

Among all the kidney organoids we have discussed here, adult renal tissue-derived organoids have not been extensively used for modelling kidney diseases, possibly due to the technical challenges in generating tubuloids and tumoroids. Renal cancer-derived tumoroids offer a new means for evaluating prospective drug effects in a patient-specific manner. However, out of the few drugs tested, not all drugs show similar reaction in tumoroids as previously exhibited in primary tumours (Grassi et al., 2019). Moreover, different mutations and previous exposure to chemo-drugs could confer distinctive dose-response curve in tumoroids (Calandrini et al., 2020).

In spite of all these limitations, kidney organoids represent a unique model system that enables us to interrogate human-specific kidney disease phenotypes with a resolution that has never been achieved (Figure 2). Nevertheless, the explosion of organoid biology does not take away the value of conventional models. On the contrary, the availability of different model systems allows researchers to leverage on results obtained from different models, leading to even more comprehensive interpretation of kidney diseases.

## PERSPECTIVE

The establishment of kidney organoids have provided unprecedented opportunities for modelling various types of human kidney diseases with complex pathological phenotypes. Human PSC-derived kidney organoids have shown remarkable advantages in presenting phenotypes involving complex tissue architecture while retaining patient genetic composition, ushering a new era of personalized medicine. To address the limitations of hPSC-derived kidney organoids, multiple bioengineering approaches are being developed and incorporated into organoid culture. Microfluidic device has successfully facilitated vascularization and maturation of *in vitro* kidney organoid culture (Homan et al., 2019). Furthermore, microfluidic device has also enabled the functional interaction between nephron epithelial and vascular cells, which is required for the realization of proximal tubular

reabsorption (Lin et al., 2019) and glomerular filtration (Musah et al., 2017). To circumvent inter-organoid variability, as well as to scale up organoid production, several high-throughput culture methods are available, including 3D extrusion bioprinting (Lawlor et al., 2021), microwell culture (Czerniecki et al., 2018), and suspension bioreactor culture (Przepiorski et al., 2018; Kumar et al., 2019).

Comparing with hPSC-derived kidney organoids, adult renal tissue-derived organoids are expected to show greater potential in modelling kidney diseases that manifest during adulthood. While patient-derived tubuloids facilitate the investigation of genetic diseases and infectious diseases (Schutgens et al., 2019), healthy adult-derived tubuloids may provide a novel model system for studying renal tubule regeneration. In comparison with animal models or cancer cell lines, kidney cancer-derived tumoroids represent a great alternative for studying tumor heterogeneity and progression, as well as for patient-specific drug validation. Although much remains to be done for efficient and consistent derivation of tumoroids from kidney cancer biopsies, patient-specific tumoroids offer exciting opportunities to look into the interaction between tumor cells and autologous immune cells, enabling immune-oncology investigation within the tumor microenvironment and personalized immunotherapy testing (Neal et al., 2018).

During the last ten exciting years, the development of novel organoid models has substantially expanded our capability to investigate human kidney development and diseases within a 3D tissue microenvironment *in vitro*. Alongside animal models and monolayer cell culture models, kidney organoids will undoubtedly advance our understanding of kidney diseases and facilitate the development of novel therapeutics.

## AUTHOR CONTRIBUTIONS

ML and AC contributed equally to this manuscript.

## FUNDING

This work is supported by MOE Grants (MOE2019-T2-1-072, MOE-T2EP30220-0008, and MOE-MOET32020-0004), NMRC Grant (NMRC/OFIRG/0076/2018), and Nanyang Assistant Professorship.

## REFERENCES

- Andres, G. A., Morgan, C., Hsu, K. C., Rifkind, R. A., and Seegal, B. C. (1962). Use of Ferritin-Conjugated Antibody to Identify Nephrotoxic Sera in Renal Tissue by Electron Microscopy. *Nature* 194, 590–591. doi:10.1038/194590a0
- Bantounas, I., Ranjzad, P., Tengku, F., Silajdzic, E., Forster, D., Asselin, M.-C., et al. (2018). Generation of Functioning Nephrons by Implanting Human Pluripotent Stem Cell-Derived Kidney Progenitors. *Stem Cell Rep.* 10, 766–779. doi:10.1016/j.stemcr.2018.01.008
- Bergmann, C., Guay-Woodford, L. M., Harris, P. C., Horie, S., Peters, D. J. M., and Torres, V. E. (2018). Polycystic Kidney Disease. *Nat. Rev. Dis. Primer* 4, 50. doi:10.1038/s41572-018-0047-y
- Betz, B., and Conway, B. R. (2016). An Update on the Use of Animal Models in Diabetic Nephropathy Research. *Curr. Diab. Rep.* 16, 18. doi:10.1007/s11892-015-0706-2
- Bikbov, B., Purcell, C. A., Levey, A. S., Smith, M., Abdoli, A., Abebe, M., et al. (2020). Global, Regional, and National burden of Chronic Kidney Disease, 1990–2017: a Systematic Analysis for the Global Burden of Disease Study 2017. *The Lancet* 395, 709–733. doi:10.1016/S0140-6736(20)30045-3
- Boertien, W. E., Meijer, E., Li, J., Bost, J. E., Struck, J., Flessner, M. F., et al. (2013). Relationship of Copeptin, a Surrogate Marker for Arginine Vasopressin, with Change in Total Kidney Volume and GFR Decline in Autosomal Dominant Polycystic Kidney Disease: Results from the CRISP Cohort. *Am. J. Kidney Dis. Off. J. Natl. Kidney Found.* 61, 420–429. doi:10.1053/j.ajkd.2012.08.038



- Boletta, A., Qian, F., Onuchic, L. F., Bhunia, A. K., Phakdeekitcharoen, B., Hanaoka, K., et al. (2000). Polycystin-1, the Gene Product of PKD1, Induces Resistance to Apoptosis and Spontaneous Tubulogenesis in MDCK Cells. *Mol. Cell* 6, 1267–1273. doi:10.1016/S1097-2765(00)00123-4
- Boute, N., Gribouval, O., Roselli, S., Benessy, F., Lee, H., Fuchshuber, A., et al. (2000). NPHS2, Encoding the Glomerular Protein Podocin, Is Mutated in Autosomal Recessive Steroid-Resistant Nephrotic Syndrome. *Nat. Genet.* 24, 349–354. doi:10.1038/74166
- Brosius, F. C., and Alpers, C. E. (2013). New Targets for Treatment of Diabetic Nephropathy: what We Have Learned from Animal Models. *Curr. Opin. Nephrol. Hypertens.* 22, 17–25. doi:10.1097/MNH.0b013e32835b3766
- Brosius, F. C., Alpers, C. E., Bottinger, E. P., Breyer, M. D., Coffman, T. M., Gurley, S. B., et al. (2009). Mouse Models of Diabetic Nephropathy. *J. Am. Soc. Nephrol.* JASN 20, 2503–2512. doi:10.1681/ASN.2009070721
- Broutier, L., Mastrogianni, G., Versteegen, M. M., Francies, H. E., Gavarró, L. M., Bradshaw, C. R., et al. (2017). Human Primary Liver Cancer–Derived Organoid Cultures for Disease Modeling and Drug Screening. *Nat. Med.* 23, 1424–1435. doi:10.1038/nm.4438
- Brown, A. C., Muthukrishnan, S. D., and Oxburgh, L. (2015). A Synthetic Niche for Nephron Progenitor Cells. *Dev. Cell* 34, 229–241. doi:10.1016/j.devcel.2015.06.021
- Calandrin, C., Schutgens, F., Oka, R., Margaritis, T., Candelli, T., Mathijssen, L., et al. (2020). An Organoid Biobank for Childhood Kidney Cancers that Captures Disease and Tissue Heterogeneity. *Nat. Commun.* 11, 1310. doi:10.1038/s41467-020-15155-6
- Combes, A. N., Phipson, B., Lawlor, K. T., Dorison, A., Patrick, R., Zappia, L., et al. (2019a). Single Cell Analysis of the Developing Mouse Kidney Provides Deeper Insight into Marker Gene Expression and Ligand-Receptor Crosstalk. *Development* 146, dev178673. doi:10.1242/dev.178673
- Combes, A. N., Zappia, L., Er, P. X., Oshlack, A., and Little, M. H. (2019b). Single-cell Analysis Reveals Congruence between Kidney Organoids and Human Fetal Kidney. *Genome Med.* 11, 3. doi:10.1186/s13073-019-0615-0
- Coppo, R., Chiesa, M., Cirina, P., Peruzzi, L., Amore, A., and IgACE, European. (2002). Study Group In Human IgA Nephropathy Uteroglobin Does Not Play the Role Inferred from Transgenic Mice. *Am. J. Kidney Dis. Off. J. Natl. Kidney Found.* 40, 495–503. doi:10.1053/ajkd.2002.34890
- Cristofori, P., Zanetti, E., Fregona, D., Piaia, A., and Trevisan, A. (2007). Renal Proximal Tubule Segment-specific Nephrotoxicity: An Overview on Biomarkers and Histopathology. *Toxicol. Pathol.* 35, 270–275. doi:10.1080/01926230601187430
- Cruz, N. M., Song, X., Czerniecki, S. M., Gulieva, R. E., Churchill, A. J., Kim, Y. K., et al. (2017). Organoid Cystogenesis Reveals a Critical Role of Microenvironment in Human Polycystic Kidney Disease. *Nat. Mater.* 16, 1112–1119. doi:10.1038/nmat4994
- Czerniecki, S. M., Cruz, N. M., Harder, J. L., Menon, R., Annis, J., Otto, E. A., et al. (2018). High-Throughput Screening Enhances Kidney Organoid Differentiation from Human Pluripotent Stem Cells and Enables Automated Multidimensional Phenotyping. *Cell Stem Cell* 22, 929–940. doi:10.1016/j.stem.2018.04.022
- Daehn, I. S., and Duffield, J. S. (2021). The Glomerular Filtration Barrier: a Structural Target for Novel Kidney Therapies. *Nat. Rev. Drug Discov.* 20, 1–19. doi:10.1038/s41573-021-00242-0
- Davidow, C. J., Maser, R. L., Rome, L. A., Calvet, J. P., and Grantham, J. J. (1996). The Cystic Fibrosis Transmembrane Conductance Regulator Mediates Transepithelial Fluid Secretion by Human Autosomal Dominant Polycystic Kidney Disease Epithelium *In Vitro*. *Kidney Int.* 50, 208–218. doi:10.1038/ki.1996.304
- Doyonnas, R., Kershaw, D. B., Duhme, C., Merckens, H., Chelliah, S., Graf, T., et al. (2001). Anuria, Omphalocele, and Perinatal Lethality in Mice Lacking the Cd34-Related Protein Podocalyxin. *J. Exp. Med.* 194, 13–28. doi:10.1084/jem.194.1.13
- Dvela-Levitt, M., Kost-Alimova, M., Emani, M., Kohnert, E., Thompson, R., Sidhom, E.-H., et al. (2019). Small Molecule Targets TMED9 and Promotes Lysosomal Degradation to Reverse Proteinopathy. *Cell* 178, 521–535. doi:10.1016/j.cell.2019.07.002
- Eilat, D., Schechter, A. N., and Steinberg, A. D. (1976). Antibodies to Native tRNA in NZB/NZW Mice. *Nature* 259, 141–143. doi:10.1038/259141a0
- England, A. R., Chaney, C. P., Das, A., Patel, M., Malewska, A., Armendariz, D., et al. (2020). Identification and Characterization of Cellular Heterogeneity within the Developing Renal Interstitium. *Development* 147, dev190108. doi:10.1242/dev.190108
- Fang, L., Karakiulakis, G., and Roth, M. (2020). Are Patients with Hypertension and Diabetes Mellitus at Increased Risk for COVID-19 Infection? *Lancet Respir. Med.* 8, e21. doi:10.1016/S2213-2600(20)30116-8
- Fendler, A., Bauer, D., Busch, J., Jung, K., Wulf-Goldenberg, A., Kunz, S., et al. (2020). Inhibiting WNT and NOTCH in Renal Cancer Stem Cells and the Implications for Human Patients. *Nat. Commun.* 11, 929. doi:10.1038/s41467-020-14700-7
- Freedman, B. S., Brooks, C. R., Lam, A. Q., Fu, H., Morizane, R., Agrawal, V., et al. (2015). Modelling Kidney Disease with CRISPR-Mutant Kidney Organoids Derived from Human Pluripotent Epiblast Spheroids. *nature.com/remotex.ntu.edu.sg/munications* 6, 1–13. doi:10.1038/ncomms9715
- Fujii, M., Shimokawa, M., Date, S., Takano, A., Matano, M., Nanki, K., et al. (2016). A Colorectal Tumor Organoid Library Demonstrates Progressive Loss of Niche Factor Requirements during Tumorigenesis. *Cell Stem Cell* 18, 827–838. doi:10.1016/j.stem.2016.04.003
- Gansevoort, R. T., Correa-Rotter, R., Hemmelgarn, B. R., Jafar, T. H., Heerspink, H. J. L., Mann, J. F., et al. (2013). Chronic Kidney Disease and Cardiovascular Risk: Epidemiology, Mechanisms, and Prevention. *The Lancet* 382, 339–352. doi:10.1016/S0140-6736(13)60595-4
- Garreta, E., Prado, P., Tarantino, C., Oria, R., Fanlo, L., Martí, E., et al. (2019). Fine Tuning the Extracellular Environment Accelerates the Derivation of Kidney Organoids from Human Pluripotent Stem Cells. *Nat. Mater.* 18, 397–405. doi:10.1038/s41563-019-0287-6
- Go, A. S., Chertow, G. M., Fan, D., McCulloch, C. E., and Hsu, C. (2004). Chronic Kidney Disease and the Risks of Death, Cardiovascular Events, and Hospitalization. *N. Engl. J. Med.* 351, 1296–1305. doi:10.1056/NEJMoa041031
- Grassi, L., Alfonsi, R., Francescangeli, F., Signore, M., Angelis De, M. L., Addario, A., et al. (2019). Organoids as a New Model for Improving Regenerative Medicine and Cancer Personalized Therapy in Renal Diseases. *Cell Death Dis.* 10, 1–15. doi:10.1038/s41419-019-1453-0
- Gu, Y.-F., Cohn, S., Christie, A., McKenzie, T., Wolff, N., Do, Q. N., et al. (2017). Modeling Renal Cell Carcinoma in Mice: Bap1 and Pbrm1 Inactivation Drive Tumor Grade. *Cancer Discov.* 7, 900–917. doi:10.1158/2159-8290.CD-17-0292
- Gunay-Aygun, M., Avner, E. D., Bacallao, R. L., Choyke, P. L., Flynn, J. T., Germino, G. G., et al. (2006). Autosomal Recessive Polycystic Kidney Disease and Congenital Hepatic Fibrosis: Summary Statement of a First National Institutes of Health/Office of Rare Diseases Conference. *J. Pediatr.* 149, 159–164. doi:10.1016/j.jpeds.2006.03.014
- Hale, L. J., Howden, S. E., Phipson, B., Lonsdale, A., Er, P. X., Ghobrial, I., et al. (2018). 3D Organoid-Derived Human Glomeruli for Personalised Podocyte Disease Modelling and Drug Screening. *Nat. Commun.* 9, 5167. doi:10.1038/s41467-018-07594-z
- Happé, H., and Peters, D. J. M. (2014). Translational Research in ADPKD: Lessons from Animal Models. *Nat. Rev. Nephrol.* 10, 587–601. doi:10.1038/nrneph.2014.137
- Harlander, S., Schönenberger, D., Toussaint, N. C., Prummer, M., Catalano, A., Brandt, L., et al. (2017). Combined Mutation in Vhl, Trp53 and Rb1 Causes clear Cell Renal Cell Carcinoma in Mice. *Nat. Med.* 23, 869–877. doi:10.1038/nm.4343
- Henderson, J. M., Al-Waheeb, S., Weins, A., Dandapani, S. V., and Pollak, M. R. (2008). Mice with Altered Alpha-Actinin-4 Expression Have Distinct Morphologic Patterns of Glomerular Disease. *Kidney Int.* 73, 741–750. doi:10.1038/sj.ki.5002751
- Herron, B. J., Lu, W., Rao, C., Liu, S., Peters, H., Bronson, R. T., et al. (2002). Efficient Generation and Mapping of Recessive Developmental Mutations Using ENU Mutagenesis. *Nat. Genet.* 30, 185–189. doi:10.1038/ng812
- Hildebrandt, F. (2010). Genetic Kidney Diseases. *The Lancet* 375, 1287–1295. doi:10.1016/S0140-6736(10)60236-X
- Hirsch, H. H., Brennan, D. C., Drachenberg, C. B., Ginevri, F., Gordon, J., Limaye, A. P., et al. (2005). Polyomavirus-Associated Nephropathy in Renal Transplantation: Interdisciplinary Analyses and Recommendations. *Transplantation* 79, 1277–1286. doi:10.1097/01.TP.0000156165.83160.09
- Hollywood, J. A., Przepiorski, A., D'Souza, R. F., Sreebhavan, S., Wolvetang, E. J., Harrison, P. T., et al. (2020). Use of Human Induced Pluripotent Stem Cells and

- Kidney Organoids to Develop a Cysteamine/mTOR Inhibition Combination Therapy for Cystinosis. *J. Am. Soc. Nephrol. JASN* 31, 962–982. doi:10.1681/ASN.2019070712
- Homan, K. A., Gupta, N., Kroll, K. T., Kolesky, D. B., Skylar-Scott, M., Miyoshi, T., et al. (2019). Flow-enhanced Vascularization and Maturation of Kidney Organoids *In Vitro*. *Nat. Methods* 16, 255–262. doi:10.1038/s41592-019-0325-y
- Howden, S. E., Wilson, S. B., Groenewegen, E., Starks, L., Forbes, T. A., Tan, K. S., et al. (2021). Plasticity of Distal Nephron Epithelia from Human Kidney Organoids Enables the Induction of Ureteric Tip and Stalk. *Cell Stem Cell* 28, 671–684. doi:10.1016/j.stem.2020.12.001
- Hwang, D.-Y., Dworschak, G. C., Kohl, S., Saisawat, P., Vivante, A., Hilger, A. C., et al. (2014). Mutations in 12 Known Dominant Disease-Causing Genes Clarify many Congenital Anomalies of the Kidney and Urinary Tract. *Kidney Int.* 85, 1429–1433. doi:10.1038/ki.2013.508
- Jansen, J., Reimer, K. C., Nagai, J. S., Varghese, F. S., Overheul, G. J., Beerde, M., et al. (2021). SARS-CoV-2 Infects the Human Kidney and Drives Fibrosis in Kidney Organoids. *Cell Stem Cell* 29, 217–231. doi:10.1016/j.stem.2021.12.010
- Kaminski, M. M., Tomic, J., Kresbach, C., Engel, H., Klockenbusch, J., Müller, A.-L., et al. (2016). *Nat. Cell Biol.* 18, 1269–1280. doi:10.1038/ncb3437
- Kanai, Y., Lee, W. S., You, G., Brown, D., and Hediger, M. A. (1994). The Human Kidney Low Affinity Na<sup>+</sup>/glucose Cotransporter SGLT2. Delineation of the Major Renal Reabsorptive Mechanism for D-Glucose. *J. Clin. Invest.* 93, 397–404. doi:10.1172/JCI116972
- Kapitsinou, P. P., and Haase, V. H. (2008). The VHL Tumor Suppressor and HIF: Insights from Genetic Studies in Mice. *Cell Death Differ.* 15, 650–659. doi:10.1038/sj.cdd.4402313
- Kaplan, J. M., Kim, H. S., North, K. N., Rennke, H., Correia, A. L., Tong, H.-Q., et al. (2000). Mutations in ACTN4, encoding  $\alpha$ -actinin-4, cause familial focal segmental glomerulosclerosis. *Nat. Genet.* 24, 251–256. doi:10.1038/73456
- Kim, D., and Dressler, G. R. (2005). Nephrogenic Factors Promote Differentiation of Mouse Embryonic Stem Cells into Renal Epithelia. *J. Am. Soc. Nephrol.* 16, 3527–3534. doi:10.1681/ASN.2005050544
- Kim, Y. K., Refaeli, I., Brooks, C. R., Jing, P., Gulieva, R. E., Hughes, M. R., et al. (2017). Gene-Edited Human Kidney Organoids Reveal Mechanisms of Disease in Podocyte Development. *STEM CELLS* 35, 2366–2378. doi:10.1002/stem.2707
- Kirby, A., Gnirke, A., Jaffe, D. B., Barešová, V., Pochet, N., Blumenstiel, B., et al. (2013). Mutations Causing Medullary Cystic Kidney Disease Type 1 Lie in a Large VNTR in MUC1 Missed by Massively Parallel Sequencing. *Nat. Genet.* 45, 299–303. doi:10.1038/ng.2543
- Kopper, O., de Witte, C. J., Löhmußaar, K., Valle-Inclán, J. E., Hami, N., Kester, L., et al. (2019). An Organoid Platform for Ovarian Cancer Captures Intra- and Interpatient Heterogeneity. *Nat. Med.* 25, 838–849. doi:10.1038/s41591-019-0422-6
- Koptides, M., and Deltas, C. C. (2000). Autosomal Dominant Polycystic Kidney Disease: Molecular Genetics and Molecular Pathogenesis. *Hum. Genet.* 107, 115–126. doi:10.1007/s004390000347
- Krendel, M., Kim, S. V., Willinger, T., Wang, T., Kashgarian, M., Flavell, R. A., et al. (2009). Disruption of Myosin 1e promotes podocyte injury. *J. Am. Soc. Nephrol. JASN* 20, 86–94. doi:10.1681/ASN.2007111172
- Kumar, S. V., Er, P. X., Lawlor, K. T., Motazedian, A., Scurr, M., Ghobrial, I., et al. (2019). Kidney Micro-organoids in Suspension Culture as a Scalable Source of Human Pluripotent Stem Cell-Derived Kidney Cells. *Dev. Camb. Engl.* 146, dev172361. doi:10.1242/dev.172361
- Kuraoka, S., Tanigawa, S., Taguchi, A., Hotta, A., Nakazato, H., Osafune, K., et al. (2020). PKD1-Dependent Renal Cystogenesis in Human Induced Pluripotent Stem Cell-Derived Ureteric Bud/Collecting Duct Organoids. *J. Am. Soc. Nephrol. JASN* 31, 2355–2371. doi:10.1681/ASN.2020030378
- Lager, D. J., Qian, Q., Bengal, R. J., Ishibashi, M., and Torres, V. E. (2001). The Pck Rat: A New Model that Resembles Human Autosomal Dominant Polycystic Kidney and Liver Disease. *Kidney Int.* 59, 126–136. doi:10.1046/j.1523-1755.2001.00473.x
- Launay, P., Grossetête, B., Arcos-Fajardo, M., Gaudin, E., Torres, S. P., Beaudoin, L., et al. (2000). Fc $\alpha$  Receptor (CD89) Mediates the Development of Immunoglobulin A (IgA) Nephropathy (Berger's Disease). Evidence for Pathogenic Soluble Receptor-IgA Complexes in Patients and CD89 Transgenic Mice. *J. Exp. Med.* 191, 1999–2009. doi:10.1084/jem.191.11.1999
- Lawlor, K. T., Vanslambrouck, J. M., Higgins, J. W., Chambon, A., Bishard, K., Arndt, D., et al. (2021). Cellular Extrusion Bioprinting Improves Kidney Organoid Reproducibility and Conformation. *Nat. Mater.* 20, 260–271. doi:10.1038/s41563-020-00853-9
- Lee, C.-H., and Motzer, R. J. (2017). The Evolution of Anti-angiogenic Therapy for Kidney Cancer. *Nat. Rev. Nephrol.* 13, 69–70. doi:10.1038/nrneph.2016.194
- Lee, G.-H., Proenca, R., Montez, J. M., Carroll, K. M., Darvishzadeh, J. G., Lee, J. I., et al. (1996). Abnormal Splicing of the Leptin Receptor in Diabetic Mice. *Nature* 379, 632–635. doi:10.1038/379632a0
- Leeuwen Lantinga-van, I. S., Dauwerse, J. G., Baelde, H. J., Leonhard, W. N., van de Wal, A., Ward, C. J., et al. (2004). Lowering of Pkd1 Expression Is Sufficient to Cause Polycystic Kidney Disease. *Hum. Mol. Genet.* 13, 3069–3077. doi:10.1093/hmg/ddh336
- Leiter, E. H. (1982). Multiple Low-Dose Streptozotocin-Induced Hyperglycemia and Insulinitis in C57BL Mice: Influence of Inbred Background, Sex, and Thymus. *Proc. Natl. Acad. Sci. U. S. A.* 79, 630–634. doi:10.1073/pnas.79.2.630
- Li, D., Qiu, Z., Shao, Y., Chen, Y., Guan, Y., Liu, M., et al. (2013). Heritable Gene Targeting in the Mouse and Rat Using a CRISPR-Cas System. *Nat. Biotechnol.* 31, 681–683. doi:10.1038/nbt.2661
- Li, Z., Araoka, T., Wu, J., Liao, H.-K., Li, M., Lazo, M., et al. (2016). 3D Culture Supports Long-Term Expansion of Mouse and Human Nephrogenic Progenitors. *Cell Stem Cell* 19, 516–529. doi:10.1016/j.stem.2016.07.016
- Li, Z., Chung, A. C., Zhou, L., Huang, X. R., Liu, F., Fu, P., et al. (2011). C-reactive Protein Promotes Acute Renal Inflammation and Fibrosis in Unilateral Ureteral Obstructive Nephropathy in Mice. *Lab. Invest.* 91, 837–851. doi:10.1038/labinvest.2011.42
- Lin, N. Y. C., Homan, K. A., Robinson, S. S., Kolesky, D. B., Duarte, N., Moisan, A., et al. (2019). Renal Reabsorption in 3D Vascularized Proximal Tubule Models. *Proc. Natl. Acad. Sci.* 116, 5399–5404. doi:10.1073/pnas.1815208116
- Low, J. H., Li, P., Chew, E. G. Y., Zhou, B., Suzuki, K., Zhang, T., et al. (2019). Generation of Human PSC-Derived Kidney Organoids with Patterned Nephron Segments and a De Novo Vascular Network. *Cell Stem Cell* 25, 373–387. doi:10.1016/j.stem.2019.06.009
- Lu, H., Galeano, M. C. R., Ott, E., Kaeslin, G., Kausalya, P. J., Kramer, C., et al. (2017). Mutations in DZIP1L, Which Encodes a Ciliary-Transition-Zone Protein, Cause Autosomal Recessive Polycystic Kidney Disease. *Nat. Genet.* 49, 1025–1034. doi:10.1038/ng.3871
- Mae, S.-I., Ryosaka, M., Sakamoto, S., Matsuse, K., Nozaki, A., Igami, M., et al. (2020). Expansion of Human iPSC-Derived Ureteric Bud Organoids with Repeated Branching Potential. *Cell Rep.* 32, 107963. doi:10.1016/j.celrep.2020.107963
- Mae, S.-I., Shono, A., Shiota, F., Yasuno, T., Kajiwara, M., Gotoda-Nishimura, N., et al. (2013). Monitoring and Robust Induction of Nephrogenic Intermediate Mesoderm from Human Pluripotent Stem Cells. *Nat. Commun.* 4, 1367. doi:10.1038/ncomms2378
- Maffei, M., Halaas, J., Ravussin, E., Pratley, R. E., Lee, G. H., Zhang, Y., et al. (1995). Leptin Levels in Human and Rodent: Measurement of Plasma Leptin and Ob RNA in Obese and Weight-Reduced Subjects. *Nat. Med.* 1, 1155–1161. doi:10.1038/nm1195-1155
- Makris, K., and Spanou, L. (2016). Acute Kidney Injury: Definition, Pathophysiology and Clinical Phenotypes. *Clin. Biochem. Rev.* 37, 85–98.
- Mango-Karim, R., Uchic, M., Lechene, C., and Grantham, J. J. (1989). Renal Epithelial Cyst Formation and Enlargement *In Vitro*: Dependence on cAMP. *Proc. Natl. Acad. Sci.* 86, 6007–6011. doi:10.1073/pnas.86.15.6007
- Matsushita, K., Coresh, J., Sang, Y., Chalmers, J., Fox, C., Gualler, E., et al. (2015). Estimated Glomerular Filtration Rate and Albuminuria for Prediction of Cardiovascular Outcomes: a Collaborative Meta-Analysis of Individual Participant Data. *Lancet Diabetes Endocrinol.* 3, 514–525. doi:10.1016/S2213-8587(15)00040-6
- McMahon, A. P. (2016). Development of the Mammalian Kidney. *Curr. Top. Dev. Biol.* 117, 31–64. doi:10.1016/bs.ctdb.2015.10.010
- Mele, C., Iatropoulos, P., Donadelli, R., Calabria, A., Maranta, R., Cassis, P., et al. (2011). MYO1E MUTATIONS AND CHILDHOOD FAMILIAL FOCAL SEGMENTAL GLOMERULOSCLEROSIS. *N. Engl. J. Med.* 365, 295–306. doi:10.1056/NEJMoa1101273
- Meyrier, A. (2005). Mechanisms of Disease: Focal Segmental Glomerulosclerosis. *Nat. Clin. Pract. Nephrol.* 1, 44–54. doi:10.1038/ncpneph0025

- Monteil, V., Kwon, H., Prado, P., Hagelkrüys, A., Wimmer, R. A., Stahl, M., et al. (2020). Inhibition of SARS-CoV-2 Infections in Engineered Human Tissues Using Clinical-Grade Soluble Human ACE2. *Cell* 181, 905–913. doi:10.1016/j.cell.2020.04.004
- Morizane, R., Lam, A. Q., Freedman, B. S., Kishi, S., Valerius, M. T., and Bonventre, J. V. (2015). Nephron Organoids Derived from Human Pluripotent Stem Cells Model Kidney Development and Injury. *Nat. Biotechnol.* 33, 1193–1200. doi:10.1038/nbt.3392
- Moura, I. C., Benhamou, M., Launay, P., Vrtovsnik, F., Blank, U., and Monteiro, R. C. (2008). The Glomerular Response to IgA Deposition in IgA Nephropathy. *Semin. Nephrol.* 28, 88–95. doi:10.1016/j.semnephrol.2007.10.010
- Mukundan, L., Odegaard, J. I., Morel, C. R., Heredia, J. E., Mwangi, J. W., Ricardo-Gonzalez, R. R., et al. (2009). PPAR- $\delta$  Senses and Orchestrates Clearance of Apoptotic Cells to Promote Tolerance. *Nat. Med.* 15, 1266–1272. doi:10.1038/nm.2048
- Mundel, P., Reiser, J., and Kriz, W. (1997). Induction of Differentiation in Cultured Rat and Human Podocytes. *J. Am. Soc. Nephrol. JASN* 8, 697–705. doi:10.1681/ASN.V85697
- Musah, S., Mammoto, A., Ferrante, T. C., Jeanty, S. S. F., Hirano-Kobayashi, M., Mammoto, T., et al. (2017). Mature Induced-Pluripotent-Stem-Cell-Derived Human Podocytes Reconstitute Kidney Glomerular-Capillary-wall Function on a Chip. *Nat. Biomed. Eng.* 1, 1–12. doi:10.1038/s41551-017-0069
- Nakanishi, K., Sweeney, W. E., Zerres, K., Guay-Woodford, L. M., and Avner, E. D. (2000). Proximal Tubular Cysts in Fetal Human Autosomal Recessive Polycystic Kidney Disease. *J. Am. Soc. Nephrol. JASN* 11, 760–763. doi:10.1681/ASN.V114760
- Nargund, A. M., Pham, C. G., Dong, Y., Wang, P. I., Osmangyoglu, H. U., Xie, Y., et al. (2017). The SWI/SNF Protein PBRM1 Restrains VHL-Loss-Driven Clear Cell Renal Cell Carcinoma. *Cell Rep.* 18, 2893–2906. doi:10.1016/j.celrep.2017.02.074
- Neal, J. T., Li, X., Zhu, J., Giangarra, V., Grzeskowiak, C. L., Ju, J., et al. (2018). Organoid Modeling of the Tumor Immune Microenvironment. *Cell* 175, 1972–1988. doi:10.1016/j.cell.2018.11.021
- Neubert, K., Meister, S., Moser, K., Weisel, F., Maseda, D., Amann, K., et al. (2008). The Proteasome Inhibitor Bortezomib Depletes Plasma Cells and Protects Mice with Lupus-like Disease from Nephritis. *Nat. Med.* 14, 748–755. doi:10.1038/nm1763
- Nicolaou, N., Renkema, K. Y., Bongers, E. M. H. F., Giles, R. H., and Knoers, N. V. A. M. (2015). Genetic, Environmental, and Epigenetic Factors Involved in CAKUT. *Nat. Rev. Nephrol.* 11, 720–731. doi:10.1038/nrneph.2015.140
- O'Brien, L. E., Zegers, M. M. P., and Mostov, K. E. (2002). Building Epithelial Architecture: Insights from Three-Dimensional Culture Models. *Nat. Rev. Mol. Cell Biol.* 3, 531–537. doi:10.1038/nrm859
- Park, J., Shrestha, R., Qiu, C., Kondo, A., Huang, S., Werth, M., et al. (2018). Single-cell Transcriptomics of the Mouse Kidney Reveals Potential Cellular Targets of Kidney Disease. *Science* 360, 758–763. doi:10.1126/science.aar2131
- Patrakka, J., Kestilä, M., Wartiovaara, J., Ruotsalainen, V., Tissari, P., Lenkkeri, U., et al. (2000). Congenital Nephrotic Syndrome (NPHS1): Features Resulting from Different Mutations in Finnish Patients. *Kidney Int.* 58, 972–980. doi:10.1046/j.1523-1755.2000.00254.x
- Pei, Y., Watnick, T., He, N., Wang, K., Liang, Y., Parfrey, P., et al. (1999). Somatic PKD2 Mutations in Individual Kidney and Liver Cysts Support a “Two-Hit” Model of Cystogenesis in Type 2 Autosomal Dominant Polycystic Kidney Disease. *J. Am. Soc. Nephrol.* 10, 1524–1529. doi:10.1681/ASN.V1071524
- Phipson, B., Er, P. X., Combes, A. N., Forbes, T. A., Howden, S. E., Zappia, L., et al. (2019). Evaluation of Variability in Human Kidney Organoids. *Nat. Methods* 16, 79–87. doi:10.1038/s41592-018-0253-2
- Piliponsky, A. M., Chen, C.-C., Nishimura, T., Metz, M., Rios, E. J., Dobner, P. R., et al. (2008). Neurotensin Increases Mortality and Mast Cells Reduce Neurotensin Levels in a Mouse Model of Sepsis. *Nat. Med.* 14, 392–398. doi:10.1038/nm1738
- Piontek, K. B., Huso, D. L., Grinberg, A., Liu, L., Bedja, D., Zhao, H., et al. (2004). A Functional Floxed Allele of Pkd1 that Can Be Conditionally Inactivated *In Vivo*. *J. Am. Soc. Nephrol. JASN* 15, 3035–3043. doi:10.1097/01.ASN.0000144204.01352.86
- Piontek, K., Menezes, L. F., Garcia-Gonzalez, M. A., Huso, D. L., and Germino, G. G. (2007). A Critical Developmental Switch Defines the Kinetics of Kidney Cyst Formation after Loss of Pkd1. *Nat. Med.* 13, 1490–1495. doi:10.1038/nm1675
- Plageman, T. F., Chauhan, B. K., Yang, C., Jaudon, F., Shang, X., Zheng, Y., et al. (2011). A Trio-RhoA-Shroom3 Pathway Is Required for Apical Constriction and Epithelial Invagination. *Dev. Camb. Engl.* 138, 5177–5188. doi:10.1242/dev.067868
- Prochazka, M., Gaskins, H. R., Shultz, L. D., and Leiter, E. H. (1992). The Nonobese Diabetic Scid Mouse: Model for Spontaneous Thymomagenesis Associated with Immunodeficiency. *Proc. Natl. Acad. Sci. U. S. A.* 89, 3290–3294. doi:10.1073/pnas.89.8.3290
- Przepiorski, A., Sander, V., Tran, T., Hollywood, J. A., Sorrenson, B., Shih, J.-H., et al. (2018). A Simple Bioreactor-Based Method to Generate Kidney Organoids from Pluripotent Stem Cells. *Stem Cell Rep.* 11, 470–484. doi:10.1016/j.stemcr.2018.06.018
- Qian, F., Watnick, T. J., Onuchic, L. F., and Germino, G. G. (1996). The Molecular Basis of Focal Cyst Formation in Human Autosomal Dominant Polycystic Kidney Disease Type I. *Cell* 87, 979–987. doi:10.1016/S0092-8674(00)81793-6
- Roberts, I. S. D. (2014). Pathology of IgA Nephropathy. *Nat. Rev. Nephrol.* 10, 445–454. doi:10.1038/nrneph.2014.92
- Rossini, A. A., Williams, R. M., Appel, M. C., and Like, A. A. (1978). Complete protection from Low-Dose Streptozotocin-Induced Diabetes in Mice. *Nature* 276, 182–184. doi:10.1038/276182a0
- Ryan, M. J., Johnson, G., Kirk, J., Fuerstenberg, S. M., Zager, R. A., and Torok-Storb, B. (1994). HK-2: An Immortalized Proximal Tubule Epithelial Cell Line from normal Adult Human Kidney. *Kidney Int.* 45, 48–57. doi:10.1038/ki.1994.6
- Saleem, M. A., O'Hare, M. J., Reiser, J., Coward, R. J., Inward, C. D., Farren, T., et al. (2002). A Conditionally Immortalized Human Podocyte Cell Line Demonstrating Nephron and Podocin Expression. *J. Am. Soc. Nephrol.* 13, 630–638. doi:10.1681/ASN.V133630
- Sander, J. D., and Joung, J. K. (2014). CRISPR-cas Systems for Editing, Regulating and Targeting Genomes. *Nat. Biotechnol.* 32, 347–355. doi:10.1038/nbt.2842
- Satoh, M., Kumar, A., Kanwar, Y. S., and Reeves, W. H. (1995). Anti-nuclear Antibody Production and Immune-Complex Glomerulonephritis in BALB/c Mice Treated with Pristane. *Proc. Natl. Acad. Sci.* 92, 10934–10938. doi:10.1073/pnas.92.24.10934
- Schutgens, F., Rookmaaker, M. B., Margaritis, T., Rios, A., Ammerlaan, C., Jansen, J., et al. (2019). Tubuloids Derived from Human Adult Kidney and Urine for Personalized Disease Modeling. *Nat. Biotechnol.* 37, 303–313. doi:10.1038/s41587-019-0048-8
- Serra, A. L., Poster, D., Kistler, A. D., Krauer, F., Raina, S., Young, J., et al. (2010). Sirolimus and Kidney Growth in Autosomal Dominant Polycystic Kidney Disease. *N. Engl. J. Med.* 363, 820–829. doi:10.1056/NEJMoa0907419
- Shankar, A. S., Du, Z., Mora, H. T., van den Bosch, T. P. P., Korevaar, S. S., van den Berg-Garrelts, I. M., et al. (2021). Human Kidney Organoids Produce Functional Renin. *Kidney Int.* 99, 134–147. doi:10.1016/j.kint.2020.08.008
- Shimizu, T., Mae, S.-I., Araoka, T., Okita, K., Hotta, A., Yamagata, K., et al. (2020). A Novel ADPKD Model Using Kidney Organoids Derived from Disease-specific Human iPSCs. *Biochem. Biophys. Res. Commun.* 529, 1186–1194. doi:10.1016/j.bbrc.2020.06.141
- Taguchi, A., Kaku, Y., Ohmori, T., Sharmin, S., Ogawa, M., Sasaki, H., et al. (2014). Redefining the *In Vivo* Origin of Metanephric Nephron Progenitors Enables Generation of Complex Kidney Structures from Pluripotent Stem Cells. *Cell Stem Cell* 14, 53–67. doi:10.1016/j.stem.2013.11.010
- Taguchi, A., and Nishinakamura, R. (2017). Higher-Order Kidney Organogenesis from Pluripotent Stem Cells. *Cell Stem Cell* 21, 730–746. doi:10.1016/j.stem.2017.10.011
- Takakura, A., Contrino, L., Beck, A. W., and Zhou, J. (2008). Pkd1 Inactivation Induced in Adulthood Produces Focal Cystic Disease. *J. Am. Soc. Nephrol. JASN* 19, 2351–2363. doi:10.1681/ASN.2007101139
- Takasato, M., Er, P. X., Becroft, M., Vanslambrouck, J. M., Stanley, E. G., Elefanti, A. G., et al. (2014). Directing Human Embryonic Stem Cell Differentiation towards a Renal Lineage Generates a Self-Organizing Kidney. *Nat. Cell Biol.* 16, 118–126. doi:10.1038/ncb2894
- Takasato, M., Er, P. X., Chiu, H. S., Maier, B., Baillie, G. J., Ferguson, C., et al. (2015). Kidney Organoids from Human iPS Cells Contain Multiple Lineages and Model Human Nephrogenesis. *Nature* 526, 564–568. doi:10.1038/nature15695
- Takasato, M., and Little, M. H. (2015). The Origin of the Mammalian Kidney: Implications for Recreating the Kidney *In Vitro*. *Dev. Camb. Engl.* 142, 1937–1947. doi:10.1242/dev.104802



- Tanigawa, S., Islam, M., Sharmin, S., Naganuma, H., Yoshimura, Y., Haque, F., et al. (2018). Organoids from Nephrotic Disease-Derived iPSCs Identify Impaired NEPHRIN Localization and Slit Diaphragm Formation in Kidney Podocytes. *Stem Cell Rep.* 11, 727–740. doi:10.1016/j.stemcr.2018.08.003
- Tanigawa, S., Tanaka, E., Miike, K., Ohmori, T., Inoue, D., Cai, C.-L., et al. (2022). Generation of the Organotypic Kidney Structure by Integrating Pluripotent Stem Cell-Derived Renal Stroma. *Nat. Commun.* 13, 611. doi:10.1038/s41467-022-28226-7
- Thomas, M. C., Brownlee, M., Susztak, K., Sharma, K., Jandeleit-Dahm, K. A. M., Zoungas, S., et al. (2015). Diabetic Kidney Disease. *Nat. Rev. Dis. Primer* 1, 1–20. doi:10.1038/nrdp.2015.18
- Tonelli, M., Wiebe, N., Knoll, G., Bello, A., Browne, S., Jadhav, D., et al. (2011). Systematic Review: Kidney Transplantation Compared with Dialysis in Clinically Relevant Outcomes. *Am. J. Transpl.* 11, 2093–2109. doi:10.1111/j.1600-6143.2011.03686.x
- Toniolo, A., Onodera, T., Yoon, J.-W., and Notkins, A. L. (1980). Induction of Diabetes by Cumulative Environmental Insults from Viruses and Chemicals. *Nature* 288, 383–385. doi:10.1038/288383a0
- Torres, V. E., Chapman, A. B., Devuyt, O., Gansevoort, R. T., Perrone, R. D., Koch, G., et al. (2017). Tolvaptan in Later-Stage Autosomal Dominant Polycystic Kidney Disease. *N. Engl. J. Med.* 377, 1930–1942. doi:10.1056/NEJMoa1710030
- Torres, V. E., and Harris, P. C. (2014). Strategies Targeting cAMP Signaling in the Treatment of Polycystic Kidney Disease. *J. Am. Soc. Nephrol. JASN* 25, 18–32. doi:10.1681/ASN.2013040398
- Uchimura, K., Wu, H., Yoshimura, Y., and Humphreys, B. D. (2020). Human Pluripotent Stem Cell-Derived Kidney Organoids with Improved Collecting Duct Maturation and Injury Modeling. *Cel Rep.* 33, 108514. doi:10.1016/j.celrep.2020.108514
- Ungricht, R., Guibbal, L., Lasbennes, M.-C., Orsini, V., Beibel, M., Waldt, A., et al. (2021). Genome-wide Screening in Human Kidney Organoids Identifies Developmental and Disease-Related Aspects of Nephrogenesis. *Cell Stem Cell* 29, 160–175. doi:10.1016/j.stem.2021.11.001
- Vaduganathan, M., Vardeny, O., Michel, T., McMurray, J. J. V., Pfeffer, M. A., and Solomon, S. D. (2020). Renin–Angiotensin–Aldosterone System Inhibitors in Patients with Covid-19. *N. Engl. J. Med.* 382, 1653–1659. doi:10.1056/NEJMs2005760
- van den Berg, C. W., Ritsma, L., Avramut, M. C., Wiersma, L. E., van den Berg, B. M., Leuning, D. G., et al. (2018). Renal Subcapsular Transplantation of PSC-Derived Kidney Organoids Induces Neo-Vasculogenesis and Significant Glomerular and Tubular Maturation in Vivo. *Stem Cell Rep.* 10, 751–765. doi:10.1016/j.stemcr.2018.01.041
- Walz, G., Budde, K., Manna, M., Nürnberger, J., Wanner, C., Sommerer, C., et al. (2010). Everolimus in Patients with Autosomal Dominant Polycystic Kidney Disease. *N. Engl. J. Med.* 363, 830–840. doi:10.1056/NEJMoa1003491
- Wang, Y., Bu, F., Royer, C., Serres, S., Larkin, J. R., Soto, M. S., et al. (2014). ASPP2 Controls Epithelial Plasticity and Inhibits Metastasis through  $\beta$ -catenin-dependent Regulation of ZEB1. *Nat. Cell Biol.* 16, 1092–1104. doi:10.1038/ncb3050
- Webster, A. C., Nagler, E. V., Morton, R. L., and Masson, P. (2017). Chronic Kidney Disease. *The Lancet* 389, 1238–1252. doi:10.1016/S0140-6736(16)32064-5
- Wilson, P. D. (2004). Polycystic Kidney Disease. *N. Engl. J. Med.* 350, 151–164. doi:10.1056/NEJMra022161
- Woollard, J. R., Punyashtiti, R., Richardson, S., Masyuk, T. V., Whelan, S., Huang, B. Q., et al. (2007). A Mouse Model of Autosomal Recessive Polycystic Kidney Disease with Biliary Duct and Proximal Tubule Dilatation. *Kidney Int.* 72, 328–336. doi:10.1038/sj.ki.5002294
- Wu, H., Uchimura, K., Donnelly, E. L., Kirita, Y., Morris, S. A., and Humphreys, B. D. (2018). Comparative Analysis and Refinement of Human PSC-Derived Kidney Organoid Differentiation with Single-Cell Transcriptomics. *Cell Stem Cell* 23, 869–881. doi:10.1016/j.stem.2018.10.010
- Wysocki, J., Ye, M., Hassler, L., Gupta, A. K., Wang, Y., Nicoleas, V., et al. (2021). A Novel Soluble ACE2 Variant with Prolonged Duration of Action Neutralizes SARS-CoV-2 Infection in Human Kidney Organoids. *J. Am. Soc. Nephrol.* 32, 795–803. doi:10.1681/ASN.2020101537
- Xia, Y., Nivet, E., Sancho-Martinez, I., Gallegos, T., Suzuki, K., Okamura, D., et al. (2013). Directed Differentiation of Human Pluripotent Cells to Ureteric Bud Kidney Progenitor-like Cells. *Nat. Cell Biol.* 15, 1507–1515. doi:10.1038/ncb2872
- Yamaguchi, T., Nagao, S., Takahashi, H., Ye, M., and Grantham, J. J. (1995). Cyst Fluid from a Murine Model of Polycystic Kidney Disease Stimulates Fluid Secretion, Cyclic Adenosine Monophosphate Accumulation, and Cell Proliferation by Madin-Darby Canine Kidney Cells *In Vitro*. *Am. J. Kidney Dis.* 25, 471–477. doi:10.1016/0272-6386(95)90111-6
- Yoshimura, Y., Taguchi, A., Tanigawa, S., Yatsuda, J., Kamba, T., Takahashi, S., et al. (2019). Manipulation of Nephron-Patterning Signals Enables Selective Induction of Podocytes from Human Pluripotent Stem Cells. *J. Am. Soc. Nephrol.* 30, 304–321. doi:10.1681/ASN.2018070747
- Yu, S., Hackmann, K., Gao, J., He, X., Piontek, K., Garcia-González, M. A., et al. (2007). Essential Role of Cleavage of Polycystin-1 at G Protein-Coupled Receptor Proteolytic Site for Kidney Tubular Structure. *Proc. Natl. Acad. Sci.* 104, 18688–18693. doi:10.1073/pnas.0708217104
- Yuri, S., Nishikawa, M., Yanagawa, N., Jo, O. D., and Yanagawa, N. (2017). Vitro Propagation and Branching Morphogenesis from Single Ureteric Bud Cells. *Stem Cell Rep.* 8, 401–416. doi:10.1016/j.stemcr.2016.12.011
- Zeng, Z., Huang, B., Parvez, R. K., Li, Y., Chen, J., Vonk, A. C., et al. (2021). Generation of Patterned Kidney Organoids that Recapitulate the Adult Kidney Collecting Duct System from Expandable Ureteric Bud Progenitors. *Nat. Commun.* 12, 3641. doi:10.1038/s41467-021-23911-5
- Zwacka, R. M., Zhou, W., Zhang, Y., Darby, C. J., Dudus, L., Halldorson, J., et al. (1998). Redox Gene Therapy for Ischemia/reperfusion Injury of the Liver Reduces AP1 and NF- $\kappa$ B Activation. *Nat. Med.* 4, 698–704. doi:10.1038/nm0698-698

**Conflict of Interest:** The authors declare that the research was conducted in the absence of any commercial or financial relationships that could be construed as a potential conflict of interest.

**Publisher's Note:** All claims expressed in this article are solely those of the authors and do not necessarily represent those of their affiliated organizations, or those of the publisher, the editors and the reviewers. Any product that may be evaluated in this article, or claim that may be made by its manufacturer, is not guaranteed or endorsed by the publisher.

Copyright © 2022 Liu, Cardilla, Ngeow, Gong and Xia. This is an open-access article distributed under the terms of the Creative Commons Attribution License (CC BY). The use, distribution or reproduction in other forums is permitted, provided the original author(s) and the copyright owner(s) are credited and that the original publication in this journal is cited, in accordance with accepted academic practice. No use, distribution or reproduction is permitted which does not comply with these terms.



# Human Intestinal Organoids: Promise and Challenge

Jasin Taelman<sup>1,2</sup>, Mònica Diaz<sup>1,2</sup> and Jordi Guiu<sup>1,2\*</sup>

<sup>1</sup>Cell Plasticity and Regeneration Group, Regenerative Medicine Program, Institut d'Investigació Biomèdica de Bellvitge-IDIBELL, L'Hospitalet de Llobregat, Spain, <sup>2</sup>Program for advancing the Clinical Translation of Regenerative Medicine of Catalonia, P-CMR [C], L'Hospitalet de Llobregat, Spain

The study of human intestinal biology in healthy and diseased conditions has always been challenging. Primary obstacles have included limited tissue accessibility, inadequate *in vitro* maintenance and ethical constraints. The development of three-dimensional organoid cultures has transformed this entirely. Intestinal organoids are self-organized three-dimensional structures that partially recapitulate the identity, cell heterogeneity and cell behaviour of the original tissue *in vitro*. This includes the capacity of stem cells to self-renew, as well as to differentiate towards major intestinal lineages. Therefore, over the past decade, the use of human organoid cultures has been instrumental to model human intestinal development, homeostasis, disease, and regeneration. Intestinal organoids can be derived from pluripotent stem cells (PSC) or from adult somatic intestinal stem cells (ISC). Both types of organoid sources harbour their respective strengths and weaknesses. In this mini review, we describe the applications of human intestinal organoids, discussing the differences, advantages, and disadvantages of PSC-derived and ISC-derived organoids.

**Keywords:** organoids, 3D models, intestine, human intestinal organoids, enteroids

## OPEN ACCESS

### Edited by:

Keiichi Suzuki,  
Osaka University, Japan

### Reviewed by:

Nandor Nagy,  
Semmelweis University, Hungary

### \*Correspondence:

Jordi Guiu  
jgiu@idibell.cat

### Specialty section:

This article was submitted to  
Stem Cell Research,  
a section of the journal  
Frontiers in Cell and Developmental  
Biology

**Received:** 14 January 2022

**Accepted:** 24 February 2022

**Published:** 11 March 2022

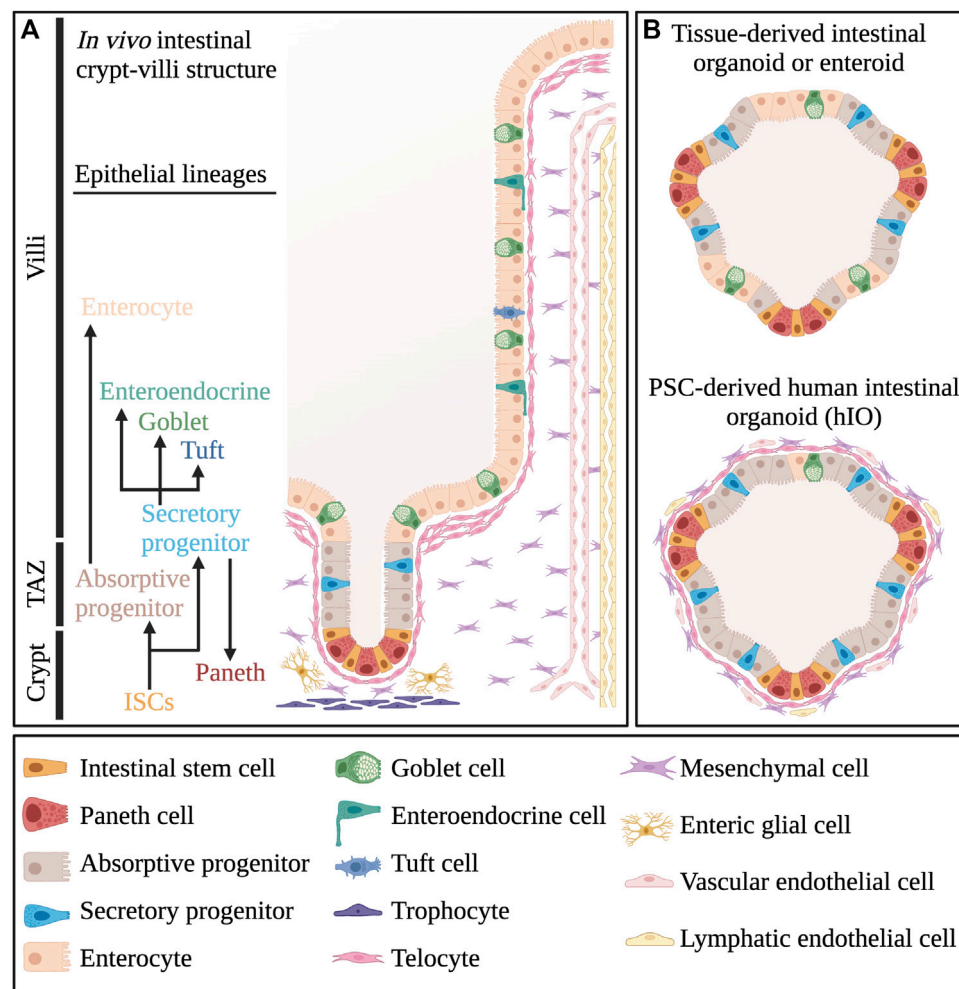
### Citation:

Taelman J, Diaz M and Guiu J (2022)  
Human Intestinal Organoids: Promise  
and Challenge.  
Front. Cell Dev. Biol. 10:854740.  
doi: 10.3389/fcell.2022.854740

## INTRODUCTION

The small intestine is a major organ that regulates digestive function and nutrient absorption. It is structured into crypts and protruding finger-like domains called villi (**Figure 1A**). The whole intestine is lined with a highly specialized epithelium, supported by a complex underlying mesenchyme (Guiu and Jensen, 2015; Gehart and Clevers, 2019; McCarthy et al., 2020a). During homeostasis, the human intestinal epithelium undergoes complete renewal every 5–7 days (Barker, 2014). This highly regenerative nature is supported by multipotent intestinal stem cells (ISCs), residing at the bottom of the crypts (Barker et al., 2007). ISCs can be identified by the expression of the R-spondin (RSPO) receptor LGR5, which plays a major role in the regulation of WNT/RSPO-signalling (Clevers, 2013). The proliferative ISC population in the crypt is maintained by neutral competition for supportive signals, including high WNT concentration, Notch signals and EGF (Snippert et al., 2010; Sato et al., 2011a). These primarily originate from Paneth cells, differentiated secretory cells that migrate away from differentiated villi regions to become interspersed with ISCs (van Es et al., 2005; Sato et al., 2011a). Paneth cells are also specialised in the secretion of antimicrobial agents such as lysozyme,  $\alpha$ -defensins and phospholipase-A2 (Porter et al., 2002). Nevertheless, ablation experiments in mice showed that Paneth cells are redundant (Kim et al., 2012; Van Es et al., 2019). While Notch-signalling can be provided by secretory lineage precursor cells, WNT and EGF signals are also supplied by multiple cell types of the subepithelial mesenchyme (Blumberg et al., 2008; Van Es et al., 2019; McCarthy et al., 2020a).





**FIGURE 1 |** Cellular composition of intestinal tissue and organoids. **(A)** Different cell types that make up the crypt-villi structure *in vivo* small intestinal tissue. **(B)** Comparative overview of the cellular composition of pluripotent stem cell-derived human intestinal organoids or hIOs and tissue-derived organoids or enteroids. TAZ, Transit Amplifying Zone. Created with BioRender.com.

One specific CD81+/Pdgfra + mesenchymal subpopulation, termed trophocytes is primarily located below the crypt epithelium and can support mouse intestinal cells *in vitro* without any additional factors (McCarthy et al., 2020a) (Figure 1A). Aside from expression of canonical Wnt ligands and Wnt-promoting Rspo proteins, trophocytes are also typified by their expression of BMP inhibitors Gremlin 1 and Noggin (McCarthy et al., 2020a). Another subpopulation, Foxl1+/Pdgfra + subepithelial myofibroblasts (SEMFs), also termed telocytes, form a loosely interconnected sheath directly below the intestinal epithelium via their far-reaching cell extensions (Shoshkes-Carmel et al., 2018). Their distribution is non-uniform as they have higher concentrations near the villus base, as well as in villus tips (Shoshkes-Carmel et al., 2018). Depending on this distribution, telocytes express multiple Bmp factors and non-canonical Wnt factors which generally counteract canonical Wnt-signalling (Shoshkes-Carmel et al., 2018; McCarthy et al., 2020b). However, telocytes also express canonical Wnt agonists,

and specific inhibition of Wnt secretion in mouse telocytes ultimately caused a dramatic reduction in ISC proliferation (Shoshkes-Carmel et al., 2018). The mesenchyme further harbours a large heterogeneous population of Pdgfra<sup>low</sup>-mesenchymal cells which can express both Bmp factors, Wnt agonists and antagonists, further contributing to a complex mesenchymal environment (McCarthy et al., 2020a; Kim JE. et al., 2020). Specific subpopulations of Gfap + enteric glial cells (EGCs), localised near crypts, also provide key yet redundant Wnt factors to ISCs (Baghdadi et al., 2022). In case of injury however, these EGCs expand and are critical to efficient intestinal regeneration (Baghdadi et al., 2022). Various types of immune cells also reside in the intestinal mesenchyme and tissue-resident lymphoid cells have been implicated in the regulation of intestinal homeostasis and regeneration by secretion of interleukin factors (Lindemans et al., 2015; Zhu et al., 2019). Furthermore, endothelial cells may also be involved in ISC maintenance, as specific inhibition of endothelial cell apoptosis

was sufficient to recover crypt homeostasis following irradiation damage (Paris et al., 2001). Lymphatic endothelial cells were also shown to express relatively high levels of Rspo3, contributing to the maintenance of intestinal homeostasis (Ogasawara et al., 2018).

Generally, factors secreted by Paneth cells and mesenchymal cells create a high WNT/Rspo-signalling environment towards the bottom of the crypt, while a high BMP-signalling environment is present towards the villi. Both gradients decrease towards the transition zone, creating a zonation with segregated environments that guide cell type identity (Sato and Clevers, 2013; Moor et al., 2018). As ISC daughter cells move from the bottom of the crypt to the villi domain, they move through these different molecular gradients, generating increasing maturation of specialized cell types (Moor et al., 2018; Shoshkes-Carmel et al., 2018; McCarthy et al., 2020a).

ISCs give rise to committed daughter cells, which differentiate into distinct absorptive and secretory lineages (Wright, 2000; Schuijers and Clevers, 2012). The absorptive lineage gives rise to nutrient-absorbing enterocytes, while the secretory lineage primarily generates diverse hormone-producing enteroendocrine cells, mucus-producing goblet cells and ISC-supporting Paneth cells (Clevers and Bevins, 2013; Beumer et al., 2018; Yang and Yu, 2021). Cells that reach the top of the villi go into apoptosis and are shed into the lumen. The relatively rapid turnover, combined with the changing molecular environments demands a high degree of plasticity from intestinal epithelial cells. This has recently been demonstrated in the mouse intestine, as all major intestinal cell types can de-differentiate to a stem cell state, in reaction to proper environmental cues. Following ablation of resident ISCs, cell-specific lineage tracing strategies demonstrated regeneration of ISCs and full crypt-villi structures from Alpi + enterocytes (Tetteh et al., 2016), Lyz + Paneth cells (Yu et al., 2018) and endocrine lineage precursor cells (Van Es et al., 2012; Barriga et al., 2017; Yan et al., 2017; Ayyaz et al., 2019). In the mouse fetal intestinal epithelium, all cells, irrespective of their location and differentiation status, actively contribute to the adult ISC pool (Guiu et al., 2019). Moreover, a recent study demonstrated that, following the loss of proliferative ISCs due to injury, de-differentiation processes are the main driving force in the generation of novel ISCs as opposed to a specialized injury-resistant reserve stem cell population (Murata et al., 2020). However, cells of the secretory lineage inherently have low proliferation rates, which may make them more resistant to routinely used forms of cell damage, such as irradiation or chemotherapy (Basak et al., 2014). This may make them more likely to be sources of de-differentiation. Interestingly, de-differentiation processes occur by a shift from an adult to a more fetal-like intestinal gene expression profile, particularly involving high YAP1-signalling (Gregorieff et al., 2015; Yui et al., 2018).

Due to limited tissue accessibility and ethical considerations, the elucidation of the cellular and molecular complexity of the intestine has relied on animal and *in vitro* model systems. In recent years, the development of three-dimensional organoids has transformed biomedical research fields, including tissue homeostasis, regeneration and stem cell differentiation

(Leushacke and Barker, 2014). In this review, we discuss the advantages and disadvantages of different organoid models.

## INTESTINAL ORGANIDS AS AN IMPROVED MODEL TO STUDY INTESTINAL FUNCTION

Mouse models have greatly enhanced our understanding of biological systems and have enabled the development of numerous therapeutic strategies. Most importantly, they have allowed us to study pathologies without involving human patients. However, insights from animal models cannot guarantee extrapolation to human tissues. For instance, the timeline of embryonic intestinal development in mice proceeds past birth, while human intestinal formation is largely completed during the second trimester (Guiu and Jensen, 2015). One major difference in these developmental schedules is the formation of Paneth cells, which in human appear during the first trimester while in mouse only by day 14 postnatally (Bry et al., 1994; Rumbo and Schiffrin, 2005). Small intestinal villi in mouse are taller than in human, even though the small intestine is proportionally about three times shorter in mice (Nguyen et al., 2015). Furthermore, EGF seems to have opposite effects on the maturation of *in vivo* intestinal epithelium in mouse and in human (Calvert et al., 1982; Ménard et al., 1988). Importantly, stable mouse organoid lines can be derived with minimal niche factors Rspo1, Noggin and EGF, while human organoids demand additional growth factors and inhibition of p38/MAPK pathways (Sato et al., 2011b; Fujii et al., 2018). In addition, studies on animal models remain encumbered by considerations of animal ethics, limiting their scalability to high-throughput use.

In the last decade, organoids have been increasingly used as *in vitro* models as they improve upon several of these shortcomings. Organoids are self-organizing three-dimensional structures, consisting of both multipotent tissue-specific stem cells, as well as their more differentiated progeny (Zachos et al., 2016). Similar to stem cell lines, they can be propagated virtually indefinitely, provided the right culture conditions are met (Sato et al., 2009; 2011b). While human intestinal organoids were the first human organoid types that were successfully established *in vitro*, many protocols have since been optimized for organoids of many other tissue types, including pancreas, liver, kidney, stomach and lung (Huch et al., 2013a, 2013b; Dye et al., 2015; Nishinakamura, 2019; Seidlitz et al., 2021). Organoids recapitulate *in vivo* tissue architecture, multiple cell type heterogeneity and interactions *in vitro*. Therefore, they will potentially model human tissue functionality and physiology more accurately than animal models or 2D models (Lancaster and Knoblich, 2014; Kim J. et al., 2020). For instance, when sufficiently matured, human intestinal organoids recapitulate budding crypt and villi domains, harbouring proliferative ISCs and progenitors, as well as differentiated enterocytes, goblet cells and Paneth cells, respectively (Onozato et al., 2021). Although organoids contain differentiated cell types, they can be cryopreserved and expanded relatively rapidly (Clinton and McWilliams-Koeppen, 2019). Organoids have proven to be

highly versatile in experimental settings, as they are compatible with routinely used imaging techniques (Mahe et al., 2013; Dekkers et al., 2019), as well as live cell imaging (Zietek et al., 2015), assessment of metabolic activity (Berger et al., 2016), genome-wide gene expression and protein analyses (Lindeboom et al., 2018; Kip et al., 2021; Norkin et al., 2021) and gene editing techniques (Koo et al., 2012; Schwank et al., 2013; Schwank and Clevers, 2016; Driehuis and Clevers, 2017). Another major advantage of organoid models is their *in vitro* scalability to high-throughput assays, in combination with their recapitulation of 3D tissue functionality (Lukonin et al., 2020; Sugimoto and Sato, 2022). As such, organoids have been increasingly used to study intestinal function, to model disease phenotypes and for drug discovery screening (Fair et al., 2018; Frum and Spence, 2021).

## PLURIPOTENT STEM CELL-DERIVED HUMAN INTESTINAL ORGANOID VS. TISSUE-DERIVED ENTEROIDS

Different types of small intestinal organoids have been described and to distinguish them, a specific nomenclature has been proposed (Stelzner et al., 2012). Human small intestinal organoids can be generated by differentiation from human pluripotent stem cells (PSCs) or by derivation from isolated multipotent stem cells and progenitor cells present in *in vivo* intestinal crypts. The former are conventionally referred to as human intestinal organoids (hIOs), while the latter are termed enteroids (Stelzner et al., 2012) (**Figure 1B**). Additionally, in the initial 24-h culture phase to generate enteroids, small circular structures are formed, which are referred to as enterospheres (Stelzner et al., 2012). The enterosphere phase is transversed by both enteroids and hIOs during their formation (Stelzner et al., 2012). In contrast to enteroids, hIOs recapitulate fetal small intestine developmental stages and are therefore an excellent tool for studying this process (Wells and Spence, 2014; Frum and Spence, 2021). However, they also differentiate into both epithelial and mesenchymal cells (Spence et al., 2011; Mahe et al., 2015). Multicellular organoids such as these are also sometimes referred to as “reconstituted intestinal organoids” (Stelzner et al., 2012). Thus, reconstituted intestinal organoids or hIOs may complicate our understanding of the molecular mechanisms occurring specifically between intestinal epithelial cells. Recently, Mithal and colleagues reported a novel strategy to generate mesenchyme-free organoids from human iPSCs (Mithal et al., 2020). On the other hand, the presence of mesenchymal cells does create an intestinal model which more closely resembles the *in vivo* tissue compared to organoids with only epithelial cells. If the goal is to study the co-dependency of both tissues during development, this is rather advantageous, as has been shown by the use of hIOs including mesenchymal cells to model fibrosis in ulcerative colitis (Sarvestani et al., 2021). However, upon establishment of hIO cultures, they largely retain fetal-like characteristics. This has been demonstrated by RNA-


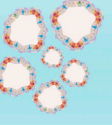
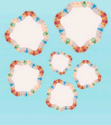
sequencing comparisons of hIOs with fetal and adult intestinal tissues and is likely caused by a lack of appropriate cues from the mesenchymal niche (Finkbeiner et al., 2015; McCarthy et al., 2020a).

In contrast, intestinal crypt-derived enteroids recapitulate adult intestinal architecture and genetic profiles of specific adult intestinal epithelial cell types more faithfully in mouse, with *Lgr5*<sup>+</sup> stem cells residing in crypt-like zones and differentiated cells residing in inter-crypt zones (Schuijers and Clevers, 2012). Interestingly, transient depletion of proliferative cells reverts mouse intestinal organoids to a more fetal-like state (Gregorieff et al., 2015). Of note, fetal-like hIOs can be matured further by transplantation under the kidney capsule of immune-deficient mice (Watson et al., 2014). One major factor involved in this maturation may originate from endothelial cells, as post-transplanted mature organoids obtain extensive vascularization (Frum and Spence, 2021). Moreover, the co-culture of hIOs with endothelial cells also promotes organoid maturation (Palikuqi et al., 2020). Nevertheless, the directed differentiation process of PSCs towards intestinal organoids takes quite some time (2–3 months), after which hIOs still largely resemble fetal intestinal homeostasis (McCracken et al., 2011; Frum and Spence, 2021). Though recently, Onozato and colleagues described a method to enhance organoid maturation *in vitro*, generating crypt-like budding and expression of villin1 (Onozato et al., 2021). Conversely, enteroids do not have to undergo sequential differentiation steps and can therefore be generated much more rapidly. Furthermore, enteroids are capable of recapitulating intestinal epithelium beyond a fetal phenotype with a higher degree of maturation (Hofer and Lutolf, 2021). However, it is important to realize that full maturation is usually not achieved with enteroids either, due to conventional culture conditions that promote proliferation. Nevertheless, due to the lack of mesenchymal cells, enteroids provide a less complex model system compared to hIOs to study epithelial cell type-specific molecular functions.

## LIMITATIONS OF INTESTINAL ORGANOID MODELS

Intestinal organoid technology has greatly enhanced research into tissue homeostasis, cell-to-cell interactions, differentiation, and physiology. However, several shortcomings still limit the model in its application to clinical research.

Firstly, while organoids are comprised of multiple cell types of the corresponding tissue, they still only include multipotent stem cells and their progeny. Enteroids therefore only include epithelial cell types. While hIOs do generate mesenchymal cells surrounding the epithelial cells, this is still rather limited compared to the *in vivo* intestine. Generally, both types of organoids lack complex mesenchymal heterogeneity and architecture, vasculature, neuronal connections and interaction with immune cells and the intestinal microbial flora. Several groups have therefore explored possible co-culture strategies to increase organoid complexity, including co-culture with endothelial (Palikuqi et al., 2020), mesenchymal (Stzepourginski et al., 2017), immune (Bar-Ephraim et al.,

	Mouse model	PSC-derived human intestinal organoids (hIOs)	Tissue-derived enteroids
			
Relative physiological complexity	High	Moderate	Low
Recapitulation of mature human physiology	Low	Moderate	High
Recapitulation of human developmental biology	Moderate	High	Low
Potential for high throughput analysis	Low	High	High
Relative time investment cost	High	Moderate	Low

**FIGURE 2 |** Strengths and weaknesses of hIOs, enteroids and mouse models. Summary of advantages and disadvantages of PSC-derived organoids or hIOs, tissue-derived organoids or enteroids and the mouse model. Created with BioRender.com.

2020) and glial cells (Baghdadi et al., 2022), as well as microbial (Finkbeiner et al., 2012; Wilson et al., 2015; Fatehullah et al., 2016; Han et al., 2019; Barron et al., 2020) and viral interactions (Zhao et al., 2021). Yet, current co-culture systems are still relatively simple, only combining one or few cell types simultaneously. In the future, both hIO and enteroid models will benefit from efforts to increase complexity of co-culture systems.

Intestinal organoids inherently form a lumen-enclosed structure. This reduces access to the absorptive apical side and leads to accumulation of apoptotic cells inside organoids. This potentially confounds drug screening and microbial co-culture studies (Altay et al., 2019). Recently, several publications have described methods to generate reversion of the apical side to the outside of organoids (Co et al., 2019, 2021; Li et al., 2020; Stroulis et al., 2021). For instance, Co. and colleagues described how inhibition of the interaction between organoid epithelial cell  $\beta 1$ -integrin receptors and the protein matrix in which they are cultured (such as Matrigel), caused spontaneous reversion of polarity (Co et al., 2019). Indeed, the localisation of the matrix used to create a supportive 3D environment, causes the apical-in polarity of organoids, similar to the extracellular matrix *in vivo*.

Conventional organoid culture mostly involves the embedding of organoids in Matrigel, a complex basement-membrane protein matrix, isolated from Engelbreth-Holm-Swarm mouse sarcoma tumor cells (Jee et al., 2019; Aisenbrey and Murphy, 2020). Matrigel provides essential ECM components to organoids, such as laminins, collagens and fibronectins (Jee et al., 2019; Aisenbrey and Murphy, 2020). Each of these components individually are capable of supporting the formation of ISC colonies, yet optimal differentiation to organoids was shown to require a delicate balancing of differential compositions (Gjorevski et al., 2016). However, due to Matrigel's highly complex composition, inherent variability and mouse origin, recent efforts are focussing on the design and study of synthetic hydrogel alternatives (Rezakhani et al., 2021). In fact, mechanical properties such as stiffness and degradability are equally vital to the formation, maintenance and differentiation of organoids in culture (Gjorevski et al., 2016). As such, the

mechanobiological properties of the protein matrix also influence the phenotype exhibited by organoids: 1) enteroids cultured in Matrigel generate budding structures that recapitulate *in vivo* behaviour (Sato et al., 2009); 2) organoids cultured in collagen I matrices acquire a foetal-like state mimicking the *in vivo* process of regeneration (Yui et al., 2018); 3) hanging drop cultures increase inter-organoid interactions, organoid fusion and can even induce continuous peristaltic movements (Ueda et al., 2010; Panek et al., 2018). Similarly, culture in floating collagen gels also generates fusion and self-organisation of intestinal organoids into tubular structures (Sachs et al., 2017). Nevertheless, as of yet, conventional organoid culture lacks the presence of *in vivo* growth factors, complex extracellular matrix composition, as well as fully optimized biomechanical properties of their environment (Guiu and Jensen, 2022). Importantly, intestinal organoid lines also possess a high degree of variability, as tissue heterogeneity (for enteroids), passaging methods, access to media components and positioning within 3D matrices impose a stochastic nature to their culture (Nikolaev et al., 2020).

Recently, novel approaches have been implemented aiming to meet several of these shortcomings. Experimentation on substrate matrix properties has allowed for improved monolayer culture of intestinal organoids, allowing access to the luminal side of intestinal cells and analysis of barrier integrity (Schweinlin et al., 2016; Altay et al., 2019). Chen and colleagues utilized a hollowed-out porous silk protein scaffold, onto which intestinal epithelial and myofibroblast cells could be seeded and maintained (Chen et al., 2015). This system recapitulated complex intestinal function and architecture, including mucus production and an accessible tubular lumen which allowed analysis of intraluminal oxygen tension and bacterial interaction (Chen et al., 2015). Future advancement of 3D bioprinting technology towards scaffold-free approaches will undoubtedly improve intestinal tissue modelling even further (Murphy and Atala, 2014; Wengerter et al., 2016). Organ-on-chip engineering has also recently been implemented to form perfusable *in vitro* mouse intestinal organoid structures, embedded in a pre-shaped matrix scaffold. Nikolaev and colleagues described the self-organization



of intestinal cells into a perfusable tube-shaped structure with crypt and villi domains and differentiation into specialised intestinal cells, inside a preformed hydrogel scaffold on a chip (Nikolaev et al., 2020). Kasendra and colleagues created an intestinal and microvascular endothelial co-culture on a chip in parallel perfusable channels. Crypt and villi structures were formed with multilineage differentiation, while interfacing with the microvascular endothelial cells (Kasendra et al., 2018). Such perfusable models allow the sequential analysis of fluid samples to quantify nutrient digestion, mucus secretion and establishment of intestinal barrier function *in vitro* (Kasendra et al., 2018; Nikolaev et al., 2020). Overall, this technology has the potential to increase robustness of crypt-villi architecture formation, nutrient absorption, co-culture strategies, larger scale intestinal architecture, as well as morphogen gradients. Moreover, multi-organ co-culture chip strategies have already been explored to investigate higher order tissue interactions and barrier function (Maschmeyer et al., 2015a; 2015b). However, the increasing complexity of organ-on-chip approaches may also limit high-throughput scalability and escalate associated costs.

## CONCLUSION

Taken together, although human organoids provide attractive *in vitro* models, it is important to keep in mind they are still simplified culture models of a much more complex *in vivo* system (Figures 1A,B) (Guiu and Jensen, 2022). Yet, they provide a highly improved model compared to 2D culture approaches in terms of recapitulation of cell type-heterogeneity, cell type-interactions and 3D architecture. Compared to mouse models, intestinal organoids circumvent animal ethics considerations, allow high-throughput scalability and provide a human model intestinal functionality (Figure 2). As such, human intestinal organoids can represent a sufficiently complex *in vitro* model of intestinal tissue from fetal to adult human stages of development, which are otherwise difficult to access. Multiple recent reports

have shown increased applicability and accuracy of organoid models, including maturation into budding organoids *in vitro*, outwards reversion of the apical side and induction of peristalsis. These improvements have increasingly benefitted potential future applications of hIOs, which could be used in a patient specific manner for drug screening and disease modelling purposes. Nevertheless, current organoid culture strategies still lack the complex interaction with *in vivo* growth factors, extracellular matrix composition and multi-organ physiology (Guiu and Jensen, 2022). Ultimately, future findings of interest from high-throughput screening studies using hIO or enteroid models should be validated *in vivo* in animal models, to provide information on the effects of the physiological environment, but also to assess whether findings from a simplified organoid structure can be recapitulated in the more complex *in vivo* intestinal tissue, albeit in an animal model.

## AUTHOR CONTRIBUTIONS

JT and JG contributed to the conception and design of the mini review. JT wrote the manuscript. JT, MD and JG edited sections and provided critical review. All authors read and approved the final version of the manuscript.

## FUNDING

This study has been funded by Instituto de Salud Carlos III through the grant CP20/00115 (Co-funded by European Social Fund. ESF investing in your future and the European Regional Development Fund “a way to build Europe”). We thank CERCA Programme/Generalitat de Catalunya for institutional support. This study has been funded by Instituto de Salud Carlos III through the project PI21/01152 (Co-funded by European Regional Development Fund. ERDF, a way to build Europe).

## REFERENCES

- Aisenbrey, E. A., and Murphy, W. L. (2020). Synthetic Alternatives to Matrigel. *Nat. Rev. Mater.* 5, 539–551. doi:10.1038/s41578-020-0199-8
- Altay, G., Larrañaga, E., Tosi, S., Barriga, F. M., Batlle, E., Fernández-Majada, V., et al. (2019). Self-organized Intestinal Epithelial Monolayers in Crypt and Villus-like Domains Show Effective Barrier Function. *Sci. Rep.* 9, 10140. doi:10.1038/s41598-019-46497-x
- Ayyaz, A., Kumar, S., Sangiorgi, B., Ghoshal, B., Gosio, J., Ouladan, S., et al. (2019). Single-cell Transcriptomes of the Regenerating Intestine Reveal a Revival Stem Cell. *Nature* 569, 121–125. doi:10.1038/s41586-019-1154-y
- Baghdadi, M. B., Ayyaz, A., Coquenlorge, S., Chu, B., Kumar, S., Streutker, C., et al. (2022). Enteric Glial Cell Heterogeneity Regulates Intestinal Stem Cell Niches. *Cell Stem Cell* 29, 86–100.e6. doi:10.1016/j.stem.2021.10.004
- Bar-Ephraim, Y. E., Kretzschmar, K., and Clevers, H. (2020). Organoids in Immunological Research. *Nat. Rev. Immunol.* 20, 279–293. doi:10.1038/s41577-019-0248-y
- Barker, N. (2014). Adult Intestinal Stem Cells: Critical Drivers of Epithelial Homeostasis and Regeneration. *Nat. Rev. Mol. Cell Biol.* 15, 19–33. doi:10.1038/nrm3721
- Barker, N., Van Es, J. H., Kuipers, J., Kujala, P., Van Den Born, M., Cozijnsen, M., et al. (2007). Identification of Stem Cells in Small Intestine and colon by Marker Gene Lgr5. *Nature* 449, 1003–1007. doi:10.1038/nature06196
- Barriga, F. M., Montagni, E., Mana, M., Mendez-Lago, M., Hernando-Momblona, X., Sevillano, M., et al. (2017). Mex3a Marks a Slowly Dividing Subpopulation of Lgr5+ Intestinal Stem Cells. *Cell Stem Cell* 20, 801–816.e7. doi:10.1016/j.stem.2017.02.007
- Barron, M. R., Cieza, R. J., Hill, D. R., Huang, S., Yadagiri, V. K., Spence, J. R., et al. (2020). The Lumen of Human Intestinal Organoids Poses Greater Stress to Bacteria Compared to the Germ-free Mouse Intestine: *Escherichia coli* Deficient in RpoS as a Colonization Probe. *mSphere* 5. doi:10.1128/mSphere.00777-20
- Basak, O., van de Born, M., Korving, J., Beumer, J., van der Elst, S., van Es, J. H., et al. (2014). Mapping Early Fate Determination in Lgr5+ Crypt Stem Cells Using a Novel Ki67-RFP Allele. *EMBO J.* 33, 2057–2068. doi:10.15252/embj.201488017
- Berger, E., Rath, E., Yuan, D., Waldschmitt, N., Khaloian, S., Allgäuer, M., et al. (2016). Mitochondrial Function Controls Intestinal Epithelial Stemness and Proliferation. *Nat. Commun.* 7, 1–17. doi:10.1038/ncomms13171
- Beumer, J., Artegiani, B., Post, Y., Reimann, F., Gribble, F., Nguyen, T. N., et al. (2018). Enteroendocrine Cells Switch Hormone Expression along the Crypt-

- To-Villus BMP Signalling Gradient. *Nat. Cel Biol.* 20, 909–916. doi:10.1038/s41556-018-0143-y
- Blumberg, R. S., Li, L., Nusrat, A., Parkos, C. A., Rubin, D. C., and Carrington, J. L. (2008). Recent Insights into the Integration of the Intestinal Epithelium within the Mucosal Environment in Health and Disease. *Mucosal Immunol.* 1, 330–334. doi:10.1038/mi.2008.29
- Bry, L., Falk, P., Huttner, K., Ouellette, A., Midtvedt, T., and Gordon, J. I. (1994). Paneth Cell Differentiation in the Developing Intestine of normal and Transgenic Mice. *Proc. Natl. Acad. Sci.* 91, 10335–10339. doi:10.1073/pnas.91.22.10335
- Calvert, R., Beaulieu, J.-F., and Ménard, D. (1982). Epidermal Growth Factor (EGF) Accelerates the Maturation of Fetal Mouse Intestinal Mucosa In Utero. *Experientia* 38, 1096–1097. doi:10.1007/bf01955387
- Chen, Y., Lin, Y., Davis, K. M., Wang, Q., Rnjak-Kovacina, J., Li, C., et al. (2015). Robust Bioengineered 3D Functional Human Intestinal Epithelium. *Sci. Rep.* 5, 13708. doi:10.1038/srep13708
- Clevers, H. C., and Bevins, C. L. (2013). Paneth Cells: Maestros of the Small Intestinal Crypts. *Annu. Rev. Physiol.* 75, 289–311. doi:10.1146/annurev-physiol-030212-183744
- Clevers, H. (2013). The Intestinal Crypt, a Prototype Stem Cell Compartment. *Cell* 154, 274–284. doi:10.1016/j.cell.2013.07.004
- Clinton, J., and McWilliams-Koeppen, P. (2019). Initiation, Expansion, and Cryopreservation of Human Primary Tissue-Derived Normal and Diseased Organoids in Embedded Three-Dimensional Culture. *Curr. Protoc. Cel Biol.* 82, e66. doi:10.1002/cpcb.66
- Co, J. Y., Margalef-Català, M., Li, X., Mah, A. T., Kuo, C. J., Monack, D. M., et al. (2019). Controlling Epithelial Polarity: A Human Enteroid Model for Host-Pathogen Interactions. *Cel Rep.* 26, 2509–2520. e4. doi:10.1016/j.celrep.2019.01.108
- Co, J. Y., Margalef-Català, M., Monack, D. M., and Amieva, M. R. (2021). Controlling the Polarity of Human Gastrointestinal Organoids to Investigate Epithelial Biology and Infectious Diseases. *Nat. Protoc.* 16, 5171–5192. doi:10.1038/s41596-021-00607-0
- Dekkers, J. F., Alieva, M., Wellens, L. M., Ariese, H. C. R., Jamieson, P. R., Vonk, A. M., et al. (2019). High-resolution 3D Imaging of Fixed and Cleared Organoids. *Nat. Protoc.* 14, 1756–1771. doi:10.1038/s41596-019-0160-8
- Driehuis, E., and Clevers, H. (2017). CRISPR/Cas 9 Genome Editing and its Applications in Organoids. *Am. J. Physiology-Gastrointestinal Liver Physiol.* 312, G257–G265. doi:10.1152/ajpgi.00410.2016
- Dye, B. R., Hill, D. R., Ferguson, M. A., Tsai, Y. H., Nagy, M. S., Dyal, R., et al. (20152015). In Vitro generation of Human Pluripotent Stem Cell Derived Lung Organoids. *Elife* 4, 1–25. doi:10.7554/eLife.05098
- Fair, K. L., Colquhoun, J., and Hannan, N. R. F. (2018). Intestinal Organoids for Modelling Intestinal Development and Disease. *Philos. Trans. R. Soc. Lond. B Biol. Sci.* 373. doi:10.1098/rstb.2017.0217
- Fatehullah, A., Tan, S. H., and Barker, N. (2016). Organoids as an In Vitro Model of Human Development and Disease. *Nat. Cel Biol.* 18, 246–254. doi:10.1038/ncb3312
- Finkbeiner, S. R., Zeng, X. L., Utama, B., Atmar, R. L., Shroyer, N. F., and Estes, M. K. (2012). Stem Cell-Derived Human Intestinal Organoids as an Infection Model for Rotaviruses. *MBio* 3, e00159–12. doi:10.1128/mBio.00159-12
- Finkbeiner, S. R., Hill, D. R., Althelm, C. H., Dedhia, P. H., Taylor, M. J., Tsai, Y.-H., et al. (2015). Transcriptome-wide Analysis Reveals Hallmarks of Human Intestine Development and Maturation In Vitro and In Vivo. *Stem Cell Rep.* 4, 1140–1155. doi:10.1016/j.stemcr.2015.04.010
- Frum, T., and Spence, J. R. (2021). hPSC-derived Organoids: Models of Human Development and Disease. *J. Mol. Med.* 99, 463–473. doi:10.1007/s00109-020-01969-w
- Fujii, M., Matano, M., Toshimitsu, K., Takano, A., Mikami, Y., Nishikori, S., et al. (2018). Human Intestinal Organoids Maintain Self-Renewal Capacity and Cellular Diversity in Niche-Inspired Culture Condition. *Cell Stem Cell* 23, 787–793. e6. doi:10.1016/j.stem.2018.11.016
- Gehart, H., and Clevers, H. (2019). Tales from the Crypt: New Insights into Intestinal Stem Cells. *Nat. Rev. Gastroenterol. Hepatol.* 16, 19–34. doi:10.1038/s41575-018-0081-y
- Gjorevski, N., Sachs, N., Manfrin, A., Giger, S., Bragina, M. E., Ordóñez-Morán, P., et al. (2016). Designer Matrices for Intestinal Stem Cell and Organoid Culture. *Nature* 539, 560–564. doi:10.1038/nature20168
- Gregorieff, A., Liu, Y., Inanlou, M. R., Khomchuk, Y., and Wrana, J. L. (2015). Yap-dependent Reprogramming of Lgr5+ Stem Cells Drives Intestinal Regeneration and Cancer. *Nature* 526, 715–718. doi:10.1038/nature15382
- Guiu, J., Hannezo, E., Yui, S., Demharter, S., Ulyanchenko, S., Maimets, M., et al. (2019). Tracing the Origin of Adult Intestinal Stem Cells. *Nature* 570, 107–111. doi:10.1038/s41586-019-1212-5
- Guiu, J., and Jensen, K. B. (2015). From Definitive Endoderm to Gut-A Process of Growth and Maturation. *Stem Cell Dev.* 24, 1972–1983. doi:10.1089/scd.2015.0017
- Guiu, J., and Jensen, K. B. (2022). In Vivo Studies Should Take Priority when Defining Mechanisms of Intestinal Crypt Morphogenesis. *Cell Mol. Gastroenterol. Hepatol.* 13, 1–3. doi:10.1016/j.jcmgh.2021.06.028
- Han, X., Lee, A., Huang, S., Gao, J., Spence, J. R., and Owyang, C. (2019). Lactobacillus Rhamnosus GG Prevents Epithelial Barrier Dysfunction Induced by Interferon-Gamma and Fecal Supernatants from Irritable Bowel Syndrome Patients in Human Intestinal Enteroids and Colonoids. *Gut Microbes* 10, 59–76. doi:10.1080/19490976.2018.1479625
- Hofer, M., and Lutolf, M. P. (2021). Engineering Organoids. *Nat. Rev. Mater.* 6, 402–420. doi:10.1038/s41578-021-00279-y
- Huch, M., Bonfanti, P., Boj, S. F., Sato, T., Loomans, C. J. M., Van De Wetering, M., et al. (2013a). Unlimited In Vitro Expansion of Adult Bi-potent Pancreas Progenitors through the Lgr5/R-Spondin axis. *EMBO J.* 32, 2708–2721. doi:10.1038/emboj.2013.204
- Huch, M., Dorrell, C., Boj, S. F., Van Es, J. H., Li, V. S. W., Van De Wetering, M., et al. (2013b). In Vitro expansion of Single Lgr5+ Liver Stem Cells Induced by Wnt-Driven Regeneration. *Nature* 494, 247–250. doi:10.1038/nature11826
- Jee, J. H., Lee, D. H., Ko, J., Hahn, S., Jeong, S. Y., Kim, H. K., et al. (2019). Development of Collagen-Based 3D Matrix for Gastrointestinal Tract-Derived Organoid Culture. *Stem Cell Int* 2019. doi:10.1155/2019/8472712
- Kasendra, M., Tovaglieri, A., Sontheimer-Phelps, A., Jalili-Firoozinezhad, S., Bein, A., Chalkiadaki, A., et al. (2018). Development of a Primary Human Small Intestine-On-A-Chip Using Biopsy-Derived Organoids. *Sci. Rep.* 8, 2871. doi:10.1038/s41598-018-21201-7
- Kim, J. E., Fei, L., Yin, W. C., Coquenlorge, S., Rao-Bhatia, A., Zhang, X., et al. (2020b). Single Cell and Genetic Analyses Reveal Conserved Populations and Signaling Mechanisms of Gastrointestinal Stromal Niches. *Nat. Commun.* 11, 334. doi:10.1038/s41467-019-14058-5
- Kim, J., Koo, B.-K., and Knoblich, J. A. (2020a). Human Organoids: Model Systems for Human Biology and Medicine. *Nat. Rev. Mol. Cel Biol.* 21, 571–584. doi:10.1038/s41580-020-0259-3
- Kim, T.-H., Escudero, S., and Shivdasani, R. A. (2012). Intact Function of Lgr5 Receptor-Expressing Intestinal Stem Cells in the Absence of Paneth Cells. *Proc. Natl. Acad. Sci.* 109, 3932–3937. doi:10.1073/pnas.1113890109
- Kip, A. M., Soons, Z., Mohren, R., Duivenvoorden, A. A. M., Röth, A. A. J., Cillero-Pastor, B., et al. (2021). Proteomics Analysis of Human Intestinal Organoids during Hypoxia and Reoxygenation as a Model to Study Ischemia-Reperfusion Injury. *Cel Death Dis.* 12, 95–13. doi:10.1038/s41419-020-03379-9
- Koo, B.-K., Stange, D. E., Sato, T., Karthaus, W., Farin, H. F., Huch, M., et al. (2012). Controlled Gene Expression in Primary Lgr5 Organoid Cultures. *Nat. Methods* 9, 81–83. doi:10.1038/nmeth.1802
- Lancaster, M. A., and Knoblich, J. A. (2014). Organogenesis in a Dish: Modeling Development and Disease Using Organoid Technologies. *Science* 345, 1247125. doi:10.1126/science.1247125
- Leushacke, M., and Barker, N. (2014). Ex Vivo culture of the Intestinal Epithelium: Strategies and Applications. *Gut* 63, 1345–1354. doi:10.1136/gutjnl-2014-307204
- Li, Y., Yang, N., Chen, J., Huang, X., Zhang, N., Yang, S., et al. (2020). Next-Generation Porcine Intestinal Organoids: an Apical-Out Organoid Model for Swine Enteric Virus Infection and Immune Response Investigations. *J. Virol.* 94. doi:10.1128/JVI.01006-20
- Lindeboom, R. G., van Voorthuisen, L., Oost, K. C., Rodriguez-Colman, M. J., Luna-Velez, M. V., Furlan, C., et al. (2018). Integrative Multi-Omics Analysis of Intestinal Organoid Differentiation. *Mol. Syst. Biol.* 14, e8227. doi:10.15252/msb.20188227
- Lindemans, C. A., Calafiore, M., Mertelsmann, A. M., O'Connor, M. H., Dudakov, J. A., Jenq, R. R., et al. (2015). Interleukin-22 Promotes Intestinal-Stem-Cell-Mediated Epithelial Regeneration. *Nature* 528, 560–564. doi:10.1038/nature16460
- Lukonin, I., Serra, D., Challet Meylan, L., Volkmann, K., Baaten, J., Zhao, R., et al. (2020). Phenotypic Landscape of Intestinal Organoid Regeneration. *Nature* 586, 275–280. doi:10.1038/s41586-020-2776-9

- Mahe, M. M., Sundaram, N., Watson, C. L., Shroyer, N. F., and Helmrath, M. A. (2015/2015). Establishment of Human Epithelial Enteroids and Colonoids from Whole Tissue and Biopsy. *J. Vis. Exp.* doi:10.3791/52483
- Mahe, M. M., Aihara, E., Schumacher, M. A., Zavros, Y., Montrose, M. H., Helmrath, M. A., et al. (2013). Establishment of Gastrointestinal Epithelial Organoids. *Curr. Protoc. Mouse Biol.* 3, 217–240. doi:10.1002/9780470942390.mol130179
- Maschmeyer, I., Hasenberg, T., Jaenicke, A., Lindner, M., Lorenz, A. K., Zech, J., et al. (2015a). Chip-based Human Liver-Intestine and Liver-Skin Co-cultures - A First Step toward Systemic Repeated Dose Substance Testing *In Vitro*. *Eur. J. Pharmaceutics Biopharmaceutics* 95, 77–87. doi:10.1016/j.ejpb.2015.03.002
- Maschmeyer, I., Lorenz, A. K., Schimek, K., Hasenberg, T., Ramme, A. P., Hübner, J., et al. (2015b). A Four-Organ-Chip for Interconnected Long-Term Co-culture of Human Intestine, Liver, Skin and Kidney Equivalents. *Lab. Chip* 15, 2688–2699. doi:10.1039/c5lc00392j
- McCarthy, N., Kraiczy, J., and Shivdasani, R. A. (2020a). Cellular and Molecular Architecture of the Intestinal Stem Cell Niche. *Nat. Cell Biol.* 22, 1033–1041. doi:10.1038/s41556-020-0567-z
- McCarthy, N., Manieri, E., Storm, E. E., Saadatpour, A., Luoma, A. M., Kapoor, V. N., et al. (2020b). Distinct Mesenchymal Cell Populations Generate the Essential Intestinal BMP Signaling Gradient. *Cell Stem Cell* 26, 391–402.e5. doi:10.1016/j.stem.2020.01.008
- McCracken, K. W., Howell, J. C., Wells, J. M., and Spence, J. R. (2011). Generating Human Intestinal Tissue from Pluripotent Stem Cells *In Vitro*. *Nat. Protoc.* 6, 1920–1928. doi:10.1038/nprot.2011.410
- Ménard, D., Arsenault, P., and Pothier, P. (1988). Biologic Effects of Epidermal Growth Factor in Human Fetal Jejunum. *Gastroenterology* 94, 656–663.
- Mithal, A., Capilla, A., Heinze, D., Berical, A., Villacorta-Martin, C., Vedaie, M., et al. (2020). Generation of Mesenchyme Free Intestinal Organoids from Human Induced Pluripotent Stem Cells. *Nat. Commun.* 11, 215. doi:10.1038/s41467-019-13916-6
- Moor, A. E., Harnik, Y., Ben-Moshe, S., Massasa, E. E., Rozenberg, M., Eilam, R., et al. (2018). Spatial Reconstruction of Single Enterocytes Uncovers Broad Zonation along the Intestinal Villus Axis. *Cell* 175, 1156–1167.e15. doi:10.1016/j.cell.2018.08.063
- Murata, K., Jadhav, U., Madha, S., van Es, J., Dean, J., Cavazza, A., et al. (2020). Ascl2-Dependent Cell Dedifferentiation Drives Regeneration of Ablated Intestinal Stem Cells. *Cell Stem Cell* 26, 377–390.e6. doi:10.1016/j.stem.2019.12.011
- Murphy, S. V., and Atala, A. (2014). 3D Bioprinting of Tissues and Organs. *Nat. Biotechnol.* 32, 773–785. doi:10.1038/nbt.2958
- Nguyen, T. L. A., Vieira-Silva, S., Liston, A., and Raes, J. (2015). How Informative Is the Mouse for Human Gut Microbiota Research? *Dis. Model. Mech.* 8, 1–16. doi:10.1242/dmm.017400
- Nikolaev, M., Mitrofanova, O., Brogiere, N., Geraldo, S., Dutta, D., Tabata, Y., et al. (2020). Homeostatic Mini-Intestines through Scaffold-Guided Organoid Morphogenesis. *Nature* 585, 574–578. doi:10.1038/s41586-020-2724-8
- Nishinakamura, R. (2019). Human Kidney Organoids: Progress and Remaining Challenges. *Nat. Rev. Nephrol.* 15, 613–624. doi:10.1038/s41581-019-0176-x
- Norkin, M., Ordóñez-Morán, P., and Huelsen, J. (2021). High-content, Targeted RNA-Seq Screening in Organoids for Drug Discovery in Colorectal Cancer. *Cel Rep.* 35, 109026. doi:10.1016/j.celrep.2021.109026
- Ogasawara, R., Hashimoto, D., Kimura, S., Hayase, E., Ara, T., Takahashi, S., et al. (2018). Intestinal Lymphatic Endothelial Cells Produce R-Spondin3. *Sci. Rep.* 8, 10719–9. doi:10.1038/s41598-018-29100-7
- Onozato, D., Ogawa, I., Kida, Y., Mizuno, S., Hashita, T., Iwao, T., et al. (2021). Generation of Budding-like Intestinal Organoids from Human Induced Pluripotent Stem Cells. *J. Pharm. Sci.* 110, 2637–2650. doi:10.1016/j.xphs.2021.03.014
- Palikuqi, B., Nguyen, D.-H. T., Li, G., Schreiner, R., Pellegata, A. F., Liu, Y., et al. (2020). Adaptable Haemodynamic Endothelial Cells for Organogenesis and Tumorigenesis. *Nature* 585, 426–432. doi:10.1038/s41586-020-2712-z
- Panek, M., Grabacka, M., and Pierzchalska, M. (2018). The Formation of Intestinal Organoids in a Hanging Drop Culture. *Cytotechnology* 70, 1085–1095. doi:10.1007/s10616-018-0194-8
- Paris, F., Fuks, Z., Kang, A., Capodiceci, P., Juan, G., Ehleiter, D., et al. (2001). Endothelial Apoptosis as the Primary Lesion Initiating Intestinal Radiation Damage in Mice. *Science* 80–293, 293–297. doi:10.1126/science.1060191
- Porter, E. M., Bevins, C. L., Ghosh, D., and Ganz, T. (2002). The Multifaceted Paneth Cell. *Cell Mol. Life Sci. (Cmls)* 59, 156–170. doi:10.1007/s00018-002-8412-z
- Rezakhani, S., Gjorevski, N., and Lutolf, M. P. (2021). Extracellular Matrix Requirements for Gastrointestinal Organoid Cultures. *Biomaterials* 276, 121020. doi:10.1016/j.biomaterials.2021.121020
- Rumbo, M., and Schiffrin, E. J. (2005). Intestinal Epithelial Barrier and Mucosal Immunity. *Cmls, Cel. Mol. Life Sci.* 62, 1288–1296. doi:10.1007/s00018-005-5033-3
- Sachs, N., Tsukamoto, Y., Kujala, P., Peters, P. J., and Clevers, H. (2017). Intestinal Epithelial Organoids Fuse to Form Self-Organizing Tubes in Floating Collagen Gels. *Dev* 144, 1107–1112. doi:10.1242/dev.143933
- Sarvestani, S. K., Signs, S., Hu, B., Yeu, Y., Feng, H., Ni, Y., et al. (2021). Induced Organoids Derived from Patients with Ulcerative Colitis Recapitulate Colitic Reactivity. *Nat. Commun.* 12, 1–18. doi:10.1038/s41467-020-20351-5
- Sato, T., and Clevers, H. (2013). Growing Self-Organizing Mini-Guts from a Single Intestinal Stem Cell: Mechanism and Applications. *Science* 340 (80-), 1190–1194. doi:10.1126/science.1234852
- Sato, T., Stange, D. E., Ferrante, M., Vries, R. G. J., Van Es, J. H., Van Den Brink, S., et al. (2011b). Long-term Expansion of Epithelial Organoids from Human Colon, Adenoma, Adenocarcinoma, and Barrett's Epithelium. *Gastroenterology* 141, 1762–1772. doi:10.1053/j.gastro.2011.07.050
- Sato, T., Van Es, J. H., Snippert, H. J., Stange, D. E., Vries, R. G., Van Den Born, M., et al. (2011a). Paneth Cells Constitute the Niche for Lgr5 Stem Cells in Intestinal Crypts. *Nature* 469, 415–418. doi:10.1038/nature09637
- Sato, T., Vries, R. G., Snippert, H. J., Van De Wetering, M., Barker, N., Stange, D. E., et al. (2009). Single Lgr5 Stem Cells Build Crypt-Villus Structures *In Vitro* without a Mesenchymal Niche. *Nature* 459, 262–265. doi:10.1038/nature07935
- Schuijers, J., and Clevers, H. (2012). Adult Mammalian Stem Cells: The Role of Wnt, Lgr5 and R-Spondins. *EMBO J.* 31, 2685–2696. doi:10.1038/emboj.2012.149
- Schwank, G., and Clevers, H. (2016). CRISPR/Cas9-Mediated Genome Editing of Mouse Small Intestinal Organoids. *Methods Mol. Biol.* 1422, 3–11. doi:10.1007/978-1-4939-3603-8\_1
- Schwank, G., Koo, B.-K., Sasselli, V., Dekkers, J. F., Heo, I., Demircan, T., et al. (2013). Functional Repair of CFTR by CRISPR/Cas9 in Intestinal Stem Cell Organoids of Cystic Fibrosis Patients. *Cell Stem Cell* 13, 653–658. doi:10.1016/j.stem.2013.11.002
- Schweinlin, M., Wilhelm, S., Schwedhelm, I., Hansmann, J., Rietscher, R., Jurowich, C., et al. (2016). Development of an Advanced Primary Human *In Vitro* Model of the Small Intestine. *Tissue Eng. C. Methods* 22, 873–883. doi:10.1089/ten.tec.2016.0101
- Seidlitz, T., Koo, B.-K., and Stange, D. E. (2021). Gastric Organoids-An *In Vitro* Model System for the Study of Gastric Development and Road to Personalized Medicine. *Cell Death Differ* 28, 68–83. doi:10.1038/s41418-020-00662-2
- Shoshkes-Carmel, M., Wang, Y. J., Wangenstein, K. J., Tóth, B., Kondo, A., Massasa, E. E., et al. (2018). Subepithelial Telocytes Are an Important Source of Wnts that Supports Intestinal Crypts. *Nature* 557, 242–246. doi:10.1038/s41586-018-0084-4
- Snippert, H. J., van der Flier, L. G., Sato, T., van Es, J. H., van den Born, M., Kroon-Veenboer, C., et al. (2010). Intestinal Crypt Homeostasis Results from Neutral Competition between Symmetrically Dividing Lgr5 Stem Cells. *Cell* 143, 134–144. doi:10.1016/j.cell.2010.09.016
- Spence, J. R., Mayhew, C. N., Rankin, S. A., Kuhar, M. F., Vallance, J. E., Tolle, K., et al. (2011). Directed Differentiation of Human Pluripotent Stem Cells into Intestinal Tissue *In Vitro*. *Nature* 470, 105–109. doi:10.1038/nature09691
- Stelzner, M., Helmrath, M., Dunn, J. C. Y., Henning, S. J., Houchen, C. W., Kuo, C., et al. (2012). A Nomenclature for Intestinal *In Vitro* Cultures. *Am. J. Physiology-Gastrointestinal Liver Physiol.* 302, G1359–G1363. doi:10.1152/ajpgi.00493.2011
- Stroulios, G., Stahl, M., Elstone, F., Chang, W., Louis, S., Eaves, A., et al. (2021). Culture Methods to Study Apical-specific Interactions Using Intestinal Organoid Models. *J. Vis. Exp.* 2021. doi:10.3791/62330
- Stzepourginski, I., Nigro, G., Jacob, J.-M., Dulauroy, S., Sansonetti, P. J., Eberl, G., et al. (2017). CD34+ Mesenchymal Cells Are a Major Component of the Intestinal Stem Cells Niche at Homeostasis and after Injury. *Proc. Natl. Acad. Sci. USA* 114, E506–E513. doi:10.1073/pnas.1620059114

- Sugimoto, S., and Sato, T. (2022). Organoid vs *In Vivo* Mouse Model: Which Is Better Research Tool to Understand the Biologic Mechanisms of Intestinal Epithelium? *Cell Mol. Gastroenterol. Hepatol.* 13, 195–197. doi:10.1016/j.jcmgh.2021.06.027
- Tetteh, P. W., Basak, O., Farin, H. F., Wiebrands, K., Kretschmar, K., Begthel, H., et al. (2016). Replacement of Lost Lgr5-Positive Stem Cells through Plasticity of Their Enterocyte-Lineage Daughters. *Cell Stem Cell* 18, 203–213. doi:10.1016/j.stem.2016.01.001
- Ueda, T., Yamada, T., Hokuto, D., Koyama, F., Kasuda, S., Kanehiro, H., et al. (2010). Generation of Functional Gut-like Organ from Mouse Induced Pluripotent Stem Cells. *Biochem. Biophysical Res. Commun.* 391, 38–42. doi:10.1016/j.bbrc.2009.10.157
- van Es, J. H., Jay, P., Gregorieff, A., van Gijn, M. E., Jonkheer, S., Hatzis, P., et al. (2005). Wnt Signalling Induces Maturation of Paneth Cells in Intestinal Crypts. *Nat. Cell Biol.* 7, 381–386. doi:10.1038/ncb1240
- Van Es, J. H., Sato, T., Van De Wetering, M., Lyubimova, A., Yee Nee, A. N., Gregorieff, A., et al. (2012). Dll1+ Secretory Progenitor Cells Revert to Stem Cells upon Crypt Damage. *Nat. Cell Biol.* 14, 1099–1104. doi:10.1038/ncb2581
- Van Es, J. H., Wiebrands, K., López-Iglesias, C., Van De Wetering, M., Zeinstra, L., Van Den Born, M., et al. (2019). Enteroendocrine and Tuft Cells Support Lgr5 Stem Cells on Paneth Cell Depletion. *Proc. Natl. Acad. Sci. USA* 116, 26599–26605. doi:10.1073/pnas.1801888117
- Watson, C. L., Mahe, M. M., Múnera, J., Howell, J. C., Sundaram, N., Poling, H. M., et al. (2014). An *In Vivo* Model of Human Small Intestine Using Pluripotent Stem Cells. *Nat. Med.* 20, 1310–1314. doi:10.1038/nm.3737
- Wells, J. M., and Spence, J. R. (2014). How to Make an Intestine. *Dev* 141, 752–760. doi:10.1242/dev.097386
- Wengert, B. C., Emre, G., Park, J. Y., and Geibel, J. (2016). Three-dimensional Printing in the Intestine. *Clin. Gastroenterol. Hepatol.* 14, 1081–1085. doi:10.1016/j.cgh.2016.05.008
- Wilson, S. S., Tocchi, A., Holly, M. K., Parks, W. C., and Smith, J. G. (2015). A Small Intestinal Organoid Model of Non-invasive Enteric Pathogen-Epithelial Cell Interactions. *Mucosal Immunol.* 8, 352–361. doi:10.1038/mi.2014.72
- Wright, N. A. (2000). Epithelial Stem Cell Repertoire in the Gut: Clues to the Origin of Cell Lineages, Proliferative Units and Cancer. *Int. J. Exp. Pathol.* 81, 117–143. doi:10.1046/j.1365-2613.2000.00146.x
- Yan, K. S., Gevaert, O., Zheng, G. X. Y., Anchang, B., Probert, C. S., Larkin, K. A., et al. (2017). Intestinal Enteroendocrine Lineage Cells Possess Homeostatic and Injury-Inducible Stem Cell Activity. *Cell Stem Cell* 21, 78–90. e6. doi:10.1016/j.stem.2017.06.014
- Yang, S., and Yu, M. (2021). Role of Goblet Cells in Intestinal Barrier and Mucosal Immunity. *Jir* Vol. 14, 3171–3183. doi:10.2147/jir.s318327
- Yu, S., Tong, K., Zhao, Y., Balasubramanian, I., Yap, G. S., Ferraris, R. P., et al. (2018). Paneth Cell Multipotency Induced by Notch Activation Following Injury. *Cell Stem Cell* 23, 46–59.e5. doi:10.1016/j.stem.2018.05.002
- Yui, S., Azzolin, L., Maimets, M., Pedersen, M. T., Fordham, R. P., Hansen, S. L., et al. (2018). YAP/TAZ-Dependent Reprogramming of Colonic Epithelium Links ECM Remodeling to Tissue Regeneration. *Cell Stem Cell* 22, 35–49.e7. doi:10.1016/j.stem.2017.11.001
- Zachos, N. C., Kovbasnjuk, O., Foulke-Abel, J., In, J., Blutt, S. E., de Jonge, H. R., et al. (2016). Human Enteroids/colonoids and Intestinal Organoids Functionally Recapitulate normal Intestinal Physiology and Pathophysiology. *J. Biol. Chem.* 291, 3759–3766. doi:10.1074/jbc.r114.635995
- Zhao, X., Li, C., Liu, X., Chiu, M. C., Wang, D., Wei, Y., et al. (2021). Human Intestinal Organoids Recapitulate Enteric Infections of Enterovirus and Coronavirus. *Stem Cell Rep.* 16, 493–504. doi:10.1016/j.stemcr.2021.02.009
- Zhu, P., Zhu, X., Wu, J., He, L., Lu, T., Wang, Y., et al. (2019). IL-13 Secreted by ILC2s Promotes the Self-Renewal of Intestinal Stem Cells through Circular RNA circPan3. *Nat. Immunol.* 20, 183–194. doi:10.1038/s41590-018-0297-6
- Zietek, T., Rath, E., Haller, D., and Daniel, H. (2015). Intestinal Organoids for Assessing Nutrient Transport, Sensing and Incretin Secretion. *Sci. Rep.* 5, 1–10. doi:10.1038/srep16831

**Conflict of Interest:** The authors declare that the research was conducted in the absence of any commercial or financial relationships that could be construed as a potential conflict of interest.

**Publisher's Note:** All claims expressed in this article are solely those of the authors and do not necessarily represent those of their affiliated organizations, or those of the publisher, the editors and the reviewers. Any product that may be evaluated in this article, or claim that may be made by its manufacturer, is not guaranteed or endorsed by the publisher.

Copyright © 2022 Taelman, Diaz and Guiu. This is an open-access article distributed under the terms of the Creative Commons Attribution License (CC BY). The use, distribution or reproduction in other forums is permitted, provided the original author(s) and the copyright owner(s) are credited and that the original publication in this journal is cited, in accordance with accepted academic practice. No use, distribution or reproduction is permitted which does not comply with these terms.





# From Mice to Men: Generation of Human Blastocyst-Like Structures *In Vitro*

Dorian Luijkx, Vinidhra Shankar, Clemens van Blitterswijk, Stefan Giselbrecht<sup>\*†</sup> and Erik Vrij<sup>\*†</sup>

Department of Instructive Biomaterial Engineering, MERLN Institute for Technology-Inspired Regenerative Medicine, Maastricht University, Maastricht, Netherlands

## OPEN ACCESS

### Edited by:

Ying Gu,  
Beijing Genomics Institute (BGI), China

### Reviewed by:

Yang Yu,  
Peking University Third Hospital, China  
Yong Fan,  
Guangzhou Medical University, China  
Kiichiro Tomoda,  
Gladstone Institute of Cardiovascular  
Disease, United States

### \*Correspondence:

Erik Vrij  
e.vrij@maastrichtuniversity.nl  
Stefan Giselbrecht  
s.giselbrecht@  
maastrichtuniversity.nl

<sup>†</sup>These authors have contributed  
equally to this work

### Specialty section:

This article was submitted to  
Stem Cell Research,  
a section of the journal  
Frontiers in Cell and Developmental  
Biology

**Received:** 17 December 2021

**Accepted:** 26 January 2022

**Published:** 11 March 2022

### Citation:

Luijkx D, Shankar V, van Blitterswijk C,  
Giselbrecht S and Vrij E (2022) From  
Mice to Men: Generation of Human  
Blastocyst-Like Structures *In Vitro*.  
Front. Cell Dev. Biol. 10:838356.  
doi: 10.3389/fcell.2022.838356

Advances in the field of stem cell-based models have in recent years lead to the development of blastocyst-like structures termed blastoids. Blastoids can be used to study key events in mammalian pre-implantation development, as they mimic the blastocyst morphologically and transcriptionally, can progress to the post-implantation stage and can be generated in large numbers. Blastoids were originally developed using mouse pluripotent stem cells, and since several groups have successfully generated blastocyst models of the human system. Here we provide a comparison of the mouse and human protocols with the aim of deriving the core requirements for blastoid formation, discuss the models' current ability to mimic blastocysts and give an outlook on potential future applications.

**Keywords:** blastoids, human blastocyst-like structures, embryonic development, pluripotent stem cells, implantation

## INTRODUCTION

In the past few years, a set of novel stem cell-based embryo models named blastoids have seen the light that recapitulate the pre-implantation blastocyst-stage embryo. Blastoids are well-poised to complement research on natural embryos as they contain both the embryonic and extraembryonic cell types, can be formed in large numbers with similar genetic makeup, are amenable to new modes of experimental manipulation including genetic screens and show features of post-implantation morphogenesis when exposed to appropriate culture conditions. In particular, human blastoids may provide promising alternatives to the use of human embryos, which are scarce and come with substantial ethical concerns (Pereira Daoud et al., 2020).

Several days after conception the blastomeric cells of the mammalian embryo compact into a tight polarized cluster named the morula. This conserved morphological event initiates, in part *via* aPKC/Hippo-mediated signaling, the first lineage bifurcation into the embryonic inner cell mass (ICM) and the extra-embryonic trophoblast (TE), that will form the fetal placenta (Cockburn and Rossant, 2010; Gerri et al., 2020a). The TE then forms an epithelium, starts pumping fluid inside and forms a cavitated sphere encasing the ICM on one side of the cavity, which is called the blastocyst (Molè et al., 2020). Interestingly, in human, commitment to either the ICM or TE does not occur until the start of cavitation (Meistermann et al., 2021). Around embryonic day 3.5 in mouse and day 5.0 in human, the ICM undergoes a second bifurcation and specifies into the epiblast (EPI), which forms the embryo proper, and primitive endoderm [PrE; named hypoblast in human (HYPO)], which gives rise to extra-embryonic endoderm tissues including parts of the yolk sac (Molè et al., 2020). In mouse, EPI and PrE cells are initially mixed in a salt/pepper-like distribution after which the PrE segregates and forms an epithelium on top of the EPI, facing the blastocyst cavity. There is evidence of HYPO

formation and subsequent segregation taking place in human embryos as well, although it is not clear whether the initial distribution of HYPO cells in the ICM follows a similar salt and pepper-like pattern as observed in mouse (Roode et al., 2012). Meanwhile the TE differentiates and can be subdivided in the polar and mural TE. The polar TE refers to the TE directly in contact with the EPI and in mouse acts as a stem cell pool for the TE, whereas the mural TE is on the opposite side of the cavity. A striking difference between mouse and human development is that the mouse blastocyst attaches to the uterine wall with the mural side, while the human blastocyst is believed to attach with the polar side (Molè et al., 2020).

Thus, phenomenologically, pre-implantation development seems largely conserved between mouse and human, however the molecular underpinnings may differ. These differences become more pronounced in early post-implantation morphogenesis when also the embryo architecture and the maternal/fetal interface deviate from mouse [reviewed in Gerri et al. (2020b), Molè et al. (2020)]. As such, there is a clear need for a sophisticated model of the human pre- and peri-implantation embryo. In addition, the wide use of mouse as a model species and subsequent vast amounts of data available on mouse embryology and gene function form a solid foundation for generating and testing embryo models (Taft, 2008). Furthermore, in contrast to human, mouse embryo models may be amenable to model full organismal development.

For faithful recapitulation of blastocysts, it is essential that blastoids contain the EPI, HYPO/PrE and TE lineages. Embryonic stem cells (ESC) (Evans and Kaufman, 1981; Martin, 1981; Thomson et al., 1998), trophoblast stem cells (TSC) (Tanaka et al., 1998; Kubaczka et al., 2014; Okae et al., 2018; Frias-Aldeguer et al., 2020), and extra-embryonic endoderm cells (XEN) (Niakan et al., 2013; Anderson et al., 2017; Linneberg-Agerholm et al., 2019) form *in vitro* analogues of the EPI, TE and PrE/HYPO, respectively, and can generally be maintained as 2D monolayer cultures. More recently, chemically defined culture conditions have been identified that permit the expansion of multiple levels of pluripotent cells that reflect different developmental states of the pre-to early post-implantation EPI (Ying et al., 2008; Theunissen et al., 2014; Yang J. et al., 2017; Yang Y. et al., 2017; Guo et al., 2017; Gao et al., 2019; Bayerl et al., 2021; Shen et al., 2021). These 2D cultures form the basis of the more complex 3D models, such as blastoids, that are designed to capture both the specification of cell types and their spatiotemporal organization. As formation of 3D models relies heavily on self-organization, the starting conditions of the 2D cultures are critical for the successful generation of 3D models. On top of the stem cells themselves and the chemical cues that direct self-organization, the 3D culture platforms play an important role in providing the freedom to re-organize, as well as enabling *in situ* imaging-based readouts and enabling high-throughput screening assays.

The first report on the generation of blastoids recapitulated the mouse blastocyst formation by using a co-culture of mouse ESCs, which resemble the pre-implantation EPI (Evans and Kaufman, 1981; Martin, 1981), and mouse TSCs, which resemble the TE (Tanaka et al., 1998). When these types were combined through

sequential seeding into microwells and exposed to a mixture of growth factors and small molecule signaling pathway modulators they formed blastocyst-like structures (Rivron et al., 2018). Following this report, several other labs have reported modified methods for blastoid generation that all recapitulate the blastocysts' overall morphology and contain the three distinct cell lineages (Rivron et al., 2018; Kime et al., 2019; Li et al., 2019; Sozen et al., 2019; Zhang et al., 2019).

Although the culture of human ESCs and later TSCs has been possible for some time (Thomson et al., 1998; Okae et al., 2018), practical and ethical restrictions have impeded advances in human embryo models. Much of the work on human models consequently relies on preceding findings in mouse. However, this gap is closing with the recent accumulation of studies in both species, including the improved understanding of the similarities and differences in pluripotency (Brons et al., 2007; Tesar et al., 2007; Weinberger et al., 2016), methods to culture blastocysts towards the post-implantation stage *in vitro* (Bedzhov et al., 2014; Deglincerti et al., 2016; Shahbazi et al., 2016), advanced single cell omics studies to demarcate cell identities and regulatory networks that underlie EPI, PrE/HYPO and TE specification (Nakamura et al., 2015; Nakamura et al., 2016; Meistermann et al., 2021), and the *in vitro* differentiation of TE and its derivatives (Castel et al., 2020; Io et al., 2021). Through the use of human extended pluripotent/expanded potential stem cells (EPSCs), induced pluripotent stem cells (iPSCs) and naïve ESCs, several groups have reported their first successes with human blastoid generation (Fan et al., 2021; Kagawa et al., 2021; Liu et al., 2021; Sozen et al., 2021; Yanagida et al., 2021; Yu et al., 2021). The methods employed have yet some marked differences between the groups, underlining the different angles and controversies surrounding the cellular subtypes and signaling pathways involved in early human development.

In this review, we aim to give an overview of the current mouse and human blastoid protocols, compare mouse and human protocols to identify core requirements for blastoid formation and discuss to what extent current blastoids mimic blastocysts.

First, we will address several of the key components in the generation of mouse and human blastoids: the starting cell lines and their flavor of pluripotency, the soluble signaling pathways modulators used to steer differentiation of cells towards the blastocyst lineages and the culture platforms applied to facilitate 3D self-organization. Additionally, we will compare the timelines of the protocols and the extent of successful lineage specification. Next, we will delineate the capacity of blastoids to recapitulate principles of blastocyst development and the potential for post-implantation progression *in vitro*. Finally, we will provide an outlook on the future applications of both mouse and human blastoids.

## GENERATION OF MOUSE AND HUMAN BLASTOCYST MODELS *IN VITRO*

### Cell Sources and Flavors of Pluripotency

As delineated above, the pre-implantation mammalian blastocyst is comprised of three lineages: the TE, the PrE/HYPO and the

EPI. In mouse, stem cell analogues can be derived from all these three primary cell types and propagated as self-renewing stem cells, namely TSCs (Tanaka et al., 1998), XEN cells (Kunath et al., 2005; Anderson et al., 2017), and pluripotent ESCs (Evans and Kaufman, 1981; Martin, 1981), respectively. The term pluripotency describes the capacity of cells to form all cell types of the mature body in response to developmental cues (Silva and Smith, 2008). Leukemia inhibitory factor (LIF) was originally found to maintain pluripotency in mouse ESCs (Williams et al., 1988). Since, Ying et al., identified that the addition of the two inhibitors PD0325901 (ERK/MAPK inhibitor) and CHIR99021 (GSK3 $\beta$  inhibitor) can sustain mouse ESCs in a so-called pluripotent ground-state, which closely reflects the late blastocyst-stage epiblast and exhibits lower cell-to-cell variability and thereby manifests in more homogenous *in vitro* cultures (Ying et al., 2008). In the mouse embryo, progression of the EPI towards the post-implantation stage is characterized by a transiently evolving transcriptional and epigenetic signature of pluripotency, from which *in vitro* analogues can be captured in discrete states (Morgani et al., 2017; Neagu et al., 2020; Kinoshita et al., 2021), including the pluripotency endpoint (i.e., primed) post-implantation EPI cells named epiblast-derived stem cells (EpiSCs) (Brons et al., 2007; Tesar et al., 2007). *In vitro* at least, the pluripotency domain appears non-linear since additional states have been identified [reviewed in Morgani et al. (2017)], including so-called extended and expanded PSCs (EPSCs) (Yang J. et al., 2017; Yang Y. et al., 2017) that, reportedly, are able to also give rise to both the extraembryonic PrE and TE cell types. Although EPSCs do robustly form PrE, transcriptomic comparisons performed by Posfai et al. contested the claim of murine EPSC' ability to form *bona fide* TE (Posfai et al., 2021). In fact, the data suggest that EPSC do not have an additional totipotent character relative to native ESC and cluster instead closer to early post-implantation pluripotent cells (Posfai et al., 2021).

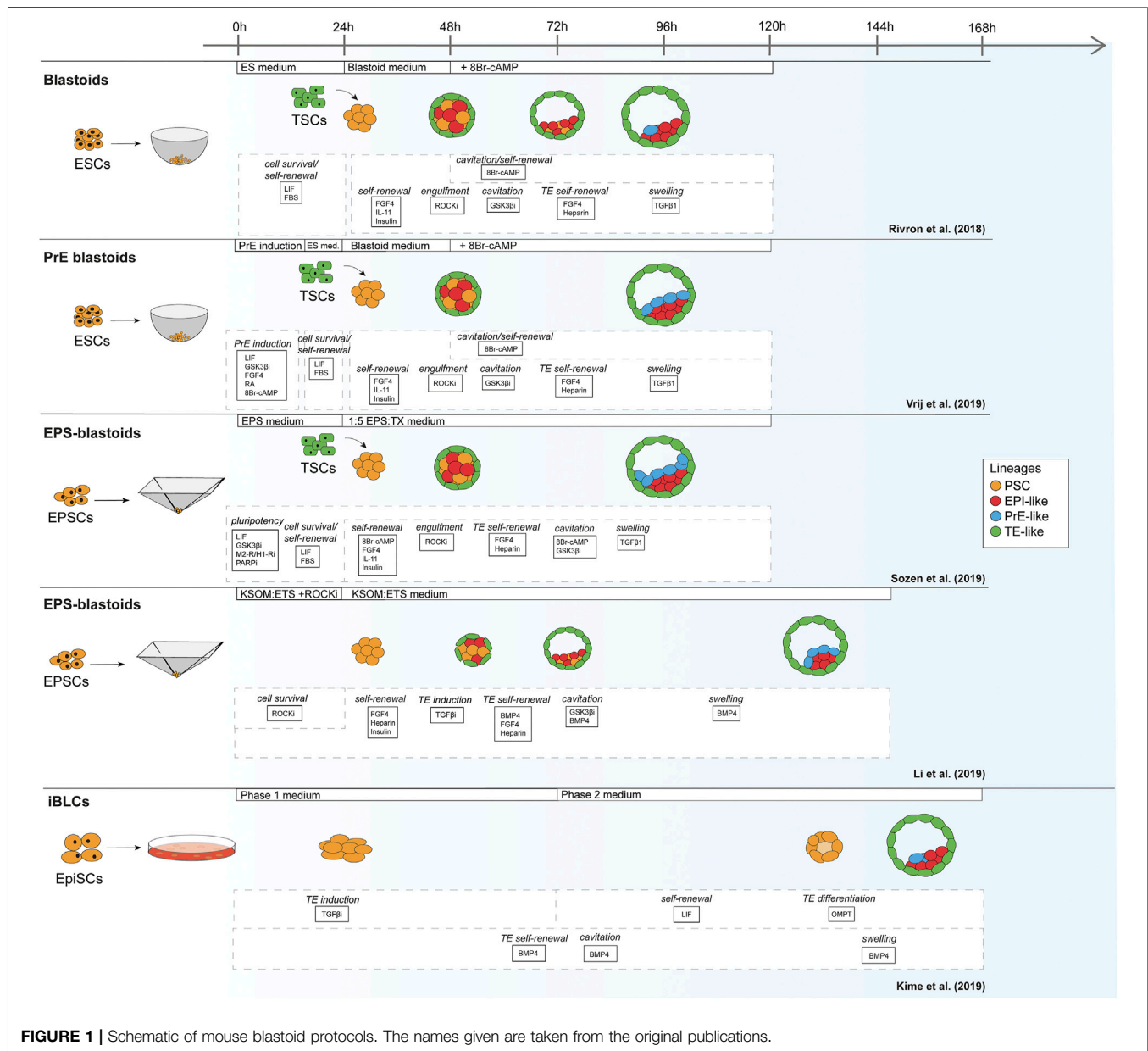
In contrast to mouse, human blastocyst-derived ESCs were originally maintained *in vitro* in a so-called primed state that reflects more the post-implantation EPI (Thomson et al., 1998) rather than the blastocyst-stage EPI. Later, numerous regulatory cocktails have been developed that claim the expansion of human ESCs and iPSCs in a naïve state (Chan et al., 2013; Gafni et al., 2013; Takashima et al., 2014; Theunissen et al., 2014; Ware et al., 2014; Bredenkamp et al., 2019b; Bayerl et al., 2021) that shares features with mouse ground-state ESCs such as their dome-like colonies, predominant activation of the OCT4 distal enhancer, germline potency and pre-X-chromosome inactivation (Weinberger et al., 2016; Devika et al., 2019; Yilmaz and Benvenisty, 2019). Moreover, methods for culturing mouse EPSCs have been translated to human as well and termed human EPSCs (Gao et al., 2019). Nevertheless, establishing a consistent and pure human naïve line can be challenging as is evidenced by current efforts to optimize the combinations of factors that permit robust expansion of human naïve pluripotent PSCs from diverse genetic backgrounds (Bredenkamp et al., 2019a; Bayerl et al., 2021; Khan et al., 2021). The progress in the field of naïve pluripotency over the past decade has been covered extensively elsewhere and will therefore not be discussed

in detail here (Weinberger et al., 2015; Smith, 2017; Yilmaz and Benvenisty, 2019; Taei et al., 2020). Important to note, whereas mouse PSC cannot readily differentiate into TE lineages, human ESCs appear to have a certain capacity to do so (Xu et al., 2002; Amita et al., 2013). Although there is no consensus yet about whether primed hPSC form *bona fide* trophoblast cells or something related (e.g., mesoderm or amnion), it appears that hPSCs maintained in EPSC and naïve conditions do form stable self-renewing lines reminiscent of early post-implantation trophoblast (Castel et al., 2020; Cinkornpumin et al., 2020; Guo et al., 2021; Io et al., 2021). Robust expansion cultures of pre-implantation TE have not been reported to date, however. Besides the differentiation to trophoblast, human naïve ESCs were reported capable of differentiating into HYPO-like cells (Linneberg-Agerholm et al., 2019).

Of note, it is important that, independent of the expansion protocol that is used, the maintenance of pure and uniform pluripotent cell populations is an essential starting point to form blastoids for both mouse and human.

For mouse, the first blastoids were formed using ESCs cultured in the 2i/LIF ground-state condition in order to form EPI and PrE, combined with multipotent TSCs to mimic the TE (**Figure 1**) (Rivron et al., 2018). In contrast to the protocols based on mouse ESCs, Li et al. reported blastoids based on murine EPSCs without addition of TSCs (EPSC-only blastoids; **Table 1**) (Rivron et al., 2018; Li et al., 2019; Sozen et al., 2019; Vrij et al., 2019). As mentioned before, while mouse ESCs are committed to the EPI lineage, mouse EPSCs are reportedly able to give rise to all cell types of the conceptus (Yang J. et al., 2017; Yang Y. et al., 2017). Although EPSCs do form PrE in blastocysts and in blastoids the claim of murine EPSC ability to form *bona fide* TE is contested (Posfai et al., 2021). Strikingly, although EPSC-only blastoids can form blastoids with fewer exogenous cues than the other models, the efficiency of blastoid generation appears higher when using TSCs for the TE compartment rather than TE induction from EPSCs alone (15 vs. 60% formation efficiency) (Li et al., 2019; Sozen et al., 2019). This is also supported by the findings of Kime et al. (2019). This group used their previously developed protocol for converting post-implantation mouse EPI cells to naïve mouse PSCs (Kime et al., 2016) and found that these converted cells could give rise to blastocyst-like structures on their own, albeit at a low efficiency (Kime et al., 2019).

Similar to the mouse models, human blastoid models were created with various types of PSCs that are believed to confer different pluripotency states (**Figure 2**). While some labs use human ESCs and iPSCs grown in naïve conditions (Kagawa et al., 2021; Yanagida et al., 2021; Yu et al., 2021), others have used EPSC conditions (Fan et al., 2021; Sozen et al., 2021) and one group has used direct reprogramming of fibroblasts over a course of 21 days into cells that form blastoids (Liu et al., 2021). This diversity in starting material likely contributes to the variation between methods in blastoid generation efficiency and capacity for lineage specification (**Table 2**). Moreover, depending on the pluripotency state, triggers for directing the founding cells towards an organized blastocyst-like structure vary as well, as is also observed in the mouse protocols (Rivron et al., 2018; Li et al., 2019; Sozen et al., 2019; Vrij et al., 2019).



As noted before, human PSCs appear more readily able to contribute to the TE lineage when they are in a naïve or EPSC conditions than mouse PSCs. This might explain why, contrary to murine blastoids, the majority of human blastoids have been formed from a single cell type and higher yields were reported in some of the single cell type approaches (Kagawa et al., 2021; Sozen et al., 2021; Yanagida et al., 2021) compared to the approach of Fan et al. that combines induced TE-like cells with EPSCs (Table 2) (Fan et al., 2021).

## Blastoid Culture Conditions

In addition to 2D PSC cultures in the appropriate pluripotency state, several other conditions must be met to generate blastoids. The PSCs need to be exposed to the right signaling molecules at

the right time to direct their differentiation towards the blastocyst lineages and they need the appropriate microenvironment to undergo their morphogenetic changes.

Signaling pathways that are involved in blastocyst formation have been thoroughly studied over the past decades in mouse [reviewed in Rossant and Tam (2009), Frum and Ralston (2015)]. While in mouse, *in vitro* work on the effects of pathway activation can be complemented with *in vivo* work, this is not the case for human due to ethical concerns. Much of what we know about signaling pathways in human development therefore stems from findings in the mouse and/or comparisons between mouse and human ESCs *in vitro*, substantiated with (single cell) omics approaches applied to human (Yan et al., 2013; Blakeley et al., 2015; Petropoulos et al., 2016) and mouse embryos in the recent



**TABLE 1 |** Overview of mouse blastoid protocols, summarizing culture conditions, experimental time lines, blastocyst marker expression, characterization experiments performed, post-implantation progression and limitations of the individual protocols.

	<b>Rivron, N.C., Frias-Aldeguer, J., Vrij, E.J. et al. Blastocyst-like structures generated solely from stem cells. <i>Nature</i> (2018)</b>	<b>Vrij, E.J., Scholte op Reimer, Y.S., Frias Aldeguer, J., et al. Chemically-defined induction of a primitive endoderm and epiblast-like niche supports post-implantation progression from blastoids. <i>bioRxiv</i> (2019)</b>	<b>Sozen, B., Cox, A.L., De Jonghe, J., et al. Self-Organization of Mouse Stem Cells into an Extended Potential Blastoid. <i>Developmental Cell</i> (2019)</b>	<b>Li, R., Zhong, C., Yu, Y., Liu, H., et al. Generation of Blastocyst-like Structures from Mouse Embryonic and Adult Cell Cultures. <i>Cell</i> (2019)</b>	<b>Kime, C., Kiyonari, H., Ohtsuka, S., et al. Induced 2C Expression and Implantation-Competent Blastocyst-like Cysts from Primed Pluripotent Stem Cells. <i>Stem Cell Reports</i> (2019)</b>
Cell lines	ES: V6.5, H2B-RFP V6.5 sub-clone, PDGFR $\alpha$ -H2B-GFP, SOX17-GFP and IB10 TS: F4, F1 and CDX2-eGFP	ES: PDGFR $\alpha$ -H2B-GFP/+, GATA6-H2B-Venus/+, H2B-RFP V6.5 sub-clone, ColA1 TetO-GATA4-mCherry/+, R26 M2rtTA/TS: F4 and F1	ES: PDGFR $\alpha$ ESCs or EPSCs, CAG: GFP ESCs or EPSCs, ROSA-mTmG ESCs or EPSCs TS: WT- and EGFP-TSCs	EPSC: EPS1 (tdTomato+), EPS2 (tdTomato+), ES: B6N-22, B6 GFP + ES iPSC from ear fibroblasts	EpiSC: mEpiSCs, XGFP mEpiSCs with MERVL-DSRed /mCherry or EOS:DSRed/mCherry
Maintenance medium	ES: 2i/Lif N2B27 medium (Ying et al., 2008) TS: TX medium (Kubaczka et al., 2014)	ES: 2i/Lif N2B27 medium TS: (modified) TX medium	ES: 2i/Lif N2B27 medium TS: TX medium	EPSC: N2B27-LCDM (Yang et al., 2017b) ES: 2i/Lif N2B7 medium	EpiSC: ND227 medium (Ying et al., 2008) + Activin A + bFGF
Oxygen during maintenance	20%	20%	20%	20%	20%
Platform	Agarose hydrogel microwells, 200 $\mu$ m $\varnothing$	Agarose hydrogel microwells, 200 $\mu$ m $\varnothing$	AggreWell™ plates 400 $\mu$ m $\varnothing$	AggreWell™ plates 400 $\mu$ m $\varnothing$	Fibronectin-coated 6 wells plate
Mouse blastoid protocol (Day 0 = seeding ESC/EPSC on platform)	<u>0 h</u> ES medium <u>24 h</u> Seed TSC  Blastoid medium <u>48 h</u> Blastoid medium + 8Br-cAMP	<u>0 h</u> PrE induction medium <u>At 21 h</u> ES medium <u>24 h</u> Seed TSC Blastoid medium <u>48 h</u> Blastoid medium + 8Br-cAMP	<u>0 h</u> EPS medium <u>24 h</u> Seed TSC EPS:TX medium (1:5)	<u>0 h</u> KSOM:ETS medium (1:1) [ETS = N2B27:basal TSC medium (1:1)] + ROCKi <u>24 h</u> KSOM:ETS medium (1:1)	<u>-14-16 h</u> ND227 medium + Activin A + bFGF <u>0 h</u> Phase 1 medium <u>96 h</u> Phase 2 medium
Oxygen during blastoid formation	20%	20%	20% during the first 24 h 5% after TSC seeding	20%	20%
Initial cell seeding number	5 ESCs + 12 TSCs per microwell	7 ESCs + 17 TSCs per microwell	4 E(P)SCs + 8 TSCs per microwell	5 EPSCs per microwell	30–50,000 mEpiSC cells/well
Aggregation	24 h	24 h	24 h	24 h	N/A
Cavitation	48–65 h	48–65 h	72–96 h	72 h	~120 h
Specification of tissues	96 h: NANOG (EPI), GATA6 (PrE), CDX2 (TE)	96 h: NANOG (EPI), GATA6 (PrE)	96 h: NANOG (EPI), FOX2A (PrE), PDGFR $\alpha$ (PrE), CDX2 (TE)	24 h: SOX2 (ICM/EPI) 48 h: active YAP (TE) 120–144: GATA4 (PrE)	168 h: NANOG (EPI), OCT4 (EPI), GATA4/6 (PrE), PDGFR $\alpha$ (PrE), CDX2 (TE), TROMA-1 (TE)
Formation completed	96 h	96 h	96 h	120–144 h	168 h
Yield of cavitated structures with EPI, TE and HYPO	12%	36%	15%	15% (~2.7% for clonal EPS-blastoids)	5–30 per well
Embryonic timeline	E3.5–4.5	E3.5–4.5	E3.5–5.0	E3.5–4.5	unknown

(Continued on following page)

**TABLE 1 |** (Continued) Overview of mouse blastoid protocols, summarizing culture conditions, experimental time lines, blastocyst marker expression, characterization experiments performed, post-implantation progression and limitations of the individual protocols.

Characterization	Immunohistochemistry qRT-PCR scRNA-seq Derivation of ES and TS cells Injection into mouse blastocysts Post-implantation progression	Immunohistochemistry Post-implantation progression	Immunohistochemistry qRT-PCR scRNA-seq Post-implantation progression	Immunohistochemistry sc-RNAseq bulk RNA-seq Derivation of ES and TS cells Injection into mouse blastocyst Post-implantation progression	Immunohistochemistry qRT-PCR Derivation of ES and TS Post-implantation progression
Markers used	EPI: NANOG, OCT4, PrE: GATA6, PDGFR $\alpha$ TE: CDX2, KRT18	EPI: NANOG, OCT4 PrE: GATA6, PDGFR $\alpha$	EPI: NANOG, OCT4 PrE: SOX17, PDGFR $\alpha$ , FOX2A, GATA4, GATA6 TE: CDX2, KRT8, TFAP2C	EPI: NANOG, OCT4, SOX2 PrE: GATA4, GATA6 TE: CDX2, CK8, KRT8, TFAP2C	EPI: NANOG, OCT4, PrE: GATA4/6, PDGFR $\alpha$ TE: CDX2, GATA3, TROMA-1 TE/CM: YAP
Post-implantation progression (attached culture)	<i>In vivo</i> in uteri mus musculus decidualization occurred CDX2, ELF5, TEAD4, HAND1, ASCL2 and proliferin (TE) positive cells observed	<i>In vitro</i> on tissue-culture glass or polystyrene plastic in IVC1 medium for 96 h OCT4+ (EPI) and GATA6+ (PrE) present	<i>In vivo</i> in uteri mus musculus decidualization occurred PDGFR $\alpha$ + (PrE), CDX2+ and KRT18+ (TE) present <i>In vitro</i> on ibidi-u plates coated with Matrigel in IVC1 medium (24 h), followed by IVC2 (next 48 h) PDGFR $\alpha$ + (PrE), GFP (TE) and OCT4+ (EPI) present	<i>In vivo</i> in uteri mus musculus decidualization occurred <i>In vitro</i> on $\mu$ -Slide 8-well in IVC1 medium and IVC2 medium; culture for 48–96 h	<i>In vivo</i> in uteri mus musculus decidualization occurred in 6.7% of the cases TROMA-1+ (TE) cells were observed invading maternal tissue PL-1 (visceral endoderm) present
Limitations	PrE is underdeveloped and structures arrest in post-implantation development	Structures arrest in post-implantation development	PaE is not fully formed and structures lack Reichert's membrane	EPSCs' ability to form TE is contested, therefore they can't be considered equivalent to totipotent blastomeres	Low efficiency No high throughput platform blastoids are resorbed during post-implantation development

years (Deng et al., 2014; Boroviak et al., 2015; Nakamura et al., 2016). Based on these studies, we are now able to attribute the activity of several pathways to the development of the blastocyst lineages in both mouse and human. Consequently, small molecules that regulate these pathways are applied in blastoid generation. Here we will discuss all pathway regulators that have reportedly been used so far to generate blastoids and explain their function(s) in blastoid formation (summarized in **Tables 3, 4**).

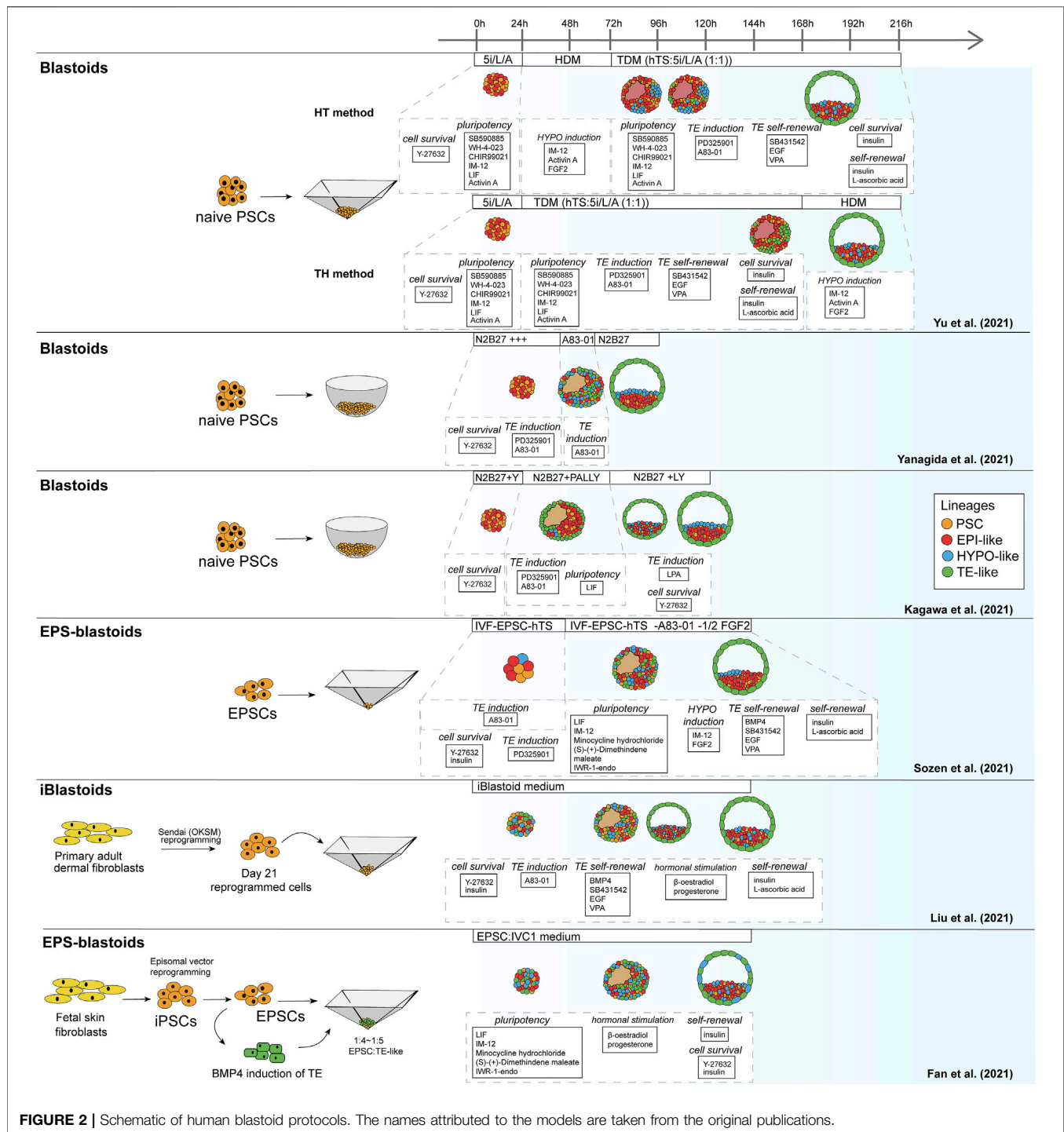
## Wnt Pathway Modulators

Wnt signaling is found to play an important role in both mouse and human development, although its role during pre-implantation remains controversial [reviewed in De Jaime-Soguero et al. (2018)]. Regardless of the disputes surrounding Wnt activity during pre-implantation stages, CHIR99201 (CHIR), a GSK3 $\beta$  inhibitor and subsequent canonical Wnt/ $\beta$ -catenin activator, is included in all mouse blastoid protocols except the one from Kime et al. Addition of CHIR significantly increased the yield of mouse blastoid formation (Rivron et al., 2018; Li et al., 2019) and Wnt inhibitors XAV939 and IWR-1-endo significantly inhibited blastoid formation (Rivron et al., 2018; Li et al., 2019). Additionally, it enhanced blastoid cavitation size (Rivron et al., 2018) and PrE induction (Rivron et al., 2018; Vrij et al., 2019).

CHIR is included in several of the human protocols (Fan et al., 2021; Sozen et al., 2021; Yu et al., 2021) and has similar functions as in mouse, namely, to maintain pluripotency of the human PSCs and support HYPO induction. Sozen et al. even found that human 3D cultures did not survive without CHIR (Sozen et al., 2021). However, CHIR is not the only Wnt regulator employed. The naïve pluripotency medium 5i/L/A that is used for blastoid generation by Yu et al. includes the selective GSK3 $\beta$  inhibitor IM-12 (Theunissen et al., 2014). In blastoid protocols based on human EPSCs, EPSC medium rather than naïve medium is used to maintain a pluripotent compartment. EPSC medium also contains CHIR and is paradoxically complemented with a canonical Wnt/ $\beta$ -catenin signaling inhibitor, IWR-endo-1 (Yang Y. et al., 2017; Fan et al., 2021; Sozen et al., 2021), that possibly mediates an effect by further increasing Axin2 levels (Kim et al., 2013).

## ERK/MAPK Pathway Modulators

The ERK/MAPK pathway too is unanimously recognized as a key player. Downregulation of ERK/MAPK signaling was first described in murine ESC cultures to maintain naïve



pluripotency alongside Wnt pathway activation (Ying et al., 2008). Through the inhibitor PD0325901, ERK/MAPK signaling is blocked, resulting in sustained pluripotency and self-renewal in both murine and human ESCs (Li et al., 2007; Ying et al., 2008; Nichols et al., 2009). As MEK inhibitors are suppressors of differentiation, they are omitted from mouse blastoid protocols to facilitate lineage specification.

In human however, maintaining ERK/MAPK inhibition in 3D culture supports the specification of the TE lineage and is therefore included in several protocols for human blastoids (Guo et al., 2021; Kagawa et al., 2021; Yanagida et al., 2021). Additionally, the previously mentioned human naïve pluripotency medium 5i/L/A contains both PD0325901 and a BRAF inhibitor, which is also linked to

**TABLE 2 |** Overview human blastoid protocols, summarizing culture conditions, experimental time lines, blastocyst marker expression.

	<b>Yu, L., Wei, Y. et al. Blastocyst-like structures generated from human pluripotent stem cells. Nature (2021)</b>	<b>Liu, X., Tan, J.P. et al. Modelling human blastocysts by reprogramming fibroblasts into iBlastoids. Nature (2021)</b>	<b>Yong Fan, Zhe-Ying Min, et al. Generation of human blastocyst-like structures from pluripotent stem cells. bioRxiv (2021)</b>	<b>Berna Sozen, Victoria Jorgensen. et al. Reconstructing human early embryogenesis in vitro with pluripotent stem cells. bioRxiv (2021)</b>	<b>Yanagida, A., Spindlow, D., et al. Naive stem cell blastocyst model captures human embryo lineage segregation. Cell Stem Cell (2021)</b>	<b>Kagawa, H., Javali, A., et al. Human blastoids model blastocyst development and implantation. Nature (2021)</b>
Cell lines	WIBR3 (OCT4-2A-GFP) hES cells, Human (fore)skin fibroblasts (neonatal origin) <b>reprogrammed to iPS cells</b>	Primary human adult dermal fibroblasts <b>reprogrammed to iPS cells</b>	Human fetal skin fibroblasts <b>reprogrammed to iPS cells and EPS cells</b>	RUES2-RLG (SOX2-GFP), H9 and ESI0017 reprogrammed to EPS cells	HNES1-GATA3:mKO2, niPSC HDF75 and cR-Shef6 reprogrammed to naïve hES cells	HNES1, H9, cR-Shef6, NIPSC16.2.b and cR-NCRM2 reprogrammed to naïve hES cells
Maintenance medium	5i/L/A medium on imEFs (Theunissen et al., 2014) or PXGL medium on imEFs (Bredenkamp et al., 2019)	Fibroblast medium	EPSC medium (Yang et al., 2017) on ICR imEFs	EPSC medium (Yang et al., 2017) on CF1 imEFs	PXGL medium on imEFs (Bredenkamp et al., 2019)	PXGL medium on imEFs (Bredenkamp et al., 2019)
Oxygen during maintenance	20%	20%	20%	20%	5%	5%
Platform	AggreWell™ plates 400 µm Ø	AggreWell™ plates 400 µm Ø	AggreWell™ plates 400 µm Ø	AggreWell™ plates 400 µm Ø	ultra-low attachment multiple-well plate (Corning Coster) + non-adherent, 'U'-bottomed 96-well (Greiner)	Non-adherent hydrogel microwells (Vrij et al., 2016)
Human blastoid protocol (Day 0 = seeding on platform)	<u>Day 0</u>  5i/L/A medium  HT <u>Day 1</u> HDM medium <u>Day 3</u> TDM medium	<u>Day 0</u> Human iBlastoid medium + 10 µM ROCKi  <u>Day 1</u> Human iBlastoid medium  TH <u>Day 1</u> TDM medium <u>Day 6-7</u> HDM medium	<u>Day -4 to 0</u> TE induction of EPSC (BMP4 medium)  <u>Day 0</u> TE-like cell:EPSC = 5:1~4:1 EPSC:IVC1 medium = 1.5:1	<u>Day 0</u> IVF-hEP-hTS (2:1:1) medium + 40 ng/ml FGF2 + TGFβi  <u>Day 2</u> IVF-hEP-hTS (2:1:1) medium + 20 ng/ml FGF2	<u>Day 0</u> N2B27 + 1.5 µM MEKi + 1 µM TGFβi + 10 µM ROCKi  <u>Day 2</u> N2B27 + 0.5 µM TGFβi  <u>Day 3</u> N2B27	<u>Day 0</u> N2B27+ 10 µM ROCKi  <u>Day 1</u> N2B27 + PALLY  <u>Day 3</u> N2B27 + 0.5 µM LPA + 10 µM ROCKi
Oxygen during blastoid formation	20%	5%	20%	5%	5%	5%
Initial cell seeding number	25 cells per microwell	100 cells per microwell	Total 100 cells per microwell (80–83 TSC + 17–20 EPSC)	5–6 cells per microwell	50–200 cells per microwell	3.0 × 10 <sup>4</sup> cells per well (calculated ~70 per microwell)
Aggregation	12 h	24 h	24 h	24 h	24 h	0–24 h
Cavitation	Day 4 Not present in 85.5% (HT) and 84.3% (TH)	Day 3–4	Day 4	Day 3–4	Day 2	Day 3

(Continued on following page)



# DEVELOPMENTAL MODELS 2.0

Topic Editors:

**Mo Li**, King Abdullah University of Science and Technology, Saudi Arabia

**Keiichiro Suzuki**, Osaka University, Japan

**Alessandra Giorgetti**, Institut d'Investigació Biomedica de Bellvitge (IDIBELL), Spain

**Ying Gu**, Beijing Genomics Institute (BGI), China

*Dr. Ying Gu is employed by BGI-Research, all other Topic Editors declare no conflicts of interest.*

**Citation:** Li, M., Suzuki, K., Giorgetti, A., Gu, Y., eds. (2022). Developmental Models 2.0. Lausanne: Frontiers Media SA. doi: 10.3389/978-2-83250-597-7

**TABLE 2 |** (Continued) Overview human blastoid protocols, summarizing culture conditions, experimental time lines, blastocyst marker expression.

Limitations	Low yield Variable efficiency ~80% of cells don't differentiate or acquire a clear embryonic identity Low post-implantation progression efficiency Cell loss due to extensive procedure for mEF depletion	Low yield No defined HYPO layer No signs of gastrulation Reported TE more similar to amnion (Zhao et al., 2021)	Low yield More total cells and fewer cells in the inner cell mass (ICM) ~50% blastoids don't have correct OCT4+ (EPI) or CK8+ (TE) localization Large variation in lineage specification	hEPSCs only partly able to specify TE Induced TSCs don't recapitulate pre-implantation TE, but post-implantation	Variable efficiency HYPO cell number varies No evidence of lineage specification potential (no derivation experiment)	Discontinuous HYPO layer? Organization of the three lineages during in vitro post-implantation does not reflect in vivo organisation at this stage
-------------	---	--	---	---	---	---

the inhibition of ERK/MAPK signaling (Theunissen et al., 2014).

TGFβ Pathway Modulators

Then, there are several members of the TGFβ-superfamily that are involved in the regulation of blastoid formation. Most mouse blastoid protocols apply low levels of TGFβ1 to maintain TE self-renewal and modulate swelling of the caviated structures (Rivron et al., 2018; Sozen et al., 2019; Vrij et al., 2019). Notably, studies in mouse identified TGFβ1 as a co-regulator with FGF4 for TSC self-renewal (Erlebacher et al., 2004). Therefore it is striking that, when murine blastoids are generated from EPSCs alone, they are exposed to Activin/Nodal/ALK4/5/7 inhibitor A83-01 to induce the TE identity in EPSCs (Li et al., 2019). Similarly, Kime et al. apply Activin/Nodal/ALK4/5/7 inhibitor SB431542 in their blastoid protocol (Kime et al., 2019). Regarding the other branch of the TGFβ-superfamily, BMP4, is included in mouse blastoid cultures (Rivron et al., 2018; Kime et al., 2019; Li et al., 2019) to support cavitation, swelling and TE self-renewal (Coucouvanis and Martin, 1999; Hayashi et al., 2010).

Similar to aforementioned murine EPSC-only blastoids and EpiSC-based blastoids, human blastoids are formed in the presence of TGFβ inhibitors. In human naïve PSCs and EPSCs alike, A83-01 in combination with PD0325901 induces a TE identity, while the less potent inhibitor SB431542 is included to support TE self-renewal (Tojo et al., 2005; Okae et al., 2018; Guo et al., 2021). Through the other TGFβ signaling branch, BMP4 contributes to TE self-renewal as well (Xu et al., 2002; Amita et al., 2013; Okae et al., 2018). In one of the human protocols, TE induction before 3D culture is even performed with BMP4 alone (Fan et al., 2021). Whether it can give rise to pre-implantation TE-like cells is unclear, as most studies on BMP4-mediated induction observe trophoblast markers that are expressed by peri- and post-implantation trophoblast cell types (Li and Parast, 2014; Jain et al., 2017; Gao et al., 2019; Fan et al., 2021). Lastly, Activin A, an activator of Activin/Nodal/ALK4/5/7 signaling, is applied in human PSC culture to maintain naïve pluripotency (Theunissen et al., 2014; Bayerl et al., 2021). In combination with Wnt and FGF pathway regulators, Activin A is also used to induce HYPO differentiation (Linneberg-Agerholm et al., 2019; Yu et al., 2021).

FGF Pathway Modulators

In mice, FGF signaling is most notably involved in directing differentiation of ESCs during pre-implantation. FGF4 specifically is indispensable for mouse ESC differentiation towards the PrE lineage (Kunath et al., 2007; Nichols et al., 2009; Lanner and Rossant, 2010; Yamanaka et al., 2010; Krawchuk et al., 2013). Moreover, FGF4 does not only direct mouse ESCs towards the PrE, but also supports TE self-renewal (Tanaka et al., 1998; Goldin and Papaioannou, 2003). Overall, FGF4, including its chaperone heparin, is an all-round crucial factor for murine blastocyst formation (Allen and Rapraeger 2003; Furue et al., 2008) and therefore it is included in nearly all mouse blastoid models (Rivron et al., 2018; Li et al., 2019; Sozen et al., 2019; Vrij et al., 2019).

**TABLE 3 |** Small molecules applied in mouse blastoid protocols. When a protocol is listed in brackets, the molecule is used in a screening or cell culture maintenance medium, but not included in the standard blastoid generation protocol.

Compound name	Pathway	Activator/inhibitor	Promotes	Protocols
(2S)-OMPT	LPA	activator	TE induction	Kime
8Br-cAMP	PKA	activator	PrE induction, self-renewal, swelling	Rivron, Vrij
BMP4	BMP/Smad	activator	cavitation, swelling, TE self-renewal	Kime, Li (, Rivron)
CHIR99201	Wnt	activator	cavitation, pluripotency, PrE induction	Li, Rivron, Sozen, Vrij
(S)-(+)-Dimethindene maleate	M2 muscarinic receptor	inhibitor	pluripotency	(Li,)Sozen
FGF4	FGF	activator	PrE induction, (TE) self-renewal	Li, Rivron, Sozen, Vrij
IL-11	JAK/STAT	activator	decidualization	Rivron, Sozen, Vrij
Insulin	PI3K	activator	proliferation	Li, Rivron, Sozen, Vrij
IWR-endo1	Tankyrase/Wnt	inhibitor	pluripotency	Sozen
LIF	JAK/STAT	activator	cell survival	Kime, Rivron, Sozen, Vrij
Minocycline hydrochloride	PARP	inhibitor	pluripotency	(Li,)Sozen
Retinoic acid	Receptor on the DNA	activator	PrE induction	Vrij
SB431542	TGF $\beta$	inhibitor	TE induction	Kime
TGF $\beta$ 1	TGF $\beta$	activator	TE-renewal; inhibits swelling	Rivron, Sozen, Vrij
Y-27632	ROCK	inhibitor	cell survival; TSC engulfment	Li, Rivron, Sozen, Vrij

**TABLE 4 |** Small molecules applied in human blastoid protocols. When a protocol is listed in brackets, the molecule is used in a screening or cell culture maintenance medium, but not included in the blastoid generation protocol.

Compound name	Pathway	Activator/inhibitor	Promotes	Protocols
b-oestradiol	estrogen receptor	activator	decidualization	Fan, Liu
A83-01	TGF $\beta$ (Nodal/Activin/ALK4/5/7)	inhibitor	TE induction	Kagawa, Liu, Sozen, Yanagida
Activin A	TGF $\beta$ (Nodal/Activin)	activator	HYPO induction	Yu
BMP4	BMP/Smad	activator	cavitation, TE self-renewal	(Fan,) Liu, Sozen
CHIR99201	Wnt	activator	HYPO induction, pluripotency	Fan, Liu, Sozen, Yu
(S)-(+)-Dimethindene maleate	M2 muscarinic receptor	inhibitor	pluripotency	Fan, Sozen
EGF	Erk/MAPK	activator	TE self-renewal, cavity expansion	Liu, Sozen, Yu
FGF2/bFGF	FGF/Erk	activator	HYPO induction	Sozen, Yu
IM-12	Wnt	activator	pluripotency	Yu
Insulin	PI3K	activator	proliferation	Fan, Liu, Sozen, Yu
IWR-endo1	Tankyrase/Wnt	inhibitor	pluripotency	Fan, Sozen
LIF	JAK/STAT	activator	cell survival	Fan, Kagawa, Sozen, Yu
L-ascorbic acid	antioxidant	-	self-renewal	Liu, Sozen, Yu
Lysophosphatidic Acid (LPA)	Hippo	inhibitor	TE induction	Kagawa
Minocycline hydrochloride	PARP	inhibitor	pluripotency	Fan, Sozen
PD325901	Erk/MAPK	inhibitor	pluripotency	Kagawa, Yanagida
Progesterone	progesterone receptor	activator	decidualization	Fan, Liu
SB431542	TGF $\beta$ (Nodal/Activin/ALK4/5/7)	inhibitor	TE self-renewal	Liu, Sozen, Yu
SB590885	BRAF	inhibitor	pluripotency	Yu
VPA	HDAC	inhibitor	TE self-renewal	Liu, Sozen, Yu
WH-4-023	SRC	inhibitor	pluripotency	Yu
Y-27632	ROCK	inhibitor	cell survival	Fan, Kagawa, Liu, Sozen, Yanagida, Yu

In human HYPO development on the other hand, FGF signaling is dispensable, showcasing a marked difference between mouse and human in the regulation of the second lineage bifurcation (Roode et al., 2012). While it might not be essential, FGF signaling through the protein FGF2/bFGF does support HYPO induction, alongside other pathways as mentioned above (Linneberg-Agerholm et al., 2019). Furthermore, it is well-established that FGF2/bFGF supports human ESC self-renewal in the conventional primed pluripotency state (Xu et al., 2005), indicating its importance for maintenance of the post-implantation epiblast.

## JAK/STAT Pathway Modulators

One of the vital factors for mouse ESC proliferation and self-renewal is the JAK/STAT3 pathway activator LIF which is produced by the preimplantation TE and feeds the EPI (Williams et al., 1988). In addition to maintaining pluripotency and EPI identity, LIF also promotes PrE specification in blastocysts (Morgani and Brickman, 2015). A related activator of the JAK/STAT3 pathway, IL-11, complements FGF4 in the maintenance of TE self-renewal in blastoids (Rivron et al., 2018).

Several factors in the JAK/STAT3 pathway are applied in human blastoid protocols as well (Fan et al., 2021; Kagawa et al., 2021; Liu et al., 2021; Sozen et al., 2021; Yu et al., 2021). LIF is

widely included to maintain the pluripotent EPI (Fan et al., 2021; Kagawa et al., 2021; Sozen et al., 2021; Yu et al., 2021), even though it appears less crucial for proliferation and self-renewal in human as it is in mouse (Humphrey et al., 2004; Dahéron et al., 2008). Meanwhile EGF is included in several blastoid protocols (Liu et al., 2021; Sozen et al., 2021; Yu et al., 2021) for its support of TE differentiation and self-renewal (Okae et al., 2018).

## ROCK Inhibitor

One universally applied compound in blastoid protocols is the ROCK inhibitor Y-27632. In mouse blastoids, it was found to improve the engulfment of ESC aggregates by TSCs and was subsequently used in all protocols where TSCs are added separately (Rivron et al., 2018). Interestingly, studies in murine blastocysts indicate that ROCK inhibitor prevents cavitation *in vivo* and hampers TE induction through Hippo signaling (Kawagishi et al., 2004; Kono et al., 2014). Whether it similarly obstructs blastoid formation in some way *in vitro* is currently unknown.

For human PSC culture, ROCK inhibitor is a common addition to prevent apoptosis when human PSCs are reseeded as single cells (Watanabe et al., 2007). As such, it is included at least for the first 24 h in every human blastoid protocol to enhance single cell survival before aggregation.

## Hippo Pathway Modulators

The mouse blastoid study by Kime et al. and the human blastoid study by Kagawa et al. show that Hippo signaling inhibition is key for TE specification in blastoids (Kime et al., 2019; Kagawa et al., 2021), similar to mouse (Yu et al., 2016) and human embryos (Gerri et al., 2020a). Kime et al. applied OMPT, an agonist of Hippo inhibitor Lysophosphatidic Acid (LPA) in their phase 2 medium (Kime et al., 2019), after they previously found that LPA promotes the conversion of EpiSCs to naïve PSCs (Kime et al., 2016). In the human blastoid system, Kagawa et al. added LPA and found that this significantly increased the blastoid formation efficiency (Kagawa et al., 2021).

## cAMP Modulation in Mouse Blastoids

In most mouse blastoid models, 8Br-cAMP, a synthetic cyclic AMP analog, is applied in order to support both maintenance of the TE through upregulation of CDX2 expression, as well as to enhance cavitation of the blastoids (Rivron et al., 2018; Sozen et al., 2019; Vrij et al., 2019). This compound has however not been included in any of the human blastoid protocols.

## Modulators Specific for Human Blastoids

Besides signaling pathway modulators with a clear connection to developmental processes, some of the human blastoid protocols include a number of small molecules that have no apparent strong connection to established developmental signaling pathways. Several of these, SRCi, M2-R/H1-Ri, and PARPi, are added to maintain the pluripotent compartment in the blastoids (Theunissen et al., 2014; Yang Y. et al., 2017). The histone deacetylase inhibitor valproic acid (VPA) is included as a component of the previously defined human trophoblast medium (Okae et al., 2018). Notably, the use of either VPA or

a similar histone deacetylase inhibitor facilitates the induction of naïve pluripotency *via* resetting of the epigenome (Guo et al., 2017).

## Hormones

Several hormones are also included in some of the models. Insulin has become a standard component of both mouse and human TSC medium compositions and as such is now also present in blastoid protocols of both species (Kubaczka et al., 2014; Okae et al., 2018). Insulin is a well-established activator of the PI3K pathway, through which it promotes cell survival and proliferation (Taniguchi et al., 2006). This support of cell survival and proliferation led to the inclusion of insulin in the media for human PSC cultures, alongside FGF2 and ascorbic acid (Chen et al., 2011). Correspondingly, insulin appears to give naïve human PSCs a growth advantage and thus curbs HYPO differentiation (Anderson et al., 2017). Finally, there are the two sex hormones,  $\beta$ -oestradiol and progesterone, which are known to increase endometrial receptivity in human and mice and upregulate cytokines that support implantation of the murine blastocyst (Norwitz et al., 2001; Basak et al., 2002; Young, 2013). Both hormones have been applied in human blastoid cultures, as components of a medium called “*in vitro* culture 1” (IVC1). This medium is developed for and typically used to permit *in vitro* post-implantation progression of blastocysts rather than for pre-implantation embryo culture (Morris et al., 2012; Bedzhov et al., 2014).

To summarize, there is evidently a myriad of components that have so far been included in blastoid protocols, especially in the human ones. This can be attributed to the fact that most of the currently published human protocols use mixes of pre-existing media to induce the blastocyst lineages in 3D cultures. Notably, the protocols developed by Yanagida et al. and Kagawa et al. only include a handful of pathway regulators and are therefore surprisingly minimalist compared to the others. This begs the question which of the compounds applied so far are truly indispensable for human blastoid generation, particularly when using PSCs maintained in the naïve state.

## Culture Platforms

Regulating the mechanical environment of stem cells to direct assembly, trigger differentiation and guide development has recently gained traction, since an increasing number of studies show a relation between physical properties of the microenvironment and stem cell behavior (Guilak et al., 2009; Han et al., 2014). For a review on the potential of *in vitro* models to study mechanical and geometrical cues in early mammalian embryogenesis, refer to (Vianello and Lutolf, 2019).

In the case of blastoids, the culture platforms need to facilitate several requirements. Firstly, after initial seeding, cells need to be in each other's proximity to aggregate. Secondly, the cells/aggregates require the efficient exchange of nutrients, signaling molecules and growth factors to support their growth, differentiation and proliferation. Thirdly, it is important to take into account that mechanical cues also directly affect the signaling pathways involved in development (e.g., Hippo signaling) (Barzegari et al., 2020). As blastoids are a pre-



implantation model, adherence to the culture platform should be prevented. Usually, this is established either through the use of a suitable, non-adherent material [e.g., agarose or polyethylene glycol (PEG) for hydrogel microwells], by pre-coating culture plates with an anti-adherence solution [e.g., polyethylene-oxide polypropylene-oxide (hydrophilic-hydrophobic)] block copolymers for Aggrewells or by using pre-treated plates (ultra-low attachment plates). Finally, through the use of microwells arrays, large quantities of blastoids can be produced for one experiment, facilitating high-throughput analysis.

For murine blastoids, either in-house produced agarose hydrogel microwells or commercial Aggrewell microwells have been used (**Table 1**). Both set-ups contain a large quantity of microwells (400–1200 per well of a well-plate) (Vrij et al., 2016). Advantages of agarose hydrogel microwells over hard-plastic Aggrewell microwells may be the aid in diffusion of nutrients and waste products throughout the gel and the circular geometry that is less obstructive compared to the inverted pyramidal-shape of Aggrewell microwells. Moreover, agarose hydrogel microwells are amenable to *in situ* bright-field and epi-fluorescence imaging and downstream analysis and therefore blastoids do not require transfer to other platforms prior to analysis. The disadvantage of agarose-hydrogel microwells however is that diffusion of soluble components into the gel hampers abrupt and complete switches in medium conditions. Additionally, transfer of blastoids is still required for high resolution (i.e., confocal-based) imaging.

Similar to mouse, most human blastoid protocols are developed using Aggrewell microwells. However, Kagawa et al. used the agarose hydrogel microwells and Yanagida et al. reported using ultra-low attachment multiwell plates and non-adherent, “U”-bottomed 96-wells plates (**Table 2**). Yanagida et al.’s method of manually transferring structures to new media conditions however is very laborious, time-consuming, likely leading to the loss of (developing) blastoids and not amenable to high-throughput screenings.

Although Aggrewell microwells are widely used and support the culture of more than 1000 structures per well, they too come with several disadvantages. While it may seem arbitrary, a technical issue due to their pyramidal shape is the difficulty of changing media without disturbing the forming structures. As such, switching media for sequential inductions of blastocyst lineages is practically hindered. In contrast, agarose hydrogel microwells are far less sensitive for flow disturbances due to their cylindrical geometry. Another disadvantage of Aggrewell microwells is that the inverted pyramidal shape significantly hinders the *in situ* imaging quality and thus image-based readouts of the structures. As a result, blastoids need to be manually transferred to different platforms for imaging and further analysis, which poses the same issues as listed above for the method employed by Yanagida et al. All in all, among the currently reported microwell platforms for blastoid generation, a platform in which blastoids can be imaged directly with high quality is still lacking.

## Recapitulation of Development

The formation of blastoids consists of roughly the same steps in mouse and human protocols: aggregation, cavitation and maturation. First, upon seeding, the PSCs need to aggregate into spherical structures. This invariably occurs in the first 24 h with both mouse and human cells. Generally, media still mainly contain factors to support maintenance of pluripotency at this stage. Once the PSCs have clumped together, the medium composition is often changed to induce lineage specification and self-renewal of these lineages. For methods that require TSCs separately, TSCs are added after the first 24 h. Subsequently, the TSCs engulf the aggregated PSCs. From this stage onward, the forming blastoid structures self-organize and undergo cavitation, followed by a maturation process in which the blastoid increases in size, forms distinct EPI and PrE cells and occasionally organize themselves by sorting out a continuous epithelial layer of PrE cells overlying the EPI within the blastoid. Lineage specification takes place in parallel with these morphological changes. Thus, blastoids undergo embryonic events reminiscent of the pre-implantation embryo (Takaoka and Hamada, 2012).

*In vivo*, mouse and human development occur at a different pace. While the mouse embryo grows from a zygote to a blastocyst in approximately 3.5 days and implants around day 4.5–5, the human embryo reaches the blastocyst stage around day 5 and implants between day 7 and 8 (Molè et al., 2020). Interestingly, this difference in developmental pace between species can to some extent also be observed *in vitro*. Mouse blastoids generated with naïve ESCs have been reported to cavitate as early as 48 h after adding TSCs to ESC aggregates, while protocols using mouse EPSCs report cavitation around 72–96 h post TSC seeding. When using EpiSCs, cavitation may even occur as late as after 120 h, however this protocol is difficult to compare with the others, since the 3D structures arise from a converting 2D culture, rather than a 3D setup (**Table 1**). Similar to mouse EPSC-based blastoids, most human blastoids form a cavity between 72 and 96 h (**Table 2**). The blastoids from Kagawa et al. and Yanagida et al. based on naïve PSCs deviate from this timing. These blastoids were observed to have a cavity as early as at the 48-h time point (Yanagida et al.) or at the 60-h time point (Kagawa et al.).

When blastoids contain all three lineages and their morphology resembles the blastocyst, they are considered fully formed and their generation is complete. At what time point this stage is reached varies hugely between models. Mouse blastoids are generally fully formed at 96 h, except for the Li et al. EPSC-only blastoids, which are fully formed at 120–144 h, and the EpiSC-based blastoids from Kime et al., which may take up to 168 h. Completion of human blastoid generation on the other hand varies between 96 and 216 h. While naïve PSC-based blastoids by Yanagida et al. and Kagawa et al. are fully formed in 96–120 h (Kagawa et al., 2021; Yanagida et al., 2021), similar to the timeline for human morula to blastocyst development (Niakan et al., 2012; Rossant and Tam, 2017), Yu et al. report that their protocol, also based on naïve PSCs, takes 7–9 days (168–216 h) (Yu et al., 2021). The iBlastoids from Liu et al. and both EPSC-based blastoid models require approximately 144 h (Fan et al., 2021; Liu et al., 2021; Sozen et al., 2021). The difference

in timing between mouse and human likely reflects the different rates of development also observed between the blastocysts of these species. The variation observed between models of the same species on the other hand may reflect the efficiency of PSC commitment to the blastocyst lineages and the efficiency of the subsequent interactions between lineages.

It is precisely the proper commitment of PSCs to the blastocyst lineages that is one of the general challenges in both mouse and human blastoid models. In mouse models, the initial naïve ESC-based blastoids often lack a well-defined PrE compartment (Rivron et al., 2018). Subsequent studies led to a modified protocol that specifically induces PrE formation in blastoids (Vrij et al., 2019). Notably, blastoids based on EPSCs form PrE more readily, which Sozen et al. linked to the enhanced pluripotency state of EPSCs compared to mouse ESCs (Sozen et al., 2019). Despite this enhanced potential, EPSC-only blastoids from Li et al. contain mislocalized EPI/PrE- or TE-like cells as well as significant cell populations that might consist of either uncommitted PSCs remaining in the EPSC state or intermediates between lineages (Li et al., 2019).

The presence of cell types *in vitro* that are not present in the natural blastocyst is usually ascribed to incomplete induction. These off-target cell types can either be entirely uncommitted to any lineage, intermediates between EPI, PrE/HYPO and/or TE, or they correspond to a later stage of development. For many of the current human blastoid models, either one or multiple types of off-target cells have been described. Further inspection of lineage markers in the iBlastoids led to the conclusion that the majority of the cells in these structures are not conclusively committed to a specific lineage, but express markers from at least two different lineages (Liu et al., 2021; Yanagida et al., 2021). Similar overlap in marker gene expression was observed by Fan et al. in their EPSC-based blastoids (Fan et al., 2021). The naïve cell-based blastoids from Yu et al. also contain a large fraction of off-target cells, but these seemingly remain in a naïve-like, uncommitted state (Yanagida et al., 2021; Yu et al., 2021). These uncommitted cells most resemble EPI and far outnumber the TE-like cells, while in the blastocyst TE is the most abundant of the three lineages (Yanagida et al., 2021). In contrast, Yanagida et al. showed that the majority of cells in their blastoids commit to the TE lineage. This is confirmed by the mutually exclusive expression of GATA2 in their TE compartment and expression of OCT4 and naïve marker KLF17 in the ICM compartment. In the same line, Kagawa et al. show that between 50 and 80% of the cells in their blastoids can be attributed to the TE lineage based on immunofluorescence staining. Additionally, they report that less than 3% of cells were transcriptionally similar to post-implantation tissues (amnion and extra-embryonic mesoderm), when comparing the single cell transcriptomes of blastoid cells to blastocysts, *in vitro* outgrowths of blastocysts and gastrulation-stage embryos (Petropoulos et al., 2016; Zhou et al., 2019; Tyser et al., 2020). All other cells matched pre-implantation blastocyst lineages.

While blastoids from Yu et al. contain cells stuck in a developmental stage preceding the blastocyst stage, the iBlastoids appear to contain cells that correspond to the post-

implantation stage. When comparing their single cell transcriptomic data with post-implantation blastocysts, the cell population within iBlastoids that was identified as TE is found to more closely resemble amnion-like cells, rather than TE (Zhao et al., 2021). This could suggest that the cells used to make iBlastoids are not completely reprogrammed towards a state of pluripotency similar to naïve PSCs and therefore less able to give rise to the TE compartment (Zheng et al., 2019; Cinkornpumin et al., 2020; Guo et al., 2021). Sozen et al. found that their human EPSC-based blastoids too have only partially specified TE, as the TE compartment could not form a cohesive epithelium. Moreover, some of these EPSC-based blastoids contain multiple cavities (Sozen et al., 2021). Besides the specification of the TE, current human blastoid models also struggle with formation of the HYPO compartment. As was the case for the first mouse blastoids (Rivron et al., 2018), the human models often appear to lack the proper localization and/or HYPO cell numbers (Fan et al., 2021; Liu et al., 2021; Sozen et al., 2021; Yanagida et al., 2021; Yu et al., 2021).

## COMPARISON OF BLASTOIDS WITH BLASTOCYSTS

In order to prove the functionality of blastoids as models of blastocysts, two experiments are generally conducted. First, following the identification and correct spatial allocation of the EPI, PrE/HYPO and TE lineages (e.g., through single cell RNAseq and immunohistochemistry), cell lines are derived from these cell types as a functional assay to verify their propagation potential *in vitro* and their downstream differentiation potential. The second experiment is to test the capacity of complete blastoids to undergo post-implantation progression.

### Derivation of Stem Cell Lines

Originally developed for derivation from natural mouse blastocysts, the general approach to obtain stem cell lines from blastoids is to seed the blastoids on a culture plate with either ESC, TSC or PrE/hypoblast-like cell culture medium (Evans and Kaufman, 1981; Martin, 1981; Tanaka et al., 1998; Ying et al., 2008; Niakan et al., 2013; Okae et al., 2018; Linneberg-Agerholm et al., 2019) that selectively favors the desired cell type over several passages. The mouse naïve PSC-based blastoids of Rivron et al., the mouse EPSC-only blastoids of Li et al. and mouse EpiSC-based blastoids of Kime et al. all confirmed the presence of EPI and TE lineages in their blastoids with this approach (Rivron et al., 2018; Kime et al., 2019; Li et al., 2019). Additionally, blastocyst chimera assays confirmed the contribution of these cell lines to the expected compartments when grown out *in utero*. Moreover, besides the chimeric contribution of EPI and TE lineages, the PrE line derived from mouse EPSC-only blastoids contributed to the yolk sac.

As for the human blastoid models, derivation experiments were performed on the naïve PSC-based blastoids of Kagawa et al. and Yu et al., the EPSC-based blastoids of Fan et al. and the iBlastoids of Liu et al., though only Yu et al. included a culture selecting for HYPO-like cells (Linneberg-Agerholm et al., 2019;

Yu et al., 2021). Remarkably, despite the low number of TE-like cells, Yu et al. was able to derive TSC cells from single plated blastoids, as well as naïve PSCs and naïve endoderm cells. The identity of these cell lines was confirmed with immunostaining, differentiation assays and injection of the derived cells into mouse blastocysts. Kagawa et al. were able to derive naïve PSCs and TSCs from their blastoid model. These derived TSCs differentiate towards syncytiotrophoblast and extravillous trophoblast cell fates in 3–6 days, as was confirmed through immunostaining and RT-qPCR of several markers. Strikingly, blastoid-derived naïve PSCs could be used to generate a second generation of blastoids. Also Liu et al. derived TSCs and naïve PSCs from their iBlastoids. The naïve PSCs were confirmed to be pluripotent through a tri-lineage differentiation assay and the TSCs were differentiated towards TE derivatives, with immunostainings supporting the presence of marker genes. Finally, Fan et al. derived PSCs and TSCs from their blastoids, which they confirmed with immunostainings of several lineage markers.

Though these derivations say little about the developmental potential of the blastoids as complete structures, they do indicate that blastoids contain PSCs or cells with similar potential capable of differentiating towards post-implantation cell types.

## Post-Implantation Development *In Vitro*

Culture media that permit the *in vitro* post-implantation progression of blastocysts have in recent years contributed to embryo phenotyping and mechanistic understanding, particularly for human since this stage is non-accessible *in vivo* (Bedzhov et al., 2014; Deglincerti et al., 2016; Shahbazi et al., 2016; Xiang et al., 2020).

*In vitro*, blastocysts are transferred to a plastic or glass substrate and cultured in optimized *in vitro* culture (IVC) medium containing for the first 2 days serum, to promote growth and attachment of the TE cells, which is later substituted by knockout serum (Bedzhov et al., 2014). With this method, post-implantation morphological changes in the embryo, in particular the EPI transformation into the egg cylinder with concomitant visceral endoderm patterning, can easily be tracked for up to 5 days of development. Likewise, blastoids can be exposed to similar culture conditions to assess their potential for early post-implantation development. Naïve mouse ESC-based blastoids reportedly only continue development rarely in the *in vitro* system. The PrE-induced blastoids on the other hand manage to occasionally grow out into post-implantation epiblast-like structures encasing pro-amniotic-like cavities- and surrounded by a visceral endoderm-like epithelium (Vrij et al., 2019). Vrij et al. suggested this developmental potential is dependent on the abundance of PrE-like cells in the blastoids prior to post-implantation culture (Vrij et al., 2019). This is supported by the *in vitro* post-implantation assays performed with EPSC-based blastoids, which form PrE more robustly. In line with the development of blastocysts and post-implantation embryo models (Bedzhov et al., 2014), both EPSC-based mouse blastoid models could form egg cylinder-like structures (Li et al., 2019; Sozen et al., 2019). These structures contained cells similar to EPI, and post-implantation PrE and TE derivatives, visceral endoderm and extraembryonic ectoderm, respectively. Moreover, Li et al. observed that these structures recapitulated post-implantation polarization events on the molecular level (Li

et al., 2019). Importantly, however, current 2D *in vitro* culture methods for post-implantation morphogenesis of blastocysts and blastoids do not readily permit the formation of mural trophoblast, associated parietal endoderm and the ectoplacental cone [current gaps in embryo model development are reviewed in Shankar et al. (2021)].

The golden standard for mouse models however, is the injection of blastoids into the uteri of pseudo-pregnant mice to assess their capacity for full placentation and development beyond implantation. Rivron et al. reported the ability of naïve ESC-based blastoids to induce decidualization *in utero* (between 10 and 20% of injected blastoids implanted), but structures failed to develop further, similar to the *in vitro* findings. The EPSC-only blastoids of Li et al. resembled naïve ESC-based blastoids in that they could implant in the uterine wall and trigger decidualization (with ~7% efficiency) but failed to continue development in this more stringent assay (Li et al., 2019). Sozen et al. reported similar findings for their EPSC-based blastoids. Upon closer inspection, they found that although the blastoids physically attached to the maternal tissue, they did not develop a Reichert's membrane (Sozen et al., 2021). This membrane was found to play an important role in post-implantation morphogenesis (Ueda et al., 2020), therefore the lack of this structure in the post-implantation progression of blastoids may prevent further development.

Although it is possible to perform *in vivo* post-implantation assays for mouse blastoids, this is obviously unacceptable for the human equivalent. Therefore, human blastoids were only tested for their post-implantation developmental potential *in vitro*. Most groups use roughly the same attached culture method as described above for mouse blastoids and blastocysts (Bedzhov et al., 2014), adapted to support human blastocyst development *in vitro* (Deglincerti et al., 2016). Notably, all the groups that applied this method report a flattening of the blastoid structures upon attachment as is also observed in *in vitro* post-implantation blastocyst culture (Deglincerti et al., 2016; Shahbazi et al., 2016). Moreover, all confirm the presence of markers of at least two of the three blastocyst lineages and provide evidence of the onset of amniotic cavity formation. Additionally, Yu et al. and Yanagida et al. report indications of the onset of yolk sac formation. However, the success rates for the formation of post-implantation structures are quite low. Yu et al. obtained post-implantation-like structures from 10% of the blastoids, while 20–30% of the iBlastoids plated for attached culture formed these structures. Sozen et al. confirmed that ~60% of their attached structures had clear EPI and TE compartments, but this rate is lower for structures that also contain a HYPO marker. What fraction of these post-implantation structures contains a pro-amniotic-like cavity is not quite clear. Meanwhile Fan et al. and Yanagida et al. reported post-implantation-like structures as well but did not include the formation efficiency.

Kawaga et al. had a slightly different approach for mimicking post-implantation progression. They applied a method similar to the common one described above, but theirs was adapted from a protocol designed for cynomolgus monkey embryos, rather than mouse (Ma et al., 2019). Using this attached culture method, they reported the differentiation and expansion of all three blastocyst

lineages and the formation of an amniotic cavity in some attached blastoids. Their post-implantation culture could be maintained for 6 days, to a day 13 equivalent stage, however these cultures did not recapitulate the spatial organization of this developmental stage *in vivo*.

Taken together, the results of the assays discussed above indicate that both the current mouse and human blastoid models are capable of mimicking some of the morphogenetic events typical for the post-implantation blastocyst *in vitro*, albeit at a low efficiency. However, the more stringent *in vivo* experiments with mouse blastoids and the failure of human blastoids to comprehensively recapitulate spatial tissue organization of post-implantation development, underline that the developmental potential of current blastoid systems and/or post-implantation culture methods is still limited for both species. More sophisticated bioengineered 3D culture methods may be needed to overcome this barrier.

## Modelling Processes of Blastocyst Development

Besides investigations of the potential of blastoid models to continue development to a post-implantation stage, some groups reported additional findings to showcase the capacity of their blastoid models to recapitulate essential processes during pre-implantation development.

In mouse blastoids, Rivron et al. found that the EPI maintains the self-renewal and epithelial identity in the adjacent polar TE (Rivron et al., 2018). This is in line with findings from Gardner et al. that trophoblast cells in contact with the ICM don't terminally differentiate, but instead contribute to the proliferating polar TE-derived ectoplacental cone (Gardner and Johnson, 1972; Gardner et al., 1973).

Furthermore, Li et al. demonstrated that their EPSC-only blastoids accumulated ZO1 and E-Cadherin at cell-cell junctions during the aggregation of the EPSCs which resembles compaction in the 8-cell stage. They also provide evidence of apical enrichment of PARD6 expression during blastoid formation (Li et al., 2019), which is an indication of polarization (Chazaud and Yamanaka, 2016). Additionally, they show nuclear YAP expression in the outer cells and cytoplasmic YAP expression in the inner cells in about 60% of their EPSC-only blastoids on day 5 (Li et al., 2019). This intracellular localization pattern of YAP, part of the Hippo signaling, is proposed to play a role in TE specification in human and mouse during blastocyst formation (Gerri et al., 2020a).

Similar evidence of processes preceding blastocyst formation *in vivo*, such as compaction and polarization, was found in human blastoids as well. Sozen et al. observed the baso-lateral expression of E-cadherin and apical enrichment of F-actin and PARD6 (Sozen et al., 2021). In previous studies, the PLC-PKC pathway was suggested to play a role in cell polarization and TE specification in human embryos (Zhu et al., 2020). Using their blastoid system, Sozen et al. could observe that both PLC-specific inhibition and depletion reduced the expression of GATA3, one of the early TE markers, in outer cells of aggregates (Sozen et al., 2021). Simultaneously, the apical expression of PARD6, which

marks polarization, was reduced too. Natural human embryos have a comparable response to *in vitro* PLC inhibition and depletion treatments (Zhu et al., 2020), supporting the capacity of the blastoid system to recapitulate pre-implantation processes.

Furthermore, Sozen et al. investigated the effect of WNT3A. In mouse blastoids, WNT3A supports cavitation and increased blastoid yield (Rivron et al., 2018). However, addition of WNT3A does not improve cavitation in human blastoid cultures. This may indicate a different role for WNT3A in human development (Sozen et al., 2021).

In line with the study of the PLC-PKC pathway by Sozen et al., Yu et al. more extensively investigated the presence of tight junctions in their blastoids and found that, similar to murine blastocysts (Eckert et al., 2004a; Eckert et al., 2004b), their blastoids required the activity of specific PKC for cavitation (Yu et al., 2021).

Kagawa et al. further complimented these findings by their study of Hippo signaling in their blastoids. They found that atypical PKC inhibition strongly reduced nuclear accumulation of YAP1. As aforementioned, as a downstream effector of Hippo signaling, YAP1 is widely established to be involved TE specification in both mouse and human *in vivo* (Gerri et al., 2020a). Kagawa et al. confirmed the same is true in their blastoids, as aPKC inhibition and reduced YAP1 nuclear accumulation also correlated with reduced number of GATA3-positive cells and overall failure of human PSC aggregates to form blastoids. In addition, they show that YAP1 overexpression accelerated cavitation of their blastoids (Kagawa et al., 2021). They further elucidated on the process of cavitation by demonstrating that, similar to the mouse blastocyst (Dumortier et al., 2019), the cavity of their blastoids forms through the merging of multiple fluid-filled cavities (Kagawa et al., 2021).

Beyond the processes of blastocyst formation prior to implantation, blastoids can be used to model the earliest maternal-embryo interaction. In fact, Kagawa et al. present an *in vitro* model of embryo adhesion, the first step in implantation, by combining their blastoid model with so-called open-faced endometrial layers (OFELs) that mimic the endometrium. Using this set-up, Kagawa et al. demonstrate that their blastoids are capable of attaching to receptive endometrium cells and repelling it. Moreover, they show blastoids specifically attach to OFELs with their polar TE region. This is the region of the TE that directly borders on the EPI cluster. Kagawa et al. generated several types of trophospheres, which are blastoids without an EPI compartment, and none of these trophospheres were unable to attach to receptive OFELs, neither did post-implantation stage TSCs and human PSC aggregates. Thus Kagawa et al. provide evidence that the TE receives cues from the EPI that enable it to interact with the endometrium. *In silico* ligand-receptor pair analysis performed by Kagawa et al. using single-cell transcriptomics data yielded a list of potential molecular interactions between TE and endometrium epithelium, which may provide clues for future studies on implantation.

All in all, both mouse and human blastoids, despite the abundance of off-target cell types detected, especially in some of the current human models, already show great potential for



investigating pre-implantation processes, such as polarization and cavitation. Notably, Kagawa et al. demonstrated that human blastoids can be used to model implantation *in vitro* when combined with maternal endometrium epithelium cell types. Although it remains unknown whether blastoids fully mimic pre-implantation development while their lineage specification remains (partially) incomplete, current results indicate that some processes underlying blastocyst formation *in vivo* may be faithfully recapitulated *in vitro*.

## CONCLUSION AND PROSPECTS

There can be little doubt that blastoids are a valuable addition to the collection of stem cell-based models. Compared to other stem cell-based embryo-like structures, including gastruloids, 2D micropatterned stem cells, post-implantation amniotic sac embryoids and embryonic-extraembryonic fusion embryoids [reviewed in Fu et al. (2021), Shankar et al. (2021)], blastoids have the unique potential to recapitulate the pre-implantation embryo and are therefore the singular model for studying this early stage of development *in vitro*.

The development of mouse blastoids several years ago has paved the way for the recent development of the human blastoid model. Although there are clear differences between mouse and human in terms of signaling pathway regulation, they share similar core signaling pathways that are tightly regulated during early embryogenesis. This knowledge has guided studies towards medium compositions that are now used to induce the three founding blastocyst lineages in the human blastoid. Moreover, microwell culture platforms first applied to mouse models, as well as several lineage markers originally identified in mice have been adopted for the human system as well. Improvements are still required for blastoids to more convincingly mimic peri- and post-implantation development, particularly regarding the extra-embryonic mesoderm, HYPO and TE compartments. Nevertheless, the first results are promising, as they show that the current models undergo morphological changes and upon attachment partly mimic the architecture of post-implantation embryonic and several extra-embryonic structures *in vitro*. More importantly, pre-implantation development is at least partially recapitulated and blastoids can be used to study cell-cell interactions typical for the blastocyst stage as well as molecular pathways involved in lineage specification.

The possibility of mimicking the pre-implantation embryo has huge implications for a plethora of studies, such as aneuploidy studies, toxicity screens, development of improved IVF compounds and studies on peri-implantation cell differentiation. Combined with more sophisticated, bioengineered *in vitro* models of the uterine wall, human blastoids may become an attractive tool for studying the process of implantation in humans. New insights in this area will indubitably deepen our understanding of key requirements

for successful implantation and subsequently aid the development of new contraceptives and therapeutic routes towards treating implantation failure in the future.

The introduction of the human blastoids to the arena of stem cell-based embryo models does certainly not make the mouse models redundant, however. On the contrary, increasingly meaningful comparisons can be made as these models are further developed to more faithfully recapitulate early embryogenesis. Comparisons between mice and human embryogenesis are relevant from an evolutionary perspective, but may also serve the field of medicine, particularly when considering implantation-related complications, as mentioned above. The more extensively studied mouse model may provide more clues for specific pathways and mechanisms to probe in the human system, saving both time and human material. Moreover, while the first reports of human blastoids have sparked debates on the ethical restrictions on research performed with human embryo (-like) structures (Pereira Daoud et al., 2020; Clark et al., 2021), the mouse embryo models may remain the favored models for more ethically challenging experiments, e.g., involving gene-editing techniques. Additionally, mouse models may be able to help chart post-implantation to a stage that human models will not be allowed to reach for ethical and legal reasons, such as *in vitro* and *in utero* advanced organogenesis or organismal development. In conclusion, these two model systems will continue to develop alongside each other and together have broad future application, both for fundamental and clinical research.

## AUTHOR CONTRIBUTIONS

DL, SG, and EV wrote the manuscript. VS collected and processed the data for the different blastoid protocols. CB helped to direct the manuscript. All the authors discussed and corrected the manuscript. SG and EV contributed equally to the manuscript.

## FUNDING

This research has received funding from the European Research Council (ERC) under the European Union's Horizon 2020 Research and Innovation Programme grant agreement No 694801. The authors gratefully acknowledge the Gravitation Program "Materials Driven Regeneration", funded by the Netherlands Organization for Scientific Research (024.003.013).

## ACKNOWLEDGMENTS

The authors acknowledge financial support from Stichting De Weijerhorst and from the Dutch Province of Limburg (program "Limburg INvesteert in haar Kenniseconomie/LINK").

## REFERENCES

- Allen, B. L., and Rapraeger, A. C. (2003). Spatial and Temporal Expression of Heparan Sulfate in Mouse Development Regulates FGF and FGF Receptor Assembly. *J. Cel Biol.* 163, 637–648. doi:10.1083/jcb.200307053
- Amita, M., Adachi, K., Alexenko, A. P., Sinha, S., Schust, D. J., Schulz, L. C., et al. (2013). Complete and Unidirectional Conversion of Human Embryonic Stem Cells to Trophoblast by BMP4. *Proc. Natl. Acad. Sci.* 110, E1212–E1221. doi:10.1073/pnas.1303094110
- Anderson, K. G. V., Hamilton, W. B., Roske, F. V., Azad, A., Knudsen, T. E., Canham, M. A., et al. (2017). Insulin fine-tunes Self-Renewal Pathways Governing Naive Pluripotency and Extra-embryonic Endoderm. *Nat. Cel Biol* 19, 1164–1177. doi:10.1038/ncb3617
- Barzegari, A., Gueguen, V., Omid, Y., Ostadrahimi, A., Nouri, M., and Pavon-Djavid, G. (2020). The Role of Hippo Signaling Pathway and Mechanotransduction in Tuning Embryoid Body Formation and Differentiation. *J. Cel Physiol* 235, 5072–5083. doi:10.1002/jcp.29455
- Basak, S., Dubanchet, S., Zourbas, S., Chaouat, G., and Das, C. (2002). Expression of Pro-inflammatory Cytokines in Mouse Blastocysts during Implantation: Modulation by Steroid Hormones. *Am. J. Reprod. Immunol.* 47, 2–11. doi:10.1034/j.1600-0897.2002.10047.x
- Bayerl, J., Ayyash, M., Shani, T., Manor, Y. S., Gafni, O., Massarwa, R., et al. (2021). Principles of Signaling Pathway Modulation for Enhancing Human Naive Pluripotency Induction. *Cell Stem Cell* 28 (9), 1549–1565. e12. doi:10.1016/j.stem.2021.04.001
- Bedzhov, I., Leung, C. Y., Bialecka, M., and Zernicka-Goetz, M. (2014). *In Vitro* culture of Mouse Blastocysts beyond the Implantation Stages. *Nat. Protoc.* 9, 2732–2739. doi:10.1038/nprot.2014.186
- Blakeley, P., Fogarty, N. M., del Valle, I., Wamaita, S. E., Hu, T. X., Elder, K., et al. (2015). Defining the Three Cell Lineages of the Human Blastocyst by Single-Cell RNA-Seq. *Development* 142, 3151–3165. doi:10.1242/dev.123547
- Boroviak, T., Loos, R., Lombard, P., Okahara, J., Behr, R., Sasaki, E., et al. (2015). Lineage-Specific Profiling Delineates the Emergence and Progression of Naive Pluripotency in Mammalian Embryogenesis. *Developmental Cel* 35, 366–382. doi:10.1016/j.devcel.2015.10.011
- Bredenkamp, N., Stirparo, G. G., Nichols, J., Smith, A., and Guo, G. (2019a). The Cell-Surface Marker Sushi Containing Domain 2 Facilitates Establishment of Human Naive Pluripotent Stem Cells. *Stem Cel Rep.* 12, 1212–1222. doi:10.1016/j.stemcr.2019.03.014
- Bredenkamp, N., Yang, J., Clarke, J., Stirparo, G. G., von Meyenn, F., Dietmann, S., et al. (2019b). Wnt Inhibition Facilitates RNA-Mediated Reprogramming of Human Somatic Cells to Naive Pluripotency. *Stem Cel Rep.* 13, 1083–1098. doi:10.1016/j.stemcr.2019.10.009
- Brons, I. G. M., Smithers, L. E., Trotter, M. W. B., Rugg-Gunn, P., Sun, B., Chuva de Sousa Lopes, S. M., et al. (2007). Derivation of Pluripotent Epiblast Stem Cells from Mammalian Embryos. *Nature* 448, 191–195. doi:10.1038/nature05950
- Castel, G., Meistermann, D., Bretin, B., Firmin, J., Blin, J., Loubersac, S., et al. (2020). Induction of Human Trophoblast Stem Cells from Somatic Cells and Pluripotent Stem Cells. *Cell Rep* 33, 108419. doi:10.1016/j.celrep.2020.108419
- Chan, Y.-S., Göke, J., Ng, J.-H., Lu, X., Gonzales, K. A. U., Tan, C.-P., et al. (2013). Induction of a Human Pluripotent State with Distinct Regulatory Circuitry that Resembles Preimplantation Epiblast. *Cell Stem Cell* 13, 663–675. doi:10.1016/j.stem.2013.11.015
- Chazaud, C., and Yamanaka, Y. (2016). Lineage Specification in the Mouse Preimplantation Embryo. *Development* 143, 1063–1074. doi:10.1242/dev.128314
- Chen, G., Gulbranson, D. R., Hou, Z., Bolin, J. M., Ruotti, V., Probasco, M. D., et al. (2011). Chemically Defined Conditions for Human iPSC Derivation and Culture. *Nat. Methods* 8, 424–429. doi:10.1038/nmeth.1593
- Cinkornpumin, J. K., Kwon, S. Y., Guo, Y., Hossain, I., Sirois, J., Russett, C. S., et al. (2020). Naive Human Embryonic Stem Cells Can Give Rise to Cells with a Trophoblast-like Transcriptome and Methylation. *Stem Cel Rep.* 15, 198–213. doi:10.1016/j.stemcr.2020.06.003
- Clark, A. T., Brivanlou, A., Fu, J., Kato, K., Mathews, D., Niakan, K. K., et al. (2021). Human Embryo Research, Stem Cell-Derived Embryo Models and *In Vitro* Gametogenesis: Considerations Leading to the Revised ISSCR Guidelines. *Stem Cel Rep.* 16, 1416–1424. doi:10.1016/j.stemcr.2021.05.008
- Cockburn, K., and Rossant, J. (2010). Making the Blastocyst: Lessons from the Mouse. *J. Clin. Invest.* 120, 995–1003. doi:10.1172/jci41229
- Coucouvanis, E., and Martin, G. R. (1999). BMP Signaling Plays a Role in Visceral Endoderm Differentiation and Cavitation in the Early Mouse Embryo. *Development* 126, 535–546. doi:10.1242/dev.126.3.535
- Dahéron, L., Opitz, S. L., Zaehres, H., Lensch, W. M., Andrews, P. W., Itskovitz-Eldor, J., et al. (2008). LIF/STAT3 Signaling Fails to Maintain Self-Renewal of Human Embryonic Stem Cells. *STEM CELLS* 22, 770–778. doi:10.1634/stemcells.22-5-770
- De Jaime-Soguero, A., Abreu de Oliveira, W., and Lluis, F. (2018). The Pleiotropic Effects of the Canonical Wnt Pathway in Early Development and Pluripotency. *Genes* 9, 93. doi:10.3390/genes9020093
- Degincerti, A., Croft, G. F., Pietila, L. N., Zernicka-Goetz, M., Siggia, E. D., and Brivanlou, A. H. (2016). Self-organization of the *In Vitro* Attached Human Embryo. *Nature* 533, 251–254. doi:10.1038/nature17948
- Deng, Q., Ramsköld, D., Reinus, B., and Sandberg, R. (2014). Single-cell RNA-Seq Reveals Dynamic, Random Monoallelic Gene Expression in Mammalian Cells. *Science* 343, 193–196. doi:10.1126/science.1245316
- Devika, A. S., Wruck, W., Adjaye, J., and Sudheer, S. (2019). The Quest for Pluripotency: a Comparative Analysis across Mammalian Species. *Reproduction* 158, R97–R111. doi:10.1530/REP-18-0083
- Dumortier, J. G., Le Verge-Serandour, M., Tortorelli, A. F., Mielke, A., de Plater, L., Turlier, H., et al. (2019). Hydraulic Fracturing and Active Coarsening Position the Lumen of the Mouse Blastocyst. *Science* 365, 465–468. doi:10.1126/science.aaw7709
- Eckert, J. J., McCallum, A., Mears, A., Rumsby, M. G., Cameron, I. T., and Fleming, T. P. (2004a). PKC Signalling Regulates Tight junction Membrane Assembly in the Pre-implantation Mouse Embryo. *Reproduction* 127, 653–667. doi:10.1530/rep.1.00150
- Eckert, J. J., McCallum, A., Mears, A., Rumsby, M. G., Cameron, I. T., and Fleming, T. P. (2004b). Specific PKC Isoforms Regulate Blastocoel Formation during Mouse Preimplantation Development. *Developmental Biol.* 274, 384–401. doi:10.1016/j.ydbio.2004.07.027
- Erlebacher, A., Price, K. A., and Glimcher, L. H. (2004). Maintenance of Mouse Trophoblast Stem Cell Proliferation by TGF- $\beta$ /activin. *Developmental Biol.* 275, 158–169. doi:10.1016/j.ydbio.2004.07.032
- Evans, M. J., and Kaufman, M. H. (1981). Establishment in Culture of Pluripotent Cells from Mouse Embryos. *Nature* 292, 154–156. doi:10.1038/292154a0
- Fan, Y., Min, Z., Alsolami, S., Ma, Z., Zhang, E., Chen, W., et al. (2021). Generation of Human Blastocyst-like Structures from Pluripotent Stem Cells. *Cell Discov* 7, 81. doi:10.1038/s41421-021-00316-8
- Frias-Aldeguez, J., Kip, M., Vivié, J., Li, L., Alemany, A., Korving, J., et al. (2020). *Embryonic Signals Perpetuate Polar-like Trophoblast Stem Cells and Pattern the Blastocyst axis.* bioRxiv, 510362.
- Frum, T., and Ralston, A. (2015). Cell Signaling and Transcription Factors Regulating Cell Fate during Formation of the Mouse Blastocyst. *Trends Genet.* 31, 402–410. doi:10.1016/j.tig.2015.04.002
- Fu, J., Warmflash, A., and Lutolf, M. P. (2021). Stem-cell-based Embryo Models for Fundamental Research and Translation. *Nat. Mater.* 20, 132–144. doi:10.1038/s41563-020-00829-9
- Furue, M. K., Na, J., Jackson, J. P., Okamoto, T., Jones, M., Baker, D., et al. (2008). Heparin Promotes the Growth of Human Embryonic Stem Cells in a Defined Serum-free Medium. *Proc. Natl. Acad. Sci.* 105, 13409–13414. doi:10.1073/pnas.0806136105
- Gafni, O., Weinberger, L., Mansour, A. A., Manor, Y. S., Chomsky, E., Ben-Yosef, D., et al. (2013). Derivation of Novel Human Ground State Naive Pluripotent Stem Cells. *Nature* 504, 282–286. doi:10.1038/nature12745
- Gao, X., Nowak-Imialek, M., Chen, X., Chen, D., Herrmann, D., Ruan, D., et al. (2019). Establishment of Porcine and Human Expanded Potential Stem Cells. *Nat. Cel Biol* 21, 687–699. doi:10.1038/s41556-019-0333-2
- Gardner, R. L., and Johnson, M. H. (1972). An Investigation of Inner Cell Mass and Trophoblast Tissues Following Their Isolation from the Mouse Blastocyst. *J. Embryol. Exp. Morphol.* 28 (2), 279–312. doi:10.1242/dev.28.2.279

- Gardner, R. L., Papaioannou, V. E., and Barton, S. C. (1973). Origin of the Ectoplacental Cone and Secondary Giant Cells in Mouse Blastocysts Reconstituted from Isolated Trophoblast and Inner Cell Mass. *J. Embryol. Exp. Morphol.* 30, 561–572. doi:10.1016/j.jeb.2019.03.001
- Gerri, C., McCarthy, A., Alanis-Lobato, G., Demtschenko, A., Bruneau, A., Loubersac, S., et al. (2020a). Initiation of a Conserved Trophoblast Program in Human, Cow and Mouse Embryos. *Nature* 587, 443–447. doi:10.1038/s41586-020-2759-x
- Gerri, C., Menchero, S., Mahadevaiah, S. K., Turner, J. M. A., and Niakan, K. K. (2020b). Human Embryogenesis: A Comparative Perspective. *Annu. Rev. Cell Dev. Biol.* 36, 411–440. doi:10.1146/annurev-cellbio-022020-024900
- Goldin, S. N., and Papaioannou, V. E. (2003). Paracrine Action of FGF4 during Periimplantation Development Maintains Trophoblast and Primitive Endoderm. *Genesis* 36, 40–47. doi:10.1002/gene.10192
- Guilak, F., Cohen, D. M., Estes, B. T., Gimble, J. M., Liedtke, W., and Chen, C. S. (2009). Control of Stem Cell Fate by Physical Interactions with the Extracellular Matrix. *Cell Stem Cell* 5, 17–26. doi:10.1016/j.stem.2009.06.016
- Guo, G., Stirparo, G. G., Strawbridge, S. E., Spindlow, D., Yang, J., Clarke, J., et al. (2021). Human Naive Epiblast Cells Possess Unrestricted Lineage Potential. *Cell Stem Cell* 28, 1040–1056. e1046. doi:10.1016/j.stem.2021.02.025
- Guo, G., von Meyenn, F., Rostovskaya, M., Clarke, J., Dietmann, S., Baker, D., et al. (2017). Epigenetic Resetting of Human Pluripotency. *Development* 144, 2748–2763. doi:10.1242/dev.146811
- Han, Y. L., Wang, S., Zhang, X., Li, Y., Huang, G., Qi, H., et al. (2014). Engineering Physical Microenvironment for Stem Cell Based Regenerative Medicine. *Drug Discov. Today* 19, 763–773. doi:10.1016/j.drudis.2014.01.015
- Hayashi, Y., Furue, M. K., Tanaka, S., Hirose, M., Wakisaka, N., Danno, H., et al. (2010). BMP4 Induction of Trophoblast from Mouse Embryonic Stem Cells in Defined Culture Conditions on Laminin. *In Vitro Cell.Dev.Biol.-Animal* 46, 416–430. doi:10.1007/s11626-009-9266-6
- Humphrey, R. K., Beattie, G. M., Lopez, A. D., Bucay, N., King, C. C., Firpo, M. T., et al. (2004). Maintenance of Pluripotency in Human Embryonic Stem Cells Is STAT3 Independent. *STEM CELLS* 22, 522–530. doi:10.1634/stemcells.22-4-522
- Io, S., Kabata, M., Iemura, Y., Semi, K., Morone, N., Minagawa, A., et al. (2021). Capturing Human Trophoblast Development with Naive Pluripotent Stem Cells *In Vitro*. *Cell Stem Cell* 28, 1023–1039. e1013. doi:10.1016/j.stem.2021.03.013
- Jain, A., Ezashi, T., Roberts, R. M., and Tuteja, G. (2017). Deciphering Transcriptional Regulation in Human Embryonic Stem Cells Specified towards a Trophoblast Fate. *Sci. Rep.* 7, 17257. doi:10.1038/s41598-017-17614-5
- Kagawa, H., Javali, A., Khoei, H. H., Sommer, T. M., Sestini, G., Novatchkova, M., et al. (2021). Human Blastoids Model Blastocyst Development and Implantation. *Nature* 601 (7894), 600–605. doi:10.1038/s41586-021-04267-8
- Kawagishi, R., Tahara, M., Sawada, K., Ikebuchi, Y., Morishige, K., Sakata, M., et al. (2004). Rho-kinase Is Involved in Mouse Blastocyst Cavity Formation. *Biochem. Biophysical Res. Commun.* 319, 643–648. doi:10.1016/j.bbrc.2004.05.040
- Khan, S. A., Park, K. M., Fischer, L. A., Dong, C., Lungjangwa, T., Jimenez, M., et al. (2021). Probing the Signaling Requirements for Naive Human Pluripotency by High-Throughput Chemical Screening. *Cel Rep* 35, 109233. doi:10.1016/j.celrep.2021.109233
- Kim, H., Wu, J., Ye, S., Tai, C.-I., Zhou, X., Yan, H., et al. (2013). Modulation of  $\beta$ -catenin Function Maintains Mouse Epiblast Stem Cell and Human Embryonic Stem Cell Self-Renewal. *Nat. Commun.* 4, 2403. doi:10.1038/ncomms3403
- Kime, C., Kiyonari, H., Ohtsuka, S., Kohbayashi, E., Asahi, M., Yamanaka, S., et al. (2019). Induced 2C Expression and Implantation-Competent Blastocyst-like Cysts from Primed Pluripotent Stem Cells. *Stem Cell Rep.* 13, 485–498. doi:10.1016/j.stemcr.2019.07.011
- Kime, C., Sakaki-Yumoto, M., Goodrich, L., Hayashi, Y., Sami, S., Derynck, R., et al. (2016). Autotaxin-mediated Lipid Signaling Intersects with LIF and BMP Signaling to Promote the Naive Pluripotency Transcription Factor Program. *Proc. Natl. Acad. Sci. USA* 113, 12478–12483. doi:10.1073/pnas.1608564113
- Kinoshita, M., Barber, M., Mansfield, W., Cui, Y., Spindlow, D., Stirparo, G. G., et al. (2021). Capture of Mouse and Human Stem Cells with Features of Formative Pluripotency. *Cell Stem Cell* 28, 453–471. e458. doi:10.1016/j.stem.2020.11.005
- Kono, K., Tamashiro, D. A. A., and Alarcon, V. B. (2014). Inhibition of RHO-ROCK Signaling Enhances ICM and Suppresses TE Characteristics through Activation of Hippo Signaling in the Mouse Blastocyst. *Developmental Biol.* 394, 142–155. doi:10.1016/j.ydbio.2014.06.023
- Krawchuk, D., Honma-Yamanaka, N., Anani, S., and Yamanaka, Y. (2013). FGF4 Is a Limiting Factor Controlling the Proportions of Primitive Endoderm and Epiblast in the ICM of the Mouse Blastocyst. *Developmental Biol.* 384, 65–71. doi:10.1016/j.ydbio.2013.09.023
- Kubaczka, C., Senner, C., Araújo-Bravo, M. J., Sharma, N., Kuckenberger, P., Becker, A., et al. (2014). Derivation and Maintenance of Murine Trophoblast Stem Cells under Defined Conditions. *Stem Cell Rep.* 2, 232–242. doi:10.1016/j.stemcr.2013.12.013
- Kunath, T., Arnaud, D., Uy, G. D., Okamoto, I., Chureau, C., Yamanaka, Y., et al. (2005). Imprinted X-Inactivation in Extra-embryonic Endoderm Cell Lines from Mouse Blastocysts. *Development* 132, 1649–1661. doi:10.1242/dev.01715
- Kunath, T., Saba-El-Leil, M. K., Almousailleakh, M., Wray, J., Meloche, S., and Smith, A. (2007). FGF Stimulation of the Erk1/2 Signalling cascade Triggers Transition of Pluripotent Embryonic Stem Cells from Self-Renewal to Lineage Commitment. *Development* 134, 2895–2902. doi:10.1242/dev.02880
- Lanner, F., and Rossant, J. (2010). The Role of FGF/Erk Signaling in Pluripotent Cells. *Development* 137, 3351–3360. doi:10.1242/dev.050146
- Li, J., Wang, G., Wang, C., Zhao, Y., Zhang, H., Tan, Z., et al. (2007). MEK/ERK Signaling Contributes to the Maintenance of Human Embryonic Stem Cell Self-Renewal. *Differentiation* 75, 299–307. doi:10.1111/j.1432-0436.2006.00143.x
- Li, R., Zhong, C., Yu, Y., Liu, H., Sakurai, M., Yu, L., et al. (2019). Generation of Blastocyst-like Structures from Mouse Embryonic and Adult Cell Cultures. *Cell* 179, 687–702. e618. doi:10.1016/j.cell.2019.09.029
- Li, Y., and Parast, M. M. (2014). BMP4 Regulation of Human Trophoblast Development. *Int. J. Dev. Biol.* 58, 239–246. doi:10.1387/ijdb.130341mp
- Linneberg-Agerholm, M., Wong, Y. F., Romero Herrera, J. A., Monteiro, R. S., Anderson, K. G. V., and Brickman, J. M. (2019). Naïve Human Pluripotent Stem Cells Respond to Wnt, Nodal and LIF Signalling to Produce Expandable Naïve Extra-embryonic Endoderm. *Development* 146 (24), dev180620. doi:10.1242/dev.180620
- Liu, X., Tan, J. P., Schröder, J., Aberkane, A., Ouyang, J. F., Mohenska, M., et al. (2021). Modelling Human Blastocysts by Reprogramming Fibroblasts into iBlastoids. *Nature* 591, 627–632. doi:10.1038/s41586-021-03372-y
- Ma, H., Zhai, J., Wan, H., Jiang, X., Wang, X., Wang, L., et al. (2019). *In Vitro* culture of Cynomolgus Monkey Embryos beyond Early Gastrulation. *Science* 366, eaax7890. doi:10.1126/science.aax7890
- Martin, G. R. (1981). Isolation of a Pluripotent Cell Line from Early Mouse Embryos Cultured in Medium Conditioned by Teratocarcinoma Stem Cells. *Proc. Natl. Acad. Sci.* 78, 7634–7638. doi:10.1073/pnas.78.12.7634
- Meistermann, D., Bruneau, A., Loubersac, S., Reignier, A., Firmin, J., François-Campion, V., et al. (2021). Integrated Pseudotime Analysis of Human Pre-implantation Embryo Single-Cell Transcriptomes Reveals the Dynamics of Lineage Specification. *Cell Stem Cell* 28, 1625–1640. e1626. doi:10.1016/j.stem.2021.04.027
- Molè, M. A., Weberling, A., and Zernicka-Goetz, M. (2020). “Comparative Analysis of Human and Mouse Development: From Zygote to Pre-gastrulation,” in *Current Topics in Developmental Biology*. Editor L. Solnica-Krezel (Academic Press), 113–138. doi:10.1016/bs.ctdb.2019.10.002
- Morgani, S. M., and Brickman, J. M. (2015). LIF Supports Primitive Endoderm Expansion during Pre-implantation Development. *Development* 142, 3488–3499. doi:10.1242/dev.125021
- Morgani, S., Nichols, J., and Hadjantonakis, A.-K. (2017). The many Faces of Pluripotency: *In Vitro* Adaptations of a Continuum of *In Vivo* States. *BMC Dev. Biol.* 17, 7. doi:10.1186/s12861-017-0150-4
- Morris, S. A., Grewal, S., Barrios, F., Patankar, S. N., Strauss, B., Buttery, L., et al. (2012). Dynamics of Anterior-Posterior axis Formation in the Developing Mouse Embryo. *Nat. Commun.* 3, 673. doi:10.1038/ncomms1671
- Nakamura, T., Okamoto, I., Sasaki, K., Yabuta, Y., Iwatani, C., Tsuchiya, H., et al. (2016). A Developmental Coordinate of Pluripotency Among Mice, Monkeys and Humans. *Nature* 537, 57–62. doi:10.1038/nature19096
- Nakamura, T., Yabuta, Y., Okamoto, I., Aramaki, S., Yokobayashi, S., Kurimoto, K., et al. (2015). SC3-seq: a Method for Highly Parallel and Quantitative

- Measurement of Single-Cell Gene Expression. *Nucleic Acids Res.* 43, e60. doi:10.1093/nar/gkv134
- Neagu, A., van Genderen, E., Escudero, I., Verwegen, L., Kurek, D., Lehmann, J., et al. (2020). *In Vitro* capture and Characterization of Embryonic Rosette-Stage Pluripotency between Naïve and Primed States. *Nat. Cell Biol.* 22, 534–545. doi:10.1038/s41556-020-0508-x
- Niakan, K. K., Han, J., Pedersen, R. A., Simon, C., and Pera, R. A. R. (2012). Human Pre-implantation Embryo Development. *Development* 139, 829–841. doi:10.1242/dev.060426
- Niakan, K. K., Schrodde, N., Cho, L. T. Y., and Hadjantonakis, A.-K. (2013). Derivation of Extraembryonic Endoderm Stem (XEN) Cells from Mouse Embryos and Embryonic Stem Cells. *Nat. Protoc.* 8, 1028–1041. doi:10.1038/nprot.2013.049
- Nichols, J., Silva, J., Roode, M., and Smith, A. (2009). Suppression of Erk Signalling Promotes Ground State Pluripotency in the Mouse Embryo. *Development* 136, 3215–3222. doi:10.1242/dev.038893
- Norwitz, E. R., Schust, D. J., and Fisher, S. J. (2001). Implantation and the Survival of Early Pregnancy. *N. Engl. J. Med.* 345, 1400–1408. doi:10.1056/nejmra000763
- Okae, H., Toh, H., Sato, T., Hiura, H., Takahashi, S., Shirane, K., et al. (2018). Derivation of Human Trophoblast Stem Cells. *Cell Stem Cell* 22, 50–63. e56. doi:10.1016/j.stem.2017.11.004
- Pereira Daoud, A. M., Popovic, M., Dondorp, W. J., Trani Bustos, M., Bredenoord, A. L., Chuva de Sousa Lopes, S. M., et al. (2020). Modelling Human Embryogenesis: Embryo-like Structures Spark Ethical and Policy Debate. *Hum. Reprod. Update* 26, 779–798. doi:10.1093/humupd/dmaa027
- Petropoulos, S., Edsgård, D., Reinius, B., Deng, Q., Panula, S. P., Codeluppi, S., et al. (2016). Single-Cell RNA-Seq Reveals Lineage and X Chromosome Dynamics in Human Preimplantation Embryos. *Cell* 165, 1012–1026. doi:10.1016/j.cell.2016.03.023
- Posfai, E., Schell, J. P., Janiszewski, A., Rovic, I., Murray, A., Bradshaw, B., et al. (2021). Evaluating Totipotency Using Criteria of Increasing Stringency. *Nat. Cell Biol.* 23, 49–60. doi:10.1038/s41556-020-00609-2
- Rivron, N. C., Frias-Aldeguer, J., Vrij, E. J., Boisset, J.-C., Korving, J., Vivié, J., et al. (2018). Blastocyst-like Structures Generated Solely from Stem Cells. *Nature* 557, 106–111. doi:10.1038/s41586-018-0051-0
- Roode, M., Blair, K., Snell, P., Elder, K., Marchant, S., Smith, A., et al. (2012). Human Hypoblast Formation Is Not Dependent on FGF Signalling. *Developmental Biol.* 361, 358–363. doi:10.1016/j.ydbio.2011.10.030
- Rossant, J., and Tam, P. P. L. (2009). Blastocyst Lineage Formation, Early Embryonic Asymmetries and axis Patterning in the Mouse. *Development* 136, 701–713. doi:10.1242/dev.017178
- Rossant, J., and Tam, P. P. L. (2017). New Insights into Early Human Development: Lessons for Stem Cell Derivation and Differentiation. *Cell Stem Cell* 20, 18–28. doi:10.1016/j.stem.2016.12.004
- Shahbazi, M. N., Jedrusik, A., Vuoristo, S., Recher, G., Hupalowska, A., Bolton, V., et al. (2016). Self-organization of the Human Embryo in the Absence of Maternal Tissues. *Nat. Cell Biol.* 18, 700–708. doi:10.1038/ncb3347
- Shankar, V., Blitterswijk, C., Vrij, E., and Giselsbrecht, S. (2021). From Snapshots to Development: Identifying the Gaps in the Development of Stem Cell-based Embryo Models along the Embryonic Timeline. *Adv. Sci.* 8, 2004250. doi:10.1002/advs.202004250
- Shen, H., Yang, M., Li, S., Zhang, J., Peng, B., Wang, C., et al. (2021). Mouse Totipotent Stem Cells Captured and Maintained through Spliceosomal Repression. *Cell* 184, 2843–2859. e2820. doi:10.1016/j.cell.2021.04.020
- Silva, J., and Smith, A. (2008). Capturing Pluripotency. *Cell* 132, 532–536. doi:10.1016/j.cell.2008.02.006
- Smith, A. (2017). Formative Pluripotency: the Executive Phase in a Developmental Continuum. *Development* 144, 365–373. doi:10.1242/dev.142679
- Sozen, B., Cox, A. L., De Jonghe, J., Bao, M., Hollfelder, F., Glover, D. M., et al. (2019). Self-Organization of Mouse Stem Cells into an Extended Potential Blastoid. *Developmental Cell* 51, 698–712. e698. doi:10.1016/j.devcel.2019.11.014
- Sozen, B., Jorgensen, V., Weatherbee, B. A. T., Chen, S., Zhu, M., and Zernicka-Goetz, M. (2021). Reconstructing Aspects of Human Embryogenesis with Pluripotent Stem Cells. *Nat. Commun.* 12, 5550. doi:10.1038/s41467-021-25853-4
- Taei, A., Rasooli, P., Braun, T., Hassani, S.-N., and Baharvand, H. (2020). Signal Regulators of Human Naïve Pluripotency. *Exp. Cell Res.* 389, 111924. doi:10.1016/j.yexcr.2020.111924
- Taft, R. A. (2008). Virtues and Limitations of the Preimplantation Mouse Embryo as a Model System. *Theriogenology* 69, 10–16. doi:10.1016/j.theriogenology.2007.09.032
- Takaoka, K., and Hamada, H. (2012). Cell Fate Decisions and axis Determination in the Early Mouse Embryo. *Development* 139, 3–14. doi:10.1242/dev.060095
- Takashima, Y., Guo, G., Loos, R., Nichols, J., Ficiz, G., Krueger, F., et al. (2014). Resetting Transcription Factor Control Circuitry toward Ground-State Pluripotency in Human. *Cell* 158, 1254–1269. doi:10.1016/j.cell.2014.08.029
- Tanaka, S., Kunath, T., Hadjantonakis, A.-K., Nagy, A., and Rossant, J. (1998). Promotion of Trophoblast Stem Cell Proliferation by FGF4. *Science* 282, 2072–2075. doi:10.1126/science.282.5396.2072
- Taniguchi, C. M., Emanuelli, B., and Kahn, C. R. (2006). Critical Nodes in Signalling Pathways: Insights into Insulin Action. *Nat. Rev. Mol. Cell Biol.* 7, 85–96. doi:10.1038/nrm1837
- Tesar, P. J., Chenoweth, J. G., Brook, F. A., Davies, T. J., Evans, E. P., Mack, D. L., et al. (2007). New Cell Lines from Mouse Epiblast Share Defining Features with Human Embryonic Stem Cells. *Nature* 448, 196–199. doi:10.1038/nature05972
- Theunissen, T. W., Powell, B. E., Wang, H., Mitalipova, M., Faddah, D. A., Reddy, J., et al. (2014). Systematic Identification of Culture Conditions for Induction and Maintenance of Naïve Human Pluripotency. *Cell Stem Cell* 15, 471–487. doi:10.1016/j.stem.2014.07.002
- Thomson, J. A., Itskovitz-Eldor, J., Shapiro, S. S., Waknitz, M. A., Swiergiel, J. J., Marshall, V. S., et al. (1998). Embryonic Stem Cell Lines Derived from Human Blastocysts. *Science* 282, 1145–1147. doi:10.1126/science.282.5391.1145
- Tojo, M., Hamashima, Y., Hanyu, A., Kajimoto, T., Saitoh, M., Miyazono, K., et al. (2005). The ALK-5 Inhibitor A-83-01 Inhibits Smad Signaling and Epithelial-To-Mesenchymal Transition by Transforming Growth Factor-Beta. *Cancer Sci.* 96, 791–800. doi:10.1111/j.1349-7006.2005.00103.x
- Tyler, R. C. V., Mahammadov, E., Nakanoh, S., Vallier, L., Scialdone, A., and Srinivas, S. (2020/2020). A Spatially Resolved Single Cell Atlas of Human Gastrulation. *bioRxiv* 2007, 213512. doi:10.1101/2020.07.21.213512v1
- Ueda, Y., Kimura-Yoshida, C., Mochida, K., Tsume, M., Kameo, Y., Adachi, T., et al. (2020). Intrauterine Pressures Adjusted by Reichert's Membrane Are Crucial for Early Mouse Morphogenesis. *Cell Rep.* 31, 107637. doi:10.1016/j.celrep.2020.107637
- Vianello, S., and Lutolf, M. P. (2019). Understanding the Mechanobiology of Early Mammalian Development through Bioengineered Models. *Developmental Cell* 48, 751–763. doi:10.1016/j.devcel.2019.02.024
- Vrij, E. J., Scholte op Reimer, Y. S., Frias Aldeguer, J., Misteli Guerreiro, I., Kind, J., Koo, B.-K., et al. (2019). Chemically-defined Induction of a Primitive Endoderm and Epiblast-like Niche Supports post-implantation Progression from Blastoids. *bioRxiv* 1, 510396. doi:10.1101/510396
- Vrij, E., Rouwkema, J., LaPointe, V., van Blitterswijk, C., Truckenmüller, R., and Rivron, N. (2016). Directed Assembly and Development of Material-free Tissues with Complex Architectures. *Adv. Mater.* 28, 4032–4039. doi:10.1002/adma.201505723
- Ware, C. B., Nelson, A. M., Mecham, B., Hesson, J., Zhou, W., Jonlin, E. C., et al. (2014). Derivation of Naïve Human Embryonic Stem Cells. *Proc. Natl. Acad. Sci.* 111, 4484–4489. doi:10.1073/pnas.1319738111
- Watanabe, K., Ueno, M., Kamiya, D., Nishiyama, A., Matsumura, M., Wataya, T., et al. (2007). A ROCK Inhibitor Permits Survival of Dissociated Human Embryonic Stem Cells. *Nat. Biotechnol.* 25, 681–686. doi:10.1038/nbt1310
- Weinberger, L., Ayyash, M., Novershtern, N., and Hanna, J. H. (2016). Dynamic Stem Cell States: Naïve to Primed Pluripotency in Rodents and Humans. *Nat. Rev. Mol. Cell Biol.* 17, 155–169. doi:10.1038/nrm.2015.28
- Weinberger, L., Ayyash, M., Novershtern, N., and Hanna, J. H. (2015). Understanding Stem Cell States: Naïve to Primed Pluripotency in Rodents and Humans. *bioRxiv* 1, 030676. doi:10.1101/030676
- Williams, R. L., Hilton, D. J., Pease, S., Willson, T. A., Stewart, C. L., Gearing, D. P., et al. (1988). Myeloid Leukaemia Inhibitory Factor Maintains the Developmental Potential of Embryonic Stem Cells. *Nature* 336, 684–687. doi:10.1038/336684a0
- Xiang, L., Yin, Y., Zheng, Y., Ma, Y., Li, Y., Zhao, Z., et al. (2020). A Developmental Landscape of 3D-Cultured Human Pre-gastrulation Embryos. *Nature* 577, 537–542. doi:10.1038/s41586-019-1875-y



- Xu, R.-H., Chen, X., Li, D. S., Li, R., Addicks, G. C., Glennon, C., et al. (2002). BMP4 Initiates Human Embryonic Stem Cell Differentiation to Trophoblast. *Nat. Biotechnol.* 20, 1261–1264. doi:10.1038/nbt761
- Xu, R.-H., Peck, R. M., Li, D. S., Feng, X., Ludwig, T., and Thomson, J. A. (2005). Basic FGF and Suppression of BMP Signaling Sustain Undifferentiated Proliferation of Human ES Cells. *Nat. Methods* 2, 185–190. doi:10.1038/nmeth744
- Yamanaka, Y., Lanner, F., and Rossant, J. (2010). FGF Signal-dependent Segregation of Primitive Endoderm and Epiblast in the Mouse Blastocyst. *Development* 137, 715–724. doi:10.1242/dev.043471
- Yan, L., Yang, M., Guo, H., Yang, L., Wu, J., Li, R., et al. (2013). Single-cell RNA-Seq Profiling of Human Preimplantation Embryos and Embryonic Stem Cells. *Nat. Struct. Mol. Biol.* 20, 1131–1139. doi:10.1038/nsmb.2660
- Yanagida, A., Spindlow, D., Nichols, J., Dattani, A., Smith, A., and Guo, G. (2021). Naive Stem Cell Blastocyst Model Captures Human Embryo Lineage Segregation. *Cell Stem Cell* 28 (6), 1016–1022. e4. doi:10.1016/j.stem.2021.04.031
- Yang, J., Ryan, D. J., Wang, W., Tsang, J. C.-H., Lan, G., Masaki, H., et al. (2017a). Establishment of Mouse Expanded Potential Stem Cells. *Nature* 550, 393–397. doi:10.1038/nature24052
- Yang, Y., Liu, B., Xu, J., Wang, J., Wu, J., Shi, C., et al. (2017b). Derivation of Pluripotent Stem Cells with *In Vivo* Embryonic and Extraembryonic Potency. *Cell* 169, 243–257. e225. doi:10.1016/j.cell.2017.02.005
- Yilmaz, A., and Benvenisty, N. (2019). Defining Human Pluripotency. *Cell Stem Cell* 25, 9–22. doi:10.1016/j.stem.2019.06.010
- Ying, Q.-L., Wray, J., Nichols, J., Batlle-Morera, L., Doble, B., Woodgett, J., et al. (2008). The Ground State of Embryonic Stem Cell Self-Renewal. *Nature* 453, 519–523. doi:10.1038/nature06968
- Young, S. L. (2013). Oestrogen and Progesterone Action on Endometrium: a Translational Approach to Understanding Endometrial Receptivity. *Reprod. BioMedicine Online* 27, 497–505. doi:10.1016/j.rbmo.2013.06.010
- Yu, C., Ji, S.-Y., Dang, Y.-J., Sha, Q.-Q., Yuan, Y.-F., Zhou, J.-J., et al. (2016). Oocyte-expressed Yes-Associated Protein Is a Key Activator of the Early Zygotic Genome in Mouse. *Cell Res* 26, 275–287. doi:10.1038/cr.2016.20
- Yu, L., Wei, Y., Duan, J., Schmitz, D. A., Sakurai, M., Wang, L., et al. (2021). Blastocyst-like Structures Generated from Human Pluripotent Stem Cells. *Nature* 591, 620–626. doi:10.1038/s41586-021-03356-y
- Zhang, S., Chen, T., Chen, N., Gao, D., Shi, B., Kong, S., et al. (2019). Implantation Initiation of Self-Assembled Embryo-like Structures Generated Using Three Types of Mouse Blastocyst-Derived Stem Cells. *Nat. Commun.* 10, 496. doi:10.1038/s41467-019-08378-9
- Zhao, C., Reyes, A. P., Schell, J. P., Weltner, J., Ortega, N., Zheng, Y., et al. (2021/2021). Reprogrammed iBlastoids Contain Amnion-like Cells but Not Trophectoderm. *bioRxiv* 2005, 442980. doi:10.1101/2021.05.07.442980
- Zheng, Y., Xue, X., Shao, Y., Wang, S., Esfahani, S. N., Li, Z., et al. (2019). Controlled Modelling of Human Epiblast and Amnion Development Using Stem Cells. *Nature* 573, 421–425. doi:10.1038/s41586-019-1535-2
- Zhou, F., Wang, R., Yuan, P., Ren, Y., Mao, Y., Li, R., et al. (2019). Reconstituting the Transcriptome and DNA Methylome Landscapes of Human Implantation. *Nature* 572, 660–664. doi:10.1038/s41586-019-1500-0
- Zhu, M., Shahbazi, M. N., Martin, A., Zhang, C., Sozen, B., Borsos, M., et al. (2020/2020). Mechanism of Cell Polarisation and First Lineage Segregation in the Human Embryo. *bioRxiv* 2009, 1. doi:10.1101/2020.09.23.310680v1

**Conflict of Interest:** The authors declare that the research was conducted in the absence of any commercial or financial relationships that could be construed as a potential conflict of interest.

**Publisher's Note:** All claims expressed in this article are solely those of the authors and do not necessarily represent those of their affiliated organizations, or those of the publisher, the editors and the reviewers. Any product that may be evaluated in this article, or claim that may be made by its manufacturer, is not guaranteed or endorsed by the publisher.

Copyright © 2022 Luijckx, Shankar, van Blitterswijk, Giselbrecht and Vrij. This is an open-access article distributed under the terms of the Creative Commons Attribution License (CC BY). The use, distribution or reproduction in other forums is permitted, provided the original author(s) and the copyright owner(s) are credited and that the original publication in this journal is cited, in accordance with accepted academic practice. No use, distribution or reproduction is permitted which does not comply with these terms.



# Integrative Single-Cell RNA-Seq and ATAC-Seq Analysis of Mesenchymal Stem/Stromal Cells Derived from Human Placenta

Jinlu Li<sup>1,2†</sup>, Quanlei Wang<sup>2,3†</sup>, Yanru An<sup>2</sup>, Xiaoyan Chen<sup>2</sup>, Yanan Xing<sup>1,2</sup>, Qiuting Deng<sup>1,2</sup>, Zelong Li<sup>1,2</sup>, Shengpeng Wang<sup>1,2</sup>, Xi Dai<sup>1,2</sup>, Ning Liang<sup>2</sup>, Yong Hou<sup>2</sup>, Huanming Yang<sup>2,4</sup> and Zhouchun Shang<sup>1,2,5\*</sup>

## OPEN ACCESS

### Edited by:

Mo Li,  
King Abdullah University of Science  
and Technology, Saudi Arabia

### Reviewed by:

Xi Chen,  
Southern University of Science and  
Technology, China  
Hongmei Wang,  
Institute of Zoology (CAS), China

### \*Correspondence:

Zhouchun Shang  
shangzhouchun@genomics.cn

<sup>†</sup>These authors have contributed  
equally to this work and share first  
authorship

### Specialty section:

This article was submitted to  
Stem Cell Research,  
a section of the journal  
Frontiers in Cell and Developmental  
Biology

**Received:** 16 December 2021

**Accepted:** 09 February 2022

**Published:** 05 April 2022

### Citation:

Li J, Wang Q, An Y, Chen X, Xing Y,  
Deng Q, Li Z, Wang S, Dai X, Liang N,  
Hou Y, Yang H and Shang Z (2022)  
Integrative Single-Cell RNA-Seq and  
ATAC-Seq Analysis of Mesenchymal  
Stem/Stromal Cells Derived from  
Human Placenta.  
Front. Cell Dev. Biol. 10:836887.  
doi: 10.3389/fcell.2022.836887

<sup>1</sup>College of Life Sciences, University of Chinese Academy of Sciences, Beijing, China, <sup>2</sup>BGI-Shenzhen, Shenzhen, China, <sup>3</sup>Key Laboratory of Regenerative Medicine of Ministry of Education, Biology Postdoctoral Research Station, Jinan University, Guangzhou, China, <sup>4</sup>James D. Watson Institute of Genome Sciences, Hangzhou, China, <sup>5</sup>BGI College, Northwest University, Xi'an, China

Mesenchymal stem/stromal cells derived from placenta (PMSCs) are an attractive source for regenerative medicine because of their multidifferentiation potential and immunomodulatory capabilities. However, the cellular and molecular heterogeneity of PMSCs has not been fully characterized. Here, we applied single-cell RNA sequencing (scRNA-seq) and assay for transposase-accessible chromatin sequencing (scATAC-seq) techniques to cultured PMSCs from human full-term placenta. Based on the inferred characteristics of cell clusters, we identify several distinct subsets of PMSCs with specific characteristics, including immunomodulatory-potential and highly proliferative cell states. Furthermore, integrative analysis of gene expression and chromatin accessibility showed a clearer chromatin accessibility signature than those at the transcriptional level on immunomodulatory-related genes. Cell cycle gene-related heterogeneity can be more easily distinguished at the transcriptional than the chromatin accessibility level in PMSCs. We further reveal putative subset-specific *cis*-regulatory elements regulating the expression of immunomodulatory- and proliferation-related genes in the immunomodulatory-potential and proliferative subpopulations, respectively. Moreover, we infer a novel transcription factor *PRDM1*, which might play a crucial role in maintaining immunomodulatory capability by activating *PRDM1*-regulon loop. Collectively, our study first provides a comprehensive and integrative view of the transcriptomic and epigenomic features of PMSCs, which paves the way for a deeper understanding of cellular heterogeneity and offers fundamental biological insight of PMSC subset-based cell therapy.

**Keywords:** single-cell RNA-seq, single-cell ATAC-seq, human placenta, cell heterogeneity, mesenchymal stem cells, immunomodulatory-potential

## INTRODUCTION

Mesenchymal stem/stromal cells (MSCs) are promising cell candidates for regenerative medicine and cell therapy owing to their differentiation potential and cytokine regulation capability. For multidirectional differentiation, MSCs can differentiate into mesodermal lineage cells, such as adipocytes, osteocytes, and chondrocytes, as well as other cell lineages, such as endodermic and neuroectodermic cells (Petersen et al., 1999; Macias et al., 2010). In addition, MSCs have broad anti-inflammatory and immunomodulation properties as they can secrete several cytokines, such as growth factors or anti-inflammatory mediators, to modulate immune cell populations (Shi et al., 2018; Pittenger et al., 2019). Substantial progress has been made in the exploration of MSCs in regenerative and immunomodulation treatment (Rodríguez-Fuentes et al., 2021). Recently published phase I/II clinical trials about MSCs infusion in COVID-19 patients show that MSC infusion is safe and well-tolerated (Guo Z. et al., 2020; Feng et al., 2020; Meng et al., 2020), and it shows an efficient improvement trend in patients and reduces the mortality rate (Shu et al., 2020). Meanwhile, patients with MSC infusion show a faster recovery and significantly elevated lymphocyte counts (Guo Z. et al., 2020; Shu et al., 2020) and improvements in CD4<sup>+</sup> T cells, CD8<sup>+</sup> T cells, and NK cell counts (Feng et al., 2020), indicating significant immunomodulation effects of MSCs.

MSCs can be isolated from various tissues (da Silva Meirelles et al., 2006), such as bone marrow (Prockop, 1997), adipose tissue (Zuk et al., 2003), umbilical cord (Romanov et al., 2003), and placenta (Fukuchi et al., 2004). Placenta-derived MSCs (PMSCs) are differentiated toward the neural lineages, such as neurons, oligodendrocytes (Portmann-Lanz et al., 2010), glial cells (Martini et al., 2013), and dopaminergic neurons (Chen et al., 2009). In addition, PMSCs show more attractive characteristics for cellular therapy and transplantation than other tissue-derived MSCs owing to their abundance, easy accessibility, fewer ethical concerns, noninvasiveness to the donors, and low immunogenicity *in vitro* and *in vivo* (Bailo et al., 2004; Yen et al., 2005; Vegh et al., 2013). Furthermore, PMSCs show an additional immunomodulatory capability over bone marrow, adipose, and umbilical MSCs (Lee et al., 2012; Talwadekar et al., 2015). Thus, PMSCs are widely applied to preclinical and clinical trials, including cardiovascular, neurological, bone and cartilage, and intestinal inflammatory diseases (Torre et al., 2019). To date, 54 clinical trials involving PMSCs are registered on ClinicalTrials.gov.

Previous works reveal that MSCs are heterogeneous under seeming homogeneity within and across different tissues at single-cell resolution (Zheng et al., 2020). The heterogeneity of MSCs may affect the therapeutic effect and give rise to inconsistencies in MSC-based clinical trials (Phinney, 2012). The use of certain functional subpopulations of MSCs may reduce the presence of interfering cells in an attempt to improve their particular ability for certain situations (Mo et al., 2016) while advanced insights into their properties and optimal selection for clinical indications require a deeper understanding of the molecular processes involved in MSCs.

Therefore, there is a necessity to understand the full repertoire of MSCs and their gene expression profiles and accessible chromatin profile characteristics as the most basic and critical step to design more effective therapy strategies.

Single-cell sequencing, including single-cell RNA sequencing (scRNA-seq) and assay for transposase-accessible chromatin sequencing (scATAC-seq) are powerful tools to explore the molecular and cellular heterogeneity of MSCs derived from various tissues. It is reported that MSCs derived from umbilical cords possess limited heterogeneity during *in vitro* expansion by analysis of 361 culture-expanded MSCs and proved that cell heterogeneity is dominated by cell cycle status (Huang et al., 2019). It is reported that heterogeneity of gene expression and distinct subpopulations exist in human primary Wharton's jelly-derived MSCs by scRNA-seq (Sun et al., 2020). Moreover, our previous study reveals molecular heterogeneity in human umbilical cord tissue and culture-expanded MSCs using scRNA-seq (Wang et al., 2021). However, unlike the bone marrow-, adipose-, and umbilical cord-derived MSCs (Liu et al., 2019; Sun et al., 2020; Wang et al., 2021), our knowledge about the heterogeneity of PMSCs at the single-cell level is still limited, especially the intersection between transcriptome and chromatin accessibility. Here, we integrate scRNA-seq and scATAC-seq tools to explore the molecular processes involved in PMSCs and provide a comprehensive and advanced resource revealing the cellular heterogeneity of PMSCs at single cell multiomics level.

## MATERIALS AND METHODS

### Single-Cell Dissociation and Cell Culture

The human full-term placenta from five donors were mechanically separated before serial enzyme digestions as previously reported (Fukuchi et al., 2004). Briefly, the placenta villus tissue was washed using DPBS 2–3 times and sliced into 2 mm<sup>3</sup> or smaller fragments. Then, the samples were dissociated in Dulbecco's modified Eagle medium (DMEM, Gibco) with 100 U/ml collagenase type IV and 1% penicillin streptomycin solution (P/S). After 1 h of incubation at 37°C, 0.05% TrypLE™ Express (Thermo Fisher Scientific) was added for another 15 min incubation. The dissociation was terminated by adding 2 ml standard MSC culture medium (DMEM +10% FBS +2 mM Gln +1% P/S). Cell suspension was centrifugated at 300 g for 5 min, and the supernatant was discarded. The cell pellet was resuspended in standard MSC culture medium and cultured at 37°C in a 5% CO<sub>2</sub> incubator. The cells were dissociated using TrypLE™ Express and passaged every 2–3 days five times. Cells were harvested when reaching around 80% confluence at passage 5.

### Library Preparation for scRNA-Seq and scATAC-Seq

The PMSCs at passage five were filtered through a 40 µm cell strainer and washed twice using DPBS before trypan blue staining. Then, the cell suspension with 80% viability or above

was processed using 10X Genomics GemCode Single Cell Platform in 0.4% BSA-DPBS at  $8 \times 10^5$  cells/ml. Briefly, 10,000 cells from each sample were loaded to respective channels. The cells were then partitioned into gel beads in emulsion in the GemCode instrument, followed by reverse transcription, cDNA amplification, shearing, and adaptor-sample index attachment. Then, the 10X Genomics libraries were further prepared for the DNBSEQ platform as previously reported (Wang et al., 2021). Briefly, the single-cell libraries were amplified using 10 cycles of polymerase chain reaction (PCR) and circularized by incubating with splint oligo (BGI) and T4 DNA ligase (BGI), followed by fragment size selection with PEG32 (BGI), rolling circle amplification (RCA), and sequenced using 100 bp paired-end on the DNBSEQ platform.

The PMSCs at passage 5 (from three of a total five samples in our study) were filtered through a 40- $\mu$ m cell strainer, and the cell suspension with 80% viability or above was lysed and nuclei prepared based on a previous study (Yu et al., 2021). Approximately 100,000 nuclei were mixed with 25  $\mu$ l transposition reaction mixture containing 10 mM TAPS-NaOH (pH 8.5), 5 mM MgCl<sub>2</sub>, 10% DMF, and 4  $\mu$ l of in-house Tn5 transposase. Then, they were subjected for single-cell ATAC library preparation using the DNBelab C Series Single-Cell ATAC Library Prep Set (MGI, #1000021878), which includes droplet encapsulation, preamplification, emulsion breakage, ATAC reads captured beads collection, DNA amplification, and purification. The single cell ATAC sequencing libraries were sequenced on the DNBSEQ platform at China National GeneBank (CNGB). Read structure was 70 bp for read1, inclusive of 10 bp cell barcode1, 10 bp cell barcode2, and 50 bp insert DNA; 50 bp for read2, and 10 bp for sample index.

## Flow Cytometry

The culture-expanded PMSCs at passage 5 were harvested and dissociated into single cells by 0.05% TrypLE™ Express. To determine cell surface antigen expression, the cells were processed with the Human MSC Analysis Kit (BD Stemflow™) and incubated with antibodies, including CD73, CD90, CD105, CD34, CD45, CD11b, CD19, and HLA-DR. Upon completion of the incubation, the cells were analyzed using a flow cytometer (BD Biosciences) and gated by forward and side scatter.

## Immunofluorescence Staining

PMSCs at passage 5 were fixed in 4% paraformaldehyde in PBS for 10 min and permeabilized with 0.5% Triton X-100 in PBS for 5 min at room temperature. After 120 min blocking with 3% BSA (SIGMA), cells were incubated with primary antibody overnight at 4°C. The next day, cells were washed and stained with secondary antibodies (1:300, goat antirabbit IgG-Cy3; or 1:300, goat antimouse IgG-FITC) for 60 min at room temperature and then washed three times with phosphate-buffered saline (PBS). The primary antibodies for respective cells include PRDM1 (1:100, Abcam), CXCL8 (1:300, SANTA CRUZ), TOP2A (1:200, Abcam), MKI67 (1:100, Abcam), DEDD2 (1:100, Abcam), THY1 (1:100, Abcam), CITED2 (1:100, Abcam), and IGFBP6 (1:100, Abcam). Cell nuclei were counterstained with DAPI (4',6-

diamidino-2-phenylindole) (1:500). The images were captured using Olympus IX73 and further analyzed with ImageJ software.

## Single-Cell RNA Sequencing and Data Processing

Single-cell RNA-seq FASTQ data were aligned to the GRCh38 human genome, and unique molecular identifiers (UMIs) were counted by Cell Ranger Software (Zheng et al., 2017) (cellranger-2.0.0, 10x Genomics). Genes that were expressed in less than 0.1% of total cells were removed. Cells with a detected gene number less than 800 or percentage of reads that mapped to the mitochondrial genome higher than 10% were filtered out. In addition, cells defined as outliers using a boxplot for gene number statistics were also removed. Data normalization, highly variable feature identification, dimensionality reduction, clustering, and tSNE visualization were performed with the Seurat 3.2 R package (Stuart et al., 2019). Differentially expressed genes (DEGs) of each cluster were defined by the FindAllMarkers function in Seurat with the parameter test.use = "bimod." The aample batch effect was corrected by the IntegrateData function, cell cycle phase assignment for each cell was generated by the CellCycleScoring function, and the cell cycle batch effect was corrected by the ScaleData function with the parameter vars.to.regress = "CC.Difference" within Seurat. Constructing the trajectory and ordering single cells in pseudotime were performed with monocle (Qiu et al., 2017) (Version 2.10.1) using the top 2500 highly variable genes found by Seurat. Cluster0, one, and two were down-sampled to have the same cell number as Cluster3.

## Single-Cell ATAC Sequencing and Data Processing

The raw sequencing reads were processed by PISA<sup>1</sup> and aligned to the hg38 reference genome by the BWA mem function (Li, 2013) and then deconvoluted using bap2 (Lareau et al., 2019) to create the fragment file of each scATAC-seq library for the following analysis. The TSS enrichment score and fragments of each single cell were calculated by ArchR (Granja et al., 2021) (version 0.9.5). Cells with a TSS score less than 4 or total fragments fewer than 1000 were filtered. Then, we filtered doublets based on the doublet score calculated by the function "addDoubletScores" and "filterDoublets" in ArchR. The parameter "filterRatio = 2" was used. Dimensionality reduction and clustering were also performed with ArchR using an iterative latent semantic indexing (LSI) clustering. Briefly, we created 500-bp windows tiled across the genome and determined whether each cell was accessible within each window. Next, we performed LSI dimensionality reduction with parameter "iterations = 7, dimsToUse = 1:15 sampleCells = 15,000" using the addIterativeLSI function followed by Harmony (Thi et al., 2020) for sample batch correction. Then, Seurat's FindClusters function with parameters "reducedDims = 'Harmony', method = 'Seurat', resolution = 0.1" was used for clustering. Gene scores were

<sup>1</sup><https://github.com/shiquan/PISA>



calculated by the `addGeneScoreMatrix` function with default parameters, and the different gene scores of each cluster were calculated by `getMarkerFeatures` function using ArchR. For each cluster, peak calling on the Tn5-corrected insertions (each end of the Tn5-corrected fragments) was performed using the MACS2 (Zhang et al., 2008) `callpeak` command with the default parameters. Then, the marker peaks of each cluster were defined by the `getMarkerFeatures` function, and Motif enrichment was performed by the `FindMotifs` function in Signac (Stuart et al., 2020) (Version 1.1) with parameter “background = NULL” in the significant marker peaks ( $\text{FDR} \leq 0.01$ ,  $\text{Log2FC} \geq 1$ ). TF activity was measured by `chromVAR` (Schep et al., 2017). Peak-to-gene links were identified by the `addPeak2GeneLinks` function (reducedDims = “Harmony”, `dimsToUse` = 1:15), Only links with  $\text{FDR} < 0.0001$ , `corCutOff`  $> 0.4$ , and `varCutOff`  $> 0.25$  were selected by the `plotPeak2GeneHeatmap` function.

## GO Enrichment Analysis

Gene ontology (GO) term analysis was performed by DAVID (Huang et al., 2009b; 2009a). GO terms with a  $p$ -value less than .05 were considered significantly enriched. The DEGs of each cluster in scRNA-seq and the differentially accessible genes based on gene score were used as input.

## Integration of scRNA-Seq and scATAC-Seq Data and Label Transfer

Integration of scRNA-seq and scATAC-seq was performed by the `FindTransferAnchors` function from the Seurat package. Briefly, it can align cells from scATAC-seq with cells from scRNA-seq by comparing the scATAC-seq gene score matrix with the scRNA-seq gene expression matrix to capture the shared feature correlation structure between two data sets.

## Transcription Factor Regulons Predicted Using SCENIC

We predicted transcription factor regulons using SCENIC (Aibar et al., 2017) following the standard pipeline as described previously. The gene expression matrix of PMSCs was used as input.

## Hierarchical Clustering Analysis

First, we selected the common genes between the gene expression data matrix and gene score matrix. We then normalized the mean gene expression/accessibility for each cluster to between zero and one using the maximum difference normalization method. Next, we performed hierarchical clustering analysis using the “`hclust`” function based on the Manhattan distance calculated by the “`dist`” function in R.

# RESULTS

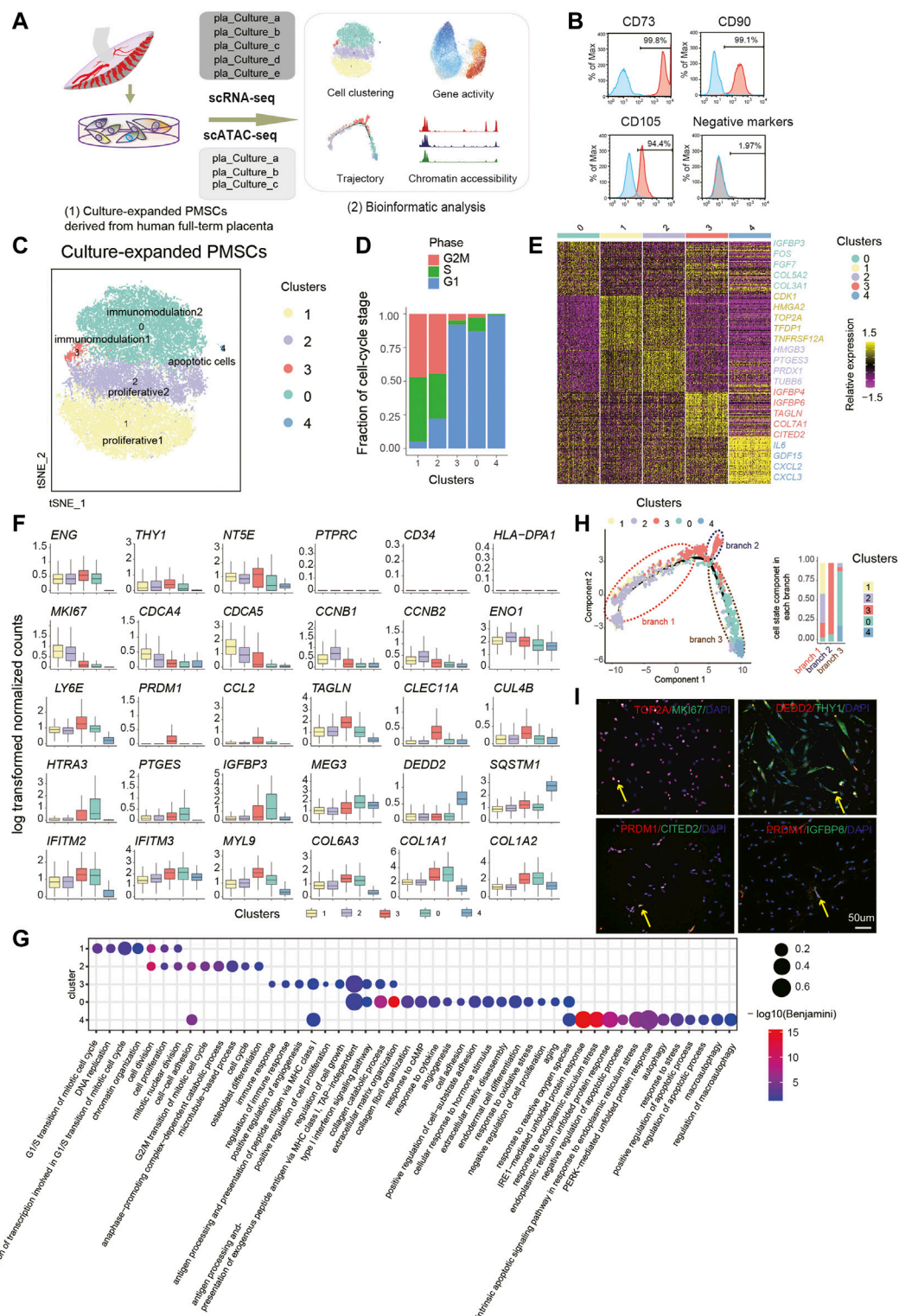
## The heterogeneity of PMSCs Revealed by scRNA-Seq

To explore the heterogeneous states of PMSCs at single-cell resolution, culture-expanded human PMSCs (passage 5) were

subjected to flow cytometry, scRNA-seq ( $n = 5$ , `pla_Culture_a/b/c/d/e`) and scATAC-seq ( $n = 3$ , `pla_Culture_a/b/c`) (Figure 1A). The flow cytometry results show high expression levels of MSC positive markers in PMSCs, including CD105 (ENG), CD73 (NT5E), and CD90 (THY1), and a lack of expression of MSC negative markers, including CD45 (PTPRC), CD34, CD11b (ITGAM), and HLA-DR (Figure 1B), which is consistent with the standard criteria for defining MSCs according to the International Society for Cellular Therapy (ISCT) in 2006 (Dominici et al., 2006). After quality control (see Methods), we kept 31,219 single cells for further transcriptomic analysis, namely, a median of 62,800 UMI counts, 6832 genes per cell, an average of 6243 cells and 209,769 mean reads per donor (Supplementary Table S1; Supplementary Figure 1B).

To generate a census of PMSCs populations, the sample batch and cell cycle effects were well excluded before deeper data mining (Figure 1D; see Methods). Five PMSC clusters with distinct features were identified based on the DEGs and the GO enrichment analysis (Figure 1C). Intriguingly, the well-known cell proliferation marker MKI67 was highly expressed in both Cluster1 and Cluster2, indicating their high proliferative capacity (Figure 1F). Besides this, genes that are strongly associated with cell proliferation and growth (e.g., *HMGA2* and *TOP2A*) (Yu et al., 2013; Lee and Berger, 2019) and cell division (e.g., *CDCA4* and *CDCA5*) were expressed at high levels in Cluster1 (Figure 1E, F). In Cluster2, we observed that *CCNB1*, *CCNB2*, and *EN O 1* were differently expressed (Figure 1E, F). A previous study shows that *CCNB1* and *CCNB2* are cell-cycle regulatory genes (Gong and Ferrell, 2010), and especially *CCNB1* is predominantly expressed in the G2/M phase of cell division (Xing et al., 2021); moreover, *CCNB1* is a cell-cell adherence term associated gene along with *EN O 1*. In line with the gene expression results above, GO analysis of the DEGs in these two clusters showed several overlapped GO terms, including cell division, cell proliferation, and mitotic nuclear division (Figure 1G). However, Cluster1 DEGs were enriched in the G1/S transition of the mitotic cell cycle and Cluster2 DEGs in the G2/M transition of cell cycle, anaphase of mitosis related terms. Notably, two MSC-featured terms, cell-cell adhesion and osteoblast differentiation potency, were only observed in Cluster2 (Figure 1G). These results suggest that Cluster1 and Cluster2 might be highly proliferative subpopulations. Cluster1 cells could be in a highly proliferative, multipotent progenitor cell state with 94.8% of cells in the G2M/S phase (Figure 1C), and Cluster2 might be in a precommitted MSC cell state, which are poised to differentiated cell state with 77.8% of cells in G2M/S phase (Figure 1C). Above all, we named Cluster1 and Cluster2 as proliferative1 and proliferative2, respectively.

Besides this, we identified two immunomodulatory-related PMSCs subgroups, Cluster3 and Cluster0, which were named as immunomodulation1 and immunomodulation2, respectively. Several well-known immunomodulation-associated genes (e.g., *IFITM2*, *IFITM3*, and *MYL9*) and collagen genes (e.g., *COL6A3*, *COL1A1*, and *COL1A2*) were commonly expressed in both clusters (Figure 1F). Moreover, immunomodulation1 and immunomodulation2 cells showed their own specific immunomodulation signatures. For example, *CCL2*, *PRDM1*,



**FIGURE 1 |** Single-Cell Transcriptome Analysis of PMSC. **(A)** Schematic overview of the workflow. MSCs derived from human placenta were processed for scRNA-seq ( $n = 5$ ) and scATAC-seq ( $n = 3$ ). **(B)** Representative flow cytometric histogram of PMSCs showing the presence of positive MSC markers (CD73, CD90 and CD105) and absence of negative MSC markers (CD34, CD45, CD11b, CD19, and HLA-DR were merged). **(C)** t-SNE visualization of 31,219 PMSC cells from five samples reveals heterogeneous cell states at the single-cell RNA seq level. Each dot represents a single cell ( $n=31,219$ ), colored by its corresponding cluster. **(D)** Bar plot showing the fraction of cell cycle component in each cluster (bottom). **(E)** A heat map shows genes (rows) that are differentially expressed across five clusters, (Continued)

**FIGURE 1** | colored by relative gene expression (z-score). Gold: high expression; Purple: low expression. Representative genes are highlighted ( $p < .05$ ,  $\log FC > 0.25$ , top90 in each cluster). **(F)** Boxplot showing the expression level of selected representative DEGs in five clusters. **(G)** GO terms enrichment of DEGs respective to indicated PMSC clusters. **(H)** Pseudotemporal developmental trajectory of PMSCs inferred by Monocle. Bar plot showing the fraction of each cluster component in each branch (bottom). **(I)** Immunostaining of MKI67, TOP2A, DEDD2, THY1(CD90), PRDM1, CITED2, and IGFBP6 in PMSCs.

and LY6E were specifically highly expressed in immunomodulation1, and HTRA3 and PTGES were solely expressed in immunomodulation2 (**Figure 1F**). All these genes are involved in different immunomodulating processes based on previous studies (Rafei et al., 2008; Fu et al., 2017; Wang T. et al., 2020; Ji et al., 2020; Pfaender et al., 2020) (**Figure 1E**). In line with this, we also observed overlapped features of immunomodulation and extracellular matrix-related GO terms in the two clusters, which are important for the maintenance of MSC functions (**Figure 1G**). Besides this, a few more immunomodulation-related terms were enriched in immunomodulation1, whereas immunomodulation2 showed more significant features in extracellular matrix organization-, collagen formation-, and cell adhesion-related terms (**Figure 1G**).

In addition, immunomodulation2 showed high expression of *FOS*, *IGFBP3*, and *MEG3* (**Figure 1E, F**), which are reported to be involved in promoting MSC differentiation (Komori, 2006; ZHUANG et al., 2015; Deng et al., 2018). In contrast, immunomodulation1 showed high expression of *CLEC11A*, *TAGLN*, *CUL4B*, *IGFBP6*, and *COX7A1* (**Figure 1E, F**). *CLEC11A*, also known as stem cell growth factor, promotes the proliferation and differentiation of hematopoietic stem/progenitor cells (Wang M. et al., 2020). Moreover, studies indicate that *CLEC11A* can promote the proliferation of islet cells and as the potentially pro-osteogenic gene to mark the related adipogenic population (Merrick et al., 2019; Shi et al., 2019). *COX7A1*, as a potential mammalian embryonic-fetal transition (EFT) marker that is upregulated in post-EFT murine and adult stem cells (West et al., 2018), was also highly expressed in immunomodulation1. Previous studies show that the addition of *IGFBP6* significantly increases pluripotency and differentiation-associated markers in PMSCs, and silencing *IGFBP6* decreases both of them (Aboalola and Han, 2017). In addition, knocking down *IGFBP6* in vascular smooth muscle cells significantly reduces cell proliferation and induces S phase arrest in the cell cycle (Wang Z. et al., 2020). In line with this, immunomodulation2-specific genes were more enriched in the negative regulation of cell proliferation, aging, response to reactive oxygen species et al., whereas immunomodulation1 was more related to positive regulation of cell proliferation and regulation of cell growth. All the above results suggest that immunomodulation1 could be related to the immunomodulation capacity cell state that shares many properties with immunomodulation2 but is more energetic, and immunomodulation2 could be in a mature immunomodulation capacity cell state with more committed differentiation.

Meanwhile, we also observed a small group of cells, Cluster4, contributing 0.33% of the total PMSCs cells but with high expression of apoptotic-related genes, including *GDF15*, *SQSTM1*, and *DEDD2*. Besides this, *CXCL2*, *CXCL3*, and *IL-6*/

24 were also highly expressed in this cluster (**Figure 1E, F**). The GO enrichment analysis showed that DEGs upregulated in Cluster4 were highly enriched in autophagy and apoptosis-related terms (**Figure 1G**), which was consistent with apoptotic MSCs showing immunomodulation functions *in vivo* (Galleu et al., 2017). Thus, we inferred that Cluster4 might be an apoptotic cell state.

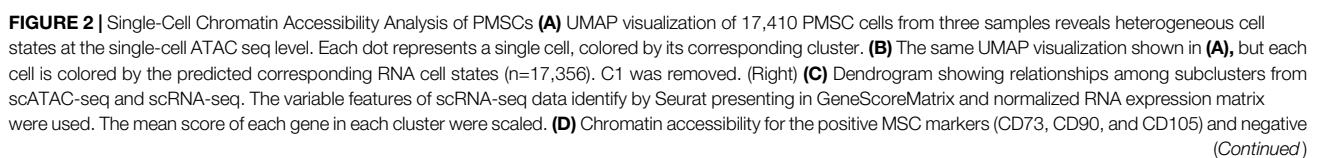
We observed distinct subpopulations with specific molecular features, and a previous study shown that *in vitro* expansion of MSCs induces spontaneous differentiation with expression of developmental markers and tissue-specific genes (Tsai et al., 2011), which inspired us to dissect the trajectory of the above clusters. Thus, we performed the pseudotime analysis using the PMSCs subpopulations. Consistently, our unsupervised trajectory analysis by Monocle2 showed that proliferative1 and proliferative2 were at the root of the trajectory. Immunomodulation1 was located in the middle of the trajectory with a minor branch, and immunomodulation2 was clustered in the further branches with apoptotic cells at the end (**Figure 1H**). The above results, combined with immunostaining of MKI67, TOP2A, PRDM1, CITED2, IGFBP6, DEDD2, and THY1 (**Figure 1I**), clearly showed the heterogeneous cellular states of PMSCs at the single-cell transcriptional level.

## Single-Cell Chromatin Accessibility Landscape of PMSCs

To explore the epigenetic characteristics of PMSCs, we harvested 17,410 scATAC-seq data sets from three individuals (pla\_Culture\_a/b/c) after quality control (**Figure 1A**; see Methods). The integrated single-cell ATAC-seq data set from all three samples showed high numbers of unique nuclear fragments per cell and signal-to-background ratio indicated by transcription start site (TSS) score (**Supplementary Figure 1D**). In addition, the distribution of expected fragment size with strong enrichment signal at TSS (**Supplementary Figure 1E**) indicated the high data quality used in our study. We identified four distinct clusters (C1, C2, C3, C4) (**Figure 2A**) when the data were projected to a low-dimensional space using ArchR based on the characteristics of peaks after batch effect removal by Harmony (**Supplementary Figure 1F**). C1 was fewer than 100 cells (54 cells, 0.3% of total) and showed no unique molecular feature pattern. Thus, only the C2, C3, and C4 were used for the following analysis.

To further dissect the epigenetic characteristics of PMSC subgroups and review the association between the transcriptional and epigenetic layer, we transferred cell states from scRNA-seq data to scATAC-seq data based on gene expression and the gene body accessibility matrix (see Methods; **Figure 2B**). Two proliferative clusters, proliferative1 and proliferative2 in scRNA-seq data, were both transferred to







**FIGURE 2 |** MSC markers (CD34, PTPRC(CD45), CD19, and HLA-DR). **(E)** scATAC-seq heat map of differentially activity gene across five clusters, colored by relative gene-activity scores (z-score). Gene-activity was converted from accessible peaks calculated in ArchR using Cicero. Gold: high activity; blue: low activity. Representative genes from scRNA-seq and relative function are highlighted. ( $\log_2$  fold change (LFC) > 0.15 and false discovery rate (FDR) < 0.01) **(F)** UMAP visualization show the gene activity of representative genes select from scRNA-seq in corresponding scATAC-seq clusters. **(G)** Aggregated scATAC-seq tracks denoting marker chromatin accessibility peaks for each cluster. **(H)** GO terms enrichment of different activities gene respective to indicated scATAC-seq clusters.

one scATAC-seq cluster, C4, although they showed distinct cell states at the transcriptional level. The small immunomodulation1 cluster (1.38% in scRNA-seq data, **Figure 1C**) was transferred to a large cluster, C2, in scATAC-seq data (5,031 cells, 29% of total); moreover, immunomodulation2 was assigned into C3.

To further identify the assignment relationship of the cell states, we performed hierarchical clustering analysis for both scRNA-seq and scATAC-seq subgroups based on the distance using all common genes (see Methods). The hierarchical clustering results also showed that proliferative1 and proliferative2 were classified together with C4, immunomodulation1 and immunomodulation2 were gathered with C2 and C3, respectively (**Figure 2C**). These data further confirm the predicted annotations by Seurat. The above results suggest that the heterogeneity of cell states in PMSCs could also be reflected by chromatin accessibility, and there are corresponding correlations but significant differences across transcriptional and epigenetic levels.

To further explore the relationship between gene expression and chromatin accessibility of PMSCs subgroups, we identified genes with differential activity based on the inferred gene-activity score (**Figure 2E**) and performed GO enrichment analysis (**Figure 2H**). We observed that the enriched genes in immunomodulation1 population, including *PRRX1*, *PRDM1*, *CCL2*, *LY6E*, *IGFBP4*, *IGFBP6*, *COX7A1*, and *CLEC11A*, showed higher accessibility in C2 than others (**Figure 2E–G**). Moreover, some cytokine superfamily members, including the CCL chemokine family, CXC chemokine family, interleukins family, and HLA major histocompatibility complex (MHC) class I protein members, only had significantly differential chromatin accessibility in C2. Please note that not all of these genes were consistently highly expressed at the transcriptional level, suggesting that the chromatin accessibility of immunomodulatory-related genes may be poised and keep more open accessibility for initiating the expression of these genes in PMSCs (**Figure 2E**). Note that immunomodulation-related terms, including “type I interferon signaling pathway,” “monocyte chemotaxis,” “antigen processing and presentation,” and “interferon- $\gamma$ -mediated signaling pathway,” were only observed in C2 (**Figure 2H**).

In addition, MSC differentiation and extracellular matrix-related genes that were highly enriched in immunomodulation2 in the scRNA-seq data (e.g., *FOS*, *SOX4*, *MEG3*, *IGFBP3*, *COL3A1*, and *COL5A2*), showed higher accessibility in C3, indicating the differentiation but not immunomodulation characteristics of PMSCs were more prominent in C3 at the chromatin accessibility level (**Figure 2E–G**). It is worth mentioning that, GO terms including “cell cycle arrest,” “cAMP response,” and “cytokine response,” were also enriched in C3 as what we observed in

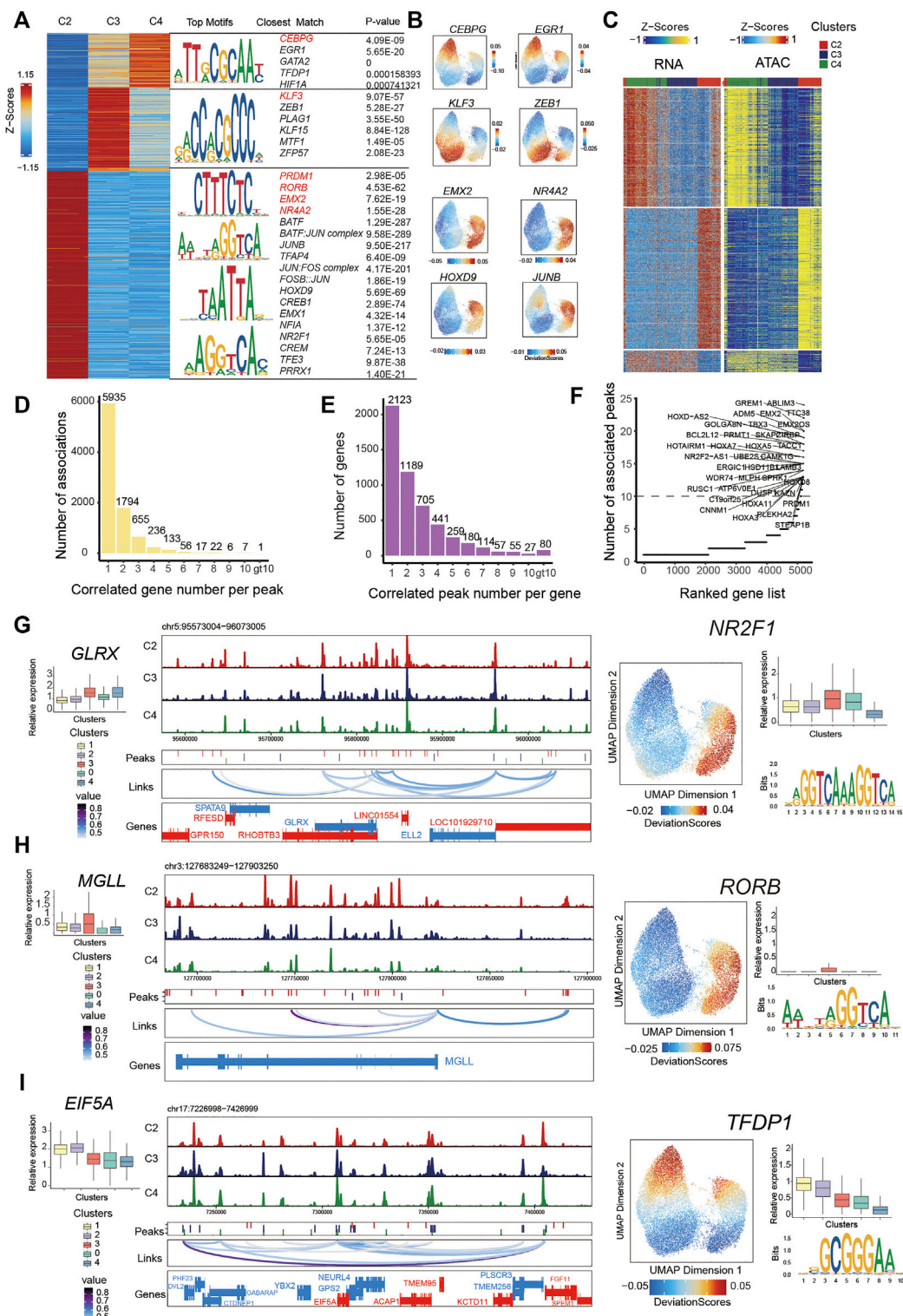
immunomodulation2 with scRNA-seq data. Besides this, functional characteristics of classic MSCs, such as “extracellular matrix organization,” “cell–cell adhesion,” and “cell migration,” MSC differentiation potential-related terms were relatively upregulated in C3. These results suggest that immunomodulation-related genes showed a clearer chromatin accessibility signature than those at the transcriptional level in PMSCs, and the chromatin accessibility of immunomodulation-related genes is being poised for immunomodulation specification.

As expected, cell proliferation- and cell cycle-related genes, such as *TOP2A*, *MKI67*, *CCNB1*, *CDC20*, *ADK1C1*, *AURKA*, and *UBE2S*, showed differential chromatin accessibility in C4, which confirmed the definition of subpopulations in scATAC-seq data based on the transfer method as described above (**Figure 2E–G**). However, the cell cycle-related genes did not show as significant a difference at the chromatin accessibility level among the three clusters as those at the transcriptional level (**Figure 3G**). Interestingly, genes with a highly predicted gene score in C4 were significantly enriched in sensory-, neuro-, and cell adhesion-related GO terms with few terms related to the cell cycle (**Figure 2H**). Above all, we inferred that cell cycle gene-related heterogeneity has more distinct characteristics at the transcriptional level than those at the chromatin accessibility level in PMSCs.

Collectively, the above results suggest that transcriptomic and epigenetic data could largely reflect each other in cell state identification. However, these two omics layers are not always consistent and are able to provide complementary information for better understanding of the heterogeneity of PMSCs.

## Characterization of the Cell State-specific Epigenetic Regulators in Inferred PMSCs Subgroups

To characterize the cell state-specific regulatory networks involved in regulating chromatin accessibility across different cell states, we conducted a Wilcoxon test to find differential peaks for each PMSC subpopulation. In total, we found 55,149 significantly accessible chromatin peaks ( $\log_2$ FC > 1 and FDR < 0.05) in at least one PMSC subpopulation across three cell states (clusters C2, C3, and C4) (**Figure 3A**). These peaks were clustered into three major groups representing the specific chromatin-accessible sites of each PMSC subgroup. Based on the marker peaks in each subgroup, we then performed motif enrichment using the FindMotifs function in Signac. As a complementary approach, some of them also showed high TFs activity calculated by ChromVAR at a per-cell level. Using this combined motif enrichment approach, we observed enrichment of the binding motif of *PRDM1*, *RORB*, *EMX2*, *BATF*:*JUN* complex, *JUNB*, and



**FIGURE 3 |** Integrated analysis of cell state-specific epigenetic regulators in inferred PMSC subgroups. **(A)** Heat map representing PMSC cell states marker peaks. Each row represents an individual marker peak, colored by the normalized marker peak accessibility score (Z-score) (Left). Transcription factor motifs and transcription factor and P-value enriched in each cell state marker peak sequence. Transcription factor motifs selected in red. **(B)** The same UMAP visualization shown in Figure 2A, but each cell is colored by the enrichment of TF activity score (deviations) calculated in ArchR using ChromVAR. **(C)** Heat maps of RNA and ATAC accessibility scores across clusters. **(D)** Heat maps of RNA and ATAC accessibility scores across clusters. Top, peak-to-gene links that are links across cell states (FDR<0.0001; corCutOff > 0.4; varCutOff > 0.25 when selecting links by plotPeak2GeneHeatmap function). Top, peak-to-gene links that are (Continued)

**FIGURE 3** | identified almost within C4. Middle, peak-to-gene links that are unique to C2. Bottom, peak-to-gene links identified in both C3 and C4. **(D)** The number of significant peak-gene links for all peaks. **(E)** The number of significant peak-gene links for all genes. **(F)** The number of significantly correlated peaks for each gene. Putative DORCs are highlighted. **(G-I)** Aggregated scATAC-seq tracks showing genomic regions near *GLRX*(G), *MGLL* (H), and *EIF5A* (I) genes. Different peaks in clusters are shown in the second line. The loop in the third line height represents the significance of peak-to-gene links (corCutOff = 0.45, FDRCutOff = 1e-04, varCutOffATAC = 0.25, varCutOffRNA = 0.25). The RNA expressions are present on the left boxplot. The motif enrichment for associated peaks (shown in **(C)**) are shown in the right and the UMAP show the enrichment of TF activity score (deviations); the boxplot shows the RNA expression of the enriched TF.

*JUN:FOS* complex (AP-1 family members) in C2; *KLF3*, *PLAG1*, and *ZEB1* in C3; and *CEBPG*, *EGR1*, *GATA2*, and *TFDP1* in C4, respectively (**Figure 3A,B**).

The pattern of chromatin accessibility reflects the possible physical interactions among enhancers, promoters, insulators, and chromatin-binding factors, all of which could cooperatively regulate gene expression (Klemm et al., 2019). Cell type-specific gene expression in eukaryotic cells was regulated by *cis*-acting DNA elements, including enhancers and promoters, and *trans*-acting factors, such as transcription factors (Roadmap Epigenomics Consortium et al., 2015). To infer the *cis*-regulatory elements of target genes in chromatin accessibility peaks, we first identified the putative 499,568 peak-gene linkages that significantly paired (within 250 kb of a gene promoter, FDR < 0.05) and used the most significant 13,863 peak-gene association for the following analysis (correlation > 0.45; FDR < 1e-04; the minimum variance quantile of the ATAC peak accessibility and the minimum variance quantile of the RNA gene expression > 0.25; **Figure 3C**). These results reveal specific peak-to-gene links in C2 and C4 and a conserved subset that is shared across both C3 and C4 (**Figure 3C**). Meanwhile, we found that most peaks were only associated with one gene, and most genes were only associated with one peak (**Figure 3D,E**), which is in line with a previous study (Ma et al., 2020).

A previous study demonstrates that domains of regulatory chromatin (DORCs, with an exceptionally large (>10) number of significant peak-gene associations) referring to peak-gene-associated regions with high density, were strongly enriched for lineage-determining genes (Ma et al., 2020). To find out the key cell state-determining genes, we inferred DORC-regulated genes as previously reported (Ma et al., 2020) (**Figure 3F**). As expected, a subset of genes was significantly associated with more than 10 peaks. For example, *GREM1*, *MGLL*, *GLRX*, *PRMT1*, *EIF5A*, and *PRDM1* showed both a differential expression pattern and chromatin accessibility state across different cell subgroups. A total of 22 peaks were significantly associated with *GREM1* and 11 peaks with *MGLL* and *GLRX*. These genes all showed differential chromatin accessibility and gene expression in immunomodulatory-capability cell subgroups. These results are consistent with the previous report that *MGLL* and *GLRX* are associated with immunity in cancer (Xiang et al., 2018; Chang et al., 2020) and *GREM1* inhibits osteogenic differentiation, senescence, and BMP transcription of adipose-derived stem cells (Liu et al., 2021). Additionally, 18 peaks were significantly associated with *PRMT1* and 11 peaks with *EIF5A*, and they both showed differential chromatin accessibility and gene expression in proliferative subgroups (**Figure 3G-I**). Consistently, previous reports indicate that *EIF5A* and *PRMT1*

promote cell proliferation in the case of several human cancers (Kaiser, 2012; Song et al., 2020). Based on the above findings, we propose that these identified peaks from significant peak-gene linkages might be specific *cis*-regulatory elements for cell state-related genes.

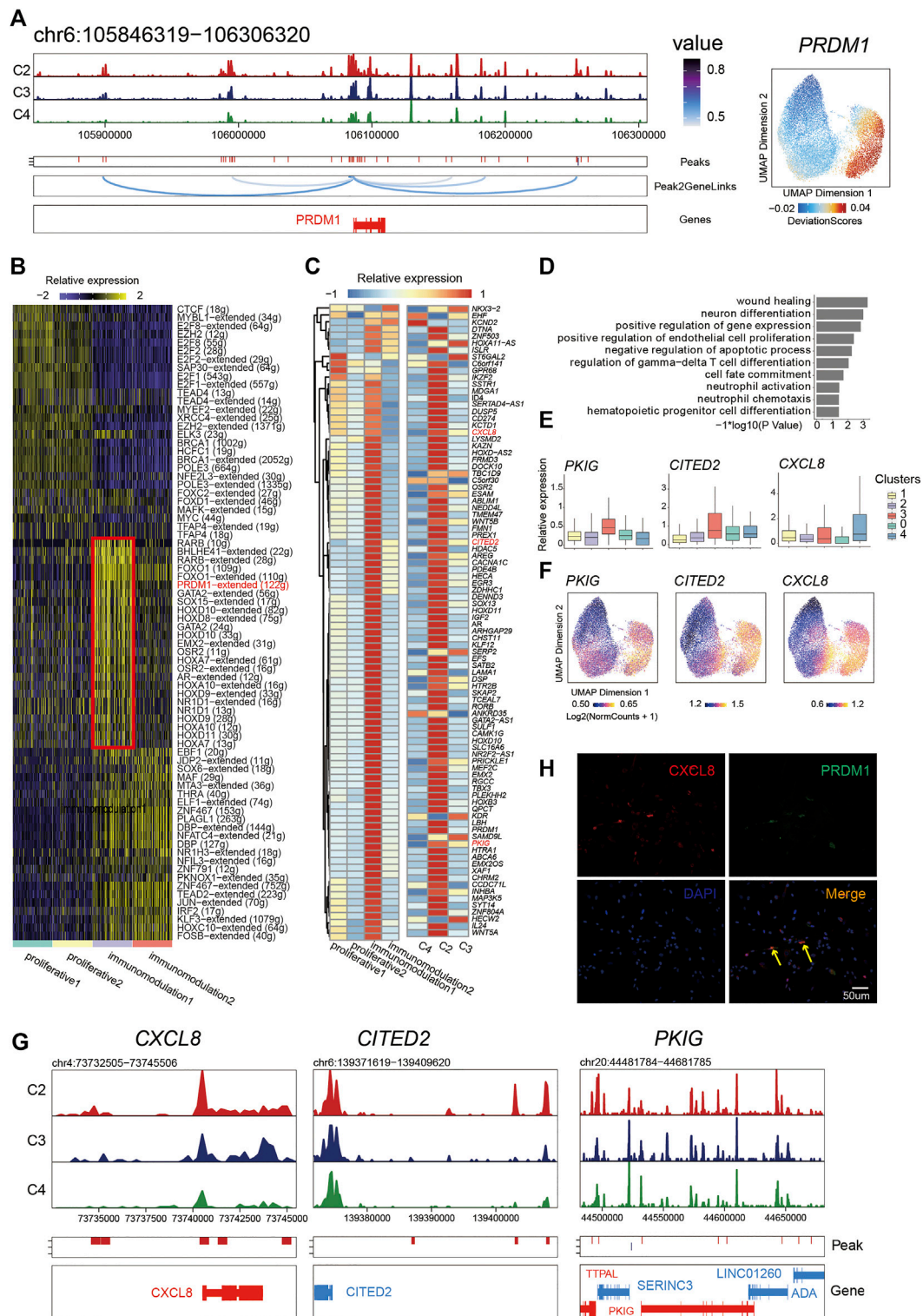
To further dissect the *cis*-regulatory elements directing the expression of those genes, we performed motif enrichment analysis on the significantly associated peaks. We found transcription factor binding sites (TFBSs) for *NR2F1* in *GLRX*-associated peaks, *RORB* in *MGLL*-associated peaks, and *TFDP1* for *EIF5A*-associated peaks. They had high TF activity in C2 or C4 (**Figure 3G-I**). Based on the temporal specificity of scATAC-seq peaks and the existence of TFs motifs in these regions, we propose that those elements might be cell state-specific *cis*-regulatory elements to regulate the expression of PMSC regulators that cause heterogeneity. Overall, our data not only present some well-known TFs that are previously reported for MSC functional phenotype, but also highlight some putative TFs for regulating PMSCs heterogeneity at the epigenomic level, which may pave the way for deeper understanding of the MSC functional mechanism.

### ***PRDM1* Plays a Crucial Role in Maintaining Immunomodulatory Capability by Activating *PRDM1*-Regulon Loop**

TFs play important roles in dictating the identity and fate of individual cells in multicellular organisms by differentially regulating the gene expression upon internal and external stimuli (Lee and Young, 2013). Previous studies show that *PRDM1* play vital roles in regulating the cell development and differentiation process (Turner et al., 1994; Ohinata et al., 2005; Kallies et al., 2006); however, its role in MSCs is still largely unknown. Here, we found *PRDM1* also showed up in the list of DORC-regulated genes with differential expression in the immunomodulation1 cell state and chromatin accessibility in C2 (**Figure 3F**; **Figure 2F**; **Figure 4A**). In addition, *PRDM1* motifs were highly enriched in differential peaks of C2 and showed high TF activity (**Figure 3A**; **Figure 4A**). Meanwhile, *PRDM1* also showed a differentially high TF regulon activity based on Single-Cell regulatory Network Inference and Clustering (SCENIC) (Aibar et al., 2017) calculated AUC scores in immunomodulation1 (**Figure 4B**). These results indicate that *PRDM1* might contribute to the regulation of immunomodulation cell state in PMSCs.

Thus, we further extracted the putative target genes of *PRDM1* inferred by SCENIC and identified the chromatin accessibility and expression profiles of them to investigate the relationship between the chromatin structure remodeling and gene expression





**FIGURE 4 |** *PRDM1* played a crucial role in maintaining immunomodulatory capability of PMSC subgroup. **(A)** Aggregated scATAC-seq tracks showing genomic regions near *PRDM1* (Left). The UMAP shows the enrichment of *PRDM1* activity score (deviations). **(B)** Heat map of different regulons identified by SCENIC. **(C)** Heat map of *PRDM1* target genes expression (left) and chromatin accessibility (right). **(D)** GO enrichment for *PRDM1* target genes. **(E)** Boxplot showing the expression level of selected representative *PRDM1* target genes *PKIG*, *CITED2*, and *CXCL8*. **(F)** The UMAP show the enrichment of *PRDM1* target genes (*PKIG*, *CITED2*, and *CXCL8*) activity score (deviations). **(G)** Aggregated scATAC-seq tracks showing genomic regions near *PKIG*, *CITED2*, and *CXCL8*, respectively. **(H)** Immunostaining of *PRDM1* and *CXCL8* in PMSCs.



in the *PRDM1* regulon network. Notably, we found that most target genes showed an enriched expression in immunomodulation1 and a significant pattern of chromatin accessibility in C2 (Figure 4C). Moreover, we observed synchronous dynamics of those targets; for instance, the target *CXCL8*, *CITED2*, and *PKIG* showed high gene expression (Figure 4E) and chromatin accessibility (Figures 4F,G), suggesting an important role in maintaining the immunomodulation cellular phenotype. In addition, the GO enrichment analysis for *PRDM1*-target genes showed that “wound healing,” “neuron differentiation,” “positive regulation of endothelial cell proliferation,” “regulation of gamma-delta T cell differentiation,” “cell fate commitment,” “neutrophil activation,” and “hematopoietic progenitor cell differentiation and neutrophil chemotaxis” were highly enriched (Figure 4D). The immunostaining result was in line with the above analysis; namely, *PRDM1* and target gene *CXCL8* were co-expressed in some PMSC single cells (Figure 4H). Collectively, our results indicate that, as a significant character in this cell state, *PRDM1*-regulon genes might be important for maintaining of immunomodulatory potential cell state in PMSCs.

## DISCUSSION

MSCs are a promising cell source for clinical application. More and more studies indicate that MSCs, even though all meet ISCT criteria, are cell mixtures in aspects of phenotypical, functional, and biochemical characteristics. MSC subpopulations with distinctive surface markers display different biological potential and corresponding therapeutic effects (Tormin et al., 2009; Phinney, 2012; Mo et al., 2016). Even single-cell-derived colonies of human MSCs are heterogenous in morphology, self-renewing ability, and the potential for multilineage differentiation, migration, and tissue engraftment (Colter et al., 2001; Prockop et al., 2001; Ryang et al., 2006). The knowledge regarding what leads to the heterogeneity of MSCs is largely unexplored. In our study, we generated a transcriptional map and a complementary chromatin-accessibility map of human PMSCs. In line with previous multiomics studies (Ma et al., 2020), the cell state heterogeneity in PMSCs can be reflected across the transcriptional and epigenetic landscape. A previous study proposes that the mesengenic process represents a complex sequence of events (Caplan, 2008). It is reported that *in vitro* expansion of MSCs also induced spontaneous differentiation with expression of developmental markers and tissue-specific genes (Tsai et al., 2011). Consistently, we also observed such phenomenon using unsupervised trajectory analysis by Monocle2 (Figure 1H), which may be attributed to intrinsic subsets with specific molecular features existing in cultured PMSCs as well as adopting FBS in PMSCs culture medium in the current study.

Based on multiomics analysis, we reveal that PMSCs show significantly enriched immunomodulatory capability at single cell resolution. The immunomodulatory capability of PMSCs are also reported in a previous study by using traditional tools. For example, PMSCs could inhibit the inflammatory response by

regulating CD4<sup>+</sup> T cell and macrophage polarization, inhibiting the inflammatory factors *IFN-γ* and *IL-17*, and upregulating the anti-inflammatory factor *TGF-β* and *IL-10* expression to attenuate renal fibrosis in rats (Zhu et al., 2020).

We identified one PMSC subgroup, C2, as main immunomodulatory potential cell state at the single-cell chromatin accessibility level, in which *LY6E*, *CCL2*, *GREM1*, *PRDM1*, and many other cytokine genes showed significant chromatin accessibilities. These genes were also highly expressed in the corresponding immunomodulatory1 cell state at the single-cell transcriptional level. Furthermore, estimates of immunomodulatory-related gene activity on the basis of correlated variation in promoter and distal-peak accessibility (Cicero) broadly repeats this pattern, including *IGFBP4*, *IGFBP6*, *CCL2*, *PRDM1*, and *LY6E* as well as other chemokine, CXC chemokine, and interleukin family members. GO enrichment analysis for genes with differential expression from the scRNA-seq data set and differential gene activity from the scATAC-seq data set in this immunomodulatory-potential cell state indicate common terms in immune- and collagen-related biological processes (Figure 1G, Figure 2E). Collectively, immunomodulatory potential cell state characteristics in PMSCs were consistently reflected across both the transcriptional and epigenetic maps (Figure 1F; Figure 2E,F).

It is reported that the therapeutic effect of MSCs are not primarily influenced by their differentiation potential but rather by the secretion of growth factors and cytokines in many cases (Caplan, 2008). MSCs can secrete cytokines and other factors, such as *TGFβ*, *IL-6*, *CCL2*, and *HLA-G* to exert the immunomodulatory effect (Choi et al., 2014; Maffioli et al., 2017). Owing to the immunomodulatory abilities, MSCs are used for many preclinical studies and clinical trials, including graft-vs-host disease, autoimmune diseases, inflammatory illnesses, lung injuries, etc. (Ringdén et al., 2006; Li and Flavell, 2008; Lee et al., 2009; Matthay et al., 2010). It is worth noting that MSCs show their efficacy in alleviating comorbidities associated with COVID-19 by directly mitigating inflammation, reversing lung dysfunction via normalizing the pulmonary microenvironment, preventing pulmonary fibrosis, and so on (Song et al., 2021).

Besides the cytokines and chemokines mentioned above, *LY6E* and *IFITM2/3* (interferon-induced transmembrane proteins 2/3) were identified in our data with differential expression levels across the clusters (Figure 1F). It is reported that *LY6E* could control CoV infection and pathogenesis and confer immune control of viral diseases, including SARS-CoV-2 (Pfaender et al., 2020; Zhao et al., 2020). *IFITM2/3* are restriction factors that block the entry of many viruses, including SARS-CoV-2 (Lee et al., 2013; Shi et al., 2021). In addition, it is reported that MSCs have an antimicrobial role and therapeutic effects on bacterial infection-caused lung injury (Lee et al., 2013). Based on the results presented in our study, PMSCs might be a better choice with promising potential to be used in COVID-19 treatment. However, more work still needs to be done for further validation.

Interestingly, the immunomodulatory-potential cell state in the scATAC-seq data, compared with that from the scRNA-seq

data, has more obvious immunomodulatory characteristics with an increased ratio in cell composition (1.38% up to 29%; **Figure 1; Figure 2A**) and high chromatin accessibility of immunomodulatory-related genes (**Figure 2E–G**). A previous study reveals that immunomodulatory activity of MSCs was seriously influenced by the inflammation microenvironment during tissue regeneration (Shi et al., 2018). Instead of being immunosuppressive in nature, MSCs might have different immunoregulatory properties depending on the immune scene and disease condition (Song et al., 2021). The fate of the implanted MSCs is locally regulated by the new environment, and their further development is selective and not directive (Pittenger et al., 2019). Prior studies observe that changes in histone modifications and chromatin accessibility for sequence-specific transcription factors might precede and prefigure changes in gene expression, and chromatin accessibility lineage-priming states could predict cell fate decisions (Rada-Iglesias et al., 2011; Lara-Astiaso et al., 2014; Ma et al., 2020). Based on our results and previous reports, we suggest that MSCs' immunomodulatory potential might be characterized to be latent at the epigenomic level when there is no specific inflammatory stimulus. The chromatin accessibility of the immunomodulatory-related genes precedes and foreshadows gene expression by creating primed chromatin states to activate their expression and fulfill the immunomodulatory potential.

Moreover, we also present two proliferative cell states in PMSCs. Compared with immunomodulatory cell states, the proliferative cell states show increased expression of genes related to the cell cycle, cell proliferation, and mitotic nuclear division and reduced expression of differentiation-related genes. After removing the cell cycle effect, we still observed that cell cycle composition was considerably inconsistent among various groups. The cell cycle state may have intrinsic characteristics of cultured cells, and this phenomenon is also previously described in other scRNA-seq studies (Kowalczyk et al., 2015; Harman et al., 2020). Meanwhile, two proliferative cell states in single-cell transcriptome data were both transferred to C4 in the single-cell chromatin accessibility data. Moreover, cell cycle-related genes, including *DKC1*, *AURKA*, *CCNB1*, *CDC20*, and *UBE2S*, showed moderate but significant differential chromatin accessibility. Furthermore, other than regulation of the fibroblast growth factor receptor signaling pathway and negative regulation of cell differentiation- and cell adhesion-related terms, the extensive chromatin priming of genes was also related to nervous system development and the neuropeptide signaling pathway. It is reported that PMSCs are capable of being induced to several neural cell types (Chen et al., 2009; Portmann-Lanz et al., 2010; Martini et al., 2013) and can be used in neurological disease treatment (Torre et al., 2019). For example, PMSCs could be differentiated into neural progenitors *in vitro*, and these progenitors could further differentiate into dopaminergic neurons to alleviate asymmetric rotational behavior after being transplanted into the striatum of Parkinson's disease model rats (Park et al., 2012). Moreover, it is demonstrated that PMSCs could modulate the inflammatory response in an Alzheimer's disease mouse model and increase the levels of  $\beta$ -amyloid degrading enzymes, resulting in an

improvement of memory function (Kim et al., 2013). The current accuracy of computational approaches that pair data from scATAC-seq and scRNA-seq from separately measured cells is variable (74.9% in skin and 36.7% in mouse brain) (Ma et al., 2020). A more scalable and better integrated approach, namely, not only sequencing technology but computational pairing approaches, would be useful for better understanding the relationship between the transcriptome and epigenome.

Chromatin accessibility regulates gene expression by modulating the interactions of transcriptional factors with their target DNA, which plays an essential role in establishing and maintaining cell identity (Klemm et al., 2019). Interactions among chromatin regulators, transcription factors, and *cis*-regulatory elements are the main drivers to shape context-specific chromatin accessibility and maintain the gene expression profile (Duren et al., 2017). In our work, we discovered that there were specific correlations between gene expression and peak accessibility at different cell states (**Figure 3C**). We linked differentially accessible regions, which were inferred as the specific *cis*-regulatory elements for cell state-related genes to DORC-regulated genes, such as *MELL*, *GLRX*, and *EIF5A*. Meanwhile, we identified the key TFs that regulate these genes using ChromVAR (**Figure 3G–I**). We found that *PRDM1* motifs were highly enriched in C2, and as a DORC, *PRDM1* showed significant chromatin accessibility. In addition, *PRDM1* was significantly upregulated in the immunomodulatory cell state. Moreover, target genes of *PRDM1* inferred by SCENIC had a coordinated pattern in gene expression and chromatin accessibility in the immunomodulatory cell state. The results of GO enrichment analysis showed that *PRDM1*-target genes were significantly enriched in wound healing, regulation of gamma-delta T cell differentiation, cell fate commitment, and neutrophil activation, etc. Previous studies shown that *PRDM1* serves as a master regulator of the development and differentiation of immunoglobulin-secreting B cells (Turner et al., 1994). Besides this, *PRDM1* is also important for thymocyte survival, T cell homeostasis (Kallies et al., 2006; Martins et al., 2006), T helper differentiation (Kallies et al., 2006), and cytokine production (Heinemann et al., 2014). It is also reported that *PRDM1* plays a critical role in the process of mouse germ cell lineage formation (Ohinata et al., 2005). Taken together, *PRDM1* would play a potential role in maintaining immunomodulatory capability by activating the *PRDM1*-regulon loop. Our work reveals potential regulatory factors and an important pathway for PMSC cell state commitment at the single cell multi-omics level for the first time, which may further support the application of PMSCs in regenerative and immunomodulation treatment. Future validation studies in chromatin accessibility and gene expression on PMSCs will increase our knowledge of the regulatory network associated with the heterogeneity of PMSCs and optimize the clinical application of MSCs.

## DATA AVAILABILITY STATEMENT

The data that support the findings of this study have been deposited into CNGB Sequence Archive (CNSA) (Guo et al., 2020) of China National GeneBank DataBase (CNGBdb) (Chen

et al., 2020) (link: <https://db.cngb.org/search/project/CNP0001689/>), accession number CNP0001689.

## ETHICS STATEMENT

The study was approved by the Institutional Review Board on Bioethics and Biosafety of BGI (Permit No. BGI-IRB 19145), and the Shenzhen Second People's Hospital (Permit No. KS20191031002). All the participants signed informed consents and voluntarily donated the samples in this study.

## AUTHOR CONTRIBUTIONS

ZS and JL conceived the idea and designed the entire project; JL performed the scRNA-seq data and scATAC-seq data analysis, generated figures, and wrote the manuscript. QW contributed to sample collection, the scRNA-seq library and scATAC-seq library

construction and functional assays. YA, XH, YX, and QD contributed to experiments and discussion. YH and HY contributed insightful comments. All authors approved the submitted version.

## FUNDING

We sincerely thank the support provided by China National Gene Bank. This study was supported by Science, Technology and Innovation Commission of Shenzhen Municipality Grant (number JCYJ20180507183628543).

## SUPPLEMENTARY MATERIAL

The Supplementary Material for this article can be found online at: <https://www.frontiersin.org/articles/10.3389/fcell.2022.836887/full#supplementary-material>

## REFERENCES

- Aboalola, D., and Han, V. K. M. (2017). Insulin-Like Growth Factor Binding Protein-6 Alters Skeletal Muscle Differentiation of Human Mesenchymal Stem Cells. *Stem Cell Int.* 2017, 1–17. doi:10.1155/2017/2348485
- Aibar, S., González-Blas, C. B., Moerman, T., Huynh-Thu, V. A., Imrichova, H., Hulselmans, G., et al. (2017). SCENIC: Single-Cell Regulatory Network Inference and Clustering. *Nat. Methods* 14, 1083–1086. doi:10.1038/nmeth.4463
- Bailo, M., Soncini, M., Vertua, E., Signoroni, P. B., Sanzone, S., Lombardi, G., et al. (2004). Engraftment Potential of Human Amnion and Chorion Cells Derived from Term Placenta. *Transplantation* 78, 1439–1448. doi:10.1097/01.TP.0000144606.84234.49
- Caplan, A. (2008). Why Are MSCs Therapeutic? New Data: New Insight. *J. Pathol.* 271, 231–241. doi:10.1002/path
- Chang, Y., Li, G., Zhai, Y., Huang, L., Feng, Y., Wang, D., et al. (2020). Redox Regulator GLRX Is Associated with Tumor Immunity in Glioma. *Front. Immunol.* 11, 1–17. doi:10.3389/fimmu.2020.580934
- Chen, F. Z., You, L. J., Yang, F., Wang, L. N., Guo, X. Q., Gao, F., et al. (2020). CNGBdb: China National GeneBank DataBase. *Hereditas* 42, 799–809. doi:10.16288/j.ycz.20-080
- Chen, L., He, D.-M., and Zhang, Y. (2009). The Differentiation of Human Placenta-Derived Mesenchymal Stem Cells into Dopaminergic Cells *In Vitro*. *Cell. Mol. Biol. Lett.* 14, 528–536. doi:10.2478/s11658-009-0015-3
- Choi, J. H., Jung, J., Na, K.-H., Cho, K. J., Yoon, T. K., and Kim, G. J. (2014). Effect of Mesenchymal Stem Cells and Extracts Derived from the Placenta on Trophoblast Invasion and Immune Responses. *Stem Cell Development* 23, 132–145. doi:10.1089/scd.2012.0674
- Colter, D. C., Sekiya, I., and Prockop, D. J. (2001). Identification of a Subpopulation of Rapidly Self-Renewing and Multipotential Adult Stem Cells in Colonies of Human Marrow Stromal Cells. *Proc. Natl. Acad. Sci.* 98, 7841–7845. doi:10.1073/pnas.141221698
- de la Torre, P., Jesús Pérez-Lorenzo, M., and I. Flores, A. (2019). Human Placenta-Derived Mesenchymal Stromal Cells: A Review from Basic Research to Clinical Applications. *IntechOpen*. doi:10.5772/intechopen.76718
- Deng, M., Luo, K., Hou, T., Luo, F., Xie, Z., Zhang, Z., et al. (2018). IGFBP3 Deposited in the Human Umbilical Cord Mesenchymal Stem Cell-secreted Extracellular Matrix Promotes Bone Formation. *J. Cel. Physiol.* 233, 5792–5804. doi:10.1002/jcp.26342
- Dominici, M., Le Blanc, K., Mueller, I., Slaper-Cortenbach, I., Marini, F. C., Krause, D. S., et al. (2006). Minimal Criteria for Defining Multipotent Mesenchymal Stromal Cells. The International Society for Cellular Therapy Position Statement. *Cytotherapy* 8, 315–317. doi:10.1080/14653240600855905
- Duren, Z., Chen, X., Jiang, R., Wang, Y., and Wong, W. H. (2017). Modeling Gene Regulation from Paired Expression and Chromatin Accessibility Data. *Proc. Natl. Acad. Sci. USA* 114, E4914–E4923. doi:10.1073/pnas.1704553114
- Feng, Y., Huang, J., Wu, J., Xu, Y., Chen, B., Jiang, L., et al. (2020). Safety and Feasibility of Umbilical Cord Mesenchymal Stem Cells in Patients with COVID-19 Pneumonia: A Pilot Study. *Cell Prolif* 53, 1–8. doi:10.1111/cpr.12947
- Fu, S.-H., Yeh, L.-T., Chu, C.-C., Yen, B. L.-J., and Sytwu, H.-K. (2017). New Insights into Blimp-1 in T Lymphocytes: A Divergent Regulator of Cell Destiny and Effector Function. *J. Biomed. Sci.* 24, 1–17. doi:10.1186/s12929-017-0354-8
- Fukuchi, Y., Nakajima, H., Sugiyama, D., Hirose, I., Kitamura, T., and Tsuji, K. (2004). Human Placenta-Derived Cells Have Mesenchymal Stem/Progenitor Cell Potential. *Stem Cells* 22, 649–658. doi:10.1634/stemcells.22-5-649
- Galleu, A., Riffo-vasquez, Y., Trento, C., Lomas, C., Dolcetti, L., Cheung, T. S., et al. (2017). Apoptosis in Mesenchymal Stromal Cells Induces *In Vivo* Recipient-Mediated Immunomodulation. *Sci. Transl. Med.* 9, 1–12. doi:10.1126/scitranslmed.aam7828
- Gong, D., and Ferrell, J. E. (2010). The Roles of Cyclin A2, B1, and B2 in Early and Late Mitotic Events. *MBoC* 21, 3149–3161. doi:10.1091/mbc.E10-05-0393
- Granja, J. M., Corces, M. R., Pierce, S. E., Bagdatli, S. T., Choudhry, H., Chang, H. Y., et al. (2021). Author Correction: ArchR Is a Scalable Software Package for Integrative Single-Cell Chromatin Accessibility Analysis. *Nat. Genet.* 53, 935. doi:10.1038/s41588-021-00850-x
- Guo, X., Chen, F., Gao, F., Li, L., Liu, K., You, L., et al. (2020a). CNSA: A Data Repository for Archiving Omics Data. *Database* 2020, 1–6. doi:10.1093/database/baaa055
- Guo, Z., Chen, Y., Luo, X., He, X., Zhang, Y., and Wang, J. (2020b). Administration of Umbilical Cord Mesenchymal Stem Cells in Patients with Severe COVID-19 Pneumonia. *Crit. Care* 24, 1–3. doi:10.1186/s13054-020-03142-8
- Harman, R. M., Patel, R. S., Fan, J. C., Park, J. E., Rosenberg, B. R., and Van de Walle, G. R. (2020). Single-cell RNA Sequencing of Equine Mesenchymal Stromal Cells from Primary Donor-Matched Tissue Sources Reveals Functional Heterogeneity in Immune Modulation and Cell Motility. *Stem Cell Res. Ther.* 11, 1–15. doi:10.1186/s13287-020-02043-5
- Heinemann, C., Heink, S., Petermann, F., Vasanthakumar, A., Rothhammer, V., Doorduyn, E., et al. (2014). IL-27 and IL-12 Oppose Pro-inflammatory IL-23 in CD4+ T Cells by Inducing Blimp1. *Nat. Commun.* 5, doi:10.1038/ncomms4770
- Huang, D. W., Sherman, B. T., and Lempicki, R. A. (2009a). Bioinformatics Enrichment Tools: Paths toward the Comprehensive Functional Analysis of Large Gene Lists. *Nucleic Acids Res.* 37, 1–13. doi:10.1093/nar/gkn923

- Huang, D. W., Sherman, B. T., and Lempicki, R. A. (2009b). Systematic and Integrative Analysis of Large Gene Lists Using DAVID Bioinformatics Resources. *Nat. Protoc.* 4, 44–57. doi:10.1038/nprot.2008.211
- Huang, Y., Li, Q., Zhang, K., Hu, M., Wang, Y., Du, L., et al. (2019). Single Cell Transcriptomic Analysis of Human Mesenchymal Stem Cells Reveals Limited Heterogeneity. *Cell Death Dis* 10. doi:10.1038/s41419-019-1583-4
- Ji, C., Sun, L.-S., Xing, F., Niu, N., Gao, H.-L., Dai, J.-W., et al. (2020). HTRA3 Is a Prognostic Biomarker and Associated with Immune Infiltrates in Gastric Cancer. *Front. Oncol.* 10, 1–14. doi:10.3389/fonc.2020.603480
- Kaiser, A. (2012). Translational Control of eIF5A in Various Diseases. *Amino Acids* 42, 679–684. doi:10.1007/s00726-011-1042-8
- Kallies, A., Hawkins, E. D., Belz, G. T., Metcalf, D., Hommel, M., Corcoran, L. M., et al. (2006). Transcriptional Repressor Blimp-1 Is Essential for T Cell Homeostasis and Self-Tolerance. *Nat. Immunol.* 7, 466–474. doi:10.1038/ni1321
- Kim, K.-S., Kim, H. S., Park, J.-M., Kim, H. W., Park, M.-k., Lee, H.-S., et al. (2013). Long-term Immunomodulatory Effect of Amniotic Stem Cells in an Alzheimer's Disease Model. *Neurobiol. Aging* 34, 2408–2420. doi:10.1016/j.neurobiolaging.2013.03.029
- Klemm, S. L., Shipony, Z., and Greenleaf, W. J. (2019). Chromatin Accessibility and the Regulatory Epigenome. *Nat. Rev. Genet.* 20, 207–220. doi:10.1038/s41576-018-0089-8
- Komori, T. (2006). Regulation of Osteoblast Differentiation by Transcription Factors. *J. Cel. Biochem.* 99, 1233–1239. doi:10.1002/jcb.20958
- Kowalczyk, M. S., Tirosh, I., Heckl, D., Rao, T. N., Dixit, A., Haas, B. J., et al. (2015). Single-cell RNA-Seq Reveals Changes in Cell Cycle and Differentiation Programs upon Aging of Hematopoietic Stem Cells. *Genome Res.* 25, 1860–1872. doi:10.1101/gr.192237.115
- Roadmap Epigenomics Consortium/Kundaje, A., Kundaje, A., Meuleman, W., Ernst, J., Bilenky, M., Yen, A., et al. (2015). Integrative Analysis of 111 Reference Human Epigenomes. *Nature* 518, 317–330. doi:10.1038/nature14248
- Lara-Astiaso, D., Weiner, A., Lorenzo-Vivas, E., Zaretzky, I., Jaitin, D. A., David, E., et al. (2014). (80), 345, 943–949. doi:10.1126/science.1256271 Chromatin State Dynamics during Blood Formation *Science*
- Lareau, C. A., Duarte, F. M., Chew, J. G., Kartha, V. K., Burkett, Z. D., Kohlway, A. S., et al. (2019). Droplet-based Combinatorial Indexing for Massive-Scale Single-Cell Chromatin Accessibility. *Nat. Biotechnol.* 37, 916–924. doi:10.1038/s41587-019-0147-6
- Lee, J. H., and Berger, J. M. (2019). Cell Cycle-dependent Control and Roles of DNA Topoisomerase II. *Genes* 10, 859. doi:10.3390/genes10110859
- Lee, J. M., Jung, J., Lee, H.-J., Jeong, S. J., Cho, K. J., Hwang, S.-G., et al. (2012). Comparison of Immunomodulatory Effects of Placenta Mesenchymal Stem Cells with Bone Marrow and Adipose Mesenchymal Stem Cells. *Int. Immunopharmacology* 13, 219–224. doi:10.1016/j.intimp.2012.03.024
- Lee, J. W., Krasnodembskaya, A., McKenna, D. H., Song, Y., Abbott, J., and Matthay, M. A. (2013). Therapeutic Effects of Human Mesenchymal Stem Cells in Ex Vivo Human Lungs Injured with Live Bacteria. *Am. J. Respir. Crit. Care Med.* 187, 751–760. doi:10.1164/rccm.201206-0990OC
- Lee, R. H., Hsu, S. C., Munoz, J., Jung, J. S., Lee, N. R., Pochampally, R., et al. (2006). A Subset of Human Rapidly Self-Renewing Marrow Stromal Cells Preferentially Engraft in Mice. *Blood* 107, 2153–2161. doi:10.1182/blood-2005-07-2701
- Lee, R. H., Pulin, A. A., Seo, M. J., Kota, D. J., Ylostalo, J., Larson, B. L., et al. (2009). Intravenous hMSCs Improve Myocardial Infarction in Mice Because Cells Embolized in Lung Are Activated to Secrete the Anti-inflammatory Protein TSG-6. *Cell Stem Cell* 5, 54–63. doi:10.1016/j.stem.2009.05.003
- Lee, T. I., and Young, R. A. (2013). Transcriptional Regulation and its Misregulation in Disease. *Cell* 152, 1237–1251. doi:10.1016/j.cell.2013.02.014
- Li, H. (2013). Aligning Sequence Reads, Clone Sequences and Assembly Contigs with BWA-MEM. *arXiv:1303.3997v2 [q-bio.GN]*. 00, 1–3. Available at: <http://arxiv.org/abs/1303.3997>.
- Li, M. O., and Flavell, R. A. (2008). Contextual Regulation of Inflammation: A Duet by Transforming Growth Factor- $\beta$  and Interleukin-10. *Immunity* 28, 468–476. doi:10.1016/j.immuni.2008.03.003
- Liu, H., Han, X., Yang, H., Cao, Y., Zhang, C., Du, J., et al. (2021). GREM1 Inhibits Osteogenic Differentiation, Senescence and BMP Transcription of Adipose-Derived Stem Cells. *Connect. Tissue Res.* 62, 325–336. doi:10.1080/03008207.2020.1736054
- Liu, X., Xiang, Q., Xu, F., Huang, J., Yu, N., Zhang, Q., et al. (2019). Single-cell RNA-Seq of Cultured Human Adipose-Derived Mesenchymal Stem Cells. *Sci. Data* 6, 1–8. doi:10.1038/sdata.2019.31
- Ma, S., Zhang, B., LaFave, L. M., Earl, A. S., Chiang, Z., Hu, Y., et al. (2020). Chromatin Potential Identified by Shared Single-Cell Profiling of RNA and Chromatin. *Cell* 183, 1103–1116. e20. doi:10.1016/j.cell.2020.09.056
- Macias, M. I., Grande, J., Moreno, A., Domínguez, I., Bornstein, R., and Flores, A. I. (2010). Isolation and Characterization of True Mesenchymal Stem Cells Derived from Human Term Decidua Capable of Multilineage Differentiation into All 3 Embryonic Layers. *Am. J. Obstet. Gynecol.* 203, e9–e95. e23. doi:10.1016/j.ajog.2010.06.045
- Maffioli, E., Nonnis, S., Angioni, R., Santagata, F., Calì, B., Zanotti, L., et al. (2017). Proteomic Analysis of the Secretome of Human Bone Marrow-Derived Mesenchymal Stem Cells Primed by Pro-inflammatory Cytokines. *J. Proteomics* 166, 115–126. doi:10.1016/j.jpro.2017.07.012
- Martini, M. M., Jeremias, T. D. S., Kohler, M. C., Marostica, L. L., Trentin, A. G., and Alvarez-Silva, M. (2013). Human Placenta-Derived Mesenchymal Stem Cells Acquire Neural Phenotype under the Appropriate Niche Conditions. *DNA Cel Biol.* 32, 58–65. doi:10.1089/dna.2012.1807
- Martins, G. A., Cimmino, L., Shapiro-Shelef, M., Szabolcs, M., Herron, A., Magnusdottir, E., et al. (2006). Transcriptional Repressor Blimp-1 Regulates T Cell Homeostasis and Function. *Nat. Immunol.* 7, 457–465. doi:10.1038/ni1320
- Matthay, M. A., Goolaeerts, A., Howard, J. P., and Woo Lee, J. (2010). Mesenchymal Stem Cells for Acute Lung Injury: Preclinical Evidence. *Crit. Care Med.* 38, S569–S573. doi:10.1097/CCM.0b013e3181ff1fd
- Meirelles, L. d. S., Chagastelles, P. C., and Nardi, N. B. (2006). Mesenchymal Stem Cells Reside in Virtually All post-natal Organs and Tissues. *J. Cel Sci.* 119, 2204–2213. doi:10.1242/jcs.02932
- Meng, F., Xu, R., Wang, S., Xu, Z., Zhang, C., Li, Y., et al. (2020). Human Umbilical Cord-Derived Mesenchymal Stem Cell Therapy in Patients with COVID-19: a Phase 1 Clinical Trial. *Sig Transduct Target. Ther.* 5. doi:10.1038/s41392-020-00286-5
- Merrick, D., Sakers, A., Irgebay, Z., Okada, C., Calvert, C., Morley, M. P., et al. (2019). Identification of a Mesenchymal Progenitor Cell Hierarchy in Adipose Tissue. *Science* 364, 364. doi:10.1126/science.aav2501
- Mo, M., Wang, S., Zhou, Y., Li, H., and Wu, Y. (2016). Mesenchymal Stem Cell Subpopulations: Phenotype, Property and Therapeutic Potential. *Cell. Mol. Life Sci.* 73, 3311–3321. doi:10.1007/s00018-016-2229-7
- Ohinata, Y., Payer, B., O'Carroll, D., Ancelin, K., Ono, Y., Sano, M., et al. (2005). Blimp1 Is a Critical Determinant of the Germ Cell Lineage in Mice. *Nature* 436, 207–213. doi:10.1038/nature03813
- Park, S., Kim, E., Koh, S.-E., Maeng, S., Lee, W.-d., Lim, J., et al. (2012). Dopaminergic Differentiation of Neural Progenitors Derived from Placental Mesenchymal Stem Cells in the Brains of Parkinson's Disease Model Rats and Alleviation of Asymmetric Rotational Behavior. *Brain Res.* 1466, 158–166. doi:10.1016/j.brainres.2012.05.032
- Petersen, B. E., Bowen, W. C., Patrene, K. D., Mars, W. M., Sullivan, A. K., Murase, N., et al. (1999). Bone Marrow as a Potential Source of Hepatic Oval Cells. *Science* 284, 1168–1170. doi:10.1126/science.284.5417.1168
- Pfaender, S., Mar, K. B., Michailidis, E., Kratzel, A., Boys, I. N., V'kovski, P., et al. (2020). LY6E Impairs Coronavirus Fusion and Confers Immune Control of Viral Disease. *Nat. Microbiol.* 5, 1330–1339. doi:10.1038/s41564-020-0769-y
- Phinney, D. G. (2012). Functional Heterogeneity of Mesenchymal Stem Cells: Implications for Cell Therapy. *J. Cel. Biochem.* 113, 2806–2812. doi:10.1002/jcb.24166
- Pittenger, M. F., Discher, D. E., Péault, B. M., Phinney, D. G., Hare, J. M., and Caplan, A. I. (2019). Mesenchymal Stem Cell Perspective: Cell Biology to Clinical Progress. *Npj Regen. Med.* 4. doi:10.1038/s41536-019-0083-6
- Portmann-Lanz, C. B., Schoeberlein, A., Portmann, R., Mohr, S., Rollini, P., Sager, R., et al. (2010). Turning Placenta into Brain: Placental Mesenchymal Stem Cells Differentiate into Neurons and Oligodendrocytes. *Am. J. Obstet. Gynecol.* 202, 294e1–294e11. doi:10.1016/j.ajog.2009.10.893
- Prockop, D. J. (1997). Marrow Stromal Cells as Stem Cells for Nonhematopoietic Tissues. *Science* 276, 71–74. doi:10.1126/science.276.5309.71
- Prockop, D. J., Sekiya, I., and Colter, D. C. (2001). Isolation and Characterization of Rapidly Self-Renewing Stem Cells from Cultures of Human Marrow Stromal Cells. *Cytherapy* 3, 393–396. doi:10.1080/146532401753277229



- Qiu, X., Mao, Q., Tang, Y., Wang, L., Chawla, R., Pliner, H. A., et al. (2017). Reversed Graph Embedding Resolves Complex Single-Cell Trajectories. *Nat. Methods* 14, 979–982. doi:10.1038/nmeth.4402
- Rada-Iglesias, A., Bajpai, R., Swigut, T., Bruggmann, S. A., Flynn, R. A., and Wysocka, J. (2011). A Unique Chromatin Signature Uncovers Early Developmental Enhancers in Humans. *Nature* 470, 279–283. doi:10.1038/nature09692
- Rafei, M., Hsieh, J., Fortier, S., Li, M., Yuan, S., Birman, E., et al. (2008). Mesenchymal Stromal Cell-Derived CCL2 Suppresses Plasma Cell Immunoglobulin Production via STAT3 Inactivation and PAX5 Induction. *Blood* 112, 4991–4998. doi:10.1182/blood-2008-07-166892
- Ringdén, O., Uzunel, M., Rasmusson, I., Remberger, M., Sundberg, B., Lönnies, H., et al. (2006). Mesenchymal Stem Cells for Treatment of Therapy-Resistant Graft-Versus-Host Disease. *Transplantation* 81, 1390–1397. doi:10.1097/01.tp.0000214462.63943.14
- Rodriguez-Fuentes, D. E., Fernández-Garza, L. E., Samia-Meza, J. A., Barrera-Barrera, S. A., Caplan, A. I., and Barrera-Saldaña, H. A. (2021). Mesenchymal Stem Cells Current Clinical Applications: A Systematic Review. *Arch. Med. Res.* 52, 93–101. doi:10.1016/j.arcmed.2020.08.006
- Romanov, Y. A., Svintsitskaya, V. A., and Smirnov, V. N. (2003). Searching for Alternative Sources of Postnatal Human Mesenchymal Stem Cells: Candidate MSC-Like Cells from Umbilical Cord. *Stem Cells* 21, 105–110. doi:10.1634/stemcells.21-1-105
- Schep, A. N., Wu, B., Buenrostro, J. D., and Greenleaf, W. J. (2017). ChromVAR: Inferring Transcription-Factor-Associated Accessibility from Single-Cell Epigenomic Data. *Nat. Methods* 14, 975–978. doi:10.1038/nmeth.4401
- Shi, G., Kenney, A. D., Kudryashova, E., Zani, A., Zhang, L., Lai, K. K., et al. (2021). Opposing Activities of IFITM Proteins in SARS-CoV-2 Infection. *EMBO J.* 40, 1–12. doi:10.15252/emj.2020106501
- Shi, R., Hu, J., Li, W., Wang, Z., Pan, Y., Bai, M., et al. (2019). Protective Effects of Clec11a in Islets against Lipotoxicity via Modulation of Proliferation and Lipid Metabolism in Mice. *Exp. Cell Res.* 384, 111613. doi:10.1016/j.yexcr.2019.111613
- Shi, Y., Wang, Y., Li, Q., Liu, K., Hou, J., Shao, C., et al. (2018). Immunoregulatory Mechanisms of Mesenchymal Stem and Stromal Cells in Inflammatory Diseases. *Nat. Rev. Nephrol.* 14, 493–507. doi:10.1038/s41581-018-0023-5
- Shu, L., Niu, C., Li, R., Huang, T., Wang, Y., Huang, M., et al. (2020). Treatment of Severe COVID-19 with Human Umbilical Cord Mesenchymal Stem Cells. *Stem Cell Res. Ther.* 11, 1–11. doi:10.1186/s13287-020-01875-5
- Song, C., Chen, T., He, L., Ma, N., Li, J.-a., Rong, Y.-F., et al. (2020). PRMT1 Promotes Pancreatic Cancer Growth and Predicts Poor Prognosis. *Cell Oncol.* 43, 51–62. doi:10.1007/s13402-019-00435-1
- Song, N., Wakimoto, H., Rossignoli, F., Bhere, D., Ciccocioppo, R., Chen, K.-S., et al. (2021). Mesenchymal Stem Cell Immunomodulation: In Pursuit of Controlling COVID-19 Related Cytokine Storm. *Stem Cells* 39, 707–722. doi:10.1002/stem.3354
- Stuart, T., Butler, A., Hoffman, P., Hafemeister, C., Papalexi, E., Mauck, W. M., et al. (2019). Comprehensive Integration of Single-Cell Data. *Cell* 177, 1888–1902. e21. doi:10.1016/j.cell.2019.05.031
- Stuart, T., Srivastava, A., Lareau, C., and Satija, R. (2020). Multimodal Single-Cell Chromatin Analysis with Signac. *bioRxiv*, 1109–373613. Available at: <https://www.biorxiv.org/content/10.1101/2020.11.09.373613v1%0Ahttps://www.biorxiv.org/content/10.1101/2020.11.09.373613v1.abstract>.
- Sun, C., Wang, L., Wang, H., Huang, T., Yao, W., Li, J., et al. (2020). Single-cell RNA-Seq Highlights Heterogeneity in Human Primary Wharton's Jelly Mesenchymal Stem/stromal Cells Cultured *In Vitro*. *Stem Cell Res. Ther.* 11, 1–16. doi:10.1186/s13287-020-01660-4
- Talwadekar, M. D., Kale, V. P., and Limaye, L. S. (2015). Placenta-derived Mesenchymal Stem Cells Possess Better Immunoregulatory Properties Compared to Their Cord-Derived Counterparts-A Paired Sample Study. *Sci. Rep.* 5, 1–12. doi:10.1038/srep15784
- Tormin, A., Brune, J. C., Olsson, E., Valcich, J., Neuman, U., Olofsson, T., et al. (2009). Characterization of Bone Marrow-Derived Mesenchymal Stromal Cells (MSC) Based on Gene Expression Profiling of Functionally Defined MSC Subsets. *Cytotherapy* 11, 114–128. doi:10.1080/14653240802716590
- Tran, H. T. N., Ang, K. S., Chevrier, M., Zhang, X., Lee, N. Y. S., Goh, M., et al. (2020). A Benchmark of Batch-Effect Correction Methods for Single-Cell RNA Sequencing Data. *Genome Biol.* 21, 12–32. doi:10.1186/s13059-019-1850-9
- Tsai, C.-C., Chen, Y.-J., Yew, T.-L., Chen, L.-L., Wang, J.-Y., Chiu, C.-H., et al. (2011). Hypoxia Inhibits Senescence and Maintains Mesenchymal Stem Cell Properties through Down-Regulation of E2A-P21 by HIF-TWIST. *Blood* 117, 459–469. doi:10.1182/blood-2010-05-287508
- Turner, C. A., Mack, D. H., and Davis, M. M. (1994). Blimp-1, a Novel Zinc finger-containing Protein that Can Drive the Maturation of B Lymphocytes into Immunoglobulin-Secreting Cells. *Cell* 77, 297–306. doi:10.1016/0092-8674(94)90321-2
- Vegh, I., Grau, M., Gracia, M., Grande, J., De La Torre, P., and Flores, A. I. (2013). Decidua Mesenchymal Stem Cells Migrated toward Mammary Tumors *In Vitro* and *In Vivo* Affecting Tumor Growth and Tumor Development. *Cancer Gene Ther.* 20, 8–16. doi:10.1038/cgt.2012.71
- Wang, M., Guo, J., Zhang, L., Kuek, V., Xu, J., and Zou, J. (2020a). Molecular Structure, Expression, and Functional Role of Clec11a in Skeletal Biology and Cancers. *J. Cel. Physiol.* 235, 6357–6365. doi:10.1002/jcp.29600
- Wang, Q., Li, J., Wang, S., Deng, Q., Wang, K., Dai, X., et al. (2021). Single-cell Transcriptome Profiling Reveals Molecular Heterogeneity in Human Umbilical Cord Tissue and Culture-expanded Mesenchymal Stem Cells. *FEBS J.* 288, 5311–5330. doi:10.1111/febs.15834
- Wang, T., Jing, B., Xu, D., Liao, Y., Song, H., Sun, B., et al. (2020b). PTGES/PGE2 Signaling Links Immunosuppression and Lung Metastasis in Gprc5a-Knockout Mouse Model. *Oncogene* 39, 3179–3194. doi:10.1038/s41388-020-1207-6
- Wang, Z., Qi, Y., Wang, R., Wu, W., Li, Z., Wang, M., et al. (2020c). IGFBP6 Regulates Vascular Smooth Muscle Cell Proliferation and Morphology via Cyclin E-CDK2. *J. Cel. Physiol.* 235, 9538–9556. doi:10.1002/jcp.29762
- West, M. D., Labat, I., Sternberg, H., Larocca, D., Nasonkin, I., Chapman, K. B., et al. (2018). Use of Deep Neural Network Ensembles to Identify Embryonic-Fetal Transition Markers: Repression of COX7A1 in Embryonic and Cancer Cells. *Oncotarget* 9, 7796–7811. doi:10.18632/oncotarget.23748
- Xiang, W., Shi, R., Kang, X., Zhang, X., Chen, P., Zhang, L., et al. (2018). Monoacylglycerol Lipase Regulates Cannabinoid Receptor 2-dependent Macrophage Activation and Cancer Progression. *Nat. Commun.* 9. doi:10.1038/s41467-018-04999-8
- Xing, Z., Wang, X., Liu, J., Zhang, M., Feng, K., and Wang, X. (2021). Expression and Prognostic Value of CDK1, CCNA2, and CCNB1 Gene Clusters in Human Breast Cancer. *J. Int. Med. Res.* 49. doi:10.1177/0300060520980647
- Yen, B. L., Huang, H. I., Chien, C. C., Jui, H. Y., Ko, B. S., Yao, M., et al. (2005). Isolation of Multipotent Cells from Human Term Placenta. *Stem Cells* 23, 3–9. doi:10.1634/stemcells.2004-0098
- Yu, K.-R., Park, S.-B., Jung, J.-W., Seo, M.-S., Hong, I.-S., Kim, H.-S., et al. (2013). HMGA2 Regulates the *In Vitro* Aging and Proliferation of Human Umbilical Cord Blood-Derived Stromal Cells through the mTOR/p70S6K Signaling Pathway. *Stem Cell Res.* 10, 156–165. doi:10.1016/j.scr.2012.11.002
- Yu, Y., Wei, X., Deng, Q., Lan, Q., Guo, Y., Han, L., et al. (2021). Single-Nucleus Chromatin Accessibility Landscape Reveals Diversity in Regulatory Regions across Distinct Adult Rat Cortex. *Front. Mol. Neurosci.* 14, 1–9. doi:10.3389/fnmol.2021.651355
- Zhang, Y., Liu, T., Meyer, C. A., Eeckhoutte, J., Johnson, D. S., Bernstein, B. E., et al. (2008). Model-based Analysis of ChIP-Seq (MACS). *Genome Biol.* 9. doi:10.1186/gb-2008-9-9-r137
- Zhao, X., Zheng, S., Chen, D., Zheng, M., Li, X., Li, G., et al. (2020). LY6E Restricts the Entry of Human Coronaviruses, Including the Currently Pandemic SARS-CoV-2. *bioRxiv* 94, 1–17. doi:10.1101/2020.04.02.021469
- Zheng, G., Xie, Z.-Y., Wang, P., Wu, Y.-F., and Shen, H.-Y. (2020). Recent Advances of Single-Cell RNA Sequencing Technology in Mesenchymal Stem Cell Research. *Wjsc* 12, 438–447. doi:10.4252/WJSC.V12.I6.438
- Zheng, G. X. Y., Terry, J. M., Belgrader, P., Ryvkin, P., Bent, Z. W., Wilson, R., et al. (2017). Massively Parallel Digital Transcriptional Profiling of Single Cells. *Nat. Commun.* 8. doi:10.1038/ncomms14049
- Zhu, Z., Han, C., Xian, S., Zhuang, F., Ding, F., Zhang, W., et al. (2020). Placental Mesenchymal Stromal Cells (PMSCs) and PMSC-Derived Extracellular Vesicles (PMSC-EVs) Attenuated Renal Fibrosis in Rats with Unilateral

- Ureteral Obstruction (UUO) by Regulating CD4+ T Cell Polarization. *Stem Cell Int.* 2020, 1–12. doi:10.1155/2020/2685820
- Zhuang, W., Ge, X., Yang, S., Huang, M., Zhuang, W., Chen, P., et al. (2015). Upregulation of lncRNA MEG3 Promotes Osteogenic Differentiation of Mesenchymal Stem Cells from Multiple Myeloma Patients by Targeting BMP4 Transcription. *Stem Cells* 33, 1985–1997. doi:10.1002/stem.1989
- Zuk, P. A., Zhu, M., Ashjian, P., Ugarte, D. A. De., Huang, J. I., Mizuno, H., et al. (2003). Human Adipose Tissue Is a Source of Multipotent Stem Cells. *Mol. Biol. Cell* 14, 516–528. doi:10.1091/mbc.E02

**Conflict of Interest:** Authors JL, QW, YA, XC, YX, QD, ZL, SW, XD, NL, YH, HY and ZS were employed by the company BGI-Shenzhen.

**Publisher's Note:** All claims expressed in this article are solely those of the authors and do not necessarily represent those of their affiliated organizations, or those of the publisher, the editors and the reviewers. Any product that may be evaluated in this article, or claim that may be made by its manufacturer, is not guaranteed or endorsed by the publisher.

Copyright © 2022 Li, Wang, An, Chen, Xing, Deng, Li, Wang, Dai, Liang, Hou, Yang and Shang. This is an open-access article distributed under the terms of the Creative Commons Attribution License (CC BY). The use, distribution or reproduction in other forums is permitted, provided the original author(s) and the copyright owner(s) are credited and that the original publication in this journal is cited, in accordance with accepted academic practice. No use, distribution or reproduction is permitted which does not comply with these terms.



# Transcriptomic Profile of the Mouse Postnatal Liver Development by Single-Nucleus RNA Sequencing

Jiangshan Xu<sup>1,2†</sup>, Shijie Hao<sup>1,2†</sup>, Quan Shi<sup>2,3</sup>, Qiuting Deng<sup>1,2</sup>, Yujia Jiang<sup>2,4</sup>, Pengcheng Guo<sup>5,6</sup>, Yue Yuan<sup>1,2</sup>, Xuyang Shi<sup>1,2</sup>, Shuncheng Shangguan<sup>6,7</sup>, Huiwen Zheng<sup>2,4</sup>, Guangyao Lai<sup>6,7</sup>, Yaling Huang<sup>2</sup>, Yang Wang<sup>2</sup>, Yumo Song<sup>2</sup>, Yang Liu<sup>2</sup>, Liang Wu<sup>1,2</sup>, Zhifeng Wang<sup>2</sup>, Jiehui Cheng<sup>8</sup>, Xiaoyu Wei<sup>2</sup>, Mengnan Cheng<sup>1,2</sup>, Yiwei Lai<sup>6</sup>, Giacomo Volpe<sup>9</sup>, Miguel A. Esteban<sup>2,5,6,10</sup>, Yong Hou<sup>2</sup>, Chuanyu Liu<sup>2\*</sup> and Longqi Liu<sup>1,2\*</sup>

## OPEN ACCESS

### Edited by:

Mo Li,  
King Abdullah University of Science  
and Technology, Saudi Arabia

### Reviewed by:

Ling Shuai,  
Nankai University, China  
Tao Tan,  
Kunming University of Science and  
Technology, China

### \*Correspondence:

Chuanyu Liu  
liuchuan@genomics.cn  
Longqi Liu  
liulongqi@genomics.cn

<sup>†</sup>These authors contributed equally to  
this work

### Specialty section:

This article was submitted to  
Stem Cell Research,  
a section of the journal  
Frontiers in Cell and Developmental  
Biology

Received: 11 December 2021

Accepted: 11 March 2022

Published: 06 April 2022

### Citation:

Xu J, Hao S, Shi Q, Deng Q, Jiang Y,  
Guo P, Yuan Y, Shi X, Shangguan S,  
Zheng H, Lai G, Huang Y, Wang Y,  
Song Y, Liu Y, Wu L, Wang Z, Cheng J,  
Wei X, Cheng M, Lai Y, Volpe G,  
Esteban MA, Hou Y, Liu C and Liu L  
(2022) Transcriptomic Profile of the  
Mouse Postnatal Liver Development  
by Single-Nucleus RNA Sequencing.  
Front. Cell Dev. Biol. 10:833392.  
doi: 10.3389/fcell.2022.833392

<sup>1</sup>College of Life Sciences, University of Chinese Academy of Sciences, Beijing, China, <sup>2</sup>BGI-Shenzhen, Shenzhen, China, <sup>3</sup>Department of Biology, University of Copenhagen, Copenhagen, Denmark, <sup>4</sup>BGI College and Henan Institute of Medical and Pharmaceutical Sciences, Zhengzhou University, Zhengzhou, China, <sup>5</sup>State Key Laboratory for Zoonotic Diseases, Key Laboratory for Zoonosis Research of Ministry of Education, Institute of Zoonosis, College of Veterinary Medicine, Jilin University, Changchun, China, <sup>6</sup>Laboratory of Integrative Biology, Guangzhou Institutes of Biomedicine and Health, Chinese Academy of Sciences, Guangzhou, China, <sup>7</sup>Joint School of Life Sciences, Guangzhou Medical University and Guangzhou Institutes of Biomedicine and Health, Chinese Academy of Sciences, Guangzhou, China, <sup>8</sup>Guangdong Hospital of Traditional Chinese Medicine, Zhuhai, China, <sup>9</sup>Hematology and Cell Therapy Unit, IRCCS-Istituto Tumori 'Giovanni Paolo II', Bari, Italy, <sup>10</sup>Biological Laboratory (Guangzhou Regenerative Medicine and Health Guangdong Laboratory), Guangzhou, China

**Keywords:** postnatal liver development, single-nucleus transcriptomics, hepatocyte maturation, liver zonation, bile acid synthesis

## INTRODUCTION

The liver plays a vital role in maintaining the physiological homeostasis of mammals and is responsible for many biological processes, including detoxification, bile acid synthesis, glycolysis, and lipid metabolism (Ben-Moshe and Itzkovitz 2019). The liver consists of repeating anatomical units termed liver lobules, including parenchymal and non-parenchymal cells. Hepatocyte, the liver parenchymal cells, account for 60% of hepatic cells composition and 80% of liver mass (Godoy et al., 2013). While the liver non-parenchymal cells (NPCs), including bile duct cell (cholangiocyte), liver endothelial cell (LEC), hepatic stellate cells (HSC), Kupffer cell, and other immune cell populations, account for the remaining 20% of liver mass (MacParland et al., 2018; Aizarani et al., 2019). When the cell function is compromised or its composition becomes abnormal, it can cause many diseases, such as fatty liver disease, cirrhosis, and hepatocellular carcinoma (Saviano et al., 2020).

During embryonic development, a few cells from the endoderm begin to specialize into hepatoblasts around embryonic day (E) 8.5 - E9.0 in mouse embryos (Tremblay and Zaret 2005). By E10.5, hepatoblast, LEC, and HSC start to organize into primitive sinusoidal capillaries (Gordillo et al., 2015). Finally, hepatoblast begin to differentiate into hepatocyte and cholangiocyte approximately at E13.5 (Roskams and Desmet 2008; Yang et al., 2017). In those developmental processes, several transcription factors and signaling pathways, including *Hhex*, hepatocyte nuclear factor 4α (*Hnf4α*), fibroblast growth factors (FGFs), bone morphogenetic proteins (BMPs), Wnt/β-catenin, and Hippo pathway play essential roles (Bort et al., 2006; McLin et al., 2007; Negishi et al., 2010; Alder et al., 2014; Wang et al., 2015; Ober and Lemaigre 2018). Until E16.5, the liver is the main hematopoietic organ in the body, then gradually becomes a metabolic organ (Zaret 2002). After birth, both the nutrient metabolism and the immune system in the liver will undergo significant transformations in response to drastic changes, such as the primary source of energy switching from glucose in the cord blood to lipids in breast milk (Ehara et al., 2015). As a result, metabolic pathways, including fatty acid β-oxidation, gluconeogenesis, and *de novo* lipogenesis, are upregulated in the neonatal liver (Perichon and Bourre 1995; Sekine et al., 2007).

After a short period of adaptation, hepatocytes begin to proliferate and differentiate rapidly around postnatal day 3 (P3), as a result of increased  $\beta$ -catenin signaling (Apte et al., 2007). By P7, the liver lobule structure has been formed (Ober and Lemaigre 2018), becomes more intact, and performs several functions, including xenobiotic metabolism, steroid metabolism, and bile acids biosynthetic (Li et al., 2009; Cui et al., 2012).

In recent years, single-cell transcriptome sequencing has been developing rapidly and has been applied in many research fields, such as cell atlas construction, as well as studying embryo development and disease pathogenesis (Granja et al., 2019; Tang et al., 2019; Cao et al., 2020; Trevino et al., 2021). In terms of liver development, single-cell transcriptome sequencing has been used to elucidate the origin of hepatoblasts, the differentiation trajectory of hepatoblasts and NPCs, and the interaction among different cell types (Popescu et al., 2019; Lotto et al., 2020; Mu et al., 2020; Wang et al., 2020). However, few single-cell transcriptomic studies on liver development in mice after birth. A robust and comprehensive bulk RNA sequencing study was performed to characterize the liver development spanning E12.5 to postnatal week 8, which found that many important liver metabolic functions are acquired after birth (Gong et al., 2020). However, bulk RNA sequencing cannot distinguish the gene expression of different cell types and does not provide information about cell-cell interaction and microenvironment composition, thus calling for a more systematic single-cell transcriptome study of postnatal liver development. Moreover, single-nucleus RNA sequencing (snRNA-seq) has an obvious advantage over single-cell RNA sequencing (scRNA-seq) in detecting multiple cell types without any bias (Zeng et al., 2016; Lake et al., 2017; Bakken et al., 2018; Ding et al., 2020). This is crucial for liver tissue because hepatocytes are prone to cell death during liver single-cell isolation, and obtaining HSCs and cholangiocytes remains quite challenging. In addition, it could lead to skewed cell types ratio in scRNA-seq datasets (Donne et al., 2020; Brazovskaja et al., 2021; Guillems et al., 2022).

For this study, we performed snRNA-seq to profile 82,967 nuclei from four key time points of postnatal murine liver development (P0, P3, P7, P14). We identified 28 clusters of hepatic cell types and analyzed the dynamic changes in cells composition and functions and the hepatocyte differentiation trajectories during this process. Interestingly, we found two HSC subtypes specifically expressing some markers of LECs or Kupffer cells. In addition, the ligand-receptor interaction and transcription factor regulative activity analysis significantly increased the reliability of the new cell types.

## MATERIALS AND METHODS

### Sample Collection

All mice used in this study were in C57BL/6 background. The Institutional Review Board approved the use of mice in relevant experimental studies on the Ethics Committee of BGI (Permit No. BGI-IR20210903001). Four neonatal mice from different time points (P0, P3, P7, P14) after birth were purchased from Jiangsu

Ailingfei Biotechnology Co. LTD. and used in this study. Mice were transported to the Guangzhou Institute of Biomedicine and Health (GIBH) of the Chinese Academy of Sciences, where GIBH colleagues helped with tissue dissection. Liver tissues were harvested, resected, and snap-frozen in liquid nitrogen. The dissected mouse liver tissues were transported on dry ice to BGI-Shenzhen and were immediately stored in a liquid nitrogen tank.

### Nuclei Isolation From Frozen Tissues

Nuclei were isolated from frozen mouse liver tissue according to a published nucleus extraction method (Corces et al., 2017). All the subsequent procedures were performed on ice. Briefly, each frozen liver tissue was cut into pieces and transferred to a prechilled 2 ml tissue Dounce homogenizer (Sigma, #D8938-1SET) with 2 ml of ice-cold homogenization buffer [500 mM sucrose (Sigma, #69293), 1% BSA (Sigma, #V900933-100G) in nuclease-free water, 20 mM Tris pH 8.0 (Sigma, #T2694-1L) 50 mM KCl (Sigma, #P5405), 10 mM  $MgCl_2$  (Sigma, #2670-100g), 0.1% NP-40 (Invitrogen, #FNN0021), 1  $\times$  protease inhibitor cocktail (Thermo Scientific, #87786), 0.1 mM DTT (Sigma, #646563), and 0.12 U/ $\mu$ l RNasin Plus (Promega, #N2115)]. The tissue was incubated on ice for 5 min and homogenized by 25 strokes of the loose Dounce pestle, after which the homogenate was filtered through a 70  $\mu$ m cell strainer (Sigma, #CLS431752-50EA). Next, the filtered homogenate was further homogenized by 25 strokes of the tight pestle to release nuclei, then filtered through a 40  $\mu$ m cell strainer (Sigma, #CLS431750-50EA) into a 15 ml centrifuge tube and centrifuged at 500 g for 5 min. The sediment was resuspended in 1.5 ml blocking buffer containing 1  $\times$  phosphate buffer saline (PBS, Thermo Fisher Scientific, #10010049), 1% filtered sterilized BSA, and 0.2 U/ml RNasin Plus by pipetting up and down gently and centrifuged at 500 g for 5 min. The previous step was repeated once. The nuclei were resuspended in 0.04% BSA of PBS, then counted by DAPI (Beyotime, #C1006) staining and diluted to a concentration of 1,000 nuclei/ $\mu$ l.

### snRNA-Seq Library Preparation and Sequencing

The single-nucleus RNA-seq libraries were prepared as previously described (Liu et al., 2019) with DNBelab C Series High-throughput Single-Cell RNA Library Preparation Kit (MGI, 940-000047-00). Briefly, the single cell suspension, barcoded mRNA capture beads, and droplet generation oil were loaded into the corresponding reservoirs on the chip for droplet generation. The droplets were placed at room temperature for 20 min and then broken and collected by the bead filter. The beads pellet was resuspended with 100  $\mu$ l RT mix. The mixture was then thermal cycled as follows: 42°C for 90 min, 10 cycles of 50°C for 2 min, 42°C for 2 min. The PCR master mix was added to the beads pellet, and thermal cycled as follows: 95°C for 3 min, 15 cycles of 98°C for 20 s, 58°C for 20 s, 72°C for 3 min, and finally 72°C for 5 min. Amplified cDNA was purified using 60  $\mu$ l of DNA clean beads (VAZYME, #N411-03). According to the manufacturer protocol, the cDNA was subsequently



fragmented by NEBNext dsDNA Fragmentase (New England Biolabs, #M0348L). The indexed sequencing libraries were constructed and sequenced using the DIPSEQ T10 sequencer at the China National GeneBank.

## Raw Sequencing Data Processing

The read structure was paired-end with read 1 covering 30 bases in which the 1st–20th bases were cell barcodes, and the 21st–30th bases were unique molecular identifier (UMI) sequences. The read 2 contains 100 bp of transcript sequences. The PISA software (<https://github.com/shiquan/PISA>) was used to parse raw reads into FASTQ+ format based on the library structure and correct cell barcodes with the allow list if the hamming distance is equal or lower than one. The reformed reads were aligned to reference genome GRCm38 (mm10) by using STAR (Dobin et al., 2013) software. SAM files were transformed into BAM files and annotated with a reference gene set using PISA software. The UMIs in reads with the same cell barcode and gene annotation containing 1 bp mismatch were corrected to the most supported one. Then, we filtered the empty droplets by using R package DropletUtils (Lun et al., 2019). A final cell-x-gene matrix was generated by PISA too. The SoupX (Young and Behjati 2020) software was harnessed to remove the influence of ambient RNA.

## Doublet Filtering, Batch Effect Eliminating, and Cell Clustering

The final cell-x-gene matrix was introduced into the Seurat (v4.0.0) package to create a Seurat object followed by normalization, scaled, and dimensionality reduce by the CreateSeuratObject, NormalizeData, FindVariableFeatures, ScaleData, and RunPCA functions in turn with default parameters (Hao et al., 2021). Then, we performed the DoubletFinder (v2.0.3) package to filter the doublet cells (McGinnis et al., 2019). The CCA algorithm implemented by the FindIntegrationAnchors and IntegrateData functions in Seurat was used to integrate all the filtered objects from each sample. Finally, taking advantage of the FindNeighbors and FindClusters functions, we divided all cells into 20 clusters covering the most common hepatic cell types.

## Hepatocyte Trajectory Inference

About 10,000 hepatocytes were extracted from the integrated Seurat object and introduced into Monocle 2 (v2.18.0) by the as.CellDataSet function (Trapnell et al., 2014). Then, we reduced the dimensions by using the reduceDimension function with the method of DDRTree. At last, we inferred the pseudo-temporal cell transition process and split cells into 13 states with the orderCells function. Finally, the genes changing along pseudotime were identified using the differentialGeneTest function with the formula “~sm.ns (Pseudotime)”.

## Regulatory Network Inference

To investigate the possible regulatory network intra- or inter-cell, we performed transcript factor regulatory analysis and ligand-receptor interaction analysis by using the pySCENIC (v0.11.2) (Van de Sande et al., 2020) package and CellChat (v1.1.0) (Jin

et al., 2021) package, following the tutorials respectively. The transcript factors regulative activity matrix, exported from the pySCENIC pipeline, was inserted to the Seurat object as a new assay, and the cell type-specific regulons were identified by using the FindAllMarkers function of Seurat and visualized by the DimPlot function of Seurat. In addition, the netVisual\_circle function visualized the ligand-receptor-interaction results.

## Visualization

The marker gene dot plot and Uniform Manifold Approximation and Projection (UMAP) were visualized by the DotPlot and DimPlot functions of Seurat, respectively. The bar plot of GO term enrichment was visualized by the barplot function of the clusterProfiler package (v3.18.1) (Yu et al., 2012). The plot\_cell\_trajectory function of Monocle 2 visualized the trajectory embedding dot plot. Other dot plots, box plots, violin plots, bar plots, and stream plots were visualized by ggplot2 package (v3.3.3) with the color palette of ArchR package (v1.0.1) (Hadley 2016; Granja et al., 2021).

## RESULTS

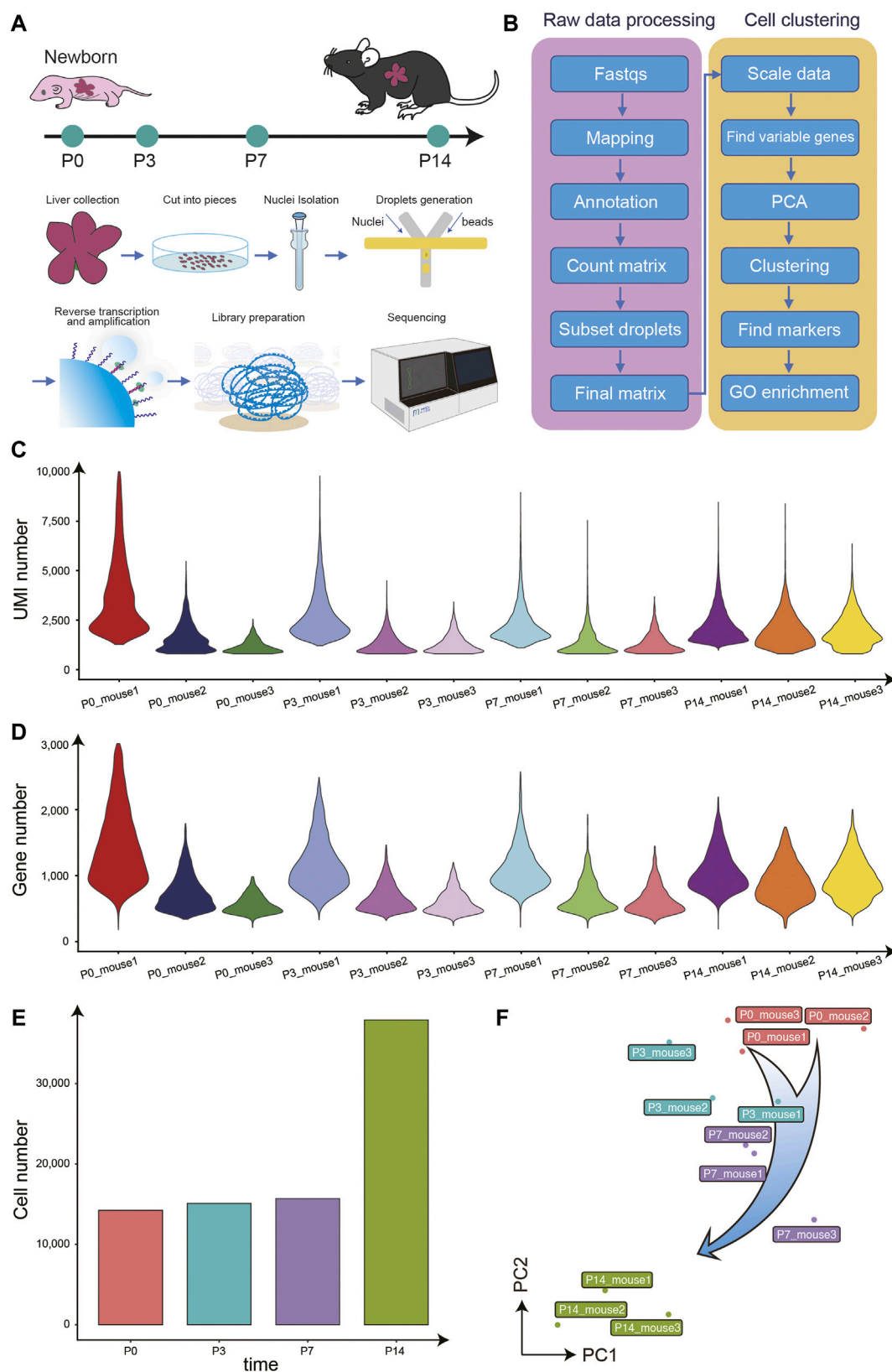
### snRNA-Seq Data Quality Control

To generate an overview of postnatal liver development at the single-cell resolution, we performed snRNA-seq on the liver of mice at P0, P3, P7, P14, and there are three biological replicates at each time point (Figure 1A). First, we evaluated the raw sequencing data quality through several parameters, including the total reads number, the fraction of reads with a valid barcode, and Q30 of reads and barcodes. Around 36,370 million of the raw reads were filtered into a total of 26,610 million clean reads (Supplementary Table 1). The average bases Q30 in reads and barcodes were 87.6 and 92.0%, respectively. Following the raw data preprocessing, we performed the data parsing, reads mapping, alignment annotation, and matrix counting. To further eliminate the effect of doublets in snRNA-seq data, we performed one round of doublet filtering (Figure 1B).

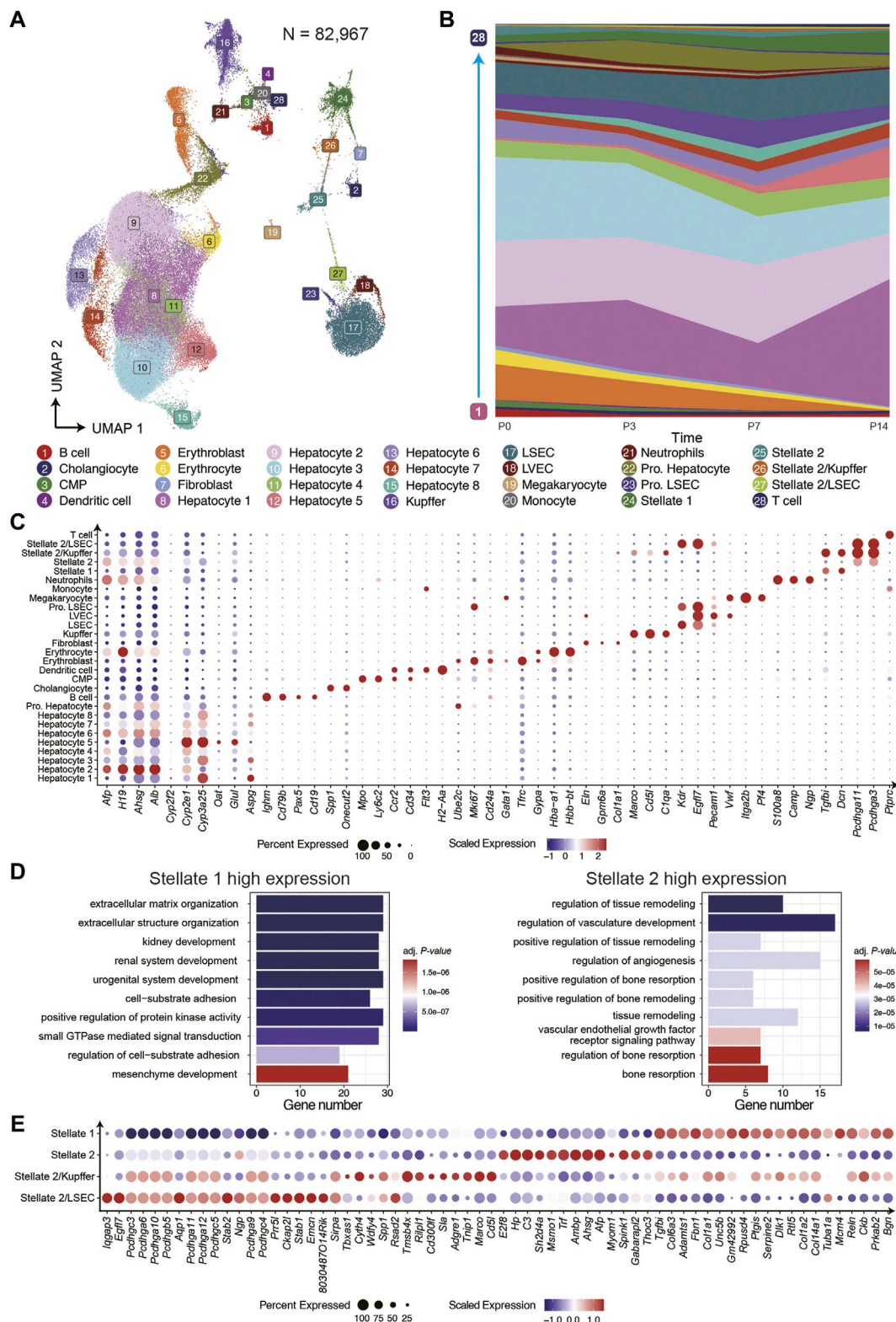
In total, 82,967 single nucleus transcriptomes from the 39 snRNA-seq libraries passed quality control, with a median number of 2,254 UMIs and 1,005 genes per cell (Figures 1C–E). Besides, the principal component analysis (PCA) showed that samples from the same time point clustered together and the P14 libraries were far away from the libraries of the other three time points, consistent with previous reports (Gong et al., 2020; Chembazhi et al., 2021), indicating the high library quality and repeatability (Figure 1F).

### Cell Types Composition During Postnatal Liver Development

To investigate the cells composition and the functional diversity of different cell types during postnatal liver development at single-cell resolution, we integrated all snRNA-seq data from four time points and clustered them into 28 clusters with eliminated batch effect by using Seurat (Figure 2A; Supplementary Figure 1). We further annotated the 28



**FIGURE 1 |** Overview of the experimental design, data analysis workflow, and snRNA-seq data quality control. **(A)** The mouse liver samples of four different time points after birth were collected for snRNA-seq profiling. **(B)** The analysis workflow for snRNA-seq profiles. **(C)** The violin plot for the UMIs number of each library. **(D)** The violin plot for the genes number of each library. **(E)** The histogram for the cell numbers each time point. **(F)** The PCA analysis for all libraries.



**FIGURE 2 |** The cell type composition of postnatal liver development. **(A)** The UMAP of snRNA-seq data displayed 28 clusters in four time points. **(B)** The cell composition was dynamic at four time points. **(C)** The dot plot for cell-type-specific genes expression in 28 clusters. **(D)** The GO term enrichment analysis of differential genes of two hepatic stellate clusters. **(E)** Highly expressed genes in hepatic stellate cell subtypes

clusters to the known liver resident cell types based on the distinct expression of canonical marker genes and analyzed the changes of cell composition at different time points. (**Figures 2B,C; Supplementary Figure 2**).

For hepatocytes, we identified nine subtypes at different stages of differentiation. The hepatocytes 2, 3, and 6 were immature cells in the early stage of postnatal liver development. These cells highly expressed *Afp*, *H19*, and *Ahsg*, which were essential factors for hepatocyte differentiation and tumorigenesis in hepatocellular carcinoma (HCC) (Lazarevich 2000; Kalabay et al., 2007; Pope et al., 2017). The hepatocytes 1, 4, 5, 7, and 8 were characterized by the high expression of genes related to liver metabolic functions, and the proportion of these cells increased gradually during postnatal liver development. The genes exclusively expressed in hepatocyte 1 contained many periportal exhibited features in the adult mouse liver, such as *Apsg*, *Sds*, and *Cyp2f2* (Halpern et al., 2017; Ben-Moshe et al., 2019). On the contrary, the genes highly expressed in the hepatocyte 5 contained more pericentral features of the liver zonation, such as *Glul*, *Cyp2e1*, and *Oat*. The Pro. Hepatocyte group consisted of proliferating hepatocytes and highly expressed proliferation genes, such as *Mki67* and *Ube2c*, with those cells being more abundant in P3 and P7. The Cholangiocytes were detected at all time points, specifically expressing *Spp1* and *Onecut2*. And the latter one may be a new marker gene.

Regarding the liver resident non-parenchymal cells, including LEC, HSC, Kupffer cell, we identified many cell subtypes and compared their cell proportion at all time points. Besides, the Kupffer cells increased significantly at P3 and P7 but decreased sharply at P14, suggesting more immune challenges to respond to drastic environmental changes after birth. On the other hand, three LEC clusters, including liver sinusoidal endothelial cell (LSEC), proliferating endothelial cell, and liver vessel endothelial cell (LVEC), that specifically expressed *Vwf* were discovered. For mesenchymal cells, we identified two HSCs subtypes and fibroblast. The fibroblast distinctively expressed *Eln*, *Colla1*, and *Gpm6a*. In addition, both the HSC subtypes expressed classical marker genes *Dcn*, *Reln*, and *Fgfb*.

Interestingly, the stellate 2 exclusively expressed many genes of the protocadherin family, indicating a critical role in establishing the specific cell-cell connections (Hirayama et al., 2012). Next, we compared the differential expressed genes (DEGs) of these two groups of HSCs and performed the Gene Ontology (GO) terms enrichment analysis. We found that stellate 1 highly expressed genes related to extracellular matrix organization and cell adhesion, while the DEGs of stellate 2 were mainly enriched in signaling pathways related to angiogenesis and hypoxia response (**Figure 2D**). The cluster stellate 2 displayed a transitional pattern in UMAP spanning LSEC to Stellate 1, indicating its composition complexity. For a deeper understanding of stellate 2, we regrouped it into three subgroups and identified the marker genes in each population (**Figure 2E**). There were two new heterogeneous cell types in these three subgroups, one of which expressing *Cd51* and *Marco* was annotated as Stellate 2/Kupffer, which was recently

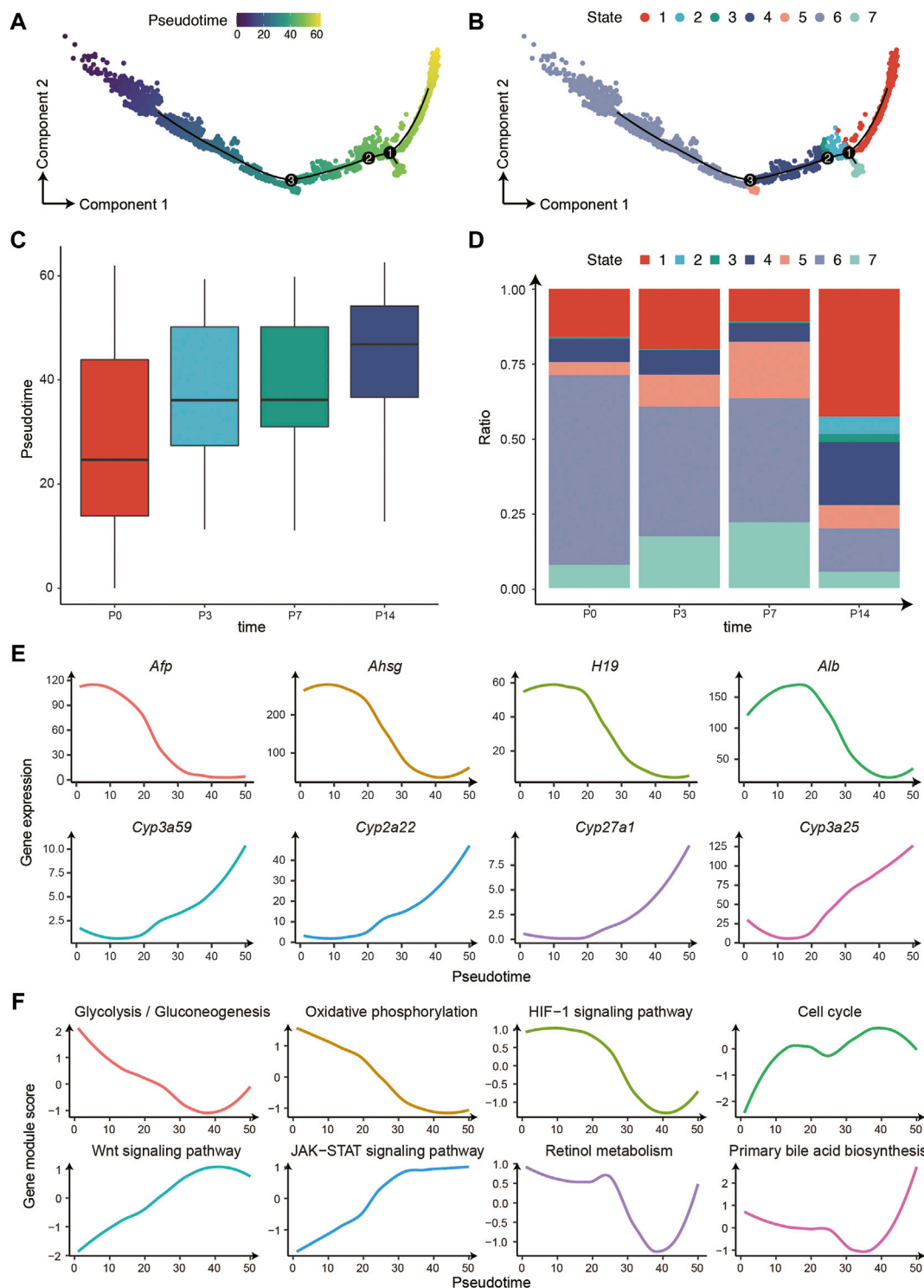
mentioned by a published paper (Liang et al., 2022). Another heterozygous group expressing *Kdr* and *Egfl7* was annotated as Stellate 2/LSEC. Further, we analyzed the ligand-receptor interactions between stellate and other cell types and found the multiplex functions of these two heterogeneous subgroups (**Supplementary Figure 3**). For example, the VEGF signaling pathway is enriched in Stellate 2/LSEC cell and LSEC; the AGT signaling pathway is more enriched in Stellate 2/Kupffer cell and Kupffer. These results further suggest that the newly discovered cell types are reliable. Moreover, we found the CDH signaling pathway enriched among hepatocytes, proliferating hepatocytes, and stellate 2, indicating the effect of stellate 2 on hepatocyte proliferation.

We also identified many NPCs cell types of hematopoietic origin that can be grouped into three main lineages: lymphoid, myeloid, and erythroid. We observed several clusters of B cells at different stages of differentiation, as characterized by the expression of genes involved in regulating B cells differentiation and maturation, such as *Pax5*, *Cd79b*, and *Cd19*. In our study, T cells were also found expressing *Ptprc* (*Cd45*). The myeloid cells identified in our datasets consisted of common myeloid progenitor (CMP), neutrophils, monocytes, and dendritic cells, expressing classic marker genes, such as *Mpo*, *S100a8*, *Ccr2*, and *H2-Aa*, respectively. The erythroid lineage contained erythroblast and immature erythrocyte, both of which highly expressed *Hba-a1* and *Hbb-bt*. The erythroblast, also highly expressed *Gypa* and *Gata1* are a critical determinant of erythrocyte differentiation (Cao et al., 2020). In addition, we observed the expression of genes associated with platelet formation, such as *Pf4* and *Plek*, in megakaryocytes (Italiano and Shivdasani 2003) (**Figure 2C; Supplementary Figure 2**). Almost all these developing hematopoietic cells except for T cells gradually decreased during liver development and eventually disappeared by P14, which is consistent with the conclusion of a paper published in the journal of Hepatology in 2018 (Nakagaki et al., 2018).

## Cellular Trajectory of Hepatocyte Differentiation

To further characterize the hepatocyte differentiation process and the liver metabolic function dynamics, we used Monocle 2 to establish the developing trajectory and calculated the pseudotime for each nucleus (**Figure 3A**). There was a clear differentiation trajectory from left to right, consisting of three branching points that divide all hepatocytes into 7 states (**Figure 3B**). In addition, the pseudotime distribution and cell state composition across four time points displayed great coordination, further confirming the validity of our trajectory analysis (**Figures 3C,D**). Furthermore, we analyzed the variation of a series of essential genes related to liver development and found that the expression of marker genes of immature hepatocytes decreased gradually along the trajectory, such as *Afp*, *Ahsg*, and *H19*. In contrast, the expression of liver metabolism-related genes increased significantly, such as *Cyp3a59*, *Cyp2a22*, *Cyp27a1*, and





**FIGURE 3 |** The differentiation trajectory of hepatocytes. **(A)** The trajectory of hepatocyte development from P0 to P14 with Monocle 2. The colors from blue to yellow indicate an increased pseudotime. **(B)** The trajectory is the same as **(A)**. The colors represent 7 different states. **(C)** The boxplot for the pseudotime distribution in four time points. **(D)** The histogram displayed the hepatocyte numbers of 7 states in four time points. **(E)** The gene expression changes patterns along the trajectory. **(F)** The pathway changes patterns along the trajectory.

*Cyp3a25* (Figure 3E). Therefore, the trajectory reconstructed the procession of hepatocyte maturation.

Moreover, we investigated the pathway changes along the differentiation trajectory of hepatocytes (Figure 3F). The dynamic of these pathways can be further divided into three main categories: 1) The decreased pathways including glycolysis/gluconeogenesis, oxidative phosphorylation, and *HIF-1* signaling pathway, possibly owing to the changes of oxygen and nutrients supply after birth (Bohme et al., 1983); 2) Pathways that increased in P3 and P7 and decreased in P14, including cell cycle and WNT signaling pathway, which regulates the proliferative capacity of hepatocytes; 3) The increased pathways including the JAK-STAT signaling pathway, retinol metabolism, and bile secretion, that are mainly involved in the acquisition of metabolic function of hepatocytes post birth.

## Cell Type-Specific Transcription Factor Activity Analysis

Finally, we investigate the essential regulatory genes in the mouse liver development process after birth. We performed single-cell regulatory network inference and clustering (SCENIC) analysis (Aibar et al., 2017). And we captured 12 cell type-specific transcription factors (Regulon) that may significantly affect the fate of hepatic cells and liver function in adults (Supplementary Figure 4). For instance, FOXA2 (Hepatocyte Nuclear Factor 3-Beta, HNF3B), HNF4A, and SOX9 are essential in determining the differentiation of hepatoblast (Gordillo et al., 2015), had higher regulative activity in hepatocytes or cholangiocytes. Besides, NR1H4, NR1I2, and CEBPB can affect multiple liver functions, including bile acid synthesis and transport, detoxification, and regeneration (Milnes et al., 2008; Jakobsen et al., 2013; Haeusler et al., 2016) had different regulative activity in different hepatocyte subgroups, implying their various functions in hepatocyte development. For the liver non-parenchymal cells, we found that: TCF4 is enriched explicitly in LEC; MAFB is enriched explicitly in Kupffer cell; GATA6 and FOXF1 are enriched in fibroblast and stellate, 1 respectively. Mainly TFAP4 was extremely cell type-specific in stellate 2, a gene that promotes tumorigenic capability and activates the Wnt/ $\beta$ -catenin pathway in hepatocellular carcinoma in previous studies (Zhao and Duncan 2005; Song et al., 2018).

## CONCLUSION

In summary, we profiled the single-nucleus transcriptome of mouse postnatal liver development at four time points, identified 28 different hepatic cell types, and investigated the dynamic of cells composition. Interestingly, we identified a new subtype of hepatic stellate cells that exclusively expressed many genes of the protocadherin family, such as *Pcdhg3* and *Pcdhg11*, which may be of great importance in the establishment of specific cell-cell connections. Furthermore, by regrouping and annotation,

we obtained two new heterogeneous cell subtypes in stellate 2, respectively expressed markers of LEC and Kupffer cell, including *Egfl7*, *Kdr*, *Cd5l*, and *Macro*. Moreover, the CellChat analysis showed that the CDH signaling pathway only enriched among hepatocyte clusters and stellate 2, which may influence the proliferation of hepatocyte. For hepatic parenchyme cell, we identified several immature hepatocyte subtypes and cholangiocyte, respectively highly expressed *Afp*, *Ahsg*, *Spp1*, and *Onecut2*. But we do not find the liver stem cell population (hepatoblast) by checked the expression levels of classic marker genes, such as *Dlk1*, *Nope*, *Cd24a*, *Prom1* and *Epcam*, which is consistent with the known fact that hepatoblast differentiation mainly occurs from E13.5 to E18.5 during mouse embryonic development (Miyajima et al., 2014; Gordillo et al., 2015; So et al., 2020; Wang et al., 2020). Consider that two important recent studies by lineage tracing in mice have reported that there are no adult stem cells in the liver, but that there are differences in the regional hepatocyte proliferation of the liver lobule (He et al., 2021; Wei et al., 2021), so we think that there are only immature hepatic cells in the mouse liver after birth according to the data of this study, which requires further experimental verification by assays including chimera or organoid (Leeb and Wutz 2011; Leeb and Wutz 2012; Takebe et al., 2017; Li et al., 2018). Such immature hepatic cells during liver development are very important for the study of expanded culture of hepatocytes *in vitro*, organoid and disease models, because they have some similar characteristics to hepatocyte progenitor cells and strong cellular plasticity (Li et al., 2020). In addition, we found that several signaling pathways changed along the hepatocytic differentiation trajectory, such as glycolysis/gluconeogenesis, oxidative phosphorylation, bile secretion, JAK-STAT, WNT signaling pathway, among others. Finally, we identified key transcription factors activity enriched in different cell clusters, including FOXA2 (HNF3B), HNF4A, and SOX9. Both FOXA2 and HNF4A are pioneer hepatocyte transcription factors for the differentiation of embryonic stem cell from the foregut endoderm into hepatoblast during embryonic development, which activated liver-specific genes such as *Alb* and *Ttr* (Olsen and Jeffery 1997; Alder et al., 2014; Gordillo et al., 2015). SOX9 significantly affect hepatoblast differentiated into cholangiocyte and has been used as a marker gene for liver progenitor cell in certain conditions for a period of time (Antonioni et al., 2009; Tarlow et al., 2014). In a word, this dataset will be a valuable resource to understand the fundamental biological events in postnatal liver development, such as the differentiation process of hepatocytes, angiogenesis, and the postnatal acquisition of metabolic functions.

## DATA AVAILABILITY STATEMENT

The datasets presented in this study can be found in online repositories. The names of the repository/repositories and accession number(s) can be found below: BioProject:

PRJNA790690 and China National GeneBank DataBase (CNCBdb) Project accession : CNP0002461.

## ETHICS STATEMENT

The animal study was reviewed and approved by The Ethics Committee of BGI.

## AUTHOR CONTRIBUTIONS

JX, SH, CL, and LL conceived the idea. PG, SS, and GL collected the samples. JX generated the data. QD, YJ, YY, MC, ZW, JC, PG, XS, SS, GL, YLH, YW and YH assisted with the experiments. SH analyzed the data with the assistance of QS, HZ, XW, YL, LW and YS. JX wrote the manuscript with the input of SH. CL and LL supervised the study. YL, ME, YH and GV provided helpful comments on this study and revised the manuscript. All authors contributed to the article and approved the submitted version.

## FUNDING

LL was supported by the Shenzhen Basic Research Project for Excellent Young Scholars (RCYX20200714114644191). ME was supported by the Innovative Team Program of Bioland Laboratory (Guangzhou Regenerative Medicine and Health

Guangdong Laboratory) (2018GZR110103001) and a Guangdong Basic and Applied Basic Research Foundation (2021B1515120075).

## ACKNOWLEDGMENTS

We thank all members of the Center for Digitizing Cells from the Institute of SuperCells (BGI) for helpful comments and colleagues from Guangzhou Institutes of Biomedicine and Health, Chinese Academy of Sciences for assistance with sample collection. We thank China National GeneBank for providing technical support.

## SUPPLEMENTARY MATERIAL

The Supplementary Material for this article can be found online at: <https://www.frontiersin.org/articles/10.3389/fcell.2022.833392/full#supplementary-material>

**Supplementary Figure 1** | The UMAP of snRNA-seq data shows 20 clusters in four time points.

**Supplementary Figure 2** | Cell-type-specific marker genes expression visualized by UMAP.

**Supplementary Figure 3** | HSCs related ligand-receptor interaction network.

**Supplementary Figure 4** | Cell-type-specific transcription factors regulation activity visualized by UMAP.

**Supplementary Table 1** | snRNA-seq raw data statistics.

## REFERENCES

- Aibar, S., González-Blas, C. B., Moerman, T., Huynh-Thu, V. A., Imrichova, H., Hulselmans, G., et al. (2017). SCENIC: Single-Cell Regulatory Network Inference and Clustering. *Nat. Methods* 14 (11), 1083–1086. doi:10.1038/nmeth.4463
- Aizarani, N., Saviano, A., Sagar, Mailly, L., DurandHerman, S. J. S., Herman, J. S., et al. (2019). A Human Liver Cell Atlas Reveals Heterogeneity and Epithelial Progenitors. *Nature* 572 (7768), 199–204. doi:10.1038/s41586-019-1373-2
- Alder, O., Cullum, R., Lee, S., Kan, A. C., Wei, W., Yi, Y., et al. (2014). Hippo Signaling Influences HNF4A and FOXA2 Enhancer Switching during Hepatocyte Differentiation. *Cel Rep.* 9 (1), 261–271. doi:10.1016/j.celrep.2014.08.046
- Antoniou, A., Raynaud, P., Cordi, S., Zong, Y., Tronche, F., Stanger, B. Z., et al. (2009). Intrahepatic Bile Ducts Develop According to a New Mode of Tubulogenesis Regulated by the Transcription Factor SOX9. *Gastroenterology* 136 (7), 2325–2333. doi:10.1053/j.gastro.2009.02.051
- Apte, U., Zeng, G., Thompson, M. D., Muller, P., Micsenyi, A., Cieply, B., et al. (2007).  $\beta$ -Catenin Is Critical for Early Postnatal Liver Growth. *Am. J. Physiology-Gastrointestinal Liver Physiol.* 292 (6), G1578–G1585. doi:10.1152/ajpgi.00359.2006
- Bakken, T. E., Hodge, R. D., Miller, J. A., Yao, Z., Nguyen, T. N., Aeversmann, B., et al. (2018). Single-nucleus and Single-Cell Transcriptomes Compared in Matched Cortical Cell Types. *PLoS One* 13 (12), e0209648. doi:10.1371/journal.pone.0209648
- Ben-Moshe, S., and Itzkovitz, S. (2019). Spatial Heterogeneity in the Mammalian Liver. *Nat. Rev. Gastroenterol. Hepatol.* 16 (7), 395–410. doi:10.1038/s41575-019-0134-x
- Ben-Moshe, S., Shapira, Y., Moor, A. E., Manco, R., Veg, T., Bahar Halpern, K., et al. (2019). Spatial Sorting Enables Comprehensive Characterization of Liver Zonation. *Nat. Metab.* 1 (9), 899–911. doi:10.1038/s42255-019-0109-9
- Böhme, H.-J., Sparmann, G., and Hofmann, E. (1983). Biochemistry of Liver Development in the Perinatal Period. *Experientia* 39 (5), 473–483. doi:10.1007/bf01965164
- Bort, R., Signore, M., Tremblay, K., Barbera, J. P. M., and Zaret, K. S. (2006). Hex Homeobox Gene Controls the Transition of the Endoderm to a Pseudostratified, Cell Emergent Epithelium for Liver Bud Development. *Develop. Biol.* 290 (1), 44–56. doi:10.1016/j.ydbio.2005.11.006
- Brazovskaja, A., Gomes, T., Körner, C., He, Z., Schaffer, T., Eckel, J. C., et al. (2021). Cell Atlas of the Regenerating Human Liver after portal Vein Embolization. *BioRxiv*. doi:10.1101/2021.06.03.444016
- Cao, J., O'Day, D. R., Pliner, H. A., Kingsley, P. D., Deng, M., Daza, R. M., et al. (2020). A Human Cell Atlas of Fetal Gene Expression. *Science* 370 (6518), eaba7721. doi:10.1126/science.aba7721
- Chembazhi, U. V., Bangru, S., Hernaez, M., and Kalsotra, A. (2021). Cellular Plasticity Balances the Metabolic and Proliferation Dynamics of a Regenerating Liver. *Genome Res.* 31 (4), 576–591. doi:10.1101/gr.267013.120
- Corces, M. R., Trevino, A. E., Hamilton, E. G., Greenside, P. G., Sinnott-Armstrong, N. A., Vesuna, S., et al. (2017). An Improved ATAC-Seq Protocol Reduces Background and Enables Interrogation of Frozen Tissues. *Nat. Methods* 14 (10), 959–962. doi:10.1038/nmeth.4396
- Cui, J. Y., Renaud, H. J., and Klaassen, C. D. (2012). Ontogeny of Novel Cytochrome P450 Gene Isoforms during Postnatal Liver Maturation in Mice. *Drug Metab. Dispos* 40 (6), 1226–1237. doi:10.1124/dmd.111.042697
- Ding, J., Adiconis, X., Simmons, S. K., Kowalczyk, M. S., Hession, C. C., Marjanovic, N. D., et al. (2020). Systematic Comparison of Single-Cell and Single-Nucleus RNA-Sequencing Methods. *Nat. Biotechnol.* 38 (6), 737–746. doi:10.1038/s41587-020-0465-8

- Dobin, A., Davis, C. A., Schlesinger, F., Drenkow, J., Zaleski, C., Jha, S., et al. (2013). STAR: Ultrafast Universal RNA-Seq Aligner. *Bioinformatics* 29 (1), 15–21. doi:10.1093/bioinformatics/bts635
- Donne, R., Saroul-Ainama, M., Cordier, P., Celton-Morizur, S., and Desdouets, C. (2020). Polyploidy in Liver Development, Homeostasis and Disease. *Nat. Rev. Gastroenterol. Hepatol.* 17 (7), 391–405. doi:10.1038/s41575-020-0284-x
- Ehara, T., Kamei, Y., Yuan, X., Takahashi, M., Kanai, S., Tamura, E., et al. (2015). Ligand-Activated PPAR $\alpha$ -dependent DNA Demethylation Regulates the Fatty Acid  $\beta$ -Oxidation Genes in the Postnatal Liver. *Diabetes* 64 (3), 775–784. doi:10.2337/db14-0158
- Godoy, P., Hewitt, N. J., Albrecht, U., Andersen, M. E., Ansari, N., Bhattacharya, S., et al. (2013). Recent Advances in 2D and 3D *In Vitro* Systems Using Primary Hepatocytes, Alternative Hepatocyte Sources and Non-parenchymal Liver Cells and Their Use in Investigating Mechanisms of Hepatotoxicity, Cell Signaling and ADME. *Arch. Toxicol.* 87 (8), 1315–1530. doi:10.1007/s00204-013-1078-5
- Gong, T., Zhang, C., Ni, X., Li, X., Li, J. e., Liu, M., et al. (2020). A Time-Resolved Multi-Omic Atlas of the Developing Mouse Liver. *Genome Res.* 30 (2), 263–275. doi:10.1101/gr.253328.119
- Gordillo, M., Evans, T., and Gouon-Evans, V. (2015). Orchestrating Liver Development. *Development* 142 (12), 2094–2108. doi:10.1242/dev.114215
- Granja, J. M., Corces, M. R., Pierce, S. E., Bagdatli, S. T., Choudhry, H., Chang, H. Y., et al. (2021). ArchR Is a Scalable Software Package for Integrative Single-Cell Chromatin Accessibility Analysis. *Nat. Genet.* 53 (3), 403–411. doi:10.1038/s41588-021-00790-6
- Granja, J. M., Klemm, S., McGinnis, L. M., Kathiria, A. S., Mezger, A., Corces, M. R., et al. (2019). Single-cell Multiomic Analysis Identifies Regulatory Programs in Mixed-Phenotype Acute Leukemia. *Nat. Biotechnol.* 37 (12), 1458–1465. doi:10.1038/s41587-019-0332-7
- Guilliams, M., Bonnardel, J., Haest, B., Vanderborght, B., Wagner, C., Remmerie, A., et al. (2022). Spatial Proteogenomics Reveals Distinct and Evolutionarily-Conserved Hepatic Macrophage Niches. *Cell* 185 (2), 379–396.e338. doi:10.1016/j.cell.2021.12.018
- Hadley, W. (2016). *ggplot2: Elegant Graphics for Data Analysis*. New York: Springer-Verlag.
- Haeusler, R. A., Camastra, S., Nannipieri, M., Astiarraga, B., Castro-Perez, J., Xie, D., et al. (2016). Increased Bile Acid Synthesis and Impaired Bile Acid Transport in Human Obesity. *J. Clin. Endocrinol. Metab.* 101 (5), 1935–1944. doi:10.1210/jc.2015-2583
- Halpern, K. B., Shenhav, R., Matcovitch-Natan, O., Tóth, B., Lemze, D., Golan, M., et al. (2017). Single-cell Spatial Reconstruction Reveals Global Division of Labour in the Mammalian Liver. *Nature* 542 (7641), 352–356. doi:10.1038/nature21065
- Hao, Y., Hao, S., Andersen-Nissen, E., Mauck, W. M., 3rd, Zheng, S., Butler, A., et al. (2021). Integrated Analysis of Multimodal Single-Cell Data. *Cell* 184 (13), 3573–3587. e3529. doi:10.1016/j.cell.2021.04.048
- He, L., Pu, W., Liu, X., Zhang, Z., Han, M., Li, Y., et al. (2021). Proliferation Tracing Reveals Regional Hepatocyte Generation in Liver Homeostasis and Repair. *Science* 371 (6532), eabc4346. doi:10.1126/science.abc4346
- Hirayama, T., Tarusawa, E., Yoshimura, Y., Galjart, N., and Yagi, T. (2012). CTCF Is Required for Neural Development and Stochastic Expression of Clustered Pcdh Genes in Neurons. *Cel Rep.* 2 (2), 345–357. doi:10.1016/j.celrep.2012.06.014
- Italiano, J. E., Jr., and Shivdasani, R. A. (2003). Megakaryocytes and beyond: the Birth of Platelets. *J. Thromb. Haemost.* 1 (6), 1174–1182. doi:10.1046/j.1538-7836.2003.00290.x
- Jakobsen, J. S., Waage, J., Rapin, N., Bisgaard, H. C., Larsen, F. S., and Porse, B. T. (2013). Temporal Mapping of CEBPA and CEBPB Binding during Liver Regeneration Reveals Dynamic Occupancy and Specific Regulatory Codes for Homeostatic and Cell Cycle Gene Batteries. *Genome Res.* 23 (4), 592–603. doi:10.1101/gr.146399.112
- Jin, S., Guerrero-Juarez, C. F., Zhang, L., Chang, I., Ramos, R., Kuan, C.-H., et al. (2021). Inference and Analysis of Cell-Cell Communication Using CellChat. *Nat. Commun.* 12 (1), 1088. doi:10.1038/s41467-021-21246-9
- Kalabay, L., Gráf, L., Vörös, K., Jakab, L., Benkő, Z., Telegdy, L., et al. (2007). Human Serum Fetuin A/ $\alpha$ 2HS-glycoprotein Level Is Associated with Long-Term Survival in Patients with Alcoholic Liver Cirrhosis, Comparison with the Child-Pugh and MELD Scores. *BMC Gastroenterol.* 7, 15. doi:10.1186/1471-230x-7-15
- Lake, B. B., Codeluppi, S., Yung, Y. C., Gao, D., Chun, J., Kharchenko, P. V., et al. (2017). A Comparative Strategy for Single-Nucleus and Single-Cell Transcriptomes Confirms Accuracy in Predicted Cell-type Expression from Nuclear RNA. *Sci. Rep.* 7 (1), 6031. doi:10.1038/s41598-017-04426-w
- Lazarevich, N. L. (2000). Molecular Mechanisms of Alpha-Fetoprotein Gene Expression. *Biochemistry (Mosc)* 65 (1), 117–133.
- Leeb, M., and Wutz, A. (2011). Derivation of Haploid Embryonic Stem Cells from Mouse Embryos. *Nature* 479 (7371), 131–134. doi:10.1038/nature10448
- Leeb, M., and Wutz, A. (2012). Establishment of Epigenetic Patterns in Development. *Chromosoma* 121 (3), 251–262. doi:10.1007/s00412-012-0365-x
- Li, T., Huang, J., Jiang, Y., Zeng, Y., He, F., Zhang, M. Q., et al. (2009). Multi-stage Analysis of Gene Expression and Transcription Regulation in C57/B6 Mouse Liver Development. *Genomics* 93 (3), 235–242. doi:10.1016/j.ygeno.2008.10.006
- Li, T., Wang, L., Zhang, X., Jiang, L., Li, Y., Mao, J., et al. (2018). Generation of Rat-Mouse Chimeras by Introducing Single Cells of Rat Inner Cell Masses into Mouse Blastocysts. *J. Genet. Genomics* 142 (5), 787–799. doi:10.1016/j.jgg.2018.03.006
- Li, W., Li, L., and Hui, L. (2020). Cell Plasticity in Liver Regeneration. *Trends Cel Biol.* 30 (4), 329–338. doi:10.1016/j.tcb.2020.01.007
- Liang, Y., Kaneko, K., Xin, B., Lee, J., Sun, X., Zhang, K., et al. (2022). Temporal Analyses of Postnatal Liver Development and Maturation by Single-Cell Transcriptomics. *Develop. Cel* 57 (3), 398–414. doi:10.1016/j.devcel.2022.01.004
- Liu, C., Wu, T., Fan, F., Liu, Y., Wu, L., Junkin, M., et al. (2019). A Portable and Cost-Effective Microfluidic System for Massively Parallel Singlecell Transcriptome Profiling. *BioRxiv*. doi:10.1101/818450
- Lotto, J., Drissler, S., Cullum, R., Wei, W., Setty, M., Bell, E. M., et al. (2020). Single-Cell Transcriptomics Reveals Early Emergence of Liver Parenchymal and Non-parenchymal Cell Lineages. *Cell* 183 (3), 702–716. doi:10.1016/j.cell.2020.09.012
- Lun, A. T. L., Riesenfeld, S., Riesenfeld, S., Andrews, T., Dao, T. P., and Marioni, T. J. C. (2019). J. Participants in the 1st Human Cell Atlas and JEmptyDrops: Distinguishing Cells from Empty Droplets in Droplet-Based Single-Cell RNA Sequencing Data. *Genome Biol.* 20 (1), 63. doi:10.1186/s13059-019-1662-y
- MacParland, S. A., Liu, J. C., Ma, X.-Z., Innes, B. T., Bartczak, A. M., Gage, B. K., et al. (2018). Single Cell RNA Sequencing of Human Liver Reveals Distinct Intrahepatic Macrophage Populations. *Nat. Commun.* 9 (1), 4383. doi:10.1038/s41467-018-06318-7
- McGinnis, C. S., Murrow, L. M., and Gartner, Z. J. (2019). DoubletFinder: Doublet Detection in Single-Cell RNA Sequencing Data Using Artificial Nearest Neighbors. *Cel Syst.* 8 (4), 329–337. e324. doi:10.1016/j.cels.2019.03.003
- McLIn, V. A., Rankin, S. A., and Zorn, A. M. (2007). Repression of Wnt/ $\beta$ -Catenin Signaling in the Anterior Endoderm Is Essential for Liver and Pancreas Development. *Development* 134 (12), 2207–2217. doi:10.1242/dev.001230
- Milnes, M. R., Garcia, A., Grossman, E., Grün, F., Shiotsugu, J., Tabb, M. M., et al. (2008). Activation of Steroid and Xenobiotic Receptor (SXR, NR1I2) and its Orthologs in Laboratory, Toxicologic, and Genome Model Species. *Environ. Health Perspect.* 116 (7), 880–885. doi:10.1289/ehp.10853
- Miyajima, A., Tanaka, M., and Itoh, T. (2014). Stem/progenitor Cells in Liver Development, Homeostasis, Regeneration, and Reprogramming. *Cell Stem Cell* 14 (5), 561–574. doi:10.1016/j.stem.2014.04.010
- Mu, T., Xu, L., Zhong, Y., Liu, X., Zhao, Z., Huang, C., et al. (2020). Embryonic Liver Developmental Trajectory Revealed by Single-Cell RNA Sequencing in the Foxa2eGFP Mouse. *Commun. Biol.* 3 (1), 642. doi:10.1038/s42003-020-01364-8
- Nakagaki, B. N., Mafra, K., de Carvalho, É., Lopes, M. E., Carvalho-Gontijo, R., de Castro-Oliveira, H. M., et al. (2018). Immune and Metabolic Shifts during Neonatal Development Reprogram Liver Identity and Function. *J. Hepatol.* 69 (6), 1294–1307. doi:10.1016/j.jhep.2018.08.018
- Negishi, T., Nagai, Y., Asaoka, Y., Ohno, M., Namae, M., Mitani, H., et al. (2010). Retinoic Acid Signaling Positively Regulates Liver Specification by Inducingwnt2bbgene Expression in Medaka. *Hepatology* 51 (3), 1037–1045. doi:10.1002/hep.23387
- Ober, E. A., and Lemaigre, F. P. (2018). Development of the Liver: Insights into Organ and Tissue Morphogenesis. *J. Hepatol.* 68 (5), 1049–1062. doi:10.1016/j.jhep.2018.01.005
- Olsen, C. L., and Jeffery, W. R. (1997). A Forkhead Gene Related to HNF-3 $\beta$  Is Required for Gastrulation and axis Formation in the Ascidian Embryo. *Development* 124 (18), 3609–3619. doi:10.1242/dev.124.18.3609



- Périchon, R., and Bourre, J. M. (1995). Peroxisomal  $\beta$ -oxidation Activity and Catalase Activity during Development and Aging in Mouse Liver. *Biochimie* 77 (4), 288–293. doi:10.1016/0300-9084(96)88138-7
- Pope, C., Piekos, S. C., Chen, L., Mishra, S., and Zhong, X.-b. (2017). The Role of H19, a Long Non-coding RNA, in Mouse Liver Postnatal Maturation. *PLoS One* 12 (11), e0187557. doi:10.1371/journal.pone.0187557
- Popescu, D.-M., Botting, R. A., Stephenson, E., Green, K., Webb, S., Jardine, L., et al. (2019). Decoding Human Fetal Liver Haematopoiesis. *Nature* 574 (7778), 365–371. doi:10.1038/s41586-019-1652-y
- Roskams, T., and Desmet, V. (2008). Embryology of Extra- and Intrahepatic Bile Ducts, the Ductal Plate. *Anat. Rec.* 291 (6), 628–635. doi:10.1002/ar.20710
- Saviano, A., Henderson, N. C., and Baumert, T. F. (2020). Single-cell Genomics and Spatial Transcriptomics: Discovery of Novel Cell States and Cellular Interactions in Liver Physiology and Disease Biology. *J. Hepatol.* 73 (5), 1219–1230. doi:10.1016/j.jhep.2020.06.004
- Sekine, K., Chen, Y.-R., Kojima, N., Ogata, K., Fukamizu, A., and Miyajima, A. (2007). Foxo1 Links Insulin Signaling to C/EBP $\alpha$  and Regulates Gluconeogenesis during Liver Development. *EMBO J.* 26 (15), 3607–3615. doi:10.1038/sj.emboj.7601784
- So, J., Kim, A., Lee, S.-H., and Shin, D. (2020). Liver Progenitor Cell-Driven Liver Regeneration. *Exp. Mol. Med.* 52 (8), 1230–1238. doi:10.1038/s12276-020-0483-0
- Song, J., Xie, C., Jiang, L., Wu, G., Zhu, J., Zhang, S., et al. (2018). Transcription Factor AP-4 Promotes Tumorigenic Capability and Activates the Wnt/ $\beta$ -Catenin Pathway in Hepatocellular Carcinoma. *Theranostics* 8 (13), 3571–3583. doi:10.7150/thno.25194
- Takebe, T., Sekine, K., Kimura, M., Yoshizawa, E., Ayano, S., Koido, M., et al. (2017). Massive and Reproducible Production of Liver Buds Entirely from Human Pluripotent Stem Cells. *Cel Rep.* 21 (10), 2661–2670. doi:10.1016/j.celrep.2017.11.005
- Tang, X., Huang, Y., Lei, J., Luo, H., and Zhu, X. (2019). The Single-Cell Sequencing: New Developments and Medical Applications. *Cell Biosci* 9, 53. doi:10.1186/s13578-019-0314-y
- Tarlow, B. D., Finegold, M. J., and Grompe, M. (2014). Clonal Tracing of Sox9+ Liver Progenitors in Mouse Oval Cell Injury. *Hepatology* 60 (1), 278–289. doi:10.1002/hep.27084
- Trapnell, C., Cacchiarelli, D., Grimsby, J., Pokharel, P., Li, S., Morse, M., et al. (2014). The Dynamics and Regulators of Cell Fate Decisions Are Revealed by Pseudotemporal Ordering of Single Cells. *Nat. Biotechnol.* 32 (4), 381–386. doi:10.1038/nbt.2859
- Tremblay, K. D., and Zaret, K. S. (2005). Distinct Populations of Endoderm Cells Converge to Generate the Embryonic Liver Bud and Ventral Foregut Tissues. *Develop. Biol.* 280 (1), 87–99. doi:10.1016/j.ydbio.2005.01.003
- Trevino, A. E., Müller, F., Andersen, J., Sundaram, L., Kathiria, A., Shcherbina, A., et al. (2021). Chromatin and Gene-Regulatory Dynamics of the Developing Human Cerebral Cortex at Single-Cell Resolution. *Cell* 184 (19), 5053–5069. e5023. doi:10.1016/j.cell.2021.07.039
- Van de Sande, B., Flerin, C., Davie, K., De Waegeneer, M., Hulselmans, G., Aibar, S., et al. (2020). A Scalable SCENIC Workflow for Single-Cell Gene Regulatory Network Analysis. *Nat. Protoc.* 15 (7), 2247–2276. doi:10.1038/s41596-020-0336-2
- Wang, J., Rhee, S., Palaria, A., and Tremblay, K. D. (2015). FGF Signaling Is Required for Anterior but Not Posterior Specification of the Murine Liver Bud. *Dev. Dyn.* 244 (3), 431–443. doi:10.1002/dvdy.24215
- Wang, X., Yang, L., Wang, Y.-C., Xu, Z.-R., Feng, Y., Zhang, J., et al. (2020). Comparative Analysis of Cell Lineage Differentiation during Hepatogenesis in Humans and Mice at the Single-Cell Transcriptome Level. *Cell Res* 30 (12), 1109–1126. doi:10.1038/s41422-020-0378-6
- Wei, Y., Wang, Y. G., Jia, Y., Li, L., Yoon, J., Zhang, S., et al. (2021). Liver Homeostasis Is Maintained by Midlobular Zone 2 Hepatocytes. *Science* 371 (6532), eabb1625. doi:10.1126/science.abb1625
- Yang, L., Wang, W. H., Qiu, W. L., Guo, Z., Bi, E., and Xu, C. R. (2017). A Single-cell Transcriptomic Analysis Reveals Precise Pathways and Regulatory Mechanisms Underlying Hepatoblast Differentiation. *Hepatology* 66 (5), 1387–1401. doi:10.1002/hep.29353
- Young, M. D., and Behjati, S. (2020). SoupX Removes Ambient RNA Contamination from Droplet-Based Single-Cell RNA Sequencing Data. *Gigascience* 9 (12), gaa151. doi:10.1093/gigascience/gaa151
- Yu, G., Wang, L.-G., Han, Y., and He, Q.-Y. (2012). clusterProfiler: an R Package for Comparing Biological Themes Among Gene Clusters. *OMICS: A J. Integr. Biol.* 16 (5), 284–287. doi:10.1089/omi.2011.0118
- Zaret, K. S. (2002). Regulatory Phases of Early Liver Development: Paradigms of Organogenesis. *Nat. Rev. Genet.* 3 (7), 499–512. doi:10.1038/nrg837
- Zeng, W., Jiang, S., Kong, X., El-Ali, N., Ball, A. R., Jr., Ma, C. I., et al. (2016). Single-nucleus RNA-Seq of Differentiating Human Myoblasts Reveals the Extent of Fate Heterogeneity. *Nucleic Acids Res.* 44 (21), e158. doi:10.1093/nar/gkw739
- Zhao, R., and Duncan, S. A. (2005). Embryonic Development of the Liver. *Hepatology* 41 (5), 956–967. doi:10.1002/hep.20691

**Conflict of Interest:** The authors JX, SH, QS, QD, YJ, YY, XS, HZ, YH, YW, YS, YL, LW, ZW, XW, MC, YH, CL, and LL were employed by BGI group.

The remaining authors declare that the research was conducted in the absence of any commercial or financial relationships that could be construed as a potential conflict of interest.

**Publisher's Note:** All claims expressed in this article are solely those of the authors and do not necessarily represent those of their affiliated organizations, or those of the publisher, the editors and the reviewers. Any product that may be evaluated in this article, or claim that may be made by its manufacturer, is not guaranteed or endorsed by the publisher.

Copyright © 2022 Xu, Hao, Shi, Deng, Jiang, Guo, Yuan, Shi, Shangguan, Zheng, Lai, Huang, Wang, Song, Liu, Wu, Wang, Cheng, Wei, Cheng, Lai, Volpe, Esteban, Hou, Liu and Liu. This is an open-access article distributed under the terms of the Creative Commons Attribution License (CC BY). The use, distribution or reproduction in other forums is permitted, provided the original author(s) and the copyright owner(s) are credited and that the original publication in this journal is cited, in accordance with accepted academic practice. No use, distribution or reproduction is permitted which does not comply with these terms.



# Adapting Physiology in Functional Human Islet Organogenesis

Eiji Yoshihara<sup>1,2\*</sup>

<sup>1</sup>Lundquist Institute for Biomedical Innovation at Harbor-UCLA Medical Center, Torrance, CA, United States, <sup>2</sup>David Geffen School of Medicine at University of California, Los Angeles, CA, United States

Generation of three-dimensional (3D)-structured functional human islets is expected to be an alternative cell source for cadaveric human islet transplantation for the treatment of insulin-dependent diabetes. Human pluripotent stem cells (hPSCs), such as human embryonic stem cells (hESCs) and human induced pluripotent stem cells (hiPSCs), offer infinite resources for newly synthesized human islets. Recent advancements in hPSCs technology have enabled direct differentiation to human islet-like clusters, which can sense glucose and secrete insulin, and those islet clusters can ameliorate diabetes when transplanted into rodents or non-human primates (NHPs). However, the generated hPSC-derived human islet-like clusters are functionally immature compared with primary human islets. There remains a challenge to establish a technology to create fully functional human islets *in vitro*, which are functionally and transcriptionally indistinguishable from cadaveric human islets. Understanding the complex differentiation and maturation pathway is necessary to generate fully functional human islets for a tremendous supply of high-quality human islets with less batch-to-batch difference for millions of patients. In this review, I summarized the current progress in the generation of 3D-structured human islets from pluripotent stem cells and discussed the importance of adapting physiology for *in vitro* functional human islet organogenesis and possible improvements with environmental cues.

**Keywords:** human islet-like organoids, nuclear receptors, physiology, human pluripotent stem cells, diabetes

## OPEN ACCESS

### Edited by:

Keiichiro Suzuki,  
Osaka University, Japan

### Reviewed by:

Hirotake Komatsu,  
Beckman Research Institute, City of  
Hope, United States

### \*Correspondence:

Eiji Yoshihara  
eiji.yoshihara@lundquist.org

### Specialty section:

This article was submitted to  
Stem Cell Research,  
a section of the journal  
Frontiers in Cell and Developmental  
Biology

**Received:** 14 January 2022

**Accepted:** 22 March 2022

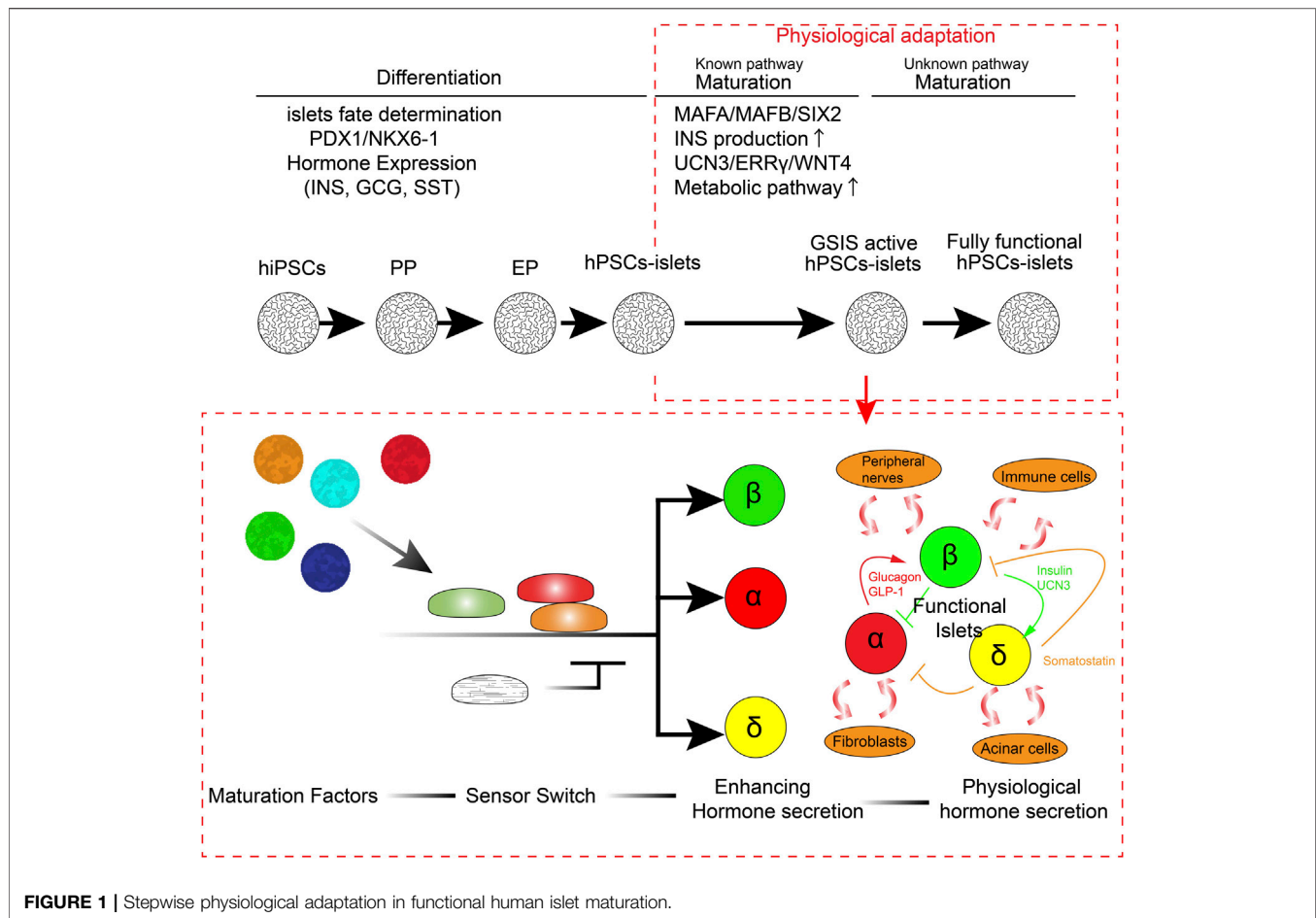
**Published:** 26 April 2022

### Citation:

Yoshihara E (2022) Adapting  
Physiology in Functional Human  
Islet Organogenesis.  
Front. Cell Dev. Biol. 10:854604.  
doi: 10.3389/fcell.2022.854604

## INTRODUCTION

Diabetes is a complicated chronic disease that affects more than 450 million people worldwide (Cho et al., 2018; Huang et al., 2018; Rogers et al., 2020; Rogers and Kim, 2020; Shah et al., 2020; Smalls et al., 2020; Tan et al., 2020). Microvasculature defects caused by diabetes lead to stroke, blindness, and kidney failure in some patients (Creager et al., 2003; Luscher et al., 2003; Beckman et al., 2013; Paneni et al., 2013; Cayabyab et al., 2021). Although the discovery of insulin a century ago made significant improvements in diabetic therapeutics, from lethal to treatable, even modern insulin therapy cannot be an alternative to endogenous functional insulin-producing  $\beta$  cells. Insulin treatment requires manual glucose monitoring and adjustment of insulin injection in both amount and timing every day, which also means the high maintenance and economic impact for the patients and expenditure on healthcare in all countries. Continuous, rapid fine-tuning of glucose or other nutrition-sensing insulin secretion is necessary for functional cure of diabetes. Cadaveric islet transplantation provides a functional cure for insulin-dependent type 1 diabetes (T1D) with a success rate of more than 90%, and its efficacy has been sustained for over 20 years in some cases (Lemos et al., 2021). The short supply and requirement of immunosuppressants, which



increase the risk of adverse effects, limit the islet transplantation for the treatment of diabetes. Owing to their pluripotency and self-renewal function, human pluripotent stem cells (hPSCs), such as human induced pluripotent stem cells (hiPSCs) (Takahashi et al., 2007) and human embryonic stem cells (hESCs) (Thomson et al., 1998), offer an alternative cell resource for human cadaveric islets. Step-by-step treatment of small chemicals and recombinant proteins, which induce differentiation from hPSCs, was developed by integrating the knowledge of specific signaling pathways that contribute to the pancreatic lineage specification and islet differentiation. While recent advances in this approach have made it possible to reproducibly generate functional hPSC-derived insulin-producing  $\beta$ -like cells, which are capable of sensing glucose concentration and secreting insulin, there are several major limitations to our knowledge in generating fully functional human  $\beta$  cells or human islets. First, we have not yet clarified the pathway to induce each endocrine cell type separately. Although there are several reports on the production of more biasedly  $\alpha$  cells rather than  $\beta$  cells from hPSCs (Rezania et al., 2011; Peterson et al., 2020), these established protocols do not generate a single-cell type but rather contain other cell types together with differentiation. Second, we have not completely understood the pathway of postnatal functional islet maturation,

which typically occurs a few years after birth in humans. hPSC-derived insulin-producing cells are generated either by  $\beta$ -like cells (hPSC-derived  $\beta$ -like cells; monolayer or isolated insulin-producing cells) or human islet-like organoid clusters (hPSC-derived islets;  $\alpha$ ,  $\beta$ ,  $\gamma$ -cells containing 3D-structured cell cluster). Therefore, the current protocol of generating fully functional hPSC-derived  $\beta$ -like cells or islets remains a challenge. Identifying such a pathway is necessary to improve the immaturity of generated islets and reduce the risk of batch-to-batch differences. In this review, I aimed to outline the current progress in generating functional human pancreatic islets from the perspective of 1) pancreatic lineage specification, 2) postnatal functional maturation, 3) differences between primary human islets and hPSC-derived islets, 4) missing factors, and 5) further adaptation of the environmental physiological responses (Figure 1). Additionally, I aimed to discuss future perspectives to improve the current protocol for generating functional human islets from hPSCs.

## Pancreatic Lineage Specification

Since the establishment of hESCs (Thomson et al., 1998), insulin-producing  $\beta$  cells have been identified in spontaneously differentiated cells from hESCs (Lumelsky et al., 2001; Assady et al., 2001). In addition with the efforts to identify the essential

pathways for pancreatic lineage specification, efficient endodermal differentiation (D'Amour et al., 2005) and pancreatic progenitor (PP) differentiation (D'Amour et al., 2006) protocols have been developed. hESC- or hiPSC-derived PPs are capable to differentiate into mature functional  $\beta$  cells *in vivo* within a couple of months of transplantation (Kroon et al., 2008), suggesting that these protocols represent the right track for generating functional  $\beta$  cells *in vitro*. The key features of stage-specific differentiation are controlled by stage-specific transcriptional factors (TFs) and key identity genes (Tahbaz and Yoshihara, 2021). hPSCs undergo definitive endodermal (DE) differentiation by targeting the Activin A pathway and canonical Wnt (cWnt) pathway, Wnt3A, SRY-box transcription factor 17 (SOX17) and Forkhead box A2/box2 (FOXA2) are prominent DE markers. Fibroblast growth factor 7 (FGF7/KGF) induces a primitive gut tube (PGT). Hepatocyte nuclear factor 1 $\beta$  (HNF1 $\beta$ ) and hepatocyte nuclear factor-4 $\alpha$  (HNF4 $\alpha$ ) are well-known PGT markers. Retinoic acid (RA) signaling activation, combined with sonic hedgehog (SSH) inhibition, bone morphogenetic protein (BMP) signal inhibition, and protein kinase C (PKC) activation, leads to PPs. PPs are pancreatic and duodenal homeobox 1 (PDX-1) and NK6 homeobox 1 (NKX6-1) double-positive cells, which can further generate mono-hormonal  $\beta$  cells,  $\alpha$  cells (glucagon producing), and  $\delta$  cells (somatostatin producing). RAs activation, SSH inhibition, BMP signal inhibition, transforming growth factor  $\beta$  (TGF $\beta$ ) signal inhibition, and thyroid hormone signaling activation (THR) lead to endocrine progenitor (EP) generation. NEUROG3 (NGN3) is the key transcriptional factor of EP. It has been recently observed that targeting the cytoskeleton by inhibiting actin polymerization enhances NGN3 expression in the endocrine stage (Mamidi et al., 2018; Hogrebe et al., 2020).  $\gamma$ -secretase inhibition, BMP signal inhibition, TGF $\beta$  signal inhibition, and THR activation lead to the generation of endocrine hormone-producing cells ( $\alpha$ ,  $\beta$ , and  $\gamma$  cells). Prematured glucose-response  $\beta$ -like cells are generated (Pagliuca et al., 2014; Rezanian et al., 2014; Russ et al., 2015). Although these previous studies established reproducible GSIS, impaired glucose-stimulated  $\text{Ca}^{2+}$  flux, reduced production of insulin, and many transcriptional differences have been observed in hPSC-derived  $\beta$ -like cells compared to those of primary  $\beta$  cells or islets (Veres et al., 2019; Augsornworawat et al., 2020; Yoshihara et al., 2020; Balboa et al., 2022). These results suggested that hPSC-derived  $\beta$ -like cells may remain a feature of the juvenile/neonatal stage of  $\beta$  cells (Hrvatin et al., 2014).

## Postnatal Functional Maturation

Increasing evidence suggests that multiple functional maturation pathways play an important role in the postnatal acquisition of robust GSIS function (Alvarez-Dominguez and Melton, 2021). Therefore, the current focus on improving the protocol for generating functional islets relies on the identification of the new pathways for functional maturation. Islet functional maturation is accelerated after birth to adapt to oxygen- and nutrition-rich environments. There are a number of transcriptional factors and key  $\beta$ -cell marker gene expressions such as *INSULIN* (*INS*), MAF bZIP transcription factor A

(*MAFA*), SIX homeobox 2 (*SIX2*), glucose-6-phosphatase catalytic subunit 2 (*G6PC2*), and urocortin 3 (*UCN3*), which are lower in hPSC-derived  $\beta$ -like cells generated *in vitro* (Balboa et al., 2022). Chromatin remodeling and miRNA expression have been suggested to control the gene expression for functional  $\beta$ -cell maturation (Xie et al., 2013; Dhawan et al., 2015; Jacovetti et al., 2015). *MAFA* expression, regulated by T3 and other unknown signals, is important for *INS* and *G6PC2* transcription (Martin et al., 2008; Artner et al., 2010; Aguayo-Mazzucato et al., 2011; Hang and Stein, 2011). *G6PC2* expression suppresses low-glucose concentration-stimulated insulin secretion, leading to amplification of the GSIS function. MAF BZIP transcription factor B (*MAFB*) alternatively regulates *INS* gene expression in human  $\beta$  cells (Russell et al., 2020). Metabolic shift triggered by weaning enhances GSIS (Jacovetti et al., 2015; Stolovich-Rain et al., 2015). *SIX2* is important for sustaining key  $\beta$ -cell lineage and metabolic genes (Arda et al., 2016; Velazco-Cruz et al., 2020a; Bevacqua et al., 2021). ATP and other nutrients, including glucose, have been reported to enhance the maturity of juvenile/neonate  $\beta$  cells in rodents (Rorsman et al., 1989; Hellerstrom and Swenne, 1991). We have previously demonstrated that estrogen-related receptor- $\gamma$  (ERR $\gamma$ ) and related metabolic genes are upregulated during postnatal development in mouse islets (Yoshihara et al., 2016). ERR $\gamma$  directly regulates gene clusters related to mitochondrial pyruvate metabolism, tricarboxylic acid (TCA) cycle, and oxidative phosphorylation (OxPhos), causing enhanced glucose-stimulated ATP production and insulin secretion (Yoshihara et al., 2016; Ahmadian et al., 2018; Fan et al., 2018). These metabolic reprogramming may be postnatally coordinated by the non-canonical WNT pathway (ncWNT4) (Bader et al., 2016; Yoshihara et al., 2020). Flattop (Fltp), a receptor of Wnt4, is upregulated postnatally in murine  $\beta$  cells, and Wnt4 enhances the maturation of  $\beta$  cells in mice and humans. We demonstrated that Wnt4 expression is significantly lower in murine neonatal islets or hPSC-derived  $\beta$ -like cells than that in murine adult  $\beta$  cells or primary adult human islets (Bader et al., 2016; Yoshihara et al., 2016; Yoshihara et al., 2020). Additionally, Wnt4 treatment enhances oxidative features and GSIS function in hPSC-derived 3D-structured human islet-like organoids (HILOs). These studies indicate that not only lineage commitment but also metabolic adaptation is important for enhancing the functional maturation of hPSC-derived  $\beta$ -like cells or islets. Other lineage-dependent transcriptional factors (LDTFs) and signal-dependent transcriptional factors (SDTFs), which collaboratively modulate functional maturation, have been discussed elsewhere (Wortham and Sander, 2021). The  $\beta$ -cell function is enhanced through aging in rodents, and p16 plays a key role in reducing cell proliferation and enhancing GSIS function. Circadian rhythms acquired during development also play an important role in  $\beta$ -cell maturation (Alvarez-Dominguez et al., 2020). Recent advances in single-cell technologies have enabled recapturing of the gene clusters involved in the differentiation and *in vivo* maturation of hPSC-derived  $\beta$ -like cells (Veres et al., 2019; Augsornworawat et al., 2021; Balboa et al., 2022). Several key  $\beta$ -cell genes in hPSC-derived  $\beta$ -like cells, including *INS*, *MAFA*, *G6PC2*, and *UCN3*,



have been observed to be expressed in equivalent amounts only after *in vivo* maturation (Veres et al., 2019; Augsornworawat et al., 2021; Balboa et al., 2022). From these studies, the key changes during functional  $\beta$ -cell maturation seem to be advanced lineage commitment, metabolic reprogramming to a more oxidative status with efficient glucose utilization, cell cycle reduction, and adaptation to environmental physiological changes *in vivo*.

## Differences Between Primary Human Islets and hPSC-Derived Islets

Although there has been a better understanding of the pancreatic differentiation, islets maturation, and the technologies mimicking human organogenesis, there are many differences between the primary human islets supplied by the human donors and the generated hPSC-derived islets. Generally, hPSC-derived islets exhibit lower insulin production and GSIS fold changes than adult human primary islets (Pagliuca et al., 2014; Rezanian et al., 2014; Velazco-Cruz et al., 2020b; Yoshihara et al., 2020). These functional differences may be insufficiently represented since the primary adult islets functionally differ among individuals, and the donor islets were typically shipped at 4°C overnight or a few days, which makes the condition of primary human islets unideal. This suggests that the functional differences between hPSC-derived islets and primary adult islets may be even bigger than the ones described or thought of previously. In 2014, Hrvatin et al. (2014) revealed that the hPSC-derived  $\beta$ -like cells resemble human fetal  $\beta$  cells more transcriptionally rather than adult  $\beta$  cells. Remarkable technological advances have been made to create more glucose-responsive hPSC-derived  $\beta$ -like cells, which are capable of secreting insulin in response to high glucose, to produce mono-hormonal insulin-producing cells rather than poly-hormonal insulin-producing cells, and for improved differentiation efficacy to create insulin-producing cells to about ~70%. The insulin production levels are significantly higher than those in previous protocols (Pagliuca et al., 2014; Rezanian et al., 2014; Russ et al., 2015). Although considerable progress has been made in creating functional islets from hPSCs, there are still significant differences between hPSC-derived  $\beta$ -like cells and human primary  $\beta$  cells.  $\text{Ca}^{2+}$  influx, which is triggered by the closure of the  $\text{K}^{\text{ATP}}$  channel in response to ATP amplification typically induced by glucose metabolism in the mitochondria of hPSC-derived  $\beta$ -like cells, is much slower and abnormal compared with that in the primary human islets<sup>23,24,4</sup>. This is linked to the slower and fewer insulin secretion responses in hPSC-derived  $\beta$ -like cells (Pagliuca et al., 2014; Rezanian et al., 2014; Nair et al., 2019). Patch-clamp recordings revealed heterogeneity and aberrant ion current such as  $\text{Na}^+$  (Balboa et al., 2022). Aberrant metabolic features in hPSC-derived  $\beta$ -like cells or islets, such as glycolysis, TCA cycle, and OxPhos, were observed and demonstrated as the target pathways to improve GSIS (Yoshihara et al., 2016; Nair et al., 2019; Davis et al., 2020; Balboa et al., 2022). It has been observed that longer culturing time of hPSC-derived islets at the maturation stage *in vitro* improves some maturation marker gene expression and GSIS; however, it has been identified that *in vivo* engraftment for

6 months is necessary to promote further maturation (Veres et al., 2019; Augsornworawat et al., 2020; Balboa et al., 2022). There remain several missing factors to understand how pancreatic islets adapt to the physiological environment during functional maturation. These factors should be considered to further improve the generation of functional human islets from hPSCs (Figure 1).

## Current Progress and Missing Factors for Generating Fully Functional Human Islets Dynamic Metabolic Circulation

Blood glucose levels are elevated postnatally triggered by weaning owing to the alternation of nutritional sources from fat-rich breast milk to a carbohydrate-rich chow diet (Stolovich-Rain et al., 2015). Glucose has been identified as a maturation factor in rodent  $\beta$  cells (Hellerstrom and Swenne, 1991). Therefore, the current protocol for *in vitro*  $\beta$ -cell generation is intended to increase glucose concentration during differentiation from the PP stage to the  $\beta$ -cell maturation stage (Yoshihara et al., 2020). The bottleneck of glycolysis (Davis et al., 2020) or mitochondrial metabolism (Yoshihara et al., 2016) in hPSC-derived  $\beta$ -like cells may limit the glucose-induced maturation efficacy. Improving  $\beta$ -cell metabolism has been highlighted as the target for improving maturation. We have previously demonstrated that forced expression of estrogen-related receptor  $\gamma$  (ERR $\gamma$ ), a master regulator of mitochondrial gene expression, including pyruvate metabolism, the TCA cycle, and OxPhos improves GSIS in hPSC-derived  $\beta$ -like cells (Yoshihara et al., 2016). Reaggregation (Nair et al., 2019) or the ncWnt4/planar cell polarity (PCP) pathway (Bader et al., 2016; Yoshihara et al., 2020) enhances mitochondrial metabolism, which enhances GSIS function in hPSC-derived  $\beta$ -like cells. ncWnt/PCP effector Flattop (Fltp) expression increases during postnatal  $\beta$  cell maturation and is heterogeneously expressed in mature  $\beta$  cells. Fltp-positive (Fltp+)  $\beta$  cells are characterized by higher mitochondrial gene expression and activity (Bader et al., 2016). Wnt4, a component of ncWnt pathway increases during postnatal  $\beta$  cell maturation, and Wnt4 expression is lower in hPSC-derived  $\beta$ -like cells than that in the primary human  $\beta$  cells. Wnt4 stimulation enhances expression in mitochondrial gene expression and activity and GSIS function in hPSC-derived human islet-like organoids (HILOs). We have reported that ERR $\gamma$  is a downstream factor of Wnt4 signaling to regulate mitochondrial gene expression and activity (Yoshihara et al., 2020). Declining mammalian target of rapamycin complex 1 (mTORC1) signaling from neonate to adult maturation has been observed (Ni et al., 2017; Jaafar et al., 2019; Helman et al., 2020). The constitutively active mTORC pathway in mouse  $\beta$  cells increases  $\beta$ -cell proliferation while reducing  $\beta$  cells' maturation gene expressions such as *Ins1*, *Ucn3*, *Mafa*, and *G6pc2* and mitochondrial metabolic genes (Jaafar et al., 2019). mTORC1 enhances the responses of amino acid-stimulated insulin secretion, which increases insulin secretion at low glucose concentrations and reduces GSIS thresholds (Helman et al., 2020). In addition to mitochondria metabolism, glycolysis is impaired in hPSC-derived  $\beta$ -like cells, which limits the

pyruvate and related fuel mitochondrial metabolite production. The enzymatic activity, but not the expression of glyceraldehyde 3-phosphate dehydrogenase (GAPDH) and phosphoglycerate kinase 1 (PGK1), which are important for the enzymatic conversion of glyceraldehyde 3-phosphate to 3-phosphoglycerate in glycolysis in hPSC-derived  $\beta$ -like cells, is defective (Davis et al., 2020). This bottleneck of enzymatic activity slows down the glycolysis activity, limiting the production of phosphoenolpyruvate to fuel ATP generation through the mitochondria. Cell-permeable intermediate metabolites such as methyl-succinate and methyl-pyruvates partially rescue the GSIS defect in hPSC-derived  $\beta$ -like cells. Since most of the hPSC-derived  $\beta$ -like cells generated *in vitro* present significantly lower maximum respiration of the mitochondria, efficient supply of the mitochondria and improvement of the mitochondria are some of the key features of immature hPSC-derived  $\beta$ -like cells.

Dynamic continuous nutritional exchange is the natural condition for endogenous functional  $\beta$ -like cells; however, it has not been replicated for *in vitro*-cultured hPSC-derived  $\beta$ -like cells. The current protocol relies on feeding nutrition-rich media during  $\beta$ -like cell differentiation every day or every other day. In this setting, glucose is utilized without refill for more than 24–48 h and waste such as lactate from the cells continues to accumulate in the culture condition. Lactate and pyruvate transporters, such as monocarboxylate transporter 1 (MCT1), are disallowance genes in functional  $\beta$  cells, and their expression has been observed in neonates or hPSC-derived  $\beta$ -like cells (Yoshihara et al., 2016). This notion raises the concern that accumulated lactate not only oxidizes the media but is also re-absorbed in the hPSC-derived  $\beta$ -like cells to interrupt the proper metabolic activity and differentiation in  $\beta$  cells. In addition, a recent study found that hPSC-derived islets are hyper-sensitive to pyruvate-induced insulin secretion, which typically is not observed in primary adult islets (Balboa et al., 2022). Aberrant pyruvate transporter expression may contribute to this abnormal phenotype of hPSC-derived islets. *In vivo*-mimicking continuous nutritional exchange by techniques such as microfluidic perfusion (Jun et al., 2019) may aid in improving the metabolic disorder in hPSC-derived  $\beta$ -like cells.

### Oxygen Supply

In addition to nutrition, oxygen is a critical factor responsible for the functionality of  $\beta$  cells. Mature islets are surrounded by microvessels, which provide circulating oxygen tension (approximately 100 mmHg) (Jansson and Hellerstrom, 1983). It has been observed that *in vitro*-cultured human islet viability, especially hypoxia-induced necrosis in the center of islets, is improved by hyperoxia (approximately 350 mmHg) (Komatsu et al., 2016; Komatsu et al., 2017). Since there is no oxygen supply from microvessel *in vitro*-cultured hPSC-derived islets, current typical cell culture conditions, 5% CO<sub>2</sub>, 20% O<sub>2</sub> (approximately 160 mmHg), may not be ideal for differentiation and maintenance. The inner cell mass of blastocyst is likely to maintain low O<sub>2</sub> condition (approximately 5% O<sub>2</sub>) (Rodesch et al., 1992; Clark et al., 2006; Harvey, 2007; Lees et al., 2019). This is reasonable since hPSC metabolism is characterized by being highly dependent on glycolysis and up to 70% of glucose is

converted to lactate (Lees et al., 2019). During differentiation and maturation, this metabolism is shifted to a more oxidative mitochondria-dependent process (Varum et al., 2011). High O<sub>2</sub> levels (approximately 35% O<sub>2</sub>) promote the growth of *ex vivo*-cultured mouse pancreatic buds (Fraker et al., 2007). Similarly, rat pancreata cultured with high O<sub>2</sub> (60–80% O<sub>2</sub>) promotes  $\beta$ -cell differentiation (Heinis et al., 2010). Mechanistically, hypoxia activates hypoxia-inducible factor 1 $\alpha$  (HIF1 $\alpha$ ), which in turn activates the hairy and enhancer of split (HES1) to prevent  $\beta$ -cell differentiation (Heinis et al., 2010). High O<sub>2</sub> (60% O<sub>2</sub>) exposure between the endoderm and EP stage facilitated differentiation of EPs by activating cWnt signaling and suppressing HIF1 $\alpha$  and HES1 expression, which leads to the promotion of NGN3 expression in the insulin-producing cell differentiation model of mouse and human ES cells (Cechin et al., 2014; Hakim et al., 2014). In contrast, an excessive amount of O<sub>2</sub> may increase the reactive oxygen species (ROS) and cause oxidative stress which triggers  $\beta$ -cell dysfunction (Robertson et al., 2004; Gerber and Rutter, 2017). Both hypoxia and oxidative stress/ROS induce thioredoxin-interacting protein (Txnip), a major cause of  $\beta$ -cell dysfunction in diabetes (Yoshihara et al., 2010a; Yoshihara et al., 2010b; Yoshihara et al., 2014; Yoshihara, 2020). Therefore, rather than a continuous supply of excessive O<sub>2</sub>, more dynamic regulation of O<sub>2</sub> supply should be considered to improve the current protocol for the differentiation of the  $\beta$  cells. Monitoring the dynamic O<sub>2</sub> supply will benefit the better differentiation and function of hPSC-derived  $\beta$  cells.

### Fibroblasts, Pancreatic Exocrine, and Immune Cell Interactions

Islet microenvironments consist of pancreatic fibroblasts, acinar cells, vasculature cells, and immune cells such as macrophages. Increasing evidence suggests that exocrine acinar cells play a critical role in maintaining islet function and defects in exocrine link to the pathogenesis of some types of diabetes (Rickels et al., 2020; Chiou et al., 2021). The pancreatic organ-matched mesenchyme promotes self-renewal of the hPSC-derived PPs without further direct differentiation (Sneddon et al., 2012). These studies suggest that the islet microenvironment created by non-endocrine cells contributes to islet development and functional regulation. Further investigation of the spatiotemporal interaction between the endocrine cells and non-endocrine cells in islets is required to identify the key pathway that facilitates islet differentiation and physiological activity during fetal and postnatal development.

### Peripheral Neuro-Vasculature System

It has been widely recognized that central and peripheral neurons play an important role in regulating the exocrine and endocrine pancreas (Buijs et al., 2001; Chandra and Liddle, 2013). Neural projections from the dorsal motor neuron (dMN) in the brain stem innervate the pancreas and regulate enzymatic and hormonal secretions in the exocrine and endocrine systems, respectively. Tyrosine hydroxylase (TH)-positive sympathetic nerves have been detected in the fetal pancreas starting from the early stages, such as 8 weeks post-conception (w.p.c) (Krivova et al., 2021). The sympathetic nerve innervation of mouse islets is

**TABLE 1 |** Physiological role of nuclear receptors in functional  $\beta$  cells.

Common name	Symbol	Abbreviation	Ligands	Function	Human islets (FPKM)	Mouse islets (FPKM)	References
Thyroid hormone receptor- $\alpha$	NR1A1	TR $\alpha$	Thyroid hormone	Upregulation MAFA, GCK gene expression. Enhances GSIS, insulin production	>10	>20	Aguayo-Mazzucato et al. (2013)
Thyroid hormone receptor- $\beta$	NR1A1	TR $\beta$		Upregulation MAFA, GCK gene expression. Enhances GSIS, insulin production	>1	>2	Aguayo-Mazzucato et al. (2013)
Retinoic acid receptor- $\alpha$	NR1B1	RAR $\alpha$	Vitamin A, retinoic acids	Endocrine differentiation. Regulation of $\beta$ -cell mass	>5	>5	Brun et al. (2015), Matthews et al. (2004), Stafford and Prince, (2002)
Retinoic acid receptor- $\beta$	NR1B2	RAR $\beta$		Endocrine differentiation	>0.5	>0.4	Perez et al. (2013), Fedullo et al. (2021), Stafford and Prince, (2002)
Retinoic acid receptor- $\gamma$	NR1B3	RAR $\gamma$		Endocrine differentiation	>1	>10	Fedullo et al. (2021), Stafford and Prince, (2002)
Peroxisome proliferator-activated receptor- $\alpha$	NR1C1	PPAR $\alpha$	Fatty acids, prostaglandins	Enhances fatty acid oxidation and insulin secretion	>3	>0.3	Lalloyer et al. (2006), Zhou et al. (1998)
Peroxisome proliferator-activated receptor- $\delta$	NR1C2	PPAR $\delta$		Enhances fatty acid oxidation and insulin secretion	>6	>12	Tang et al. (2013)
Peroxisome proliferator-activated receptor- $\gamma$	NR1C3	PPAR $\gamma$		Enhances fatty acid oxidation and insulin secretion	>0.3	>5	Dubois et al. (2000), Rosen et al. (2003)
Rev-ErbA $\alpha$	NR1D1	Rev-ErbA $\alpha$	Heme	Circadian oscillation	>14	>30	Saini et al. (2016), Pulimeno et al. (2013)
Rev-ErbA $\alpha$	NR1D2	Rev-ErbA $\beta$		Circadian oscillation	>20	>30	Saini et al. (2016), Pulimeno et al. (2013)
RAR-related orphan receptor- $\alpha$	NR1F1	ROR $\alpha$	Cholesterol, retinoic acids	Suppresses GSIS. Circadian oscillation	>3	>1	Muhlbauer et al. (2013)
RAR-related orphan receptor- $\beta$	NR1F2	ROR $\beta$		Suppresses GSIS. Circadian oscillation	>1	>0.01	Taneera et al. (2019), Muhlbauer et al. (2013)
RAR-related orphan receptor- $\gamma$	NR1F3	ROR $\gamma$		Suppresses GSIS. Circadian oscillation	>7	>10	Taneera et al. (2019), Muhlbauer et al. (2013)
Liver X receptor- $\beta$	NR1H2	LXR $\beta$	Cholesterol	Enhances glycerol/fatty acids cycling	>13	>30	Efanov et al. (2004), Zitzer et al. (2006), Gerin et al. (2005)
Liver X receptor- $\alpha$	NR1H3	LXR $\alpha$		Enhances glycerol/fatty acids cycling	>2	>5	Efanov et al. (2004)
Farnesoid X receptor- $\alpha$	NR1H4	FXR $\alpha$	Bile acids	Upregulation of INS, GLP1R gene expression	>1	>9	Renga et al. (2010), Kong et al. (2019a), Kong et al. (2019b), Dufer et al. (2012), Kong et al. (2021)
Farnesoid X receptor- $\beta$	NR1H5	FXR $\beta$		-	-	>0.01	-
Vitamin D receptor	NR1I1	VDR	Vitamin D	Suppresses inflammation and prevents cytokine induced $\beta$ -cell dedifferentiation. Modulation of BAF complex	>3	>40	Wei et al. (2018)
Pregnane X receptor	NR1I2	PXR	Xenobiotics	Unclear	>0.01	>0.05	-
Constitutive androstane receptor	NR1I3	CAR	Androstane	Unclear	>0.1	>0.03	-
Hepatocyte nuclear factor-4- $\alpha$	NR2A1	HNF4 $\alpha$	Fatty acids	Responsible gene for MODY1	>3	>10	Yamagata et al. (1996)
Hepatocyte nuclear factor-4- $\gamma$	NR2A2	HNF4 $\gamma$		Pancreatic differentiation	>0.2	>2	Boj et al. (2001)
Retinoid X receptor- $\alpha$	NR2B1	RXR $\alpha$	Retinoic acids	Pancreatic differentiation	>10	>12	Kane et al. (2010), Kadison et al. (2001)
Retinoid X receptor- $\beta$	NR2B2	RXR $\beta$		Attenuates GSIS	>18	>18	Kane et al. (2010), Kadison et al. (2001)
Retinoid X receptor- $\gamma$	NR2B3	RXR $\gamma$		Pancreatic differentiation	>5	>0.1	Kane et al. (2010), Kadison et al. (2001)
Testicular receptor 2	NR2C1	TR2	-	Unclear	>3	>3	-
Testicular receptor 4	NR2C2	TR4		Unclear	>6	>6	-

(Continued on following page)

**TABLE 1 |** (Continued) Physiological role of nuclear receptors in functional  $\beta$  cells.

Common name	Symbol	Abbreviation	Ligands	Function	Human islets (FPKM)	Mouse islets (FPKM)	References
Homolog of the <i>Drosophila</i> tailless gene	NR2E1	TLX	-	Enhances $\beta$ -cell proliferation	>0.01	-	Shi et al. (2019), Shi et al. (2015)
Photoreceptor cell-specific nuclear receptor	NR2E3	PNR	-	Unclear	>0.01	>0.01	-
Chicken ovalbumin upstream promoter- $\alpha$	NR2F1	COUP-TF $\alpha$	-	Negatively regulates the mouse INS2 gene	>0.5	>0.3	Zhang et al. (2017), Boutant et al. (2012), Qin et al. (2010), Perilhou et al. (2008), Bardoux et al. (2005)
Chicken ovalbumin upstream promoter- $\beta$	NR2F2	COUP-TF $\beta$	-	Positively regulates $\beta$ -cell proliferation. Islet tumorigenesis	>6	>1	Qin et al. (2010), Boutant et al. (2012)
Chicken ovalbumin upstream promoter- $\gamma$	NR2F6	COUP-TF $\gamma$	-	Unclear	>25	>23	-
Estrogen receptor- $\alpha$	NR3A1	ER $\alpha$	Estrogens	Regulates insulin synthesis. Suppresses lipid synthesis	>1	>0.03	Alonso-Magdalena et al. (2008), Wong et al. (2010), Tiano et al. (2011)
Estrogen receptor- $\beta$	NR3A2	ER $\beta$	-	Regulates insulin synthesis. Suppresses lipid synthesis	>0.01	>0.02	Tiano et al. (2011), Wong et al. (2010), Alonso-Magdalena et al. (2008)
Estrogen-related receptor- $\alpha$	NR3B1	ERR $\alpha$	-	Unclear/possibly upregulates mitochondrial gene expression and enhances oxidative metabolism	>23	>10	-
Estrogen-related receptor- $\beta$	NR3B2	ERR $\beta$	-	Unclear	>0.1	>0.1	-
Estrogen-related receptor- $\gamma$	NR3B3	ERR $\gamma$	-	Upregulates mitochondrial gene expression and enhances oxidative metabolism and postnatal maturation	>2	>2	Yoshihara et al. (2016), Yoshihara et al. (2020)
Glucocorticoid receptor	NR3C1	GR	Cortisol	Promotes pancreatic differentiation. Induces apoptosis	>14	>17	Aylward et al. (2021), Ghazali et al. (2018), Reich et al. (2012), Matthews and Hanley, (2011), Ranta et al. (2006), Gesina et al. (2006), Shapiro et al. (2000)
Mineralocorticoid receptor	NR3C2	MR	Aldosterone	Enhances insulin secretion through $\alpha$ -cell GLP1 secretion	>5	>2.5	Goto et al. (2019)
Progesterone receptor	NR3C3	PR	Progesterone	Negatively regulates $\beta$ -cell proliferation	>2	>0.05	Picard et al. (2002)
Androgen receptor	NR3C4	AR	Testosterone	Enhances GSIS	>0.2	>0.1	Navarro et al. (2016)
Nerve growth factor IB	NR4A1	NGFIB	-	Positively and negatively regulates $\beta$ -cell proliferation	>2	>15	Yu et al. (2015), Tessem et al. (2014), Briand et al. (2012)
Nuclear receptor related 1	NR4A2	NURR1	-	Positively regulates $\beta$ -cell proliferation	>1	>1	Close et al. (2019)
Neuron-derived orphan receptor 1	NR4A3	NOR1	-	Positively and negatively regulates $\beta$ -cell proliferation	>0.5	>0.05	Tessem et al. (2014), Briand et al. (2012), Close et al. (2019)
Steroidogenic factor 1	NR5A1	SF-1	Phosphatidylinositols	Unclear	-	-	-
Liver receptor homolog-1	NR5A2	LRH-1	-	Pancreas organogenesis. Protects from stress-induced $\beta$ -cell apoptosis	>2	>0.4	Hale et al. (2014), Baquie et al. (2018), Cobo-Vuilleumier et al. (2018)
Germ cell nuclear factor	NR6A1	GCNF	-	Unclear	>0.2	>2.5	-
Dosage-sensitive sex reversal, adrenal hypoplasia critical region, on chromosome X, gene 1	NR0B1	DAX1	-	Unclear	>17	-	-
Small heterodimer partner	NR0B2	SHP	-	Negatively regulates $\beta$ -cell survival	>7	>0.01	Noh et al. (2013), Seo et al. (2008), Park et al. (2007), Suh et al. (2004)



reported to be a critical factor for proper islet architecture and function in a  $\beta$ -adrenergic dependent manner (Borden et al., 2013). Although how the innervation of peripheral nerves in human islets is important for organizing islet architecture, development, and function is still controversial or remains unknown, many receptors for neurotransmitters are expressed in human islets and regulate hormone secretion (Ahren, 2000; Burns et al., 2015; Rosario et al., 2016; Lin et al., 2021).

### Paracrine Regulation

Islets are multicellular mini-organs consisting of differential hormone-expressing cells with paracrine hormone regulation (Huising, 2020).  $\alpha$  cells secrete glucagon and glucagon-like peptide-1 (GLP-1), which enhance insulin secretion in  $\beta$  cells.  $\delta$  cells secrete somatostatin, which suppresses insulin secretion in  $\beta$  cells and glucagon secretion from  $\alpha$  cells (Strowski et al., 2000). Insulin inhibits glucagon secretion by stimulating somatostatin secretion by sodium-glucose co-transporter-2 (SGLT2) (Vergari et al., 2019). UCN3, co-secreted with insulin, also stimulates somatostatin secretion from  $\delta$  cells to enhance paracrine feedback regulation of  $\beta$  cells (van der Meulen et al., 2015). Although this paracrine hormone regulation plays an important role in proper insulin secretion in islets, the effect of paracrine signaling on islet differentiation and maturation has not yet been elucidated.

### Organ–Organ Interaction

Islets are embedded in the exocrine pancreas while through the nervous innervation and vasculature network receiving the signals from outside the pancreas. The intestine plays a central role in regulating  $\beta$ -cell function through the enteroendocrine hormone secretion directly or via the vagus nerve–brain–pancreas axis. Adipokines and hepatokines also play an important role in  $\beta$ -cell function (El Ouamari et al., 2013; Prentice et al., 2021). These signals from outside the pancreas influence the differentiation and maturation of islets remain poorly understood. Since the organs are simultaneously differentiated and mature during fetal and postnatal development, it is possible that organ–organ interactions also play an important role in islet differentiation and maturation.

### Adapting Physiology

Adapting to physiological environmental stimuli is a hallmark of mature adult organs, which are broadly regulated by nuclear hormone receptor (NR) signaling (Evans and Mangelsdorf, 2014). NR, a superfamily of 48 transcriptional factors in humans, regulates gene expression in response to various hormones, lipids, and metabolites and plays a master role in development and physiology (Evans and Mangelsdorf, 2014). Many NRs are expressed in rodent and human islets and are related to the  $\beta$ -cell physiology in response to lipid metabolism (Chuang et al., 2008) (Table 1). Free fatty acids, such as palmitate, stimulate insulin secretion for the short term, whereas chronic exposure to high concentrations of free fatty acids induces compensatory  $\beta$ -cell expansion and eventually leads to  $\beta$ -cell growth arrest and apoptosis. Nuclear receptor subfamily 4 group A member 1 (NR4A1) is translocated to the nucleus in response

to free fatty acids and plays a key role in lipotoxicity-induced  $\beta$ -cell apoptosis (Susini et al., 1998; Roche et al., 1999; Briand et al., 2012; Yu et al., 2015; Close et al., 2019). Mechanistically, NR4A1 binds to Foxo1 at the *MafA* promoter region and suppresses its expression to reduce *insulin* transcription (Briand et al., 2012). NR4A1 is required for Nkx6-1-mediated  $\beta$ -cell mass expansion (Tessem et al., 2014). Cholesterol sensor Liver X receptor (LXR; LXR $\alpha$  and LXR $\beta$ ) stimulates GSIS and insulin biosynthesis (Efanov et al., 2004; Zitzer et al., 2006). LXR $\beta$ KO mice exhibit a glucose-intolerant phenotype secondary to blunted GSIS *in vivo* (Gerin et al., 2005; Zitzer et al., 2006). Peroxisome proliferator-activated receptors (PPARs; PPAR $\gamma$ , PPAR $\alpha$ , and PPAR $\delta$ ) broadly regulate fatty acid oxidation, thereby enhancing GSIS and reducing lipotoxic effects in  $\beta$  cells. Estrogen receptors (ERs; ER $\alpha$  and ER $\beta$ ) also protect against lipotoxicity, especially in females. Testosterone-mediated androgen receptor (AR) signaling enhances GSIS and glucagon-like peptide-1 (GLP-1)-mediated insulin secretion in males (Navarro et al., 2016). Vitamin D receptor (VDR) regulates SWI/SNF chromatin remodeling together with bromodomain-containing protein 7 (BRD7) and BRD9, and protection from cytokines induces dedifferentiation of  $\beta$  cells in rodents and hPSC-derived  $\beta$ -like cells (Wei et al., 2018). Estrogen-related receptor  $\gamma$  (ERR $\gamma$ ) regulates mitochondrial gene expression related to the TCA cycle and OxPhos (Yoshihara et al., 2016). Farnesoid X receptors (FXRs; FXR $\alpha$  and FXR $\beta$ ) regulate *Ins* (Renga et al., 2010), adenylyl cyclase 8 (*Adcy8*) (Kong et al., 2019a), transient receptor potential ankyrin 1 (*Trpa1*) (Kong et al., 2019b), and GLP-1 receptor (*Glp1r*) (Kong et al., 2021) gene expression and protect from lipotoxicity (Popescu et al., 2010) in the rodents. Glucocorticoids and steroids are known to induce hyperglycemia, which may cause diabetes. Glucocorticoid receptor (GR) signaling through dexamethasone was initially believed to have a negative impact on islet physiology by reducing insulin synthesis and insulin secretion and inducing apoptosis in murine  $\beta$  cells (Philippe and Missotten, 1990; Goodman et al., 1996; Ranta et al., 2006; Reich et al., 2012; Aylward et al., 2021). In contrast, GR plays an essential role in human fetal and adult islet development by controlling  $\beta$ -cell transcriptomes, such as *PDX-1*, *GCK*, *GLUT2*, *SIX2*, and *SIX3* (Gesina et al., 2006; Matthews and Hanley, 2011; Ghazalli et al., 2018). Thyroid hormone receptors (TRs; TR $\alpha$  and TR $\beta$ ) regulate *MafA* expression during postnatal rat  $\beta$ -cell maturation (Aguayo-Mazzucato et al., 2013). Hypothyroidism impairs hPSC-PP maturation in mice suggesting the importance of TRs signaling *in vivo* functional  $\beta$ -cell maturation (Bruin et al., 2016). Circadian rhythms regulate  $\beta$ -cell maturation and physiology (Marcheva et al., 2010; Perelis et al., 2015; Alvarez-Dominguez et al., 2020). The clock protein REV-ERV $\alpha$  regulates the circadian rhythms in  $\beta$  cells, and downregulation of REV-ERV $\alpha$  impairs time-dependent GSIS (Vieira et al., 2012). REV-ERV $\alpha$  may be an important physiological regulator of  $\beta$  cells in time-restricted feeding or preventing pathogenesis of T2D by modulating  $\beta$ -cell rhythmic transcriptional regulation by adapting to environmental changes over time (Petrenko et al., 2020; Brown et al., 2021). Hepatic nuclear receptor 4- $\alpha$  (HNF4 $\alpha$ ) is responsible for maturity-onset diabetes of the young 1 (MODY1) (Yamagata et al., 1996).

Although NRs integrate gene regulation and cell function to adapt to environmental physiological stimulation, the contribution of NRs to functional maturation to adapt to environmental stimulation in islets is largely unknown. Understanding how these factors cooperatively regulate  $\beta$ -cell differentiation and physiological adaptation may improve generation of a physiological level of functional  $\beta$  cells.

## CONCLUSION

I discussed the existing limitations of the technology to generate human islets from pluripotent stem cells. The current protocol is generated on the basis of lineage specification; however, sufficient number of integrated functional maturation pathways are not there. The challenge remains to create cells with protocols within a few weeks of additional maturation, which exhibit equal functionality with primary human islets in terms of 1) amount of insulin secretion, 2) speed and accuracy of response to glucose, 3) transcriptome, and 4) controlled differentiation to individual endocrine cell types by integrating the new pathways adapting to environmental physiological stimulation. The key challenge in the field is that maturation may not only be coordinated by single signaling but corporately regulates by multiple signaling as the environmental sensor switch (Figure 1). Additionally, the required signaling may not be constitutively activated or suppressed; however, it is dynamically regulated by adapting to environmental physiological situations to work flexibly and properly in the spatiotemporal physiological situation. The future challenge of developing new technology should focus on dissecting many differential signaling and transcriptional networks that are involved in postnatal functional maturation and integrating how those signaling pathways synergistically regulate islet maturation. The robustness of scalability, consistency of high quality, and less batch-to-batch generation of different human islets *in vitro* should be continuously improved. One important notion for adapting to environmental signals is the duration and timing of the stimulation of those signals. The current protocol generates glucose-responsive hPSC-derived  $\beta$ -like cells or islets within

4–10 weeks of culturing *in vitro*. However, it takes approximately 40 weeks of differentiation and a few years of postnatal functional islet maturation in human body. This significant gap in the developmental time may need to be considered adapting to environmental cues in functional human islet organogenesis. A deeper understanding of islet differentiation and maturation is critical for generating fully functional human islets *in vitro*. Integrating the microenvironmental cues that mimic *in vivo* situations may help in further improving the protocol.

## DATA AVAILABILITY STATEMENT

The original contributions presented in the study are included in the article/Supplementary Material, further inquiries can be directed to the corresponding author.

## AUTHOR CONTRIBUTIONS

EY conceptualized and wrote the manuscript.

## FUNDING

This work was supported by the California Institute for Regenerative Medicine (CIRM)-DISC2 discovery award and Allen Foundation. EY was supported by the JDRF (formerly known as Juvenile Diabetes Research Foundation) career development award, which was made possible through collaboration between JDRF International and the Leona M. and Harry B. Helmsley Charitable Trust.

## SUPPLEMENTARY MATERIAL

The Supplementary Material for this article can be found online at: <https://www.frontiersin.org/articles/10.3389/fcell.2022.854604/full#supplementary-material>

## REFERENCES

- Aguayo-Mazzucato, C., Koh, A., El Khattabi, I., Li, W.-C., Toschi, E., Jermendy, A., et al. (2011). MafA Expression Enhances Glucose-Responsive Insulin Secretion in Neonatal Rat Beta Cells. *Diabetologia* 54, 583–593. doi:10.1007/s00125-010-2026-z
- Aguayo-Mazzucato, C., Zavacki, A. M., Marinellarena, A., Hollister-Lock, J., El Khattabi, I., Marsili, A., et al. (2013). Thyroid Hormone Promotes Postnatal Rat Pancreatic  $\beta$ -Cell Development and Glucose-Responsive Insulin Secretion through MAFA. *Diabetes* 62, 1569–1580. doi:10.2337/db12-0849
- Ahmadian, M., Liu, S., Reilly, S. M., Hah, N., Fan, W., Yoshihara, E., et al. (2018). ERR $\gamma$  Preserves Brown Fat Innate Thermogenic Activity. *Cel Rep.* 22, 2849–2859. doi:10.1016/j.celrep.2018.02.061
- Ahrén, B. (2000). Autonomic Regulation of Islet Hormone Secretion - Implications for Health and Disease. *Diabetologia* 43, 393–410. doi:10.1007/s001250051322
- Alonso-Magdalena, P., Ropero, A. B., Carrera, M. P., Cederroth, C. R., Baquié, M., Gauthier, B. R., et al. (2008). Pancreatic Insulin Content Regulation by the Estrogen Receptor ER $\alpha$ . *PLoS One* 3, e2069. doi:10.1371/journal.pone.0002069
- Alvarez-Dominguez, J. R., Donaghey, J., Rasouli, N., Kenty, J. H. R., Helman, A., Charlton, J., et al. (2020). Circadian Entrainment Triggers Maturation of Human *In Vitro* Islets. *Cell Stem Cell* 26, 108–122. e10. doi:10.1016/j.stem.2019.11.011
- Alvarez-Dominguez, J. R., and Melton, D. A. (2021). Cell Maturation: Hallmarks, Triggers, and Manipulation. *Cell* 185, 235.
- Arda, H. E., Li, L., Tsai, J., Torre, E. A., Rosli, Y., Peiris, H., et al. (2016). Age-Dependent Pancreatic Gene Regulation Reveals Mechanisms Governing Human  $\beta$  Cell Function. *Cel Metab.* 23, 909–920. doi:10.1016/j.cmet.2016.04.002
- Artner, I., Hang, Y., Mazur, M., Yamamoto, T., Guo, M., Lindner, J., et al. (2010). MafA and MafB Regulate Genes Critical to  $\beta$ -Cells in a Unique Temporal Manner. *Diabetes* 59, 2530–2539. doi:10.2337/db10-0190

- Assady, S., Maor, G., Amit, M., Itskovitz-Eldor, J., Skorecki, K. L., and Tzukerman, M. (2001). Insulin Production by Human Embryonic Stem Cells. *Diabetes* 50 (8), 1691–7. doi:10.2337/diabetes.50.8.1691
- Augsornworawat, P., Maxwell, K. G., Velazco-Cruz, L., and Millman, J. R. (2020). Single-Cell Transcriptome Profiling Reveals  $\beta$  Cell Maturation in Stem Cell-Derived Islets after Transplantation. *Cel Rep.* 32, 108067. doi:10.1016/j.celrep.2020.108067
- Augsornworawat, P., Maxwell, K. G., Velazco-Cruz, L., and Millman, J. R. (2021). Single-cell Transcriptome Profiling Reveals  $\beta$  Cell Maturation in Stem Cell-Derived Islets after Transplantation. *Cel Rep.* 34, 108850. doi:10.1016/j.celrep.2021.108850
- Aylward, A., Okino, M.-L., Benaglio, P., Chiou, J., Beebe, E., Padilla, J. A., et al. (2021). Glucocorticoid Signaling in Pancreatic Islets Modulates Gene Regulatory Programs and Genetic Risk of Type 2 Diabetes. *Plos Genet.* 17, e1009531. doi:10.1371/journal.pgen.1009531
- Bader, E., Migliorini, A., Gegg, M., Moruzzi, N., Gerdes, J., Roscioni, S. S., et al. (2016). Identification of Proliferative and Mature  $\beta$ -cells in the Islets of Langerhans. *Nature* 535, 430–434. doi:10.1038/nature18624
- Balboa, D., Barsby, T., Lithovius, V., Saarimäki-Vire, J., Omar-Hmeadi, M., Dyachok, O., et al. (2022). Functional, Metabolic and Transcriptional Maturation of Human Pancreatic Islets Derived from Stem Cells. *Nat. Biotechnol.* doi:10.1038/s41587-022-01219-z
- Baquié, M., St-Onge, L., Kerr-Conte, J., Cobo-Vuilleumier, N., Lorenzo, P. I., Jimenez Moreno, C. M., et al. (2018). The Liver Receptor Homolog-1 (LRH-1) Is Expressed in Human Islets and Protects  $\beta$ -cells against Stress-Induced Apoptosis. *Hum. Mol. Genet.* 27, 406. doi:10.1093/hmg/ddx402
- Bardoux, P., Zhang, P., Flamez, D., Perilhou, A., Lavin, T. A., Tanti, J.-F., et al. (2005). Essential Role of Chicken Ovalbumin Upstream Promoter-Transcription Factor II in Insulin Secretion and Insulin Sensitivity Revealed by Conditional Gene Knockout. *Diabetes* 54, 1357–1363. doi:10.2337/diabetes.54.5.1357
- Beckman, J. A., Paneni, F., Cosentino, F., and Creager, M. A. (2013). Diabetes and Vascular Disease: Pathophysiology, Clinical Consequences, and Medical Therapy: Part II. *Eur. Heart J.* 34, 2444–2452. doi:10.1093/eurheartj/eh142
- Bevacqua, R. J., Lam, J. Y., Peiris, H., Whitener, R. L., Kim, S., Gu, X., et al. (2021). SIX2 and SIX3 Coordinately Regulate Functional Maturity and Fate of Human Pancreatic  $\beta$  Cells. *Genes Dev.* 35, 234–249. doi:10.1101/gad.342378.120
- Boj, S. F., Párrizas, M., Maestros, M. A., and Ferrer, J. (2001). A Transcription Factor Regulatory Circuit in Differentiated Pancreatic Cells. *Proc. Natl. Acad. Sci. U.S.A.* 98, 14481–14486. doi:10.1073/pnas.241349398
- Borden, P., Houtz, J., Leach, S. D., and Kuruvilla, R. (2013). Sympathetic Innervation during Development Is Necessary for Pancreatic Islet Architecture and Functional Maturation. *Cel Rep.* 4, 287–301. doi:10.1016/j.celrep.2013.06.019
- Boutant, M., Ramos, O. H. P., Tourrel-Cuzin, C., Movassat, J., Ilias, A., Vallois, D., et al. (2012). COUP-TFII Controls Mouse Pancreatic  $\beta$ -Cell Mass through GLP-1- $\beta$ -Catenin Signaling Pathways. *PLoS One* 7, e30847. doi:10.1371/journal.pone.0030847
- Briand, O., Helleboid-Chapman, A., Ploton, M., Hennuyer, N., Carpentier, R., Pattou, F., et al. (2012). The Nuclear Orphan Receptor Nur77 Is a Lipotoxicity Sensor Regulating Glucose-Induced Insulin Secretion in Pancreatic  $\beta$ -Cells. *Mol. Endocrinol.* 26, 399–413. doi:10.1210/me.2011-1317
- Brown, M. R., Sen, S. K., Mazzone, A., Her, T. K., Xiong, Y., Lee, J. H., et al. (2021). Time-restricted Feeding Prevents Deleterious Metabolic Effects of Circadian Disruption through Epigenetic Control of  $\beta$  Cell Function. *Sci. Adv.* 7, eabg6856. doi:10.1126/sciadv.abg6856
- Bruin, J. E., Saber, N., O'Dwyer, S., Fox, J. K., Mojibian, M., Arora, P., et al. (2016). Hypothyroidism Impairs Human Stem Cell-Derived Pancreatic Progenitor Cell Maturation in Mice. *Diabetes* 65, 1297–1309. doi:10.2337/db15-1439
- Brun, P. J., Grijalva, A., Rausch, R., Watson, E., Yuen, J. J., Das, B. C., et al. (2015). Retinoic Acid Receptor Signaling Is Required to Maintain Glucose-stimulated Insulin Secretion and  $\beta$ -cell Mass. *FASEB j.* 29, 671–683. doi:10.1096/fj.14-256743
- Buijs, R. M., Chun, S. J., Nijima, A., Romijn, H. J., and Nagai, K. (2001). Parasympathetic and Sympathetic Control of the Pancreas: a Role for the Suprachiasmatic Nucleus and Other Hypothalamic Centers that Are Involved in the Regulation of Food Intake. *J. Comp. Neurol.* 431, 405–423. doi:10.1002/1096-9861(20010319)431:4<405::aid-cne1079>3.0.co;2-d
- Burns, S. M., Vetere, A., Walpita, D., Dančik, V., Khodier, C., Perez, J., et al. (2015). High-throughput Luminescent Reporter of Insulin Secretion for Discovering Regulators of Pancreatic Beta-Cell Function. *Cel Metab.* 21, 126–137. doi:10.1016/j.cmet.2014.12.010
- Cayabyab, F., Nih, L. R., and Yoshihara, E. (2021). Advances in Pancreatic Islet Transplantation Sites for the Treatment of Diabetes. *Front. Endocrinol.* 12, 732431. doi:10.3389/fendo.2021.732431
- Cechin, S., Álvarez-Cubela, S., Giraldo, J. A., Molano, R. D., Villate, S., Ricordi, C., et al. (2014). Influence of *In Vitro* and *In Vivo* Oxygen Modulation on  $\beta$  Cell Differentiation from Human Embryonic Stem Cells. *Stem Cell Transl Med* 3, 277–289. doi:10.5966/sctm.2013-0160
- Chandra, R., and Liddle, R. A. (2013). Modulation of Pancreatic Exocrine and Endocrine Secretion. *Curr. Opin. Gastroenterol.* 29, 517–522. doi:10.1097/mog.0b013e3283639326
- Chiou, J., Geusz, R. J., Okino, M.-L., Han, J. Y., Miller, M., Melton, R., et al. (2021). Interpreting Type 1 Diabetes Risk with Genetics and Single-Cell Epigenomics. *Nature* 594, 398–402. doi:10.1038/s41586-021-03552-w
- Cho, N. H., Shaw, J. E., Karuranga, S., Huang, Y., Da Rocha Fernandes, J. D., Ohlrogge, A. W., et al. (2018). IDF Diabetes Atlas: Global Estimates of Diabetes Prevalence for 2017 and Projections for 2045. *Diabetes Res. Clin. Pract.* 138, 271–281. doi:10.1016/j.diabres.2018.02.023
- Chuang, J.-C., Cha, J.-Y., Garmey, J. C., Mirmira, R. G., and Joyce, J. J. (2008). Research Resource: Nuclear Hormone Receptor Expression in the Endocrine Pancreas. *Mol. Endocrinol.* 22, 2353–2363. doi:10.1210/me.2007-0568
- Clark, A. R., Stokes, Y. M., Lane, M., and Thompson, J. G. (2006). Mathematical Modelling of Oxygen Concentration in Bovine and Murine Cumulus-Oocyte Complexes. *Reproduction* 131, 999–1006. doi:10.1530/rep.1.00974
- Close, A.-F., Dadheech, N., Villela, B. S., Rouillard, C., and Buteau, J. (2019). The Orphan Nuclear Receptor Nor1/Nr4a3 Is a Negative Regulator of  $\beta$ -cell Mass. *J. Biol. Chem.* 294, 4889–4897. doi:10.1074/jbc.ra118.005135
- Cobo-Vuilleumier, N., Lorenzo, P. I., Rodríguez, N. G., Herrera Gómez, I. d. G., Fuente-Martín, E., López-Noriega, L., et al. (2018). LRH-1 Agonism Favours an Immune-Islet Dialogue Which Protects against Diabetes Mellitus. *Nat. Commun.* 9, 1488. doi:10.1038/s41467-018-03943-0
- Creager, M. A., Lüscher, T. F., Cosentino, F., and Beckman, J. A. (2003). Diabetes and Vascular Disease. *Circulation* 108, 1527–1532. doi:10.1161/01.cir.0000091257.27563.32
- D'Amour, K. A., Agulnick, A. D., Eliazar, S., Kelly, O. G., Kroon, E., and Baetge, E. E. (2005). Efficient Differentiation of Human Embryonic Stem Cells to Definitive Endoderm. *Nat. Biotechnol.* 23, 1534–1541. doi:10.1038/nbt1163
- D'Amour, K. A., Bang, A. G., Eliazar, S., Kelly, O. G., Agulnick, A. D., Smart, N. G., et al. (2006). Production of Pancreatic Hormone-Expressing Endocrine Cells from Human Embryonic Stem Cells. *Nat. Biotechnol.* 24, 1392–1401. doi:10.1038/nbt1259
- Davis, J. C., Alves, T. C., Helman, A., Chen, J. C., Kenty, J. H., Cardone, R. L., et al. (2020). Glucose Response by Stem Cell-Derived  $\beta$  Cells *In Vitro* Is Inhibited by a Bottleneck in Glycolysis. *Cel Rep.* 31, 107623. doi:10.1016/j.celrep.2020.107623
- Dhawan, S., Tschen, S.-I., Zeng, C., Guo, T., Hebrok, M., Matveyenko, A., et al. (2015). DNA Methylation Directs Functional Maturation of Pancreatic  $\beta$  Cells. *J. Clin. Invest.* 125, 2851–2860. doi:10.1172/jci79956
- Dubois, M., Pattou, F., Kerr-Conte, J., Gmyr, V., Vandewalle, B., Desreumaux, P., et al. (2000). Expression of Peroxisome Proliferator-Activated Receptor  $\gamma$  (PPAR $\gamma$ ) in normal Human Pancreatic Islet Cells. *Diabetologia* 43, 1165–1169. doi:10.1007/s001250051508
- Düfer, M., Hörth, K., Wagner, R., Schittenhelm, B., Prowald, S., Wagner, T. F. J., et al. (2012). Bile Acids Acutely Stimulate Insulin Secretion of Mouse  $\beta$ -Cells via Farnesoid X Receptor Activation and KATP Channel Inhibition. *Diabetes* 61, 1479–1489. doi:10.2337/db11-0815
- Efanov, A. M., Sewing, S., Bokvist, K., and Gromada, J. (2004). Liver X Receptor Activation Stimulates Insulin Secretion via Modulation of Glucose and Lipid Metabolism in Pancreatic Beta-Cells. *Diabetes* 53 (Suppl. 3), S75–S78. doi:10.2337/diabetes.53.suppl\_3.s75
- El Ouamari, A., Kawamori, D., Dirice, E., Liew, C. W., Shadrach, J. L., Hu, J., et al. (2013). Liver-derived Systemic Factors Drive  $\beta$  Cell Hyperplasia in Insulin-Resistant States. *Cell Rep* 3, 401–410. doi:10.1016/j.celrep.2013.01.007

- Evans, R. M., and Mangelsdorf, D. J. (2014). Nuclear Receptors, RXR, and the Big Bang. *Cell* 157, 255–266. doi:10.1016/j.cell.2014.03.012
- Fan, W., He, N., Lin, C. S., Wei, Z., Hah, N., Waizenegger, W., et al. (2018). ERR $\gamma$  Promotes Angiogenesis, Mitochondrial Biogenesis, and Oxidative Remodeling in PGC1 $\alpha$ / $\beta$ -Deficient Muscle. *Cel Rep.* 22, 2521–2529. doi:10.1016/j.celrep.2018.02.047
- Fedullo, A. L., Schiattarella, A., Morlando, M., Raguzzini, A., Toti, E., De Franciscis, P., et al. (2021). Mediterranean Diet for the Prevention of Gestational Diabetes in the Covid-19 Era: Implications of IL-6 in Diabesity. *Int. J. Mol. Sci.* 22. doi:10.3390/ijms22031213
- Fraker, C. A., Álvarez, S., Papadopoulos, P., Giraldo, J., Gu, W., Ricordi, C., et al. (2007). Enhanced Oxygenation Promotes  $\beta$ -Cell Differentiation *In Vitro*. *Stem Cells* 25, 3155–3164. doi:10.1634/stemcells.2007-0445
- Gerber, P. A., and Rutter, G. A. (2017). The Role of Oxidative Stress and Hypoxia in Pancreatic Beta-Cell Dysfunction in Diabetes Mellitus. *Antioxid. Redox Signaling* 26, 501–518. doi:10.1089/ars.2016.6755
- Gerin, I., Dolinsky, V. W., Shackman, J. G., Kennedy, R. T., Chiang, S.-H., Burant, C. F., et al. (2005). LXR $\beta$  Is Required for Adipocyte Growth, Glucose Homeostasis, and  $\beta$  Cell Function. *J. Biol. Chem.* 280, 23024–23031. doi:10.1074/jbc.m412564200
- Gesina, E., Blondeau, B., Milet, A., Le Nin, I., Duchene, B., Czernichow, P., et al. (2006). Glucocorticoid Signalling Affects Pancreatic Development through Both Direct and Indirect Effects. *Diabetologia* 49, 2939–2947. doi:10.1007/s00125-006-0449-3
- Ghazalli, N., Wu, X., Walker, S., Trieu, N., Hsin, L.-Y., Choe, J., et al. (2018). Glucocorticoid Signaling Enhances Expression of Glucose-Sensing Molecules in Immature Pancreatic Beta-like Cells Derived from Murine Embryonic Stem Cells *In Vitro*. *Stem Cell Develop.* 27, 898–909. doi:10.1089/scd.2017.0160
- Goodman, P. A., Medina-Martinez, O., and Fernandez-Mejia, C. (1996). Identification of the Human Insulin Negative Regulatory Element as a Negative Glucocorticoid Response Element. *Mol. Cell Endocrinol.* 120, 139–146. doi:10.1016/0303-7207(96)03830-0
- Goto, R., Kondo, T., Ono, K., Kitano, S., Miyakawa, N., Watanabe, T., et al. (2019). Mineralocorticoid Receptor May Regulate Glucose Homeostasis through the Induction of Interleukin-6 and Glucagon-like Peptide-1 in Pancreatic Islets. *J. Clin. Med.* 8. doi:10.3390/jcm8050674
- Hakim, F., Kaitsuka, T., Raed, J. M., Wei, F.-Y., Shiraki, N., Akagi, T., et al. (2014). High Oxygen Condition Facilitates the Differentiation of Mouse and Human Pluripotent Stem Cells into Pancreatic Progenitors and Insulin-Producing Cells. *J. Biol. Chem.* 289, 9623–9638. doi:10.1074/jbc.m113.524363
- Hale, M. A., Swift, G. H., Hoang, C. Q., Deering, T. G., Masui, T., Lee, Y.-K., et al. (2014). The Nuclear Hormone Receptor Family Member NR5A2 Controls Aspects of Multipotent Progenitor Cell Formation and Acinar Differentiation during Pancreatic Organogenesis. *Development* 141, 3123–3133. doi:10.1242/dev.109405
- Hang, Y., and Stein, R. (2011). MafA and MafB Activity in Pancreatic  $\beta$  Cells. *Trends Endocrinol. Metab.* 22, 364–373. doi:10.1016/j.tem.2011.05.003
- Harvey, A. J. (2007). The Role of Oxygen in Ruminant Preimplantation Embryo Development and Metabolism. *Anim. Reprod. Sci.* 98, 113–128. doi:10.1016/j.anireprosci.2006.10.008
- Heinis, M., Simon, M.-T., Ilc, K., Mazure, N. M., Pouyssegur, J., Scharfmann, R., et al. (2010). Oxygen Tension Regulates Pancreatic  $\beta$ -Cell Differentiation through Hypoxia-Inducible Factor 1 $\alpha$ . *Diabetes* 59, 662–669. doi:10.2337/db09-0891
- Hellerström, C., and Swenne, I. (1991). Functional Maturation and Proliferation of Fetal Pancreatic Beta-Cells. *Diabetes* 40 (Suppl. 2), 89–93. doi:10.2337/diab.40.2.s89
- Helman, A., Cangelosi, A. L., Davis, J. C., Pham, Q., Rothman, A., Faust, A. L., et al. (2020). A Nutrient-Sensing Transition at Birth Triggers Glucose-Responsive Insulin Secretion. *Cel Metab.* 31, 1004–1016. e5. doi:10.1016/j.cmet.2020.04.004
- Hogrebe, N. J., Augsornworawat, P., Maxwell, K. G., Velazco-Cruz, L., and Millman, J. R. (2020). Targeting the Cytoskeleton to Direct Pancreatic Differentiation of Human Pluripotent Stem Cells. *Nat. Biotechnol.* 38, 460–470. doi:10.1038/s41587-020-0430-6
- Hrvatin, S., O'Donnell, C. W., Deng, F., Millman, J. R., Pagliuca, F. W., Diiorio, P., et al. (2014). Differentiated Human Stem Cells Resemble Fetal, Not Adult,  $\beta$  Cells. *Proc. Natl. Acad. Sci. U.S.A.* 111, 3038–3043. doi:10.1073/pnas.1400709111
- Huang, Y., Karuranga, S., Malanda, B., and Williams, D. R. R. (2018). Call for Data Contribution to the IDF Diabetes Atlas 9th Edition 2019. *Diabetes Res. Clin. Pract.* 140, 351–352. doi:10.1016/j.diabres.2018.05.033
- Huising, M. O. (2020). Paracrine Regulation of Insulin Secretion. *Diabetologia* 63, 2057–2063. doi:10.1007/s00125-020-05213-5
- Jaafar, R., Tran, S., Shah, A. N., Sun, G., Valdearcos, M., Marchetti, P., et al. (2019). mTORC1 to AMPK Switching Underlies  $\beta$ -cell Metabolic Plasticity during Maturation and Diabetes. *J. Clin. Invest.* 129, 4124–4137. doi:10.1172/JCI127021
- Jacovetti, C., Matkovich, S. J., Rodriguez-Trejo, A., Guay, C., and Regazzi, R. (2015). Postnatal  $\beta$ -cell Maturation Is Associated with Islet-specific microRNA Changes Induced by Nutrient Shifts at Weaning. *Nat. Commun.* 6, 8084. doi:10.1038/ncomms9084
- Jansson, L., and Hellerström, C. (1983). Stimulation by Glucose of the Blood Flow to the Pancreatic Islets of the Rat. *Diabetologia* 25, 45–50. doi:10.1007/BF00251896
- Jun, Y., Lee, J., Choi, S., Yang, J. H., Sander, M., Chung, S., et al. (2019). In Vivo-mimicking Microfluidic Perfusion Culture of Pancreatic Islet Spheroids. *Sci. Adv.* 5, eaax4520. doi:10.1126/sciadv.aax4520
- Kadison, A., Kim, J., Maldonado, T., Crisera, C., Prasad, K., Manna, P., et al. (2001). Retinoid Signaling Directs Secondary Lineage Selection in Pancreatic Organogenesis. *J. Pediatr. Surg.* 36, 1150–1156. doi:10.1053/jpsu.2001.25734
- Kane, M. A., Folias, A. E., Pingitore, A., Perri, M., Obrochta, K. M., Krois, C. R., et al. (2010). Identification of 9- Cis -retinoic Acid as a Pancreas-specific Autocoid that Attenuates Glucose-Stimulated Insulin Secretion. *Proc. Natl. Acad. Sci. U.S.A.* 107, 21884–21889. doi:10.1073/pnas.1008859107
- Komatsu, H., Cook, C., Wang, C.-H., Medrano, L., Lin, H., Kandeel, F., et al. (2017). Oxygen Environment and Islet Size Are the Primary Limiting Factors of Isolated Pancreatic Islet Survival. *PLoS One* 12, e0183780. doi:10.1371/journal.pone.0183780
- Komatsu, H., Kang, D., Medrano, L., Barriga, A., Mendez, D., Rawson, J., et al. (2016). Isolated Human Islets Require Hyperoxia to Maintain Islet Mass, Metabolism, and Function. *Biochem. Biophysical Res. Commun.* 470, 534–538. doi:10.1016/j.bbrc.2016.01.110
- Kong, X., Li, B., Deng, Y., and Ma, X. (2019a). FXR Mediates Adenylyl Cyclase 8 Expression in Pancreatic  $\beta$ -Cells. *J. Diabetes Res.* 2019, 8915818. doi:10.1155/2019/8915818
- Kong, X., Feng, L., Yan, D., Li, B., Yang, Y., and Ma, X. (2021). FXR-mediated Epigenetic Regulation of GLP-1R Expression Contributes to Enhanced Incretin Effect in Diabetes after RYGB. *J. Cel Mol Med.*
- Kong, X., Tu, Y., Li, B., Zhang, L., Feng, L., Wang, L., et al. (2019b). Roux-en-Y Gastric Bypass Enhances Insulin Secretion in Type 2 Diabetes via FXR-Mediated TRPA1 Expression. *Mol. Metab.* 29, 1–11. doi:10.1016/j.molmet.2019.08.009
- Krivova, Y. S., Proshchina, A. E., Otyga, D. A., Leonova, O. G., and Saveliev, S. V. (2022). Prenatal Development of Sympathetic Innervation of the Human Pancreas. *Ann. Anat.* 240, 151880. doi:10.1016/j.aanat.2021.151880
- Kroon, E., Martinson, L. A., Kadoya, K., Bang, A. G., Kelly, O. G., Eliazar, S., et al. (2008). Pancreatic Endoderm Derived from Human Embryonic Stem Cells Generates Glucose-Responsive Insulin-Secreting Cells *In Vivo*. *Nat. Biotechnol.* 26, 443–452. doi:10.1038/nbt1393
- Lalloyer, F., Vandewalle, B., Percevault, F., Torpier, G., Kerr-Conte, J., Oosterveer, M., et al. (2006). Peroxisome Proliferator-Activated Receptor  $\alpha$  Improves Pancreatic Adaptation to Insulin Resistance in Obese Mice and Reduces Lipotoxicity in Human Islets. *Diabetes* 55, 1605–1613. doi:10.2337/db06-0016
- Lees, J. G., Cliff, T. S., Gammilonghi, A., Ryall, J. G., Dalton, S., Gardner, D. K., et al. (2019). Oxygen Regulates Human Pluripotent Stem Cell Metabolic Flux. *Stem Cell Int* 2019, 8195614. doi:10.1155/2019/8195614
- Lemos, J. R. N., Baidal, D. A., Ricordi, C., Fuenmayor, V., Alvarez, A., and Alejandro, R. (2021). Survival after Islet Transplantation in Subjects with Type 1 Diabetes: Twenty-Year Follow-Up. *Diabetes Care* 44, e67–e68. doi:10.2337/dc20-2458
- Lin, E. E., Scott-Solomon, E., and Kuruvilla, R. (2021). Peripheral Innervation in the Regulation of Glucose Homeostasis. *Trends Neurosciences* 44, 189–202. doi:10.1016/j.tins.2020.10.015
- Lumelsky, N., Blondel, O., Laeng, P., Velasco, I., Ravin, R., and McKay, R. (2001). Differentiation of Embryonic Stem Cells to Insulin-Secreting Structures Similar to Pancreatic Islets. *Science* 292 (5520), 1389–94. doi:10.1126/science.1058866



- Lüscher, T. F., Creager, M. A., Beckman, J. A., and Cosentino, F. (2003). Diabetes and Vascular Disease: Pathophysiology, Clinical Consequences, and Medical Therapy: Part II. *Circulation* 108, 1655–1661. doi:10.1161/01.CIR.0000089189.70578.E2
- Mamidi, A., Prawiro, C., Seymour, P. A., De Lichtenberg, K. H., Jackson, A., Serup, P., et al. (2018). Mechanosignalling via Integrins Directs Fate Decisions of Pancreatic Progenitors. *Nature* 564, 114–118. doi:10.1038/s41586-018-0762-2
- Marcheva, B., Ramsey, K. M., Buhr, E. D., Kobayashi, Y., Su, H., Ko, C. H., et al. (2010). Disruption of the Clock Components CLOCK and BMAL1 Leads to Hypoinsulinaemia and Diabetes. *Nature* 466, 627–631. doi:10.1038/nature09253
- Martin, C. C., Flemming, B. P., Wang, Y., Oeser, J. K., and O'Brien, R. M. (2008). Foxa2 and MafA Regulate Islet-specific Glucose-6-Phosphatase Catalytic Subunit-Related Protein Gene Expression. *J. Mol. Endocrinol.* 41, 315–328. doi:10.1677/jme-08-0062
- Matthews, K. A., Rhoten, W. B., Driscoll, H. K., and Chertow, B. S. (2004). Vitamin A Deficiency Impairs Fetal Islet Development and Causes Subsequent Glucose Intolerance in Adult Rats. *J. Nutr.* 134, 1958–1963. doi:10.1093/jn/134.8.1958
- Matthews, L. C., and Hanley, N. A. (2011). The Stress of Starvation: Glucocorticoid Restraint of Beta Cell Development. *Diabetologia* 54, 223–226. doi:10.1007/s00125-010-1963-x
- Mühlbauer, E., Bazwinsky-Wutschke, I., Wolgast, S., Labucay, K., and Peschke, E. (2013). Differential and Day-Time Dependent Expression of Nuclear Receptors ROR $\alpha$ , ROR $\beta$ , ROR $\gamma$  and RXR $\alpha$  in the Rodent Pancreas and Islet. *Mol. Cell Endocrinol.* 365, 129–138. doi:10.1016/j.mce.2012.10.001
- Nair, G. G., Liu, J. S., Russ, H. A., Tran, S., Saxton, M. S., Chen, R., et al. (2019). Recapitulating Endocrine Cell Clustering in Culture Promotes Maturation of Human Stem-Cell-Derived  $\beta$  Cells. *Nat. Cell Biol.* 21, 263–274. doi:10.1038/s41556-018-0271-4
- Navarro, G., Xu, W., Jacobson, D. A., Wicksteed, B., Allard, C., Zhang, G., et al. (2016). Extranuclear Actions of the Androgen Receptor Enhance Glucose-Stimulated Insulin Secretion in the Male. *Cel Metab.* 23, 837–851. doi:10.1016/j.cmet.2016.03.015
- Ni, Q., Gu, Y., Xie, Y., Yin, Q., Zhang, H., Nie, A., et al. (2017). Raptor Regulates Functional Maturation of Murine Beta Cells. *Nat. Commun.* 8, 15755. doi:10.1038/ncomms15755
- Noh, J.-R., Hwang, J. H., Kim, Y.-H., Kim, K.-S., Gang, G.-T., Kim, S.-W., et al. (2013). The Orphan Nuclear Receptor Small Heterodimer Partner Negatively Regulates Pancreatic Beta Cell Survival and Hyperglycemia in Multiple Low-Dose Streptozotocin-Induced Type 1 Diabetic Mice. *Int. J. Biochem. Cell Biol.* 45, 1538–1545. doi:10.1016/j.biocel.2013.05.004
- Pagliuca, F. W., Millman, J. R., Gürtler, M., Segel, M., Van Dervort, A., Ryu, J. H., et al. (2014). Generation of Functional Human Pancreatic  $\beta$  Cells *In Vitro*. *Cell* 159, 428–439. doi:10.1016/j.cell.2014.09.040
- Paneni, F., Beckman, J. A., Creager, M. A., and Cosentino, F. (2013). Diabetes and Vascular Disease: Pathophysiology, Clinical Consequences, and Medical Therapy: Part I. *Eur. Heart J.* 34, 2436–2443. doi:10.1093/eurheartj/eh149
- Park, K.-G., Lee, K.-M., Seo, H.-Y., Suh, J.-H., Kim, H.-S., Wang, L., et al. (2007). Glucotoxicity in the INS-1 Rat Insulinoma Cell Line Is Mediated by the Orphan Nuclear Receptor Small Heterodimer Partner. *Diabetes* 56, 431–437. doi:10.2337/db06-0753
- Perelis, M., Marcheva, B., Ramsey, K. M., Schipma, M. J., Hutchison, A. L., Taguchi, A., et al. (2015). Pancreatic  $\beta$  Cell Enhancers Regulate Rhythmic Transcription of Genes Controlling Insulin Secretion. *Science* 350, aac4250. doi:10.1126/science.aac4250
- Pérez, R. J., Benoit, Y. D., and Gudas, L. J. (2013). Deletion of Retinoic Acid Receptor  $\beta$  (RAR $\beta$ ) Impairs Pancreatic Endocrine Differentiation. *Exp. Cell Res.* 319, 2196–2204. doi:10.1016/j.yexcr.2013.05.032
- Perilhou, A., Tourrel-Cuzin, C., Zhang, P., Kharoubi, I., Wang, H., Fauveau, V., et al. (2008). The MODY1 Gene for Hepatocyte Nuclear Factor 4 $\alpha$  and a Feedback Loop Control COUP-TFII Expression in Pancreatic Beta Cells. *Mol. Cell Biol.* 28, 4588–4597. doi:10.1128/mcb.01191-07
- Peterson, Q. P., Veres, A., Chen, L., Slama, M. Q., Kenty, J. H. R., Hassoun, S., et al. (2020). A Method for the Generation of Human Stem Cell-Derived Alpha Cells. *Nat. Commun.* 11, 2241. doi:10.1038/s41467-020-16049-3
- Petrenko, V., Gandasi, N. R., Sage, D., Tengholm, A., Barg, S., and Dibner, C. (2020). In Pancreatic Islets from Type 2 Diabetes Patients, the Dampened Circadian Oscillators lead to Reduced Insulin and Glucagon Exocytosis. *Proc. Natl. Acad. Sci. U.S.A.* 117, 2484–2495. doi:10.1073/pnas.1916539117
- Philippe, J., and Missotten, M. (1990). Dexamethasone Inhibits Insulin Biosynthesis by Destabilizing Insulin Messenger Ribonucleic Acid in Hamster Insulinoma Cells. *Endocrinology* 127, 1640–1645. doi:10.1210/endo-127-4-1640
- Picard, F., Wanatabe, M., Schoonjans, K., Lydon, J., O'Malley, B. W., and Auwerx, J. (2002). Progesterone Receptor Knockout Mice Have an Improved Glucose Homeostasis Secondary to  $\beta$ -cell Proliferation. *Proc. Natl. Acad. Sci. U.S.A.* 99, 15644–15648. doi:10.1073/pnas.202612199
- Popescu, I. R., Helleboid-Chapman, A., Lucas, A., Vandewalle, B., Dumont, J., Bouchaert, E., et al. (2010). The Nuclear Receptor FXR Is Expressed in Pancreatic  $\beta$ -cells and Protects Human Islets from Lipotoxicity. *FEBS Lett.* 584, 2845–2851. doi:10.1016/j.febslet.2010.04.068
- Prentice, K. J., Saksi, J., Robertson, L. T., Lee, G. Y., Inouye, K. E., Eguchi, K., et al. (2021). A Hormone Complex of FABP4 and Nucleoside Kinases Regulates Islet Function. *Nature* 600, 720. doi:10.1038/s41586-021-04137-3
- Pulimeno, P., Mannic, T., Sage, D., Giovannoni, L., Salmon, P., Lemeille, S., et al. (2013). Autonomous and Self-Sustained Circadian Oscillators Displayed in Human Islet Cells. *Diabetologia* 56, 497–507. doi:10.1007/s00125-012-2779-7
- Qin, J., Chen, X., Yu-Lee, L.-y., Tsai, M.-J., and Tsai, S. Y. (2010). Nuclear Receptor COUP-TFII Controls Pancreatic Islet Tumor Angiogenesis by Regulating Vascular Endothelial Growth Factor/vascular Endothelial Growth Factor Receptor-2 Signaling. *Cancer Res.* 70, 8812–8821. doi:10.1158/0008-5472.can-10-0551
- Ranta, F., Avram, D., Berchtold, S., Düfer, M., Drews, G., Lang, F., et al. (2006). Dexamethasone Induces Cell Death in Insulin-Secreting Cells, an Effect Reversed by Exendin-4. *Diabetes* 55, 1380–1390. doi:10.2337/db05-1220
- Reich, E., Tamary, A., Sionov, R. V., and Melloul, D. (2012). Involvement of Thioredoxin-Interacting Protein (TXNIP) in Glucocorticoid-Mediated Beta Cell Death. *Diabetologia* 55, 1048–1057. doi:10.1007/s00125-011-2422-z
- Renga, B., Mencarelli, A., Vavassori, P., Brancalione, V., and Fiorucci, S. (2010). The Bile Acid Sensor FXR Regulates Insulin Transcription and Secretion. *Biochim. Biophys. Acta (Bba) - Mol. Basis Dis.* 1802, 363–372. doi:10.1016/j.bbadis.2010.01.002
- Rezania, A., Bruin, J. E., Arora, P., Rubin, A., Batushansky, I., Asadi, A., et al. (2014). Reversal of Diabetes with Insulin-Producing Cells Derived *In Vitro* from Human Pluripotent Stem Cells. *Nat. Biotechnol.* 32, 1121–1133. doi:10.1038/nbt.3033
- Rezania, A., Riedel, M. J., Wideman, R. D., Karanu, F., Ao, Z., Warnock, G. L., et al. (2011). Production of Functional Glucagon-Secreting  $\alpha$ -Cells from Human Embryonic Stem Cells. *Diabetes* 60, 239–247. doi:10.2337/db10-0573
- Rickels, M. R., Norris, A. W., and Hull, R. L. (2020). A Tale of Two Pancreases: Exocrine Pathology and Endocrine Dysfunction. *Diabetologia* 63, 2030–2039. doi:10.1007/s00125-020-05210-8
- Robertson, R. P., Harmon, J., Tran, P. O., and Poirout, V. (2004). Beta-cell Glucose Toxicity, Lipotoxicity, and Chronic Oxidative Stress in Type 2 Diabetes. *Diabetes* 53 (Suppl. 1), S119–S124. doi:10.2337/diabetes.53.2007.s119
- Roche, E., Buteau, J., Aniento, I., Reig, J. A., Soria, B., and Prentki, M. (1999). Palmitate and Oleate Induce the Immediate-Early Response Genes C-Fos and Nur-77 in the Pancreatic Beta-Cell Line INS-1. *Diabetes* 48, 2007–2014. doi:10.2337/diabetes.48.10.2007
- Rodesch, F., Simon, P., Donner, C., and Jauniaux, E. (1992). Oxygen Measurements in Endometrial and Trophoblastic Tissues during Early Pregnancy. *Obstet. Gynecol.* 80, 283–285.
- Rogers, M. A. M., and Kim, C. (2020). Congenital Infections as Contributors to the Onset of Diabetes in Children: A Longitudinal Study in the United States, 2001–2017. *Pediatr. Diabetes* 21, 456–459. doi:10.1111/pedi.12957
- Rogers, M. A. M., Wei, M. Y., Kim, C., and Lee, J. M. (2020). Sex Differences in Autoimmune Multimorbidity in Type 1 Diabetes Mellitus and the Risk of Cardiovascular and Renal Disease: A Longitudinal Study in the United States, 2001–2017. *J. Women's Health* 29, 511–519. doi:10.1089/jwh.2019.7935
- Rorsman, P., Arkhammar, P., Bokvist, K., Hellerström, C., Nilsson, T., Welsh, M., et al. (1989). Failure of Glucose to Elicit a normal Secretory Response in Fetal Pancreatic Beta Cells Results from Glucose Insensitivity of the ATP-Regulated K<sup>+</sup> Channels. *Proc. Natl. Acad. Sci. U.S.A.* 86, 4505–4509. doi:10.1073/pnas.86.12.4505

- Rosario, W., Singh, I., Wautlet, A., Patterson, C., Flak, J., Becker, T. C., et al. (2016). The Brain-To-Pancreatic Islet Neuronal Map Reveals Differential Glucose Regulation from Distinct Hypothalamic Regions. *Diabetes* 65, 2711–2723. doi:10.2337/db15-0629
- Rosen, E. D., Kulkarni, R. N., Sarraf, P., Ozcan, U., Okada, T., Hsu, C.-H., et al. (2003). Targeted Elimination of Peroxisome Proliferator-Activated Receptor  $\gamma$  in  $\beta$  Cells Leads to Abnormalities in Islet Mass without Compromising Glucose Homeostasis. *Mol. Cell Biol.* 23, 7222–7229. doi:10.1128/mcb.23.20.7222-7229.2003
- Russ, H. A., Parent, A. V., Ringler, J. J., Hennings, T. G., Nair, G. G., Shveygert, M., et al. (2015). Controlled Induction of Human Pancreatic Progenitors Produces Functional Beta-like Cells *In Vitro*. *EMBO J.* 34, 1759–1772. doi:10.15252/embj.201591058
- Russell, R., Carnese, P. P., Hennings, T. G., Walker, E. M., Russ, H. A., Liu, J. S., et al. (2020). Loss of the Transcription Factor MAFB Limits  $\beta$ -cell Derivation from Human PSCs. *Nat. Commun.* 11, 2742. doi:10.1038/s41467-020-16550-9
- Saini, C., Petrenko, V., Pulimeno, P., Giovannoni, L., Berney, T., Hebrok, M., et al. (2016). A Functional Circadian Clock Is Required for Proper Insulin Secretion by Human Pancreatic Islet Cells. *Diabetes Obes. Metab.* 18, 355–365. doi:10.1111/dom.12616
- Seo, H.-Y., Kim, Y. D., Lee, K.-M., Min, A.-K., Kim, M.-K., Kim, H.-S., et al. (2008). Endoplasmic Reticulum Stress-Induced Activation of Activating Transcription Factor 6 Decreases Insulin Gene Expression via Up-Regulation of Orphan Nuclear Receptor Small Heterodimer Partner. *Endocrinology* 149, 3832–3841. doi:10.1210/en.2008-0015
- Shah, V. N., Grimsman, J. M., Foster, N. C., Dost, A., Miller, K. M., Pavel, M., et al. (2020). Undertreatment of Cardiovascular Risk Factors in the Type 1 Diabetes Exchange Clinic Network ( United States ) and the Prospective Diabetes Follow-up (Germany/Austria) Registries. *Diabetes Obes. Metab.* 22, 1577–1585. doi:10.1111/dom.14069
- Shapiro, A. M. J., Lakey, J. R. T., Ryan, E. A., Korbitt, G. S., Toth, E., Warnock, G. L., et al. (2000). Islet Transplantation in Seven Patients with Type 1 Diabetes Mellitus Using a Glucocorticoid-free Immunosuppressive Regimen. *N. Engl. J. Med.* 343, 230–238. doi:10.1056/nejm200007273430401
- Shi, X., Ma, D., Li, M., Zeng, L., Chen, J., and Yang, Y. (2019). Nuclear Receptor TLX Regulates Islet Beta Cell Proliferation via E2F6. *Biochem. Biophysical Res. Commun.* 513, 560–566. doi:10.1016/j.bbrc.2019.04.033
- Shi, X., Xiong, X., Dai, Z., Deng, H., Sun, L., Hu, X., et al. (2015). Nuclear Orphan Receptor TLX Affects Gene Expression, Proliferation and Cell Apoptosis in Beta Cells. *Biochem. Biophysical Res. Commun.* 468, 387–393. doi:10.1016/j.bbrc.2015.10.042
- Small, B. L., Ritchwood, T. D., Bishu, K. G., and Egede, L. E. (2020). Racial/Ethnic Differences in Glycemic Control in Older Adults with Type 2 Diabetes: United States 2003–2014. *Int. J. Environ. Res. Public Health* 17. doi:10.3390/ijerph17030950
- Sneddon, J. B., Borowiak, M., and Melton, D. A. (2012). Self-renewal of Embryonic-Stem-Cell-Derived Progenitors by Organ-Matched Mesenchyme. *Nature* 491, 765–768. doi:10.1038/nature11463
- Stafford, D., and Prince, V. E. (2002). Retinoic Acid Signaling Is Required for a Critical Early Step in Zebrafish Pancreatic Development. *Curr. Biol.* 12, 1215–1220. doi:10.1016/s0960-9822(02)00929-6
- Stolovich-Rain, M., Enk, J., Vikesa, J., Nielsen, F. C., Saada, A., Glaser, B., et al. (2015). Weaning Triggers a Maturation Step of Pancreatic  $\beta$  Cells. *Develop. Cell* 32, 535–545. doi:10.1016/j.devcel.2015.01.002
- Strowski, M. Z., Parmar, R. M., Blake, A. D., and Schaeffer, J. M. (2000). Somatostatin Inhibits Insulin and Glucagon Secretion via Two Receptor Subtypes: An *In Vitro* Study of Pancreatic Islets from Somatostatin Receptor 2 Knockout Mice\*. *Endocrinology* 141, 111–117. doi:10.1210/endo.141.1.7263
- Suh, Y.-H., Kim, S.-Y., Lee, H.-Y., Jang, B. C., Bae, J. H., Sohn, J.-N., et al. (2004). Overexpression of Short Heterodimer Partner Recovers Impaired Glucose-Stimulated Insulin Secretion of Pancreatic  $\beta$ -cells Overexpressing UCP2. *J. Endocrinol.* 183, 133–144. doi:10.1677/joe.1.05675
- Susini, S., Roche, E., Prentki, M., and Schlegel, W. (1998). Glucose and Glucocorticoid Peptides Synergize to Induce C- Fos , C- Jun , junB , Zif -268, and Nur- 77 Gene Expression in Pancreatic  $\beta$ (INS-1) Cells. *FASEB J.* 12, 1173–1182. doi:10.1096/fasebj.12.12.1173
- Tabbaz, M., and Yoshihara, E. (2021). Immune Protection of Stem Cell-Derived Islet Cell Therapy for Treating Diabetes. *Front. Endocrinol.* 12, 716625. doi:10.3389/fendo.2021.716625
- Takahashi, K., Tanabe, K., Ohnuki, M., Narita, M., Ichisaka, T., Tomoda, K., et al. (2007). Induction of Pluripotent Stem Cells from Adult Human Fibroblasts by Defined Factors. *Cell* 131, 861–872. doi:10.1016/j.cell.2007.11.019
- Tan, X., Lee, L. K., Huynh, S., Pawaskar, M., and Rajpathak, S. (2020). Sociodemographic Disparities in the Management of Type 2 Diabetes in the United States. *Curr. Med. Res. Opin.* 36, 967–976. doi:10.1080/03007995.2020.1756764
- Taneera, J., Mohammed, A. K., Dhaiban, S., Hamad, M., Prasad, R. B., Sulaiman, N., et al. (2019). ROR $\beta$  and ROR $\gamma$  Associate with Human Islet Dysfunction and Inhibit Insulin Secretion in INS-1 Cells. *Islets* 11, 10–20. doi:10.1080/19382014.2019.1566684
- Tang, T., Abbott, M. J., Ahmadian, M., Lopes, A. B., Wang, Y., and Sul, H. S. (2013). Desnutrin/ATGL Activates PPAR $\delta$  to Promote Mitochondrial Function for Insulin Secretion in Islet  $\beta$  Cells. *Cell Metab.* 18, 883–895. doi:10.1016/j.cmet.2013.10.012
- Tessem, J. S., Moss, L. G., Chao, L. C., Arlotto, M., Lu, D., Jensen, M. V., et al. (2014). Nkx6.1 Regulates Islet  $\beta$ -cell Proliferation via Nr4a1 and Nr4a3 Nuclear Receptors. *Proc. Natl. Acad. Sci. U.S.A.* 111, 5242–5247. doi:10.1073/pnas.1320953111
- Thomson, J. A., Itskovitz-Eldor, J., Shapiro, S. S., Waknitz, M. A., Swiergiel, J. J., Marshall, V. S., et al. (1998). Embryonic Stem Cell Lines Derived from Human Blastocysts. *Science* 282, 1145–1147. doi:10.1126/science.282.5391.1145
- Tiano, J. P., Delghingaro-Augusto, V., Le May, C., Liu, S., Kaw, M. K., Khuder, S. S., et al. (2011). Estrogen Receptor Activation Reduces Lipid Synthesis in Pancreatic Islets and Prevents  $\beta$  Cell Failure in Rodent Models of Type 2 Diabetes. *J. Clin. Invest.* 121, 3331–3342. doi:10.1172/jci44564
- van der Meulen, T., Donaldson, C. J., Cáceres, E., Hunter, A. E., Cowing-Zitron, C., Pound, L. D., et al. (2015). Urocortin3 Mediates Somatostatin-dependent Negative Feedback Control of Insulin Secretion. *Nat. Med.* 21, 769–776. doi:10.1038/nm.3872
- Varum, S., Rodrigues, A. S., Moura, M. B., Momcilovic, O., Easley, C. A., Ramalho-Santos, J., et al. (2011). Energy Metabolism in Human Pluripotent Stem Cells and Their Differentiated Counterparts. *PLoS One* 6, e20914. doi:10.1371/journal.pone.0020914
- Velazco-Cruz, L., Goedegebuure, M. M., Maxwell, K. G., Augsornworawat, P., Hogrebe, N. J., and Millman, J. R. (2020a). SIX2 Regulates Human  $\beta$  Cell Differentiation from Stem Cells and Functional Maturation *In Vitro*. *Cell Rep.* 31, 107687. doi:10.1016/j.celrep.2020.107687
- Velazco-Cruz, L., Goedegebuure, M. M., and Millman, J. R. (2020b). Advances toward Engineering Functionally Mature Human Pluripotent Stem Cell-Derived  $\beta$  Cells. *Front. Bioeng. Biotechnol.* 8, 786. doi:10.3389/fbioe.2020.00786
- Veres, A., Faust, A. L., Bushnell, H. L., Engquist, E. N., Kenty, J. H.-R., Harb, G., et al. (2019). Charting Cellular Identity during Human *In Vitro*  $\beta$ -cell Differentiation. *Nature* 569, 368–373. doi:10.1038/s41586-019-1168-5
- Vergari, E., Knudsen, J. G., Ramracheya, R., Salehi, A., Zhang, Q., Adam, J., et al. (2019). Insulin Inhibits Glucagon Release by SGLT2-Induced Stimulation of Somatostatin Secretion. *Nat. Commun.* 10, 139. doi:10.1038/s41467-018-08193-8
- Vieira, E., Marroquí, L., Batista, T. M., Caballero-Garrido, E., Carneiro, E. M., Boscherio, A. C., et al. (2012). The Clock Gene Rev-Erba Regulates Pancreatic  $\beta$ -Cell Function: Modulation by Leptin and High-Fat Diet. *Endocrinology* 153, 592–601. doi:10.1210/en.2011-1595
- Wei, Z., Yoshihara, E., He, N., Hah, N., Fan, W., Pinto, A. F. M., et al. (2018). Vitamin D Switches BAF Complexes to Protect  $\beta$  Cells. *Cell* 173, 1135–1149. doi:10.1016/j.cell.2018.04.013
- Wong, W. P. S., Tiano, J. P., Liu, S., Hewitt, S. C., Le May, C., Dalle, S., et al. (2010). Extracellular Estrogen Receptor- $\alpha$  Stimulates NeuroD1 Binding to the Insulin Promoter and Favors Insulin Synthesis. *Proc. Natl. Acad. Sci. U.S.A.* 107, 13057–13062. doi:10.1073/pnas.0914501107
- Wortham, M., and Sander, M. (2021). Transcriptional Mechanisms of Pancreatic Beta-Cell Maturation and Functional Adaptation. *Trends Endocrinol. Metab.*
- Xie, R., Everett, L. J., Lim, H.-W., Patel, N. A., Schug, J., Kroon, E., et al. (2013). Dynamic Chromatin Remodeling Mediated by Polycomb Proteins Orchestrates

- Pancreatic Differentiation of Human Embryonic Stem Cells. *Cell Stem Cell* 12, 224–237. doi:10.1016/j.stem.2012.11.023
- Yamagata, K., Furuta, H., Oda, N., Kaisaki, P. J., Menzel, S., Cox, N. J., et al. (1996). Mutations in the Hepatocyte Nuclear Factor-4 $\alpha$  Gene in Maturity-Onset Diabetes of the Young (MODY1). *Nature* 384, 458–460. doi:10.1038/384458a0
- Yoshihara, E. (2020). TXNIP/TBP-2: A Master Regulator for Glucose Homeostasis. *Antioxidants (Basel)* 9. doi:10.3390/antiox9080765
- Yoshihara, E., Chen, Z., Matsuo, Y., Masutani, H., and Yodoi, J. (2010a). Thiol Redox Transitions by Thioredoxin and Thioredoxin-Binding Protein-2 in Cell Signaling. *Methods Enzymol.* 474, 67–82. doi:10.1016/s0076-6879(10)74005-2
- Yoshihara, E., Fujimoto, S., Inagaki, N., Okawa, K., Masaki, S., Yodoi, J., et al. (2010b). Disruption of TBP-2 Ameliorates Insulin Sensitivity and Secretion without Affecting Obesity. *Nat. Commun.* 1, 127. doi:10.1038/ncomms1127
- Yoshihara, E., Masaki, S., Matsuo, Y., Chen, Z., Tian, H., and Yodoi, J. (2014). Thioredoxin/Txnip: Redoxosome, as a Redox Switch for the Pathogenesis of Diseases. *Front. Immunol.* 4, 514. doi:10.3389/fimmu.2013.00514
- Yoshihara, E., O'Connor, C., Gasser, E., Wei, Z., Oh, T. G., Tseng, T. W., et al. (2020). Immune-evasive Human Islet-like Organoids Ameliorate Diabetes. *Nature* 586, 606–611. doi:10.1038/s41586-020-2631-z
- Yoshihara, E., Wei, Z., Lin, C. S., Fang, S., Ahmadian, M., Kida, Y., et al. (2016). ERR $\gamma$  Is Required for the Metabolic Maturation of Therapeutically Functional Glucose-Responsive  $\beta$  Cells. *Cel Metab.* 23, 622–634. doi:10.1016/j.cmet.2016.03.005
- Yu, C., Cui, S., Zong, C., Gao, W., Xu, T., Gao, P., et al. (2015). The Orphan Nuclear Receptor NR4A1 Protects Pancreatic  $\beta$ -Cells from Endoplasmic Reticulum (ER) Stress-Mediated Apoptosis. *J. Biol. Chem.* 290, 20687–20699. doi:10.1074/jbc.m115.654863
- Zhang, T., Li, X.-H., Zhang, D.-B., Liu, X.-Y., Zhao, F., Lin, X.-W., et al. (2017). Repression of COUP-TFI Improves Bone Marrow-Derived Mesenchymal Stem Cell Differentiation into Insulin-Producing Cells. *Mol. Ther. - Nucleic Acids* 8, 220–231. doi:10.1016/j.omtn.2017.06.016
- Zhou, Y.-T., Shimabukuro, M., Wang, M.-Y., Lee, Y., Higa, M., Milburn, J. L., et al. (1998). Role of Peroxisome Proliferator-Activated Receptor  $\alpha$  in Disease of Pancreatic  $\beta$  Cells. *Proc. Natl. Acad. Sci. U.S.A.* 95, 8898–8903. doi:10.1073/pnas.95.15.8898
- Zitzer, H., Wente, W., Brenner, M. B., Sewing, S., Buschard, K., Gromada, J., et al. (2006). Sterol Regulatory Element-Binding Protein 1 Mediates Liver X Receptor- $\beta$ -Induced Increases in Insulin Secretion and Insulin Messenger Ribonucleic Acid Levels. *Endocrinology* 147, 3898–3905. doi:10.1210/en.2005-1483

**Conflict of Interest:** EY is an inventor on licensed patents and patent applications related to the HILO technology described in this manuscript.

**Publisher's Note:** All claims expressed in this article are solely those of the authors and do not necessarily represent those of their affiliated organizations, or those of the publisher, the editors, and the reviewers. Any product that may be evaluated in this article, or claim that may be made by its manufacturer, is not guaranteed, or endorsed by the publisher.

Copyright © 2022 Yoshihara. This is an open-access article distributed under the terms of the Creative Commons Attribution License (CC BY). The use, distribution or reproduction in other forums is permitted, provided the original author(s) and the copyright owner(s) are credited and that the original publication in this journal is cited, in accordance with accepted academic practice. No use, distribution or reproduction is permitted which does not comply with these terms.



# Archetypal Architecture Construction, Patterning, and Scaling Invariance in a 3D Embryoid Body Differentiation Model

Olga Gordeeva<sup>1\*</sup>, Andrey Gordeev<sup>2</sup> and Pavel Erokhov<sup>1</sup>

<sup>1</sup>Koltzov Institute of Developmental Biology, Russian Academy of Sciences, Moscow, Russia, <sup>2</sup>National Institutes of Health's National Library of Medicine, Bethesda, MD, United States

## OPEN ACCESS

### Edited by:

Ying Gu,  
Beijing Genomics Institute (BGI), China

### Reviewed by:

Giseok Jeong,  
University of Ulsan, South Korea  
Jianhui Yue,  
Beijing Genomics Institute (BGI), China

### \*Correspondence:

Olga Gordeeva  
olgagordeeva@yandex.ru

### Specialty section:

This article was submitted to  
Stem Cell Research,  
a section of the journal  
Frontiers in Cell and Developmental  
Biology

**Received:** 10 January 2022

**Accepted:** 11 April 2022

**Published:** 27 April 2022

### Citation:

Gordeeva O, Gordeev A and Erokhov P  
(2022) Archetypal Architecture  
Construction, Patterning, and Scaling  
Invariance in a 3D Embryoid Body  
Differentiation Model.  
Front. Cell Dev. Biol. 10:852071.  
doi: 10.3389/fcell.2022.852071

Self-organized patterning and architecture construction studying is a priority goal for fundamental developmental and stem cell biology. To study the spatiotemporal patterning of pluripotent stem cells of different origins, we developed a three-dimensional embryoid body (EB) differentiation model quantifying volumetric parameters and investigated how the EB architecture formation, patterning, and scaling depend on the proliferation, cavitation, and differentiation dynamics, external environmental factors, and cell numbers. We identified three similar spatiotemporal patterns in the EB architectures, regardless of cell origin, which constitute the EB archetype and mimic the pre-gastrulation embryonic patterns. We found that the EB patterning depends strongly on cellular positional information, culture media factor/morphogen content, and free diffusion from the external environment and between EB cell layers. However, the EB archetype formation is independent of the EB size and initial cell numbers forming EBs; therefore, it is capable of scaling invariance and patterning regulation. Our findings indicate that the underlying principles of reaction-diffusion and positional information concepts can serve as the basis for EB architecture construction, patterning, and scaling. Thus, the 3D EB differentiation model represents a highly reproducible and reliable platform for experimental and theoretical research on developmental and stem cell biology issues.

**Keywords:** embryoid bodies (EBs), pluripotent stem cell, differentiation, morphogenesis, patterning, self-organisation

## INTRODUCTION

Pluripotent stem cells develop into all tissues and organs after their reintegration with an early embryo or *in vitro* recapitulate the developmental events after their self-assembly and self-organization in 3D cellular structures (Doetschman et al., 1985; Robertson et al., 1986; Morris et al., 2012). The 3D models based on pluripotent stem cells—embryoid bodies (EBs), blastoids, gastruloids, bi- (pluripotent and trophoblast) and tri-compartmental (pluripotent, trophoblast and extraembryonic endoderm) embryo-like aggregates (ET- and ETX-embryos, respectively)—facilitate studying the spatiotemporal patterning and dynamics of cellular processes under various experimental conditions (Bratt-Leal et al., 2009; Giobbe et al., 2012; Van Den Brink et al., 2014; Harrison et al., 2017; Flamier, 2018; Rivron et al., 2018; Rossi et al., 2018; Shahbazi et al., 2019; Sozen et al., 2019; Kim et al., 2020; Kagawa et al., 2021; Yu et al., 2021). These 3D cellular models can



reproduce the complex architecture of mammalian embryonic structures and are considered promising *in vitro* models for fundamental studies, drug discovery, and toxicological screening. The combination of 3D embryonic cell models and new experimental technologies allows more profound exploration of fundamental questions in mammalian and human developmental biology, such as self-organization, symmetry breaking, patterning, and scaling, which are also relevant to teratology and developmental toxicology (Bauwens et al., 2008; Van Den Brink et al., 2014; Deglincerti et al., 2016; Warkus et al., 2016; Dutta et al., 2017; Kang et al., 2017; Tewary et al., 2017; Sozen et al., 2021; van den Brink and van Oudenaarden, 2021; Wahlin et al., 2021).

Previous studies facilitated the development of efficient protocols for *in vitro* pluripotent stem cell differentiation to reconstruct the developmental trajectories for multiple cell types (Oh and Jang, 2019; El Azhar and Sonnen, 2021; van den Brink and van Oudenaarden, 2021). Numerous 2D and 3D engineered embryonic cell models allowed the investigation of the developmental mechanisms at different levels previously studied only in animal embryos (Camacho-Aguilar and Warmflash, 2020). However, regardless of the significant progress in creating and studying embryo-like models, there are remain insufficiently explored possible 3D morphological archetypes generated by combining different embryonic cells and the cellular mechanisms coordinating the architecture construction (Renner et al., 2017; Sozen et al., 2018; Zheng et al., 2019; van den Brink et al., 2020; Zhu and Zernicka-Goetz, 2020; El Azhar and Sonnen, 2021; Guo et al., 2021; Jerber et al., 2021; Molè et al., 2021). Therefore, further studies of the 3D embryonic cell models with different “starting” cell populations, including cancer cells, are needed for disclosing the mechanisms of morphogenesis and architecture construction in different environments. Moreover, addressing these issues is critical for standardizing protocols that reduce variability and improve reproducibility in the embryoid and organoid models for basic and pharmacological research.

In the presented study, the standardized and well-scalable 3D EB differentiation model was used to analyze the architecture creation *via* self-organization, morphogenesis, patterning, and differentiation of the embryonic stem (ESC), embryonic germ (EGC), and teratocarcinoma (ECC) cells, which differ in genetic and epigenetic states and spontaneous differentiation potentials *in vitro* and *in vivo* (Rizzino and Crowley, 1980; Andrews, 1988; Wobus and Boheler, 2005; Sharova et al., 2007; Shim et al., 2008; Weinberger et al., 2016; Kelly and Gatie, 2017; Liu et al., 2020). We used these cell lines to test the hypothesis about the equifinality in the EB architecture construction, i.e., whether these cells of different origins are capable of forming similar morphological structures mimicking early developmental events. We sought to identify the basic principles and specific features in creating the architecture of EBs, formed by cell lines of various origins, analyzing proliferation, differentiation, and cavitation dynamics in different environments. Pursuing our goals, we identified three similar spatiotemporal patterns in the EB architecture regardless of cell origin, which constitute the EB archetype and mimic the embryonic patterns at the

pre-gastrulation stages. We found that the EB patterning strongly depends on external environmental factors and the position of cell layers, but not on the initial number of cells forming EBs, and these general properties contribute to scaling invariance and patterning regulation. We assume that the basic principles of both reaction-diffusion (RD) (Turing, 1952) and positional information (PI) (Wolpert, 1981) concepts can serve as the basis for the EB architecture patterning. Therefore, the 3D EB differentiation model can be used as a highly effective and reliable platform for experimental, theoretical, and computational analyses of cell and developmental biology issues.

## MATERIALS AND METHODS

### Cell Lines and Culture

Mouse R1 embryonic stem cells (ESCs) and EGC-10 embryonic germ cells (EGCs) were kindly provided by Dr. A. Nagy (Mount Sinai Hospital, Toronto, Canada) and Dr. A. McLaren (WTCC Institute of Cancer and Developmental Biology, Cambridge, UK). The F9 embryonic teratocarcinoma cell line (ECCs) was obtained from the Russian Cell Culture Collection (<http://www.rccc.cytspb.rssi.ru/>). The ESCs, EGCs, and ECCs were routinely cultivated on gelatin-coated dishes (3%, Sigma-Aldrich) in fetal bovine serum-containing media (FBS; (SH30071.04, HyClone) at 5% CO<sub>2</sub> and 37°C, as described previously (Gordeeva et al., 2019). For undifferentiated ESCs and EGCs, media was supplemented with leukemia inhibitory factor (LIF, L-5158; 1000 U/ml, Sigma-Aldrich). All cell lines were routinely tested using MycoFluor™ *Mycoplasma* Detection Kit (M7006; Invitrogen). Cells were routinely passaged as single cells every 3 days using 0.05% Trypsin-EDTA (25-300-120; Gibco). To analyze the numbers of viable cells, the ESCs were stained with 0.4% trypan blue dye (15250-061; Gibco/Thermo Fisher Scientific) and non-stained cell numbers were counted using an Improved Neubauer Hemocytometer (Hausser Scientific, Horsham, PA, United States).

### Mouse Embryo Experiments

All animal experiments were approved by the Ethics Committee of Institute of Developmental Biology of Russian Academy of Sciences and performed in accordance with the Russian Federation legislation (Order of the Ministry of Health and Social Development of the Russian Federation No 708n, 28 August 2010) based on the European Convention for the Protection of Vertebrate Animals Used for Experimental and Other Scientific Purposes. C57Bl/6 mice at the age of 10–12 weeks were obtained from the Animal Breeding Facility-Branch “Pushchino” of the Institute of Bioorganic Chemistry, Russian Academy of Sciences. To obtain the embryos, females were mated with males overnight and vaginal plugs were tested on the following morning (embryonic stage E0.5). Fertilized females were sacrificed by cervical dislocation and embryos at the morula (E2.5) and blastocyst (E3.5 and E4.5) and egg cylinder (E6.5) stages were recovered from the oviduct and uterus and placed in the M2 medium with HEPES (M7167; Sigma-Aldrich). The epiblasts with adjacent extraembryonic endoderm of

E6.0–6.5 embryos were isolated after dissection of the uterus tissues, trophectoderm and ectoplacental cone.

## EB Generation and Differentiation

The EBs were generated using the “hanging drop” method by placing the cell suspension drops (usually 500 cells per drop, and 50, 100, 500, and 1,000 cells for differently sized EBs) on the dish lids (10-cm dish, Greiner Bio-One International GmbH) for 48 h. After formation, the ESBs, EGBs, and ECBs, formed by ESCs, EGCs, and ECCs, respectively, were collected and cultured in low adhesion plates (Greiner Bio-One International GmbH and Nunclon Sphera/ThermoFisher Scientific) in LIF-free media in the following 10 days. To maintain the EB spherical shape, the low adhesion plates with EBs were continuously shaken during the cultivation.

To study the growth and differentiation dynamics, the EBs were cultured in FBS- and KSR-media for 10 days. FBS-media consisted of the DMEM (SH30285.01) supplemented with 2 mM L-glutamine (SH30034.01), 1% non-essential amino acids (SH3023801), 15% Characterized Fetal Bovine Serum (SH30071.04) (all from HyClone), and 0.1 mM  $\beta$ -mercaptoethanol (M3148; Sigma-Aldrich). KSR-media consisted of the KnockOut DMEM (10829018), 2 mM L-glutamine (A2916801), 1% non-essential amino acids (11140050), 15% KnockOut Serum Replacement (KSR; A3181501) (all from Gibco/ThermoFisher Scientific), and 0.1 mM  $\beta$ -mercaptoethanol (Sigma-Aldrich). LIF (1000 U/ml, Sigma-Aldrich) and all-trans-retinoic acid ( $10^{-6}$  M RA; R2625, Sigma-Aldrich) were added to study their influence on the EB growth and differentiation for 5 days.

To study the patterns' regulation, merging EBs at different stages were placed in hanging drops on the 60 mm dish lid (Nuclon) or in culture medium drops covered with mineral oil (Sigma-Aldrich) in 35 mm dishes (Nuclon) for 1–2 days (5 EBs per stages for each cell line; three experiments; N = 60 for each cell line). EBs separated by a scalpel under a stereomicroscope (5 EBs per stages for each cell line; three experiments; N = 45 for each cell line) were cultured in 4-well plates (Nuclon) for 1–2 days and then analyzed. To study pattern desorganization-reconstruction, individual EBs at day10 (5 EBs/per stage for each cell line; three experiments; N = 60 for each cell line) were dissociated into single cells using 0.05% Trypsin-EDTA (25-300-120; Gibco) at 37°C for 5 min, followed by gentle mechanical dissociation with a pipette. For *de novo* EB formation, the cell suspension from individual EBs was placed in hanging drops (100 cells/per drop) on the lid of 60 mm dish (Nuclon) for 72 h.

## EB Growth and Patterning Analysis

To evaluate EB growth dynamics and patterning, the EBs (24 EBs/per stage; three experiments; N = 288 for each cell line) cultivated in 12 or 96-well plates with a low-attachment surface (Greiner Bio-One International GmbH and Nunclon Sphera; Nuclon) and imaged at the studied stages. The EB images were captured using Olympus CK40 inverted microscope equipped with a Camedia C-4040 camera (Olympus). EB diameters were measured in 2–8 directions for average calculation using ImageJ/Fiji software (<https://imagej.nih.gov/ij/>) with prior set up absolute scale

calibration (see **Supplementary Methods**). EB volumes, volumetric pattern sizes and their ratios were calculated using Excel.

## Histological and Electron Microscopy Analyses

To prepare semi-thin and ultrathin sections, EBs were fixed by 2.5% glutaraldehyde (Sigma-Aldrich) in 100 mM sodium cacodylate buffer (Serva, Germany), pH 7.0 for 24 h at 4°C and then post-fixed with 1% osmium tetroxide (Serva, Germany) in 100 mM cacodylate buffer, pH 7.0 (all from Sigma-Aldrich) within 1 h at 4°C. After dehydration procedures in serial ethanol and acetone solutions and impregnation in resin, the specimens were embedded into the Spurr's resin (Spurr kit, Sigma) or Araldite (Fluka). The EB sections were prepared using Ultratome 3 (LKB, Germany). Semi-thin sections were stained with toluidine blue in 1% sodium tetraborate (Sigma-Aldrich). Ultra-thin sections were placed on the grids and stained with aqueous uranyl acetate (Merck, Germany) and lead citrate (Serva, Germany). The sections were examined under a JEM 100CXII electron microscope (Jeol, Japan).

## EdU-Labeling and Caspase Activity Assays

For the analysis of cells in the S-phase of the cell cycle, the EBs were incubated with 10  $\mu$ M 5-ethynyl-2-deoxyuridine (EdU) for 1 h at 37°C and 5% CO<sub>2</sub> and then with a reaction solution from the Click-iT EdU Imaging Kit with Azide-Alexa 488 (C10083; Molecular Probes) according to the protocol recommended by the manufacturer. After the completion of the Click-iT EdU reaction, the EBs were fixed with 3% paraformaldehyde (P6148; Sigma-Aldrich) in PBS, washed with PBS and stained with Hoechst 33342 (1  $\mu$ g/ml; H3570; Molecular Probes). EBs were cleared in glycerol-PBS, placed on 18-well  $\mu$ -Slides (81826; Ibidi, Martinsried, Germany) in a mounting medium (50001; Ibidi) and imaged under a Leica TSC SPE confocal microscope.

The Vybrant FAM Poly Caspases Assay Kit (V35117, Molecular Probes) for the detection of caspase-1, -3-9 activity was used according to the manufacturer's recommendations. The EBs were incubated in culture media containing FLICA reagent (FAM-VAD-FMK poly caspases reagent) for 1 h at 37°C and 5% CO<sub>2</sub> and Hoechst 33342 (1  $\mu$ g/ml) and propidium iodide (PI; 1  $\mu$ g/ml) were added to the culture media for 15 min. After washing with PBS, the EBs were mounted on 15-well  $\mu$ -Slides (81506; Ibidi) and immediately examined under a confocal microscope.

## Alkaline Phosphatase Activity and Immunofluorescence Analyses

For alkaline phosphatase activity (ALP) assay, EBs were fixed by 2% paraformaldehyde in PBS, pH 7.0 within 15 min, washed with PBS and incubated in a solution containing 10 ml 0.02 M Tris-HCl buffer, pH 8.7 (T1503), 1 mg Naphthol-AS-B1-phosphate (N2125), and 5 mg Fast Red TR dye (305464) (all reagents from Sigma-Aldrich) at 37°C for 1 h.

For immunofluorescence analysis, mouse embryos and EBs were fixed with 3% paraformaldehyde in PBS for 1 h, washed with PBS, and then permeabilized and blocked with 0.5% Triton X-100 (T9284; Sigma-Aldrich) and 3% Bovine Serum Albumin, Fraction V (85040C; Sigma-Aldrich) in PBS within 1–3 h. Primary antibodies were incubated in PBS with 0.25% Tween 20 (P1379; Sigma-Aldrich) at 4°C overnight. The following dilutions of primary antibodies were used: Oct4 (1:150; rabbit IgG, sc-9081, Santa Cruz Biotechnology), Gata4 (1:150; goat IgG, sc-1237, Santa Cruz Biotechnology), and ZO-1 protein (1:100, rabbit IgG, 61–7,300, Invitrogen). After extensive washing in PBS, secondary Alexa Fluor 488 and 594 chicken anti-rabbit antibodies (1:800; A-21441 and A-21442, Molecular Probes), Alexa Fluor 488 donkey anti-goat antibodies (1:800; A-11055, Molecular Probes) and Alexa Fluor 594 chicken anti-goat antibodies (1:800; A-11058, Molecular Probes) were applied for 3–4 h. After staining and extensive washing, the embryos and EBs were cleared in increasing concentrations of glycerol in PBS (30, 50, 75, and 90%), mounted on 18-well  $\mu$ -Slides (Ibidi) in a glycerol-based mounting medium (Ibidi), and imaged.

## Confocal Microscopy Image Acquisitions, Processing, and Quantitative Analysis

The embryos and EBs were placed on the 18- and 15-well  $\mu$ -Slides (Ibidi) and studied under Leica TSC SPE and SP5 confocal microscopes using the 405, 488, and 596 lasers and HCX PL APO CS 20.0  $\times$  0.70 IMM UV and 40.0  $\times$  1.25 OIL UV objectives. Z-stacks of optical sections were acquired with 0.3–1  $\mu$ m z-steps at 100–120  $\mu$ m depth of specimen scanning. To generate the 3D volume reconstruction for EBs and embryos, the confocal z-stacks were processed using 3D Viewer Plugins of ImageJ/Fiji software.

To analyze the proliferative cell domain, the numbers of EdU-labeled and the total Hoechst-stained nuclei in the EBs were counted using the 2D Automated Cell Counter tool in ImageJ software (<https://imagej.nih.gov/ij/plugins/cell-counter.html>) for confocal stacks, as previously described (Gordeeva and Gordeev, 2021). The cell counts were based on the object-level identification of Hoechst- and EdU-stained nuclei in each plane of confocal z-stack, which were counted in two separate channels. For the segmentation of merged nuclei, each image was run through the watershed algorithm and manually corrected. The square range for counted nuclei was set at 15–350  $\mu$ m<sup>2</sup> based on prior nuclei measurements. At least 20–25 images were processed for each confocal z-stack of EBs (7 EB per stage for each cell line, three experiments; total N = 84 per cell line). The percentage of EdU-labeled nuclei in relation to the total number of Hoechst-stained nuclei for each image and the average percentages for each analyzed confocal z-stack were calculated and used for the analysis of volume ratios of proliferation domains (see **Supplementary Methods**).

To determine the regional immunofluorescence intensity of Oct4 and Gata4 expression along the EB diameter, ImageJ/Fiji software was used to identify the associated fluorescence intensity within the identified region of interest (ROI manager). The line plots depicting diametral trends of proteins of interest in

individual EB were created with the ROI/Multi plot tool. A plot of intensity values across the EB diameters in middle sections of the z-stack (for several planes) was generated in each channel. Additionally, plots of z-axis profiles of EBs were generated with the Image/Stack/Plot z-axis profile tool for analyzing intensity values through the z-axis within an ROI (100  $\times$  100  $\mu$ m) on the stacks for EBs at different stages. All measurements were carried out after checking the background intensity in each channel.

## Live-Cell Analysis of Small Molecule and Protein Diffusion Into Embryoid Bodies

The fluorescent tracers were used for the live-cell analysis of free diffusion of small molecules and proteins from culture media into the EBs and early embryos. Rodamine B isothiocyanate (RITC, MW 536; 283924, Sigma-Aldrich) was used for small molecule diffusion analysis. The fluorescent protein tracers (20 and 43 kDa) were prepared by FITC conjugating using the protocol for protein labeling (see **Supplementary Methods**). For diffusion analysis, the EBs and embryos were placed on the 35 mm  $\mu$ -dishes or on 18 well-flat  $\mu$ -slides with coverglass bottoms (Ibidi) in phenol red-free DMEM media with HEPES and L-glutamine (21063029, Gibco) supplemented with RITC or fluorescent protein tracers (final concentration 2  $\mu$ g/ml) and exposed for 5, 15, 30, and 60 min. The EBs and embryos were examined under a Leica TSC SP5 confocal microscope with a temperature control system (at 37°C) using the 488 and 596 lasers and APO CS 20.0  $\times$  0.70 IMM UV and 40.0  $\times$  1.25 OIL UV objectives. A z-series of optical sections were done with 1–3  $\mu$ m z-steps to 100–120  $\mu$ m depth of specimen scanning. The RITC solution (10–15  $\mu$ l) was injected into the inner cavity of EB10 under a stereomicroscope (Zeiss) using a glass capillary with an inner diameter 50–70  $\mu$ m connected with CellTram Vario Microinjector (Eppendorf) and analyzed within 15–60 min after injection under Leica TSC SP5 microscope.

## Gene Expression Analysis

For the gene expression analysis, we collected the samples of EBs grown in FBS and KSR culture media supplemented with different combinations of LIF and RA and differently sized EBs (early and small EBs: N = 200–300 per sample for each cell number, stage, and cell line; and late and large EBs: N = 100 per sample for each cell number, stage, and cell line). Total RNAs isolated from EBs using Trizol (15596-018; Invitrogen) were treated with TURBO DNase (AM 1907; Ambion/Invitrogen) according to the manufacturer's recommendations and the RNA yield and quality were analyzed using NanoDrop 2000 (Thermo Scientific). cDNAs were synthesized using an oligo-dT18 primer (SO131; Fermentas) and reverse transcriptase SuperScript III (18080044; Invitrogen) according to the manufacturer's protocols. Gene expression analysis was carried out with the qRT-PCR master mix with SYBR Green stain and ROX reference dye (PK156L; Evrogen, Russia) using the Applied Biosystems 7500 Real-Time PCR System (Life Technologies). The expression levels of target genes were normalized to the expression of the reference gene hypoxanthine-guanine

phosphoribosyltransferase (*Hprt*). All experiments were run in triplicate. The relative levels of target gene expression were calculated using the comparative  $2^{-\Delta\Delta C_t}$  method (ABI Relative Quantification Study software, Applied Biosystems). Specific primers were designed using the Beacon Designer 8.0 software (Premier Biosoft) (**Supplementary Table S1**).

## Statistics and Data Analysis

Statistical analyses of EB growth were performed using one-way ANOVA and Student-Newman-Keuls test for post hoc analysis using the R v.3.2.3 software (<http://www.r-project.org>). Data presented as mean  $\pm$  s.d. for three independent experiments. Analyses of EB10-to-EB1 volumetric ratios were performed using two-tailed Student's unpaired *t*-test for normalized data collected from three experiments. The gene expression data were subjected to statistical analysis using the R v.3.2.3 software. The averaged  $\Delta C_t$  values for the target gene obtained from three independent experiments ( $n = 3$ ) were used for statistical analysis using one-way ANOVA followed by a Tukey post-hoc test. The heatmaps were constructed using a hierarchical clustering algorithm with Euclidean distances measurement based on the averaged  $\Delta C_t$  values of studied genes after data scaling using the R v.3.2.3 software.

## RESULTS

### Architecture Construction and Patterning of the EBs Formed by ESCs, EGCs, and ECCs

To standardize the 3D EB differentiation model, we used mouse ESCs, EGCs, and ECCs with the same genetic background based on the male genotype of the 129/Sv/Ev mouse strain (Bernstine et al., 1973; Nagy et al., 1993; Durcova-Hills et al., 2003). This allowed us to exclude the genotypic influence since mouse ESCs and EGCs displayed more variation in global gene expression between lines with different genotypes than between lines of various origins, while ECCs lines showed significant differences between sub-lines (Rizzino and Crowley, 1980; Moore et al., 1986; Sharova et al., 2007; Shim et al., 2008). F9 ECC line has limited spontaneous differentiation potential in conventional *in vitro* culture and after transplantation into nude mice but is capable of induced differentiation and EB formation (Gordeeva and Nikonova, 2013; Gordeeva and Khaydukov, 2017). The use of pluripotent stem and malignant teratocarcinoma cell lines allow us to focus on extracting the basic principles and specific features in the architecture construction of the EB of different cell origin (ESBs, EGBs, and ECBs).

Minimal EB size variability was achieved for all cell lines (CV EB diameters = 2.6–4.0% and 4.9–7.2% at day 1–3 and 5–10, respectively), indicating high reproducibility of model performance (**Supplementary Table S2**). To quantify the volumetric spherical parameters of whole EBs and their patterns at the studied stages, we first analyzed the shape descriptors, such as circularity, aspect ratio, roundness, skewness, and density, in three projections/views of the same EBs in different images. A high degree of circularity and roundness (approx. 0.9), indicating the spherical shape, was

determined for the EBs at all stages. Therefore, we calculated spherical volumes of total EBs and different EB domains (see **Supplementary Materials and Supplementary Table S2**).

We studied the architecture of ESBs, EGBs, and ECBs at four differentiation stages (EB1, EB3, EB5, and EB10) for 10 days when critical morphogenetic events occur (**Figures 1A–C,E**). The ESBs, EGBs, and ECBs developed similar stage-specific cellular patterns and architectures (**Figures 1B,C**). Early EBs (EB1 and EB3) represented uniform cell spheroids, while the EB5 and EB10 were mature cellular spheroids with spatially segregated outer cell rings of extraembryonic endoderm (ExEn) and inner epiblast-like (Epi-I) epithelialized cell layers with an internal cavity (**Figures 1B,C**). Histological analysis revealed the key elements of morphogenetic transformation in the EBs at the studied differentiation stages mimicking some early developmental events (Martin and Evans, 1975; Martin et al., 1977; Ducibella et al., 1982; Loebel et al., 2003; White et al., 2018): the compaction of spheroid surface similar to that of the late morulas (**Figure 1D1**); epithelialization of the outer and inner cell layers with the formation of a thick basement membrane resembling embryo Reichart's membrane (**Figure 1D2,D4**); the formation of central cavities like the pro-amniotic cavity of an embryo (**Figure 1D3**); and the overgrowth of multilayer ExEn that leads to an irregular, asymmetric architecture like during the gastrulation stage (**Figure 1D4**).

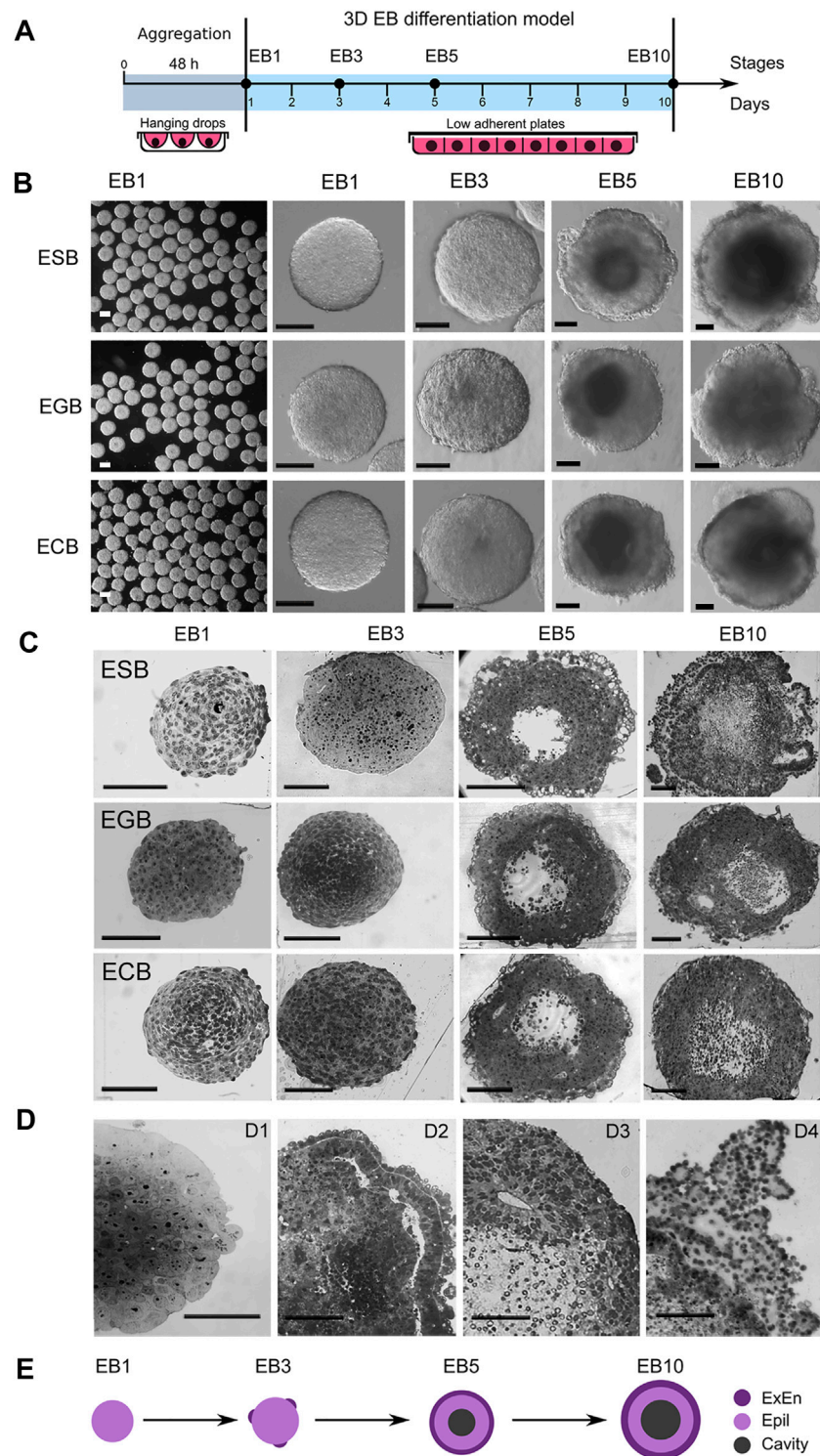
Summarizing morphological data, we concluded that despite different cell origins, the ESBs, EGBs and ECBs develop similar EB architectures at the corresponding stages due to a similar spatial patterning and timing of morphogenetic events. During differentiation and morphogenesis, EBs of different origins establish the EB archetype homologous to the embryoblast covered with ExEn at the E5.5–E6.5 stages. The EB archetype represents a radially symmetrical 3D cell structure consisting of three spatial patterns: two distinct epithelialized cell layers separated by a thick extracellular matrix membrane and an internal cavity (**Figure 1E**). At later stages, the deviation from the EB archetype may occur due to asymmetric overgrowths of the ExEn on the EB surface.

### Contribution of Proliferation and Cavitation to the Formation of Embryoid Body Architecture

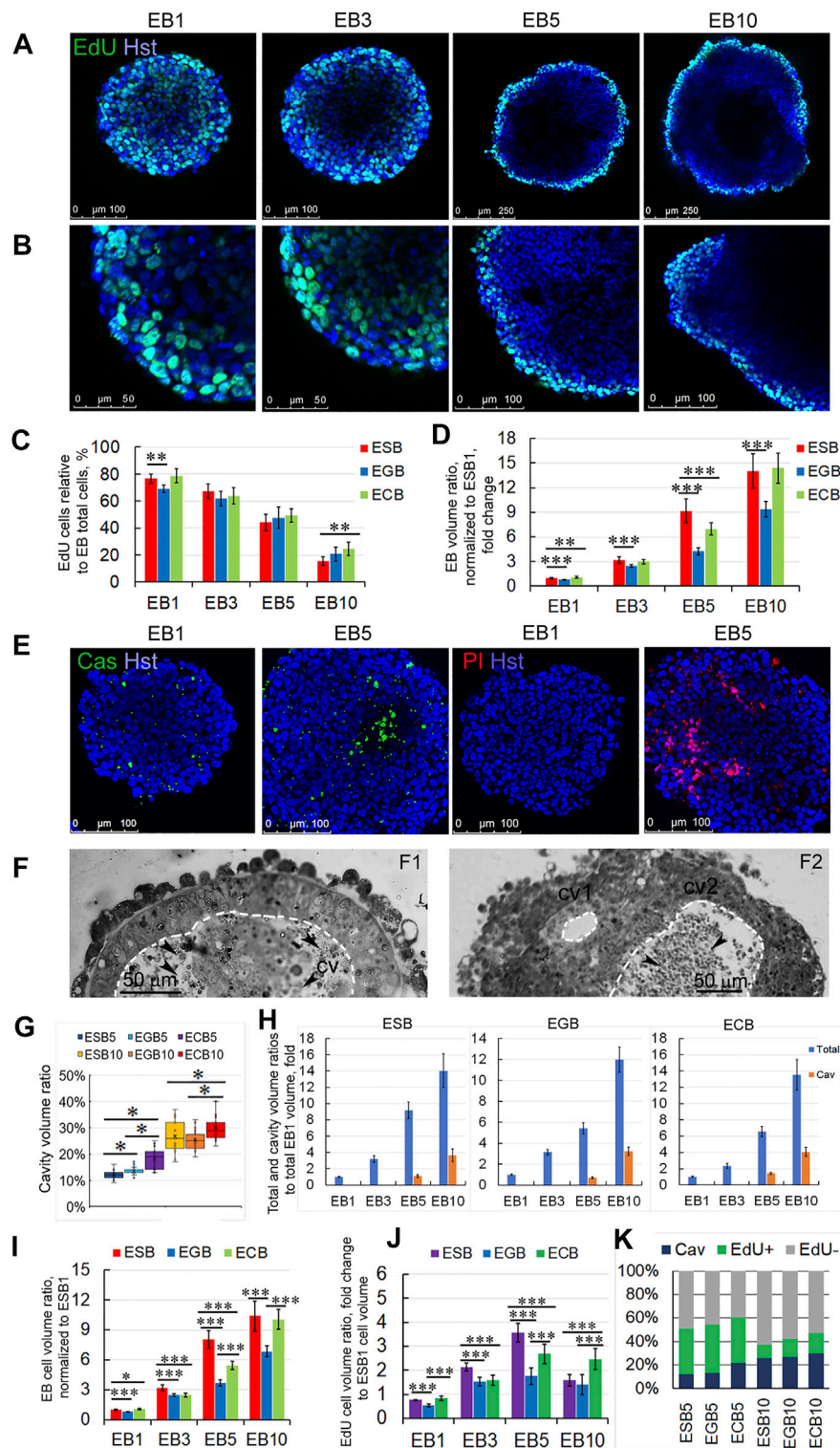
During development, patterning is regulated through balancing cell proliferation, differentiation, and death. To understand the contribution of these processes in the EB architecture construction, first, the spatiotemporal dynamics of the cell proliferation and cavitation domains were analyzed in the EB differentiation model.

Analysis of proliferative dynamics of the ESBs, EGBs, and ECBs revealed that the cells in the S-phase of the cell cycle (EdU-labeled) uniformly distributed throughout the EB1 and EB3 volumes and predominantly in the surface cell layers in EB5 and EB10 (**Figures 2A,B**). The number of EdU-labeled cells gradually decreased in the range from 70–80% cells in EB1 to 15–20% cells in EB10, respectively. The number of EdU-labeled cells differed significantly between ESBs and EGBs at the EB1





**FIGURE 1 |** 3D EB differentiation model: architectures and dynamics of ESBs, EGBs, and ECBs. **(A)** Schematic timeline for 3D EB differentiation model: EB formation in hanging drops and differentiation in suspension culture system for 10 days at EB1, EB3, EB5, and EB10 stages. **(B)** Representative images of differentiating ESB, EGBs, and ECBs with similar morphological patterns at the corresponding stages. **(C,D)** Histological sections of differentiating ESB, EGBs, and ECBs. **(C)** Similar spatiotemporal differentiation dynamics of ESB, EGBs, and ECBs and the formation of the EB archetype containing three morphologically distinct patterns. **[(D), D1–D4]** Morphogenetic events during EB differentiation: compaction **[(D),D1]** epithelization of extraembryonic endoderm (ExEn) and epiblast-like (Epi-I) cell patterns and delamination of inner cell layers **[(D),D2]** formation of internal cavities via the delamination and apoptosis **[(D),D3]**, and hypertrophy of ExEn immersed in the thick extracellular matrix **[(D),D4]**. **(E)** Schematic timeline for forming of the EB archetype with three distinct patterns: ExEn and Epi-I cellular patterns and inner cavity. **(B,C,D)** Scale bars: 100  $\mu$ m.



**FIGURE 2** | Spatiotemporal growth dynamics of ESB, EGBs, and ECBs. **(A,B)** Representative immunofluorescence confocal images of EdU-labeled cells in EBs at EB1, EB3, EB5, and EB10 stages. **(B)** Higher magnification images of A images. Nuclei were stained with Hoechst 33342 (Hst). The spatial distribution of EdU-labeled cells in EBs changes from uniform to surface during differentiation. **(C)** Proportions of the EdU-labeled cells to total cell numbers (Hst) in differentiating ESB, EGBs, and ECBs were counted using the ImageJ/Fiji cell counting tool ( $n = 7 \times 4$  stages for each cell line; total  $N = 84$ ). The data are presented as means  $\pm$  s.d., \*\* $p < 0.01$ , ANOVA. **(D)** EB volume growth dynamics significantly differed between ESB, EGBs, and ECBs (24 EBs/per stage; three experiments;  $N = 288$  for each cell line). Total EB volumes at all stages were normalized to ESB1 volume. **(E)** Representative immunofluorescence confocal images of caspase activity (Cas), PI-stained necrotic cells, and

(Continued)

**FIGURE 2 |** total nuclei staining (Hst) in EB1 and EB5. **(F)** Histological sections showing internal EB cavities with (cv2) or without (cv2) dead cells. Cavities marked by dashed lines. **(G)** The ratios of cavity-to-total volume in EB5 and EB10 differ between cell lines (24 EBs per stage; three experiments;  $N = 144$  for each cell line). Data presented as a boxplot with means and the 25th and 75th percentile range; whiskers indicate maximum and minimum values.  $**p < 0.01$ ,  $***p < 0.001$ , two-tailed Student's unpaired *t*-test. **(H)** Total and cavity volume dynamics in ESB, EGBs, and ECBs normalized to corresponding EB1 volumes (24 EBs/per stage; three experiments;  $N = 288$  for each cell line). **(I)** The ratios of cellular-to-total EB volumes differ between ESB, EGBs, and ECBs (24 EBs/per stage; three experiments;  $N = 288$  for each cell line). **(J)** Calculated volumetric ratios of EdU-labeled cell domains to total EB volumes normalized to ESB1 increase at EB1-EB5 stages and decrease at EB5-EB10 stages (24 EBs/per stage; three experiments;  $N = 288$  for each cell line). **(K)** The stacked barplots show the percentages of volumetric ratios of EdU-labeled and unlabeled cell domains and cavity to total EB volumes: the prevalence of the cell proliferation domain during EB1-EB5 stages and the cavitation at EB5-EB10 stages (24 EBs/per stage; three experiments;  $N = 288$  for each cell line). The data are presented as averaged normalized means collected from three independent experiments. **(D, H,I,J)** The data at all graphs are presented as averaged means  $\pm$  s.d. collected from three independent experiments.  $*p < 0.05$ ,  $**p < 0.01$ ,  $***p < 0.001$ , ANOVA.

stage, ESBs and ECBs at the EB10 stage (**Figure 2C**). Despite a decrease in the number of cells in the S-phase of the cell cycle, the total EB volumes increased 10–14 times from the EB1 to EB10 stages. Significant differences in total volumes were found between ESB, EGB, and ECB at all stages (**Figure 2D**). Such differences in their EB growth dynamics can have several explanations: different proliferation rates due to different cell cycle lengths for ESBs, EGBs, and ECBs at the studied stages; different dynamics of the internal cavity formation associated with cell death; and different differentiation dynamics. The most significant differences in the total volume between the cell lines (**Figure 2D**) were found at the EB5 stage, at which cell death and differentiation intensified (see below).

Live-cell and histological analyses revealed that cell death significantly contributes to the internal EB cavity formation (cavitation). Multiple apoptotic and necrotic cells were identified using live-cell analysis of caspase activity (Cas) and with propidium iodide (PI) and Hoechst 33342 staining in the EB5 (**Figure 2E**). Additionally, we identified the small cell rosettes with the lumen (**Figures 1D3, 2F2**), which resembled those during the pro-amniotic cavity formation (Bedzhov and Zernicka-Goetz, 2014; Orietti et al., 2021). These observations suggest that the EB central cavity may form through mixed mechanisms—apoptotic and hollowing-like (Datta et al., 2011)—in different local sites (**Figure 2F**). Probably, the central cavity is formed by the fusion of multiple cavities with the obligate involvement of apoptosis to remove overabundant cells during the epithelialization of inner cell layers. This assumption is consistent with previous data on EB cavitation and new data on the pro-amniotic cavity formation in double embryos (Coucounanis and Martin, 1995; Orietti et al., 2021).

Analysis of the EB cavity volume dynamics showed an increase in the cavity to total volume ratios from 12–22% to 25–29% for EB5 and EB10, respectively (**Figure 2G**). The cavity volumes corresponded to 0.4–1.4- and 3.2–4.0-fold of the EB1 total volume at the EB5 and EB10 stages, respectively (**Figure 2H**). The differences in ratios of the cavity to total EB volume between ESBs, EGBs, and ECBs were more significant at EB5 than at the EB10 stage (**Figure 2G**). These data are consistent with the volumetric ratios of the pro-amniotic cavity to total embryo volume (Epi, ExEn and cavity), which were 20% and 27% for the E6.0 and E 6.5 embryos, respectively (**Supplementary Figure S1**).

To understand the integrated volumetric dynamics during the EB architecture construction, we calculated the increase in the EB cellular volume considering the proportion of EdU-labeled

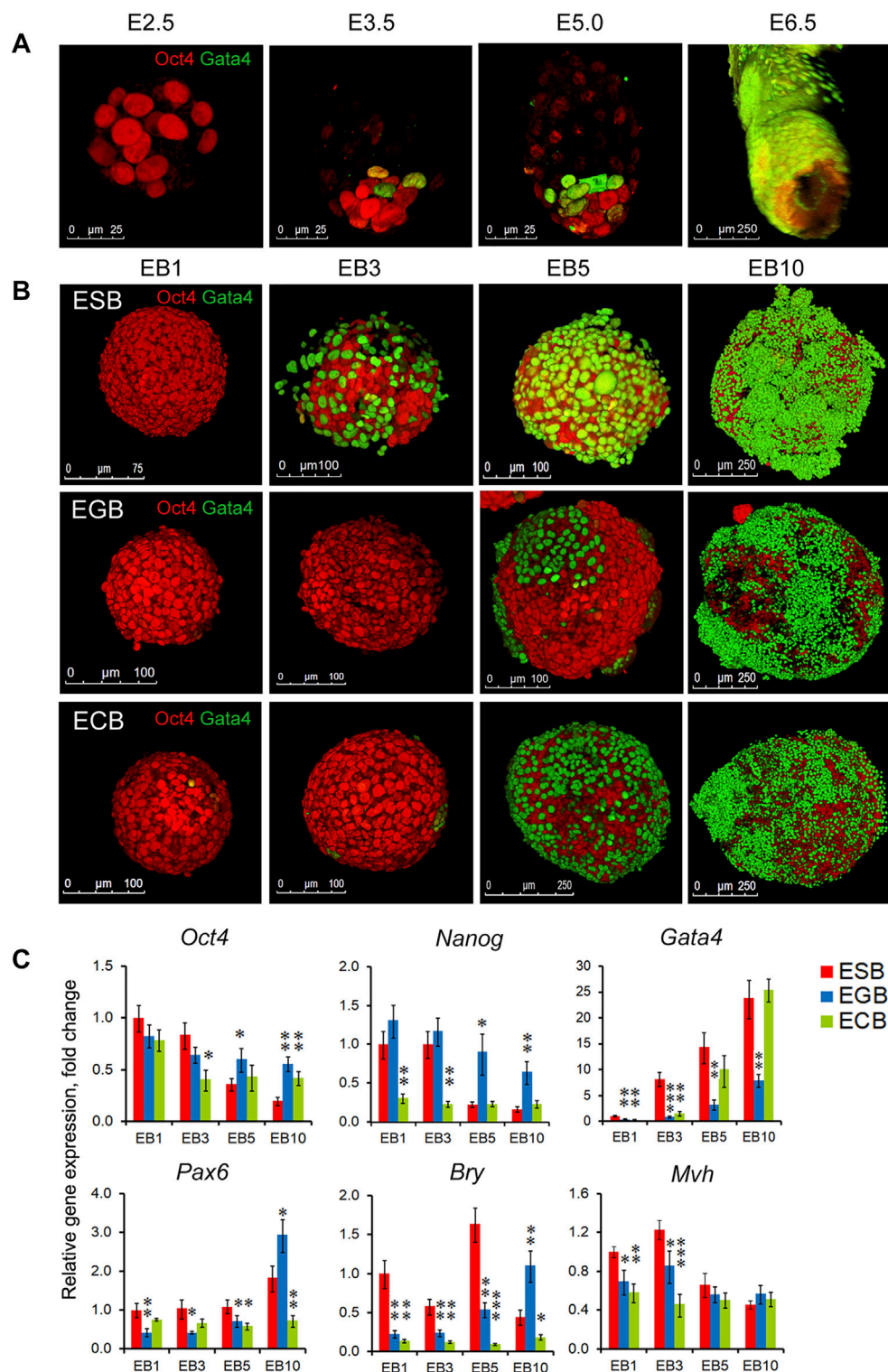
cells at each stage and the loss of EB cellular volume during the cavitation in EB5 and EB10. In general, the changes in EB cellular volumes (total volume minus the cavity volume) correlated with the gradual increase of the total volumes of ESBs, EGBs, and ECBs (**Figures 2C,I**). However, calculated changes in EB cellular volumes associated with the EdU-labeled cell domains indicated the increase in the volumetric proportion of proliferating cell domains from the EB1 to EB5 stages and the decrease from the EB5 to EB10 stages (**Figures 2I–K**). The dynamics of proliferation and cavitation domains were different between ESBs, EGBs and ECBs at most stages and the rank of gain-and-loss of EB cellular volume to EB10 stage increases in the EGBs—ESBs—ECBs row (**Figures 2H–K**). Thus, two opposite tendencies during the EB architecture construction were revealed: the prevalence of the cell proliferation domain during the EB1-EB5 stages and the cell death/cavitation domain during the EB5-EB10 stages (**Figure 2K**). ESBs, EGBs, and ECBs showed similar spatiotemporal dynamics for cell proliferation and cavitation domains but with different rate of these processes.

## Spatiotemporal Patterning and Differentiation Dynamics of ESBs, EGBs, and ECBs Consistent With the Early Developmental Trajectory

Along with cell proliferation and cavitation dynamics, the differentiation dynamics of two EB cellular patterns also play a significant role in the EB architecture construction. To understand the consistency of earliest morphogenetic and differentiation events in the EBs and embryos, we analyzed spatiotemporal patterns for the ExEn and Epi-l cells expressing Gata4 and Oct4, respectively, at four EB differentiation stages and the E2.5, E3.5, E4.5–5.0, and E6.0 stages using 3D reconstructed models from the confocal z-stacks (**Figures 3A,B**). Despite the significant difference in the developmental states of cells in EBs and early embryos, morphogenetic events associated with the spatial patterning of early populations of pluripotent and ExEn cells have some similar aspects.

Early mouse embryos at the pre-implantation stages (E2.5–E5.0) progress from an 8-cell aggregate through the formation of the trophectoderm, inner cell mass, and primitive ExEn in blastocyst to the early egg cylinder stage (E6.0), consisting of the pro-amniotic cavity and five embryonic populations, trophectoderm, extraembryonic ectoderm, and visceral and parietal extraembryonic endoderm and epiblast





**FIGURE 3 |** Spatiotemporal differentiation dynamics of ESB, EGBs, ECBs, and early embryos. **(A)** 3D reconstructed models of spatiotemporal patterns of the pluripotent (*Oct4*) and ExEn (*Gata4*) cells in mouse embryos at the E2.5, E3.5, E5.0, and E6.0 stages. Confocal z-stack images were processed using ImageJ/Fiji 3D Viewer tool. **(B)** 3D reconstructed models of spatiotemporal patterns of the Epi-l (*Oct4*) and ExEn (*Gata4*) cells in ESB, EGBs, and ECBs at the EB1, EB3, EB5, and EB10 stages. **(C)** Expression profiles of embryonic lineage markers in differentiating EBs: pluripotent - *Oct4* and *Nanog*, ExEn—*Gata4*, neuroectodermal—*Pax6*, mesodermal—*Bry*, germline—*Mvh*. Relative gene expression for each marker was evaluated relative to expression levels in ESB1. Data are shown as means  $\pm$  s.d. from three experiments. \* $p < 0.05$ , \*\* $p < 0.01$ , \*\*\* $p < 0.001$ , ANOVA.



(Figure 3A, Supplementary Movie S1, S2). Each new embryonic population arises in strict coordination with the others (Tam and Behringer, 1997; Beddington and Robertson, 1999).

The EB patterning is also associated with successive ExEn and Epi-I differentiation stages. Initially, the EB1 consists of a uniform aggregate of Oct4 expressing cells (Figure 3B, Supplementary Movie S3), whereas at the EB3 stage, single primitive ExEn cells expressing Gata4 emerge at several surface sites of a core aggregate of Oct4 expressing cells (Figure 3B, Supplementary Movies S4, S5). The timing of ExEn emerging was slightly different for ESBs, EGBs, and ECBs: the EB2-3 for the ESBs and ECBs (36–48 h) and the EB3-4 for the EGBs (48–72 h). At the EB5 stage, all three characteristic patterns develop in ESBs, EGBs, and ECBs (Figure 3B, Supplementary Movie S6). Based on the analysis of reconstructed EB models, we hypothesize that the ExEn pattern was likely formed through propagation and epiboly of individual cells rather than delaminating the entire surface cell layer in EBs. The internal cellular layers form the Epi-I pattern consisting of Oct4 expressing cells adjacent to the ExEn pattern and a cavity in the central cellular area. Finally, at the EB10 stage, the EB architecture consists of three well-formed patterns (Figure 3B, Supplementary Movie S7). Irregular ExEn outgrowths in the EB10 surface probably arise due to the absence of the trophoctoderm, which is required as a spatial regulator for ExEn morphogenesis and polarity axes establishment (Tam and Behringer, 1997; Weberling and Zernicka-Goetz, 2021).

Differential expression of the early embryonic lineage markers with the most significant differences in the expression of *Nanog*, *Gata4*, *Pax6*, and *Bry* was revealed between ESBs, EGBs, and ECBs (Figure 3C). Similarly, across expression profiles of TGF $\beta$  family factors, the most significant differences were identified in the expression of *ActivinA*, *Lefty1*, *Bmp4*, and *Gdf3* (Supplementary Figure S2). Nevertheless, the gene expression profiles indicate a reproducible track of the early embryonic lineages during EB differentiation, with the greatest expression dynamics of *Gata4* and *Oct4/Nanog* and significantly lesser expression dynamics of three germ layer markers. These data are consistent with the developmental trajectory of two early embryonic lineages at the E2.5–E6.5 stages and highlight the reproducible differences in gene expression profiles and differentiation timing between ESBs, EGBs, and ECBs. However, despite common EB archetype for ESBs, EGBs, and ECBs *in vitro*, the *in vivo* differentiation patterns of EB1 and EB10 formed after transplantation into Nude mice were strictly consistent with those of undifferentiated cells of parental lines and resulted in a formation of teratomas with the derivatives of the three germ layers (ESBs and EGBs) and teratocarcinomas (ECBs) consisting undifferentiated tumor cells (Supplementary Figure S3, and Supplementary Material).

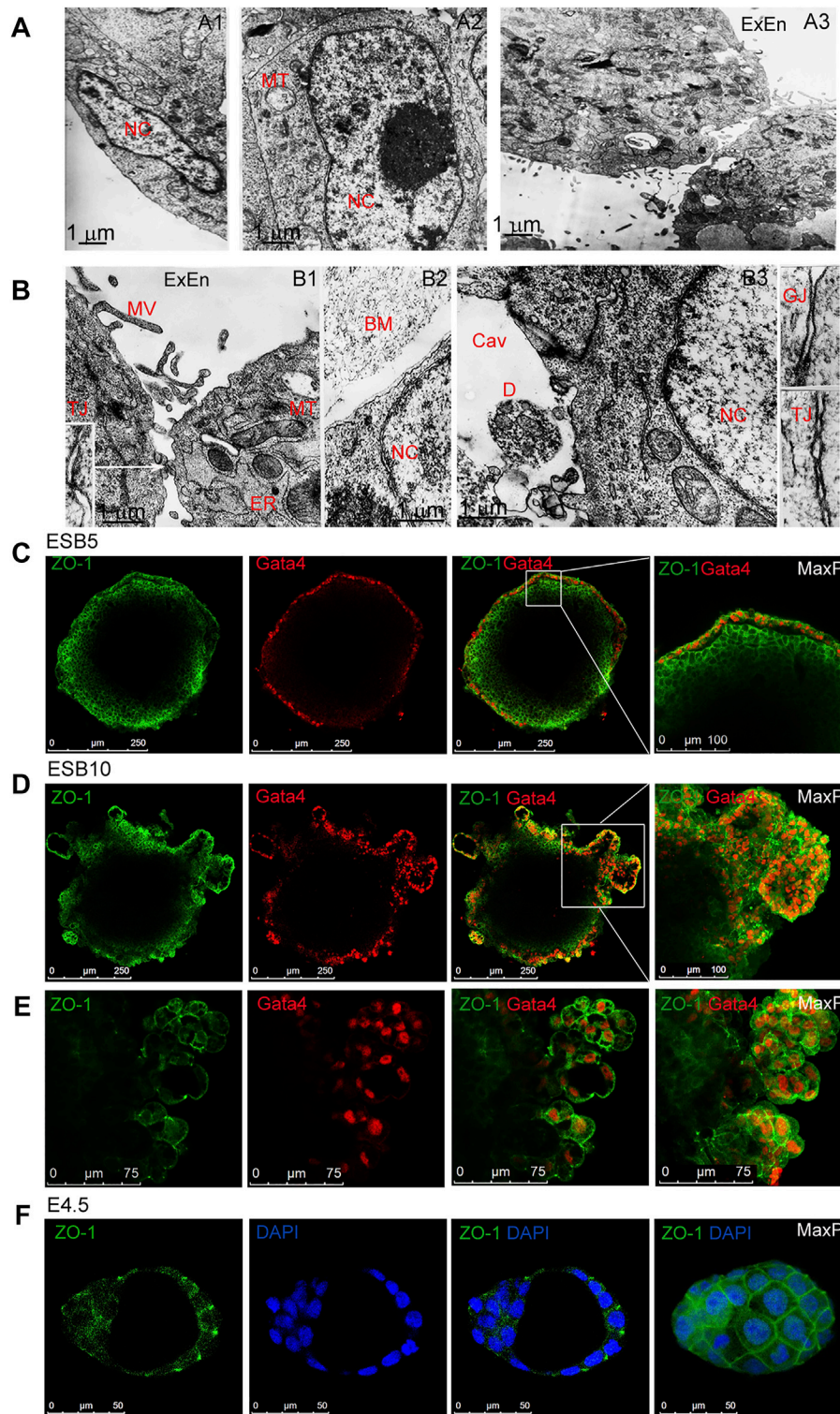
## Cell Contacts and Free Diffusion From External Environment During ESB, EGB, and ECB Differentiation and Patterning

In the formation of EB architecture, the structuring and communication of cell layers significantly depend on

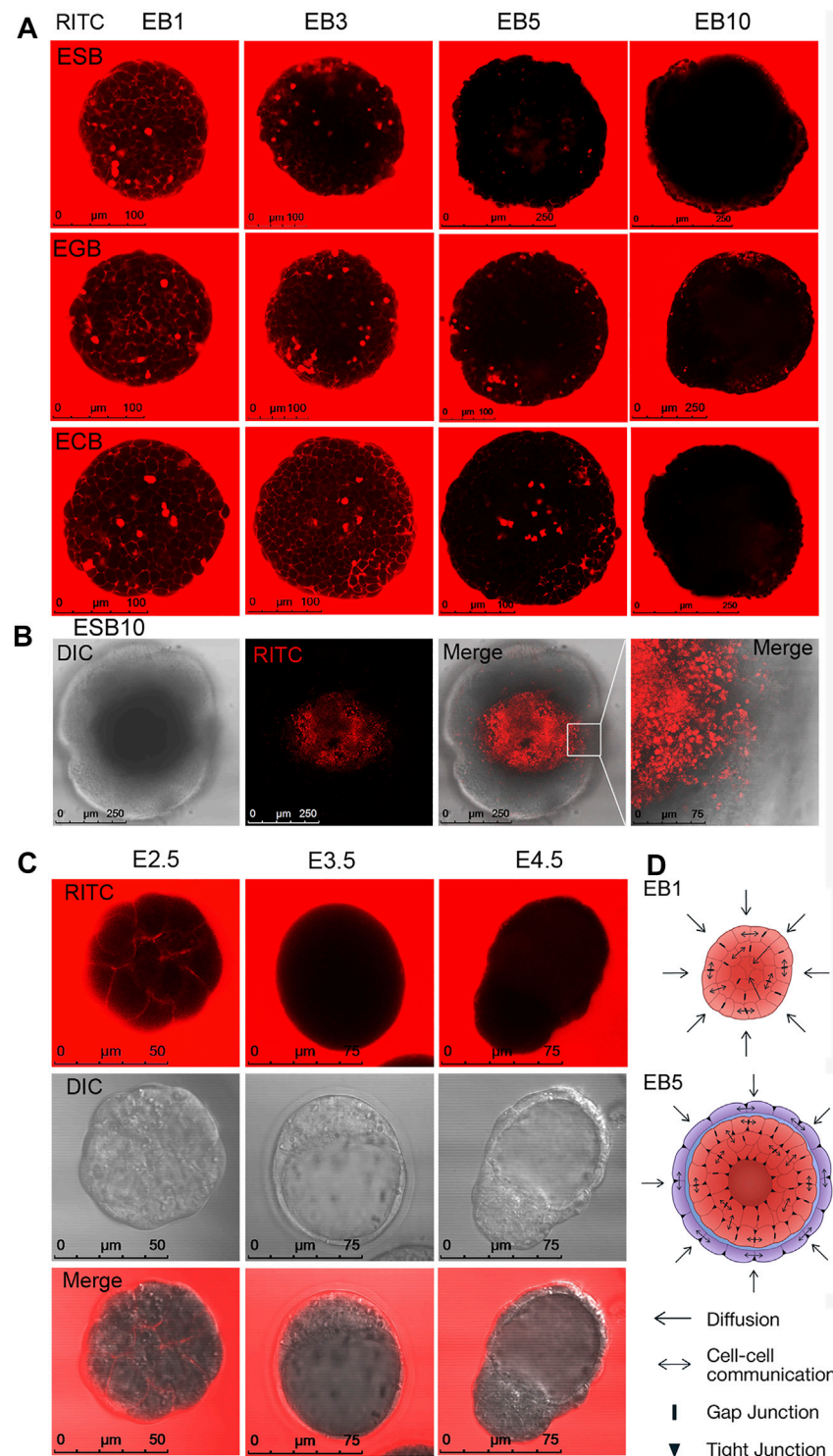
intercellular contacts. Electron microscopic analysis revealed the dynamics of cell contacts, which determine the EB architecture and influence most functions of the EB cells (Figures 4A,B). In ESB1, cells of outer and inner layers had different cell and nuclei shapes while similar low nuclear-cytoplasmic ratio and cell ultrastructure with low-developed endoplasmic reticulum and multiple mitochondria (Figure 4A1,A2). In ESB5, the outer ExEn cells contained numerous microvilli and a well-developed endoplasmic reticulum secreting components of the extracellular matrix for a multilayered basement membrane that separates ExEn from the inner cells (Figure 4A3, 4B1,B2). In early EBs, only the gap junctions were detected among all cells, while both gap and tight junctions were identified in the later EBs (Figure 4B1,B3). Moreover, tight junctions were detected between the inner cells adjacent to the internal cavity of ESB5 (Figure 4B3). Immunofluorescent staining of ESBs, EGBs, and ECBs detected the ZO-1 tight junction protein in the epithelialized ExEn cells and adjacent inner Epi-I cells at the EB5 stages (Figure 4C), and afterward, in the cells of ExEn outgrowths at the EB10 stage (Figures 4D,E).

Live-cell confocal microscopy was used to study communications between the external environment and EB patterns. Free diffusion of the fluorescent flow tracers, fluorescent dye RITC and fluorescently labeled proteins with molecular weights of 20 and 43 kDa, was analyzed in ESBs, EGBs, and ECBs at all stages (Figure 5A, Supplementary Figures S4, S5). In accordance with the distribution of intercellular contacts, diffusion of all fluorescent tracers was detected in the intercellular space between all cells at the EB1 and EB3 stages after 5 min incubation. Intracellular diffusion of studied tracers was observed only in the dead cells (Figure 5A, Supplementary Figures S4, S5). However, at the EB5 stage, the diffusion of all tracers in the intercellular space was identified mainly between outer cell layers and sometimes between inner cells locally. Finally, at the EB10 stage, no diffusion was determined in the inner EB layers even after incubation for 1 h; although all fluorescent tracers were detected between some ExEn cells at the EB10 stage (Figure 5A, Supplementary Figures S4, S5). Moreover, no diffusion between inner cells (only dead cells staining) was detected after the RITC injection into the internal cavity of EB10 (Figure 5B). Similarly, free RITC diffusion was detected in the intercellular space between the blastomeres of the E2.5 morula but not in the E3.5 and E4.5 blastocysts, confirming the integrity of tight junctions in the trophoctoderm (Figure 5C).

All these data show that during the formation of the EB archetype, there is a gradual restriction of diffusion with the external environment and between cells of different EB patterns (Figure 5D). The limitation of diffusion of small molecules and proteins in differentiating EBs occurs after forming tight junctions and a powerful basement membrane and contributes to the further EB patterning. Interestingly, the multilayered ExEn can partially compensate for the barrier function of the trophoctoderm, which provides selective transport of active substances and drugs to the embryo

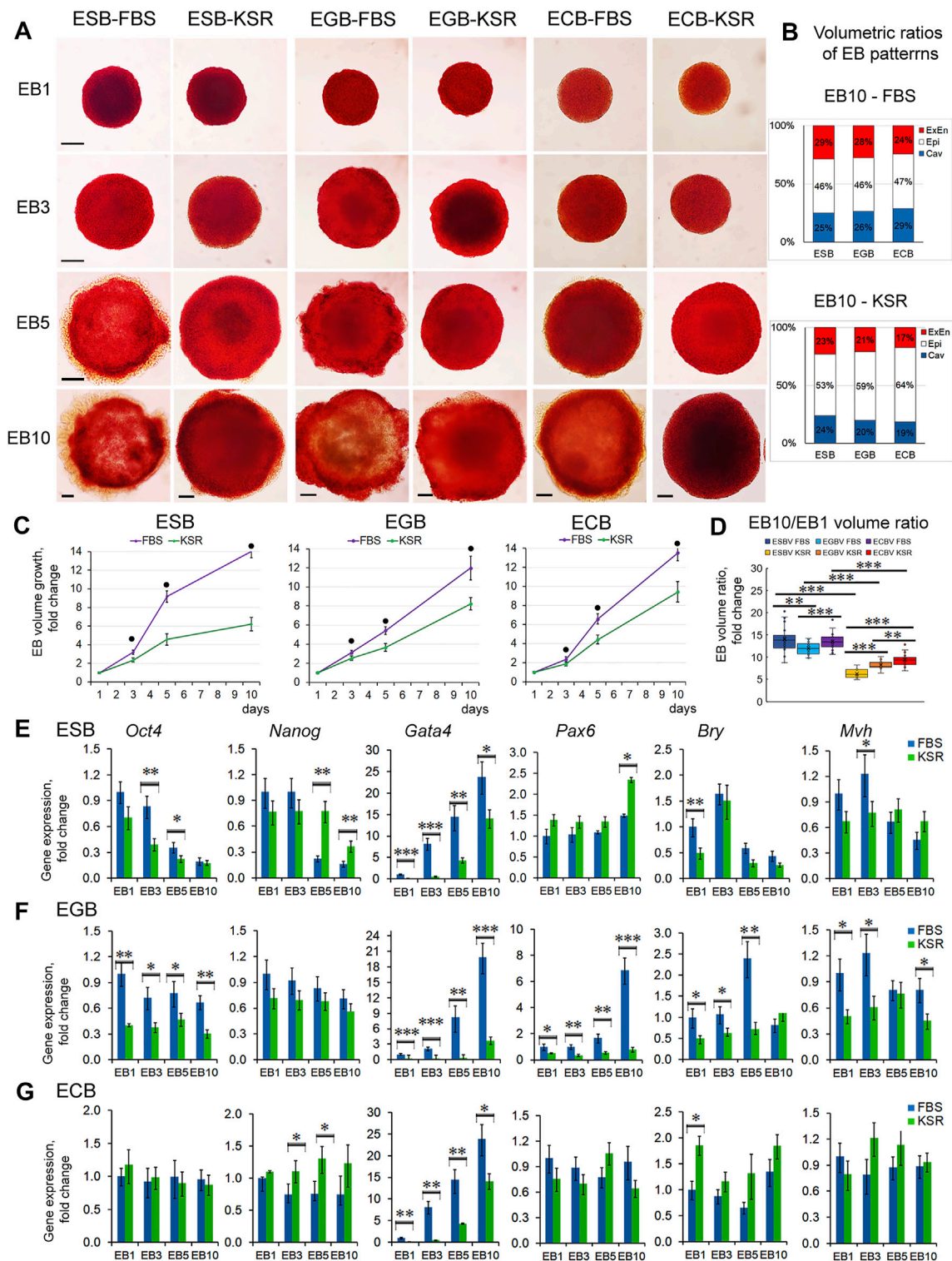


**FIGURE 4 |** Cellular ultrastructure and contacts in differentiating EBs. **(A,B)** Electron microscopy images of outer and inner cells of EB1 **[(A),A1,A2]** and EB5 **[(A),A3], [(B),B1–B3]**. Gap (GJ) and tight (TJ) junctions between the ExEn and Epi-I cells in sidebars (140000x magnification). Nc, nucleus, MT, mitochondria, MV, microvillus; ER, endoplasmic reticulum; BM, basal membrane; Cav, inner cavity, D, cell debris. **(C,D,E)** Representative confocal images and maximal projections of ZO-1 and Gata4 double staining in ExEn and Epi-I cells of EB5 **(C)** and overgrown ExEn structures of EB10 **(D,E)**. **(F)** Representative images and maximal projections of ZO-1 and DAPI double staining in the E4.5 mouse embryo.



**FIGURE 5 |** Cellular communications and small molecule diffusion in differentiating EBs and early embryos. **(A)** Representative images of live cell analysis of RITC diffusion in ESB, EGBs, and ECBs at the EB1-EB10 stages. Free RITC diffusion was detected in the intercellular space of the outer and inner cell layers of EB1 and EB3, partial diffusion in the intercellular space of EB5, and no free diffusion in EB10. **(B)** No free diffusion was detected after the RITC injection into the internal cavity of EB10 (only dead cells staining). **(C)** Free RITC diffusion was detected in the intercellular space between the blastomeres of the E2.5 morula but not in the E3.5 and E4.5 blastocysts. **(D)** The scheme of cellular communications and the diffusion of substances from the external environment modulated by intercellular contacts in EB1 and EB5. Epi-I—red, ExEn—purple, basement membrane—blue.





**FIGURE 6** | EB growth, differentiation, and patterning in different culture conditions. **(A)** Morphological analysis and ALP-staining of differentiating ESBs, EGBs, and ECBs grown in KSR- and FBS-media. **(B)** The stacked barplots indicate the percentages of volumetric ratios of ExEn, Epi-l, and cavity patterns in ESBs, EGBs, and ECBs at day 10 in the KSR- and FBS-media (24 EBs/per group; three experiments; N = 144 for each cell line). **(C)** Different EB growth dynamics in KSR- and FBS-media for all cell lines (24 EBs/per stage for each group; three experiments; N = 576 for each cell line). The data are shown as averaged means  $\pm$  s.d. from three

(Continued)



**FIGURE 6 |** experiments. •  $p < 0.001$ , ANOVA. **(D)** Volumetric ratios of EB10 to EB1 for KSR- and FBS-media (24 EBs/per stage for each group, collected from three experiments;  $N = 288$  for each cell line). Data presented as boxplots with means and the 25th and 75th percentile range; whiskers indicate maximum and minimum values. \*\* $p < 0.01$ , \*\*\* $p < 0.001$ , two-tailed Student's unpaired  $t$ -test. **(E,F,G)** Expression of embryonic lineages markers in differentiating ESBs, EGBs, and ECBs grown in KSR- and FBS-media. Relative gene expression for each marker was evaluated relative to expression levels in EB1-FBS. The data are presented as means  $\pm$  s.d. from three experiments. \* $p < 0.05$ , \*\* $p < 0.01$ , \*\*\* $p < 0.001$ , ANOVA.

(Marikawa and Alarcon, 2012; Eliesen et al., 2021; Gordeeva and Gordeev, 2021).

## Spatiotemporal Growth and Differentiation Dynamics of ESBs, EGBs, and ECBs Depend on External Environmental Factors

To address how the EB archetype formation is influenced by external factors/morphogens, we studied the growth and differentiation dynamics of ESBs, EGBs, and ECBs in serum (FBS) and serum-free (KSR) media with different content of growth factors. The FBS is known to contain growth factors such as IGF, FGF-2, PDGF, and TGF $\beta$  at varying concentrations in different batches, while KSR contains insulin, transferrin, and albumin at defined concentrations (Zheng et al., 2006; Chaudhry et al., 2008; Garcia-Gonzalo and Belmonte, 2008; van der Valk et al., 2010). Morphological analysis of ESBs, EGBs, and ECBs differentiating in these media revealed similar EB architectures matching the EB archetype but with different proportions and differentiation dynamics of EB patterns (**Figures 6A,B**). All the EBs developed thicker ExEn layers (24–29% vs. 17–23%) and larger cavities (25–29% vs. 19–24%) in FBS-media compared to KSR-media, while thicker Epi-l layers were in KSR-media (53–64% vs. 46–47%) (**Figures 6A,B**). These data also indicate the regular proportionality of the EB patterns: a direct relationship between the ExEn and cavity volumes and their inverse relationship with the Epi-l layer volume.

The EB growth dynamics were also significantly slower in KSR-media since the total EB10 volumes were 2.3-, 1.5-, and 1.4-fold less for ESBs, EGBs, and ECBs maintained in KSR-media than FBS-media, respectively (**Figure 6C**). The ratios of total volumes of EB10 to EB1 were 14, 12, and 13 vs. 6, 8, and 9 for ESBs, EGBs, and ECBs in FBS- and in KSR-media, respectively (**Figure 6C**). Moreover, the differences in the EB growth dynamics are retained in both KSR-media and FBS-media with various supplement combinations of LIF, which promotes self-renewal of undifferentiated pluripotent cells and retinoic acid (RA), which induces differentiation (**Supplementary Figures S6**). The down-regulating growth effects of RA were revealed for EB5s of all cell lines, while LIF enhanced the growth of ESBs and EGBs only. Expectedly, LIF and RA combination annihilated the growth effects in ESBs and EGBs (**Supplementary Figures S6A,B**).

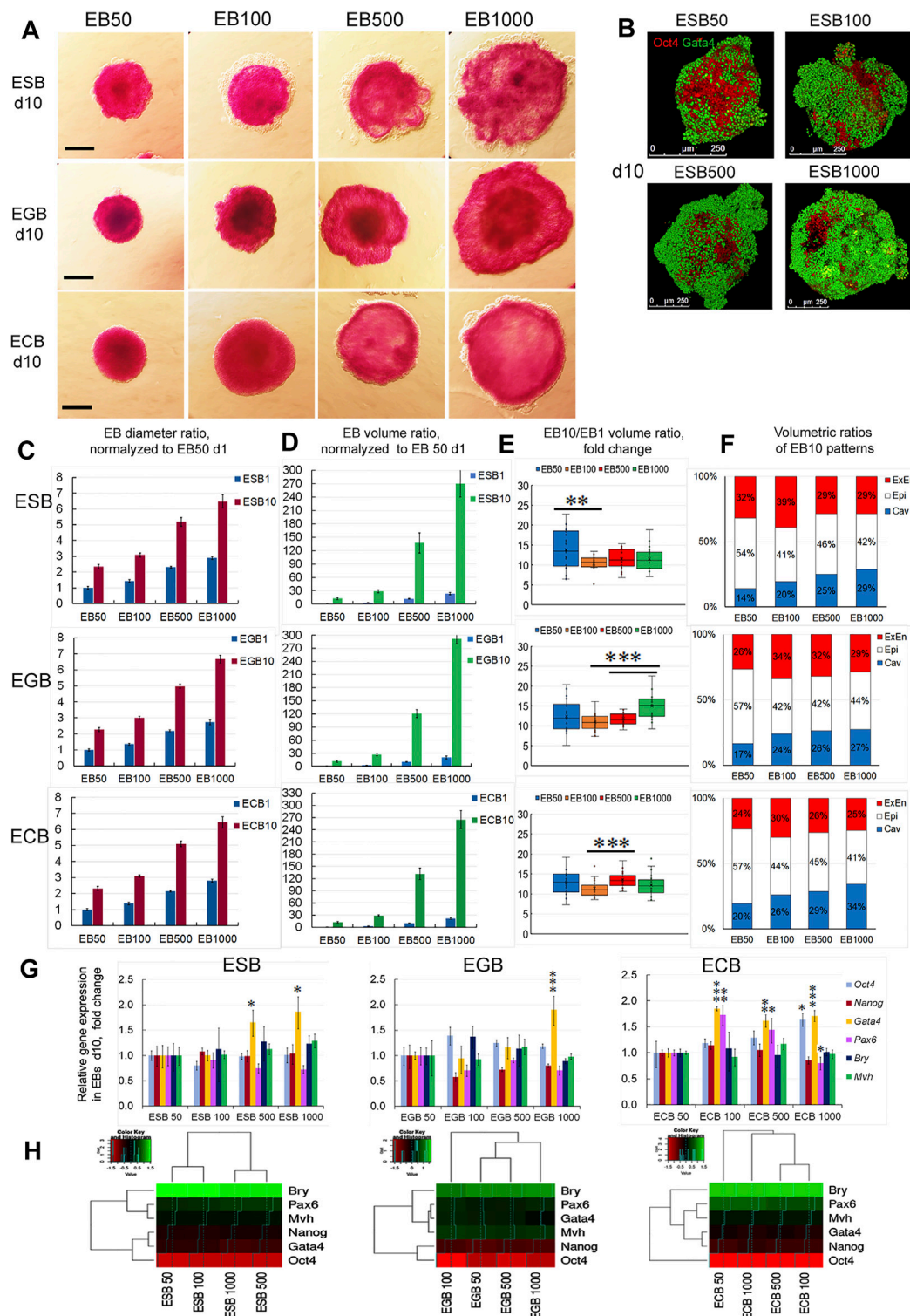
Different differentiation dynamics were also confirmed by quantitative gene expression analysis of embryonic lineage markers in ESBs, EGBs, and ECBs grown in KSR-media and FBS-media (**Figures 6E–G**). The lesser differences in the marker gene expression between EBs cultivated in KSR- and FBS-media were characteristic for ECBs, and the largest for EGBs. For all EBs, the expression dynamics of *Gata4* were most different, while the

*Pax6*, *Bry*, and *Mvh* expressions faintly differed in ESBs and ECBs, but significantly differed in EGBs. Cell line- and stage-specific differences in the *Oct4* and *Nanog* expression were found but were most pronounced at the EB5 stage. Opposite expression dynamics of *Oct4* and *Gata4* were identified in EB5 treated with the LIF and RA: up-regulated expression of *Oct4* after LIF treatment and *Gata4* after RA treatment, compared with untreated control (**Supplementary Figures S5C,D**).

These data suggest that variable dynamics of marker gene expression in spontaneously differentiating ESBs, EGBs, and ECBs may be caused by their different epigenetic states and mutations in ECCs. The epigenetic and genetic variations can lead to different responses to growth factors eliciting embryonic lineages in different environments (Ortmann and Vallier, 2017). Although, even in the absence of differentiation-promoting factors in KSR-media, all EBs can differentiate into the earliest ExEn lineage by inducing the *Gata4* expression. Simultaneously, gene markers of later lineages (*Pax6*, *Bry*, and *Mvh*) were expressed at a low level in all EBs in both media but significantly lower in the KSR-media. Similarly, the *Oct4* and *Nanog* expression dynamics were significantly less in the KSR medium. Under differentiation-promoting conditions with RA treatment, the *Oct4* and *Gata4* expressions were less different, both in all EB5s (**Supplementary Figures S6**) and 2D culture systems (Sharova et al., 2007; Gordeeva et al., 2019). All these results indicate the critical role of the levels of differentiation factors/morphogens in embryonic lineage induction. Consequently, the growth and differentiation dynamics of ESBs, EGBs, and ECBs significantly depend on both external environmental factors and cell states. The cellular composition and proportions of EB cellular patterns can be regulated by a specific combination of growth and differentiation factors.

## Spatiotemporal Growth and Differentiation Dynamics of ESBs, EGBs and ECBs Are Independent on Cell Numbers and EB Size

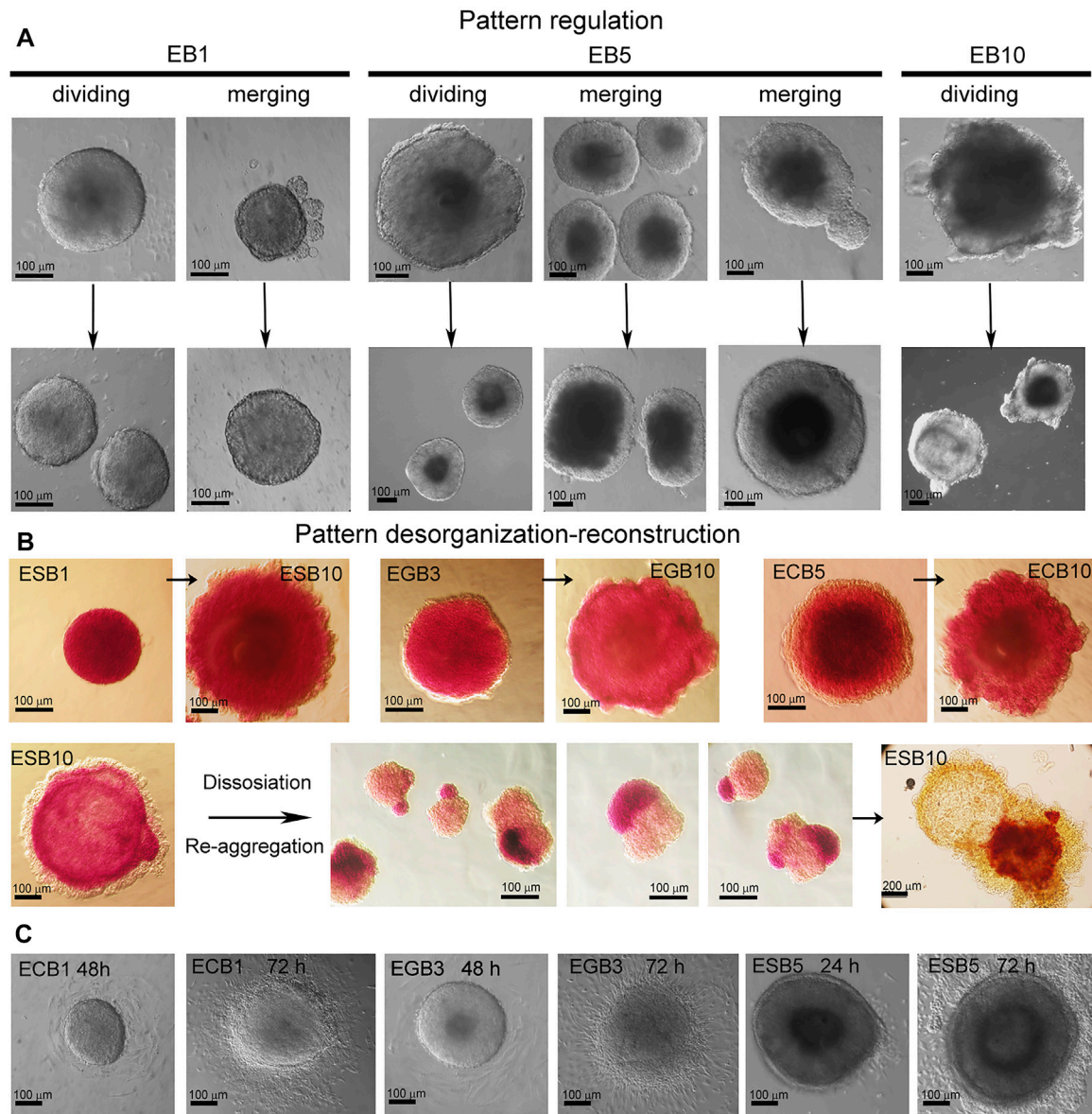
To understand size control mechanisms in the EB differentiation model, we investigated spatiotemporal growth and differentiation dynamics of differently sized EBs formed by various cell numbers. Analysis of differentiating ESBs, EGBs, and ECBs formed by 50, 100, 500, and 1,000 cells revealed no differences in their temporal dynamics and the final architectures at the EB10 stage, despite their significantly different sizes (**Figures 7A–E**). The time of appearance and spreading the ExEn and cavity occurred at an almost similar pace in all EBs. However, EB50 for all cell lines displayed a smaller ExEn cell pattern and internal cavity (**Figure 7F**), and therefore, their volumetric proportions differed from other sized EBs. The differences in the EB50 patterns' proportions



**FIGURE 7 |** Growth, differentiation, and patterning of EBs formed by different cell numbers. **(A)** ALP-staining of ESBs, EGBs, and ECBs formed by 50, 100, 500, and 1,000 cells at the 10th day of differentiation. **(B)** 3D reconstructed models of spatial patterns of the Oct4 and Gata4 expressing cells in ESBs formed by different cell numbers at day 10. **(C, D)** Diameter and volume ratios for differently sized ESBs, EGBs, and ECBs normalized to respective EB50 at day1 (24 EBs/per group for each cell line; three experiments; N = 288 for each cell line), data presented as averaged means  $\pm$  s.d. **(E)** Volumetric ratios of EB10 to EB1 for differently sized ESBs, EGBs, and ECBs day1 (24 EBs/per group for each cell line; three experiments; N = 576 for each cell line). Data presented as boxplots with means and the 25th and 75th percentile range; whiskers indicate maximum and minimum values.  $**p < 0.01$ ,  $***p < 0.001$ , two-tailed Student's unpaired *t*-test. **(F)** The stacked barplots indicate the

(Continued)

**FIGURE 7 |** percentages of normalized volumetric ratios of ExEn, Epi-I, and cavity patterns for differently sized ESBs, EGBs, and ECBs at day 10 (24 EBs/per group for each cell line; three experiments; N = 288 for each cell line) **(G,H)** Expression of embryonic lineages markers **(G)** and profile clustering **(H)** for differently sized ESBs, EGBs, and ECBs at day10. Relative gene expression for each marker was evaluated relative to expression levels in EB50 for each cell line. Heatmaps and hierarchical dendrograms show the gene expression profile clustering for differently sized EB of each cell line at day10. The data are presented as means  $\pm$  s.d. from three experiments. \* $p < 0.05$ , \*\* $p < 0.01$ , \*\*\* $p < 0.001$ , ANOVA.



**FIGURE 8 |** EB pattern regulation after dividing, merging, and disorganization. **(A)** Representative images of pattern regulation in the EB1, EB5, and EB10 after dividing and merging. After merging or dividing, the resulting EBs restored their patterns and architecture and continued further differentiation in all cases (100%) (10 EBs/per stage per cell line; three experiments; N = 120 for each cell line). **(B)** Pattern disorganization-reconstruction by dissociating EBs and re-aggregating cell suspension for 72 h (5 EBs/per stage for each cell line; three experiments; N = 60 for each cell line). Dissociated EB10 cells (100 cells/per drop) *de novo* self-organize and sort within the aggregate into arbitrary spatial arranged cellular domains consisting of homogeneous populations of ExEn and EpiI cells. During further differentiation, all three typical EB patterns are restored but with varying degrees of symmetry. Cavities are formed within the EpiI and sometimes ExEn domains. ALP activity was detected in EBs and reconstructed cell aggregates with asymmetrical patterns. **(C)** Representative images of spherical shape loss and pattern disorganization after the attachment of EB1, EB3, and EB5 to cell culture dishes at 24–72 h. EB1–5 cells can attach to the dish surface and migrate, while EB10 can not.



may be due to the greatest size variability during the formation and the slower cavitation.

Growth dynamics of differently sized EBs was proportional to the initial EB1 volume since the volumetric ratios of EB10 to EB1 were in the similar ranges of 10–14, 11–15, and 11–13 for ESBs, EGBs, and ECBs, respectively. Differences in these values between EB50, EB100, EB500, and EB1000 were mostly insignificant within each cell line (**Figures 7C–E**). However, differences in growth rate between some EB groups of each line were found and need further studies to identify possible technical and biological causes.

Analysis of embryonic lineage marker expression in the ESBs, EGBs, and ECBs formed by 50–1,000 cells on day 10 detected significant differences in the *Gata4* expression for most EB500 and EB1000, although the differences in expression levels were no more than two times (**Figure 7G**). Among the ECBs, differences in the *Pax6* expression were also found between EB100 and EB500 compared to EB50 (**Figure 7G**). Simultaneously, the expression of *Oct4* and *Nanog* did not differ significantly between most differently sized EBs for all cell lines (**Figure 7G**). Hierarchical clustering of marker expression profiles in differently sized EBs reveals no general trends since the most distinct and similar EB groups were specific for each cell line (**Figure 7H**).

Thus, ESBs, EGBs, and ECBs can maintain the invariant proportions of the archetypal EB structure and do not adjust the growth and differentiation rate relative to their size and initial cell numbers. Whilst experimentally enlarged or reduced early mouse embryos can regulate their size during the pre-gastrulation stages (E5.5–E5.75) and develop into normal-sized pups (Tarkowski, 1963; Buehr and McLaren, 1974; Lewis and Rossant, 1982; Orietti et al., 2021). These data suggest that EBs can scale their spatiotemporal patterns during architecture construction.

## Pattern Regulating and Scaling in the EB Differentiation Model

Given our finding that the morphogenesis of the EB archetype is independent of cell numbers forming EBs (**Figure 7**), we next analyzed the possibility of the pattern regulation after experimental dividing, merging, and deconstruction-reconstruction of ESBs, EGBs, and ECBs. First, we examined the EB pattern regulation after dividing or merging (**Figure 8A**). These experiments demonstrated that early EB1 and later EB5 and EB10 can restore their patterns and continue further differentiation and patterning after merging or dividing. In the case of merging EBs at different differentiation stages (EB1–EB3 and EB1–EB5), the resulting patterns and architecture corresponded to a later stage. Early EBs (EB1–EB3) easily regained their spherical shape for 2–4 h, while EB5 restored shape and patterns for 24–48 h after merging or dividing. Although the EB10s never merged, dividing EB10 resulted in two EB10s with partially restored and asymmetric patterns for 48 h. Thus, these results showed that, like in the EBs formed by different numbers of cells, overall sizes of merging or dividing EBs

are not regulated, but EB patterns and architecture are restored during the following days of differentiation.

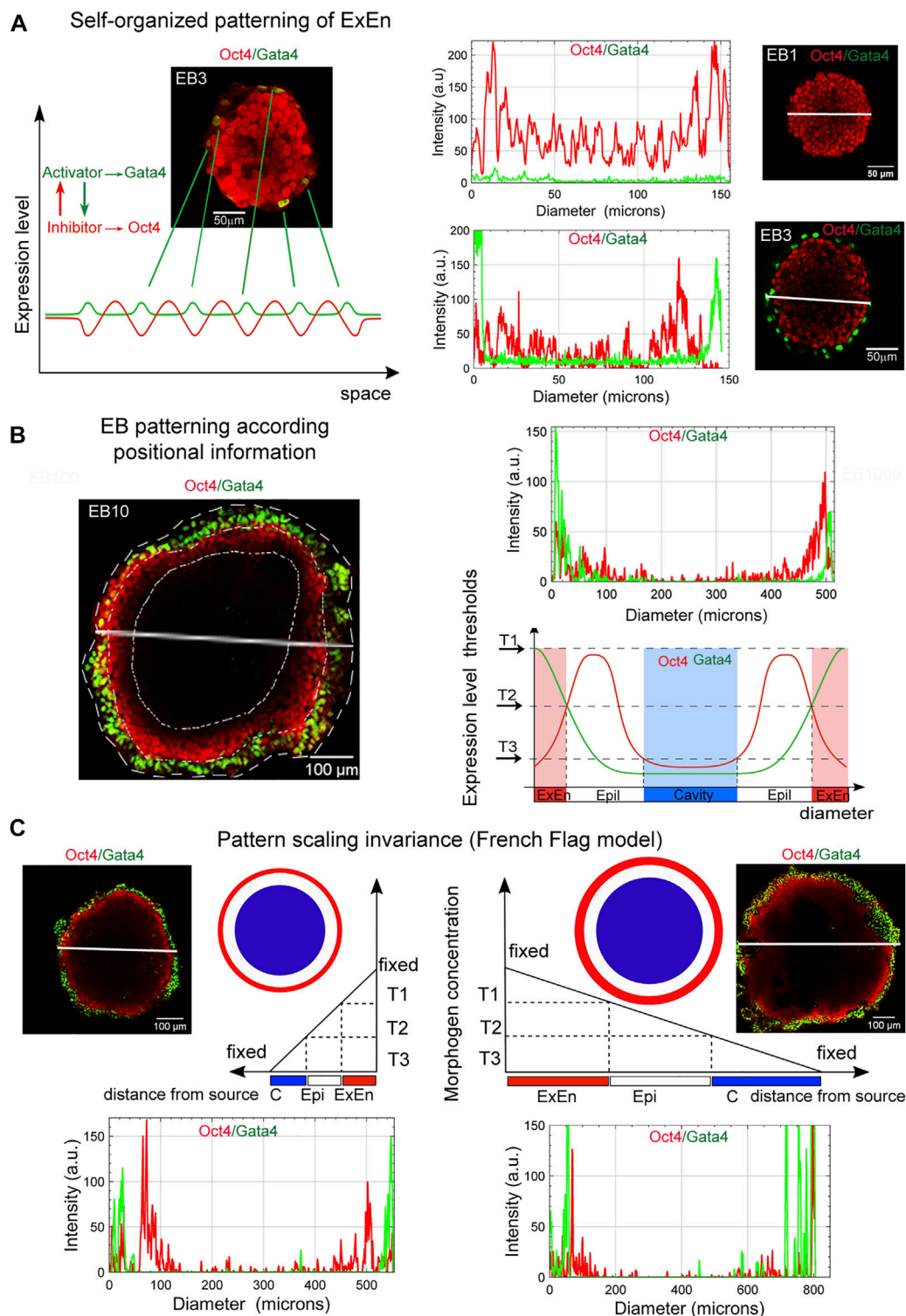
We next examined whether EB patterns are regulated after dissociating ESBs, EGBs, and ECBs at different stages. The experiments with pattern disorganization-reconstruction by EB dissociation and re-aggregation of cell suspension (100 cells in hanging drops for 72 h) revealed *de novo* self-assembly and architecture construction for the EB1, EB3, and EB5 (**Figure 8B**). In contrast, dissociated EB10 cells re-aggregated and sorted within the aggregate into arbitrary spatial arranged cellular domains consisting of homogeneous ExEn and Epi-l cell populations (**Figure 8B**). During further differentiation, the Epi-l domain becomes internal due to the spreading of ExEn cells over its surface, and then cavities are formed within the Epi-l and sometimes ExEn domains. Thus, all three archetypal EB patterns are restored but with varying symmetry degrees. ESBs, EGBs, and ECBs showed similar features in restoring their patterns during these experiments.

Together, these results demonstrate that EB1, EB3, and EB5 easily regain their spherical shape and patterns, as their cellular fates are not fully determined. Additionally, EB1–EB5 cells retain their migration ability, as they easily adhere and migrate over the culture dish surface (**Figure 8C**). In EB10, no fusion, adherence, and reorganization of shape and cellular patterns proceeded, probably due to the fixed spatial position of differentiated cells through specific contacts. However, after EB10 dissociation, ExEn and Epi-l cell migration significantly contributes to *de novo* self-organizing EB structure. These results are consistent with previous studies of the capacity to re-establish experimentally disorganized patterns through cell sorting and spreading based on differential adhesion (Armstrong, 1989; Maeda et al., 2007; Choi et al., 2016; Revell et al., 2019; Scalise et al., 2021).

## DISCUSSION

In this study, we explored a highly reproducible experimental platform, the 3D EB differentiation model, which generates the EB archetype mimicking architectures and developmental trajectories of the early embryos (Beddington and Robertson, 1999; Rivera-Pérez and Hadjantonakis, 2015; White et al., 2018; Sozen et al., 2019). The EB archetype, consisting of three individual morphological patterns—ExEn, Epi-l, and internal cavity—was established by the ESCs, EGCs, and ECCs without the involvement of the trophoctoderm lineage. This suggests the possible independence in the architecture construction for the earliest epiblast covered with extraembryonic endoderm from the trophoblast, which selectively isolates the embryo from external influences and plays a significant role in the formation of the polarity axes of the early embryo (Smith, 1980; Marikawa and Alarcon, 2012; Weberling and Zernicka-Goetz, 2021). Therefore, the EB archetype represents a radially symmetric 3D cell structure without the polarity axes. Interestingly, even in the ETX-embryos containing trophoctodermal cells, only the proximal-distal axis, but not the anteroposterior axis, is set in them (Sozen et al., 2019). Moreover, the appropriate embryonic patterns were identified in





**FIGURE 9 |** Basic principles in EB patterning and scaling. **(A)** The ExEn pattern in early EBs can emerge due to random changes in the Gata4 and Oct4 expression in surface cells, which may correspond to the RD model of self-organizing patterns in homogeneous systems. Representative plots of spatial trends for the intensity of the Oct4 and Gata4 expression across diameters (marked by white lines) in respective images of EB1 and EB3 demonstrate changes in Gata4 expression in surface cell layers. Similar trends in signal intensity changes were observed when analyzing the along the z-axis (see **Supplementary Figure S7A,B**). **(B)** Three morphological patterns in EBs, ExEn, Epi-1, and the cavity, can presumably form in accordance with the position of the cell layers under conditions of a morphogen concentration gradient and free diffusion from the external environment. The EB archetype patterning may be consistent with the French Flag paradigm. The highest morphogens' (Continued)

**FIGURE 9 |** concentrations (T1) can induce the ExEn pattern ( $\text{Gata4}^{\text{high}}/\text{Oct4}^{\text{low}}$ ), moderate concentrations (T2) can contribute to maintaining the Epi-I pattern ( $\text{Oct4}^{\text{high}}/\text{Gata4}^{\text{low}}$ ), and low concentrations (T3) can trigger apoptosis and cavitation ( $\text{Oct4}^{\text{low}}/\text{Gata4}^{\text{low}}$ ). A representative plot of spatial trends for the intensity of expression of Oct4 and Gata4 across EB10 diameter (marked by a white line) shows the distribution of expression levels of these marker proteins in accordance with the EB patterns depicted in the diagram below. **(C)** A scheme showing the expected EB pattern scaling invariance model (French flag model for volumetric scaling). Pattern scaling in differently sized EBs may be consistent with the models of scaling by specific boundary conditions and a diffusion modulator. T1, T2, and T3 threshold levels of morphogens (constant concentration in cell culture media) can define similar ExEn, Epi-I, and cavity proportions in small and large EBs (see **Figure 7F**). Representative plots of spatial trends for the intensity of Oct4 and Gata4 expression in EB100 and EB1000 indicate the similar distributions of expression of these marker proteins across diameters in accordance with the EB patterns depicted in the pictures above. Similar trends in signal intensity changes are observed along the z-axis scanning of EB100 and EB1000 (**Supplementary Figure S7C,D**). Distributions of Gata4 and Oct4 staining intensity along the z-axis indicate ExEn and Epi-I patterns of different sizes in EB100 and EB1000.

only 20% and 30% of formed ET- and ETX-embryos, respectively (Sozen et al., 2018, 2019).

All stages of the EB architecture formation are closely related to the symmetry breaking. Although, at all differentiation stages, EBs remain predominantly radially symmetric 3D cellular structures at a large-scale level, the formation of all three patterns is associated with symmetry-breaking events at a smaller local scale (**Figures 1B,D, 3B**). As mentioned above, the first symmetry-breaking event is associated with the appearance of single ExEn cells and the initiation of external cell patterning. Subsequent symmetry-breaking events are related to the establishing apical-basal polarity in the ExEn and Epi-I cell layers, which lead to the formation of two functionally distinct types of epithelium (**Figures 1C, 4**). Local symmetry breaking continues with further differentiation of these cell patterns, resulting in asymmetric outgrowths in the ExEn pattern and cavity formation in the Epi-I pattern (**Figures 1C,D, 3B**). It can be assumed that all these symmetry-breaking events can be triggered by changes in the morphogens' diffusion from the external environment (**Figure 5, Supplementary Figure S4**) and changes in the expression of TGF $\beta$  factors during differentiation (**Supplementary Figure S2**). Such changes may lead to establishing local morphogens' gradients within these patterns. However, despite the successive symmetry-breaking events during EB patterning, no morphological signs of the presumptive polarity axes were observed in mature EB10 (**Figures 1B,C**). The lack of spatial boundaries formed by the trophoblast and the blastocyst cavity may explain the disturbance in establishing the EB proximal-distal axis, but not the anterior-posterior axis. Therefore, further research is needed to identify the mechanisms that may underlay the polarity axes formation in the EB differentiation model.

Analyzing the contribution of cell proliferation, death, differentiation, patterning, and intercellular communication in the EB architecture construction, we found changing trends in the ratio of the cell proliferation and death domains (**Figure 2**) and a gradual restriction of diffusion from the external environment and between cellular layers (**Figure 5, Supplementary Figures S4, S5**). Presumably, the restricted communication between cellular patterns through diffusion modulating (tight junctions and thick basement membrane) can drive further pattern development contributing to internal morphogens' gradient and the mechanical stress for epithelialized cell layers. On the one hand, the extensive contact with the external environment can lead to hypertrophy of the ExEn pattern (**Figures 1D4, 3B, 7B**). On the other hand, the restriction of free diffusion of growth

factors/morphogens from the culture media to EB5-EB10 inner cellular layers (**Figure 5, Supplementary Figures S4, S5**) can result to the prevalence of cell death/cavitation domain over proliferation domain (**Figure 2K**). With EB cavity patterning, the Epi-I cells adjacent to the basement membrane preferentially survive and proliferate (**Figures 2A,F**), as previously shown for early embryos and ETX-embryos (Bedzhov and Zernicka-Goetz, 2014; Harrison et al., 2017). To promote more advanced EB stages, the EB cavitation and ExEn regulation mechanisms require further investigation.

Given our finding that the formation of the EB archetype during ESB, EGB, and ECB morphogenesis can recapitulate some aspects of the early development, we next considered whether the basic principles of RD and PI morphogenetic concepts could be involved in the self-organization, patterning, and scaling in the 3D EB differentiation model. According to our observations, the onset of EB patterning is associated with the appearance of single ExEn cells at several surface locations after LIF withdrawal in culture media (**Figure 3B, Supplementary Movie S4**). We assumed that the ExEn cell type may appear due to random changes in the Oct4 and Gata4 expression (activator-inhibitor TFs) in surface cells (**Figure 9A**), which are stimulated through several intermediate steps in Erk/Mek and TGF $\beta$  family signaling pathways (Burdon et al., 1999; Fujikura et al., 2002; Frankenberg et al., 2011).

The triggering of the differentiation of pluripotent cells due to the random changes of transcription factor expression in single cells was previously examined experimentally (Plachta et al., 2011; Pantazis and Bollenbach, 2012) and by theoretical modeling (Halley et al., 2009, 2012; Greaves et al., 2017). The developed conceptual model proposes that stochastic gene expression within a stem cell gene regulatory network self-organizes to a critical-like state, which primes various transcriptional programs associated with different cell lineages. This model is consistent with the concept of a self-organizing pattern in the RD system, which postulates that a new pattern can arise during chemical morphogenesis after interactions of two homogeneously distributed substances (morphogenes), which generate stable periodic pattern even from a random or uniform initial condition. These patterns represent local differences in the concentrations of the two substances (Turing, 1952).

Based on our observations, we hypothesized that the PI interpretation by EB cells might also determine cell fate during EB patterning. Thus, the external EB cell layer has the largest contact area with the external environment and can be exposed to

the maximum concentrations of growth factors/morphogens. Hence, they are probably the first to respond to the stimulation (**Figure 9A**). We have detected the ExEn pattern only on the surface of EBs, even in media with different growth factors' contents (**Figures 3B, 6**). Therefore, we believe that the outer ExEn pattern is most likely formed due to the proliferation and spread of initiator cells over the surface until an enclosed cell layer is formed (**Figure 3B, Supplementary movies S3, S5, S6**). However, this assumption needs to be confirmed by live-cell analysis. Simultaneously, EB inner cells retained a low-differentiated state since they continued to express Oct4 and ALP (**Figures 3B, 5, 6**). Two possibilities can explain this: firstly, by the remoteness from the source of differentiation factors, and secondly, by establishing tight junctions and the basement membrane limiting diffusion in late EBs. The EB patterning is fundamentally different from the 2D gastruloid and peri-gastrulation-like patterning for hESC colonies with simultaneously arising radial cell layers of lineage progenitors (Warmflash et al., 2014; Deglincerti et al., 2016; Etoc et al., 2016; Tewary et al., 2017). These differences may reflect mouse and human specific features of embryonic stem cell patterning and the differences between 2D and 3D models.

Next, we considered whether the EB patterning is consistent with the classic French flag paradigm (Wolpert, 1981). The PI conceptual model describes embryonic patterning in terms of a coordinate system determining polarity as the direction in which positional information is specified or measured (Wolpert, 1981; Umulis and Othmer, 2013; Green and Sharpe, 2015; Čapek and Müller, 2019). In the French flag paradigm, the ability of the system to adjust the pattern when parts are removed or added and to demonstrate size invariance is related to the ability of cells to change positional information and interpret it. In the EB archetype, the cell fate in each EB pattern presumably may be determined by the PI of cell layers as a distance from the morphogens' source (**Figures 9B,C**). According to the PI concept, these three patterns might be formed due to the morphogen concentration gradient arising *via* free diffusion from the external environment. The spatial distribution gradient of soluble growth factors, nutrients, and oxygen may be formed due to uneven diffusive mass transfer within EBs. The modeling and direct measurement of oxygen and cytokine concentrations suggest that the size of EB strongly affects the threshold at which the system becomes mass transfer limited (Wartenberg et al., 2001; Van Winkle et al., 2012). If such gradients are formed, the highest threshold concentrations of morphogens can give rise to the ExEn pattern ( $Gata4^{high}/Oct4^{low}$ ), moderate concentrations can maintain the Epi-I pattern ( $Oct4^{high}/Gata4^{low}$ ), and low threshold concentrations of morphogens can trigger apoptosis and cavitation ( $Oct4^{low}/Gata4^{low}$ ) (**Figure 9B**). The differentiation rate and the size of the ExEn pattern can depend on the concentration of growth factors/morphogens from the external environment since thicker ExEn patterns and higher *Gata4* expression were detected in EBs cultured in FBS-media compared to KSR-media (**Figures 6A,B,E-G**). Notably, the final ExEn pattern formation does not depend on the free EB surface area and continues in ExEn outgrowths hereafter (**Figure 3B**). After establishing all three

patterns, the ExEn and Epi-I patterns continue their development, possibly following a new morphogen gradient.

Analyzing the scale invariance in the EB differentiation model (**Figures 7, 8**), we suggested that pattern scaling in differently sized EBs may be explained *via* the models of scaling by specific boundary conditions and diffusion modulators (Čapek and Müller, 2019). It can be assumed that the ExEn pattern in small and large EBs is formed by the different numbers of initiator cells under free diffusion and maximum morphogen concentrations (**Figure 9C**). However, with fixed boundary conditions (growth factor concentrations and EB surface area) and emerging diffusion modulators (tight junctions and the basement membrane), morphogens' gradient can probably remain proportional to the EB surface area and volume. Additionally, the concentrations of secreted morphogens and extracellular matrix proteins may remain proportional to the number of ExEn cells.

Previous studies and our current study have shown that EB differentiation and patterning are highly dependent on the growth factors/morphogens from the culture media with FBS and KSR and their endogenous gene expression of TGF $\beta$  family factors (Dang et al., 2002; Bauwens et al., 2008; ten Berge et al., 2008; Bratt-Leal et al., 2009; Giobbe et al., 2012; Chhabra et al., 2019). Our study found that the growth factors/morphogens' concentration in the culture media does not affect the EB archetype structure, even for the ECBs, whereas it affects growth and differentiation dynamics, cellular composition, and patterns' proportions (**Figure 6, Supplementary Figures S5**). All EBs formed more voluminous ExEn and cavity patterns but less voluminous Epi-I patterns in the FBS medium than in the KSR medium. Importantly, the ESBs, EGBs, and ECBs with different expression levels of TGF $\beta$  factors (**Supplementary Figures S2**) form similar EB architectures (**Figures 1B,C, 3B**), i.e., strived for the unified EB archetype. All these data can serve as a basis for experimental engineering and theoretical modeling of EB patterns through modulation by various morphogens/signaling pathways, like previously developed peri-gastrulation-like patterning models for hESC colonies (Warmflash et al., 2014; Deglincerti et al., 2016; Etoc et al., 2016; Tewary et al., 2017). These studies demonstrated how the modulation of BMP4 concentration in culture medium induces self-organization of pSMAD1 gradient in hESC colonies, which stimulates a radial pre-patterning cell fates with the trophectoderm-like fate (CDX2) at the colony edge, followed by the endoderm-like (SOX17) and primitive streak-like (BRA) regions, and the ectoderm-like (SOX2) region at the colony center (Etoc et al., 2016; Tewary et al., 2017). The cell fate acquisition depends on both the pSMAD1 signaling strength and duration of induction and is consistent with the positional information of cells. The formation of such a pre-patterning may depend on the colony size and cell density in the colonies that correlate with the "edge-sensing" basolateral or apical distribution of BMP receptors in the hESC membranes and can be adjusted by the morphogen concentration according to the colony size. Interestingly, the trophectoderm-like fate pre-pattern identified at the hESC colony edge never forms in mouse EBs with an external ExEn pattern. It should be considered that both the EB and hPSC colony patterning depend

on the exogenous and endogenous morphogens and coordinated interaction of multiple signaling pathways, which need further investigations using the principles of RD and PI concepts.

Taking together our considerations and assumptions, we can conclude that both RD and PI concepts may be parallel involved in the EB archetype formation. RD may initiate the self-organizing ExEn patterning consistent with the PI of EB surface cells. The subsequent formation of ExEn, Epi-I, and cavity patterns could also be determined by their PI, as the distance of cell layers from the external morphogens' source, and the morphogens' concentration gradient, which can be formed in accordance with RD. However, the upstream or downstream mode of RD and PI at specific stages of the EB patterning is challenging to define, and further experimental research is needed.

In conclusion, the developed 3D EB differentiation model of self-organized patterning and architecture construction provides an opportunity for experimental and computational modeling and analyzing the mechanisms of cellular diversity and spatiotemporal patterns under the morphogen influence. The presented model is free from ethical concerns and can be used for drug discovery and toxicological research. This model is physiologically approximated to *in vivo* conditions and imitates some early developmental events. Our investigative approaches to studying the formation of EB archetypal structure can also be helpful for organoid and cancer spheroid research.

## DATA AVAILABILITY STATEMENT

The original contributions presented in the study are included in the article/**Supplementary Material**, further inquiries can be directed to the corresponding author.

## ETHICS STATEMENT

The animal study was reviewed and approved by the Ethics Committee of Institute of Developmental Biology of Russian Academy of Sciences and performed in accordance with the

Russian Federation legislation (Order of the Ministry of Health and Social Development of the Russian Federation No. 708n, 28 August 2010) based on the European Convention for the Protection of Vertebrate Animals Used for Experimental and Other Scientific Purposes.

## AUTHOR CONTRIBUTIONS

Data collecting and analysis: OG, AG, and PE; Methodology: OG, AG, and PE; Writing, editing, reviewing of manuscript: OG, AG, and PE; Visualization: OG and AG; Funding and project administration: OG. All authors contributed to the article and approved the final version.

## FUNDING

This work was supported by the Russian Foundation for Basic Research (grants 06-04-08279 and 11-04-00379).

## ACKNOWLEDGMENTS

The authors thank D. Gulyaev and T. Tortunova (IDB RAS) for help with electron microscopy and semi-thin sections, M. Gorobets and A. Golub (IDB RAS) for help with animal care, E. Tsitrin and V. Pochaev (Core Facility on Cell Technologies and Optical Research Methods in IDB RAS) for help with confocal microscopy, N. Lifantseva (IDB RAS) for help with qRT-PCR, and T. Nikonova for help with cell transplantations and animal surgery.

## SUPPLEMENTARY MATERIAL

The Supplementary Material for this article can be found online at: <https://www.frontiersin.org/articles/10.3389/fcell.2022.852071/full#supplementary-material>

## REFERENCES

- Andrews, P. W. (1988). Human Teratocarcinomas. *Biochim. Biophys. Acta (Bba) - Rev. Cancer* 948, 17–36. Available at: <http://view.ncbi.nlm.nih.gov/pubmed/3293662>. doi:10.1016/0304-419x(88)90003-0
- Armstrong, P. B. (1989). Cell Sorting Out: The Self-Assembly of Tissues In Vitro. *Crit. Rev. Biochem. Mol. Biol.* 24, 119–149. doi:10.3109/10409238909086396
- Bauwens, C. L., Peerani, R., Niebruegge, S., Woodhouse, K. A., Kumacheva, E., Husain, M., et al. (2008). Control of Human Embryonic Stem Cell Colony and Aggregate Size Heterogeneity Influences Differentiation Trajectories. *Stem Cells* 26, 2300–2310. doi:10.1634/stemcells.2008-0183
- Beddington, R. S. P., and Robertson, E. J. (1999). Axis Development and Early Asymmetry in Mammals. *Cell* 96, 195–209. Available at: <http://view.ncbi.nlm.nih.gov/pubmed/9988215>. doi:10.1016/s0092-8674(00)80560-7
- Bedzhov, I., and Zernicka-Goetz, M. (2014). Self-organizing Properties of Mouse Pluripotent Cells Initiate Morphogenesis upon Implantation. *Cell* 156, 1032–1044. doi:10.1016/j.cell.2014.01.023
- Bernstine, E. G., Hooper, M. L., Grandchamp, S., and Ephrussi, B. (1973). Alkaline Phosphatase Activity in Mouse Teratoma. *Proc. Natl. Acad. Sci. U.S.A.* 70, 3899–3903. doi:10.1073/pnas.70.12.3899
- Bratt-Leal, A. M., Carpenedo, R. L., and McDevitt, T. C. (2009). Engineering the Embryoid Body Microenvironment to Direct Embryonic Stem Cell Differentiation. *Biotechnol. Prog.* 25, 43–51. Available at: <http://view.ncbi.nlm.nih.gov/pubmed/19198003>. doi:10.1002/btpr.139
- Buehr, M., and McLaren, A. (1974). Size Regulation in Chimaeric Mouse Embryos. *J. Embryol. Exp. Morphol.* 31, 229–234. doi:10.1242/dev.31.1.229
- Burdon, T., Stracey, C., Chambers, I., Nichols, J., and Smith, A. (1999). Suppression of SHP-2 and ERK Signalling Promotes Self-Renewal of Mouse Embryonic Stem Cells. *Dev. Biol.* 210, 30–43. doi:10.1006/dbio.1999.9265
- Camacho-Aguilar, E., and Warmflash, A. (2020). “Insights Into Mammalian Morphogen Dynamics From Embryonic Stem Cell Systems,” in *Current Topics in Developmental Biology*, 279–305. doi:10.1016/bs.ctdb.2019.11.010
- Čapek, D., and Müller, P. (2019). Positional Information and Tissue Scaling during Development and Regeneration. *Dev* 146, dev17770. doi:10.1242/dev.177709
- Chaudhry, M. A., Vitalis, T. Z., Bowen, B. D., and Piret, J. M. (2008). Basal Medium Composition and Serum or Serum Replacement Concentration Influences on



- the Maintenance of Murine Embryonic Stem Cells. *Cytotechnology* 58, 173–179. doi:10.1007/s10616-008-9177-5
- Chhabra, S., Liu, L., Goh, R., Kong, X., and Warmflash, A. (2019). Dissecting the Dynamics of Signaling Events in the BMP, WNT, and NODAL cascade during Self-Organized Fate Patterning in Human Gastruloids. *Plos Biol.* 17, e3000498. doi:10.1371/journal.pbio.3000498
- Choi, J., Iich, E., and Lee, J.-H. (2016). Organogenesis of Adult Lung in a Dish: Differentiation, Disease and Therapy. *Dev. Biol.* 420, 278–286. doi:10.1016/j.ydbio.2016.10.002
- Coucouvanis, E., and Martin, G. R. (1995). Signals for Death and Survival: A Two-step Mechanism for Cavitation in the Vertebrate Embryo. *Cell* 83, 279–287. doi:10.1016/0092-8674(95)90169-8
- Dang, S. M., Kyba, M., Perlingeiro, R., Daley, G. Q., and Zandstra, P. W. (2002). Efficiency of Embryoid Body Formation and Hematopoietic Development from Embryonic Stem Cells in Different Culture Systems. *Biotechnol. Bioeng.* 78, 442–453. Available at: <http://view.ncbi.nlm.nih.gov/pubmed/11948451>. doi:10.1002/bit.10220
- Datta, A., Bryant, D. M., and Mostov, K. E. (2011). Molecular Regulation of Lumen Morphogenesis. *Curr. Biol.* 21, R126–R136. doi:10.1016/j.cub.2010.12.003
- Degincerti, A., Etoc, F., Guerra, M. C., Martyn, I., Metzger, J., Ruza, A., et al. (2016). Self-organization of Human Embryonic Stem Cells on Micropatterns. *Nat. Protoc.* 11, 2223–2232. doi:10.1038/nprot.2016.131
- Doetschman, T. C., Eistetter, H., Katz, M., Schmidt, W., and Kemler, R. (1985). The *In Vitro* Development of Blastocyst-Derived Embryonic Stem Cell Lines: Formation of Visceral Yolk Sac, Blood Islands and Myocardium. *J. Embryol. Exp. Morphol.* 87, 27–45. doi:10.1242/dev.87.1.27
- Ducibella, T., Anderson, D., Aalberg, J., and DeWolf, W. C. (1982). Cell Surface Polarization, Tight Junctions, and Eccentric Inner Cells Characterize Human Teratocarcinoma Embryoid Bodies. *Dev. Biol.* 94, 197–205. doi:10.1016/0012-1606(82)90083-5
- Durcova-Hills, G., Wianny, F., Merriman, J., Zernicka-Goetz, M., and McLaren, A. (2003). Developmental Fate of Embryonic Germ Cells (EGCs), *In Vivo* and *In Vitro*. *Differentiation* 71, 135–141. Available at: <http://view.ncbi.nlm.nih.gov/pubmed/12641567>. doi:10.1046/j.1432-0436.2003.710204.x
- Dutta, D., Heo, I., and Clevers, H. (2017). Disease Modeling in Stem Cell-Derived 3D Organoid Systems. *Trends Mol. Med.* 23, 393–410. doi:10.1016/j.molmed.2017.02.007
- El Azhar, Y., and Sonnen, K. F. (2021). Development in a Dish-In Vitro Models of Mammalian Embryonic Development. *Front. Cell Dev. Biol.* 9, 655993. doi:10.3389/fcell.2021.655993
- Eliesen, G. A. M., van Hove, H., Meijer, M. H., van den Broek, P. H. H., Pertijs, J., Roeleveld, N., et al. (2021). Toxicity of Anticancer Drugs in Human Placental Tissue Explants and Trophoblast Cell Lines. *Arch. Toxicol.* 95, 557–571. doi:10.1007/s00204-020-02925-w
- Etoc, F., Metzger, J., Ruza, A., Kirst, C., Yoney, A., Ozair, M. Z., et al. (2016). A Balance between Secreted Inhibitors and Edge Sensing Controls Gastruloid Self-Organization. *Dev. Cell* 39, 302–315. doi:10.1016/j.devcel.2016.09.016
- Flamier, A. (2018). “Use of Embryoid Bodies for the Detection of Teratogens and Analysis of Teratogenic Mechanisms,” in *Stem Cells in Birth Defects Research and Developmental Toxicology*, 59–69. doi:10.1002/9781119283249.ch3
- Frankenberg, S., Gerbe, F., Bessonard, S., Belville, C., Pouchin, P., Bardot, O., et al. (2011). Primitive Endoderm Differentiates via a Three-Step Mechanism Involving Nanog and RTK Signaling. *Dev. Cell* 21, 1005–1013. doi:10.1016/j.devcel.2011.10.019
- Fujikura, J., Yamato, E., Yonemura, S., Hosoda, K., Masui, S., Nakao, K., et al. (2002). Differentiation of Embryonic Stem Cells Is Induced by GATA Factors. *Genes Dev.* 16, 784–789. doi:10.1101/gad.968802
- Garcia-Gonzalo, F. R., and Belmonte, J. C. I. (2008). Albumin-associated Lipids Regulate Human Embryonic Stem Cell Self-Renewal. *PLoS One* 3, e1384. doi:10.1371/journal.pone.0001384
- Giobbe, G. G., Zagallo, M., Riello, M., Serena, E., Masi, G., Barzon, L., et al. (2012). Confined 3D Microenvironment Regulates Early Differentiation in Human Pluripotent Stem Cells. *Biotechnol. Bioeng.* 109, 3119–3132. Available at: <http://view.ncbi.nlm.nih.gov/pubmed/22674472>. doi:10.1002/bit.24571
- Gordeeva, O., and Gordeev, A. (2021). Comparative Assessment of Toxic Responses in 3D Embryoid Body Differentiation Model and Mouse Early Embryos Treated with 5-hydroxytryptophan. *Arch. Toxicol.* 95, 253–269. doi:10.1007/s00204-020-02909-w
- Gordeeva, O., and Khaydukov, S. (2017). Tumorigenic and Differentiation Potentials of Embryonic Stem Cells Depend on TGF  $\beta$  Family Signaling: Lessons from Teratocarcinoma Cells Stimulated to Differentiate with Retinoic Acid. *Stem Cell Int.* 2017, 1–14. doi:10.1155/2017/7284872
- Gordeeva, O. F., and Nikonova, T. M. (2013). Development of Experimental Tumors Formed by Mouse and Human Embryonic Stem and Teratocarcinoma Cells after Subcutaneous and Intraperitoneal Transplantations into Immunodeficient and Immunocompetent Mice. *Cel. Transpl.* 22, 1901–1914. doi:10.3727/096368912X657837
- Gordeeva, O., Gordeev, A., and Khaydukov, S. (2019). Expression Dynamics of Mage Family Genes during Self-Renewal and Differentiation of Mouse Pluripotent Stem and Teratocarcinoma Cells. *Oncotarget* 10, 3248–3266. doi:10.18632/oncotarget.26933
- Greaves, R. B., Dietmann, S., Smith, A., Stepney, S., and Halley, J. D. (2017). A Conceptual and Computational Framework for Modelling and Understanding the Non-equilibrium Gene Regulatory Networks of Mouse Embryonic Stem Cells. *Plos Comput. Biol.* 13, e1005713. doi:10.1371/journal.pcbi.1005713
- Green, J. B. A., and Sharpe, J. (2015). Positional Information and Reaction-Diffusion: Two Big Ideas in Developmental Biology Combine. *Dev* 142, 1203–1211. doi:10.1242/dev.114991
- Guo, J., Wang, P., Sozen, B., Qiu, H., Zhu, Y., Zhang, X., et al. (2021). Machine Learning-Assisted High-Content Analysis of Pluripotent Stem Cell-Derived Embryos *In Vitro*. *Stem Cell Rep.* 16, 1331–1346. doi:10.1016/j.stemcr.2021.03.018
- Halley, J. D., Burden, F. R., and Winkler, D. A. (2009). Stem Cell Decision Making and Critical-like Exploratory Networks. *Stem Cell Res.* 2, 165–177. doi:10.1016/j.scr.2009.03.001
- Halley, J. D., Smith-Miles, K., Winkler, D. A., Kalkan, T., Huang, S., and Smith, A. (2012). Self-organizing Circuitry and Emergent Computation in Mouse Embryonic Stem Cells. *Stem Cell Res.* 8, 324–333. doi:10.1016/j.scr.2011.11.001
- Harrison, S. E., Sozen, B., Christodoulou, N., Kyprianou, C., and Zernicka-Goetz, M. (2017). Assembly of Embryonic and Extraembryonic Stem Cells to Mimic Embryogenesis *In Vitro*. *Science* 356, eaal1810. doi:10.1126/science.aal1810
- Jerber, J., Seaton, D. D., Seaton, D. D., Cuomo, A. S. E., Kumasaka, N., Haldane, J., et al. (2021). Population-scale Single-Cell RNA-Seq Profiling across Dopaminergic Neuron Differentiation. *Nat. Genet.* 53, 304–312. doi:10.1038/s41588-021-00801-6
- Kagawa, H., Javali, A., Khoei, H. H., Sommer, T. M., Sestini, G., Novatchkova, M., et al. (2021). Human Blastoids Model Blastocyst Development and Implantation. *Nature* 601, 600–605. doi:10.1038/s41586-021-04267-8
- Kang, H. Y., Choi, Y.-K., Jo, N. R., Lee, J.-H., Ahn, C., Ahn, I. Y., et al. (2017). Advanced Developmental Toxicity Test Method Based on Embryoid Body's Area. *Reprod. Toxicol.* 72, 74–85. doi:10.1016/j.reprotox.2017.06.185
- Kelly, G. M., and Gatie, M. I. (2017). Mechanisms Regulating Stemness and Differentiation in Embryonal Carcinoma Cells. *Stem Cell Int.* 2017, 3684178. Available at: <https://view.ncbi.nlm.nih.gov/pubmed/28373885>. doi:10.1155/2017/3684178
- Kim, J., Koo, B.-K., and Knoblich, J. A. (2020). Human Organoids: Model Systems for Human Biology and Medicine. *Nat. Rev. Mol. Cell Biol.* 21, 571–584. doi:10.1038/s41580-020-0259-3
- Lewis, N. E., and Rossant, J. (1982). Mechanism of Size Regulation in Mouse Embryo Aggregates. *J. Embryol. Exp. Morphol.* 72, 169–181. doi:10.1242/dev.72.1.169
- Liu, G., David, B. T., Trawczynski, M., and Fessler, R. G. (2020). Advances in Pluripotent Stem Cells: History, Mechanisms, Technologies, and Applications. *Stem Cell Rev. Rep.* 16, 3–32. doi:10.1007/s12015-019-09935-x
- Loebel, D. A. F., Watson, C. M., De Young, R. A., and Tam, P. P. L. (2003). Lineage Choice and Differentiation in Mouse Embryos and Embryonic Stem Cells. *Dev. Biol.* 264, 1–14. Available at: <http://view.ncbi.nlm.nih.gov/pubmed/14623228>. doi:10.1016/s0012-1606(03)00390-7
- Maeda, T. T., Ajioka, I., and Nakajima, K. (2007). Computational Cell Model Based on Autonomous Cell Movement Regulated by Cell-Cell Signalling Successfully Recapitulates the “inside and outside” Pattern of Cell Sorting. *BMC Syst. Biol.* 1, 43. doi:10.1186/1752-0509-1-43
- Marikawa, Y., and Alarcon, V. B. (2012). Creation of Trophectoderm, the First Epithelium, in Mouse Preimplantation Development. *Results Probl. Cell Differ.* 55, 165–184. doi:10.1007/978-3-642-30406-4\_9

- Martin, G. R., and Evans, M. J. (1975). Differentiation of Clonal Lines of Teratocarcinoma Cells: Formation of Embryoid Bodies *In Vitro*. *Proc. Natl. Acad. Sci. U.S.A.* 72, 1441–1445. doi:10.1073/pnas.72.4.1441
- Martin, G. R., Wiley, L. M., and Damjanov, I. (1977). The Development of Cystic Embryoid Bodies *In Vitro* from Clonal Teratocarcinoma Stem Cells. *Dev. Biol.* 61, 230–244. doi:10.1016/0012-1606(77)90294-9
- Molè, M. A., Coorens, T. H. H., Shahbazi, M. N., Weberling, A., Weatherbee, B. A. T., Gantner, C. W., et al. (2021). A Single Cell Characterisation of Human Embryogenesis Identifies Pluripotency Transitions and Putative Anterior Hypoblast centre. *Nat. Commun.* 12, 3679. doi:10.1038/s41467-021-23758-w
- Moore, E. E., Mitra, N. S., and Moritz, E. A. (1986). Differentiation of F9 Embryonal Carcinoma Cells: Differences in the Effects of Retinoic Acid, 5-bromodeoxyuridine, and N'-N'-dimethylacetamide. *Differentiation* 31, 183–190. doi:10.1111/j.1432-0436.1986.tb00399.x
- Morris, S. A., Grewal, S., Barrios, F., Patankar, S. N., Strauss, B., Buttery, L., et al. (2012). Dynamics of Anterior-Posterior axis Formation in the Developing Mouse Embryo. *Nat. Commun.* 3, 673. doi:10.1038/ncomms1671
- Nagy, A., Rossant, J., Nagy, R., Abramow-Newerly, W., and Roder, J. C. (1993). Derivation of Completely Cell Culture-Derived Mice from Early-Passage Embryonic Stem Cells. *Proc. Natl. Acad. Sci. U.S.A.* 90, 8424–8428. doi:10.1073/pnas.90.18.8424
- Oh, Y., and Jang, J. (2019). Directed Differentiation of Pluripotent Stem Cells by Transcription Factors. *Mol. Cell* 42, 200–209. doi:10.14348/molcells.2019.2439
- Orietti, L. C., Rosa, V. S., Antonica, F., Kyprianou, C., Mansfield, W., Marques-Souza, H., et al. (2021). Embryo Size Regulates the Timing and Mechanism of Pluripotent Tissue Morphogenesis. *Stem Cell Rep.* 16, 1182–1196. doi:10.1016/j.stemcr.2020.09.004
- Ortmann, D., and Vallier, L. (2017). Variability of Human Pluripotent Stem Cell Lines. *Curr. Opin. Genet. Dev.* 46, 179–185. doi:10.1016/J.GDE.2017.07.004
- Pantazis, P., and Bollenbach, T. (2012). Transcription Factor Kinetics and the Emerging Asymmetry in the Early Mammalian Embryo. *Cell Cycle* 11, 2055–2058. doi:10.4161/cc.20118
- Plachta, N., Bollenbach, T., Pease, S., Fraser, S. E., and Pantazis, P. (2011). Oct4 Kinetics Predict Cell Lineage Patterning in the Early Mammalian Embryo. *Nat. Cell Biol.* 13, 117–123. doi:10.1038/ncb2154
- Renner, M., Lancaster, M. A., Bian, S., Choi, H., Ku, T., Peer, A., et al. (2017). Self-organized Developmental Patterning and Differentiation in Cerebral Organoids. *EMBO J.* 36, 1316–1329. doi:10.15252/embj.201694700
- Revell, C., Blumenfeld, R., and Chalut, K. J. (2019). Force-based Three-Dimensional Model Predicts Mechanical Drivers of Cell Sorting. *Proc. R. Soc. B.* 286, 20182495. doi:10.1098/rspb.2018.2495
- Rivera-Pérez, J. A., and Hadjantonakis, A.-K. (2015). The Dynamics of Morphogenesis in the Early Mouse Embryo. *Cold Spring Harb. Perspect. Biol.* 7, a015867. doi:10.1101/cshperspect.a015867
- Rivron, N. C., Frias-Aldeguer, J., Vrij, E. J., Boisset, J.-C., Korving, J., Vivié, J., et al. (2018). Blastocyst-like Structures Generated Solely from Stem Cells. *Nature* 557, 106–111. doi:10.1038/s41586-018-0051-0
- Rizzino, A., and Crowley, C. (1980). Growth and Differentiation of Embryonal Carcinoma Cell Line F9 in Defined media. *Proc. Natl. Acad. Sci. U.S.A.* 77, 457–461. doi:10.1073/pnas.77.1.457
- Robertson, E., Bradley, A., Kuehn, M., and Evans, M. (1986). Germ-Line Transmission of Genes Introduced into Cultured Pluripotential Cells by Retroviral Vector. *Nature* 323, 445–448. doi:10.1038/323445a0
- Rossi, G., Manfrin, A., and Lutolf, M. P. (2018). Progress and Potential in Organoid Research. *Nat. Rev. Genet.* 19, 671–687. doi:10.1038/s41576-018-0051-9
- Scalise, M., Marino, F., Salerno, L., Cianflone, E., Molinaro, C., Salerno, N., et al. (2021). From Spheroids to Organoids: The Next Generation of Model Systems of Human Cardiac Regeneration in a Dish. *Ijms* 22, 13180. doi:10.3390/ijms222413180
- Shahbazi, M. N., Siggia, E. D., and Zernicka-Goetz, M. (2019). Self-organization of Stem Cells into Embryos: A Window on Early Mammalian Development. *Science* 364, 948–951. doi:10.1126/science.aax0164
- Sharova, L. V., Sharov, A. A., Piao, Y., Shaik, N., Sullivan, T., Stewart, C. L., et al. (2007). Global Gene Expression Profiling Reveals Similarities and Differences Among Mouse Pluripotent Stem Cells of Different Origins and Strains. *Dev. Biol.* 307, 446–459. Available at: <http://view.ncbi.nlm.nih.gov/pubmed/17560561>. doi:10.1016/j.ydbio.2007.05.004
- Shim, S. W., Han, D. W., Yang, J. H., Lee, B. Y., Kim, S. B., Shim, H., et al. (2008). Derivation of Embryonic Germ Cells from post Migratory Primordial Germ Cells, and Methylation Analysis of Their Imprinted Genes by Bisulfite Genomic Sequencing. *Mol. Cell* 25, 358–367.
- Smith, L. J. (1980). Embryonic axis Orientation in the Mouse and its Correlation with Blastocyst Relationships to the Uterus. *Development* 55, 257–277. doi:10.1242/dev.55.1.257
- Sozen, B., Amadei, G., Cox, A., Wang, R., Na, E., Czukiewska, S., et al. (2018). Self-assembly of Embryonic and Two Extra-embryonic Stem Cell Types into Gastrulating Embryo-like Structures. *Nat. Cell Biol.* 20, 979–989. doi:10.1038/s41556-018-0147-7
- Sozen, B., Cox, A. L., De Jonghe, J., Bao, M., Hollfelder, F., Glover, D. M., et al. (2019). Self-Organization of Mouse Stem Cells into an Extended Potential Blastoid. *Dev. Cell* 51, 698–712.e8. doi:10.1016/j.devcel.2019.11.014
- Sozen, B., Cornwall-Scoones, J., and Zernicka-Goetz, M. (2021). The Dynamics of Morphogenesis in Stem Cell-Based Embryology: Novel Insights for Symmetry Breaking. *Dev. Biol.* 474, 82–90. doi:10.1016/j.ydbio.2020.12.005
- Tam, P. P. L., and Behringer, R. R. (1997). Mouse Gastrulation: The Formation of a Mammalian Body Plan. *Mech. Dev.* 68, 3–25. doi:10.1016/S0925-4773(97)00123-8
- Tarkowski, A. K. (1963). Studies on Mouse Chimeras Developed from Eggs Fused *In Vitro*. *Natl. Cancer Inst. Monogr.* 11, 51–71.
- ten Berge, D., Koole, W., Fuerer, C., Fish, M., Eroglu, E., and Nusse, R. (2008). Wnt Signaling Mediates Self-Organization and axis Formation in Embryoid Bodies. *Cell Stem Cell* 3, 508–518. Available at: <http://view.ncbi.nlm.nih.gov/pubmed/18983966>. doi:10.1016/j.stem.2008.09.013
- Tewary, M., Ostblom, J., Prochazka, L., Zulueta-Coarasa, T., Shakiba, N., Fernandez-Gonzalez, R., et al. (2017). A Stepwise Model of Reaction-Diffusion and Positional-Information Governs Self-Organized Human Perigastrulation-like Patterning. *Dev* 144, 4298–4312. doi:10.1242/dev.149658
- Turing, A. M. (1952). The Chemical Basis of Morphogenesis. *Philos. Trans. R. Soc. Lond. B. Biol. Sci.* 237, 37–72.
- Umulis, D. M., and Othmer, H. G. (2013). Mechanisms of Scaling in Pattern Formation. *Development* 140, 4830–4843. doi:10.1242/dev.100511
- van den Brink, S. C., and van Oudenaarden, A. (2021). 3D Gastruloids: a Novel Frontier in Stem Cell-Based *In Vitro* Modeling of Mammalian Gastrulation. *Trends Cell Biol.* 31, 747–759. doi:10.1016/j.tcb.2021.06.007
- Van Den Brink, S. C., Baillie-Johnson, P., Balayo, T., Hadjantonakis, A.-K., Nowotschin, S., Turner, D. A., et al. (2014). Symmetry Breaking, Germ Layer Specification and Axial Organisation in Aggregates of Mouse Embryonic Stem Cells. *Dev* 141, 4231–4242. doi:10.1242/dev.113001
- van den Brink, S. C., Alemany, A., van Batenburg, V., Moris, N., Blotenburg, M., Vivié, J., et al. (2020). Single-cell and Spatial Transcriptomics Reveal Somatogenesis in Gastruloids. *Nature* 582, 405–409. doi:10.1038/s41586-020-2024-3
- van der Valk, J., Brunner, D., De Smet, K., Fex Svenningsen, Å., Honegger, P., Knudsen, L. E., et al. (2010). Optimization of Chemically Defined Cell Culture media - Replacing Fetal Bovine Serum in Mammalian *In Vitro* Methods. *Toxicol. Vitro* 24, 1053–1063. doi:10.1016/j.tiv.2010.03.016
- Van Winkle, A. P., Gates, I. D., and Kallos, M. S. (2012). Mass Transfer Limitations in Embryoid Bodies during Human Embryonic Stem Cell Differentiation. *Cells Tissues Organs* 196, 34–47. doi:10.1159/000330691
- Wahlin, K. J., Cheng, J., Jurlina, S. L., Jones, M. K., Dash, N. R., Ogata, A., et al. (2021). CRISPR Generated SIX6 and POU4F2 Reporters Allow Identification of Brain and Optic Transcriptional Differences in Human PSC-Derived Organoids. *Front. Cell Dev. Biol.* 9, 3077. doi:10.3389/fcell.2021.764725
- Warkus, E. L. L., Yuen, A. A. Y. Q., Lau, C. G. Y., and Marikawa, Y. (2016). Use of *In Vitro* Morphogenesis of Mouse Embryoid Bodies to Assess Developmental Toxicity of Therapeutic Drugs Contraindicated in Pregnancy. *Toxicol. Sci.* 149, 15–30. doi:10.1093/toxsci/kfv209
- Warmflash, A., Sorre, B., Etoc, F., Siggia, E. D., and Brivanlou, A. H. (2014). A Method to Recapitulate Early Embryonic Spatial Patterning in Human Embryonic Stem Cells. *Nat. Methods* 11, 847–854. doi:10.1038/nmeth.3016
- Wartenberg, M., DÖNmez, F., C. Ling, F., Acker, H., Hescheler, J., and Sauer, H. (2001). Tumor-induced Angiogenesis Studied in Confrontation Cultures of Multicellular Tumor Spheroids and Embryoid Bodies Grown from Pluripotent Embryonic Stem Cells. *FASEB j.* 15, 995–1005. doi:10.1096/15.26.000350com

- Weberling, A., and Zernicka-Goetz, M. (2021). Trophectoderm Mechanics Direct Epiblast Shape upon Embryo Implantation. *Cel Rep.* 34, 108655. doi:10.1016/j.celrep.2020.108655
- Weinberger, L., Ayyash, M., Novershtern, N., and Hanna, J. H. (2016). Dynamic Stem Cell States: Naive to Primed Pluripotency in Rodents and Humans. *Nat. Rev. Mol. Cel Biol.* 17, 155–169. Available at: <https://view.ncbi.nlm.nih.gov/pubmed/26860365>. doi:10.1038/nrm.2015.28
- White, M. D., Zenker, J., Bissiere, S., and Plachta, N. (2018). Instructions for Assembling the Early Mammalian Embryo. *Dev. Cel.* 45, 667–679. doi:10.1016/j.devcel.2018.05.013
- Wobus, A. M., and Boheler, K. R. (2005). Embryonic Stem Cells: Prospects for Developmental Biology and Cell Therapy. *Physiol. Rev.* 85, 635–678. doi:10.1152/physrev.00054.2003
- Wolpert, L. (1981). Positional Information and Pattern Formation. *Phil. Trans. R. Soc. Lond. B* 295, 441–450. doi:10.1098/rstb.1981.0152
- Yu, L., Wei, Y., Duan, J., Schmitz, D. A., Sakurai, M., Wang, L., et al. (2021). Blastocyst-like Structures Generated from Human Pluripotent Stem Cells. *Nature* 591, 620–626. doi:10.1038/s41586-021-03356-y
- Zheng, X., Baker, H., Hancock, W. S., Fawaz, F., McCaman, M., and Pungor, E. (2006). Proteomic Analysis for the Assessment of Different Lots of Fetal Bovine Serum as a Raw Material for Cell Culture. Part IV. Application of Proteomics to the Manufacture of Biological Drugs. *Biotechnol. Prog.* 22, 1294–1300. doi:10.1021/bp060121o
- Zheng, Y., Xue, X., Shao, Y., Wang, S., Esfahani, S. N., Li, Z., et al. (2019). Controlled Modelling of Human Epiblast and Amnion Development Using Stem Cells. *Nature* 573, 421–425. doi:10.1038/s41586-019-1535-2
- Zhu, M., and Zernicka-Goetz, M. (2020). Principles of Self-Organization of the Mammalian Embryo. *Cell* 183, 1467–1478. doi:10.1016/j.cell.2020.11.003

**Conflict of Interest:** The authors declare that the research was conducted in the absence of any commercial or financial relationships that could be construed as a potential conflict of interest.

**Publisher's Note:** All claims expressed in this article are solely those of the authors and do not necessarily represent those of their affiliated organizations, or those of the publisher, the editors and the reviewers. Any product that may be evaluated in this article, or claim that may be made by its manufacturer, is not guaranteed or endorsed by the publisher.

Copyright © 2022 Gordeeva, Gordeev and Erokhov. This is an open-access article distributed under the terms of the Creative Commons Attribution License (CC BY). The use, distribution or reproduction in other forums is permitted, provided the original author(s) and the copyright owner(s) are credited and that the original publication in this journal is cited, in accordance with accepted academic practice. No use, distribution or reproduction is permitted which does not comply with these terms.



# Pancreatic Organoids for Regenerative Medicine and Cancer Research

Joan Casamitjana<sup>1,2,3</sup>, Elisa Espinet<sup>4,5\*</sup> and Meritxell Rovira<sup>1,2,3\*</sup>

<sup>1</sup>Department of Physiological Science, School of Medicine, University of Barcelona (UB), L'Hospitalet de Llobregat, Barcelona, Spain, <sup>2</sup>Pancreas Regeneration: Pancreatic Progenitors and Their Niche Group, Regenerative Medicine Program, Institut D'Investigació Biomèdica de Bellvitge (IDIBELL), L'Hospitalet de Llobregat, Barcelona, Spain, <sup>3</sup>Program for Advancing the Clinical Translation of Regenerative Medicine of Catalonia (P-CMR[C]), L'Hospitalet de Llobregat, Barcelona, Spain, <sup>4</sup>Department of Pathology and Experimental Therapy, School of Medicine, University of Barcelona (UB), L'Hospitalet de Llobregat, Barcelona, Spain, <sup>5</sup>Molecular Mechanisms and Experimental Therapy in Oncology Program (Oncobell), Institut D'Investigació Biomèdica de Bellvitge (IDIBELL), L'Hospitalet de Llobregat, Barcelona, Spain

## OPEN ACCESS

### Edited by:

Ying Gu,  
Beijing Genomics Institute (BGI), China

### Reviewed by:

Luis Arnes,  
University of Copenhagen, Denmark  
Orest William Blaschuk,  
Zonula Inc., Canada

### \*Correspondence:

Elisa Espinet  
elisa.espinet@gmail.com  
Meritxell Rovira  
mrovira@idibell.cat

### Specialty section:

This article was submitted to  
Stem Cell Research,  
a section of the journal  
Frontiers in Cell and Developmental  
Biology

**Received:** 28 February 2022

**Accepted:** 06 April 2022

**Published:** 03 May 2022

### Citation:

Casamitjana J, Espinet E and Rovira M  
(2022) Pancreatic Organoids for  
Regenerative Medicine and  
Cancer Research.  
Front. Cell Dev. Biol. 10:886153.  
doi: 10.3389/fcell.2022.886153

In recent years, the development of *ex vivo* organoid cultures has gained substantial attention as a model to study regenerative medicine and diseases in several tissues. Diabetes and pancreatic ductal adenocarcinoma (PDAC) are the two major devastating diseases affecting the pancreas. Suitable models for regenerative medicine in diabetes and to accurately study PDAC biology and treatment response are essential in the pancreatic field. Pancreatic organoids can be generated from healthy pancreas or pancreatic tumors and constitute an important translational bridge between *in vitro* and *in vivo* models. Here, we review the rapidly emerging field of pancreatic organoids and summarize the current applications of the technology to tissue regeneration, disease modelling, and drug screening.

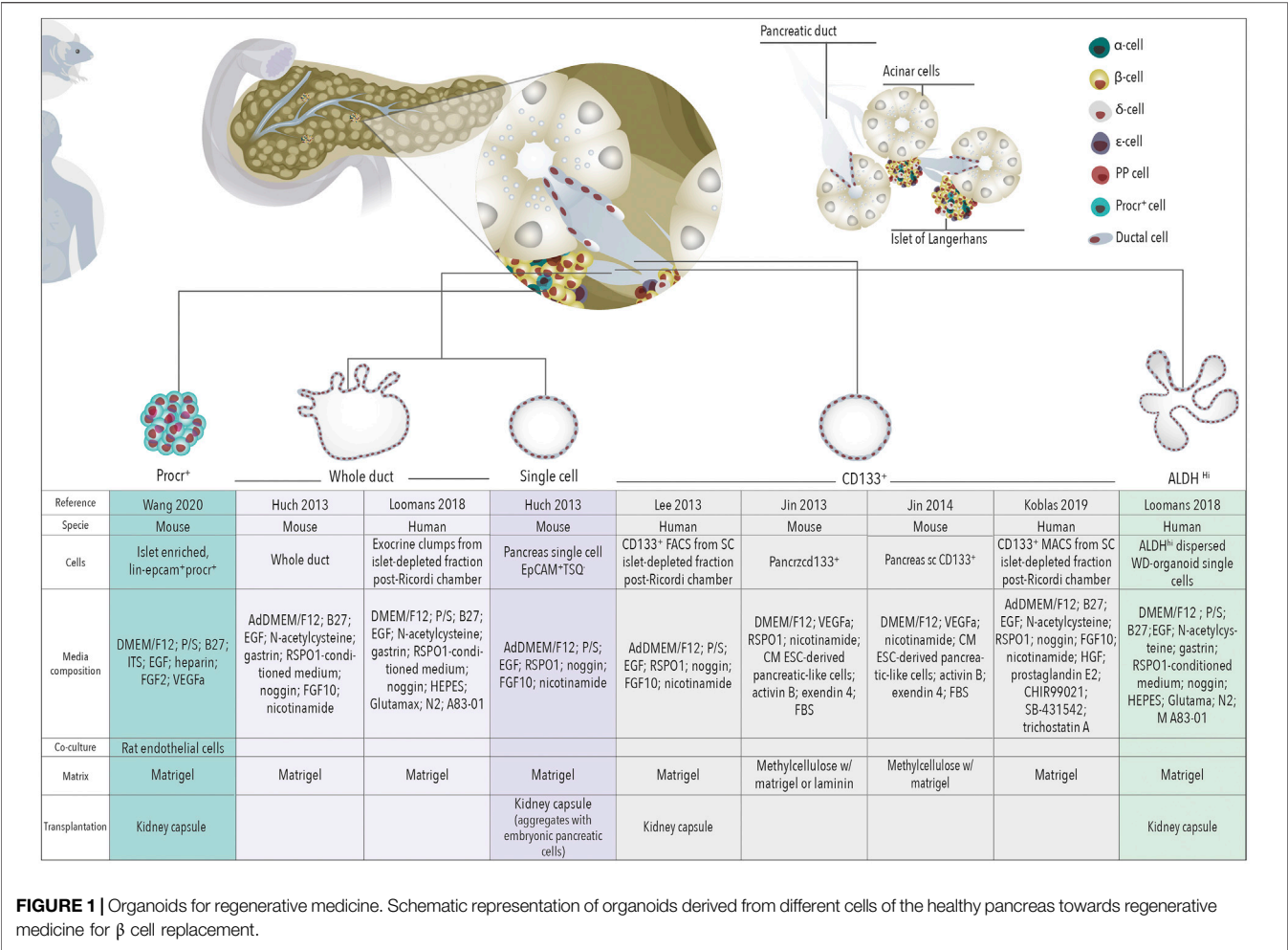
**Keywords:** organoids, pancreas, PDAC, diabetes, regenerative medicine, personalized medicine

## INTRODUCTION

The pancreas is an endoderm derived gland with an endocrine and an exocrine compartment. The endocrine compartment is formed by hormone producing cells that regulate blood glucose levels. Within the most abundant endocrine cells we find insulin producing  $\beta$  cells, glucagon producing  $\alpha$  cells, somatostatin producing  $\delta$  cells, and pancreatic polypeptide producing PP cells (**Figure 1**). They are organized in highly vascularized clusters termed Islets of Langerhans, which comprise ~1–2% of the organ (Wang et al., 2016; Marsee et al., 2021). The rest of the gland displays an exocrine function. Exocrine pancreas is mainly formed by acinar cells, organized in acini, which produce and secrete digestive enzymes that are transported into the duodenum through an intricate network of tubules formed by the other exocrine cell type, the ductal cells, which secrete bicarbonate to neutralize stomach acidity (Grapin-Botton, 2005) (**Figure 1**).

Dysregulation of either the endocrine or the exocrine pancreas results in two major diseases: diabetes mellitus and pancreatic ductal adenocarcinoma (PDAC), respectively. Diabetes is a metabolic disorder characterized by loss or dysfunction of pancreatic  $\beta$  cells. There are 537 million adults (20–79 years) living with diabetes and its prevalence is increasing and predicted to rise to 643 million by 2030 (IDF Diabetes Atlas 10th edition), making diabetes a major public health challenge worldwide. Current treatments for insulin-dependent diabetic people are based on multiple insulin injections coupled with regular blood glucose monitoring (Melton,





2021). Although there have been major advances in pharmacogenetic findings of antidiabetic agents, patients and their families still don't live free from the constant burden of monitoring blood glucose levels, insulin pumps, diet and exercise. Importantly, transplantation of cadaveric islets arose as a promising therapy option leading to impressive results on insulin independence (Hering et al., 2016; Lablanche et al., 2018; Shapiro et al., 2000). However, access to islets is limited by the number of deceased donors. Additionally, transplantation requires the life-long induced immunosuppression of the patient (Vantyghem et al., 2019). Together, these preclude the widespread use of cadaveric islet transplantation to treat diabetes. Alternative cell replacement therapies to find an unlimited source of  $\beta$  cells have been investigated for the last couple of decades. On the one hand, protocols have been developed to induce endocrine cells differentiation, specially  $\beta$  cells, from human embryonic stem cells (ESC) (Balboa et al., 2022; Rezanian et al., 2014) and induced pluripotent stem cells (iPSC) (Nostro et al., 2011). These cells have recently been reported to be able to produce insulin in human patients using macroencapsulation systems in two phase I/II clinical trials (clinicaltrials.gov). The first reports of one of the trials have been recently released showing device safety and insulin

secretion from engrafted pluripotent stem cell-derived pancreatic progenitor cells in patients with type 1 diabetes (Ramzy et al., 2021; Shapiro et al., 2021). On the other hand, multiple adult pancreatic cell types have been identified to be able to give rise to  $\beta$  cells and are being investigated as inducible endogenous progenitors (Afelik and Rovira, 2017), specially using organoid cultures.

Pancreatic ductal adenocarcinoma (PDAC) is one of the deadliest types of cancer with a 5-year survival rate of approximately 9%. PDAC is the third cause of cancer related death in the United States and Europe behind lung and colorectal cancer and its incidence is estimated to increase in the next years (Siegel et al., 2020). The main reasons for such a devastating outcome are late detection and poor response to treatment. This highlights the urgent need for appropriate models to study tumor onset and for platforms that allow the investigation of more efficacious therapies. Unfortunately, genetic mouse models do not fully recapitulate the complex human scenario and the study of human early disease is challenging as the majority of patients are diagnosed in an advanced disease stage. Similarly, access to large amounts of human primary material for direct drug testing studies is typically limited as only 20% of PDAC patients are eligible for resection and fine needle biopsies from non-resectable

patients result in recovery of too few tumor cells. Organoid models appear as an attractive model in the field of pancreatic cancer research to overcome these limitations.

Organoids are 3D *in vitro* models of self-renewing cells, which spontaneously self-organize into structures with similarities to their corresponding *in vivo* tissue (Marsee et al., 2021; **Box 1**). Organoids can be used to study healthy or diseased tissue and can be generated from embryonic progenitors, adult-derived stem/progenitor cells, tumor samples or differentiated from pluripotent stem cells (iPSC/ESC). Although the capacity of pancreatic organoids derived from healthy tissue to recapitulate tissue differentiation and architecture is limited, pancreatic organoids open a window of opportunity to develop regenerative medicine therapies for diabetes and disease modeling. Additionally, PDAC derived organoids can be used for the development of personalized medicine therapies and drug screening. In this review we highlight the advances made in the development and use of pancreatic organoids in these topics and discuss the future challenges in this fast-developing field.

## HEALTHY TISSUE DERIVED ORGANOIDS FOR REGENERATIVE MEDICINE

Highly proliferative tissues such as intestine and skin harbor a significant pool of progenitors (Gonzales and Fuchs, 2017; McCarthy et al., 2020), which comprise ~5–8% of the tissue and allow its renewal in homeostatic conditions or upon injury (Gonzales and Fuchs, 2017; Guiu et al., 2019). Other tissues such as liver, display a low turn-over of cells in homeostasis and only specific cells proliferate upon injury to regenerate the damaged tissue (Campana et al., 2021). The pancreas does not display regenerative ability in homeostasis nor upon injury and therefore has limited capacity for regeneration, specially the endocrine compartment (Zhou and Melton, 2018). Although in the last couple of decades many laboratories have investigated the presence of pancreatic progenitors in the adult tissue to

identify an unlimited source of  $\beta$  cells for replacement therapies, to date, most lineage tracing reports suggest that dedicated progenitors do not exist in this gland. Instead, some terminal differentiated pancreatic lineages, such as acinar, ductal and endocrine cells (Afelik and Rovira, 2017), have the ability to give rise to  $\beta$  cells under specific injury models pointing out at high pancreatic plasticity.

Acinar cell potential to give rise to  $\beta$  cells has been investigated showing none or extremely low efficiency in homeostasis and regenerative conditions (Pan and Wright, 2011). However, acinar cells display high plasticity or transdifferentiation capacity when compared to other pancreatic cells. Thus, acinar cells have been reprogrammed *in vivo* into insulin expressing cells upon lentiviral infection of three master regulators of endocrine differentiation, Neurog3, Pdx1, and MafA (Azzarelli et al., 2017). Recently it has been described that inflammation plays and important role in acinar to  $\beta$  transdifferentiation thus only when inflammation is attenuated, either by reducing the intensity of transcription factor expression or by depleting macrophages, the production of new  $\beta$ -like cells occur (Clayton et al., 2016). Moreover, *in vitro* murine and human acinar cells transdifferentiate into an embryonic-like phenotype (Houbracken et al., 2011; Pinho et al., 2011). Therefore, delineating acinar cell culture conditions may uncover acinar-to- $\beta$ -cell transdifferentiation in the future.

Both acinar and ductal cells can initiate organoid cultures, therefore containing proliferative cells or cells able to enter the cell cycle. Nevertheless, only ductal cells are able to form organoids that can be expanded and maintained *in vitro* over time while acinar cells cannot (Huch et al., 2013). This implies that having proliferative capacity is not sufficient to efficiently form organoids. Cells should also require a certain degree of cellular plasticity *in vitro* which seem to be exclusive to ductal cells. As the capacity of organoids to expand over numerous passages proves the presence of stem/progenitor cells in the original preparation and has been linked to the existence of adult progenitors in other tissues, these results suggest that, in the pancreas, progenitors are likely located in the ductal compartment. Although, so far, the capacity of pancreatic

### BOX 1 | Pancreatic 3D Cultures

**Aggregates:** Cell aggregates are formed by artificially forcing cells to grow together in culture. Most common methods include use of low attachment culture plates, agarose micro-wells or hanging-drop cultures that pool cells together (Cavallari et al., 2007; Hilderink et al., 2015; Ware et al., 2016; Zuellig et al., 2017; Wassmer et al., 2020).

**Spheroids:** Spheroids are spherical cellular units that are generally cultured as free-floating aggregates with no matrix component and are of low complexity. Spheroids can be generated from immortalized cell lines, primary cells or fragments of tissue and, as such, their viability is limited, as they do not contain a progenitor phenotype. Spheroids develop a necrotic core as they grow in size and possess no or limited tissue structure and a less representative tissue architecture. Sphere-forming assays have been widely used in 1) stem cell biology to assess the self-renewal and differentiation potential of a particular cell type 2) *in vitro* models to investigate solid tumors.

The first spheroids used to investigate stem cells were developed to investigate the presence of adult neuronal stem cells (neurospheres) (Reynolds and Weiss, 1992). These assays have been adopted to investigate stem cells and progenitors in a variety of tissues. A suffix is usually added to identify the tissue of origin of the spheroids, such as, mammary gland-derived mammospheres (Dontu et al., 2003), pancreas-derived pancreatospheres (Kerr-Conte et al., 1996; Seaberg et al., 2004; Smukler et al., 2011) and prostate-derived prostatospheroids (Rajasekhar et al., 2011).

**Organoids:** Organoids have been used as 3D cell culture models to study adult progenitors and tumor biology since 2009 when they were first described by Clevers' laboratory (Sato et al., 2009). Organoids are more complex than spheroids and are three-dimensional cell cultures that incorporate some of the key features of the organ of origin. These *in vitro* culture systems contain a self-renewing stem cell population that differentiates into multiple, organ-specific cell types that exhibit spatial organization like the corresponding organ and can recapitulate some functions of the organ providing a highly physiologically relevant system.

Organoids are derived from one or a few adult stem cells of a tissue, from embryonic stem cells or from induced pluripotent stem cells. Typically, they require a scaffold to grow, such as Basement Membrane Extract (BME), Matrigel or extracellular matrix components.

Tumor-derived organoids from patients have opened a window of opportunity to investigate more complex tumor microenvironment, disease modelling and personalize medicine therapies.

organoids derived from healthy tissue to recapitulate tissue differentiation and architecture is limited, pancreatic organoids hold promise for the development of regenerative medicine therapies for diabetes and disease modelling.

## Human and Mouse Ductal Derived Organoids for Diabetes Treatment: A Promise Not Yet Fulfilled

Pancreatic organoids were first described by Clevers' laboratory in 2013 (Huch et al., 2013), introducing pancreatic organoid technology as a putative unlimited source of induced-progenitors with the prospect of future differentiation into insulin secreting cells. The adult pancreas does not express the stem marker *Lgr5* in homeostatic conditions (Sato et al., 2009). However, mouse pancreatic duct fragments were shown to initiate *Lgr5* expression in RSP01-based cultures followed by organoid formation (Huch et al., 2013). Organoids derived from mouse and human pancreatic tissue expressed ductal markers (*SOX9*, *KRT19*, *MUC1*) and only organoids expressing *Sox9* were capable of long-term expansion (Huch et al., 2013; Boj et al., 2015). Together, these observations suggest that ductal cells *in vitro* display progenitor capacities. In line, organoids derived from *EpCAM*<sup>+</sup>-*TSQ*<sup>−</sup> cells (i.e., non-endocrine epithelial cells) could be induced to differentiate into ductal as well as endocrine cells upon transplantation with embryonic E13 mouse or E14 rat pancreata under the kidney capsule of non-diabetic immunodeficient mice, although the efficiency of differentiation toward endocrine lineages was ~5% (Huch et al., 2013). Later, lentivirus-mediated, doxycycline-inducible expression of *Neurog3*, *Pdx1*, and *MafA* in mouse pancreatic ductal organoids has been shown to generate cells that express insulin and resemble  $\beta$ -cells at the transcriptome level (Azzarelli et al., 2017). The combinatorial potential of these three transcriptional factors to induce endocrine differentiation was reported by Melton's laboratory to induce transdifferentiation of acinar cells to  $\beta$  cells *in vivo* (Zhou et al., 2008). Finally, efficiency of organoid-derived  $\beta$ -like cell generation can be significantly enhanced by preventing phosphorylation of the *Neurog3* protein and further augmented by conditions promoting differentiation (Azzarelli et al., 2017). This suggests that post-translational regulation of key regulators of endocrine differentiation can be exploited to enhance  $\beta$ -cell generation from organoids (Figure 1).

## ALDH Positive Ductal Derived Organoids

Pancreatic organoids have been subsequently derived from subpopulations of ductal cells defined by already identified progenitor markers. We showed that mouse ductal cells displaying high aldehyde dehydrogenase (ALDH) activity display progenitor features *in vitro*, in pancreatospheres cultures and upon transplantation into embryonic pancreas (Rovira et al., 2010). These cells demonstrated dramatic expansion in the setting of epithelial injury and pregnancy (Rovira et al., 2010; Ioannou et al., 2013; Socorro et al., 2017). *ALDH*<sup>hi</sup> cells have indeed been identified in human fetal and adult pancreas (Loomans et al., 2018; Oakie et al., 2018). Recently, Koning's laboratory (Loomans et al., 2018) showed that human

ductal pancreatic cells displaying high ALDH activity can efficiently form organoids that can be expanded and maintained overtime. Interestingly, gene expression profiling revealed that *ALDH*<sup>hi</sup> ductal expressing cells are closer to human fetal pancreatic tissue compared with adult pancreatic tissue (endocrine and exocrine). *ALDH*<sup>hi</sup> derived organoids are able to differentiate into insulin expressing cells *in vitro* and upon being engrafted into the kidney capsule, although with low efficiency (~1.5% of insulin positive cells) (Loomans et al., 2018) (Figure 1).

## CD133 Positive Ductal Derived Organoids

Similarly to ALDH, CD133 is a marker whose expression has been described as a cell surface marker in adult progenitor populations (Shmelkov et al., 2005; Li, 2013; Vassalli, 2019). CD133 is also expressed in a fraction of pancreatic ductal cells (Immervoll et al., 2008; Immervoll et al., 2011) and indeed, it has been used as surface marker to isolate ductal cells and assess their progenitor potential in cultures grown as monolayer colonies or spheres and their capacity to differentiate into endocrine cells *in vitro* (Oshima et al., 2007; Hori et al., 2008). *CD133*<sup>+</sup> cells isolated from mouse adult pancreas form organoids (Jin et al., 2013; Jin et al., 2014; Wedeken et al., 2017) but these do not display long-term self-renewal potential and are heterogeneous. However, they displayed endocrine and exocrine differentiation capacity in presence of WNT ligand R-spondin1 (Jin et al., 2013; Jin et al., 2014). In humans, *CD133*<sup>+</sup> isolated pancreatic cells form organoids with self-renewal potential (Lee et al., 2013) but their endocrine differentiation was only achieved upon adenoviral induction of the expression of *MafA*, *Neurog3*, *Pdx1* and *Pax4*, master regulators of endocrine differentiation. More recently, human pancreatic organoids derived from ductal *CD133*<sup>+</sup> cells could be differentiated into insulin<sup>+</sup> cells (at a frequency of ~4.6%) just by *in vitro* treatment with transcribed *Neurog3* mRNA and differentiation media (Koblas et al., 2019). Characterization of liver and pancreas organoid-initiating cells in mice showed that these cells are phenotypically and functionally similar and express *MIC1-1C3*<sup>+</sup>/*CD133*<sup>+</sup>/*CD26*<sup>−</sup> (Dorrell et al., 2014). Organoids derived from these ductal cells can differentiate into insulin expressing cells (at a frequency of ~5–22%) following tricistronic adenoviral administration of *MafA*, *Neurog3* and *Pdx1*. These insulin<sup>+</sup> cells showed transcriptional identity partially overlapping with murine  $\beta$  cells, but with retained expression of many off-target non- $\beta$  cell genes (Dorrell et al., 2014). In summary, pancreatic ductal-derived organoids have proven their potential for  $\beta$  cell replacement therapies although still the efficiency of organoids to differentiate into endocrine lineages is limited. A more refined reprogramming/differentiation methodology and a subpopulation of ductal cells that could produce an unlimited source of multipotent cells to generate endocrine cells is still needed (Figure 1).

To note, the media composition of the above studies comprises factors shown to be important in endocrine differentiation during development [e.g., FGFs (FGF10), EGF, RA] (Gittes, 2009; Santosa et al., 2016). These factors might also play a role in the differentiation of adult ductal organoids either

potentiating or hindering the process, a field that deserves further investigation.

## Procr Positive Islet Derived Organoids

Finally, protein C receptor (Procr) is a surface protein that has been reported to mark stem cells in several adult tissues (Balazs et al., 2006; Iwasaki et al., 2010; Wang et al., 2015; Yu et al., 2016; Zhou et al., 2016; Fares et al., 2017). Interestingly, a recent comprehensive single cell RNA-seq analysis of murine islets identified a novel Procr<sup>+</sup> population (Wang et al., 2020). Procr<sup>+</sup> cells were characterized by a transcriptional signature indicative of epithelial-to-mesenchymal transition, lacked expression of terminally differentiated endocrine and exocrine markers, and were able to form islet-like organoid-like spheroids *in vitro*. Islet-like derived organoids could be long-expanded *in vitro* and upon co-culture with endothelial cells differentiated into endocrine cells with a remarkable high efficiency: after 1 month, up to 80% of cells expressed insulin. *In vivo*, long-term cultured organoids restored glucose homeostasis in streptozotocin-induced T1D mice (Wang et al., 2020). (Figure 1).

## Limitations and Future Perspectives

Several reasons could explain the limited endocrine differentiation capacity of organoids:

First, organoid maintenance media has been established based on the intestinal organoid media with minimal modifications (Fujii et al., 2019), therefore it is possible that a modified media that best mimics pancreatic progenitors' requirements will influence positively their expansion, self-renewal and endocrine differentiation capacity. The stem cell/progenitor niche concept, initially proposed by Raymond Schofield in 1978, defines niches as compartments that are conducive for the maintenance of definitive stem cell properties (Schofield, 1978). The niche thus represents a defined anatomical compartment that provides signals to stem cells in the form of secreted and cell surface molecules to control the rate of stem cell proliferation, determine the fate of stem cell daughters and protect stem cells from exhaustion or death. Such a niche has not yet been identified in the adult pancreas. However, we know that through pancreas development the neuronal, mesenchymal and endothelial compartments are key for the proper maintenance and differentiation of embryonic progenitors into exocrine and endocrine lineages (Miralles et al., 1999; Lammert et al., 2001; Gittes, 2009; Borden et al., 2013). Potentially, complex organoid co-cultures with neuronal, mesenchymal and endothelial cells could shed light into the proper settings to mimic a progenitor niche and improve differentiation potential as it has been already proven in pluripotent stem cell cultures (Aghazadeh et al., 2021).

Second, the low regenerative capacity of the adult pancreatic tissue suggests that if a resident progenitor exists, it should be of really low abundance. Thus, not all ductal cells may bear progenitor capacity nor show similar organoid formation ability. Therefore, a better understanding of ductal heterogeneity could highlight ductal subpopulations to be studied in organoid culture and assess their endocrine differentiation capacity (Hendley et al., 2021).

Third, ductal-derived organoids could have a limited endocrine differentiation capacity due to epigenetic features. A better understanding of the differences between embryonic progenitors and organoids may identify an epigenetic brake to be modulated for proper endocrine differentiation.

Fourth, extracellular matrix (ECM) components might be crucial *in vitro*, as they are *in vivo*, for the proper morphogenesis and differentiation of the pancreatic lineages. Current organoid systems mostly rely on intrinsic or extrinsic biochemical signals (i.e., growth factors) and cell-cell interactions to control stem cell fate, but there are important elements to consider including the ECM and biophysical signals that are still unknown. This is because current *in vitro* models rely on animal-derived Matrigel which contains laminin, collagen IV, entactin, heparan sulfate, and growth factors (Rezakhani et al., 2021) in proportions that are difficult to manipulate. A controlled matrix rather than standard Matrigel could be key for organoid-to- $\beta$ -cell differentiation.

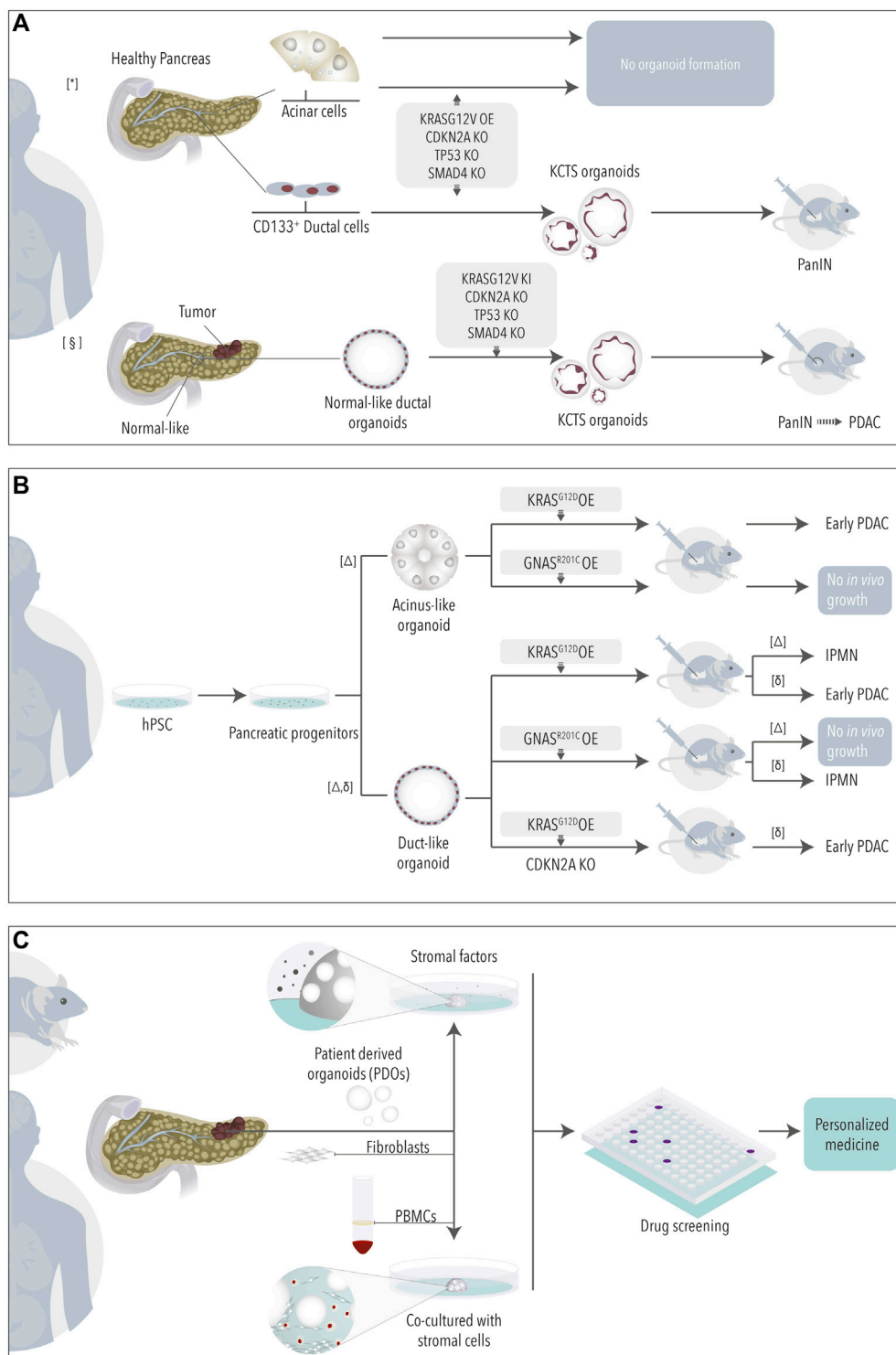
Finally, the above published studies did not analyze the possible presence of endocrine cells in the primary ductal cultures. In this scenario, it cannot be discarded that some of the insulin producing cells observed at the end of the protocol were present in the cultures from the beginning. Further studies where the absence of insulin expressing cells in the original preparation is carefully ratified prior to organoid formation are still required to properly validate and estimate the efficiency of ductal to  $\beta$  cell transdifferentiation.

## NORMAL TISSUE DERIVED ORGANOID FOR CANCER RESEARCH

### Ductal-Derived Organoids

Human healthy ductal derived organoids have also been used to model pancreatic cancer. Introduction of PDAC driver mutations in normal organoids *via* CRISPR-Cas9 or overexpression vectors has been used to study PDAC initiation and progression (Lee et al., 2017; Seino et al., 2018). Lee and colleagues (Lee et al., 2017) engineered organoids derived from healthy CD133<sup>+</sup> ductal cells to express mutant KRAS<sup>G12V</sup> (K), and deleted CDKN2A (C), TP53 (T), and SMAD4 (S) (KCTS organoids). Following orthotopic implantation, the mutant organoids gave rise to early pancreatic lesions (PanINs), but these did not progress to PDAC. Differently, KCTS organoids developed by Seino *et al.* generated *in vivo* lesions comprising the full histological transformation from PanINs to invasive PDACs (Seino et al., 2018) (Figure 2A). Instead of healthy pancreata, Seino *et al.* used ductal cells isolated from "normal-like" regions adjacent to tumor tissue. Additionally, the two studies differed in the methodology to introduce KRAS<sup>G12V</sup> (overexpression *vs.* knock-in), the culture media used to establish the organoids, and the *in vivo* implantation model (orthotopic *vs.* subcutaneous). Whether some or all of these factors influenced the results deserves further investigation and encourages working on the development of standardized models. In the meantime, it is tempting to think that the origin of ductal cells (healthy *vs.* normal-like, CD133<sup>+</sup> *vs.* bulk) may influence organoids' nature





**FIGURE 2 |** Organoids for cancer research. Non-tumoral organoids derived from healthy or normal-like tissue adjacent to tumor **(A)** or from pluripotent stem cells **(B)** have been engineered to study the role of PDAC driving mutations. **(C)** Tumoral organoids in mono- or co-cultures are used as model for drug testing. \* (Lee et al., 2017) § (Seino et al., 2018) Δ (Huang et al., 2021), δ (Breunig et al., 2021).

and that microenvironmental cues (culture media, site of implantation) will need to be adjusted in search of more representative models.

## Acinar-Derived Cultures

The above studies employed organoids derived from ductal cells to study PDAC formation. However, the cell of origin of PDAC and its implication on the progression and biology of tumors are still a matter of debate. Several studies have shown that both acinar and ductal cells can give rise to tumors in genetic mouse models (Guerra et al., 2007; Von Figura et al., 2014; Bailey et al., 2016; Ferreira et al., 2017; Lee et al., 2019; Flowers et al., 2021). Some of these studies have recently highlighted that mouse PDAC tumors arising from either acinar or ductal cells show differences at the transcriptomic and phenotypic levels (Ferreira et al., 2017; Lee et al., 2019; Flowers et al., 2021). The existence of different cells of origin shall, in part, explain the great heterogeneity observed in the PDAC human scenario (Raphael et al., 2017; Collisson et al., 2019; Backx et al., 2021a; Espinet et al., 2021). Thus, models where the impact of mutations can be studied in both acinar and ductal human cells may help us to better understand patient tumor complexity. Unfortunately, acinar cells fail to grow organoids (Seino et al., 2018) even when engineered to express the main PDAC mutations (Lee et al., 2017). In general, acinar cells are refractory to *in vitro* culture, even if successfully isolated, as they rapidly undergo transformation into ductal-like cells (acinar-to-ductal metaplasia) (Houbracken et al., 2011; Wollny et al., 2016).

## iPSC-Derived Organoids

An approach to overcome the above limitation consists in inducing the differentiation of human PSCs (hPSCs) into acinus- and ductal-like exocrine organoids (Huang et al., 2015; Hohwieler et al., 2017). To note, hPSCs have been widely studied also as a source to obtain endocrine cells *via* differentiation, a topic that will not be discussed here as it has been extensively reviewed elsewhere (Melton, 2021). hPSCs exocrine differentiation requires a sequential protocol in which ESCs are first differentiated into pancreatic progenitor-like cells and then into acinus or ductal-like cells (Huang et al., 2015; Hohwieler et al., 2017). Using this approach, Huang and colleagues recently showed that PDAC driver mutations lead indeed to cell-lineage-specific phenotypes (Huang et al., 2021). While  $KRAS^{G12D}$  in acinus-like organoids gave rise mainly to early PDAC lesions upon orthotopic transplantation,  $KRAS^{G12D}$  duct-like organoids were less efficiently engrafting and mainly developed IPMN-like lesions (Figure 2B). Differently, if presenting with a  $GNAS^{R201C}$  mutation neither acinus- nor ductal-like organoids engrafted *in vivo* (Huang et al., 2021). Another study, by Breunig and colleagues, in which ESCs were differentiated into pancreatic ductal-like organoids (PDLOs) confirmed the tropism of these different mutations, although with different results (Breunig et al., 2021). In this study,  $KRAS^{G12D}$  in PDLOs resulted in early PDAC lesions upon orthotopic engraftment while  $GNAS^{R201C}$  PDLOs developed IPMNs-like structures (Figure 2B).

## Limitations and Future Prospective

Differentiated hPSCs are a valuable model to study early mutagenic events in human cells. However, it is important to investigate the reasons behind divergent results obtained in, otherwise, similar studies. If possible, unifying protocols and definitions of hPSC-derived exocrine organoids may help conciliate the appearance of contrasting results towards a better understanding of early mutagenesis in human PDAC. Additionally, the existence of acinar and ductal heterogeneity, recently revealed by single cell sequencing technologies (Arda et al., 2016; Muraro et al., 2016; Enge et al., 2017; Martens et al., 2021; Tosti et al., 2021), will need to be considered in future studies. In promising latter single cell analyses of hPSC derived ductal-like organoids, Wiedenmann, Breunig and colleagues have shown the appearance of different types of ductal-like cells that share characteristics with ductal subsets identified in normal pancreas (Huang et al., 2021; Wiedenmann et al., 2021). This suggests that certain relevant ductal heterogeneity can be recapitulated in the hPSC model. Although scRNA-sequencing of hPSC-derived acinus-like organoids also depicted certain heterogeneity (Huang et al., 2021), overall, acinus-like organoids resembled fetal rather than mature pancreatic acini. Thus, the relevance of this observed “acinar heterogeneity” in the adult pancreas context might be questionable. Using adult mouse pancreas studies showed that only a small subset of acinar cells have long term proliferative capacity *in vivo* (Wollny et al., (2016). While these results suggest exciting functional differences in the adult acinar compartment, the study of the role of these and other acinar cells in the human and cancer scenario is still hindered by the lack of stable acinar *in vitro* models. Adaptation of the current culture conditions used to grow acinus-like organoids derived from hPSCs or from adult acini directly might result in improved acinar organoid formation. The big challenge is the fact that acinar cells rapidly lose their acinar identity upon injury or stress to move towards a ductal-like phenotype. The simple isolation of acinar cells from adult tissue might thus induce dedifferentiation of acinar cells. New studies analyzing these early events *in vitro* might help us to find the proper conditions required by acinar cells to retain their identity during longer experimental times (Backx et al., 2021b).

## PANCREATIC CANCER DERIVED ORGANIDS

Following the work in other tumor types, in 2015 Clevers and Tuveson's groups described the first protocol to establish organoids from mouse and human PDAC tissue (Boj et al., 2015). Since then, many groups have used or adapted the protocol to generate small biobanks of patient derived organoids (PDOs) with the aim to use them as avatar models to define more personalized therapies. When compared to patient derived xenografts models (PDXs), PDOs are generated faster and allow drug testing on a larger scale with lower cost (Tuveson and Clevers, 2019). Additionally, PDOs can be generated from little material obtained from fine needle biopsies, allowing the generation of models from non-resectable patients and from metastases. Thus, PDOs not only represent a model to study the biology of tumor cells, but also hold the promise of being a

platform to screen more effective drugs in a personalized and relevant-time manner. A recent comparison of the treatment of PDOs *versus* PDXs showed similar responses in the two models supporting the use of *in vitro* organoids as surrogate model (Frappart et al., 2020). Recent comparisons of the response of PDOs *versus* the actual patient response further encourage the study of organoids in the clinical setting (Frappart et al., 2020; Grossman et al., 2021).

## Pancreatic Cancer Organoids for Precision Oncology: Promises and Considerations

Two major transcriptomic epithelial subtypes have been described in PDAC after a collection of studies analyzing primary tumor samples: the classical and the basal-like subtypes (Martens et al., 2019). Tumors with a classical epithelial subtype show expression of genes characteristic of pancreatic progenitor cells and tend to be differentiated with better outcome. The basal-like epithelial subtype associates to more dedifferentiated and advanced tumors and correlates with worse outcome and lesser response to treatment (Aung et al., 2018). The emergence of PDAC PDOs offers a practical platform to study the biology of these two epithelial subtypes and to investigate subtype specific vulnerabilities. Additionally, efforts are done to generate transcriptomic signatures according to the response of different PDOs *in vitro*, that can be used to predict patient responses (Tiriac et al., 2018; Nicolle et al., 2020; Nicolle et al., 2021). The power of these signatures, some of which are currently being tested in clinical trials, will need to be carefully evaluated to find the best predictive markers.

Some studies have adapted the original PDAC-organoid media composition (Boj et al., 2015) to generate PDOs (Huang et al., 2015; Seino et al., 2018; Driehuis et al., 2019; Krieger et al., 2021). Although finding a consensus media to unify and standardize PDO growth across laboratories seems desirable, defining a unique media might be, in this case, delicate. Different tumor organoid subtypes present distinct dependency towards external soluble factors (Seino et al., 2018) likely reflecting existing differences of their tumor microenvironments (Nicolle et al., 2017; Maurer et al., 2019; Grünwald et al., 2021). Additionally, *in vivo* treatment with cytokines or implantation of organoids in different *in vivo* niches has shown to change the transcriptome of PDAC cells highlighting the plasticity of these cells under the influence of external factors (Miyabayashi et al., 2020; Tu et al., 2021). In line, the recent study by Raghavan and colleagues described that PDOs acquire culture-specific transcriptomic programs that are not present when the cells are in the tumor (Raghavan et al., 2021). More importantly, different media conditions (rather than 3D *versus* 2D structural changes) resulted in transcriptomic changes and influenced drug response of tumor cells (Raghavan et al., 2021). While we desire to move towards a standardized model as a tool for personalized medicine, these new observations question if we rather need to move towards fully personalized models first.

To add to this complex scenario, chemotherapeutic treatment has also been described to induce plasticity of PDAC tumor cells with transition from basal to classical subtype or *vice versa* having been observed (Chan-Seng-Yue et al., 2020; Hwang et al., 2020). This suggests that cancer cells undergo transcriptional subtype switching to adapt to the administered drug. In addition, Peschke, Jakubowsky and

colleagues have recently reported a classical to classical case after FOLFIRINOX treatment (Peschke et al., 2022) where PDOs derived from the pre- and the post-treated tumors showed remarkable differences to drug responses *in vitro* despite sharing genetic drivers and being both classified as classical (Peschke et al., 2022). These results indicate that a transcriptional subtype switch does not occur always, and that drug adaptation can be achieved by other, unknown, mechanisms. Together, the use of current transcriptomic classifications to predict treatment response might need to be revised in the post-treatment scenario. Further knowledge needs to be acquired to understand how the plasticity-emerged subtypes compare to the original subtypes defined in the naïve treatment scenario and how this impacts prediction of treatment response. Whenever possible, performing longitudinal functional assays with PDOs obtained pre- and post-treatment will be a valuable tool for a precision oncology approach.

## FINAL NOTES

Organoids are a very powerful tool to understand pancreatic biology and to help us to develop valuable therapies such as tissue transplantation and personalized cancer treatment. As for Spiderman, for organoids “*with great potential comes great prospects*”. Notwithstanding the above message, organoids are heterogeneous in shape and size; moreover, the absence of blood supply and interactions with other pancreatic cell types and non-pancreatic tissues limits their potential to date. For this, we need to standardize organoid cultures, including co-cultures with other cells (mesenchymal, endothelial, neuronal and immune cells), and to improve cell maturation to more faithfully model *ex vivo* the actual *in vivo* gland. In the meantime, while we continuously move towards better models, we should still acknowledge the value of standard models. Likely, the combination of models rather than a unique one will help us answer our questions.

## AUTHOR CONTRIBUTIONS

MR and EE conceived the review. MR, EE, and JC wrote the manuscript.

## FUNDING

This review was supported by Ministerio de Ciencia, Innovación y Universidades (PID2019-106160RB-I00 funded by MCIN/AEI/10.13039/501100011033) to MR and RYC-2017-21950 to MR and RYC 2020-029767 to EE (AEI/European Social Fund, UE).

## ACKNOWLEDGMENTS

We would like to thank and acknowledge Mateo Casas (mcasasengel@gmail.com) for the illustrations in the manuscript.

## REFERENCES

- Afelik, S., and Rovira, M. (2017). Pancreatic  $\beta$ -cell Regeneration: Facultative or Dedicated Progenitors? *Mol. Cell Endocrinol.* 445, 85–94. doi:10.1016/j.mce.2016.11.008
- Aghazadeh, Y., Poon, F., Sarangi, F., Wong, F. T. M., Khan, S. T., Sun, X., et al. (2021). Microvessels Support Engraftment and Functionality of Human Islets and hESC-Derived Pancreatic Progenitors in Diabetes Models. *Cell Stem Cell* 28 (11), 1936–1949. doi:10.1016/j.stem.2021.08.001
- Arda, H. E., Li, L., Tsai, J., Torre, E. A., Rosli, Y., Peiris, H., et al. (2016). Age-Dependent Pancreatic Gene Regulation Reveals Mechanisms Governing Human  $\beta$  Cell Function. *Cel. Metab.* 23 (5), 909–920. doi:10.1016/j.cmet.2016.04.002
- Aung, K. L., Fischer, S. E., Denroche, R. E., Jang, G.-H., Dodd, A., Creighton, S., et al. (2018). Genomics-Driven Precision Medicine for Advanced Pancreatic Cancer: Early Results from the COMPASS Trial. *Clin. Cancer Res.* 24 (6), 1344–1354. doi:10.1158/1078-0432.ccr-17-2994
- Azzarelli, R., Hurley, C., Sznurkowska, M. K., Rulands, S., Hardwick, L., Gamper, I., et al. (2017). Multi-Site Neurogenin3 Phosphorylation Controls Pancreatic Endocrine Differentiation. *Developmental Cel.* 41 (3), 274–286. doi:10.1016/j.devcel.2017.04.004
- Backx, E., Coolens, K., Van den Bossche, J.-L., Houbracken, I., Espinet, E., and Rooman, I. (2021). On the Origin of Pancreatic Cancer. *Cell Mol. Gastroenterol. Hepatol.* 13 (4), 1243–1253. doi:10.1016/j.jcmgh.2021.11.010
- Backx, E., Wauters, E., Baldan, J., Van Bulck, M., Michiels, E., Heremans, Y., et al. (2021). MECOM Permits Pancreatic Acinar Cell Dedifferentiation Avoiding Cell Death Under Stress Conditions. *Cell Death Differ.* 28 (9), 2601–2615. doi:10.1038/s41418-021-00771-6
- Bailey, J. M., Hendley, A. M., Lafaro, K. J., Pruski, M. A., Jones, N. C., Alsina, J., et al. (2016). P53 Mutations Cooperate with Oncogenic Kras to Promote Adenocarcinoma from Pancreatic Ductal Cells. *Oncogene* 35 (32), 4282–4288. doi:10.1038/onc.2015.441
- Balazs, A. B., Fabian, A. J., Esmon, C. T., and Mulligan, R. C. (2006). Endothelial Protein C Receptor (CD201) Explicitly Identifies Hematopoietic Stem Cells in Murine Bone Marrow. *Blood* 107 (6), 2317–2321. doi:10.1182/blood-2005-06-2249
- Balboa, D., Barsby, T., Lithovius, V., Saarimäki-Vire, J., Omar-Hmeadi, M., Dyachok, O., et al. (2022). Functional, Metabolic and Transcriptional Maturation of Human Pancreatic Islets Derived from Stem Cells. *Nat. Biotechnol.* 1, 1. doi:10.1038/s41587-022-01219-z
- Boj, S. F., Hwang, C. I., Baker, L. A., Chio, I. I., Engle, D. D., Corbo, V., et al. (2015). Organoid Models of Human and Mouse Ductal Pancreatic Cancer. *Cell* 160 (1–2), 324–338. doi:10.1016/j.cell.2014.12.021
- Borden, P., Houtz, J., Leach, S. D., and Kuruvilla, R. (2013). Sympathetic Innervation During Development Is Necessary for Pancreatic Islet Architecture and Functional Maturation. *Cel. Rep.* 4 (2), 287–301. doi:10.1016/j.celrep.2013.06.019
- Breunig, M., Merkle, J., Wagner, M., Melzer, M. K., Barth, T. F. E., Engleitner, T., et al. (2021). Modeling Plasticity and Dysplasia of Pancreatic Ductal Organoids Derived from Human Pluripotent Stem Cells. *Cell Stem Cell* 28 (6), 1105–1124. e19. doi:10.1016/j.stem.2021.03.005
- Campana, L., Esser, H., Huch, M., and Forbes, S. (2021). Liver Regeneration and Inflammation: From Fundamental Science to Clinical Applications. *Nat. Rev. Mol. Cel. Biol.* 22 (9), 608–624. doi:10.1038/s41580-021-00373-7
- Cavallari, G., Zuellig, R. A., Lehmann, R., Weber, M., and Moritz, W. (2007). Rat Pancreatic Islet Size Standardization by the “Hanging Drop” Technique. *Transplant. Proc.* 39 (6), 2018–2020. doi:10.1016/j.transproceed.2007.05.016
- Chan-Seng-Yue, M., Kim, J. C., Wilson, G. W., Ng, K., Figueroa, E. F., O’Kane, G. M., et al. (2020). Transcription Phenotypes of Pancreatic Cancer Are Driven by Genomic Events During Tumor Evolution. *Nat. Genet.* 52 (2), 231–240. doi:10.1038/s41588-019-0566-9
- Clayton, H. W., Osipovich, A. B., Stancill, J. S., Schneider, J. D., Vianna, P. G., Shanks, C. M., et al. (2016). Pancreatic Inflammation Redirects Acinar to  $\beta$  Cell Reprogramming. *Cel. Rep.* 17 (8), 2028–2041. doi:10.1016/j.celrep.2016.10.068
- Collisson, E. A., Bailey, P., Chang, D. K., and Biankin, A. V. (2019). Molecular Subtypes of Pancreatic Cancer. *Nat. Rev. Gastroenterol. Hepatol.* 16 (4), 207–220. doi:10.1038/s41575-019-0109-y
- Dontu, G., Abdallah, W. M., Foley, J. M., Jackson, K. W., Clarke, M. F., Kawamura, M. J., et al. (2003). *In Vitro* Propagation and Transcriptional Profiling of Human Mammary Stem/Progenitor Cells. *Genes Dev.* 17 (10), 1253–1270. doi:10.1101/gad.1061803
- Dorrell, C., Tarlow, B., Wang, Y., Canaday, P. S., Haft, A., Schug, J., et al. (2014). The Organoid-Initiating Cells in Mouse Pancreas and Liver Are Phenotypically and Functionally Similar. *Stem Cel. Res.* 13 (2), 275–283. doi:10.1016/j.scr.2014.07.006
- Driehuis, E., van Hoeck, A., Moore, K., Kolders, S., Francies, H. E., Gulersonmez, M. C., et al. (2019). Pancreatic Cancer Organoids Recapitulate Disease and Allow Personalized Drug Screening. *Proc. Natl. Acad. Sci. U.S.A.* 116 (52), 26580–26590. doi:10.1073/pnas.1911273116
- Engel, M., Arda, H. E., Mignardi, M., Beausang, J., Bottino, R., Kim, S. K., et al. (2017). Single-Cell Analysis of Human Pancreas Reveals Transcriptional Signatures of Aging and Somatic Mutation Patterns. *Cell* 171 (2), 321–330. doi:10.1016/j.cell.2017.09.004
- Espinet, E., Gu, Z., Imbusch, C. D., Giese, N. A., Büscher, M., Safavi, M., et al. (2021). Aggressive Pdac Show Hypomethylation of Repetitive Elements and the Execution of an Intrinsic Ifn Program Linked to a Ductal Cell of Origin. *Cancer Discov.* 11 (3), 638–659. doi:10.1158/2159-8290.cd-20-1202
- Fares, I., Chagraoui, J., Lehnertz, B., MacRae, T., Mayotte, N., Tomellini, E., et al. (2017). EPCR Expression Marks UM171-Expanded CD34+ Cord Blood Stem Cells. *Blood* 129 (25), 3344–3351. doi:10.1182/blood-2016-11-750729
- Ferreira, R. M. M., Sancho, R., Messal, H. A., Nye, E., Spencer-Dene, B., Stone, R. K., et al. (2017). Duct- and Acinar-Derived Pancreatic Ductal Adenocarcinomas Show Distinct Tumor Progression and Marker Expression. *Cel. Rep.* 21 (4), 966–978. doi:10.1016/j.celrep.2017.09.093
- Flowers, B. M., Xu, H., Mulligan, A. S., Hanson, K. J., Seoane, J. A., Vogel, H., et al. (2021). Cell of Origin Influences Pancreatic Cancer Subtype. *Cancer Discov.* 11 (3), 660–677. doi:10.1158/2159-8290.cd-20-0633
- Frappart, P. O., Walter, K., Gout, J., Beutel, A. K., Morawe, M., Arnold, F., et al. (2020). Pancreatic Cancer-derived Organoids - a Disease Modeling Tool to Predict Drug Response. *United Eur. Gastroenterol. j.* 8 (5), 594–606. doi:10.1177/2050640620905183
- Fujii, M., Clevers, H., and Sato, T. (2019). Modeling Human Digestive Diseases with CRISPR-Cas9-Modified Organoids. *Gastroenterology* 156 (3), 562–576. doi:10.1053/j.gastro.2018.11.048
- Gittes, G. K. (2009). Developmental Biology of the Pancreas: A Comprehensive Review. *Developmental Biol.* 326 (1), 4–35. doi:10.1016/j.ydbio.2008.10.024
- Gonzales, K. A. U., and Fuchs, E. (2017). Skin and its Regenerative Powers: An Alliance between Stem Cells and Their Niche. *Developmental Cel.* 43, 387–401. doi:10.1016/j.devcel.2017.10.001
- Grapin-Botton, A. (2005). Ductal Cells of the Pancreas. *Int. J. Biochem. Cel. Biol.* 37 (3), 504–510. doi:10.1016/j.biocel.2004.07.010
- Grossman, J. E., Muthuswamy, L., Huang, L., Akshinthala, D., Perea, S., Gonzalez, R. S., et al. (2021). Organoid Sensitivity Correlates with Therapeutic Response in Patients with Pancreatic Cancer. *Clin. Cancer Res.* 28, 708–718. doi:10.1158/1078-0432.ccr-20-4116
- Grünwald, B. T., Devisme, A., Andrieux, G., Vyas, F., Aliar, K., McCloskey, C. W., et al. (2021). Spatially Confined Sub-Tumor Microenvironments in Pancreatic Cancer. *Cell* 184 (22), 5577–5592. doi:10.1016/j.cell.2021.09.022
- Guerra, C., Schuhmacher, A. J., Cañamero, M., Grippo, P. J., Verdaguier, L., Pérez-Gallego, L., et al. (2007). Chronic Pancreatitis Is Essential for Induction of Pancreatic Ductal Adenocarcinoma by K-Ras Oncogenes in Adult Mice. *Cancer Cell* 11 (3), 291–302. doi:10.1016/j.ccr.2007.01.012
- Guiu, J., Hannezo, E., Yui, S., Demharther, S., Ulyanchenko, S., Maimets, M., et al. (2019). Tracing the Origin of Adult Intestinal Stem Cells. *Nature* 570 (7759), 107–111. doi:10.1038/s41586-019-1212-5
- Hendley, A. M., Rao, A. A., Leonhardt, L., Ashe, S., Smith, J. A., Giacometti, S., et al. (2021). Single-Cell Transcriptome Analysis Defines Heterogeneity of the Murine Pancreatic Ductal Tree. *Elife* 10, 1–29. doi:10.7554/elife.67776
- Hering, B. J., Clarke, W. R., Bridges, N. D., Eggerman, T. L., Alejandro, R., Bellin, M. D., et al. (2016). Phase 3 Trial of Transplantation of Human Islets in Type 1 Diabetes Complicated by Severe Hypoglycemia. *Diabetes Care* 39 (7), 1230–1240. doi:10.2337/dc15-1988
- Hilderink, J., Spijker, S., Carloti, F., Lange, L., Engelse, M., van Blitterswijk, C., et al. (2015). Controlled Aggregation of Primary Human Pancreatic Islet Cells Leads



- to Glucose-Responsive Pseudoislets Comparable to Native Islets. *J. Cel. Mol. Med.* 19 (8), 1836–1846. doi:10.1111/jcmm.12555
- Hohwieler, M., Illing, A., Hermann, P. C., Mayer, T., Stockmann, M., Perkhof, L., et al. (2017). Human Pluripotent Stem Cell-Derived Acinar/Ductal Organoids Generate Human Pancreas upon Orthotopic Transplantation and Allow Disease Modelling. *Gut* 66 (3), 473–486. doi:10.1136/gutjnl-2016-312423
- Hori, Y., Fukumoto, M., and Kuroda, Y. (2008). Enrichment of Putative Pancreatic Progenitor Cells from Mice by Sorting for Prominin1 (CD133) and Platelet-Derived Growth Factor Receptor  $\beta$ . *Stem Cells* 26 (11), 2912–2920. doi:10.1634/stemcells.2008-0192
- Houbracken, I., De Waele, E., Lardon, J., Ling, Z., Heimberg, H., Rooman, I., et al. (2011). Lineage Tracing Evidence for Transdifferentiation of Acinar to Duct Cells and Plasticity of Human Pancreas. *Gastroenterology* 141 (2), 731–741. doi:10.1053/j.gastro.2011.04.050
- Huang, L., Desai, R., Conrad, D. N., Leite, N. C., Akshinthala, D., Lim, C. M., et al. (2021). Commitment and Oncogene-Induced Plasticity of Human Stem Cell-Derived Pancreatic Acinar and Ductal Organoids. *Cell Stem Cell* 28 (6), 1090–1104. doi:10.1016/j.stem.2021.03.022
- Huang, L., Holtzinger, A., Jagan, I., Begora, M., Lohse, I., Ngai, N., et al. (2015). Ductal Pancreatic Cancer Modeling and Drug Screening Using Human Pluripotent Stem Cell- and Patient-Derived Tumor Organoids. *Nat. Med.* 21 (11), 1364–1371. doi:10.1038/nm.3973
- Huch, M., Bonfanti, P., Boj, S. F., Sato, T., Loomans, C. J. M., Van De Wetering, M., et al. (2013). Unlimited *In Vitro* Expansion of Adult Bi-Potent Pancreas Progenitors Through the Lgr5/R-Spondin axis. *EMBO J.* 32 (20), 2708–2721. doi:10.1038/emboj.2013.204
- Hwang, W. L., Jagadeesh, K. A., Guo, J. A., Hoffman, H. I., Yadollahpour, P., Mohan, R., et al. (2020). Single-Nucleus and Spatial Transcriptomics of Archival Pancreatic Cancer Reveals Multi-Compartment Reprogramming after Neoadjuvant Treatment. *bioRxiv* 1, 990456. doi:10.1101/2020.08.25.267336
- Immervoll, H., Hoem, D., Sakariassen, P. Ø., Steffensen, O. J., and Molven, A. (2008). Expression of the “Stem Cell Marker” CD133 in Pancreas and Pancreatic Ductal Adenocarcinomas. *BMC Cancer* 8, 48–14. doi:10.1186/1471-2407-8-48
- Immervoll, H., Hoem, D., Steffensen, O. J., Miletic, H., and Molven, A. (2011). Visualization of CD44 and CD133 in Normal Pancreas and Pancreatic Ductal Adenocarcinomas. *J. Histochem. Cytochem.* 59 (4), 441–455. doi:10.1369/0022155411398275
- Ioannou, M., Serafimidis, I., Arnes, L., Sussel, L., Singh, S., Vasilou, V., et al. (2013). ALDH1B1 Is a Potential Stem/Progenitor Marker for Multiple Pancreas Progenitor Pools. *Developmental Biol.* 374 (1), 153–163. doi:10.1016/j.ydbio.2012.10.030
- Iwasaki, H., Arai, F., Kubota, Y., Dahl, M., and Suda, T. (2010). Endothelial Protein C Receptor-Expressing Hematopoietic Stem Cells Reside in the Perisinusoidal Niche in Fetal Liver. *Blood* 116 (4), 544–553. doi:10.1182/blood-2009-08-240903
- Jin, L., Feng, T., Shih, H. P., Zerd, R., Luo, A., Hsu, J., et al. (2013). Colony-Forming Cells in the Adult Mouse Pancreas Are Expandable in Matrigel and Form Endocrine/Acinar Colonies in Laminin Hydrogel. *Proc. Natl. Acad. Sci. U.S.A.* 110 (10), 3907–3912. doi:10.1073/pnas.1301889110
- Jin, L., Feng, T., Zerd, R., Chen, C.-C., Riggs, A. D., and Ku, H. T. (2014). *In Vitro* Multilineage Differentiation and Self-Renewal of Single Pancreatic Colony-Forming Cells from Adult C57BL/6 Mice. *Stem Cell Development* 23 (8), 899–909. doi:10.1089/scd.2013.0466
- Kerr-Conte, J., Pattou, F., Lecomte-Houcke, M., Xia, Y., Boilly, B., Proye, C., et al. (1996). Ductal Cyst Formation in Collagen-Embedded Adult Human Islet Preparations. A Means to the Reproduction of Nesidioblastosis *In Vitro*. *Diabetes* 45 (8), 1108–1114. doi:10.2337/diabetes.45.8.1108
- Koblas, T., Leontovyc, I., Loukotova, S., and Saudek, F. (2019). Reprogramming of Human Pancreatic Organoid Cells into Insulin-Producing  $\beta$ -like Cells by Small Molecules and *In Vitro* Transcribed Modified mRNA Encoding Neurogenin 3 Transcription Factor. *Folia Biol.* 65 (3), 109–123.
- Krieger, T. G., Le Blanc, S., Jabs, J., Ten, F. W., Ishaque, N., Jechow, K., et al. (2021). Single-Cell Analysis of Patient-Derived PDAC Organoids Reveals Cell State Heterogeneity and a Conserved Developmental Hierarchy. *Nat. Commun.* 12 (1), 5826. doi:10.1038/s41467-021-26059-4
- Lablanche, S., Vantghem, M.-C., Kessler, L., Wojtuszczy, A., Borot, S., Thivolet, C., et al. (2018). Islet Transplantation versus Insulin Therapy in Patients with Type 1 Diabetes with Severe Hypoglycaemia or Poorly Controlled Glycaemia After Kidney Transplantation (TRIMECO): A Multicentre, Randomised Controlled Trial. *Lancet Diabetes Endocrinol.* 6 (7), 527–537. doi:10.1016/s2213-8587(18)30078-0
- Lammert, E., Cleaver, O., and Melton, D. (2001). Induction of Pancreatic Differentiation by Signals from Blood Vessels. *Science* 294 (5542), 564–567. doi:10.1126/science.1064344
- Lee, A. Y. L., Dubois, C. L., Sarai, K., Zarei, S., Schaeffer, D. F., Sander, M., et al. (2019). Cell of Origin Affects Tumour Development and Phenotype in Pancreatic Ductal Adenocarcinoma. *Gut* 68 (3), 487–498. doi:10.1136/gutjnl-2017-314426
- Lee, J., Snyder, E. R., Liu, Y., Gu, X., Wang, J., Flowers, B. M., et al. (2017). Reconstituting Development of Pancreatic Intraepithelial Neoplasia from Primary Human Pancreas Duct Cells. *Nat. Commun.* 8 (1), 1–14. doi:10.1038/ncomms14686
- Lee, J., Sugiyama, T., Liu, Y., Wang, J., Gu, X., Lei, J., et al. (2013). Expansion and Conversion of Human Pancreatic Ductal Cells into Insulin-Secreting Endocrine Cells. *Elife* 2 (2), e00940–22. doi:10.7554/eLife.00940
- Li, Z. (2013). CD133: A Stem Cell Biomarker and Beyond. *Exp. Hematol. Oncol.* 2, 17. doi:10.1186/2162-3619-2-17
- Loomans, C. J. M., Williams Giuliani, N., Balak, J., Ringnalda, F., van Gurp, L., Huch, M., et al. (2018). Expansion of Adult Human Pancreatic Tissue Yields Organoids Harboring Progenitor Cells with Endocrine Differentiation Potential. *Stem Cell Rep.* 10 (3), 712–724. doi:10.1016/j.stemcr.2018.02.005
- Marsee, A., Roos, F. J. M., Verstegen, M. M. A., Gehart, H., de Koning, E., Lemaigre, F., et al. (2021). Building Consensus on Definition and Nomenclature of Hepatic, Pancreatic, and Biliary Organoids. *Cell Stem Cell* 28 (5), 816–832. doi:10.1016/j.stem.2021.04.005
- Martens, S., Coolens, K., Van Bulck, M., Arsenijevic, T., Casamitjana, J., Fernandez Ruiz, A., et al. (2021). Discovery and 3D Imaging of a Novel  $\Delta$ np63-Expressing Basal Cell Type in Human Pancreatic Ducts with Implications in Disease. *Gut* 1 (0), 1–13. doi:10.1136/gutjnl-2020-322874
- Martens, S., Lefevre, P., Nicolle, R., Biankin, A. V., Puleo, F., Van Laethem, J. L., et al. (2019). Different Shades of Pancreatic Ductal Adenocarcinoma, Different Paths Towards Precision Therapeutic Applications. *Ann. Oncol.* 30 (9), 1428–1436. doi:10.1093/annonc/mdz181
- Maurer, C., Holmstrom, S. R., He, J., Laise, P., Su, T., Ahmed, A., et al. (2019). Experimental Microdissection Enables Functional Harmonisation of Pancreatic Cancer Subtypes. *Gut* 68 (6), 1034–1043. doi:10.1136/gutjnl-2018-317706
- McCarthy, N., Krawczyk, J., and Shivdasani, R. A. (2020). Cellular and Molecular Architecture of the Intestinal Stem Cell Niche. *Nat. Cel. Biol.* 22, 1033–1041. doi:10.1038/s41556-020-0567-z
- Melton, D. (2021). The Promise of Stem Cell-Derived Islet Replacement Therapy. *Diabetologia* 64 (5), 1030–1036. doi:10.1007/s00125-020-05367-2
- Miralles, F. o., Serup, P., Cluzeaud, F. o., Vewalle, A., Czernichow, P., and Scharfmann, R. (1999). Characterization of ? Cells Developed *In Vitro* from Rat Embryonic Pancreatic Epithelium. *Dev. Dyn.* 214 (2), 116–126. doi:10.1002/(sici)1097-0177(199902)214:2<116:aid-aja2>3.0.co;2-m
- Miyabayashi, K., Baker, L. A., Deschènes, A., Traub, B., Caligiuri, G., Plenker, D., et al. (2020). Intraductal Transplantation Models of Human Pancreatic Ductal Adenocarcinoma Reveal Progressive Transition of Molecular Subtypes. *Cancer Discov.* 10 (10), 1566–1589. doi:10.1158/2159-8290.cd-20-0133
- Muraro, M. J., Dharmadhikari, G., Grün, D., Groen, N., Dielen, T., Jansen, E., et al. (2016). A Single-Cell Transcriptome Atlas of the Human Pancreas. *Cel. Syst.* 3 (4), 385–394. doi:10.1016/j.cels.2016.09.002
- Nicolle, R., Blum, Y., Duconseil, P., Vanbrugghe, C., Brandone, N., Poizat, F., et al. (2020). Establishment of a Pancreatic Adenocarcinoma Molecular Gradient (PAMG) that Predicts the Clinical Outcome of Pancreatic Cancer. *EBioMedicine* 57, 102858. doi:10.1016/j.ebiom.2020.102858
- Nicolle, R., Blum, Y., Marisa, L., Loncle, C., Gayet, O., Moutardier, V., et al. (2017). Pancreatic Adenocarcinoma Therapeutic Targets Revealed by Tumor-Stroma Cross-Talk Analyses in Patient-Derived Xenografts. *Cel. Rep.* 21 (9), 2458–2470. doi:10.1016/j.celrep.2017.11.003
- Nicolle, R., Gayet, O., Duconseil, P., Vanbrugghe, C., Roques, J., Bigonnet, M., et al. (2021). A Transcriptomic Signature to Predict Adjuvant Gemcitabine Sensitivity in Pancreatic Adenocarcinoma. *Ann. Oncol.* 32 (2), 250–260. doi:10.1016/j.annonc.2020.10.601

- Nostro, M. C., Sarangi, F., Ogawa, S., Holtzinger, A., Corneo, B., Li, X., et al. (2011). Stage-Specific Signaling Through TGF $\beta$  Family Members and WNT Regulates Patterning and Pancreatic Specification of Human Pluripotent Stem Cells. *Development* 138 (7), 1445. doi:10.1242/dev.065904
- Oakie, A., Li, J., Fellows, G. F., Hess, D. A., and Wang, R. (2018). Characterization and Differentiation of Sorted Human Fetal Pancreatic ALDHhi and ALDHhi/CD133+ Cells Toward Insulin-Expressing Cells. *Stem Cell Development* 27 (4), 275–286. doi:10.1089/scd.2017.0135
- Oshima, Y., Suzuki, A., Kawashimo, K., Ishikawa, M., Ohkohchi, N., and Taniguchi, H. (2007). Isolation of Mouse Pancreatic Ductal Progenitor Cells Expressing CD133 and C-Met by Flow Cytometric Cell Sorting. *Gastroenterology* 132 (2), 720–732. doi:10.1053/j.gastro.2006.11.027
- Pan, F. C., and Wright, C. (2011). Pancreas Organogenesis: From Bud to Plexus to Gland. *Dev. Dyn.* 240 (3), 530–565. doi:10.1002/dvdy.22584
- Peschke, K., Jakubowsky, H., Schäfer, A., Maurer, C., Lange, S., Orben, F., et al. (2022). Identification of Treatment-Induced Vulnerabilities in Pancreatic Cancer Patients Using Functional Model Systems. *EMBO Mol. Med.* 14, e14876. doi:10.15252/emmm.202114876
- Pinho, A. V., Rooman, I., Reichert, M., De Medts, N., Bouwens, L., Rustgi, A. K., et al. (2011). Adult Pancreatic Acinar Cells Dedifferentiate to an Embryonic Progenitor Phenotype with Concomitant Activation of a Senescence Programme that Is Present in Chronic Pancreatitis. *Gut* 60 (7), 958–966. doi:10.1136/gut.2010.225920
- Raghavan, S., Winter, P. S., Navia, A. W., Williams, H. L., DenAdel, A., Lowder, K. E., et al. (2021). Microenvironment Drives Cell State, Plasticity, and Drug Response in Pancreatic Cancer. *Cell* 184 (25), 6119–6137. doi:10.1016/j.cell.2021.11.017
- Rajasekhar, V. K., Studer, L., Gerald, W., Socci, N. D., and Scher, H. I. (2011). Tumour-Initiating Stem-Like Cells in Human Prostate Cancer Exhibit Increased NF-Kb Signalling. *Nat. Commun.* 2, 162. doi:10.1038/ncomms1159
- Ramzy, A., Thompson, D. M., Ward-Hartstonge, K. A., Ivison, S., Cook, L., Garcia, R. V., et al. (2021). Implanted Pluripotent Stem-Cell-Derived Pancreatic Endoderm Cells Secrete Glucose-Responsive C-Peptide in Patients with Type 1 Diabetes. *Cell Stem Cell* 28 (12), 2047–2061. doi:10.1016/j.stem.2021.10.003
- Raphael, B. J., Hruban, R. H., Aguirre, A. J., Moffitt, R. A., Yeh, J. J., Stewart, C., et al. (2017). Integrated Genomic Characterization of Pancreatic Ductal Adenocarcinoma. *Cancer Cell* 32 (2), 185–e13. doi:10.1016/j.ccell.2017.07.007
- Reynolds, B. A., and Weiss, S. (1992). Generation of Neurons and Astrocytes from Isolated Cells of the Adult Mammalian Central Nervous System. *Science* 255 (5052), 1707–1710. doi:10.1126/science.1553558
- Rezakhani, S., Gjorevski, N., and Lutolf, M. P. (2021). Extracellular Matrix Requirements for Gastrointestinal Organoid Cultures. *Biomaterials* 276, 121020. doi:10.1016/j.biomaterials.2021.121020
- Rezania, A., Bruin, J. E., Arora, P., Rubin, A., Batushansky, I., Asadi, A., et al. (2014). Reversal of Diabetes with Insulin-Producing Cells Derived *In Vitro* from Human Pluripotent Stem Cells. *Nat. Biotechnol.* 32 (11), 1121–1133. doi:10.1038/nbt.3033
- Rovira, M., Scott, S.-G., Liss, A. S., Jensen, J., Thayer, S. P., and Leach, S. D. (2010). Isolation and Characterization of Centroacinar/Terminal Ductal Progenitor Cells in Adult Mouse Pancreas. *Proc. Natl. Acad. Sci. U.S.A.* 107 (1), 75–80. doi:10.1073/pnas.0912589107
- Santosa, M. M., Low, B. S., Pek, N. M., and Teo, A. K. (2016). Knowledge Gaps in Rodent Pancreas Biology: Taking Human Pluripotent Stem Cell-Derived Pancreatic Beta Cells into Our Own Hands. *Front. Endocrinol. (Lausanne)* 6, 194. doi:10.3389/fendo.2015.00194
- Sato, T., Vries, R. G., Snippert, H. J., Van De Wetering, M., Barker, N., Stange, D. E., et al. (2009). Single Lgr5 Stem Cells Build Crypt-Villus Structures *In Vitro* without a Mesenchymal Niche. *Nature* 459 (7244), 262–265. doi:10.1038/nature07935
- Schofield, R. (1978). The Relationship Between the Spleen Colony-Forming Cell and the Haemopoietic Stem Cell. *Blood Cells* 4 (1–2), 7–25.
- Seaberg, R. M., Smukler, S. R., Kieffer, T. J., Enikolopov, G., Asghar, Z., Wheeler, M. B., et al. (2004). Clonal Identification of Multipotent Precursors from Adult Mouse Pancreas that Generate Neural and Pancreatic Lineages. *Nat. Biotechnol.* 22 (9), 1115–1124. doi:10.1038/nbt1004
- Seino, T., Kawasaki, S., Shimokawa, M., Tamagawa, H., Toshimitsu, K., Fujii, M., et al. (2018). Human Pancreatic Tumor Organoids Reveal Loss of Stem Cell Niche Factor Dependence During Disease Progression. *Cell Stem Cell* 22 (3), 454–467. doi:10.1016/j.stem.2017.12.009
- Shapiro, A. M. J., Lakey, J. R. T., Ryan, E. A., Korbitt, G. S., Toth, E., Warnock, G. L., et al. (2000). Islet Transplantation in Seven Patients with Type 1 Diabetes Mellitus Using a Glucocorticoid-Free Immunosuppressive Regimen. *N. Engl. J. Med.* 343 (4), 230–238. doi:10.1056/nejm200007273430401
- Shapiro, A. M. J., Thompson, D., Donner, T. W., Bellin, M. D., Hsueh, W., Pettus, J., et al. (2021). Insulin Expression and C-Peptide in Type 1 Diabetes Subjects Implanted with Stem Cell-Derived Pancreatic Endoderm Cells in an Encapsulation Device. *Cel. Rep. Med.* 2 (12), 100466. doi:10.1016/j.xcrm.2021.100466
- Shmelkov, S. V., St.Clair, R. R., Lyden, D., and Rafii, S. (2005). AC133/CD133/Prominin-1. *Int. J. Biochem. Cel. Biol.* 37 (4), 715–719. doi:10.1016/j.biocel.2004.08.010
- Siegel, R. L., Miller, K. D., and Jemal, A. (2020). Cancer Statistics, 2020. *CA A. Cancer J. Clin.* 70 (1), 7–30. doi:10.3322/caac.21590
- Smukler, S. R., Arntfield, M. E., Razavi, R., Bikopoulos, G., Karpowicz, P., Seaberg, R., et al. (2011). The Adult Mouse and Human Pancreas Contain Rare Multipotent Stem Cells that Express Insulin. *Cell Stem Cell* 8 (3), 281–293. doi:10.1016/j.stem.2011.01.015
- Socorro, M., Criscimanna, A., Riva, P., Tandon, M., Prasadana, K., Guo, P., et al. (2017). Identification of Newly Committed Pancreatic Cells in the Adult Mouse Pancreas. *Sci. Rep.* 7 (1), 17539. doi:10.1038/s41598-017-17884-z
- Tiriak, H., Belleau, P., Engle, D. D., Plenker, D., Deschênes, A., Somerville, T. D. D., et al. (2018). Organoid Profiling Identifies Common Responders to Chemotherapy in Pancreatic Cancer. *Cancer Discov.* 8 (9), 1112–1129. doi:10.1158/2159-8290.cd-18-0349
- Tosti, L., Hang, Y., Debnath, O., Tiesmeyer, S., Trefzer, T., Steiger, K., et al. (2021). Single-Nucleus and *In Situ* RNA-Sequencing Reveal Cell Topographies in the Human Pancreas. *Gastroenterology* 160 (4), 1330–1344. e11. doi:10.1053/j.gastro.2020.11.010
- Tu, M., Klein, L., Espinet, E., Georgomanolis, T., Wegwitz, F., Li, X., et al. (2021). TNF- $\alpha$ -Producing Macrophages Determine Subtype Identity and Prognosis via AP1 Enhancer Reprogramming in Pancreatic Cancer. *Nat. Cancer* 2 (11), 1185–1203. doi:10.1038/s43018-021-00258-w
- Tuveson, D., and Clevers, H. (2019). Cancer Modeling Meets Human Organoid Technology. *Science* 364, 952–955. doi:10.1126/science.aaw6985
- Vantyghem, M.-C., de Koning, E. J. P., Pattou, F., and Rickels, M. R. (2019). Advances in  $\beta$ -cell Replacement Therapy for the Treatment of Type 1 Diabetes. *The Lancet* 394 (10205), 1274–1285. doi:10.1016/s0140-6736(19)31334-0
- Vassalli, G. (2019). Aldehyde Dehydrogenases: Not Just Markers, but Functional Regulators of Stem Cells. *Stem Cell Int.* 2019, 3904645. doi:10.1155/2019/3904645
- Von Figura, G., Fukuda, A., Roy, N., Liku, M. E., Morris Iv, J. P., Kim, G. E., et al. (2014). The Chromatin Regulator Brg1 Suppresses Formation of Intraductal Papillary Mucinous Neoplasm and Pancreatic Ductal Adenocarcinoma. *Nat. Cel. Biol.* 16 (3), 255–267. doi:10.1038/ncb2916
- Wang, D., Cai, C., Dong, X., Yu, Q. C., Zhang, X.-O., Yang, L., et al. (2015). Identification of Multipotent Mammary Stem Cells by Protein C Receptor Expression. *Nature* 517 (7532), 81–84. doi:10.1038/nature13851
- Wang, D., Wang, J., Bai, L., Pan, H., Feng, H., Clevers, H., et al. (2020). Long-Term Expansion of Pancreatic Islet Organoids from Resident Procr+ Progenitors. *Cell* 180 (6), 1198–1211. doi:10.1016/j.cell.2020.02.048
- Wang, Y. J., Schug, J., Won, K.-J., Liu, C., Naji, A., Avrahami, D., et al. (2016). Single-Cell Transcriptomics of the Human Endocrine Pancreas. *Diabetes* 65 (10), 3028–3038. doi:10.2337/db16-0405
- Ware, M. J., Colbert, K., Keshishian, V., Ho, J., Corr, S. J., Curley, S. A., et al. (2016). Generation of Homogenous Three-Dimensional Pancreatic Cancer Cell Spheroids Using an Improved Hanging Drop Technique. *Tissue Eng. C: Methods* 22 (4), 312–321. doi:10.1089/ten.tec.2015.0280
- Wassmer, C. H., Bellofatto, K., Perez, L., Lavallard, V., Cottet-Dumoulin, D., Ljubicic, S., et al. (2020). Engineering of Primary Pancreatic Islet Cell Spheroids for Three-Dimensional Culture or Transplantation: A Methodological Comparative Study. *Cel. Transpl.* 29, 963689720937292–963689720937298. doi:10.1177/0963689720937292
- Wedeken, L., Luo, A., Tremblay, J. R., Rawson, J., Jin, L., Gao, D., et al. (2017). Adult Murine Pancreatic Progenitors Require Epidermal Growth Factor and Nicotinamide for Self-Renewal and Differentiation in a Serum- and

- Conditioned Medium-Free Culture. *Stem Cell Development* 26 (8), 599–607. doi:10.1089/scd.2016.0328
- Wiedenmann, S., Breunig, M., Merkle, J., von Toerne, C., Georgiev, T., Moussus, M., et al. (2021). Single-Cell-Resolved Differentiation of Human Induced Pluripotent Stem Cells into Pancreatic Duct-Like Organoids on a Microwell Chip. *Nat. Biomed. Eng.* 5 (8), 897–913. doi:10.1038/s41551-021-00757-2
- Wollny, D., Zhao, S., Everlien, I., Lun, X., Brunken, J., Brüne, D., et al. (2016). Single-Cell Analysis Uncovers Clonal Acinar Cell Heterogeneity in the Adult Pancreas. *Developmental Cel.* 39 (3), 289–301. doi:10.1016/j.devcel.2016.10.002
- Yu, Q. C., Song, W., Wang, D., and Zeng, Y. A. (2016). Identification of Blood Vascular Endothelial Stem Cells by the Expression of Protein C Receptor. *Cell Res.* 26 (10), 1079–1098. doi:10.1038/cr.2016.85
- Zhou, F., Li, X., Wang, W., Zhu, P., Zhou, J., He, W., et al. (2016). Tracing Haematopoietic Stem Cell Formation at Single-Cell Resolution. *Nature* 533 (7604), 487–492. doi:10.1038/nature17997
- Zhou, Q., Brown, J., Kanarek, A., Rajagopal, J., and Melton, D. A. (2008). *In Vivo* Reprogramming of Adult Pancreatic Exocrine Cells to  $\beta$ -Cells. *Nature* 455 (7213), 627–632. doi:10.1038/nature07314
- Zhou, Q., and Melton, D. A. (2018). Pancreas Regeneration. *Nature* 557 (7705), 351–358. doi:10.1038/s41586-018-0088-0
- Zuellig, R. A., Cavallari, G., Gerber, P., Tschopp, O., Spinas, G. A., Moritz, W., et al. (2017). Improved Physiological Properties of Gravity-Enforced Reassembled Rat and Human Pancreatic Pseudo-Islets. *J. Tissue Eng. Regen. Med.* 11 (1), 109–120. doi:10.1002/term.1891
- Conflict of Interest:** The authors declare that the research was conducted in the absence of any commercial or financial relationships that could be construed as a potential conflict of interest.
- Publisher's Note:** All claims expressed in this article are solely those of the authors and do not necessarily represent those of their affiliated organizations, or those of the publisher, the editors and the reviewers. Any product that may be evaluated in this article, or claim that may be made by its manufacturer, is not guaranteed or endorsed by the publisher.

Copyright © 2022 Casamitjana, Espinet and Rovira. This is an open-access article distributed under the terms of the Creative Commons Attribution License (CC BY). The use, distribution or reproduction in other forums is permitted, provided the original author(s) and the copyright owner(s) are credited and that the original publication in this journal is cited, in accordance with accepted academic practice. No use, distribution or reproduction is permitted which does not comply with these terms.

## GLOSSARY

**2D** 2-dimensional

**3D** 3-dimensional

**ALDH** Aldehyde Dehydrogenase

**BME** Basal membrane extract

**BMP** Bone morphogenetic protein

**CD26** Cluster of differentiation 26, Dipeptidyl peptidase-4

**CD133** Cluster of differentiation 133, Prominin-1

**CDKN2A** Cyclin dependent kinase inhibitor 2A

**ECM** Extracellular Matrix

**EGF** Epidermal growth factor

**EpCAM** Epithelial Cell Adhesion Molecule

**ESC** Embryonic Stem Cell

**FGF** Fibroblast growth factor

**GNAS** GNAS complex locus

**IPMN** Intraductal papillary mucinous neoplasm

**iPSC** Induced Pluripotent Stem Cell

**KRAS** KRAS proto-oncogene, GTPase

**Krt19** Cytokeratin-19

**Lgr5** Leucine-rich repeat-containing G-protein coupled receptor 5

**MafA** MAF bZIP transcription factor A

**MIC1-1C3** Oval Cell Marker MIC1

**MUC1** Mucin 1, CD227

**Neurog3** Neurogenin 3

**PanIN** Pancreatic intraepithelial neoplasia

**Pax4** Paired box 4

**PDAC** Pancreatic Ductal Adenocarcinoma

**PDLO** Pancreatic ductal-like organoids

**PDO** Patient derived organoids

**PDX** Patient derived xenografts

**Pdx1** Pancreatic and duodenal homeobox 1

**PP** Pancreatic Polypeptide

**Procr** Protein C receptor

**RA** Retinoic Acid

**RSPO-1** R-spondin1

**SMAD4** SMAD family member 4

**Sox9** SRY (Sex determining region Y)-box9

**T1D** Type 1 Diabetes

**TGFβ** Transforming growth factor beta 1

**TP53** Tumor protein p53

**TSQ** Methoxy-8-p-toluenesulfonamido-quilone





# A Cellular Resolution Spatial Transcriptomic Landscape of the Medial Structures in Postnatal Mouse Brain

Mengnan Cheng<sup>1,2†</sup>, Liang Wu<sup>1,2†</sup>, Lei Han<sup>2</sup>, Xin Huang<sup>1,2</sup>, Yiwei Lai<sup>2,3</sup>, Jiangshan Xu<sup>1,2</sup>, Shuai Wang<sup>1,2</sup>, Mei Li<sup>2</sup>, Huiwen Zheng<sup>2,4</sup>, Weimin Feng<sup>1,2</sup>, Zirui Huang<sup>2</sup>, Yujia Jiang<sup>2,4</sup>, Shijie Hao<sup>1,2</sup>, Zhao Li<sup>2</sup>, Xi Chen<sup>2</sup>, Jian Peng<sup>2</sup>, Pengcheng Guo<sup>5</sup>, Xiao Zhang<sup>5</sup>, Guangyao Lai<sup>3,6</sup>, Qiuting Deng<sup>1,2</sup>, Yue Yuan<sup>2</sup>, Fangming Yang<sup>2</sup>, Xiaoyu Wei<sup>2</sup>, Sha Liao<sup>2</sup>, Ao Chen<sup>2</sup>, Giacomo Volpe<sup>7</sup>, Miguel A. Esteban<sup>2,3,5,8</sup>, Yong Hou<sup>2</sup>, Chuanyu Liu<sup>2\*</sup> and Longqi Liu<sup>1,2,4\*</sup>

## OPEN ACCESS

### Edited by:

Mo Li,  
King Abdullah University of Science  
and Technology, Saudi Arabia

### Reviewed by:

Yong Fan,  
Guangzhou Medical University, China  
Song-Lin Ding,  
Allen Institute for Brain Science,  
United States

### \*Correspondence:

Chuanyu Liu  
liuchuan@genomics.cn  
Longqi Liu  
liulongqi@genomics.cn

<sup>†</sup>These authors have contributed  
equally to this work

### Specialty section:

This article was submitted to  
Stem Cell Research,  
a section of the journal  
Frontiers in Cell and Developmental  
Biology

**Received:** 17 February 2022

**Accepted:** 31 March 2022

**Published:** 17 May 2022

### Citation:

Cheng M, Wu L, Han L, Huang X, Lai Y,  
Xu J, Wang S, Li M, Zheng H, Feng W,  
Huang Z, Jiang Y, Hao S, Li Z, Chen X,  
Peng J, Guo P, Zhang X, Lai G,  
Deng Q, Yuan Y, Yang F, Wei X, Liao S,  
Chen A, Volpe G, Esteban MA, Hou Y,  
Liu C and Liu L (2022) A Cellular  
Resolution Spatial Transcriptomic  
Landscape of the Medial Structures in  
Postnatal Mouse Brain.  
Front. Cell Dev. Biol. 10:878346.  
doi: 10.3389/fcell.2022.878346

<sup>1</sup>College of Life Sciences, University of Chinese Academy of Sciences, Beijing, China, <sup>2</sup>BGI-Shenzhen, Shenzhen, China, <sup>3</sup>Laboratory of Integrative Biology, Guangzhou Institutes of Biomedicine and Health, Chinese Academy of Sciences, Guangzhou, China, <sup>4</sup>BGI College and Henan Institute of Medical and Pharmaceutical Sciences, Zhengzhou University, Zhengzhou, China, <sup>5</sup>State Key Laboratory for Zoonotic Diseases, Key Laboratory for Zoonosis Research of Ministry of Education, Institute of Zoonosis, College of Veterinary Medicine, Jilin University, Changchun, China, <sup>6</sup>Joint School of Life Sciences, Guangzhou Institutes of Biomedicine and Health, Guangzhou Medical University, Guangzhou, China, <sup>7</sup>Hematology and Cell Therapy Unit, IRCCS Istituto Tumori "Giovanni Paolo II", Bari, Italy, <sup>8</sup>Bioland Laboratory (Guangzhou Regenerative Medicine and Health Guangdong Laboratory), Guangzhou, China

**Keywords:** spatial transcriptomics, stereo-seq, postnatal mouse brain development, single cell, brain region delineation and identification

## INTRODUCTION

Mammalian brain development is a complex process that starts from the neurulation of the early embryo to maturation and functionalization in postnatal brain development (Stiles and Jernigan, 2010). Major biological events that occur during brain development include cell proliferation, neurogenesis, cell migration, gliogenesis, and myelination, during which numerous cells are generated and migrate to specific regions to obtain corresponding functions (Jiang and Nardelli, 2016). These processes adhere to tight spatiotemporal regulation by extrinsic and intrinsic cues across different anatomical regions or layers (Martinez, 2001; Echevarria et al., 2003; Hodge and Hevner, 2011; Manuel et al., 2015). The disruption of gene expression or regulatory factors can lead to developmental dysfunction or neuropsychiatric diseases (Li et al., 2018; Parenti et al., 2020). Previous studies have mainly focused on the molecular features of specific regions; however, a complete understanding of brain development requires comprehensive characterization of cell types, molecular features, and spatial localization of each cell or gene at the whole-brain scale (Tiklova et al., 2019; Tan et al., 2021).

Mouse brain development can be broadly divided into two stages, embryonic and postnatal. During the embryonic stage, starting from embryonic day 10 (E10), a large number of neurons are generated by cell proliferation and neurogenesis. Within the first week after birth, numerous glial cells are generated, which are critical for neuronal synaptogenesis. By postnatal day 7 (P7), many neurons start forming synaptic connections to build the initial neural circuits of the brain (Han et al., 2009). Besides, some brain regions undergo dramatic changes during this period. For example, neurogenesis in the dentate gyrus of the hippocampus begins at E10 and reaches a maximum rate in the first two postnatal weeks (P0–P14) (Zhang et al., 2005). Granule cells of the cerebellum begin at E15 and undergo massive proliferation, peaking from P5 to P7 (Zhang et al., 2005; Carter et al., 2018;

Kozareva et al., 2021). Therefore, it is significant to understand the molecular, cellular, and regional characteristics of this stage.

Single-cell and spatial transcriptomic technologies have greatly accelerated the understanding of cell type taxonomy, spatial localization, and functions in both adult and developing brains (Lein et al., 2017). For example, Zeisel et al. (2018) described the transcriptional features of 19 regions in the central nervous system and peripheral nervous system of adult mice, including the olfactory bulb, cortex, nucleus (striatum, hypothalamus, and so on), midbrain, and spinal cord. Some studies have focused on specific cortical regions of the adult brain in mice or humans (Lake et al., 2016; Tasic et al., 2016; Tasic et al., 2018). The current systematic molecular description of mouse brain development comes from the Allen Institute, which used the ISH approach (Thompson et al., 2014). Primate brain development has been systematically described which covers the stage from E40 to postnatal 48 months (Bakken et al., 2016). Whole-brain coverage of spatial transcriptome (via laser microdissection) and gene expression (via ISH) are also available for prenatal human brains (Miller et al., 2014; Ding et al., 2022). Furthermore, studies have focused on resolving the developmental features of the prenatal mouse brain, ranging from E7 to E18.5 (Di Bella et al., 2021; La Manno et al., 2021); however, a comprehensive study on the spatial organization of cell types at the maturation stage in the postnatal mouse brain is yet to be performed.

The rapid evolution of cutting-edge spatial transcriptomic technologies has provided new methods to decipher complex brains (Liao et al., 2021; Ortiz et al., 2021). Although FISH-based spatial technology has allowed the study of gene expression patterns in specific regions, the limited number of detected genes and restricted brain field of view have largely hampered the global analysis of the entire brain in detail (Long et al., 2017). In this regard, spatial transcriptomic technologies based on next-generation sequencing, such as spatial transcriptomics (Stahl et al., 2016), Slide-seq (Rodriques et al., 2019), HDST (Vickovic et al., 2019), DBiT-seq (Liu et al., 2020), and Seq-Scope (Cho et al., 2021), have been employed in the field of brain development. However, these methods have limitations in terms of capture sensitivity, resolution, and field of view. To address these issues, we recently developed Stereo-seq, a DNA nanoball (DNB) patterned array-based technology that allows ultra-high resolution and spatial transcriptomics profiling with a large field of view (Chen et al., 2021). Stereo-seq enables the identification of subregions and cellular resolution analysis in complex tissues, and it has been applied to map spatial patterns of gene expression across whole mouse embryos with particular interests in the developing brains from E9.5 to E16.5 (Chen et al., 2021); however, no high-resolution spatial transcriptomic study has been performed on the neonatal developmental stage of the whole mouse brain.

In this study, we applied Stereo-seq to generate a spatially resolved transcriptomic dataset of P7 murine brain sagittal sections near the middle line. Also, we determined the subcellular distribution of 27,330 genes across the entire section. We identified 41 anatomical regions with differentially expressed genes and enriched region-specific gene regulatory

networks. Moreover, we performed image-based cell segmentation on this dataset and identified 99,365 cells, with 41 cell types localized in different regions. This study provides a comprehensive resource for future research on the cellular and molecular mechanisms of postnatal brain development. To facilitate this exploration, we created a website containing an open and interactive database (<https://db.cngb.org/stomics/datasets/STDS0000139?tab=explore>).

## MATERIALS AND METHODS

### Tissue Collection

In this study, we used P7 C57BL/6 mice purchased from Jiangsu ALF Biotechnology Co., Ltd. (<http://jsalfei.com>). The methods related to laboratory animals were approved by the Institutional Review Board of the Ethics Committee of BGI (permit no. BGI-IR20210903001). First, the mice were sacrificed via carbon dioxide asphyxiation, and the whole brain was harvested and immediately immersed in embedding molds with precooled Tissue-Tek OCT (Sakura, 4583). Then, the molds with tissue were transferred into prechilled isopentane using liquid nitrogen until the OCT was completely solid. Finally, the embedded tissue was stored at  $-80^{\circ}\text{C}$ .

### Tissue Processing and Imaging

Stereo-seq experiments were performed as previously described (Chen et al., 2021). We used a Stereo-seq capture chip with an area of  $200\text{ mm}^2$  ( $20\text{ mm} \times 10\text{ mm}$ ). First, the chip was washed with  $\text{NF-H}_2\text{O}$  supplemented with  $0.05\text{ U}/\mu\text{L}$  RNase inhibitor (NEB, M0314L) and dried at room temperature. The embedded tissue was cut to a thickness of  $10\text{ }\mu\text{m}$  using a Leica CM1950 cryostat. Cryosections were adhered to the surface of the Stereo-seq capture chip and incubated at  $37^{\circ}\text{C}$  for 5 min. The chip with the section was then fixed in precooled methanol for 40 min at  $-20^{\circ}\text{C}$ . Subsequently, the chip was removed and air-dried. The following operation was only used in section 1:  $200\text{ }\mu\text{L}$  of tissue fluorescent staining solution ( $0.1 \times \text{SSC}$  (Thermo, AM9770) with  $1/200$  nucleic acid dye (Thermo Fisher, Q10212) and  $2\text{ U}/\mu\text{L}$  RNase inhibitor) was dripped on the chip for 3 min. The staining solution was then removed, and the chip was washed using wash buffer ( $0.1 \times \text{SSC}$  supplemented with  $2\text{ U}/\mu\text{L}$  RNase inhibitor), which was also used for the subsequent washing steps. Imaging was performed using a Ti-7 Nikon Eclipse microscope of the FITC channel (objective  $\times 10$ ).

### Stereo-Seq Library Preparation

After washing,  $200\text{ }\mu\text{L}$  of a permeabilization reagent ( $0.1\%$  pepsin (Sigma, P7000) in  $0.01\text{ M}$  HCl buffer) was dripped on the chip and incubated at  $37^{\circ}\text{C}$  for 12 min. The reagent was then removed, and the chip was carefully washed. Subsequently,  $200\text{ }\mu\text{L}$  RT mix ( $1 \times$  first-strand buffer,  $10\text{ U}/\mu\text{L}$  SuperScript II (Invitrogen, 18064-014),  $1\text{ mM}$  dNTPs,  $1\text{ M}$  betaine solution,  $7.5\text{ mM}$   $\text{MgCl}_2$ ,  $5\text{ mM}$  DTT,  $2\text{ U}/\mu\text{L}$  RNase inhibitor, and  $2.5\text{ }\mu\text{M}$  Stereo-seq-TSO (5-CTGCTGACGTACTGAGAGGC/rG/rG//iXNA\_G/-3)) were dripped on the chip, which was incubated at  $42^{\circ}\text{C}$  for 2 h. After reverse transcription, the tissue was washed

twice with wash buffer and digested with tissue removal buffer (10 mM Tris-HCl, 25 mM EDTA, 100 mM NaCl, and 0.5% SDS) at 37°C for 30 min. The chip was then treated with exonuclease I (NEB, M0293L) for 1 h at 37°C and washed twice with the wash buffer. The resulting first-strand cDNAs were amplified using the KAPA HiFi Hotstart Ready Mix (Roche, KK2602) with a 0.8  $\mu$ M cDNA–polymerase chain reaction (PCR) primer (5-CTGCTGACGTACTGAGAGGC-3), followed by incubation at 95°C for 5 min, 15 cycles at 98°C for 20 s, 58°C for 20 s, and 72°C for 3 min, and a final incubation at 72°C for 5 min.

## Library Construction and Sequencing

The resulting cDNA products were quantified using the Qubit™ dsDNA Assay Kit (Thermo, Q32854) after purification using VAHTS DNA Clean Beads (Vazyme, N411-03, 0.6 $\times$ ). First, 20 ng of products was fragmented using in-house Tn5 transposase at 55°C for 10 min, after which the reaction was stopped by the addition of 0.02% SDS. The fragmentation products were then amplified using KAPA HiFi Hotstart Ready Mix with 0.3  $\mu$ M Stereo-seq-Library-F primer (5phos/CTGCTGACGTACTGAGAGG\*C\*A-3) and 0.3  $\mu$ M Stereo-seq-Library-R primer (5-GAGACGTTCTCGACTCAGCAGA-3) followed by incubation at 95°C for 5 min, 13 cycles at 98°C for 20 s, 58°C for 20 s, and 72°C for 30 s, and 1 cycle at 72°C for 5 min. Finally, the PCR products were purified using VAHTS DNA Clean Beads ( $\times$ 0.6 and  $\times$ 0.15). The library was sequenced (35 bp for read 1 and 100 bp for read 2) using an MGI DNBEQ-Tx sequencer at the China National Gene Bank.

## Processing of Stereo-Seq Raw Data

The fastq files of Stereo-seq, generated by the MGI DNBEQ-Tx sequencer, were processed in accordance with a previous study using the SAW pipeline (<https://github.com/BGIResearch/SAW>) (Chen et al., 2021). Briefly, the coordinate identity (CID) sequences of DNB were mapped to the designed coordinates of the *in situ* captured chip, which allowed one base mismatch. The unique molecular identifiers (UMIs) containing either N bases or more than two bases with a quality score lower than 10 were filtered out. Next, the CIDs and UMIs were appended to each associated read header of read 2, and read 2 was aligned to the reference genome (mm10) using STAR (Dobin et al., 2013); mapped reads with MAPQ <10 were filtered out. The retained reads were annotated to their corresponding genes. The UMIs with the same CID and gene locus collapsed, allowing one mismatch to be corrected for sequencing and PCR errors. This information was used to generate a CID-containing expression profile matrix.

## Cell Segmentation

The cells were segmented based on nucleic acid staining of the same section. We summed the UMI of each CID, converted the gene matrix into an image where each pixel corresponded to one CID, and manually aligned it with the image of the nucleic acid staining. Then, we kept the image of the nucleic acid staining in the same size as that of the CID, so that each “x” and “y” corresponded to a pixel on the image of the nucleic acid staining. After alignment, we applied the watershed algorithm of the Scikit-image to perform cell segmentation based on nucleic

acid staining using a block size of 41 and an offset of 0.003. The cells were then extracted using Euclidean distance transformation with a distance of 15 from the background. Finally, for each segmented cell, the UMI of each gene from different CIDs was aggregated, and a cell matrix was generated for downstream analysis. The differentially expressed genes (DEGs) were identified using the FindAllMarker function and were defined as those with a fold change >2, adjusted P value < 0.05, and different positive ratio between case and control >0.1.

## Spatially Constrained Clustering

The expression matrix of the P7 mouse brain was binned into bin 50 (25  $\mu$ m), and the UMIs of each gene in each bin from different CIDs were aggregated. In a previous study, the expression matrix of bin 50 was used to perform spatially constrained clustering analysis, which included spatial information during unsupervised clustering (Chen et al., 2021). The data were log-normalized in Scanpy (Wolf et al., 2018); highly variable genes were selected, and principal component analysis (PCA) reductions were performed. The spatial k-nearest neighbor (KNN) graph was built using Squidpy (Palla et al., 2022) and then collapsed with the KNN graph of gene expression, which was created using Scanpy with 30 dimensions. The combined graph was used as the input for the Leiden algorithm to identify cell clusters. The marker genes of each cluster were then calculated using Seurat with min.pct = 0.05. Each cluster was annotated based on canonical markers and anatomical annotation of the Allen Brain Atlas (Lein et al., 2007).

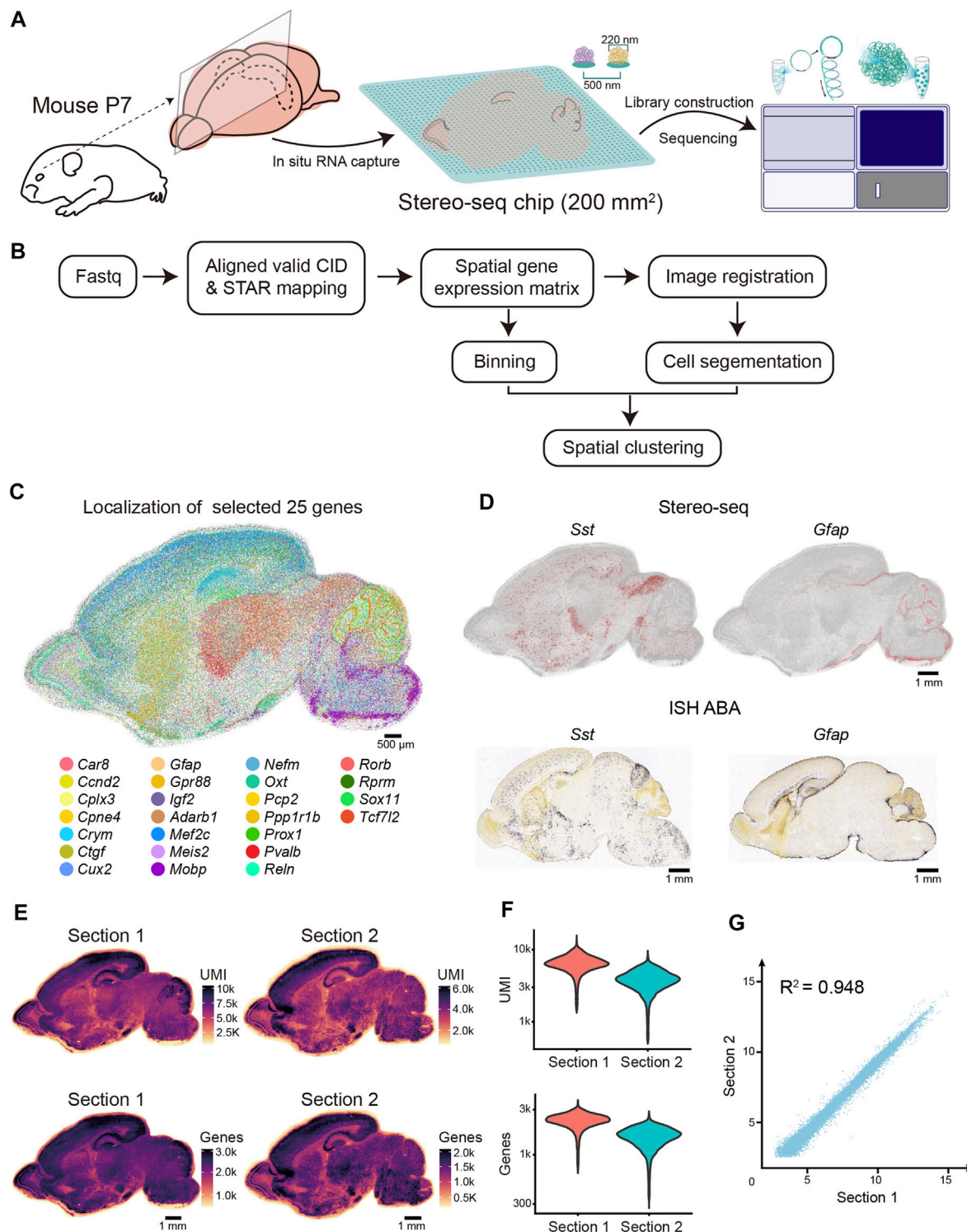
## Regulon Analysis

The regulon analysis of transcript factors followed the standard pySCENIC pipeline (Van de Sande et al., 2020). First, the gene expression profiles of bin 50 were used as the input and the GENIE3 algorithm (Huynh-Thi et al., 2010) was used to reconstruct the coexpression network between each transcript factor and the other genes. The coexpression module of each transcription factor with other genes was filtered using the cisTarget database (<https://resources.aertslab.org/cistarget/>) with default parameters. Next, the regulon activity (area under the curve, AUC) was analyzed using the AUCell function with the default threshold. Finally, the regulon enrichment of each anatomical region was defined as the mean activity of each anatomical region minus the mean activity of all bins and filtering out low regulons with enrichment of less than 0.1 in all anatomical regions.

## Unsupervised Clustering of Segmented Cells

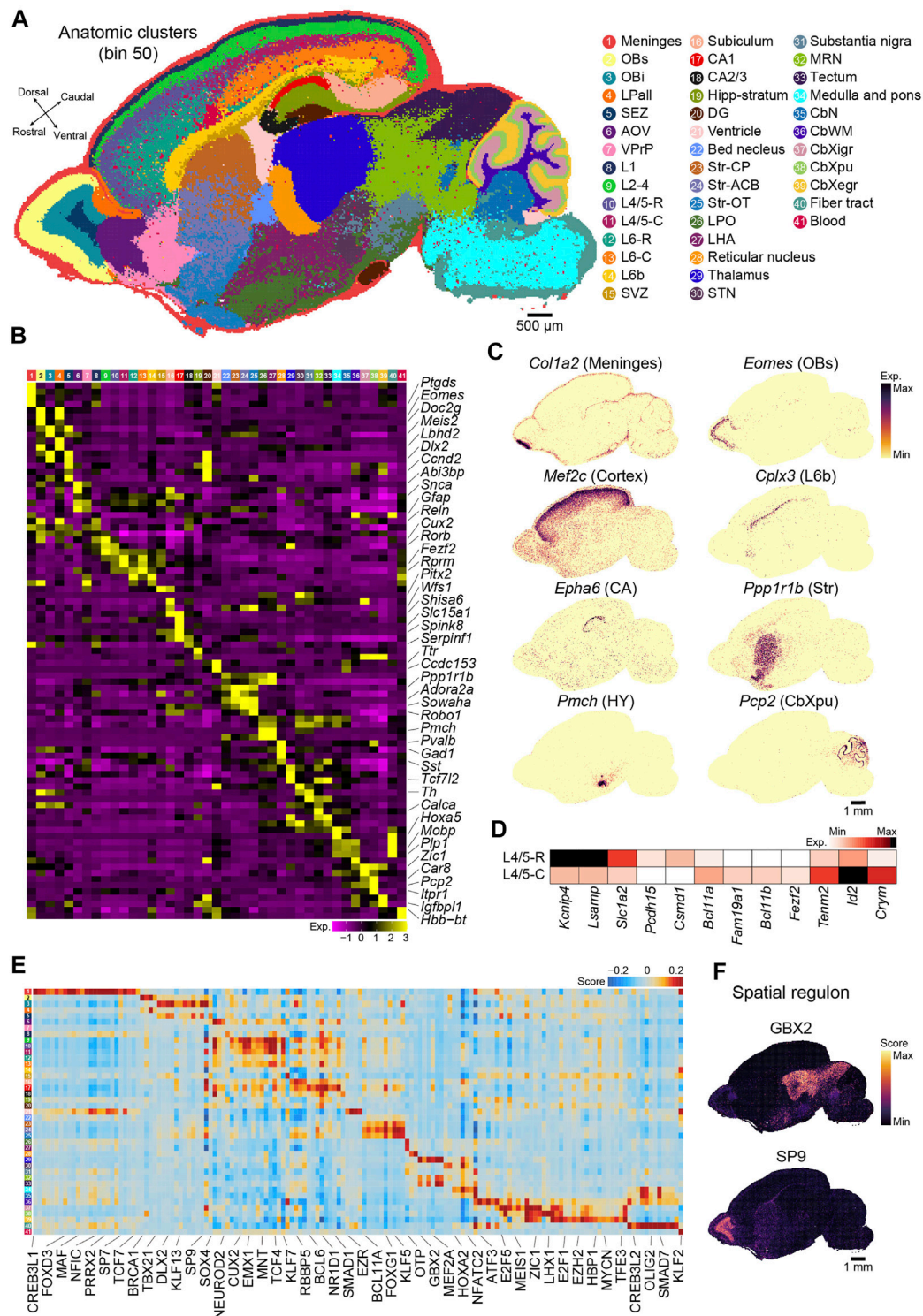
For the analysis of segmented cells in the P7 mouse brain, we filtered out cells with gene numbers less than 300 or those with a total number of detected genes ranking in the top 0.2%. The resulting cells were further processed using Seurat (Hao et al., 2021), followed by SCTransform, scaling, feature gene selection, PCA dimension reduction, and clustering with a resolution parameter of 3. Each cluster was annotated based on the marker genes of cell types.





**FIGURE 1 |** Overview of the experimental method, data analysis workflow, and Stereo-seq data quality. **(A)** Schematic representation of the Stereo-seq workflow. Left, sagittal sections near the middle line were collected for the Stereo-seq profiling. Middle, *in situ* RNA capture from tissue. The effective area of chip in this study is 200 mm<sup>2</sup>. Spot size and center-to-center distance of Stereo-seq chip are 200 nm and 500 nm respectively. Right, library construction and sequencing. **(B)** Graphic representation of Stereo-seq analytical workflow. **(C)** Molecular localization of the 25 selected genes. Each dot represents a captured gene. Scale bar, 500 μm. **(D)** Top: Spatial visualization of *Sst* and *Gfap* localization of the P7 mouse brain section. Bottom: ISH images of *Sst* and *Gfap* localization of the P4 mouse brain section taken from ABA. Scale bars, 1 mm. **(E)** Spatial distribution of UMIs and genes (bin 50) per section. Scale bars, 1 mm. **(F)** Violin plot indicating the distribution of the UMI and genes (bin 50) per section. **(G)** Pearson correlation coefficient ( $R^2 = 0.948$ ) between the two replicates.





**FIGURE 2 |** Recognition of regional and molecular characteristics of the anatomical regions based on binning. **(A)** Unsupervised spatially constrained clustering of the P7 mouse brain sagittal section 1 analyzed by Stereo-seq at bin 50 resolution. Bins are colored by their annotation. OBs, superficial stratum of olfactory bulb; OBI, intermediate stratum of olfactory bulb; LPall, lateral pallidum; SEZ, subependymal zone; AOV, anterior olfactory nucleus; VPrP, ventropallial prepiriform area; L1, cortical layer 1; L2–4, cortical layers 2–4; L4/5-R, cortical rostral layer 4/5; L4/5-C, cortical caudal layer 4/5; L6-R, cortical rostral layer 6; L6-C, cortical caudal layer 6; L6b, cortex layer 6b; SVZ, subventricular zone; CA1, cornu ammonis area 1; CA2/3, cornu ammonis area 2/3; Hipp-stratum, stratum molecular of CA and DG; DG, dentate gyrus; Str-CP, caudoputamen; Str-ACB, nucleus accumbens; Str-OT, olfactory tubercle; LPO, lateral preoptic area; LHA, lateral hypothalamus; STN, subthalamic (Continued)

**FIGURE 2 |** nucleus; MRN, midbrain reticular nucleus; CbN, cerebellar nuclei; CbWM, white matter of the cerebellum; CbXigr, internal granular layer of the cerebellum cortex; CbXpu, Purkinje cell layer of cerebellum cortex; CbXeigr, external granular layer of cerebellum cortex. Scale bar, 500  $\mu$ m. **(B)** Heatmap of normalized expression of selected marker genes for the indicated 41 clusters of the P7 mouse brain shown in **(A)**. **(C)** Spatial visualization of the indicated gene expression for meninges (*Col1a2+*), OBs (*Eomes+*), cortex (*Mef2c+*), L6b (*Cplx3+*), CA (*Epha6+*), Str (*Ppp1r1b+*), HY (*Pmch+*), and CbXpu (*Pcp2+*) in the section shown in **(A)**. Scale bar, 1 mm. **(D)** Heatmap of the differential expressed genes between L4/5-R and L4/5-C. **(E)** Heatmap of each cluster's predicted regulons for the P7 mouse brain section shown in **(A)**. **(F)** Spatial visualization of the representative regulons in **(E)**. Scale bar, 1 mm.

## RESULTS

### Stereo-Seq Data Quality Control of the P7 Mouse Brain Sections

We generated Stereo-seq libraries of two sagittal sections (sections 1 and 2) near the middle line of the P7 mouse brain (Figure 1A). We obtained 17.944 billion raw fastq reads covering a tissue area of 82.01 and 80.08 mm<sup>2</sup>, respectively (Supplementary Table S1). Simultaneously, we systematically evaluated the quality of the Stereo-seq dataset based on the quality of sequencing, the mapping ratio, the distribution of the known maker genes, the capture efficiency, and the correlation between two sections. First, we evaluated the quality of sequencing data; for section 1, the Q30 in CID was 85.21%, Q30 in UMI was 82.6%, and Q30 in insertion was 83.96% (Supplementary Table S1). The retained reads were processed using the SAW pipeline in accordance with a previous report (Figure 1B). Afterwards, for section 1, 59.3% reads with valid CID were then aligned to genome, with a mapping ratio of 87.1%. Then, the low mapping quality alignments were filtered out according to MAQP. Finally, we obtained 95.35 million CIDs with transcript capturing after registration with the image of the nuclei acid staining (Supplementary Table S1).

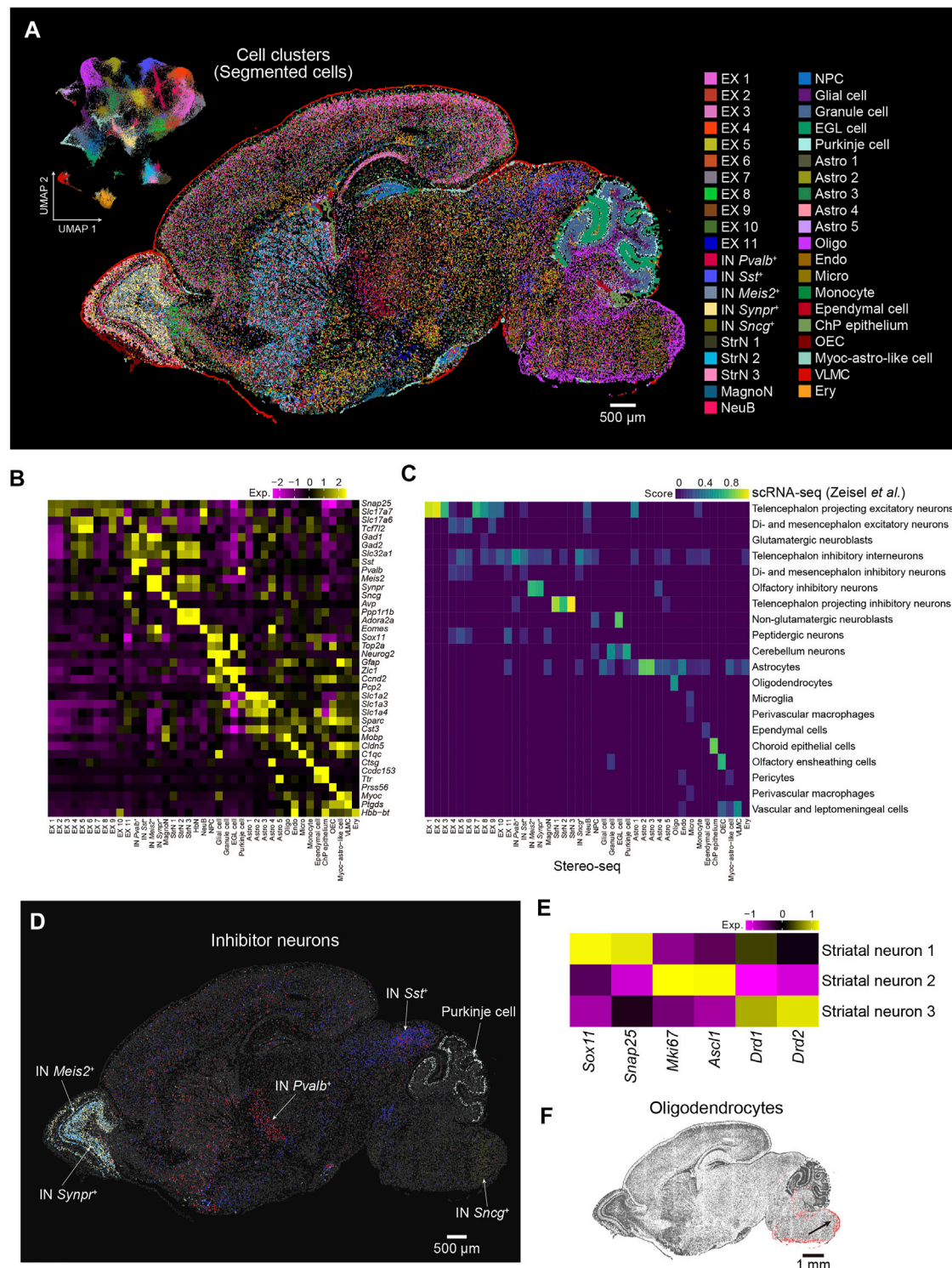
Next, to evaluate the spatial gene expression pattern of Stereo-seq, we selected 25 reported regional-specific genes from 27,330 genes to show the spatial expression patterns for section 1 of the P7 mouse brain. The anatomical regions of the brain were observed based on gene expression patterns (Figure 1C). As expected, the distribution of specific brain cell markers (*Sst* and *Gfap*) exhibited remarkable similarity to *in situ* hybridization (ISH) data from P4 mice (Allen Institute) (Lein et al., 2007) (Figure 1D). To evaluate the efficiency of the high-resolution *in situ* capture of Stereo-seq, we calculated the UMIs and gene counts of each bin (bin 50, 50  $\times$  50 DNB bins, 25  $\mu$ m diameter), which is an appropriate method to identify the different anatomical regions of the Stereo-seq data (Chen et al., 2021; Wu et al., 2021). In section 1, 27,330 genes were detected, with an average of 6,425 UMI and 2,276 genes at bin 50 resolution (Figures 1E,F and Supplementary Table S1). The Pearson correlation coefficient indicated a high correlation between the two sections ( $R^2 = 0.948$ ) (Figure 1G). Hence, our Stereo-seq dataset for the P7 mouse brain illustrates the *in situ* capture of mRNA molecules with high accuracy and efficiency and thus provides a high-quality resource for subsequent data exploration and biological interpretation.

### Region-Specific Patterns of Gene Expression and Gene Regulatory Networks

Next, we applied an unsupervised spatially constrained clustering method [(Chen et al., 2021), see Methods] to reconstruct the

spatial heterogeneity of the sagittal brain section of P7 mice at bin 50 resolution. We identified 41 anatomical regions that were carefully annotated by canonical markers in each anatomical region (Figures 2A,B and Supplementary Table S2). Tissue-specific identities were confirmed by visualizing the specific marker genes (Figure 2C and Supplementary Figure S1A). The distribution of specific markers (*Tshz1* and *Pvalb*) captured by Stereo-seq exhibited the expected similarity to *in situ* hybridization (ISH) data taken from BrainTx (Supplementary Figure S1B). The anatomical clusters included 27 clusters in the forebrain, 3 in the midbrain, 7 in the hindbrain, and 2 widely distributed throughout the brain section [meninges (*Ptgds+*) and blood (*Hbb-bt+*)]. The forebrain was divided into the main anatomical regions, including the olfactory bulb (OB), neocortex, hippocampus, striatum, and diencephalon. Six subregions across the OB were identified: the superficial stratum of the OB (OBs, *Cdhr1+*), intermediate stratum of the OB (Obi, *Tshz1+*), subependymal zone (SEZ, *Dlx1+* and *Sox11+*), lateral pallidum (LPall, *Fst+*), anterior olfactory nucleus (AOV, *Abi3bp+* and *Galnt16+*), and ventropallial prepiriform area (VPrP, *Glut+*). For the neocortex, the Stereo-seq dataset was used to identify different cortical layers based on spatially region-specific genes, including layer 1 (L1, *Gfap+*), layers 2–4 (L2–4, *Cux2+* and *Rorb2+*), layer 4/5 (L4/5, *Rorb+* and *Fezf2+*), layer 6 (L6, *Rprm+*), layer 6b (L6b, *Cplx3+* and *Ctgf+*), and the subventricular zone (SVZ, *Dlx1+*, *Dlx2+*, *Sox11+*, and *Ccnd2+*). In addition to the laminar structure, we observed significant differences along the rostral and caudal axes within deep layer, which suggested functional differences along the rostral and caudal axes in the neocortex sublayers. For example, *Lsmp* and *Kcnip4* were highly expressed in L4/5-R, whereas teneurin transmembrane protein 2 (*Tenm2*) was enriched in L4/5-C (Figure 2D). We also identified region-specific gene expression profiles in different subcortical regions, such as the ventricle, which contains the choroid plexus (*Ttr+*), and striatum, including three subregions: caudoputamen (Str-CP, *Ppp1r1b+* and *Cxcl14+*), nucleus accumbens (Str-ACB, *Ppp1r1b+* and *Adora2a+*), and olfactory tubercle (Str-OT, *Wfs1+* and *Robo1+*). In the diencephalon, we observed clusters indicative of the thalamus (*Kitl+* and *Ntng1+*), reticular nucleus (*Pvalb+* and *Gad1+*), subthalamic nucleus (STN, *Pitx2+*), lateral hypothalamus (LHA, *Pmch+*), and hypothalamus (HY, *Avp+* and *Oxt+*). The hippocampus could be subdivided into five subregions: cornu ammonis area 1 (CA1, *Fibcd1+*, *Wfs1+*, and *Shisa6+*), cornu ammonis area 2/3 (CA2/3, *Nptx1+* and *Spink8+*), dentate gyrus (DG, *Prox1+* and *Neurod1+*), subiculum (*Nts+*), and stratum molecular of CA and DG (Hipp stratum, *Camk2a+*). In the midbrain, we observed typical subanatomical regions, such as the substantia





**FIGURE 3 |** Spatial distribution of cell types in the P7 mouse brain. **(A)** Left: UMAP visualization of the segmented cells from the P7 mouse brain **section 1**. Right: Spatial visualization of cell types shown in the left panel for the whole brain **section 1**. Cells are colored by the annotations. EX, excitatory neuron; IN, inhibitory neuron; MagnaN, magnocellular neuron; StrN, striatal neuron; NeuB, neuroblast; NPC, neuron progenitor cell; EGL cell, external granular layer cell; Astro, astrocyte; Oligo, oligodendrocyte; Endo, endothelium; Micro, microglia; ChP epithelium, choroid plexus epithelium; OEC, olfactory ensheathing cell; Myoc-astro-like cell, myoc-expressing astrocyte-like cell; VLMC, vascular leptomeningeal cell; Ery, erythrocyte. Scale bar, 500  $\mu$ m. **(B)** Heatmap of normalized expression of selected marker genes for the 41 cell types of the P7 mouse brain shown in **(A)**. **(C)** Correspondence between the cell types shown in **A** by Stereo-seq and the cell clusters identified by reported scrNA-seq (Zeisel et al., 2018). **(D)** Spatial visualization of different subtypes of inhibitor neuron clusters shown in **(A)**. Scale bar, 500  $\mu$ m. **(E)** Heatmap of normalized expression of the indicated genes for the three striatal neuron types shown in **(A)**. **(F)** Spatial visualization of oligodendrocytes shown in **(A)**. Scale bar, 1 mm.

nigra (*Th+* and *Gata3+*). The cerebellum was divided into four layers and one nucleus, including the external granular layer (CbXegr, *Cenpa+*), Purkinje cell layer (CbXpu, *Car8+* and *Pcp2+*), internal granular layer of the cerebellum cortex (CbXigr, *Zic1+* and *Cbln1+*), white matter of the cerebellum (CbWM, *Gfap+* and *Spp1+*), and cerebellar nuclei (*Plp1+*) (Figures 2A–C; Supplementary Table S2).

We also employed pySCENIC (Van de Sande et al., 2020) to calculate the activity of the gene regulatory network (also known as regulon) and assess the regulatory activity of the transcription factor across all anatomical regions. The regulons showed strong regional specificity (Figure 2E; Supplementary Table S3). For example, *GBX2* was enriched in clusters 29 (thalamus) and 32 and 33 (midbrain), which was consistent with previous reports that *Gbx2* is expressed in thalamic postmitotic neuronal progenitors and is essential for the maintenance of thalamic neuronal identity (Figures 2E,F) (Nakayama et al., 2013), as well as that it is a transcriptional repressor that regulates the specification and morphogenesis of the mid-hindbrain junction (Nakayama et al., 2013). SP9, a zinc finger transcription factor, was also highly enriched in cluster 3 (Obi) (Figures 2E,F), which was consistent with its function as a regulator of GABAergic neuron production in the olfactory bulb (Zhang et al., 2016). Our analysis revealed strong heterogeneity in both gene expression and gene regulatory networks across anatomical regions in the postnatal mouse brain and suggested that our Stereo-seq data are a great resource for further exploration of molecular regulation in the brain.

## Spatial Distribution of Cell Types in the P7 Mouse Brain

Cells are fundamental elements of organs. The high resolution of the Stereo-seq technology enables the dissection of the spatial transcriptome at cellular resolution at the whole section scale. Next, we performed cell segmentation analysis by registration of the image of the nucleic acid staining and Stereo-seq data using Scikit-image. Segmented cells with gene number less than 300 or the top 0.2% cells ranked by gene number were filtered out. A total of 99,365 cells with an average number of 787 UMI and 698 genes per cell were used for downstream analysis. Subsequently, we employed Seurat to evaluate the cell heterogeneity of sagittal brain section 1 at cellular resolution and identified 41 major cell types that could be annotated using known putative markers, including 25 clusters of neurons and 16 clusters of nonneuronal cells (Figures 3A,B). These annotations were further confirmed by correlation analysis using a publicly available scRNA-seq dataset (Zeisel et al., 2018) (Figure 3C). By the analysis of differential expressed genes (DEGs), we obtained 505 DEGs across the 41 clusters (Supplementary Figure S2). For example, *Sostdc1* and *Calml4* were highly expressed in the choroid plexus epithelium (ChP epithelium). Olfactory ensheathing cell (OEC) highly expressed *Rcn3* and *Lum*. *Gm20425* and *Grb14* were highly enriched in oligodendrocyte (OLI). The spatial distribution of the cell types showed strong regional heterogeneity, which indicates specific functions in each region. For example, *Meis2+* and *Synpr+* inhibitory neurons were located in the olfactory bulb, and the distribution of the *Meis2+* inhibitory

neurons was wider. *Sst+* inhibitory neurons were highly enriched in the inferior colliculus of the midbrain, whereas *Pvalb+* inhibitory neurons were mostly enriched in the reticular nucleus and striatum. *Snca+* inhibitory neurons were mainly located in the medullary region of the hindbrain, and Purkinje cells were located in the cerebellum (Figure 3D). We identified three neuronal subclusters in the striatum, which widely expressed *Ppp1r1b* and *Adora2a*. The striatal neuron 1 cluster displayed high expression of *Sox11*, an immature neuron marker (Bergsland et al., 2006; Chen et al., 2015), whereas striatal neuron 2 expressed both proliferation (*Mki67*) and progenitor (*Ascl1*) markers. Striatal neuron 3 was characterized by high expression levels of genes related to GABAergic spiny projection neurons that receive and integrate information within the striatum, such as *Drd1* and *Drd2* (Anderson et al., 2020) (Figure 3E). We also observed that oligodendrocytes mainly appeared in the hindbrain, which suggested that neurons in the hindbrain were myelinated at this stage (Figure 3F). Overall, our results demonstrate the utility of Stereo-seq data to comprehensively characterize cell types and cell state heterogeneity at the whole-brain section level, which is paramount for understanding cell differentiation processes involving regional and subregional specificities.

## CONCLUSION

We report a high-resolution spatial transcriptomic atlas of sagittal sections from the P7 mouse brain using Stereo-seq. This dataset enables the exploration of the spatial gene expression patterns of 27,330 genes across the medial structures near the midline of the postnatal mouse brain. By applying unsupervised clustering, we identified 41 anatomical regions with differentially expressed genes and showed enrichment of gene regulatory networks, which may be associated with the functions of different regions. We also provided a single-cell resolution map of the whole brain section using image-based cell segmentation and identified 99,365 cells of 41 subtypes in different regions of the P7 mouse brain section. This dataset provides a comprehensive spatial map of anatomical regions, genes, regulons, and cell types in the P7 mouse brain and has significant implications for studies on cell differentiation, cell migration, intercellular interactions, and the underlying regulatory mechanisms. In addition, our work paves the way for studies on brain developmental disorders.

## DATA AVAILABILITY STATEMENT

The datasets presented in this study can be found in online repositories. The names of the repository/repositories and accession number(s) can be found in the article/Supplementary Material.

## ETHICS STATEMENT

The animal study was reviewed and approved by the Ethics Committee of BGI.



## AUTHOR CONTRIBUTIONS

MC, LW, CL, and LL conceived the idea. CL and LL supervised the study. MC, JX, HZ, PG, XZ, GL, and JP collected the samples. MC generated the data with the help of XH, JX, YJ, ZL, XC, QD, and YY. LW analysis the data. SW, ML, WF, and ZH provided help with the cell segmentation. MC wrote the manuscript with the input of LW. LH, SH, FY, XW, YL, SL, AC, and YH gave the relevant advice. LH, YL, GV, ME, CL, and LL provided helpful comments on this study and revised the manuscript. All authors contributed to the article and approved the submitted version.

## FUNDING

LL was supported by the Shenzhen Basic Research Project for Excellent Young Scholars (RCYX20200714114644191). ME was supported by the Innovative Team Program of Bioland Laboratory (Guangzhou Regenerative Medicine and Health Guangdong Laboratory) (2018GZR110103001) and a

Guangdong Basic and Applied Basic Research Foundation (2021B1515120075).

## ACKNOWLEDGMENTS

We thank all members of the Center for Digitizing Cells, Institute of SuperCells, BGI-Shenzhen for helpful comments. We thank China National GeneBank for providing technical support.

## SUPPLEMENTARY MATERIAL

The Supplementary Material for this article can be found online at: <https://www.frontiersin.org/articles/10.3389/fcell.2022.878346/full#supplementary-material>

**Supplementary Figure S1** | Spatial visualization of the indicated gene expression in the section shown in **Figure 2A**.

**Supplementary Figure S2** | Heatmap of the differential expressed genes of the clusters in **Figure 3A**.

## REFERENCES

- Anderson, A. G., Kulkarni, A., Harper, M., and Konopka, G. (2020). Single-Cell Analysis of Foxp1-Driven Mechanisms Essential for Striatal Development. *Cel Rep.* 30, 3051–3066. doi:10.1016/j.celrep.2020.02.030
- Bakken, T. E., Miller, J. A., Ding, S.-L., Sunkin, S. M., Smith, K. A., Ng, L., et al. (2016). A Comprehensive Transcriptional Map of Primate Brain Development. *Nature* 535, 367–375. doi:10.1038/nature18637
- Bergsland, M., Werme, M., Malewicz, M., Perlmann, T., and Muhr, J. (2006). The Establishment of Neuronal Properties Is Controlled by Sox4 and Sox11. *Genes Dev.* 20, 3475–3486. doi:10.1101/gad.403406
- Carter, R. A., Bihannic, L., Rosencrance, C., Hadley, J. L., Tong, Y., Phoenix, T. N., et al. (2018). A Single-Cell Transcriptional Atlas of the Developing Murine Cerebellum. *Curr. Biol.* 28, 2910–2920. doi:10.1016/j.cub.2018.07.062
- Chen, C., Lee, G. A., Pourmorady, A., Sock, E., and Donoghue, M. J. (2015). Orchestration of Neuronal Differentiation and Progenitor Pool Expansion in the Developing Cortex by SoxC Genes. *J. Neurosci.* 35, 10629–10642. doi:10.1523/jneurosci.1663-15.2015
- Chen, A., Liao, S., Cheng, M., Ma, K., Wu, L., Lai, Y., et al. (2021). Spatiotemporal Transcriptomic Atlas of Mouse Organogenesis Using DNA Nanoball Patterned Arrays. *bioRxiv*, 427004. doi:10.1101/2021.01.17.427004
- Cho, C.-S., Xi, J., Si, Y., Park, S.-R., Hsu, J.-E., Kim, M., et al. (2021). Microscopic Examination of Spatial Transcriptome Using Seq-Scope. *Cell* 184, 3559–3572. doi:10.1016/j.cell.2021.05.010
- Di Bella, D. J., Habibi, E., Stickels, R. R., Scalia, G., Brown, J., Yadollahpour, P., et al. (2021). Molecular Logic of Cellular Diversification in the Mouse Cerebral Cortex. *Nature* 595, 554–559. doi:10.1038/s41586-021-03670-5
- Ding, S. L., Royall, J. J., Lesnar, P., Facer, B. A. C., Smith, K. A., Wei, Y., et al. (2022). Cellular Resolution Anatomical and Molecular Atlases for Prenatal Human Brains. *J. Comp. Neurol.* 530, 6–503. doi:10.1002/cne.25243
- Dobin, A., Davis, C. A., Schlesinger, F., Drenkow, J., Zaleski, C., Jha, S., et al. (2013). STAR: Ultrafast Universal RNA-Seq Aligner. *Bioinformatics* 29, 15–21. doi:10.1093/bioinformatics/bts635
- Echevarria, D., Vieira, C., Gimeno, L., and Martínez, S. (2003). Neuroepithelial Secondary Organizers and Cell Fate Specification in the Developing Brain. *Brain Res. Brain Res. Rev.* 43, 179–191. doi:10.1016/j.brainresrev.2003.08.002
- Han, X., Wu, X., Chung, W.-Y., Li, T., Nekrutenko, A., Altman, N. S., et al. (2009). Transcriptome of Embryonic and Neonatal Mouse Cortex by High-Throughput RNA Sequencing. *Proc. Natl. Acad. Sci. U.S.A.* 106, 12741–12746. doi:10.1073/pnas.0902417106
- Hao, Y., Hao, S., Andersen-Nissen, E., Mauck, W. M., 3rd, Zheng, S., Butler, A., et al. (2021). Integrated Analysis of Multimodal Single-Cell Data. *Cell* 184, 3573–3587. doi:10.1016/j.cell.2021.04.048
- Hodge, R. D., and Hevner, R. F. (2011). Expression and Actions of Transcription Factors in Adult Hippocampal Neurogenesis. *Devel. Neurobiol.* 71, 680–689. doi:10.1002/dneu.20882
- Huynh-Thu, V. A., Irrthum, A., Wehenkel, L., and Geurts, P. (2010). Inferring Regulatory Networks from Expression Data Using Tree-Based Methods. *PLoS One* 5, e12776. doi:10.1371/journal.pone.0012776
- Jiang, X., and Nardelli, J. (2016). Cellular and Molecular Introduction to Brain Development. *Neurobiol. Dis.* 92, 3–17. doi:10.1016/j.nbd.2015.07.007
- Kozareva, V., Martin, C., Osorno, T., Rudolph, S., Guo, C., Vanderburg, C., et al. (2021). A Transcriptomic Atlas of Mouse Cerebellar Cortex Comprehensively Defines Cell Types. *Nature* 598, 214–219. doi:10.1038/s41586-021-03220-z
- La Manno, G., Siletti, K., Furlan, A., Gyllborg, D., Vinsland, E., Mossi Albiach, A., et al. (2021). Molecular Architecture of the Developing Mouse Brain. *Nature* 596, 92–96. doi:10.1038/s41586-021-03775-x
- Lake, B. B., Ai, R., Kaeser, G. E., Salathia, N. S., Yung, Y. C., Liu, R., et al. (2016). Neuronal Subtypes and Diversity Revealed by Single-Nucleus RNA Sequencing of the Human Brain. *Science* 352, 1586–1590. doi:10.1126/science.aaf1204
- Lein, E. S., Hawrylycz, M. J., Ao, N., Ayres, M., Bensinger, A., Bernard, A., et al. (2007). Genome-wide Atlas of Gene Expression in the Adult Mouse Brain. *Nature* 445, 168–176. doi:10.1038/nature05453
- Lein, E., Borm, L. E., and Linnarsson, S. (2017). The Promise of Spatial Transcriptomics for Neuroscience in the Era of Molecular Cell Typing. *Science* 358, 64–69. doi:10.1126/science.aan6827
- Li, M., Santpere, G., Imamura Kawasawa, Y., Evgrafov, O. V., Gulden, F. O., Pochareddy, S., et al. (2018). Integrative Functional Genomic Analysis of Human Brain Development and Neuropsychiatric Risks. *Science* 362, eaat7615. doi:10.1126/science.aat7615
- Liao, J., Lu, X., Shao, X., Zhu, L., and Fan, X. (2021). Uncovering an Organ's Molecular Architecture at Single-Cell Resolution by Spatially Resolved Transcriptomics. *Trends Biotechnol.* 39, 43–58. doi:10.1016/j.tibtech.2020.05.006
- Liu, Y., Yang, M., Deng, Y., Su, G., Enninfu, A., Guo, C. C., et al. (2020). High-Spatial-Resolution Multi-Omics Sequencing via Deterministic Barcoding in Tissue. *Cell* 183, 1665–1681. doi:10.1016/j.cell.2020.10.026
- Long, X., Colonell, J., Wong, A. M., Singer, R. H., and Lionnet, T. (2017). Quantitative mRNA Imaging throughout the Entire Drosophila Brain. *Nat. Methods* 14, 703–706. doi:10.1038/nmeth.4309

- Manuel, M. N., Mi, D., Mason, J. O., and Price, D. J. (2015). Regulation of Cerebral Cortical Neurogenesis by the Pax6 Transcription Factor. *Front. Cel. Neurosci.* 9, 70. doi:10.3389/fncel.2015.00070
- Martínez, S. (2001). The Isthmic Organizer and Brain Regionalization. *Int. J. Dev. Biol.* 45, 367–371. doi:10.1387/IJDB.11291867
- Miller, J. A., Ding, S.-L., Sunkin, S. M., Smith, K. A., Ng, L., Szafer, A., et al. (2014). Transcriptional Landscape of the Prenatal Human Brain. *Nature* 508, 199–206. doi:10.1038/nature13185
- Nakayama, Y., Kikuta, H., Kanai, M., Yoshikawa, K., Kawamura, A., Kobayashi, K., et al. (2013). Gbx2 Functions as a Transcriptional Repressor to Regulate the Specification and Morphogenesis of the Mid-hindbrain junction in a Dosage- and Stage-dependent Manner. *Mech. Develop.* 130, 532–552. doi:10.1016/j.mod.2013.07.004
- Ortiz, C., Carlén, M., and Meletis, K. (2021). Spatial Transcriptomics: Molecular Maps of the Mammalian Brain. *Annu. Rev. Neurosci.* 44, 547–562. doi:10.1146/annurev-neuro-100520-082639
- Palla, G., Spitzer, H., Klein, M., Fischer, D., Schaar, A. C., Kuemmerle, L. B., et al. (2022). Squidpy: a Scalable Framework for Spatial Omics Analysis. *Nat. Methods* 19, 171. doi:10.1038/s41592-021-01358-2
- Parenti, I., Rabaneda, L. G., Schoen, H., and Novarino, G. (2020). Neurodevelopmental Disorders: From Genetics to Functional Pathways. *Trends Neurosci.* 43, 608–621. doi:10.1016/j.tins.2020.05.004
- Rodrigues, S. G., Stickels, R. R., Goeva, A., Martin, C. A., Murray, E., Vanderburg, C. R., et al. (2019). Slide-seq: A Scalable Technology for Measuring Genome-wide Expression at High Spatial Resolution. *Science* 363, 1463–1467. doi:10.1126/science.aaw1219
- Stahl, P. L., Salmén, F., Vickovic, S., Lundmark, A., Navarro, J. F., Magnusson, J., et al. (2016). Visualization and Analysis of Gene Expression in Tissue Sections by Spatial Transcriptomics. *Science* 353, 78–82. doi:10.1126/science.aaf2403
- Stiles, J., and Jernigan, T. L. (2010). The Basics of Brain Development. *Neuropsychol. Rev.* 20, 327–348. doi:10.1007/s11065-010-9148-4
- Tan, L., Ma, W., Wu, H., Zheng, Y., Xing, D., Chen, R., et al. (2021). Changes in Genome Architecture and Transcriptional Dynamics Progress Independently of Sensory Experience during post-natal Brain Development. *Cell* 184, 741–758. doi:10.1016/j.cell.2020.12.032
- Tasic, B., Menon, V., Nguyen, T. N., Kim, T. K., Jarsky, T., Yao, Z., et al. (2016). Adult Mouse Cortical Cell Taxonomy Revealed by Single Cell Transcriptomics. *Nat. Neurosci.* 19, 335–346. doi:10.1038/nn.4216
- Tasic, B., Yao, Z., Graybiel, L. T., Smith, K. A., Nguyen, T. N., Bertagnoli, D., et al. (2018). Shared and Distinct Transcriptomic Cell Types across Neocortical Areas. *Nature* 563, 72–78. doi:10.1038/s41586-018-0654-5
- Thompson, C. L., Ng, L., Menon, V., Martinez, S., Lee, C.-K., Glattfelder, K., et al. (2014). A High-Resolution Spatiotemporal Atlas of Gene Expression of the Developing Mouse Brain. *Neuron* 83, 309–323. doi:10.1016/j.neuron.2014.05.033
- Tiklova, K., Björklund, Å. K., Lahti, L., Fiorenzano, A., Nolbrant, S., Gillberg, L., et al. (2019). Single-cell RNA Sequencing Reveals Midbrain Dopamine Neuron Diversity Emerging during Mouse Brain Development. *Nat. Commun.* 10, 581. doi:10.1038/s41467-019-08453-1
- Van de Sande, B., Flerin, C., Davie, K., De Waegeneer, M., Hulselmans, G., Aibar, S., et al. (2020). A Scalable SCENIC Workflow for Single-Cell Gene Regulatory Network Analysis. *Nat. Protoc.* 15, 2247–2276. doi:10.1038/s41596-020-0336-2
- Vickovic, S., Eraslan, G., Salmén, F., Klughammer, J., Stenbeck, L., Schapiro, D., et al. (2019). High-definition Spatial Transcriptomics for *In Situ* Tissue Profiling. *Nat. Methods* 16, 987–990. doi:10.1038/s41592-019-0548-y
- Wolf, F. A., Angerer, P., and Theis, F. J. (2018). SCANPY: Large-Scale Single-Cell Gene Expression Data Analysis. *Genome Biol.* 19, 15.
- Wu, L., Yan, J., Bai, Y., Chen, F., Xu, J., Zou, X., et al. (2021). Spatially-resolved Transcriptomics Analyses of Invasive Fronts in Solid Tumors. *bioRxiv*, 465135. doi:10.1101/2021.10.21.465135
- Zeisel, A., Hochgerner, H., Lönnerberg, P., Johnsson, A., Memic, F., van der Zwan, J., et al. (2018). Molecular Architecture of the Mouse Nervous System. *Cell* 174, 999–1014. doi:10.1016/j.cell.2018.06.021
- Zhang, J., Miller, M. I., Plachez, C., Richards, L. J., Yarowsky, P., van Zijl, P., et al. (2005). Mapping Postnatal Mouse Brain Development with Diffusion Tensor Microimaging. *Neuroimage* 26, 1042–1051. doi:10.1016/j.neuroimage.2005.03.009
- Zhang, Q., Zhang, Y., Wang, C., Xu, Z., Liang, Q., An, L., et al. (2016). The Zinc Finger Transcription Factor Sp9 Is Required for the Development of Striatopallidal Projection Neurons. *Cel Rep.* 16, 1431–1444. doi:10.1016/j.celrep.2016.06.090

**Conflict of Interest:** Authors MC, LW, LH, XH, YL, JX, SW, ML, HZ, WF, ZH, YJ, SH, ZL, XC, JP, QD, YY, FY, XW, SL, AC, ME, YH, CL, and LL were employed by BGI-Shenzhen.

The remaining authors declare that the research was conducted in the absence of any commercial or financial relationships that could be construed as a potential conflict of interest.

**Publisher's Note:** All claims expressed in this article are solely those of the authors and do not necessarily represent those of their affiliated organizations, or those of the publisher, the editors and the reviewers. Any product that may be evaluated in this article, or claim that may be made by its manufacturer, is not guaranteed or endorsed by the publisher.

Copyright © 2022 Cheng, Wu, Han, Huang, Lai, Xu, Wang, Li, Zheng, Feng, Huang, Jiang, Hao, Li, Chen, Peng, Guo, Zhang, Lai, Deng, Yuan, Yang, Wei, Liao, Chen, Volpe, Esteban, Hou, Liu and Liu. This is an open-access article distributed under the terms of the Creative Commons Attribution License (CC BY). The use, distribution or reproduction in other forums is permitted, provided the original author(s) and the copyright owner(s) are credited and that the original publication in this journal is cited, in accordance with accepted academic practice. No use, distribution or reproduction is permitted which does not comply with these terms.



# Calreticulin Identified as One of the Androgen Response Genes That Trigger Full Regeneration of the Only Capable Mammalian Organ, the Deer Antler

Qianqian Guo<sup>1,2</sup>, Junjun Zheng<sup>2</sup>, Hengxing Ba<sup>1</sup>, Hongmei Sun<sup>2</sup>, Jingjie Zhai<sup>3</sup>, Wenying Wang<sup>1</sup> and Chunyi Li<sup>1\*</sup>

## OPEN ACCESS

### Edited by:

Mo Li,  
King Abdullah University of Science  
and Technology, Saudi Arabia

### Reviewed by:

Bin Guo,  
Jilin University, China  
Jiannan Li,  
Jilin University, China  
Jinlan Jiang,  
Jilin University, China  
Aruna Sharma,  
Uppsala University, Sweden

### \*Correspondence:

Chunyi Li  
lichunyi1959@163.com

### Specialty section:

This article was submitted to  
Stem Cell Research,  
a section of the journal  
Frontiers in Cell and Developmental  
Biology

**Received:** 26 January 2022

**Accepted:** 22 April 2022

**Published:** 13 June 2022

### Citation:

Guo Q, Zheng J, Ba H, Sun H, Zhai J,  
Wang W and Li C (2022) Calreticulin  
Identified as One of the Androgen  
Response Genes That Trigger Full  
Regeneration of the Only Capable  
Mammalian Organ, the Deer Antler.  
Front. Cell Dev. Biol. 10:862841.  
doi: 10.3389/fcell.2022.862841

<sup>1</sup>Institute of Antler Science and Product Technology, Changchun Sci-Tech University, Jilin, China, <sup>2</sup>Institute of Special Economic Animal and Plant Sciences, Chinese Academy of Agricultural Sciences, Jilin, China, <sup>3</sup>Department of Oral Implantology, Jilin Provincial Key Laboratory of Sciences and Technology for Stomatology Nanoengineering, Hospital of Stomatology, Jilin University, Jilin, China

Deer antlers are male secondary sexual characters that develop to become bone; they are unique appendages that, once lost, can fully regenerate from the permanent bony protuberances or pedicles. Pedicle periosteum (PP) is the tissue that gives rise to the regenerating antlers with three differentiation stages, namely, dormant (DoPP), potentiated (PoPP), and activated (AcPP). Thus far, the transition from the PoPP to the AcPP has not been studied. Our results showed that the AcPP cells maintained their original stem cell features by expressing mesenchymal stem cell (MSC) markers CD73, CD90, and CD105, although they had entered the proliferation mode. The differentially expressed genes (DEGs) in the AcPP compared with those of the PoPP were mainly involved in protein processing, cell cycle, and calcium signaling pathways. Calreticulin (CALR), an androgen response gene, was significantly differentially upregulated in the AcPP cells, and its expression level was negatively regulated by androgens, in contrast to the currently known model systems where all regulation is positive. The downregulation of CALR expression in the AcPP cells *in vitro* inhibited cell proliferation, induced apoptosis, and inhibited cell cycle progression at G1-S transition. Therefore, CALR is likely a downstream mediator of androgen hormones for triggering initiation of antler regeneration. We believe that the identification of CALR has not only discovered “one critical piece” of the “jigsaw puzzle” in the initiation of antler regeneration but also helps in revealing the mechanism underlying this unique mammalian epimorphic regeneration and has also opened a new avenue for the study of the nature of CALR regulation by androgen (putative binding partners), thus facilitating the identification of potential molecule(s) for investigation as targets for clinical evaluation.

**Keywords:** antler regeneration, calreticulin, androgen response gene, antler stem cells, RNAi

## INTRODUCTION

Deer antlers are the only mammalian organ that, once lost, can fully grow back (Goss and Rosen, 1973; Price et al., 2005). Thus, they offer a unique opportunity to explore how nature has solved the problem of mammalian organ regeneration, a matter highly pertinent to the field of regenerative medicine (Nieto-Diaz et al., 2012). Each year in spring, hard antlers are cast from the permanent bony protuberances (pedicles), which triggers the regeneration of new (velvet) antlers (Kierdorf et al., 2009; Kierdorf and Kierdorf, 2011). Total or partial deletion of the pedicle periosteum (PP) prior to antler regeneration has demonstrated convincingly that it is the PP that gives rise to regenerating antlers (Li et al., 2007). Membrane insertion experiments have shown that to enable the antler to regenerate, the PP must interact with its enveloping skin, which is facilitated by close association of these two tissue types (Li et al., 2008). Based on these findings, Li et al. (2004) and Li et al. (2007) classified the PP along the longitudinal axis of a pedicle into three states proximo-distally, the dormant PP (DoPP, proximal two-thirds of the PP), characterized by loosely linked to the pedicle skin; the potentiated PP (PoPP, distal third of the PP), intimately associated with the pedicle skin; and the activated PP (AcPP, peripherally encroaching into the cast plane of the pedicle), which is intimately associated with the antler (velvet) skin.

In seeking to unveil the molecular mechanism underlying the transition from the DoPP to the PoPP, our team has carried out a series of studies. Dong et al. (2016) identified 169 differentially expressed proteins (70 upregulated and 99 downregulated) of the PoPP over the DoPP using iTRAQ-based quantitative proteomic analysis. Yang et al. (2016) found that the levels of genome-wide DNA methylation were significantly lower in the PoPP than in the DoPP. Furthermore, Dong et al. (2019) reported that the epithelial-mesenchymal transition process may participate in potentiation of the PP (using two-dimensional difference gel electrophoresis, 2D-DIGE). All of these results are consistent with our histological (Li et al., 2005) and tissue deletion (Li et al., 2007) findings. However, thus far, the mechanism underlying the transition from the PoPP to the AcPP has not been resolved, albeit that it is the indispensable step for initiation of antler blastema formation and subsequent regeneration of the antler (Li and Chu, 2016).

Antlers and their antecedent pedicles are male secondary sexual characters and, as such, their development is strictly under control of androgen hormones (Weerasekera et al., 2020). Surprisingly, except for pedicle initiation and antler calcification that require high levels of androgens, androgens seem to be detrimental to antler regeneration and growth. In this respect, initiation of antler regeneration can only start when androgens decrease to an almost undetectable level; castration at any time of stags in the hard antler stage will induce casting of the hard antler and immediate regeneration of a new antler, and further administration of exogenous androgen can effectively suppress antler regeneration (Bubenik et al., 1982; Suttie et al., 1995; Akhtar et al.,

2019). Therefore, androgens must act as a “brake” on antler regeneration likely through suppression of the activation of the PP cells. However, the identity of such androgen response gene(s) that are released from the “brake” is, thus far, unknown.

The aim of the present study was to use a range of techniques to investigate the transition from the PoPP state to the AcPP state (triggering of PP cell proliferation and thus initiation of antler regeneration) and identify candidates for the androgen response gene(s) through the analysis of differential expression. Our results showed that the AcPP cells, which had entered the proliferation state, still partly maintained the original stemness evidenced by the expression of marker genes of the mesenchymal stem cells (MSCs; CD73, CD90, and CD105). Furthermore, during this transition, calreticulin (CALR), an androgen response gene, was highly expressed in the AcPP cells. The downregulation of CALR *in vitro* had significant influence on the PP cells evidenced by reduction in the cell proliferation rate, inhibition of cell cycle progression, and induction of apoptosis. Consequently, we propose that CALR is a key androgen response factor that triggers the initiation of antler regeneration *in vivo*.

## MATERIALS AND METHODS

### Ethics Statement

All animal-related experiments in the present study were performed in accordance with the guidelines of the Animal Care and Use Committee of Jilin University and under the approval from the Temporary Animal Ethics Committee of Changchun Sci-Tech University (Permit Number: CKARI-2020-017).

### Experimental Animals and Tissue Sampling

The 3-year-old sika deer (*Cervus nippon*) stags were used in the study from Dong Ao Deer Farm. Three stags were selected from the herd at the time of hard antler button casting when the distal rim of the pedicle skin had encroached onto the casting surface peripherally and occupied one-third to one-half of the entire casting surface (Supplementary Figure S1A). Each selected animal was slaughtered immediately; the right-side pedicles were used for histology and cell culture and the left-side ones for molecular study. The detailed procedures for sampling of PoPP and AcPP tissues were reported elsewhere (Li et al., 2003). The tissue samples from the right-side pedicles were fixed in 10% formalin for histology; those from the left side were frozen in liquid nitrogen and stored at  $-80^{\circ}\text{C}$  for RNA extraction and sequencing.

### Histology

Histological procedures for processing PP tissues have been reported elsewhere (Li et al., 2005). In brief, trimmed PP tissues were embedded in paraffin wax, sectioned at  $4\mu\text{m}$ , rehydrated, and co-stained with Alcian blue (AB) and hematoxylin/eosin (HE). The stained sections were then dehydrated, mounted, examined, and photographed under a slice scanner (Leica, Germany).



## Immunohistochemistry

IHC was performed using the UltraSensitive TM SP (Mouse/Rabbit) IHC Kit (MX Biotechnologies, China), according to the manufacturer's protocol. Briefly, PP tissue sections were rehydrated and subjected to antigen retrieval. After blocking the nonspecific binding with milk powder, the sections were incubated with primary antibodies overnight at 4°C and washed with PBS three times; the sections were then incubated with biotinylated secondary antibody (MX Biotechnologies, China) for 10 min at room temperature and finally visualized using DAB (3, 3'-diaminobenzidine; MX Biotechnologies, China) staining. First antibodies used in this study included rabbit anti-ki67 (1:1000, Abcam, ab16667), rabbit anti-CD90 (1:100, Bioss, bs-0778R), mouse anti-CD105 (1:100, Elabscience, ESH135), rabbit anti-CD73 (1:100, Santa, sc-25603), and rabbit anticalreticulin (CALR; 1:50, Abcam, ab702); isotypic IgG (1:500, Abcam, ab172730) was used as the control. The images were captured by using an inverted microscope (Nikon, Japan) or a slice scanner (Leica, Germany).

## RNA-Seq

RNA-sequencing (RNA-seq) was performed by BGI Life Tech Co. Ltd. (Wuhan, China). The PP tissues were rapidly ground into fine powder in liquid nitrogen using Freezer/Mill 6770 (SPEX CertiPrep Ltd., United States), and total RNA was extracted using TRIzol reagent (Qiagen, Hilden, Germany) according to the manufacturer's procedure. RNA quality was confirmed using a bioanalyzer with a minimum RNA integrity number of 7. In total, 0.6 mg RNA was used to construct libraries according to the manufacturer's instructions (Illumina TruSeq Library Preparation Kit v3), and libraries were sequenced using an Illumina HiSeq X Ten at BGI (Shenzhen, China). SOAPnuke (v1.5.2; Cock et al., 2009) was used to filter raw reads, and high-quality reads were aligned to the *Cervus hanglu yarkandensis* (Yarkand deer) reference genome CEY\_v1 (Ba et al., 2020) by HISAT (v2.0.4; Kim et al., 2015). The transcript quantification (FPKM, fragments per kilobase per million) was calculated using RSEM (Li and Dewey, 2011). Analysis of the differential expression gene (DEG) was performed using DESeq2 software (v1.4.5; Love et al., 2014). Genes meeting the criteria set at  $|\log_2(\text{fold change})| > 0.5$ , and the false discovery rate (FDR)  $< 0.01$  were assigned as differentially expressed. Principal components analysis (PCA) was performed with the R packages factextra v1.0.6 and FactoMineR v2.2. Venn diagram and the volcano plot were drawn using Dr. Tom software (<https://biosys.bgi.com>). GO and KEGG enrichment analyses were carried out using the R package clusterProfiler (v3.4.4; Yu et al., 2012).

## Cell Culture

Procedures for culturing the AcPP and PoPP cells were as described previously (Li et al., 2012; Seo et al., 2014; Guo et al., 2015). Briefly, the cells were cultured in the medium containing DMEM (Life, United States) plus 10% FBS (Gibco, United States), 100 U/ml penicillin, and 100 µg/ml streptomycin (Invitrogen, United States) at 37°C in 5% CO<sub>2</sub>, passaged using trypsin (Sigma, United States) and stored in liquid nitrogen in freezing medium (90% FBS +10%

DMSO). When required, the cells were thawed and seeded in T75 flasks (Nest Biotechnology, United States). The cells used in this study had gone through two passages.

## Testosterone Treatment, Cell Proliferation, and Calreticulin Expression Assays

The cells were seeded in 24-well plates at a density of  $2 \times 10^4$  cells/ml/well. Each treatment was performed in triplicate. The cells were incubated for 48 h and followed by 24 h starvation in the serum-free medium (culture medium without FBS) prior to the following treatments for 24 h: 1) 1% FBS, 2) 5% FBS, 3) 10% FBS, 4) 0.0 nM T, 5) 0.5 nM T (Sigma, United States), 6) 1.0 nM T, 7) 5.0 nM T, 8) 10.0 nM T, and 9) 50.0 nM T. The cell proliferation rate and the expression level of CALR were analyzed by CCK-8 and qRT-PCR assays, respectively.

## Cell Transfection

Three short-hairpin RNAs (shRNA) targeting CALR (shCALR1: GCGGCCTGATAATACCTAT, shCALR2: GCTGGATCGAATCCAAACA, and shCALR3: GCTGGATCGAATCCAAACA) were synthesized by GenePharma Biotechnology (Shanghai, China). The 293 T-cells were transiently transfected with the recombinant lentiviral shRNA constructs or empty carrier (pLVTHM as negative control) along with the pCMVΔ8.9 and pMD2G plasmids in a ratio of 2:2:1 using Lipofectamine 3000 (Invitrogen, United States) according to the manufacturer's protocol. Virus-containing supernatants were collected at 24 and 48 h after transfection, pooled together, and then concentrated by centrifugation (5,000 g, 40 min) using the Amicon ultra centrifugal filter devices (Millipore Corporation, United States). Then, the AcPP cells were infected with the lentiviruses carrying shCALR1, shCALR2, shCALR3, or the negative control in the presence of 5 µg/ml polybrene (Sigma-Aldrich). The GFP expressing cells were sorted by flow cytometry (BD FACSAria, United States) according to the manufacturer's manual. The efficiency of CALR silencing by these shRNAs was determined using Western blotting and qRT-PCR assays.

## Western Blot Analysis

Total cellular proteins were extracted using RIPA buffer, and the cell lysates were centrifuged at 15,000 g at 4°C for 15 min. The protein concentration was measured using the BCA protein assay (Beyotime, China). Then, 30 µg protein was separated on a 10% SDS-PAGE, and the separated proteins were electro-transferred onto the 0.2-µm PVDF membranes. The membranes were then blocked in TBST containing 5% nonfat dry milk for 2 h at room temperature and hybridized with the primary antibody (rabbit anti-CALR, Abcam) overnight at 4°C. Then, the blots were probed with HRP-conjugated secondary antibodies and detected using ECL, photographed, and quantified using ImageJ software.

## Quantitative Real-Time PCR

Total RNA was isolated using TRIzol reagent and purified on a silica base spin column (SK1321, Shanghai Shenggong Inc.,

China) according to the manufacturer's protocol. The specific primers, based on the DNA sequences located in the gene coding regions, were designed using software Primer 5 (**Supplementary Table S1**). Glyceraldehyde-3-phosphate dehydrogenase (GAPDH) was used as an endogenous control. Total RNA was reverse-transcribed onto cDNA using the cDNA Synthesis Kit (Invitrogen Inc., Camarillo, CA, United States). The SYBR Kit (Applied Biosystems, Foster City, CA, United States) was used in the qRT-PCR assay according to the manufacturer's protocol. Relative expression was calculated using the  $2^{-\Delta\Delta CT}$  method to assess the fold change in expression levels of the target genes. Linear regression analysis was performed using the ggplot2 R package (Bader and Hogue, 2003).

### Cell Counting Kit-8 and Cell Colony Formation Assays

Cell viability was measured using the Cell Counting Kit-8 (Solarbio, China) according to the manufacturer's instructions. The colony formation assay was carried out using a reported methodology (Wang et al., 2019). Briefly, 200 cells in 2 ml medium were seeded into each well of 6-well plates, and the medium was replaced every 4 days; after 14 days of culture, the formed cell colonies were washed with PBS, fixed in 4% paraformaldehyde for 30 min, and stained with 0.5% crystal violet dye for 5 min. Nonspecific staining was removed by three rinses with double-distilled water, and the cells were photographed under a microscope. The colony-forming ability of cells was estimated by quantifying the number of colony-forming units (CFUs,  $\geq 50$  cells).

### EdU (5-Ethynyl-20-Deoxyuridine) Incorporation Assay

The EdU incorporation assay was performed using a KeyFluor594 Click-iT EdU Kit (KeyGEN BioTECH, China) according to the manufacturer's protocol. Briefly, the cells were first incubated with the medium supplemented with 50  $\mu$ M EdU for 3 h and fixed in 4% polyformaldehyde for 30 min. The cells were then permeabilized with 0.5% Triton X-100 and subsequently blocked with 3% bovine serum albumin (BSA) in PBS for 2 h. The nuclei of cells were counterstained with DAPI for 5 min in the dark. The specific fluorescent staining was examined under a fluorescent microscope.

### Flow Cytometry Analysis

Flow cytometry was used to analyze the cell cycle and cell apoptosis. For cell cycle analysis, the cells were collected and fixed in pre-cooled 75% ethanol overnight at  $-20^{\circ}\text{C}$ , centrifuged at 500 g, and resuspended in 500  $\mu$ l PBS containing 10  $\mu$ l RNase (50  $\mu$ g/ml; Sigma, United States) for 30 min at  $37^{\circ}\text{C}$ , followed by the incubation with propidium iodide (PI, final concentration: 50  $\mu$ g/ml) solution for 30 min in the dark, and then cell cycles were analyzed using flow cytometry.

Apoptosis was detected using the Annexin V-PE/7-AAD staining kit (Kaiji Inc., China), according to the manufacturer's instruction. Briefly,  $1-2 \times 10^6$  cells were

trypsinized using EDTA-free trypsin (Invitrogen, United States) and centrifuged at 1,500 g, washed twice in 10 ml PBS, and then labeled with 7-AAD and Annexin V-PE in binding buffer according to the manufacturer's instructions. The apoptotic cells were detected using flow cytometry.

### Statistical Analysis

The results are presented as mean  $\pm$  SD. Statistical significance was evaluated using GraphPad Prism 8.0.1 (GraphPad Software, La Jolla, CA, United States) software. Statistical analysis for the comparisons of multiple variables was performed using a two-way ANOVA, and Student's *t*-test was used to compare two variables. All experiments were performed in triplicate. The values were set at  $p < 0.05$  for statistical significance.

## RESULTS

### Activated Pedicle Periosteum Cells Were in the Proliferation Mode but Retained the Expression of Classical Mesenchymal Stem Cell Marker Genes: CD73, CD90, and CD105

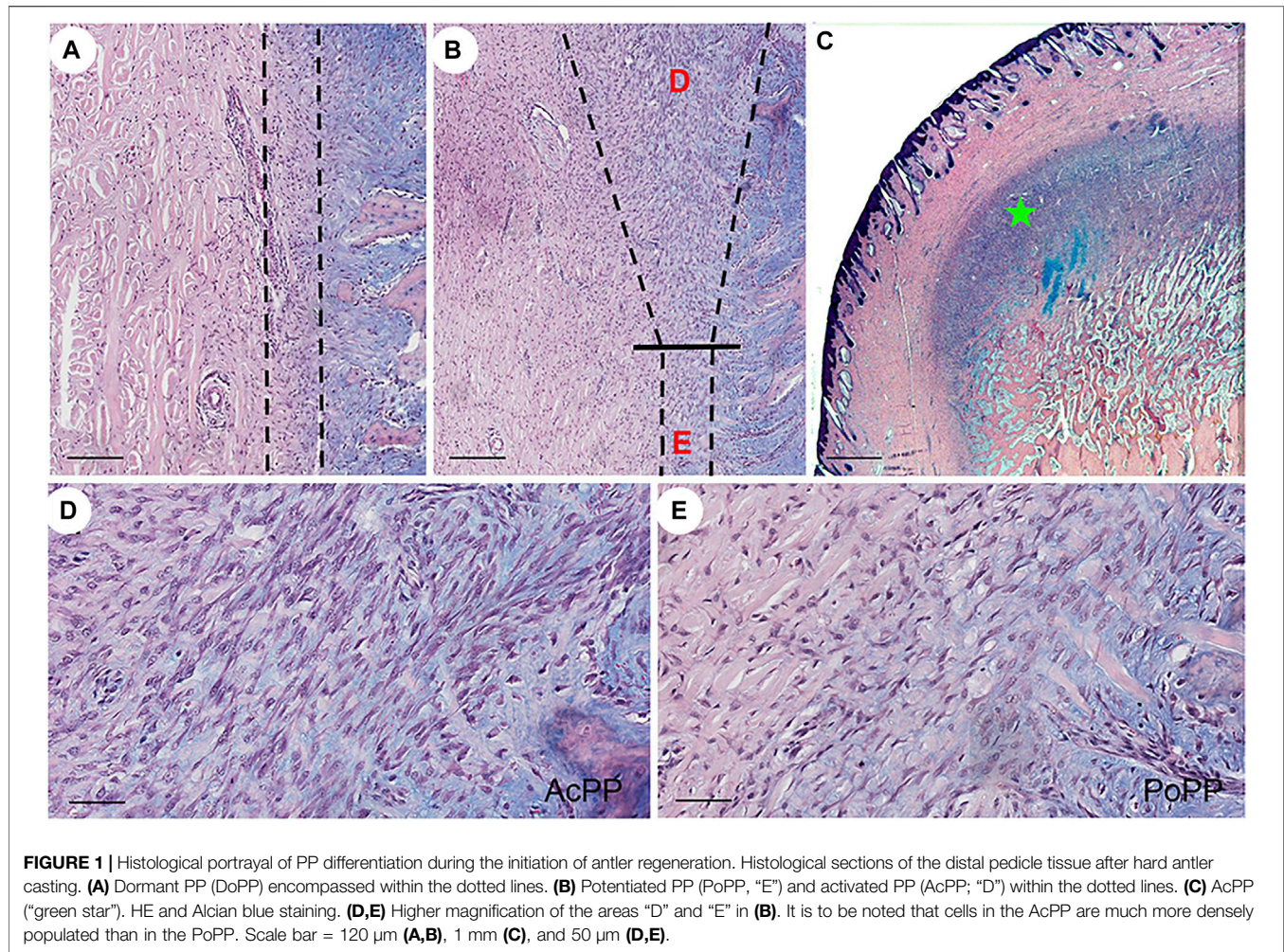
On the histologically processed tissue sections, three developmental states of the PP [DoPP (**Figure 1A**), PoPP (**Figure 1B**), and AcPP (**Figures 1B,C**)] were clearly demarcated. At a higher magnification, one could clearly see that the AcPP layer was much thickened (**Figure 1B**), and cells in the AcPP (**Figure 1D**) were more densely populated than those in the PoPP (**Figure 1E**). This indicates that immediately after hard antler casting, transition from the PoPP to the AcPP had occurred and antler regeneration had started.

To further confirm the histological results (i.e., that AcPP cells were in proliferation mode), we carried out IHC staining of Ki67, with a highly significant difference in the mitotic figures being detected; this was higher in the AcPP than in the PoPP (**Figures 2A,B**). To determine whether the AcPP cells (proliferation mode) retained their original stemness as per their antecedents, the PoPP cells, we examined the expression of three classic MSC marker genes: CD73, CD90, and CD105 (Wang et al., 2019). The results showed that all three MSC marker genes were positively stained in almost all cells of the AcPP, with no visible difference in expression levels between the AcPP and PoPP cells (**Figures 2C-H**). Therefore, even after entering the proliferation mode, PP cells still retained their MSC features with the expression of classic MSC marker genes at the AcPP stage.

### Significant Number of Differentially Expressed Genes Identified in the Cells of the Activated Pedicle Periosteum Over the Potentiated Pedicle Periosteum

A total of 42.1 Gbps of clean paired-end reads from six libraries (triplicates/group) were obtained after quality filtering (**Supplementary Table S2**). These clean reads were aligned to the reference genome, with an alignment rate of  $88.66 \pm 2.10\%$  (**Supplementary Table S3**). Principal component analysis (PCA)





**FIGURE 1 |** Histological portrayal of PP differentiation during the initiation of antler regeneration. Histological sections of the distal pedicle tissue after hard antler casting. **(A)** Dormant PP (DoPP) encompassed within the dotted lines. **(B)** Potentiated PP (PoPP; “E”) and activated PP (AcPP; “D”) within the dotted lines. **(C)** AcPP (“green star”). HE and Alcian blue staining. **(D,E)** Higher magnification of the areas “D” and “E” in **(B)**. It is to be noted that cells in the AcPP are much more densely populated than in the PoPP. Scale bar = 120  $\mu$ m **(A,B)**, 1 mm **(C)**, and 50  $\mu$ m **(D,E)**.

was carried out to determine the spatial distribution and similarities between the AcPP and PoPP. We found that different samples of the same tissue type were unambiguously grouped together (**Figure 3A**). In total, 25,311 genes were detected; of these genes, 22,016 were co-expressed in both the AcPP and the PoPP and 534 and 2,761 genes were specifically expressed in the AcPP and in the PoPP, respectively (**Figure 3B**). In total, 6,214 DEGs between the AcPP and PoPP were identified through RNA-seq, including 1,548 upregulated and 4,666 downregulated based on the criteria set at  $|\log_2(\text{fold change})| > 0.5$  and  $\text{FDR} < 0.01$ . The distribution status of the identified DEGs was visualized using a volcano plot (**Figure 3C**).

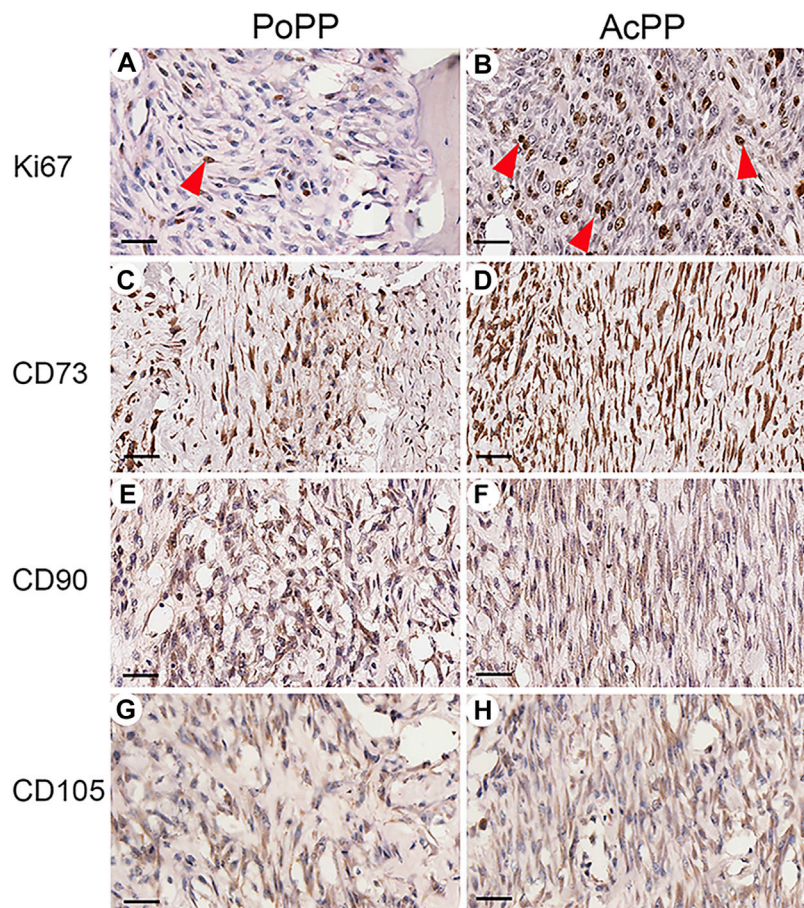
### Predicted Functions of the Differentially Expressed Genes in the Activated Pedicle Periosteum Through Analyses of Gene Ontology and Kyoto Encyclopedia of Genes and Genomes

To predict the functions of the identified DEGs in the AcPP, both Gene Ontology (GO) and Kyoto Encyclopedia of Genes and Genomes (KEGG) enrichment analyses were performed. The top

significantly upregulated BP terms were mainly related to the activation of cell proliferation and osteogenesis: mitotic nuclear division, chromosome segregation, organelle fission, mitotic sister chromatid segregation, sister chromatid segregation, and ossification (**Figure 4A**). These findings are consistent with the results of our histological observations, in that AcPP layers were significantly thickened and the number of proliferating cells was significantly increased. In contrast, the significantly downregulated BP terms were mainly related to the inhibition of immune response: T-cell activation, regulation of leukocyte activation, regulation of lymphocyte activation, and positive regulation of inflammatory response. In addition, DEGs involved in CC terms showed significant enrichment in the endoplasmic reticulum lumen, ribosome, and plasma membrane (**Figure 4B**), and DEGs involved in MF terms were mainly related to extracellular matrix structural constituent, channel activity, and cytokine receptor activity (**Figure 4C**).

KEGG analysis results showed that the most significant pathways for the upregulated DEGs were “protein procession in the endoplasmic reticulum” (e.g., CALR), “cell cycle” (e.g., CDK1, CCNB1, and E2F1), and “protein digestion and absorption” (e.g., SLC1A5; **Figure 4D**), which were consistent





**FIGURE 2 |** Immunohistochemistry (IHC) of Ki67 and MSC marker genes for the PoPP and AcPP. PoPP: (A,C,E,G); AcPP: (B,D,F,H). (A,B) IHC staining of Ki67 (red arrowheads). (C,D) IHC staining of CD73. (E,F) IHC staining of CD90. and (G,H) IHC staining of CD105. Scale bar = 50  $\mu$ m.

with the results of GO analysis, in that the upregulated DEGs were enriched in the biological process related to “cell division.” The downregulated DEGs were mainly enriched in the pathways including “the calcium signaling pathway” (e.g., IP3R, CAMK, and PKC) and “Th1 and Th2 cell differentiation” (e.g., IL6 and CXCL12).

### Validation of RNA-Seq Results

These RNA-seq results were validated using qRT-PCR, and the androgen response gene CALR was identified as one of the highly expressed DEGs in the AcPP.

Twelve key DEGs involved in the enriched signaling pathways or biological processes were selected for the verification through qRT-PCR. The results showed that expression levels of these selected DEGs from RNA-seq were confirmed being highly consistent ( $R^2 = 0.77$ ) with those from qRT-PCR (Figures 5A,B), indicating the reliability of our RNA-seq data. Among the verified DEGs, CALR was found to be one of the androgen-responsive genes and was highly differentially expressed in the AcPP cells over the PoPP cells (Figure 5A), being involved in both the upregulated pathway “protein processing in the endoplasmic reticulum” and the downregulated pathway “calcium signaling pathway” (Figure 4D). Given that antlers are the male

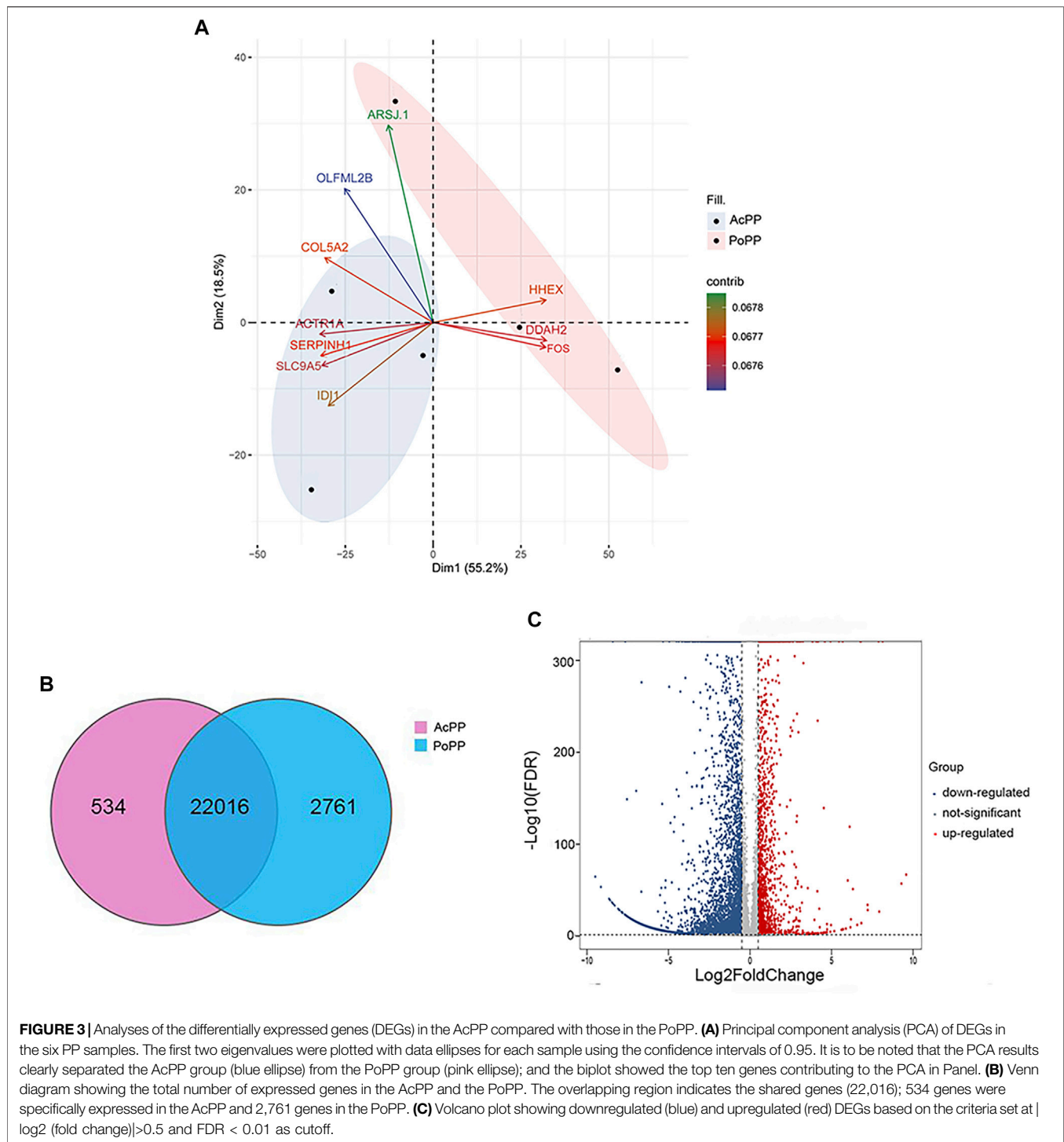
secondary sexual characters and CALR is the androgen responsive gene, this gene was, therefore, selected for further analysis.

To further confirm the findings for CALR from both RNA-seq and qRT-PCR, we carried out IHC staining. The results showed that CALR-positively stained cells were only sparsely scattered in the PoPP (Figure 5C) whereas densely populated in the AcPP (Figure 5D). Cell counting results (Figure 5E) showed that the percentage of CALR-positive cells in the AcPP ( $78.22\% \pm 6.68\%$ ) was significantly more ( $p < 0.001$ ) than that in the PoPP ( $30.00\% \pm 3.82\%$ ). Taken together, these results indicate that CALR is significantly upregulated during the activation process from the PoPP to the AcPP and may play a key role in the initiation of antler regeneration *via* the promotion of PP cell proliferation.

### Expression of Calreticulin Was not Only Associated With Changes in Androgen Hormones but Also Causally Related to Them

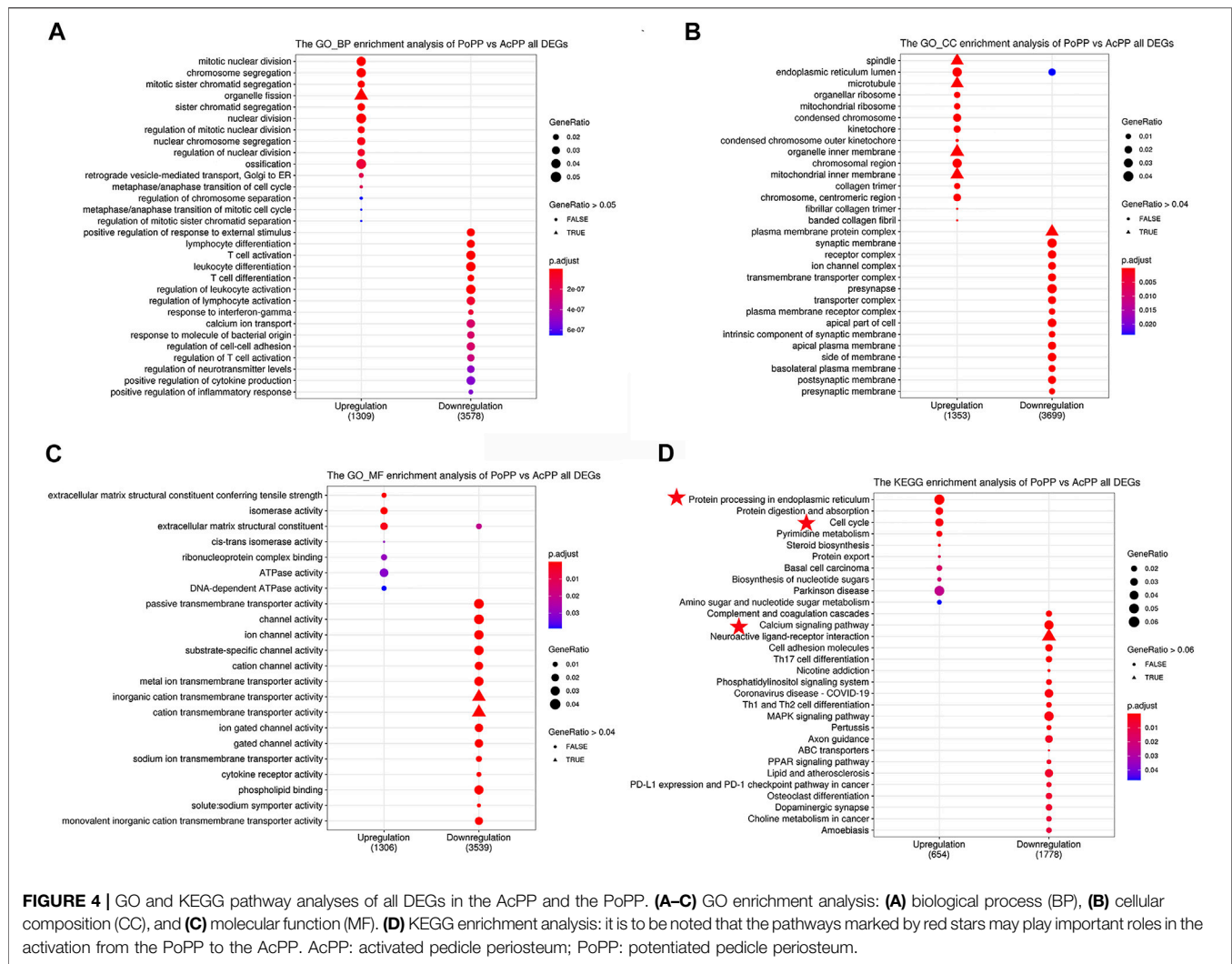
To determine whether upregulation of CALR in the AcPP is causally related to a decreasing level of circulating androgen hormones during the period of initiation of antler





regeneration, we carried out an *in vitro* assay. The results showed that the addition of a wide range of concentrations (0.5–50 nM) of testosterone (T) in serum-free medium, including physiological concentration, significantly suppressed the proliferation of both the AcPP ( $p < 0.01$ ; **Figure 6A**) and PoPP ( $p < 0.05$ ; **Figure 6C**) cells compared with those of the control. This shows that the high level of T

negatively impacts PP cell growth, hence inhibiting the initiation of antler regeneration. This result is consistent with the *in vivo* findings that antler regeneration always takes place when circulating T reaches almost an undetectable level, and administration of exogenous T at the antler growth season can effectively prevent the activation of antler regeneration (Bubenik et al., 1982;



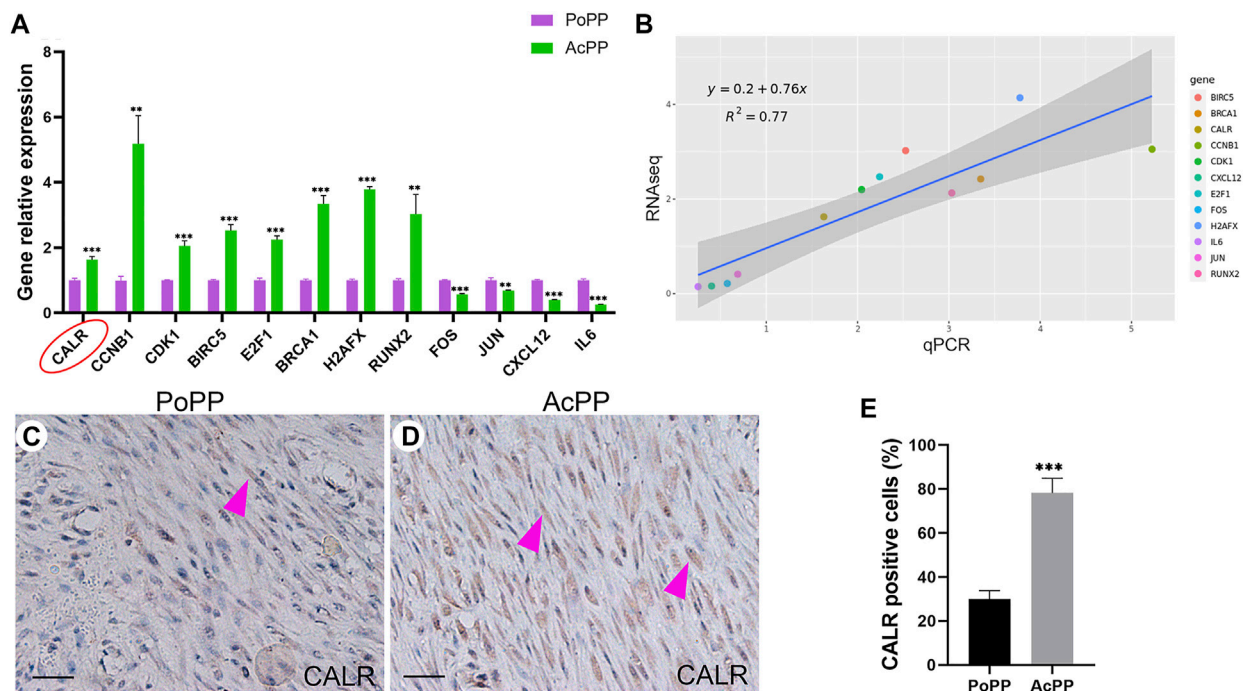
Suttie et al., 1995). Notably, in the present study, a high level of T effectively downregulated the expression of CALR in the AcPP ( $p < 0.001$ ; **Figure 6B**) and the PoPP ( $p < 0.05$ ; **Figure 6D**) compared to that in the control. Our results further confirmed that CALR is the androgen-responsive gene in the antler system and is negatively regulated by androgens.

## Downregulation of Calreticulin Expression Significantly Impaired Proliferation of the Activated Pedicle Periosteum Cells

To test the direct effects of CALR on PP cell proliferation and initiation of antler regeneration, the expression of CALR in the AcPP cells was downregulated through RNAi. The results showed that all recombinant lentiviral transfections were successful (fluorescence; **Figure 7A**); all three constructed target sequences (shCALR1, shCALR2, and shCALR3) significantly downregulated the expression of CALR at both protein ( $p < 0.01$ ; **Figures 7B,C**) and mRNA ( $p <$

0.001; **Figure 7D**) levels in the AcPP cells compared to the empty vector shRNA (vehicle) and untreated (control) groups, and shCALR1 was found to be the most effective (knockdown rate:  $67.50 \pm 2.25\%$ ) and therefore was selected for further study and denoted as the CALR-RNAi group. No significant difference was detected between the vehicle and control groups in the knockdown rate ( $p > 0.05$ ).

Fewer proliferating cells (EdU positive) were detected in the CALR-RNAi group ( $15.00 \pm 3.22\%$ ) than in the control ( $36.17 \pm 5.19\%$ ) and vehicle ( $29.50 \pm 3.72\%$ ) groups ( $p < 0.001$ ; **Figures 8A,B**). Likewise, the proliferation rate of the AcPP cells in the CALR-RNAi group was significantly lower than that of the vehicle ( $p < 0.01$ ) and control ( $p < 0.05$ ) groups from day 3 onward after seeding (**Figure 8C**). Furthermore, the results of colony-forming unit (CFU) analysis showed that the CALR-RNAi group exhibited the lowest number of CFUs compared to those of the control ( $p < 0.01$ ) and vehicle ( $p < 0.001$ ) groups (**Figures 8D,E**). Taken together, the downregulation of CALR expression can effectively inhibit the proliferation of the AcPP cells *in vitro* and thus could be expected to suppress the initiation of antler regeneration *in vivo*.



**FIGURE 5 |** RNA-seq results validated using qRT-PCR; CALR was highly significantly upregulated in the AcPP compared with the PoPP. **(A)** Histogram showing the mRNA expression levels of 12 DEGs (CCNB1, CDK1, E2F, RUNX2, BRCA1, H2AFX, CALR, FOS, JUN, BIRC5, IL6, and CXCL12, relative to that of GAPDH) in the AcPP (green) and the PoPP (pink) using qPCR. \*\*:  $p < 0.01$  and \*\*\*:  $p < 0.001$ . **(B)** Correlation analyses between the RNA-seq and qRT-PCR for the 12 DEGs, where a high correlation was detected ( $R^2 = 0.77$ ). **(C,D)** IHC of calreticulin (CALR); it is to be noted that weak positive staining was observed in cells that are sparsely populated in the PoPP but strong positive staining in cells densely populated in the AcPP. Scale bar = 50  $\mu$ m. **(E)** Percentage of CALR positive cells; it is to be noted that the percentage of CALR positive cells in the AcPP was significantly higher than that in the PoPP. \*\*\* $p < 0.001$ .

## Downregulation of Calreticulin Expression Affected Cell Cycle Progression of Activated Pedicle Periosteum Cells

To further assess the mitogenic effects of CALR on the AcPP cells, we measured the cell cycle progression using flow cytometry. The results showed that percentages of cells in the G0/G1 phase in the CALR-RNAi group ( $82.11 \pm 0.37\%$ ) were significantly higher than those in the control ( $72.85 \pm 1.46\%$ ) and vehicle ( $78.12 \pm 0.52\%$ ) groups ( $p < 0.01$ ). In contrast, cells in the S phase in the CALR-RNAi group ( $14.13 \pm 0.95\%$ ) were significantly lower than those of the control group ( $17.63\% \pm 0.96\%$ ;  $p < 0.05$ ) (Figures 9A–D). These data indicate that the downregulation of CALR in the AcPP cells can effectively induce cell cycle arrest by inhibiting G1-S phase transition.

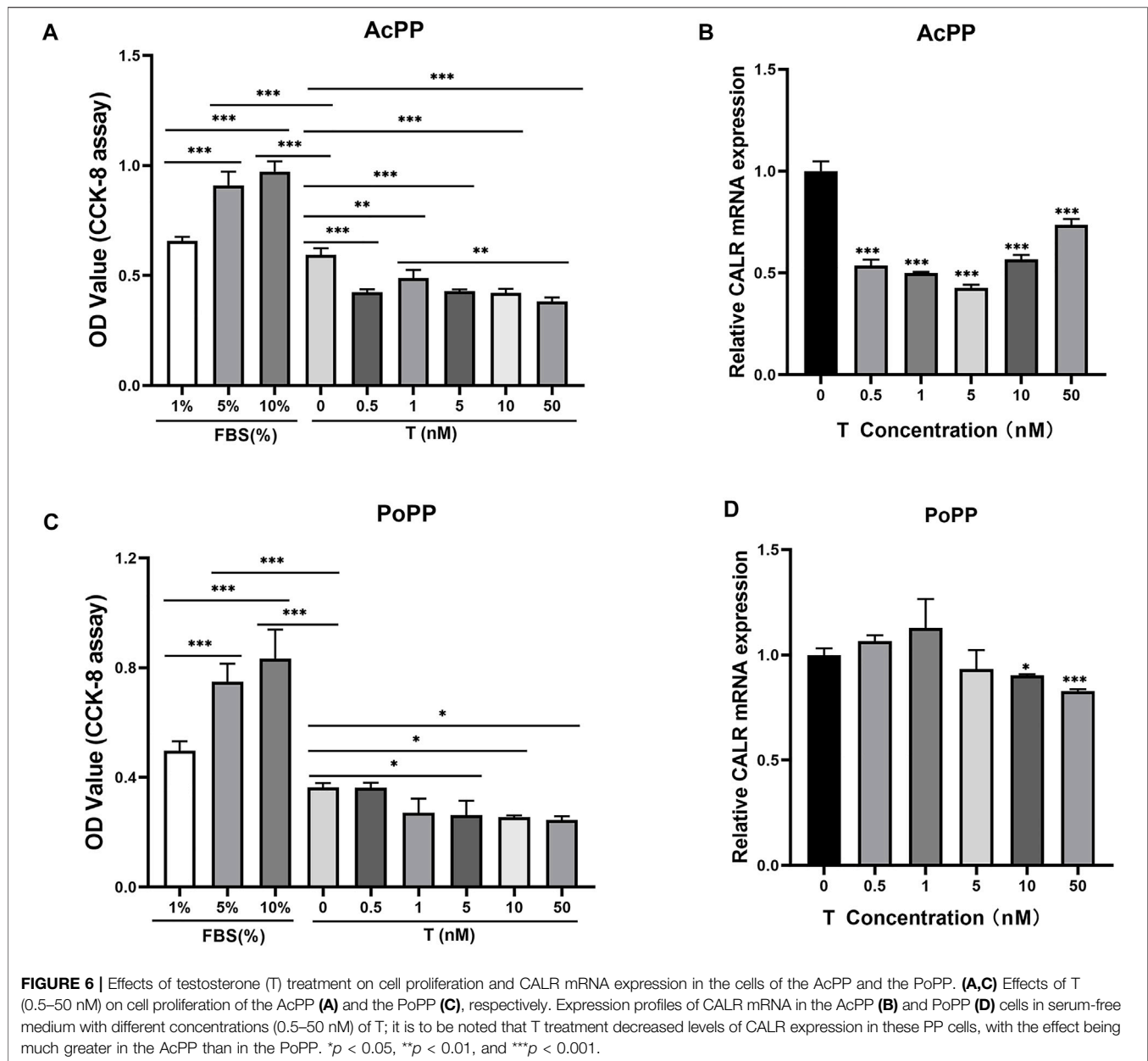
The expression status of some key regulators of G1-S phase transition was then analyzed using qRT-PCR. The results showed that mRNA levels of cyclin E2 (CCNE2) and cyclin-dependent kinase 2 (CDK2) were decreased ( $p < 0.05$ ), and the mRNA level of p27, a cell cycle inhibitor, was increased in the CALR-RNAi group compared to that in other groups ( $p < 0.05$ , Figure 9E).

## Downregulation of Calreticulin Expression Induced Apoptosis of the Activated Pedicle Periosteum Cells

Given the influence of CALR on proliferation of AcPP cells, we considered the effect of downregulation of CALR expression on apoptosis of these cells using flow cytometry. The results showed that the downregulation of CALR expression increased the apoptotic rate of the AcPP cells ( $p < 0.05$ , Figure 10), with the apoptotic rate of AcPP cells in the CALR-RNAi group ( $3.06 \pm 0.25\%$ ) being higher than that of the control ( $1.46 \pm 0.60\%$ ) and vehicle ( $2.16 \pm 0.05\%$ ) groups ( $p < 0.05$ ). These results suggest that the downregulation of CALR expression in the AcPP cells can also effectively induce AcPP cell apoptosis, besides inhibiting proliferation of these cells.

## DISCUSSION

To the best of our knowledge, the present study is the first in the antler research field to investigate the transition process from the PoPP to the AcPP using RNA-seq. Notably, the AcPP cells, although being activated entering the proliferation state still,



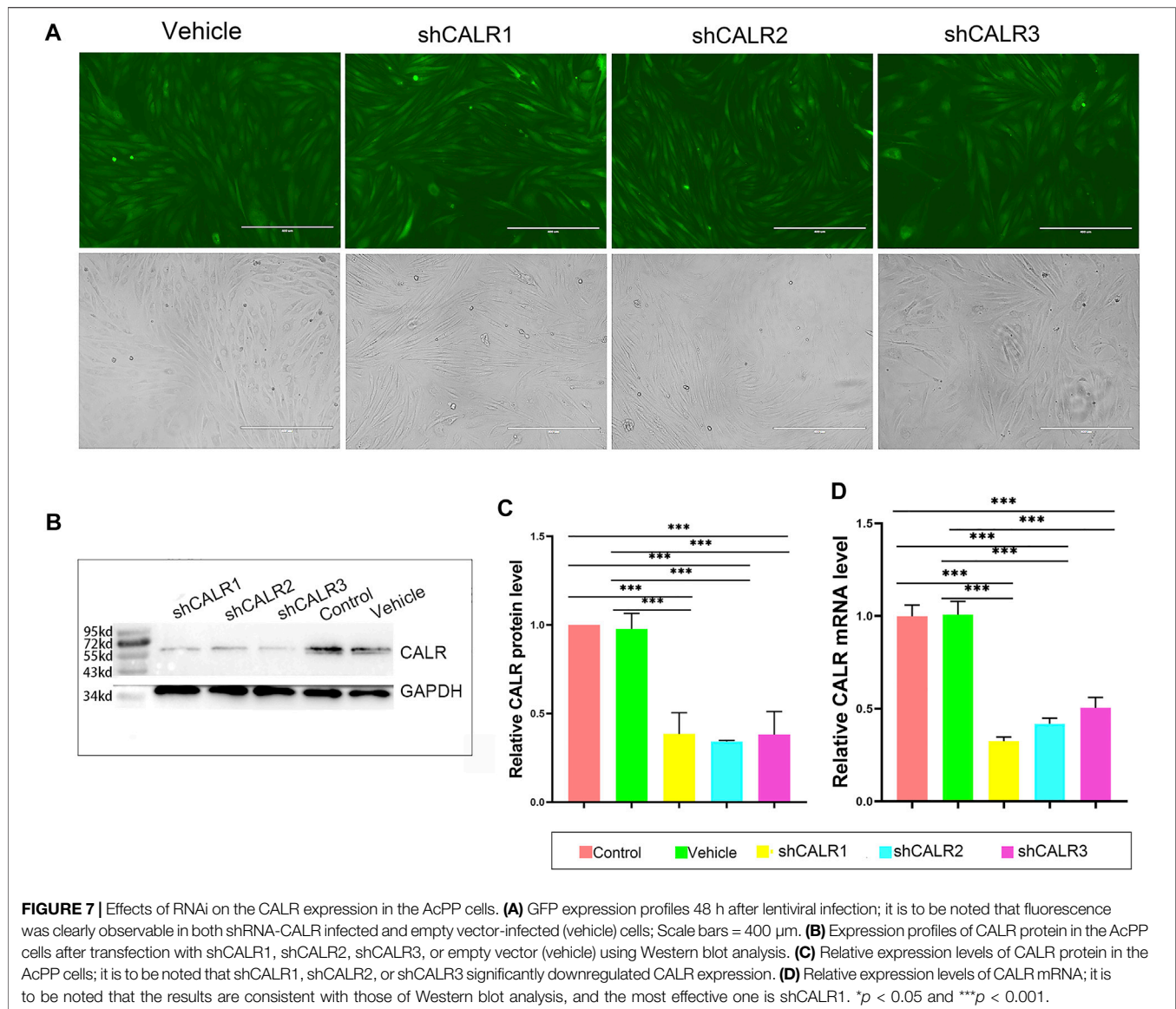
like their predecessors, the PoPP cells, retained some MSC characters, such as expression of MSC marker genes CD73, CD90, and CD105.

In total, 6,214 DEGs of the AcPP over the PoPP were detected including 1,548 upregulated and 4,666 downregulated. These DEGs were found to be mainly involved in the cell cycle pathway, protein procession in endoplasmic reticulum, calcium signaling pathway, osteogenesis, and immune response; all of these are consistent with our histological findings and functional analyses. Among these DEGs, CALR, an androgen response gene, was found to be highly significantly expressed in the cells of the AcPP over the PoPP. The expression level of CALR in these PP cells was causally related to the changes in the

androgen hormone level *in vitro*. Taken together, these findings show that it is highly likely that CALR serves as one of the key regulators that drive the formation of antler blastema by activating/permitting AcPP cell proliferation.

Although it has been known for decades that antler regeneration can only take place when circulating androgen hormones decrease to the baseline (Akhtar et al., 2019), the factor(s) that are activated by the decrease in androgens and responsible for triggering initiation of antler regeneration have proven to be elusive. With the discovery of the PP as the tissue type that gives rise to regenerating antlers (Li et al., 2007) and the definition of the three differentiation states of the PP, namely, the DoPP, PoPP, and AcPP (Li et al., 2004; Li et al., 2005; Li, 2013), we are now ready to identify this molecule(s) using modern techniques.



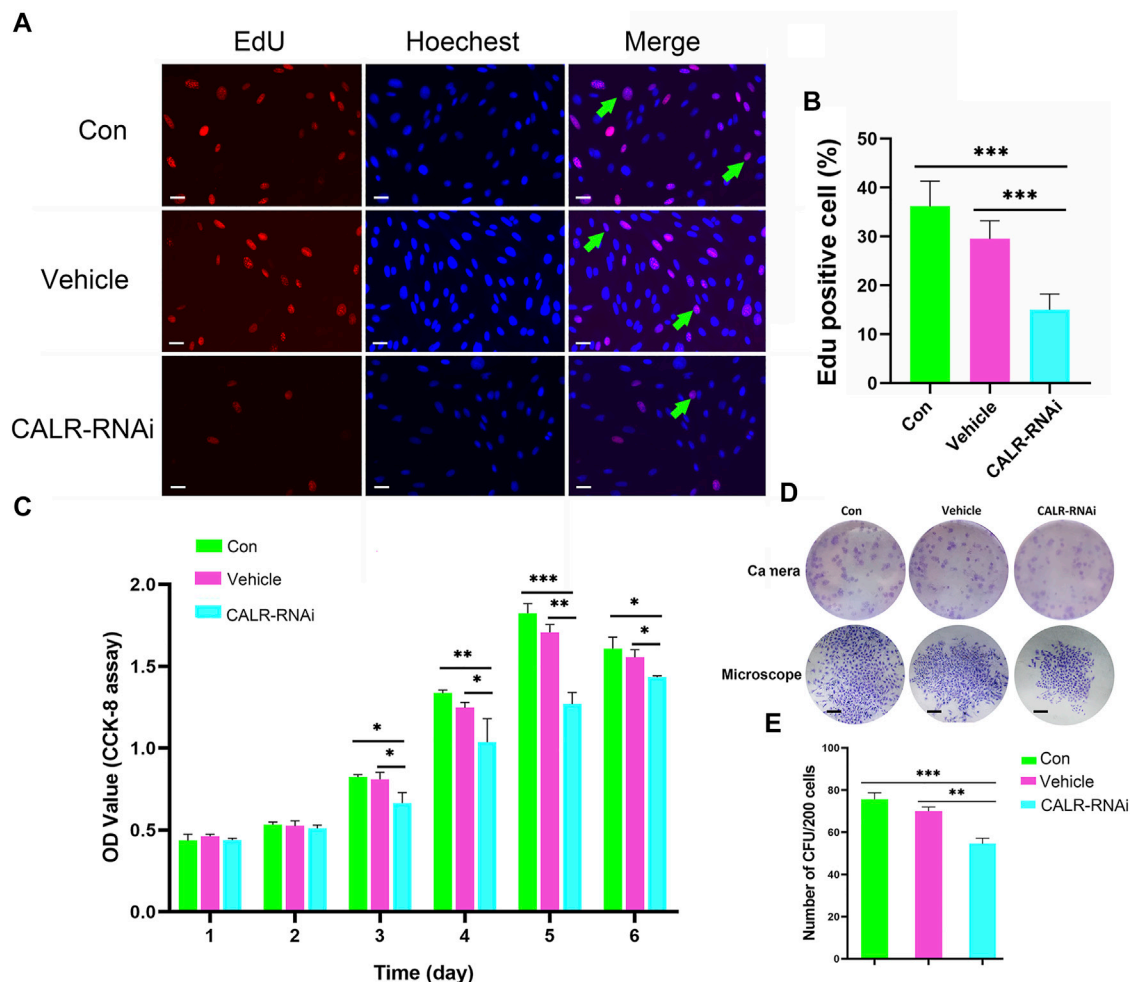


**FIGURE 7 |** Effects of RNAi on the CALR expression in the AcPP cells. **(A)** GFP expression profiles 48 h after lentiviral infection; it is to be noted that fluorescence was clearly observable in both shRNA-CALR infected and empty vector-infected (vehicle) cells; Scale bars = 400  $\mu$ m. **(B)** Expression profiles of CALR protein in the AcPP cells after transfection with shCALR1, shCALR2, shCALR3, or empty vector (vehicle) using Western blot analysis. **(C)** Relative expression levels of CALR protein in the AcPP cells; it is to be noted that shCALR1, shCALR2, or shCALR3 significantly downregulated CALR expression. **(D)** Relative expression levels of CALR mRNA; it is to be noted that the results are consistent with those of Western blot analysis, and the most effective one is shCALR1. \* $p$  < 0.05 and \*\*\* $p$  < 0.001.

In the present study, using RNA-seq, we found that CALR, an androgen response gene (Wang et al., 1997), was highly significantly expressed in the cells of the AcPP over the PoPP using both qRT-PCR and IHC. Subsequent experiments convincingly showed that the downregulation of CALR expression had significant impacts on the AcPP cells: impaired proliferation rate, inhibited G1-S phase transition in cell cycle progression, and induced apoptosis. Therefore, CALR is at least one of the androgen downstream mediators for triggering initiation of antler regeneration.

CALR is a highly conserved chaperone protein which resides primarily in the endoplasmic reticulum (Luo and Lee, 2013; Halperin et al., 2014) and is also located in the nucleus and cytoplasm, playing multiple roles in a variety of cellular processes (Coppolino et al., 1997; Krause and Michalak, 1997; Kielbik et al., 2021). CALR is reported to be involved in mediation of the effects of androgen hormones on cell proliferation and prevention of

apoptosis in male sex accessory glands. For example, castration of rats downregulates CALR expression and then causes prostate involution (apoptosis), whereas androgen replacement upregulates CALR expression and then stimulates prostate regrowth (proliferation) back to the original size (Krause and Michalak, 1997; Zhu and Wang, 1999). In a recent report (Zheng et al., 2020), CALR knockdown in a cancer cell line NKTCL significantly reduced the cell proliferation rate, inhibited G1-to-S phase transition by increasing the expression level of p27, the cell cycle inhibitor, and decreasing the levels of cyclin E2 (CCNE2) and cyclin-dependent kinase 2 (CDK2). Antler stem cell activation (from the PoPP to the AcPP) and formation of regenerating antler blastema are essentially the reflection of cell proliferation and/or prevention of cell apoptosis. In the present study, we found that the downregulation of CALR expression in the AcPP cells (antler being another male accessory sex organ) *in vitro* significantly impaired the cell



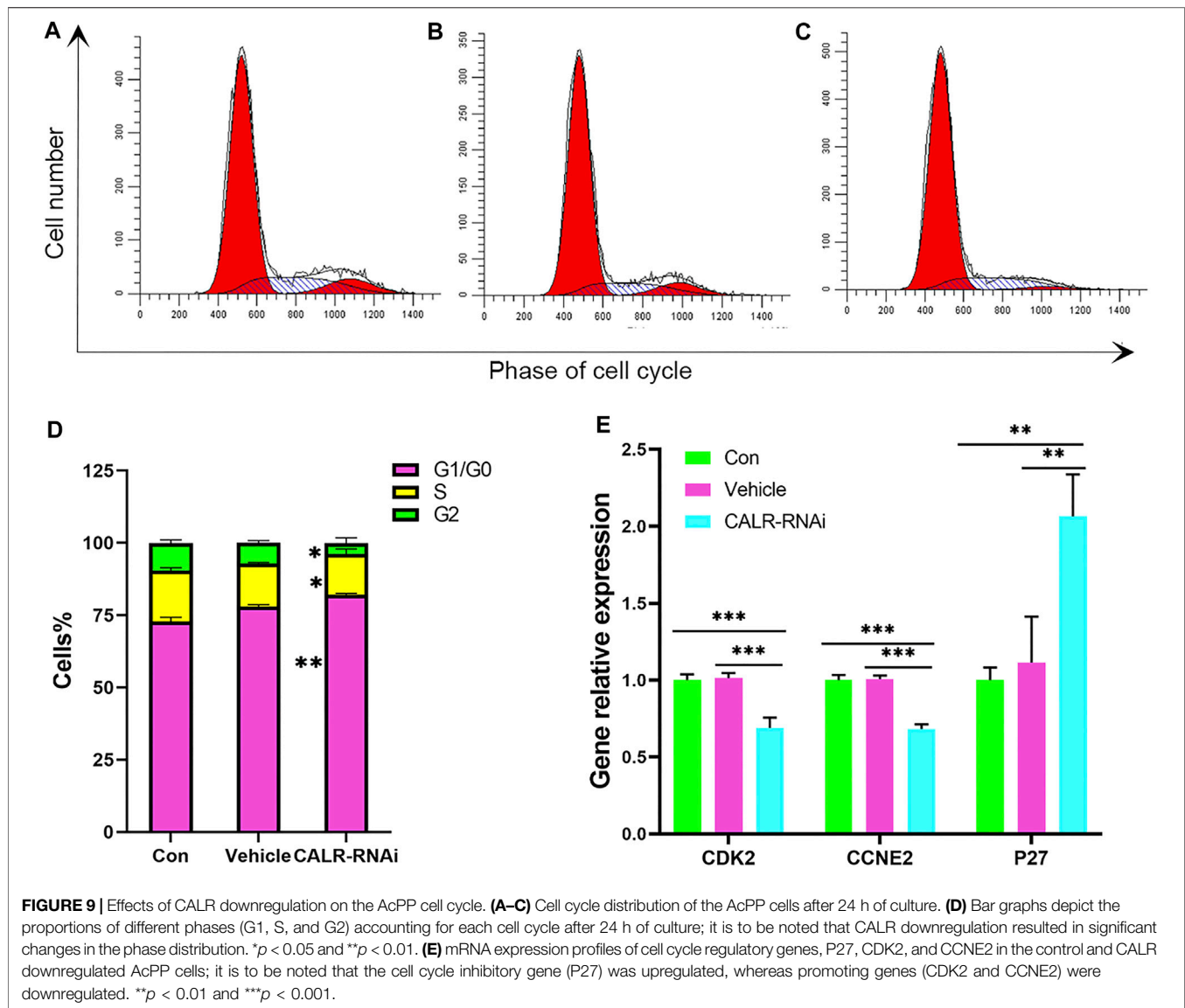
**FIGURE 8 |** Effects of CALR downregulation on AcPP cell proliferation. **(A)** Proliferation cells (red fluorescence) in the AcPP of different treatment groups determined by EdU incorporation assay; Scale bar = 25  $\mu$ m. **(B)** Percentage of EdU positive cells; it is to be noted that EdU positive cells were significantly fewer in the CALR-RNAi group than those in the other groups (\*\* $p < 0.001$ ). **(C)** Proliferation of AcPP cells evaluated by CCK-8 assay on 6-day incubation. **(D)** Colony-forming units (CFUs) (top) and a single CFU (bottom) formed by different groups of AcPP cells on day 14 (scale bar = 500  $\mu$ m). **(E)** Number of CFUs; it is to be noted that CFUs in the CALR-RNAi group were significantly fewer than those in the other groups. \*\* $p < 0.01$  and \*\*\* $p < 0.001$ .

proliferation rate, arrested more cells at the G1 phase, increased expression level of p27, and decreased expression levels of CCNE2 and CDK2. Therefore, the observed decrease in the proliferation rate of AcPP cells by the downregulation of CALR expression may be achieved *via* inhibiting cell cycle progression at the phase of G1-to-S transition.

Zhu et al. (1998) reported that CALR downregulation causes cell apoptosis likely because a low level of CALR is insufficient to buffer the cytotoxic intracellular  $\text{Ca}^{2+}$  overload. As a high capacity intracellular  $\text{Ca}^{2+}$ -binding protein, CALR alone binds approximately 50% of the  $\text{Ca}^{2+}$  stored in the endoplasmic reticulum lumen (Qiu et al., 2012; Venkatesan et al., 2021). The overexpression of CALR in a tumor cell line effectively increased the  $\text{Ca}^{2+}$  buffering capacity and protected cells against apoptosis (Bastianutto et al., 1995). In consistence with these findings, in the present study, we found that the CALR level in the AcPP cells was significantly upregulated when the level of

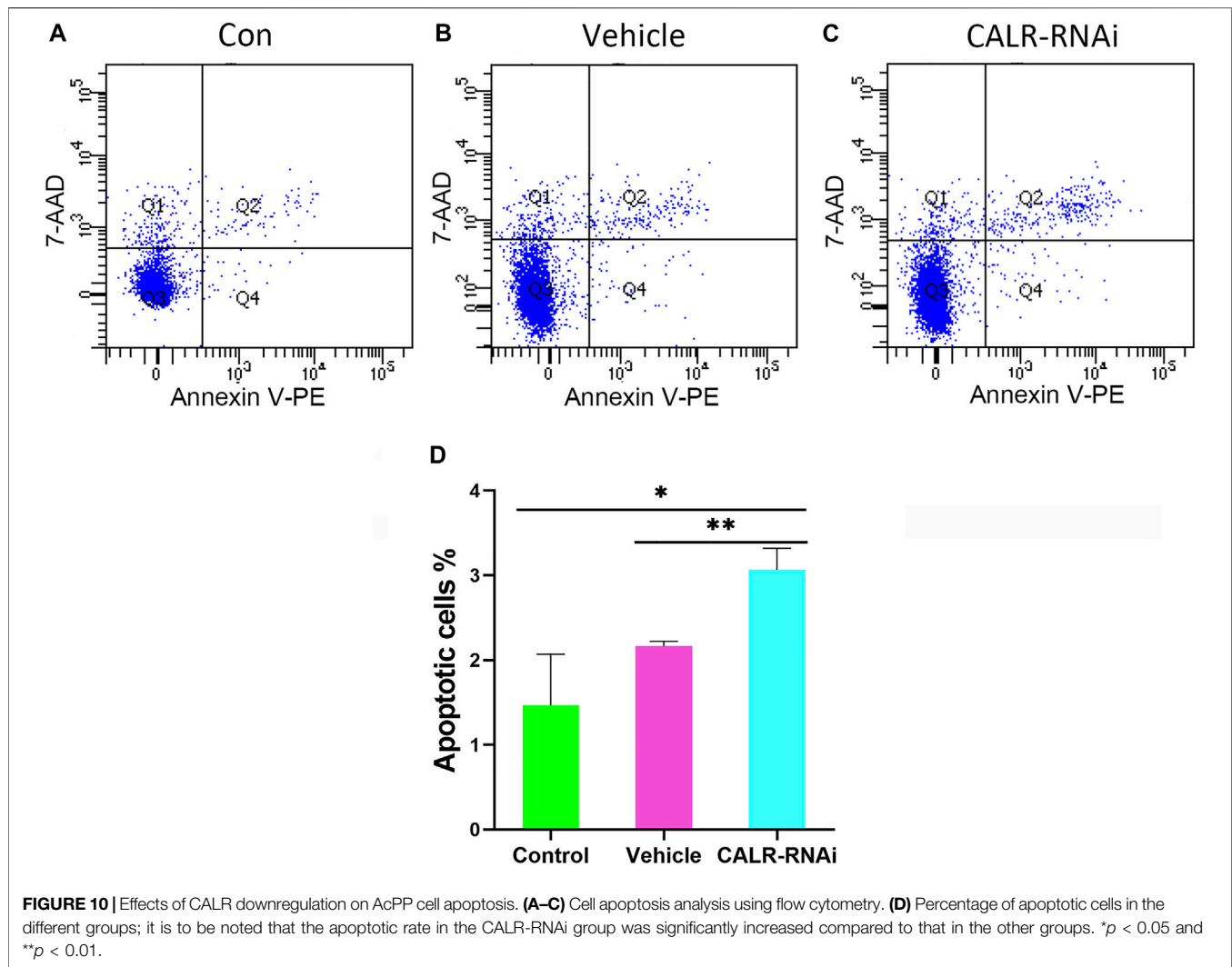
circulating androgen decreased to the baseline, while the calcium signaling pathway was downregulated. Furthermore, the downregulation of CALR expression in the AcPP cells *via* RNAi *in vitro* increased cell apoptosis. Therefore, as a key regulator for  $\text{Ca}^{2+}$  homeostasis, we propose that a high level of CALR in the AcPP cells can reduce the cell stress caused by an overload of  $\text{Ca}^{2+}$  and effectively prevent cell apoptosis.

It has been well-established that androgen plays its role *via* its receptor (AR) and that the AR is a ligand-dependent transcription factor that regulates the expression of androgen response genes (Chang et al., 1995; Funahashi et al., 2015). Thus, these genes serve as the downstream mediators for the androgen effects. Among these genes, CALR was found to be positively regulated by androgens in the male sex accessory glands such as prostate and seminal vesicles but not in other organs such as the liver, brain, kidney, heart, and muscle (Wang et al., 1997). We have shown that



CALR expression in the antler stem cells (AcPP cells) during regeneration of deer antlers was also regulated by androgens in the present study. However, unlike the other male sex accessory organs in which CALR expression is positively regulated by androgens, in the AcPP cells, it was negatively regulated; that is, a high level of CALR expression was associated with low levels of androgen. The phenomenon of androgen negatively regulating CALR has not been reported thus far in the classic sex accessory organs, but the results of the present study are supported by the findings from studies of our team: castration in the hard antler phase effectively induced hard antler casting and immediate regeneration of new antlers and at the same time triggered CALR expression in the distal PP tissue (equivalent to the AcPP; Akhtar et al., 2019); CALR was highly differentially expressed in the rapid proliferating cells in the antler growth center compared to the DoPP (dormant) cells (Dong et al., 2020).

Irrespective of negative or positive regulation by androgens, the CALR gene must be highly expressed in the activated PP cells and in the antler growth center cells as these proliferating cells require high levels of CALR for maintenance of  $\text{Ca}^{2+}$  homeostasis and prevention of apoptosis. Given that active cells demand increased protein synthesis (Feng et al., 2015), enhanced endoplasmic reticulum activity, such as the unfolded protein response (UPR), is required to facilitate protein folding and protect the cell from deleterious accumulation of unfolded proteins (Luo and Lee, 2013; Chen et al., 2022). As an endoplasmic reticulum resident protein, CALR is a well-established effector of the UPR (Schardt et al., 2011; Halperin et al., 2014), so the increased expression of CALR in activated PP cells may play a role in facilitating protein correct folding by mediating the UPR. Interestingly, recent reports have shown that androgens activate UPR signaling in both normal and cancer cells (Sheng et al., 2015; Jin and Saatcioglu, 2020). Therefore, the potential links between CALR, androgen, and UPR signaling during the



process of PoPP activation would be of interest. In addition, the expression of CALR in the AP cells, another type of antler stem cell responsible for pedicle and first antler formation, is positively regulated by androgens during the initiation of pedicle formation (Liu et al., unpublished).

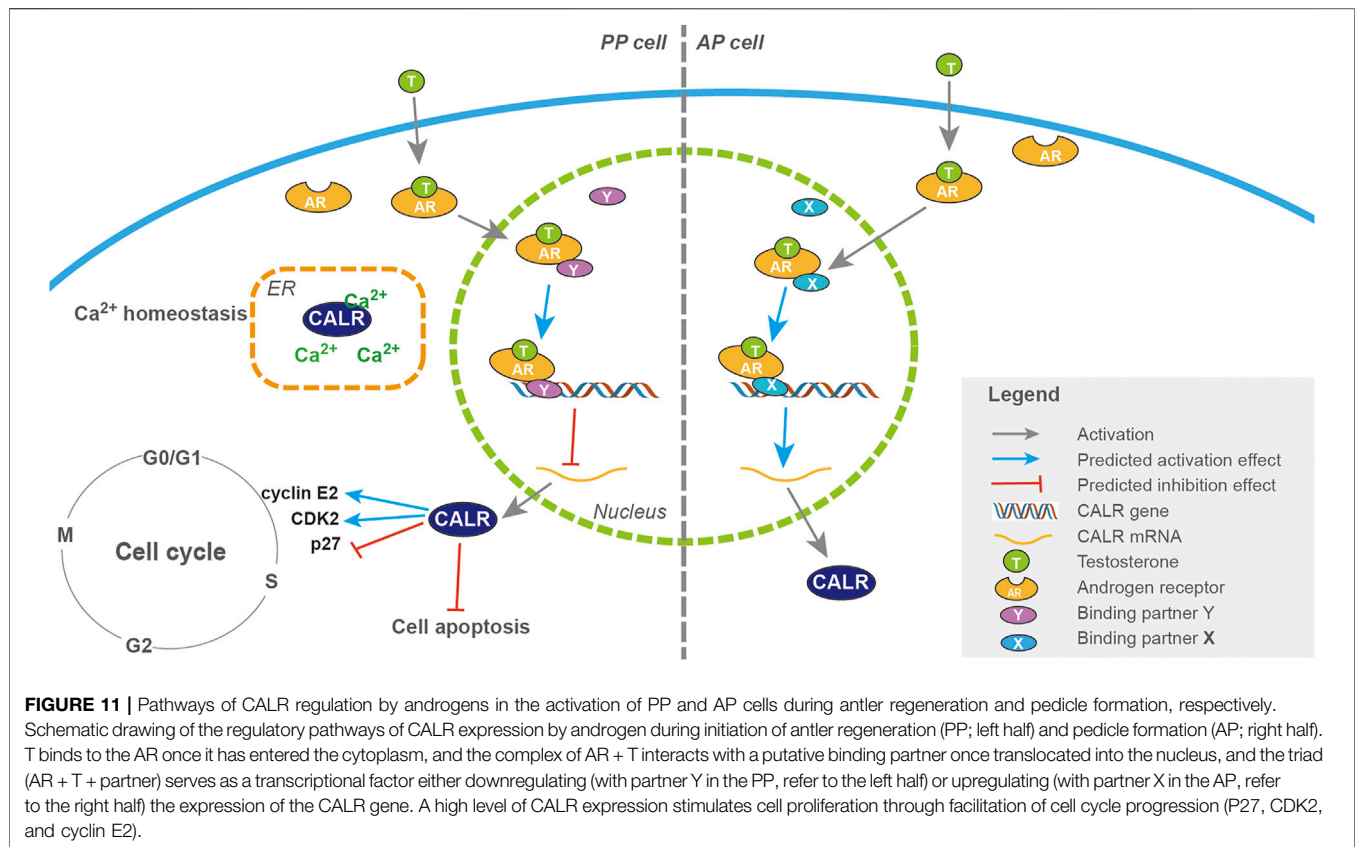
It is currently not known why and how regulation of CALR expression by androgens is altered in the antler regeneration. Zhu et al. (1998) reported that although CALR is an androgen response gene, the AR-binding site has not been identified from the CALR promoter region (Zhu et al., 1998). These authors put forward two explanations: 1) AR-binding sites may be localized far away from the transcription initiation site of the CALR promoter; 2) AR may regulate CALR gene expression without making direct contact with a DNA element(s) but rather by interacting with another DNA-binding protein.

If the second explanation (indirect regulation) applies, then the positive or negative effect of androgens on the regulation of CALR expression in the antler system would likely be dependent on the binding partners. Under this hypothesis, binding with partner X would result in positive regulation (such as with the

prostate and AP cells), whereas binding with partner Y would result in negative regulation, such as in the PP cells. Analogous to this is the dual nature of regulation in angiogenesis. Thrombospondin-1 (TSP1) is a factor that can be pro-angiogenic or antiangiogenic solely depending on the binding partner with which the TSP1 interacts (Kaur et al., 2021): TSP1 inhibits angiogenesis if interacting with CD36, whereas TSP1 stimulates angiogenesis if it interacts with some integrin heterodimers (such as  $\beta 1$  and  $\beta 3$ ). If the partner-dependent theory is true, subsequent identification and characterization of these putative binding partners would be of great significance in developing an understanding of the mechanism underlying androgen regulation of CALR expression.

With the discovery of the involvement of the androgen response gene, CALR, in the initiation of antler regeneration, we are now in the position to outline the whole picture of the initiation of antler regeneration (**Figure 11**). To help understand this regeneration process, we make an analogy with starting an automatic motor vehicle: PP at the DoPP stage is like a parked car with the brake on [gear in “P (parking)”; potentiation of the PP





(PoPP) through interactions with the enveloping skin is like turning on the car engine, but the car still remains unmoved as the gear is still in the position “P;” activation of the PP (AcPP) triggered by decreasing in the circulating androgen level to the baseline is like shifting the gear from “P” to “D (driving);” and commencement of AcPP cell proliferation under highly expressed CALR is like engagement of the motor power with the wheels so that the car is starting to move forward, provided that the fuel (high level of IGF1) is readily available in the tank.

Overall, we believe that identification of an androgen response gene, CALR, in the present study has not only discovered “one critical piece” of the “jigsaw puzzle” in the initiation of antler regeneration (helping to further reveal the mechanism underlying this unique mammalian epimorphic regeneration) but also opened up a new avenue for investigation of the nature of CALR regulation by androgen (putative binding partners). This latter aspect may be very relevant for seeking new targets for the treatment of androgen-related clinical conditions.

## DATA AVAILABILITY STATEMENT

The datasets presented in this study can be found in online repositories. The names of the repository/repositories and accession number(s) can be found below: NCBI BioSample

accession number: SAMN17863449. The link is <https://www.ncbi.nlm.nih.gov/biosample>.

## ETHICS STATEMENT

The animal study was reviewed and approved by the Temporary Animal Ethics Committee of Changchun Sci-Tech University (Permit Number: CKARI-2020-017).

## AUTHOR CONTRIBUTIONS

QG and CL conceived and designed the experiment. QG, JiZ, JuZ, and WW performed the experiments. JuZ and HB performed bioinformatics and statistical analyses. QG and CL drafted the manuscript. JuZ, WW, and CL revised the manuscript. All authors read and approved the final manuscript.

## FUNDING

This work was funded by the Strategic Priority Research Program of the Chinese Academy of Sciences (No. XDA16010105), The Youth Technology Talents Innovation

and Entrepreneurship Special Project of Changchun City (21QC04), The National Natural Science Foundation of China (U20A20403), and Provincial Natural Science Foundation of Jilin (2020201031JC).

## ACKNOWLEDGMENTS

We would like to thank Peter Fennessy for critically reading through the manuscript; and staff from the Institute of Antler Science and Product Technology Changchun Sci-Tech

University, the Stem Cell Research Group, the Institute of Special Wild Economic Animals and Plants, and Chinese Academy of Agricultural Sciences, for help the collection of antler stem cells.

## SUPPLEMENTARY MATERIAL

The Supplementary Material for this article can be found online at: <https://www.frontiersin.org/articles/10.3389/fcell.2022.862841/full#supplementary-material>

## REFERENCES

- Akhtar, R. W., Liu, Z., Wang, D., Ba, H., Shah, S. A. H., and Li, C. (2019). Identification of Proteins that Mediate the Role of Androgens in Antler Regeneration Using Label Free Proteomics in Sika Deer (*Cervus Nippon*). *General Comp. Endocrinol.* 283, 113235. doi:10.1016/j.ygcen.2019.113235
- Ba, H., Cai, Z., Gao, H., Qin, T., Liu, W., Xie, L., et al. (2020). Chromosome-level Genome Assembly of Tarim Red Deer, *Cervus elaphus* Yarkandensis. *Sci. Data* 7, 187. doi:10.1038/s41597-020-0537-0
- Bader, G. D., and Hogue, C. W. (2003). An Automated Method for Finding Molecular Complexes in Large Protein Interaction Networks. *BMC Bioinforma.* 4, 2. doi:10.1186/1471-2105-4-2
- Bastianutto, C., Clementi, E., Codazzi, F., Podini, P., De Giorgi, F., Rizzuto, R., et al. (1995). Overexpression of Calreticulin Increases the Ca<sup>2+</sup> Capacity of Rapidly Exchanging Ca<sup>2+</sup> Stores and Reveals Aspects of Their Lumenal Microenvironment and Function. *J. Cell Biol.* 130, 847–855. doi:10.1083/jcb.130.4.847
- Bubenik, G. A., Morris, J. M., Schams, D., and Claus, A. (1982). Photoperiodicity and Circannual Levels of LH, FSH, and Testosterone in Normal and Castrated Male, White-Tailed Deer. *Can. J. Physiol. Pharmacol.* 60, 788–793. doi:10.1139/y82-110
- Chang, C., Saltzman, A., Yeh, S., Young, W., Keller, E., Lee, H.-J., et al. (1995). Androgen Receptor: an Overview. *Crit. Rev. Eukar Gene Expr.* 5, 97–125. doi:10.1615/critrevueukargeneexpr.v5.i2.10
- Chen, H., Miao, Y., Bian, A., Ye, J., Wang, J., Cong, X., et al. (2022). A Novel Small-Molecule Activator of Unfolded Protein Response Suppresses Castration-Resistant Prostate Cancer Growth. *Cancer Lett.* 532, 215580. doi:10.1016/j.canlet.2022.215580
- Cock, P. J. A., Fields, C. J., Goto, N., Heuer, M. L., and Rice, P. M. (2009). The Sanger Fastq File Format for Sequences with Quality Scores, and the Solexa/Illumina Fastq Variants. *Nucleic Acids Res.* 38 (6), 1767–1771. doi:10.1093/nar/gkp1137
- Coppolino, M. G., Woodside, M. J., Demareux, N., Grinstein, S., St-Arnaud, R., and Dedhar, S. (1997). Calreticulin Is Essential for Integrin-Mediated Calcium Signalling and Cell Adhesion. *Nature* 386, 843–847. doi:10.1038/386843a0
- Dong, Z., Ba, H., Zhang, W., Coates, D., and Li, C. (2016). iTRAQ-Based Quantitative Proteomic Analysis of the Potentiated and Dormant Antler Stem Cells. *Ijms* 17, 1778. doi:10.3390/ijms17111778
- Dong, Z., Coates, D., Liu, Q., Sun, H., and Li, C. (2019). Quantitative Proteomic Analysis of Deer Antler Stem Cells as a Model of Mammalian Organ Regeneration. *J. Proteomics* 195, 98–113. doi:10.1016/j.jprot.2019.01.004
- Dong, Z., Haines, S., and Coates, D. (2020). Proteomic Profiling of Stem Cell Tissues during Regeneration of Deer Antler: A Model of Mammalian Organ Regeneration. *J. Proteome Res.* 19, 1760–1775. doi:10.1021/acs.jproteome.0c00026
- Feng, R., Ye, J., Zhou, C., Qi, L., Fu, Z., Yan, B., et al. (2015). Calreticulin Down-Regulation Inhibits the Cell Growth, Invasion and Cell Cycle Progression of Human Hepatocellular Carcinoma Cells. *Diagn Pathol.* 10, 149. doi:10.1186/s13000-015-0382-1
- Funahashi, Y., Wang, Z., O'Malley, K. J., Tyagi, P., DeFranco, D. B., Gingrich, J. R., et al. (2015). Influence of E. Coli-Induced Prostatic Inflammation on Expression of Androgen-Responsive Genes and Transforming Growth Factor Beta 1 Cascade Genes in Rats. *Prostate* 75, 381–389. doi:10.1002/pros.22924
- Goss, R. J., and Rosen, J. K. (1973). The Effect of Latitude and Photoperiod on the Growth of Antlers. *J. Reprod. Fertil. Suppl.* 19, 111–118.
- Guo, Q., Wang, D., Liu, Z., and Li, C. (2015). Effects of P21 Gene Down-Regulation through RNAi on Antler Stem Cells *In Vitro*. *PLoS One* 10, e0134268. doi:10.1371/journal.pone.0134268
- Halperin, L., Jung, J., and Michalak, M. (2014). The Many Functions of the Endoplasmic Reticulum Chaperones and Folding Enzymes. *IUBMB Life* 66, 318–326. doi:10.1002/iub.1272
- Jin, Y., and Saatcioglu, F. (2020). Targeting the Unfolded Protein Response in Hormone-Regulated Cancers. *Trends Cancer* 6 (2), 160–171. doi:10.1016/j.trecan.2019.12.001
- Kaur, S., Bronson, S. M., Pal-Nath, D., Miller, T. W., Soto-Pantoja, D. R., and Roberts, D. D. (2021). Functions of Thrombospondin-1 in the Tumor Microenvironment. *Ijms* 22, 4570. doi:10.3390/ijms22094570
- Kielbik, M., Szulc-Kielbik, I., and Klink, M. (2021). Calreticulin-Multifunctional Chaperone in Immunogenic Cell Death: Potential Significance as a Prognostic Biomarker in Ovarian Cancer Patients. *Cells* 10, 130. doi:10.3390/cells10010130
- Kierdorf, U., and Kierdorf, H. (2011). Deer Antlers - a Model of Mammalian Appendage Regeneration: an Extensive Review. *Gerontology* 57, 53–65. doi:10.1159/000300565
- Kierdorf, U., Li, C., and Price, J. S. (2009). Improbable Appendages: Deer Antler Renewal as a Unique Case of Mammalian Regeneration. *Seminars Cell & Dev. Biol.* 20, 535–542. doi:10.1016/j.semcdb.2008.11.011
- Kim, D., Langmead, B., and Salzberg, S. L. (2015). HISAT: a Fast Spliced Aligner with Low Memory Requirements. *Nat. Methods* 12, 357–360. doi:10.1038/nmeth.3317
- Krause, K.-H., and Michalak, M. (1997). Calreticulin. *Cell* 88, 439–443. doi:10.1016/s0092-8674(00)81884-x
- Li, B., and Dewey, C. N. (2011). RSEM: Accurate Transcript Quantification from RNA-Seq Data with or without a Reference Genome. *BMC Bioinforma.* 12 (1), 323–338. doi:10.1186/1471-2105-12-323
- Li, C., and Chu, W. (2016). The Regenerating Antler Blastema the Derivative of Stem Cells Resident in a Pedicle Stump. *Front. Biosci.* 21, 455–467. doi:10.2741/4401
- Li, C., Harper, A., Puddick, J., Wang, W., and McMahon, C. (2012). Proteomes and Signalling Pathways of Antler Stem Cells. *PLoS One* 7, e30026. doi:10.1371/journal.pone.0030026
- Li, C. (2013). Histogenetic Aspects of Deer Antler Development. *Front. Biosci.* E5, 479–489. doi:10.2741/e629
- Li, C., Littlejohn, R. P., Corson, I. D., and Suttie, J. M. (2003). Effects of Testosterone on Pedicle Formation and its Transformation to Antler in Castrated Male, Freemartin and Normal Female Red Deer (*Cervus elaphus*). *General Comp. Endocrinol.* 131, 21–31. doi:10.1016/s0016-6480(02)00625-1
- Li, C., Mackintosh, C. G., Martin, S. K., and Clark, D. E. (2007). Identification of Key Tissue Type for Antler Regeneration through Pedicle Periosteum Deletion. *Cell Tissue Res.* 328, 65–75. doi:10.1007/s00441-006-0333-y
- Li, C., Suttie, J. M., and Clark, D. E. (2005). Histological Examination of Antler Regeneration in Red Deer (*Cervus elaphus*). *Anat. Rec.* 282A, 163–174. doi:10.1002/ar.a.20148

- Li, C., Suttie, J. M., and Clark, D. E. (2004). Morphological Observation of Antler Regeneration in Red Deer (*Cervus elaphus*). *J. Morphol.* 262, 731–740. doi:10.1002/jmor.10273
- Li, C., Yang, F., Xing, X., Gao, X., Deng, X., Mackintosh, C., et al. (2008). Role of Heterotypic Tissue Interactions in Deer Pedicle and First Antler Formation—Revealed via a Membrane Insertion Approach. *J. Exp. Zool.* 310B, 267–277. doi:10.1002/jez.b.21210
- Love, M. I., Huber, W., and Anders, S. (2014). Moderated Estimation of Fold Change and Dispersion for Rna-Seq Data with Deseq2. *Genome Biol.* 15 (12), 550. doi:10.1186/s13059-014-0550-8
- Luo, B., and Lee, A. S. (2013). The Critical Roles of Endoplasmic Reticulum Chaperones and Unfolded Protein Response in Tumorigenesis and Anticancer Therapies. *Oncogene* 32, 805–818. doi:10.1038/onc.2012.130
- Nieto-Diaz, M., Pita-Thomas, D. W., Munoz-Galdeano, T., Martinez-Maza, C., Navarro-Ruiz, R., Reigada, D., et al. (2012). Deer Antler Innervation and Regeneration. *Front. Biosci.* 17, 1389–1401. doi:10.2741/3993
- Price, J., Fauchoux, C., and Allen, S. (2005). Deer Antlers as a Model of Mammalian Regeneration. *Curr. Top. Dev. Biol.* 67, 1–48. doi:10.1016/s0070-2153(05)67001-9
- Qiu, Y., Xi, J., Du, L., and Poovaiah, B. W. (2012). The Function of Calreticulin in Plant Immunity. *Plant Signal. Behav.* 7, 907–910. doi:10.4161/psb.20721
- Schardt, J. A., Mueller, B. U., and Pabst, T. (2011). Activation of the Unfolded Protein Response in Human Acute Myeloid Leukemia. *Methods Enzym.* 489, 227–243. doi:10.1016/b978-0-12-385116-1.00013-3
- Seo, M.-S., Park, S.-B., Choi, S.-W., Kim, J.-J., Kim, H.-S., and Kang, K.-S. (2014). Isolation and Characterization of Antler-Derived Multipotent Stem Cells. *Cell Transpl.* 23, 831–843. doi:10.3727/096368912x661391
- Sheng, X., Arnoldussen, Y. J., Storm, M., Tesikova, M., Nenseth, H. Z., Zhao, S., et al. (2015). Divergent Androgen Regulation of Unfolded Protein Response Pathways Drives Prostate Cancer. *EMBO Mol. Med.* 7, 788–801. doi:10.15252/emmm.201404509
- Suttie, J. M., Fennessy, P. F., Lapwood, K. R., and Corson, I. D. (1995). Role of Steroids in Antler Growth of Red Deer Stags. *J. Exp. Zool.* 271, 120–130. doi:10.1002/jez.1402710207
- Venkatesan, A., Satin, L. S., and Raghavan, M. (2021). Roles of Calreticulin in Protein Folding, Immunity, Calcium Signaling and Cell Transformation. *Prog. Mol. Subcell. Biol.* 59, 145–162. doi:10.1007/978-3-030-67696-4\_7
- Wang, D., Berg, D., Ba, H., Sun, H., Wang, Z., and Li, C. (2019). Deer Antler Stem Cells Are a Novel Type of Cells that Sustain Full Regeneration of a Mammalian Organ—Deer Antler. *Cell Death Dis.* 10, 443. doi:10.1038/s41419-019-1686-y
- Wang, Z., Tufts, R., Haleem, R., and Cai, X. (1997). Genes Regulated by Androgen in the Rat Ventral Prostate. *Proc. Natl. Acad. Sci. U.S.A.* 94, 12999–13004. doi:10.1073/pnas.94.24.12999
- Weerasekera, D. S., Perera, S. J., Nanayakkara, D. K. K., Herath, H. M. S. S., Rathnasekara, A. N. L., and Ranawana, K. B. (2020). The Antler Cycle and Fecal Testosterone of Male Sambar Deer *Rusa Unicolor* at the Horton Plains National Park in Sri Lanka. *BioMed Res. Int.* 2020, 1. doi:10.1155/2020/6903407
- Yang, C., Lu, X., Sun, H., Chu, W. H., and Li, C. (2016). Analysis of Genomewide DNA Methylation Reveals Differences in DNA Methylation Levels between Dormant and Naturally as Well as Artificially Potentiated Pedicle Periosteum of Sika Deer (*Cervus Nippon*). *J. Exp. Zool. Mol. Dev. Evol.* 326, 375–383. doi:10.1002/jez.b.22695
- Yu, G., Wang, L.-G., Han, Y., and He, Q.-Y. (2012). clusterProfiler: an R Package for Comparing Biological Themes Among Gene Clusters. *OMICS A J. Integr. Biol.* 16, 284–287. doi:10.1089/omi.2011.0118
- Zheng, Y., Li, C., Xin, P., Peng, Q., Zhang, W., Liu, S., et al. (2020). Calreticulin Increases Growth and Progression of Natural killer/T-Cell Lymphoma. *Aging* 12, 23822–23835. doi:10.18632/aging.104030
- Zhu, N., and Wang, Z. (1999). Calreticulin Expression Is Associated with Androgen Regulation of the Sensitivity to Calcium Ionophore-Induced Apoptosis in LNCaP Prostate Cancer Cells. *Cancer Res.* 59, 1896–1902.
- Zhu, N., Pewitt, E. B., Cai, X., Cohn, E. B., Lang, S., Chen, R., et al. (1998). Calreticulin: An Intracellular Ca<sup>++</sup>-Binding Protein Abundantly Expressed and Regulated by Androgen in Prostatic Epithelial Cells\*This Work Was Supported by Boehringer Ingelheim International GmbH, American Cancer Society, Illinois Division Grant 95-58, the Robert H. Lurie Cancer Center Grant 200, NCI 1R21 CA69851-01, a CaPCURE Award, and NIH Grant R01-DK-51193. *Endocrinology* 139, 4337–4344. doi:10.1210/endo.139.10.6242

**Conflict of Interest:** The authors declare that the research was conducted in the absence of any commercial or financial relationships that could be construed as a potential conflict of interest.

The reviewers BG, JL, and JJ declared a shared parent affiliation with the author JZ to the handling editor at the time of review.

**Publisher's Note:** All claims expressed in this article are solely those of the authors and do not necessarily represent those of their affiliated organizations, or those of the publisher, the editors, and the reviewers. Any product that may be evaluated in this article, or claim that may be made by its manufacturer, is not guaranteed or endorsed by the publisher.

Copyright © 2022 Guo, Zheng, Ba, Sun, Zhai, Wang and Li. This is an open-access article distributed under the terms of the Creative Commons Attribution License (CC BY). The use, distribution or reproduction in other forums is permitted, provided the original author(s) and the copyright owner(s) are credited and that the original publication in this journal is cited, in accordance with accepted academic practice. No use, distribution or reproduction is permitted which does not comply with these terms.



## OPEN ACCESS

## EDITED BY

Alessandra Giorgetti,  
Institut d'Investigació Biomedica de  
Bellvitge (IDIBELL), Spain

## REVIEWED BY

Yun Xia,  
Nanyang Technological University,  
Singapore  
Tiziana A. Brevini,  
University of Milan, Italy  
Tao Li,  
Second Affiliated Hospital of Hainan  
Medical University, China

## \*CORRESPONDENCE

Zhongwei Li,  
zhongwei.li@med.usc.edu

## SPECIALTY SECTION

This article was submitted to Stem Cell  
Research,  
a section of the journal  
Frontiers in Cell and Developmental  
Biology

RECEIVED 26 May 2022

ACCEPTED 01 July 2022

PUBLISHED 22 July 2022

## CITATION

Huang B, Zeng Z, Zhang CC,  
Schreiber ME and Li Z (2022),  
Approaches to kidney replacement  
therapies—opportunities  
and challenges.  
*Front. Cell Dev. Biol.* 10:953408.  
doi: 10.3389/fcell.2022.953408

## COPYRIGHT

© 2022 Huang, Zeng, Zhang, Schreiber  
and Li. This is an open-access article  
distributed under the terms of the  
[Creative Commons Attribution License  
\(CC BY\)](https://creativecommons.org/licenses/by/4.0/). The use, distribution or  
reproduction in other forums is  
permitted, provided the original  
author(s) and the copyright owner(s) are  
credited and that the original  
publication in this journal is cited, in  
accordance with accepted academic  
practice. No use, distribution or  
reproduction is permitted which does  
not comply with these terms.

# Approaches to kidney replacement therapies—opportunities and challenges

Biao Huang<sup>1,2</sup>, Zipeng Zeng<sup>1,2</sup>, Chennan C. Zhang<sup>1,2</sup>,  
Megan E. Schreiber<sup>1,2</sup> and Zhongwei Li<sup>1,2\*</sup>

<sup>1</sup>USC/UKRO Kidney Research Center, Division of Nephrology and Hypertension, Department of Medicine, Keck School of Medicine, University of Southern California, Los Angeles, CA, United States, <sup>2</sup>Department of Stem Cell Biology and Regenerative Medicine, Keck School of Medicine, University of Southern California, Los Angeles, CA, United States

One out of seven people develop chronic kidney disease (CKD). When kidney function continues to decline, CKD patients may develop end-stage renal disease (ESRD, or kidney failure). More than 2 out of 1,000 adults develop ESRD and these patients must live on dialysis or get a kidney transplant to survive. Each year, more than \$51 billion is spent to treat patients with ESRD in the United States. In addition, ESRD greatly reduces longevity and quality of life for patients. Compared to dialysis, kidney transplant offers the best chance of survival, but few donor organs are available. Thus, there is an urgent need for innovative solutions that address the shortage of kidneys available for transplantation. Here we summarize the status of current approaches that are being developed to solve the shortage of donor kidneys. These include the bioartificial kidney approach which aims to make a portable dialysis device, the recellularization approach which utilizes native kidney scaffold to make an engineered kidney, the stem cell-based approach which aims to generate a kidney *de novo* by recapitulating normal kidney organogenesis, the xenotransplantation approach which has the goal to make immunocompatible pig kidneys for transplantation, and the interspecies chimera approach which has potential to generate a human kidney in a host animal. We also discuss the interconnections among the different approaches, and the remaining challenges of translating these approaches into novel therapies.

## KEYWORDS

pluripotent stem cells, bioartificial kidney, decellularization, kidney organoid, xenotransplant, interspecies chimera, genome editing, bioengineering (general)



## Introduction

Kidneys filter our blood and remove wastes, acid and extra fluid from our bodies, and help maintain a healthy balance of water, salt, pH, and minerals in our blood. In addition, by producing hormones, kidneys regulate our blood pressure and red blood cell production and keep our bones strong. Humans and other animals cannot live without this essential organ.

During the embryonic and fetal stages, kidneys naturally form through the process of organogenesis. Overall, mouse and human kidney organogenesis share considerable similarities (McMahon, 2016; Lindström et al., 2018a; Lindström et al., 2018b; Lindström et al., 2018c). In the mouse at around embryonic day 10.5 (E10.5), part of the Wolffian duct (named “ureteric bud” or UB) invades the surrounding mesenchymal tissue (named “metanephric mesenchyme” or MM), marking the initiation of kidney organogenesis. A similar invasion of UB into MM is also observed in the human at around 5 weeks of gestational age. The developing kidney then enters the next phase with the expansion of UB and MM, coupled with repetitive mutual induction between MM and UB. Eventually, over a period of around 10 days in the mouse, and around 31 weeks in the human, the MM gives rise to all the nephrons, the functional units of the kidney (~14,000 nephrons in a mouse kidney, and ~1 million nephrons in a human kidney). Meanwhile, the UB undergoes extensive branching morphogenesis to generate a tree-like collecting duct (CD) network for processing and transporting the urine generated from the nephrons to the bladder.

However, kidney function declines with age, upon injury, or under various disease conditions, and the adult kidney has a very limited ability to regenerate itself and recover. Therefore, diminishing kidney function tends to progress down a one-way street, and it is difficult to reverse course. When kidney function decreases to a certain point, a patient develops chronic kidney disease (CKD). According to Centers for Disease Control and Prevention (CDC), 15% of the adults in the United States, or 37 million Americans, have CKD (<https://www.cdc.gov/kidneydisease/publications-resources/ckd-national-facts.html>). In the clinical setting, doctors describe the progression of CKD from stages 1–5 in increasing order of severity (Chen et al., 2019). These stages are based on glomerular filtration rate (GFR), an indicator of kidney function that calculates how fast wastes are filtered and extra fluids removed from the blood, measured in milliliters per minute (ml/min). With impaired kidney function, GFR drops correspondingly. During stages 4–5 (GFR <30), patients experience signs and symptoms, including nausea, fatigue, drowsiness, weakness, headache, loss of appetite, itching, muscle cramps, hypertension, volume overload, anemia, bone, mineral, and electrolyte abnormalities, etc. Drug treatments and a low-protein, low-salt diet can help manage signs and symptoms and slow but often not stop the progression of CKD, for which there is no cure (Chen et al.,

2019). When GFR drops to less than 15 ml/min, patients reach stage 5, or ESRD, in which remaining kidney function is not enough to support life. According to the 2021 Annual Data Report from United States Renal Data System (USRDS), currently, more than 809,103 Americans live with ESRD (more than 2 in every 1,000 people, <https://adr.usrds.org/2021>). ESRD patients need either dialysis or a kidney transplant to survive. On an annual basis, more than \$51 billion is spent to treat patients with ESRD in the United States, accounting for more than 7% of the Medicare budget. In the most common form of dialysis, hemodialysis, a machine filters wastes from the blood, which is then returned to the body. Patients typically spend 3–5 h per dialysis session 3 days per week in the dialysis center, dramatically reducing their quality of life. Moreover, even with this treatment, only 35%–50% of hemodialysis patients survive for 5 years. Kidney transplant carries a more favorable 5-year survival rate of more than 80%, but there is a severe shortage of donor organs. In 2021, 90,483 Americans were on the waiting list for donor kidneys, but only 24,670 received a transplant (<https://www.organdonor.gov>). It is estimated that 13 Americans die each day while waiting for a kidney transplant. Thus, there is an urgent need for innovative solutions that address the shortage of kidneys available for transplantation. In this review, we introduce the concept and summarize the progress of the current approaches to solving the shortage of donor kidneys (summarized in Figure 1). We also discuss the advantages and challenges of the approaches (summarized in Table 1).

## Bioartificial kidney—making a portable dialysis device

Bioartificial kidneys are built upon dialysis devices. Like dialysis, bioartificial kidneys employ artificial hemofilters to filter wastes from the blood. Furthermore, a biological component consisting of kidney's proximal tubule cells is added to enhance the performance of the dialysis device, aiming at recapitulating not only the filtration function of the kidney, but also most of the kidney's reabsorption and excretion functions (Humes et al., 2014; Salani et al., 2018). This review focuses on this type of bioartificial kidney. It is of note that other wearable artificial kidney devices aiming at miniaturizing dialysis device, without a biological component, are also being actively developed and are reviewed elsewhere (Salani et al., 2018).

The development of bioartificial kidneys started with a pioneering study from Humes and colleagues with the generation of an extracorporeal renal tubule assist device (RAD) (Humes et al., 1999a). This RAD consisted of about  $10^8$  renal proximal tubule cells grown as confluent monolayer along the inner surface of one standard hemofiltration cartridge. RAD was then connected to a conventional hemofilter to assemble the bioartificial kidney. Both *in vitro* and *in vivo*

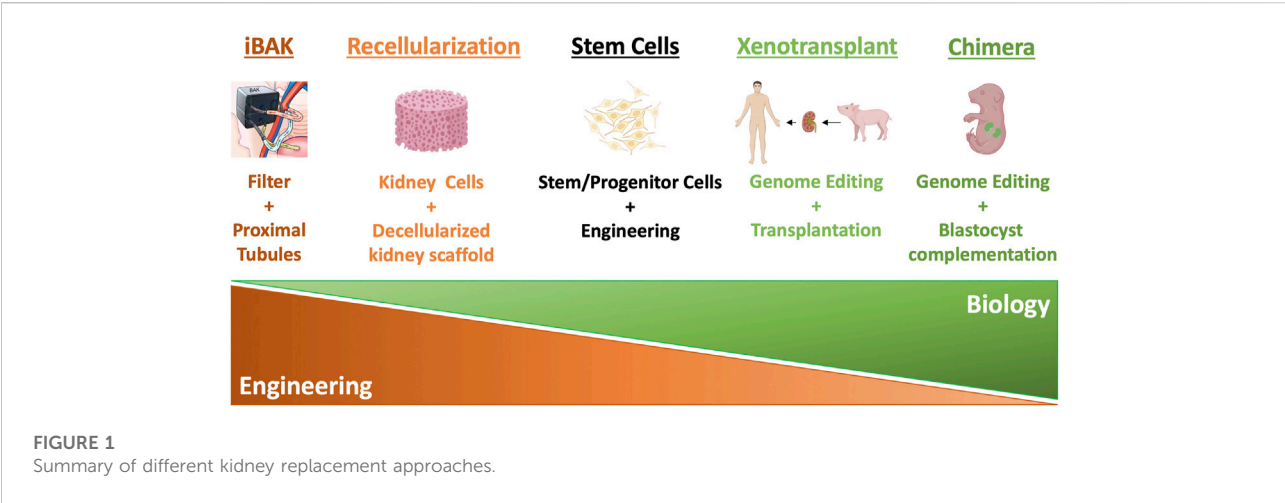


TABLE 1 Advantages and challenges of different kidney replacement approaches.

	IBAK	Recellularization	Stem cells	Xenotransplant	Chimera
Advantages	No immune rejection No ethical concerns	Native kidney scaffold No ethical concern	No immune rejection No ethical concerns	Functionality Maturity	Grow kidney <i>in vivo</i>
Challenges	Cell source Long-term efficacy Durability	Cell source Recellularization Long-term efficacy	Scalability Urine excretion Vasculature	Immunogenicity Long-term efficacy Safety concerns Ethical concerns	Xenotransplant Safety concerns Ethical concerns

studies of the system showed that the renal cells retained their normal functions, such as metabolic activities, active transport properties, and key endocrine processes (Humes et al., 1999a; Humes et al., 1999b; Fissell et al., 2003). This RAD-based bioartificial kidney was then tested in FDA-approved clinical trials for the treatment of acute renal failure (ARF), for which the mortality rate exceeding 70%, despite hemodialysis or continuous renal replacement therapy (CRRT). In an initial Phase I/II clinical trial, safety of RAD device was demonstrated for up to 24 h, with maintained viability, durability, and functionality (Humes et al., 2004). In a follow-up multicenter, randomized, Phase II clinical trial involving 58 patients who had ARF and required CRRT, patients with CRRT + RAD treatment had dramatically reduced mortality rate (33% CRRT + RAD vs. 61% CRRT-only at day 28). The risk for death in the CRRT + RAD group was estimated to be 50% of the CRRT-only group (Tumlin et al., 2008). These results highlight the potential of RAD device in the treatment of ARF.

Based on the RAD system, Roy, Fissell, and colleagues from University of California, San Francisco (UCSF) and Vanderbilt University aim to further miniaturize the device size in order to create an implantable bioartificial kidney (iBAK) as a permanent solution to ESRD (<https://pharm.ucsf.edu/kidney>). Similarly, iBAK device combines two parts: hemofilter and bioreactor.

The hemofilter is upgraded to incorporate silicon membranes with nanometer-scale slit-like pores to mimic the filtration function of the kidney’s glomeruli. These silicon membranes are fabricated using the microelectromechanical systems (MEMS) toolkit which enables the unprecedented control over nanoscale feature size and geometry in a scalable manufacturing process (Fissell et al., 2009). Importantly, to prevent coagulation of plasma in contact with silicon, the surface of the silicon membrane is modified to incorporate biomaterials which can greatly reduce the adhesion of proteins and platelets, complement activation, and coagulation (Fissell et al., 2009; Kanani et al., 2010; Melvin et al., 2010; Li et al., 2011; Muthusubramaniam et al., 2011). The hemofilter part helps filter the blood to remove waste products and toxins from blood. The other part, bioreactor, is infused with renal proximal tubule cells to rebalance electrolytes and other blood components. The bioreactor is upgraded from an earlier version of bioartificial renal epithelial cell system (BRECS) (Buffington et al., 2012). Like RAD, BRECS has human renal proximal tubule cells grown as confluent monolayer along the inner surface of a hemofiltration cartridge, but these renal proximal tubule cells are first expanded *in vitro* (Westover et al., 2012), and the whole system can be cryopreserved, enabling on-demand use for acute indications. Compared to BRECS, the upgraded bioreactor seeds

expanded renal proximal tubule cells onto the silicon scaffold but not onto the surface of the traditional hemofiltration cartridge. These renal proximal tubule cells can reabsorb salts, sugar, and most water back to bloodstream and excrete toxins to the bladder. Instead of external electrical pump used in hemodialysis, this device uses the energy from patient's own heart to pump blood through the hemofilter. Importantly, according to this group's 2021 ASN conference abstract (#PO0513), this coffee cup-sized device has been implanted into pigs for preclinical evaluation. Within 3 days after implanting this device into the retroperitoneum of pig without any anticoagulation or immunosuppression treatment, the pig showed no severe side effect including hematoma, thromboembolism or other infection (peer-reviewed article has not been published at the time of writing). Importantly, one of the great advantages of this bioartificial kidney is that it doesn't need blood thinning or immunosuppressant drugs, since the renal tubule cells in the device are separated from the recipient's immune cells or antibodies as cells or larger molecules from the blood cannot pass through the nanopores of the hemofilter.

These results are encouraging, but some major challenges need to be solved for clinical development of this approach. First, to make the bioreactor component, large quantities of high-quality human proximal tubule cells are needed for manufacturing. In the current proof-of-concept studies, these cells are sourced from deceased donor human kidneys that are determined not suitable for transplantation. However, a reliable and sustainable source of human proximal tubule cells are urgently needed for future commercialization, which could potentially be provided from the directed differentiation of human pluripotent stem cells into renal epithelial cell types (see below). Second, long-term durability and efficacy of bioartificial kidneys upon transplantation remain to be determined: the nanopores in the silicon hemofilter may clog up over time, and it also remains unknown whether the proximal tubule cells maintain their differentiated phenotypes and functionality in the long run. Third, with the current design, the patients will rely on water and electrolyte supplementation and dietary restrictions to maintain the homeostasis. It would be a great improvement if a real-time biofeedback component can be incorporated to monitor the patient's homeostatic state and regulate the function of the bioartificial kidney autonomously to maintain homeostasis.

## Recellularization—reseeding native kidney scaffold

Decellularized whole organ scaffold offers an attractive source for whole organ engineering. Decellularization can be achieved through perfusion at controlled pressure in an intact organ using detergents such as sodium dodecyl sulfate (SDS) or

Triton X-100 to remove the cellular components of the organ (Guyette et al., 2014). Over the past decade, successful decellularization of the kidney has been reported, with successes from species including rat (Song et al., 2013; Caralt et al., 2015), pig (Orlando et al., 2012; Abolbashari et al., 2016; Poornejad et al., 2017), monkey (Nakayama et al., 2010), and human (Peloso et al., 2015). In general, after decellularization, few native cells remain in the kidney, leaving an acellular scaffold with retained vasculature and tissue structures, and extracellular matrix (ECM) components. ECM contains important mechanical, biophysical, and biochemical cues that regulate cell identity and function in the organ (Hussey et al., 2018). It is thus hypothesized that, if the acellular scaffold can be properly recellularized, it will be able to reconstitute a transplantable bioengineered organ.

Proof-of-concept recellularization of a decellularized kidney scaffold to make a transplantable bioengineered kidney was reported in 2013 from Ott and colleagues (Song et al., 2013). In this study, cadaveric rat kidneys were decellularized using renal artery perfusion with 1% SDS at a constant pressure of 40 mm Hg. Cells from two sources were then utilized to recellularize the kidney scaffold. Human umbilical venous endothelial cells (HUVECs) were infused through the renal artery and rat neonatal kidney cells (NKC) were seeded through the ureter. After recellularization and additional 3–5 days of perfusion, HUVECs were found to line the vascular channels throughout the entire scaffold while NKCs were identified in the different compartments of the nephron, with podocytes appearing to preferentially engraft into the glomerular regions. Upon orthotopic transplantation, the bioengineered kidney perfused well without any evidence of bleeding from the vasculature. Importantly, urine is produced from the transplant although the volume is about 1/3 of that from a native kidney. Urinalysis, however, indicated only limited kidney function from the bioengineered kidney, reflected by much higher glucose and albumin but much lower creatinine and urea in the urine, compared with native kidney control. These results suggest that further optimization of recellularization is still needed to enhance the extent and distribution of the renal cell types across the kidney scaffold to improve the function of the bioengineered kidney.

Importantly, rapid progress in the areas of biomaterials and 3D bioprinting technologies (Murphy and Atala, 2014; Matai et al., 2020) have opened new avenues to fabricating scaffolds with designed geometrical, mechanical, biochemical, and biophysical features from either native or synthetic ECM biomaterials (Hussey et al., 2018). These new bioengineering tools might provide novel solutions to the current recellularization challenges. In addition to the optimization of recellularization, other challenges need to be overcome to move kidney organ decellularization/recellularization approach into a feasible therapy. The first consideration is the cell source for recellularization. Ideally a mixture of renal cell types representing different segments of the nephron, like the NKCs in the proof-of-

concept study mentioned above (Song et al., 2013), should be used for recellularizing a kidney scaffold. For that, induced pluripotent stem cells (iPSC)-derived kidney organoids (see next section) might be able to provide such a source. Importantly, with iPSCs isolated from a transplant recipient's own cells, in theory, it would be possible to recellularize an acellular kidney to avoid immune rejection. Second, most of the current proof-of-concept studies have been performed in rat models, but studies using human kidney scaffolds are still limited. More work will need to be done in decellularized human kidney scaffolds to show the viability of ECM scaffolding as well as proper transplantation and physiological function of a bioengineered kidney in large animal models.

## Stem cells—de novo generation of a kidney

Pluripotent stem cells (PSCs), including embryonic stem cells (ESCs) (Evans and Kaufman, 1981; Martin, 1981; Thomson et al., 1998) and induced pluripotent stem cells (iPSCs) (Takahashi and Yamanaka, 2006; Takahashi et al., 2007), have the potential to generate any cell type of the body (Robinton and Daley, 2012). With the recent progress in PSC-derived kidney progenitor cells and their derivative miniature kidney-like structures named “organoids,” PSCs hold great promise in rebuilding a kidney *de novo* by recapitulating normal kidney organogenesis.

Studies of kidney organogenesis have provided valuable insights into how we might be able to rebuild a kidney. Within UB and MM of the developing kidney, several self-renewing stem/progenitor populations drive the expansion and repetitive mutual induction of these structures. It is now clear that at least two progenitor populations are present in the MM, along with one in the UB (McMahon, 2016). *Wnt11*<sup>+</sup> UB progenitor cells (UPCs) reside at the branching tips of the UB epithelium (Majumdar et al., 2003; Rutledge et al., 2017); *Six2*<sup>+</sup> nephron progenitor cells (NPCs) are located in the inner layer of the MM, capping and contacting the UPCs (Self et al., 2006; Kobayashi et al., 2008); and *Foxd1*<sup>+</sup> interstitial progenitor cells (IPCs) are found in the outer layer of the MM, surrounding the NPCs (Kobayashi et al., 2014). In mice, lineage-tracing experiments have demonstrated that all of these progenitor populations can self-renew and differentiate, with NPCs giving rise to the nephrons, IPCs becoming the kidney stromal cell types and UPCs generating the CD network. In addition to these progenitor populations, it is thought that vascular progenitor cells (VPCs) form the blood vessels, for which less is known compared to other progenitors (McMahon, 2016). Importantly, of these progenitor populations, the interaction between NPCs and UPCs lays the foundation for kidney formation. During a typical UB branching cycle, UPCs self-renew upon receiving glial cell line-derived neurotrophic factor (GDNF) secreted from the surrounding NPCs (Durbec et al., 1996; Moore et al., 1996; Pichel

et al., 1996; Sánchez et al., 1996; Treanor et al., 1996; Cacalano et al., 1998). Meanwhile, most of the NPCs self-renew and stay in close contact with the UPCs. Upon receiving Wnt9b signals from the trunk region of the UB, the NPCs farthest from the UPCs differentiate stepwise into pretubular aggregate (PA), renal vesicle (RV), S-shaped body (SSB), eventually forming a nephron tubule (Carroll et al., 2005). Importantly, the proximal nephron, which is the segment farthest from the UB, recruits endothelial cells to form vascularized glomeruli, which will filter the blood (Eremina et al., 2003; Eremina and Quaggin, 2004). The distal nephron closest to the UB fuses seamlessly with the UB epithelium to make a continuous lumen, so that the urine will pass from the nephron tubule to the UB-derived CD (Kao et al., 2012). This process repeats itself again and again, generating new nephrons, branching morphogenesis and more self-renewing NPCs and UPCs for the next cycle (Short et al., 2014). These progenitor cells are exhausted around the time of birth (postnatal day 2 for mouse; 36 weeks gestation for human), resulting in the limited regenerative potential of the adult kidney.

Considering the progenitors, as kidney's building blocks, play central roles in kidney organogenesis, to recreate these embryonic/fetal-stage kidney progenitors from PSCs have become the focus of kidney researchers in the field of regenerative medicine in the past decade, which subsequently led to the creation of various kidney organoids that model kidney development and disease *in vitro*. Following normal developmental process, stepwise differentiation protocols have been established to generate NPCs from pluripotent stem cells, which can further generate 3D structures representing major segments of the nephron, including glomeruli, proximal tubule, loop of Henle and distal tubule (Taguchi et al., 2014; Morizane et al., 2015; Takasato et al., 2015). Similarly, UB-like cells have been generated from human PSCs in an earlier study (Xia et al., 2013), and recently, several groups have reported the generation of 3D branching UB organoids that have both UB tip and trunk segments (Taguchi and Nishinakamura, 2017; Mae et al., 2018), or have a near-pure population of the tip cells—the UPCs (Howden et al., 2020; Zeng et al., 2021). These UB organoids can further mature into CD organoids showing the expression of marker genes representative of principal cells and intercalated cells in the CD (Howden et al., 2020; Kuraoka et al., 2020; Tsujimoto et al., 2020; Zeng et al., 2021). Of note, taking a different approach than directed differentiation from PSCs, other groups have developed methods to culture and expand primary NPCs (Brown et al., 2015; Li et al., 2016; Tanigawa et al., 2016) and primary UPCs (Yuri et al., 2017; Zeng et al., 2021) that are isolated from embryonic/fetal kidneys, which can also differentiate into nephron and CD organoids, respectively. Importantly, Taguchi and Nishinakamura showed that when mouse embryonic stem cell (mESC)-derived NPCs and UB were mixed together, a self-organized higher-order kidney structure was generated, with the formation of both nephrons and CD in the same structure (Taguchi and Nishinakamura, 2017).



Recently, this group further derived mouse IPC-like cells from mESCs and by mixing NPCs, UB, and IPCs, a more complete kidney structure was formed with the addition of stroma population to nephrons and CD (Tanigawa et al., 2022). Taken together, exciting progress has been made in the past decade, enabling us to produce large quantities of kidney progenitor cells and derive miniature kidney-like organoids from them, opening new avenues for kidney regeneration and disease modeling [comprehensively reviewed elsewhere (Little and Combes, 2019)]. However, despite the encouraging progress, it is still challenging to leap from progenitors or organoids to a transplantable organ. Several technical hurdles need to be overcome.

## Scalability

Patients can live well with at least 20%–30% of normal kidney function. Mice have an average of 14,000 nephrons per kidney, so they would need 5,600–8,400 nephrons to sustain life; in humans, with an average one million nephrons per kidney, a minimum of 400,000–600,000 nephrons are needed. However, in the miniature kidney organoid systems, dozens to hundreds of nephrons can be produced through self-organization. This number is far from adequate to sustain the life of mouse or human, so scale-up of the organoid system is required. For that, bioengineering approaches such as 3D bioprinting technologies (Lawlor et al., 2021) and a recently proposed biomanufacturing via organ building blocks (OBBs) approach (Wolf et al., 2022) will likely be useful.

## Plumbing

Most of the current kidney organoids recapitulate either the kidney's nephron or CD, lacking a continuous nephron-CD structure to allow urine excretion. In the higher-order kidney organoid structure generated from mixing different types of mouse kidney progenitors (Taguchi and Nishinakamura, 2017; Tanigawa et al., 2022), the nephrons are interconnected with the CD system, allowing potential urine to drain. However, the system still lacks a single route for urine to exit. By incorporating bioengineering strategies to this system, this problem could potentially be solved in the future. It is also of note that, the higher-order kidney structures were generated using mouse PSCs, but a similar higher-order kidney structure has not yet been generated from human PSCs.

## Vasculature

For kidney to function, it is essential to have vasculature infiltrating properly into the glomeruli to generate primitive filtrate from the blood. In addition, peritubular vasculature is also important for performing reabsorption and excretion function of the kidney. However, the first generation of

kidney organoids (Taguchi et al., 2014; Freedman et al., 2015; Morizane et al., 2015; Takasato et al., 2015) have very limited vasculature. Recent improvement via the manipulation of shear force and angiogenic signals (Homan et al., 2019), and the adjustment of embryonic patterning signals (Low et al., 2019), have greatly increased vasculature formation in the kidney organoids. However, the infiltration of vasculature into the glomeruli is still rare *in vitro*. In strong contrast, when kidney organoids were transplanted into recipient animals, blood vessels were formed and grafted well into the glomeruli of the transplant (Li et al., 2016; van den Berg et al., 2018; Garreta et al., 2019; Subramanian et al., 2019). Interestingly, these blood vessels were formed almost exclusively from the recipient's own cells, paving the road for interconnecting the transplant to the circulation system of the recipient.

## Maturation

In-depth characterization of kidney organoids using single-cell sequencing technologies indicated the immature nature of the kidney organoids, resembling 1st–2nd trimester human fetal kidneys (Wu et al., 2018; Phipson et al., 2019; Subramanian et al., 2019), suggesting further maturation is needed for the kidney organoid to function properly. Interestingly, a recent study successfully generated highly patterned CD organoids that showed global gene expression profile similar to that of a postnatal kidney (Zeng et al., 2021), suggesting it is possible to further mature kidney organoid *in vitro*. Furthermore, transplanted organoids *in vivo* showed significantly improved maturity (van den Berg et al., 2018; Subramanian et al., 2019; Tran et al., 2019), suggesting the potential future use of host animals as incubators to achieve maturity and functionality of stem cell-derived kidney structures.

## Xenotransplantation—immunocompatible pig kidneys

Xenotransplantation opens the gate to an alternative source of transplantable kidney, from other animals. It also makes it possible to modify the donor, instead of treating the recipient with immunosuppressants, to overcome immune rejection. Naturally, the earliest trials were mostly using nonhuman primates (NHPs) as the kidney source, considering that they are evolutionary close to human. However, most of these trials were unsuccessful. In an early study from 1963, six patients received chimpanzee kidney xenotransplantation (REEMTSMA et al., 1964). Five of the xenotransplantation soon failed within 6 weeks from either rejection or infection. One patient did live a normal life for 9 months until eventually died possibly due to electrolyte disturbance.

Later, potential problems from using NHPs as the kidney source were noticed. These donor NHPs were mostly caught from wild that might carry infectious microorganisms or diseases.

Furthermore, significant ethical issues remain, making NHPs less likely to serve as donors to solve the problem of organ shortage (Cooper et al., 2002). Pigs, on the other hand, seem to be a better option, considering human's thousands of years of experiences in breeding them, their short period of time of maturation, and importantly, the high similarity in size, anatomy, and physiology between pig and human kidneys. In the 1990s, research focus was then turned to using pigs as xenograft donors. Nevertheless, transplantation of wild-type pig kidneys led to immediate hyperacute rejection, due to species differences.

To solve the problem, the focus has recently been shifted to genetically modify the donor pigs to generate pig strains with reduced immunogenicity. With new gene editing tools such as the CRISPR-Cas9 system (Jinek et al., 2012; Cong et al., 2013; Mali et al., 2013), it is now much easier to genetically manipulate pigs to accommodate our needs. Researchers have introduced human complement- and coagulation-regulatory proteins which significantly increased pig xenograft survival (Fodor et al., 1994; Cozzi and White, 1995; Wang et al., 2018a). On the other hand, knock-out of pig genes encoding pig xenoantigens also significantly increased pig xenograft survival as well (Kolber-Simonds et al., 2004; Yamada et al., 2005). Another problem for pig kidney xenotransplantation is the potential transferring of pathogenic microorganisms and porcine endogenous retrovirus (PERVs) to the human recipients. These problems can be solved by establishing pathogen-free breeding space (Cooper et al., 2020) and gene editing the donor animals to knock out PERV loci in the genome (Niu et al., 2017).

Pig-NHP xenotransplantation has been studied for decades which significantly contributed to our current understanding of xenotransplantation. However, success in NHPs does not predict the same outcome in humans. A model to further investigate pig-human xenotransplantation is needed. Recently, groups from New York University (Montgomery et al., 2022) and University of Alabama Birmingham (UAB) (Porrett et al., 2022) have both conducted pig-human xenotransplantation in brain-dead decedents using genetically modified pig kidneys. At NYU, a pig kidney with the knockout of a gene encoding  $\alpha$ -Gal, a major antigen mediating hyperacute rejection response, was connected to the blood vessels from the upper leg and kept outside of the body. And at UAB, two pig kidneys harboring 10 genetic modifications, were transplanted into the decedent's abdomen and connected to his bladder after his native kidneys were removed. In both cases, urine was produced normally and no hyperacute rejection was observed. Kidneys remained viable until termination of the studies after 54 and 74 h, respectively.

Although how physiology changes due to brain death might affect renal function remains unknown, these encouraging studies from NYU and UAB demonstrated that human decedent can be a good pre-clinical model to study safety and short-term effect of xenotransplantation, paving the road for establishing future clinical trials in living humans to evaluate the long-term safety and efficacy of this approach. In addition to

hyperacute rejection, future long-term xenotransplantation studies will address the extent of acute rejections (Cornell et al., 2008) (including acute cellular rejection and acute humoral rejection) which would arise weeks to months after transplantation. Furthermore, common issues observed in current kidney allotransplant surgeries, such as renal allograft thrombosis (Ponticelli et al., 2009) and chronic rejections, will also need to be determined in the xenotransplants.

## Interspecies chimera—growing a human kidney in a pig

Interspecies chimera is an emerging approach combining stem cells, genome editing, and blastocyst complementation techniques to generate a targeted organ from the donor stem cells within the body of another species (Wu et al., 2016). Conceptually, it is hypothesized that, if PSCs from one species are injected into a mutant blastocyst of another species for which development of a specific organ is defective, leaving a niche for organ development, the injected PSCs-derived cells will compensate for the defect and form the missing organ. The success of this approach will make it possible to generate replacement human organs from animal hosts.

The proof of concept for the successful generation of PSC-derived organs *in vivo* via interspecies chimera was first reported by Nakauchi and colleagues in 2010 (Kobayashi et al., 2010), in which a rat pancreas was generated in a mouse. In these recipient mice, *Pdx1*, a critical gene encoding a transcription factor essential for pancreas development, was knocked out, exhibiting pancreas agenesis. Donor rat iPSCs labeled with EGFP were injected into *Pdx1*<sup>-/-</sup> mouse embryos at the blastocyst stage and the embryos were then transferred into the uteri of pseudo pregnant mice. Live mice were born, and their pancreas were entirely composed of EGFP-marked rat iPSC-derived cells. Interestingly, these pancreases were small, of the size of a mouse pancreas. In a follow-up study from the same group, a reverse experiment was performed in which mouse iPSCs were injected into *Pdx1*<sup>-/-</sup> rat blastocysts (Yamaguchi et al., 2017). This time the pancreases were entirely composed of the mouse iPSC-derived cells but were of the size of rat pancreases. Islets were prepared from the pancreas of the mouse-rat chimera and transplanted into streptozotocin-induced diabetes mouse models. Importantly, these transplanted islets successfully maintained normal glucose levels over 1 year in the absence of immunosuppression. These experiments provide proof-of-concept evidence for the potential therapeutic effects of iPSC-derived islets generated in interspecies chimera.

Similar strategies have been adopted to generate a kidney *in vivo* from PSCs using rodent intraspecies and interspecies chimera systems. Knockout of *Sall1*, a gene encoding a transcription factor that plays critical roles in the metanephric

mesenchyme of a developing mouse kidney, led to kidney agenesis (Nishinakamura et al., 2001). However, when GFP-marked mouse PSCs were injected into *Sall1*<sup>-/-</sup> mouse blastocyst to form chimera, GFP + kidneys were formed (Usui et al., 2012). Further analysis confirmed that, the kidney's nephrons and stroma were generated from the injected mouse PSC-derived cells, but not the kidney's collecting duct, vasculature, or nerves that are not derived from metanephric mesenchyme and are thus not developmentally influenced by *Sall1* gene knockout. Importantly, these kidneys were grossly and histologically normal. In a follow-up study, loss-of-function *Sall1* mutant rats were generated using CRISPR-Cas9 genome editing tool and like *Sall1*<sup>-/-</sup> mice, anephric phenotype was observed in these *Sall1* mutant rats. Microinjection of mouse PSCs into *Sall1* mutant rat blastocysts successfully generated mouse-rat chimera with kidneys (Goto et al., 2019). Consistent with intraspecies chimera studies in *Sall1*<sup>-/-</sup> mice (Usui et al., 2012), various compartments of the nephron, including glomeruli, proximal tubule, loop of Henle and distal tubule, were entirely composed of GFP + mouse PSC-derived cells. Although the kidneys were histologically normal, both intraspecies and interspecies chimera did not survive to adulthood, likely due to the defect of milk suckling, another phenotype of *Sall1* gene knockout that affects the brain function, which might not be fully rescued in the chimera. This has prevented in-depth analysis of the functional maturation of the kidneys generated from the intraspecies and interspecies chimera.

Interspecies chimera provides a powerful platform to study xenogenic barriers and generate *in vivo* disease models. However, several major obstacles still prevent the translation of this approach into novel therapies to provide replacement human organs in the near future. One of the major issues is the difficulty of forming interspecies chimera using human PSCs. Human PSCs have been found to be able to incorporate into mouse (Gafni et al., 2013; Takashima et al., 2014; Masaki et al., 2015), pig and cow (Wu et al., 2017) embryos at very early developmental stage—the inner cell mass (ICM) stage, but they failed to contribute to the development at later developmental stages, likely due to the species differences from dozens of millions of years of evolutionary distance between human and these species. To solve this problem, alternative human PSC states are actively being developed in anticipation that different pluripotent state may enhance chimera formation efficiency (Wu et al., 2015; Yang et al., 2017). Furthermore, forced expression of anti-apoptotic proteins in the PSCs has also been shown to increase interspecies chimera competency (Masaki et al., 2016; Wang et al., 2018b). These efforts along these lines might lead to novel breakthroughs in this area. In addition to technical obstacles to overcome to demonstrate feasibility of this approach, ethical issues and safety concerns from the public still remain, in terms of animal warfare and the likelihood of achieving human cognitive abilities, human-like

appearance, or making human gametes, from the chimera (Wu et al., 2016).

## Conclusion and future perspectives

With the rapid technological development in the areas of regenerative medicine, genome editing, and bioengineering, over the past decade, several highly innovative approaches have been proposed aiming at providing solutions to the severe shortage of donor kidneys for transplantation. Here we have introduced the concepts of these approaches, summarized their current progress, and discussed potential challenges towards their future translation into novel therapies. It is of note that different approaches do not develop independently. Rather, these approaches can complement each other, and stem cell technologies appear to be at the center of these interconnections. For instance, the development of stem cell-derived kidney progenitors and organoids may be utilized to provide a reliable source of proximal tubule cells that are needed in commercializing the bioartificial kidney device. Large quantities of different kidney cell types that are required to recellularize a decellularized native kidney scaffold can also be provided from stem cell-derived kidney tissues. In addition, development of alternative PSC states with genetic modifications might overcome xenogenic barriers eventually leading to the generation of human organs in animal hosts through interspecies complementation. Taken together, in the past decade, we have seen remarkable progress in this area, and we are optimistic that novel kidney replacement therapies will likely benefit patients with kidney diseases in the next decade to come.

## Author contributions

BH, ZZ, CCZ, MES, and ZL wrote the manuscript. BH and ZL edited the manuscript.

## Funding

This work is supported by departmental startup fund, USC/UKRO Kidney Research Center fund, and Dean's Pilot Award from Keck School of USC to ZL and MES was supported by California Institute of Regenerative Medicine (CIRM) Bridges Program. ZZ was supported by USC Stem Cell Challenge Award.

## Conflict of interest

The authors declare that the research was conducted in the absence of any commercial or financial relationships that could be construed as a potential conflict of interest.

## Publisher's note

All claims expressed in this article are solely those of the authors and do not necessarily represent those of their affiliated

## References

- Abolbashari, M., Agcaoili, S. M., Lee, M. K., Ko, I. K., Aboushwareb, T., Jackson, J. D., et al. (2016). Repopulation of porcine kidney scaffold using porcine primary renal cells. *Acta Biomater.* 29, 52–61. doi:10.1016/j.actbio.2015.11.026
- Brown, A. C., Muthukrishnan, S. D., and Oxburgh, L. (2015). A synthetic niche for nephron progenitor cells. *Dev. Cell* 34, 229–241. doi:10.1016/j.devcel.2015.06.021
- Buffington, D. A., Pino, C. J., Chen, L., Westover, A. J., Hageman, G., and Humes, H. D. (2012). Bioartificial renal epithelial cell system (BRECS): A compact, cryopreservable extracorporeal renal replacement device. *Cell Med.* 4, 33–43. doi:10.3727/215517912X653328
- Cacalano, G., Farinas, I., Wang, L. C., Hagler, K., Forgie, A., Moore, M., et al. (1998). GFRalpha1 is an essential receptor component for GDNF in the developing nervous system and kidney. *Neuron* 21, 53–62. doi:10.1016/S0896-6273(00)80514-0
- Caralt, M., Uzarski, J. S., Jacob, S., Obergfell, K. P., Berg, N., Bijonowski, B. M., et al. (2015). Optimization and critical evaluation of decellularization strategies to develop renal extracellular matrix scaffolds as biological templates for organ engineering and transplantation. *Am. J. Transpl.* 15, 64–75. doi:10.1111/ajt.12999
- Carroll, T. J., Park, J. S., Hayashi, S., Majumdar, A., and McMahon, A. P. (2005). Wnt9b plays a central role in the regulation of mesenchymal to epithelial transitions underlying organogenesis of the mammalian urogenital system. *Dev. Cell* 9, 283–292. doi:10.1016/j.devcel.2005.05.016
- Chen, T. K., Knicely, D. H., and Grams, M. E. (2019). Chronic kidney disease diagnosis and management: A review. *JAMA* 322, 1294–1304. doi:10.1001/jama.2019.14745
- Cong, L., Ran, F. A., Cox, D., Lin, S., Barretto, R., Habib, N., et al. (2013). Multiplex genome engineering using CRISPR/Cas systems. *Science* 339, 819–823. doi:10.1126/science.1231143
- Cooper, D. K. C., Hara, H., Iwase, H., Yamamoto, T., Jagdale, A., Kumar, V., et al. (2020). Clinical pig kidney xenotransplantation: How close are we? *J. Am. Soc. Nephrol.* 31, 12–21. doi:10.1681/ASN.2019070651
- Cooper, D. K., Gollackner, B., and Sachs, D. H. (2002). Will the pig solve the transplantation backlog? *Annu. Rev. Med.* 53, 133–147. doi:10.1146/annurev.med.53.082901.103900
- Cornell, L. D., Smith, R. N., and Colvin, R. B. (2008). Kidney transplantation: Mechanisms of rejection and acceptance. *Annu. Rev. Pathol.* 3, 189–220. doi:10.1146/annurev.pathmechdis.3.121806.151508
- Cozzi, E., and White, D. J. (1995). The generation of transgenic pigs as potential organ donors for humans. *Nat. Med.* 1, 964–966. doi:10.1038/nm0995-964
- Durbec, P., Marcos-Gutierrez, C. V., Kilkenny, C., Grigoriou, M., Wartiovaara, K., Suvanto, P., et al. (1996). GDNF signalling through the Ret receptor tyrosine kinase. *Nature* 381, 789–793. doi:10.1038/381789a0
- Eremina, V., and Quaggin, S. E. (2004). The role of VEGF-A in glomerular development and function. *Curr. Opin. Nephrol. Hypertens.* 13, 9–15. doi:10.1097/00041552-200401000-00002
- Eremina, V., Sood, M., Haigh, J., Nagy, A., Lajoie, G., Ferrara, N., et al. (2003). Glomerular-specific alterations of VEGF-A expression lead to distinct congenital and acquired renal diseases. *J. Clin. Invest.* 111, 707–716. doi:10.1172/JCI17423
- Evans, M. J., and Kaufman, M. H. (1981). Establishment in culture of pluripotent cells from mouse embryos. *Nature* 292, 154–156. doi:10.1038/292154a0
- Fissell, W. H., Dubnisheva, A., Eldridge, A. N., Fleischman, A. J., Zydney, A. L., and Roy, S. (2009). High-performance silicon nanopore hemofiltration membranes. *J. Memb. Sci.* 326, 58–63. doi:10.1016/j.memsci.2008.09.039
- Fissell, W. H., Lou, L., Abrishami, S., Buffington, D. A., and Humes, H. D. (2003). Bioartificial kidney ameliorates gram-negative bacteria-induced septic shock in uremic animals. *J. Am. Soc. Nephrol.* 14, 454–461. doi:10.1097/01.asn.0000045046.94575.96
- Fodor, W. L., Williams, B. L., Matis, L. A., Madri, J. A., Rollins, S. A., Knight, J. W., et al. (1994). Expression of a functional human complement inhibitor in a transgenic pig as a model for the prevention of xenogeneic hyperacute organ rejection. *Proc. Natl. Acad. Sci. U. S. A.* 91, 11153–11157. doi:10.1073/pnas.91.23.11153
- Freedman, B. S., Brooks, C. R., Lam, A. Q., Fu, H., Morizane, R., Agrawal, V., et al. (2015). Modelling kidney disease with CRISPR-mutant kidney organoids derived from human pluripotent epiblast spheroids. *Nat. Commun.* 6, 8715. doi:10.1038/ncomms9715
- Gafni, O., Weinberger, L., Mansour, A. A., Manor, Y. S., Chomsky, E., Ben-Yosef, D., et al. (2013). Derivation of novel human ground state naive pluripotent stem cells. *Nature* 504, 282–286. doi:10.1038/nature12745
- Garreta, E., Prado, P., Tarantino, C., Oria, R., Fanlo, L., Marti, E., et al. (2019). Fine tuning the extracellular environment accelerates the derivation of kidney organoids from human pluripotent stem cells. *Nat. Mat.* 18, 397–405. doi:10.1038/s41563-019-0287-6
- Goto, T., Hara, H., Sanbo, M., Masaki, H., Sato, H., Yamaguchi, T., et al. (2019). Generation of pluripotent stem cell-derived mouse kidneys in Sall1-targeted anephric rats. *Nat. Commun.* 10, 451. doi:10.1038/s41467-019-08394-9
- Guyette, J. P., Gilpin, S. E., Charest, J. M., Tapias, L. F., Ren, X., and Ott, H. C. (2014). Perfusion decellularization of whole organs. *Nat. Protoc.* 9, 1451–1468. doi:10.1038/nprot.2014.097
- Homan, K. A., Gupta, N., Kroll, K. T., Kolesky, D. B., Sklyar-Scott, M., Miyoshi, T., et al. (2019). Flow-enhanced vascularization and maturation of kidney organoids *in vitro*. *Nat. Methods* 16, 255–262. doi:10.1038/s41592-019-0325-y
- Howden, S. E., Wilson, S. B., Groenewegen, E., Starks, L., Forbes, T. A., Tan, K. S., et al. (2020). Plasticity of distal nephron epithelia from human kidney organoids enables the induction of ureteric tip and stalk. *Cell Stem Cell* 28, 671–684.e6. doi:10.1016/j.stem.2020.12.001
- Humes, H. D., Buffington, D. A., MacKay, S. M., Funke, A. J., and Weitzel, W. F. (1999). Replacement of renal function in uremic animals with a tissue-engineered kidney. *Nat. Biotechnol.* 17, 451–455. doi:10.1038/8626
- Humes, H. D., Buffington, D., Westover, A. J., Roy, S., and Fissell, W. H. (2014). The bioartificial kidney: Current status and future promise. *Pediatr. Nephrol.* 29, 343–351. doi:10.1007/s00467-013-2467-y
- Humes, H. D., MacKay, S. M., Funke, A. J., and Buffington, D. A. (1999). Tissue engineering of a bioartificial renal tubule assist device: *In vitro* transport and metabolic characteristics. *Kidney Int.* 55, 2502–2514. doi:10.1046/j.1523-1755.1999.00486.x
- Humes, H. D., Weitzel, W. F., Bartlett, R. H., Swaniker, F. C., Paganini, E. P., Luderer, J. R., et al. (2004). Initial clinical results of the bioartificial kidney containing human cells in ICU patients with acute renal failure. *Kidney Int.* 66, 1578–1588. doi:10.1111/j.1523-1755.2004.00923.x
- Hussey, G. S., Dziki, J. L., and Badyrak, S. F. (2018). Extracellular matrix-based materials for regenerative medicine. *Nat. Rev. Mat.* 3, 159–173. doi:10.1038/s41578-018-0023-x
- Jinek, M., Chylinski, K., Fonfara, I., Hauer, M., Doudna, J. A., and Charpentier, E. (2012). A programmable dual-RNA-guided DNA endonuclease in adaptive bacterial immunity. *Science* 337, 816–821. doi:10.1126/science.1225829
- Kanani, D. M., Fissell, W. H., Roy, S., Dubnisheva, A., Fleischman, A., and Zydney, A. L. (2010). Permeability - selectivity analysis for ultrafiltration: Effect of pore geometry. *J. Memb. Sci.* 349, 405. doi:10.1016/j.memsci.2009.12.003
- Kao, R. M., Vasilyev, A., Miyawaki, A., Drummond, I. A., and McMahon, A. P. (2012). Invasion of distal nephron precursors associates with tubular interconnection during nephrogenesis. *J. Am. Soc. Nephrol.* 23, 1682–1690. doi:10.1681/ASN.2012030283
- Kobayashi, A., Mugford, J. W., Krautberger, A. M., Naiman, N., Liao, J., and McMahon, A. P. (2014). Identification of a multipotent self-renewing stromal progenitor population during mammalian kidney organogenesis. *Stem Cell Rep.* 3, 650–662. doi:10.1016/j.stemcr.2014.08.008
- Kobayashi, A., Valerius, M. T., Mugford, J. W., Carroll, T. J., Self, M., Oliver, G., et al. (2008). Six2 defines and regulates a multipotent self-renewing nephron progenitor population throughout mammalian kidney development. *Cell Stem Cell* 3, 169–181. doi:10.1016/j.stem.2008.05.020
- Kobayashi, T., Yamaguchi, T., Hamanaka, S., Kato-Itoh, M., Yamazaki, Y., Ibata, M., et al. (2010). Generation of rat pancreas in mouse by interspecific blastocyst injection of pluripotent stem cells. *Cell* 142, 787–799. doi:10.1016/j.cell.2010.07.039
- Kolber-Simonds, D., Lai, L., Watt, S. R., Denaro, M., Arn, S., Augenstein, M. L., et al. (2004). Production of alpha-1, 3-galactosyltransferase null pigs by means of



- nuclear transfer with fibroblasts bearing loss of heterozygosity mutations. *Proc. Natl. Acad. Sci. U. S. A.* 101, 7335–7340. doi:10.1073/pnas.0307819101
- Kuraoka, S., Tanigawa, S., Taguchi, A., Hotta, A., Nakazato, H., Osafune, K., et al. (2020). PKD1-Dependent renal cystogenesis in human induced pluripotent stem cell-derived ureteric bud/collecting duct organoids. *J. Am. Soc. Nephrol.* 31, 2355–2371. doi:10.1681/ASN.2020030378
- Lawlor, K. T., Vanslambrouck, J. M., Higgins, J. W., Chambon, A., Bishard, K., Arndt, D., et al. (2021). Cellular extrusion bioprinting improves kidney organoid reproducibility and conformation. *Nat. Mat.* 20, 260–271. doi:10.1038/s41563-020-00853-9
- Li, L., Marchant, R. E., Dubnisheva, A., Roy, S., and Fissell, W. H. (2011). Anti-biofouling sulfobetaine polymer thin films on silicon and silicon nanopore membranes. *J. Biomater. Sci. Polym. Ed.* 22, 91–106. doi:10.1163/092050609X12578498982998
- Li, Z., Araoka, T., Wu, J., Liao, H. K., Li, M., Lazo, M., et al. (2016). 3D culture supports long-term expansion of mouse and human nephrogenic progenitors. *Cell Stem Cell* 19, 516–529. doi:10.1016/j.stem.2016.07.016
- Lindström, N. O., Guo, J., Kim, A. D., Tran, T., Guo, Q., De Sena Brandine, G., et al. (2018). Conserved and divergent features of mesenchymal progenitor cell types within the cortical nephrogenic niche of the human and mouse kidney. *J. Am. Soc. Nephrol.* 29, 806–824. doi:10.1681/ASN.2017080890
- Lindström, N. O., McMahon, J. A., Guo, J., Tran, T., Guo, Q., Rutledge, E., et al. (2018). Conserved and divergent features of human and mouse kidney organogenesis. *J. Am. Soc. Nephrol.* 29, 785–805. doi:10.1681/ASN.2017080887
- Lindström, N. O., Tran, T., Guo, J., Rutledge, E., Parvez, R. K., Thornton, M. E., et al. (2018). Conserved and divergent molecular and anatomic features of human and mouse nephron patterning. *J. Am. Soc. Nephrol.* 29, 825–840. doi:10.1681/ASN.2017091036
- Little, M. H., and Combes, A. N. (2019). Kidney organoids: Accurate models or fortunate accidents. *Genes Dev.* 33, 1319–1345. doi:10.1101/gad.329573.119
- Low, J. H., Li, P., Chew, E. G. Y., Zhou, B., Suzuki, K., Zhang, T., et al. (2019). Generation of human PSC-derived kidney organoids with patterned nephron segments and a de novo vascular network. *Cell Stem Cell* 25, 373e379–387. doi:10.1016/j.stem.2019.06.009
- Mae, S. I., Ryosaka, M., Toyoda, T., Matsuse, K., Oshima, Y., Tsujimoto, H., et al. (2018). Generation of branching ureteric bud tissues from human pluripotent stem cells. *Biochem. Biophys. Res. Commun.* 495, 954–961. doi:10.1016/j.bbrc.2017.11.105
- Majumdar, A., Vainio, S., Kispert, A., McMahon, J., and McMahon, A. P. (2003). Wnt11 and Ret/Gdnf pathways cooperate in regulating ureteric branching during metanephric kidney development. *Development* 130, 3175–3185. doi:10.1242/dev.00520
- Mali, P., Yang, L., Esvelt, K. M., Aach, J., Guell, M., DiCarlo, J. E., et al. (2013). RNA-guided human genome engineering via Cas9. *Science* 339, 823–826. doi:10.1126/science.1232033
- Martin, G. R. (1981). Isolation of a pluripotent cell line from early mouse embryos cultured in medium conditioned by teratocarcinoma stem cells. *Proc. Natl. Acad. Sci. U. S. A.* 78, 7634–7638. doi:10.1073/pnas.78.12.7634
- Masaki, H., Kato-Itoh, M., Takahashi, Y., Umino, A., Sato, H., Ito, K., et al. (2016). Inhibition of apoptosis overcomes stage-related compatibility barriers to chimera formation in mouse embryos. *Cell Stem Cell* 19, 587–592. doi:10.1016/j.stem.2016.10.013
- Masaki, H., Kato-Itoh, M., Umino, A., Sato, H., Hamanaka, S., Kobayashi, T., et al. (2015). Interspecific *in vitro* assay for the chimera-forming ability of human pluripotent stem cells. *Development* 142, 3222–3230. doi:10.1242/dev.124016
- Matai, I., Kaur, G., Seyedalehi, A., McClinton, A., and Laurencin, C. T. (2020). Progress in 3D bioprinting technology for tissue/organ regenerative engineering. *Biomaterials* 226, 119536. doi:10.1016/j.biomaterials.2019.119536
- McMahon, A. P. (2016). Development of the mammalian kidney. *Curr. Top. Dev. Biol.* 117, 31–64. doi:10.1016/bs.ctdb.2015.10.010
- Melvin, M. E., Fissell, W. H., Roy, S., and Brown, D. L. (2010). Silicon induces minimal thromboinflammatory response during 28-day intravascular implant testing. *ASAIO J.* 56, 344–348. doi:10.1097/MAT.0b013e3181d98cf8
- Montgomery, R. A., Stern, J. M., Lonze, B. E., Tatapudi, V. S., Mangiola, M., Wu, M., et al. (2022). Results of two cases of pig-to-human kidney xenotransplantation. *N. Engl. J. Med.* 386, 1889–1898. doi:10.1056/NEJMoa2120238
- Moore, M. W., Klein, R. D., Farinas, I., Sauer, H., ArManini, M. P., Phillips, H., et al. (1996). Renal and neuronal abnormalities in mice lacking GDNF. *Nature* 382, 76–79. doi:10.1038/382076a0
- Morizane, R., Lam, A. Q., Freedman, B. S., Kishi, S., Valerius, M. T., and Bonventre, J. V. (2015). Nephron organoids derived from human pluripotent stem cells model kidney development and injury. *Nat. Biotechnol.* 33, 1193–1200. doi:10.1038/nbt.3392
- Murphy, S. V., and Atala, A. (2014). 3D bioprinting of tissues and organs. *Nat. Biotechnol.* 32, 773–785. doi:10.1038/nbt.2958
- Muthusubramaniam, L., Lowe, R., Fissell, W. H., Li, L., Marchant, R. E., Desai, T. A., et al. (2011). Hemocompatibility of silicon-based substrates for biomedical implant applications. *Ann. Biomed. Eng.* 39, 1296–1305. doi:10.1007/s10439-011-0256-y
- Nakayama, K. H., Batchelder, C. A., Lee, C. I., and Tarantal, A. F. (2010). Decellularized rhesus monkey kidney as a three-dimensional scaffold for renal tissue engineering. *Tissue Eng. Part A* 16, 2207–2216. doi:10.1089/ten.tea.2009.0602
- Nishinakamura, R., Matsumoto, Y., NaKao, K., NaKamura, K., Sato, A., Copeland, N. G., et al. (2001). Murine homolog of SALL1 is essential for ureteric bud invasion in kidney development. *Development* 128, 3105–3115. doi:10.1242/dev.128.16.3105
- Niu, D., Wei, H. J., Lin, L., George, H., Wang, T., Lee, I. H., et al. (2017). Inactivation of porcine endogenous retrovirus in pigs using CRISPR-Cas9. *Science* 357, 1303–1307. doi:10.1126/science.aan4187
- Orlando, G., Farney, A. C., Iskandar, S. S., Mirmalek-Sani, S. H., Sullivan, D. C., Moran, E., et al. (2012). Production and implantation of renal extracellular matrix scaffolds from porcine kidneys as a platform for renal bioengineering investigations. *Ann. Surg.* 256, 363–370. doi:10.1097/SLA.0b013e31825a02ab
- Peloso, A., Petrosyan, A., Da Sacco, S., Booth, C., Zamboni, J. P., O'Brien, T., et al. (2015). Renal extracellular matrix scaffolds from discarded kidneys maintain glomerular morphometry and vascular resilience and retains critical growth factors. *Transplantation* 99, 1807–1816. doi:10.1097/TP.0000000000000811
- Phipson, B., Er, P. X., Combes, A. N., Forbes, T. A., Howden, S. E., Zappia, L., et al. (2019). Evaluation of variability in human kidney organoids. *Nat. Methods* 16, 79–87. doi:10.1038/s41592-018-0253-2
- Pichel, J. G., Shen, L., Sheng, H. Z., Granholm, A. C., Drago, J., Grinberg, A., et al. (1996). Defects in enteric innervation and kidney development in mice lacking GDNF. *Nature* 382, 73–76. doi:10.1038/382073a0
- Ponticelli, C., Moia, M., and Montagnino, G. (2009). Renal allograft thrombosis. *Nephrol. Dial. Transpl.* 24, 1388–1393. doi:10.1093/ndt/gfp003
- Poornejad, N., Buckmiller, E., Schaumann, L., Wang, H., Wisco, J., Roeder, B., et al. (2017). Re-epithelialization of whole porcine kidneys with renal epithelial cells. *J. Tissue Eng.* 8, 2041731417718809. doi:10.1177/2041731417718809
- Porrett, P. M., Orandi, B. J., Kumar, V., Hou, J., Anderson, D., Cozette Killian, A., et al. (2022). First clinical-grade porcine kidney xenotransplant using a human decedent model. *Am. J. Transpl.* 22, 1037–1053. doi:10.1111/ajt.16930
- Reemtsma, K., McCracken, B. H., Schlegel, J. U., Pearl, M. A., Pearce, C. W., Dewitt, C. W., et al. (1964). Renal heterotransplantation in man. *Ann. Surg.* 160, 384–410. doi:10.1097/0000658-196409000-00006
- Robinton, D. A., and Daley, G. Q. (2012). The promise of induced pluripotent stem cells in research and therapy. *Nature* 481, 295–305. doi:10.1038/nature10761
- Rutledge, E. A., Benazet, J. D., and McMahon, A. P. (2017). Cellular heterogeneity in the ureteric progenitor niche and distinct profiles of branching morphogenesis in organ development. *Development* 144, 3177–3188. doi:10.1242/dev.149112
- Salani, M., Roy, S., and Fissell, W. H. (2018). Innovations in wearable and implantable artificial kidneys. *Am. J. Kidney Dis.* 72, 745–751. doi:10.1053/j.ajkd.2018.06.005
- Sánchez, M. P., Sillos-Santlago, I., Frisen, J., He, B., Lira, S. A., and Barbacid, M. (1996). Renal agenesis and the absence of enteric neurons in mice lacking GDNF. *Nature* 382, 70–73. doi:10.1038/382070a0
- Self, M., Lagutin, O. V., Bowling, B., Hendrix, J., Cai, Y., Dressler, G. R., et al. (2006). Six2 is required for suppression of nephrogenesis and progenitor renewal in the developing kidney. *EMBO J.* 25, 5214–5228. doi:10.1038/sj.emboj.7601381
- Short, K. M., Combes, A. N., Lefevre, J., Ju, A. L., Georgas, K. M., Lamberton, T., et al. (2014). Global quantification of tissue dynamics in the developing mouse kidney. *Dev. Cell* 29, 188–202. doi:10.1016/j.devcel.2014.02.017
- Song, J. J., Guyette, J. P., Gilpin, S. E., Gonzalez, G., Vacanti, J. P., and Ott, H. C. (2013). Regeneration and experimental orthotopic transplantation of a bioengineered kidney. *Nat. Med.* 19, 646–651. doi:10.1038/nm.3154
- Subramanian, A., Sidhom, E. H., Emani, M., Vernon, K., Sahakian, N., Zhou, Y., et al. (2019). Single cell census of human kidney organoids shows reproducibility and diminished off-target cells after transplantation. *Nat. Commun.* 10, 5462. doi:10.1038/s41467-019-13382-0
- Taguchi, A., Kaku, Y., Ohmori, T., Sharmin, S., Ogawa, M., Sasaki, H., et al. (2014). Redefining the *in vivo* origin of metanephric nephron progenitors enables generation of complex kidney structures from pluripotent stem cells. *Cell Stem Cell* 14, 53–67. doi:10.1016/j.stem.2013.11.010
- Taguchi, A., and Nishinakamura, R. (2017). Higher-order kidney organogenesis from pluripotent stem cells. *Cell Stem Cell* 21, 730e736–746. doi:10.1016/j.stem.2017.10.011

- Takahashi, K., Tanabe, K., Ohnuki, M., Narita, M., Ichisaka, T., Tomoda, K., et al. (2007). Induction of pluripotent stem cells from adult human fibroblasts by defined factors. *Cell* 131, 861–872. doi:10.1016/j.cell.2007.11.019
- Takahashi, K., and Yamanaka, S. (2006). Induction of pluripotent stem cells from mouse embryonic and adult fibroblast cultures by defined factors. *Cell* 126, 663–676. doi:10.1016/j.cell.2006.07.024
- Takasato, M., Er, P. X., Chiu, H. S., Maier, B., Baillie, G. J., Ferguson, C., et al. (2015). Kidney organoids from human iPS cells contain multiple lineages and model human nephrogenesis. *Nature* 526, 564–568. doi:10.1038/nature15695
- Takashima, Y., Guo, G., Loos, R., Nichols, J., Ficiz, G., Krueger, F., et al. (2014). Resetting transcription factor control circuitry toward ground-state pluripotency in human. *Cell* 158, 1254–1269. doi:10.1016/j.cell.2014.08.029
- Tanigawa, S., Taguchi, A., Sharma, N., Perantoni, A. O., and Nishinakamura, R. (2016). Selective *in vitro* propagation of nephron progenitors derived from embryos and pluripotent stem cells. *Cell Rep.* 15, 801–813. doi:10.1016/j.celrep.2016.03.076
- Tanigawa, S., Tanaka, E., Miike, K., Ohmori, T., Inoue, D., Cai, C. L., et al. (2022). Generation of the organotypic kidney structure by integrating pluripotent stem cell-derived renal stroma. *Nat. Commun.* 13, 611. doi:10.1038/s41467-022-28226-7
- Thomson, J. A., Itskovitz-Eldor, J., Shapiro, S. S., Waknitz, M. A., Swiergiel, J. J., Marshall, V. S., et al. (1998). Embryonic stem cell lines derived from human blastocysts. *Science* 282, 1145–1147. doi:10.1126/science.282.5391.1145
- Tran, T., Lindstrom, N. O., Ransick, A., De Sena Brandine, G., Guo, Q., Kim, A. D., et al. (2019). *In vivo* developmental trajectories of human podocyte inform *in vitro* differentiation of pluripotent stem cell-derived podocytes. *Dev. Cell* 50, 102–116. e106. doi:10.1016/j.devcel.2019.06.001
- Treanor, J. J., Goodman, L., de Sauvage, F., Stone, D. M., Poulsen, K. T., Beck, C. D., et al. (1996). Characterization of a multicomponent receptor for GDNF. *Nature* 382, 80–83. doi:10.1038/382080a0
- Tsujimoto, H., Kasahara, T., Sueta, S. I., Araoka, T., Sakamoto, S., Okada, C., et al. (2020). A modular differentiation system maps multiple human kidney lineages from pluripotent stem cells. *Cell Rep.* 31, 107476. doi:10.1016/j.celrep.2020.03.040
- Tumlin, J., Wali, R., Williams, W., Murray, P., Tolwani, A. J., Vinnikova, A. K., et al. (2008). Efficacy and safety of renal tubule cell therapy for acute renal failure. *J. Am. Soc. Nephrol.* 19, 1034–1040. doi:10.1681/ASN.2007080895
- Usui, J., Kobayashi, T., Yamaguchi, T., Knisely, A. S., Nishinakamura, R., and Nakauchi, H. (2012). Generation of kidney from pluripotent stem cells via blastocyst complementation. *Am. J. Pathol.* 180, 2417–2426. doi:10.1016/j.ajpath.2012.03.007
- van den Berg, C. W., Ritsma, L., Avramut, M. C., Wiersma, L. E., van den Berg, B. M., Leuning, D. G., et al. (2018). Renal subcapsular transplantation of PSC-derived kidney organoids induces neo-vasculogenesis and significant glomerular and tubular maturation *in vivo*. *Stem Cell Rep.* 10, 751–765. doi:10.1016/j.stemcr.2018.01.041
- Wang, L., Cooper, D. K. C., Burdorf, L., Wang, Y., and Iwase, H. (2018). Overcoming coagulation dysregulation in pig solid organ transplantation in nonhuman primates: Recent progress. *Transplantation* 102, 1050–1058. doi:10.1097/TP.0000000000002171
- Wang, X., Li, T., Cui, T., Yu, D., Liu, C., Jiang, L., et al. (2018). Human embryonic stem cells contribute to embryonic and extraembryonic lineages in mouse embryos upon inhibition of apoptosis. *Cell Res.* 28, 126–129. doi:10.1038/cr.2017.138
- Westover, A. J., Buffington, D. A., and Humes, H. D. (2012). Enhanced propagation of adult human renal epithelial progenitor cells to improve cell sourcing for tissue-engineered therapeutic devices for renal diseases. *J. Tissue Eng. Regen. Med.* 6, 589–597. doi:10.1002/term.471
- Wolf, K. J., Weiss, J. D., Uzel, S. G. M., Skylar-Scott, M. A., and Lewis, J. A. (2022). Biomanufacturing human tissues via organ building blocks. *Cell Stem Cell* 29, 667–677. doi:10.1016/j.stem.2022.04.012
- Wu, H., Uchimura, K., Donnelly, E. L., Kirita, Y., Morris, S. A., and Humphreys, B. D. (2018). Comparative analysis and refinement of human PSC-derived kidney organoid differentiation with single-cell transcriptomics. *Cell Stem Cell* 23, 869e868–881. doi:10.1016/j.stem.2018.10.010
- Wu, J., Greely, H. T., Jaenisch, R., Nakauchi, H., Rossant, J., and Belmonte, J. C. I. (2016). Stem cells and interspecies chimaeras. *Nature* 540, 51–59. doi:10.1038/nature20573
- Wu, J., Okamura, D., Li, M., Suzuki, K., Luo, C., Ma, L., et al. (2015). An alternative pluripotent state confers interspecies chimaeric competency. *Nature* 521, 316–321. doi:10.1038/nature14413
- Wu, J., Platero-Luengo, A., Sakurai, M., Sugawara, A., Gil, M. A., Yamauchi, T., et al. (2017). Interspecies chimerism with mammalian pluripotent stem cells. *Cell* 168, 473e415–486. doi:10.1016/j.cell.2016.12.036
- Xia, Y., Nivet, E., Sancho-Martinez, I., Gallegos, T., Suzuki, K., Okamura, D., et al. (2013). Directed differentiation of human pluripotent cells to ureteric bud kidney progenitor-like cells. *Nat. Cell Biol.* 15, 1507–1515. doi:10.1038/ncb2872
- Yamada, K., Yazawa, K., Shimizu, A., Iwanaga, T., Hisashi, Y., Nuhn, M., et al. (2005). Marked prolongation of porcine renal xenograft survival in baboons through the use of alpha1, 3-galactosyltransferase gene-knockout donors and the cotransplantation of vascularized thymic tissue. *Nat. Med.* 11, 32–34. doi:10.1038/nm1172
- Yamaguchi, T., Sato, H., Kato-Itoh, M., Goto, T., Hara, H., Sanbo, M., et al. (2017). Interspecies organogenesis generates autologous functional islets. *Nature* 542, 191–196. doi:10.1038/nature21070
- Yang, Y., Liu, B., Xu, J., Wang, J., Wu, J., Shi, C., et al. (2017). Derivation of pluripotent stem cells with *in vivo* embryonic and extraembryonic potency. *Cell* 169, 243e225–257. doi:10.1016/j.cell.2017.02.005
- Yuri, S., Nishikawa, M., Yanagawa, N., and Jo, O. D. (2017). *In vitro* propagation and branching morphogenesis from single ureteric Bud Cells. *Stem Cell Rep.* 8, 401–416. doi:10.1016/j.stemcr.2016.12.011
- Zeng, Z., Huang, B., Parvez, R. K., Li, Y., Chen, J., Vonk, A. C., et al. (2021). Generation of patterned kidney organoids that recapitulate the adult kidney collecting duct system from expandable ureteric bud progenitors. *Nat. Commun.* 12, 3641. doi:10.1038/s41467-021-23911-5



## OPEN ACCESS

## EDITED BY

Mo Li,  
King Abdullah University of Science and  
Technology, Saudi Arabia

## REVIEWED BY

Fabio Rossi,  
University of British Columbia, Canada  
Bianca Nowlan,  
QIMR Berghofer Medical Research  
Institute, The University of Queensland,  
Australia

## \*CORRESPONDENCE

Michael Kyba,  
kyba@umn.edu

## SPECIALTY SECTION

This article was submitted to Stem Cell  
Research,  
a section of the journal  
Frontiers in Cell and Developmental  
Biology

RECEIVED 21 May 2022

ACCEPTED 25 August 2022

PUBLISHED 22 September 2022

## CITATION

Shams AS, Arpke RW, Gearhart MD,  
Weiblen J, Mai B, Oyler D,  
Bosnakovski D, Mahmoud OM,  
Hassan GM and Kyba M (2022), The  
chemokine receptor CXCR4 regulates  
satellite cell activation, early expansion,  
and self-renewal, in response to skeletal  
muscle injury.  
*Front. Cell Dev. Biol.* 10:949532.  
doi: 10.3389/fcell.2022.949532

## COPYRIGHT

© 2022 Shams, Arpke, Gearhart,  
Weiblen, Mai, Oyler, Bosnakovski,  
Mahmoud, Hassan and Kyba. This is an  
open-access article distributed under  
the terms of the [Creative Commons  
Attribution License \(CC BY\)](https://creativecommons.org/licenses/by/4.0/). The use,  
distribution or reproduction in other  
forums is permitted, provided the  
original author(s) and the copyright  
owner(s) are credited and that the  
original publication in this journal is  
cited, in accordance with accepted  
academic practice. No use, distribution  
or reproduction is permitted which does  
not comply with these terms.

# The chemokine receptor CXCR4 regulates satellite cell activation, early expansion, and self-renewal, in response to skeletal muscle injury

Ahmed S. Shams<sup>1,2,3</sup>, Robert W. Arpke<sup>1,2</sup>, Micah D. Gearhart<sup>4</sup>,  
Johannes Weiblen<sup>1,2</sup>, Ben Mai<sup>1,2</sup>, David Oyler<sup>1,2</sup>,  
Darko Bosnakovski<sup>1,2</sup>, Omayma M. Mahmoud<sup>3</sup>,  
Gamal M. Hassan<sup>3</sup> and Michael Kyba<sup>1,2\*</sup>

<sup>1</sup>Lillehei Heart Institute, Minneapolis, MN, United States, <sup>2</sup>Department of Pediatrics, University of Minnesota, Minneapolis, MN, United States, <sup>3</sup>Department of Human Anatomy and Embryology, Faculty of Medicine, Suez Canal University, Ismailia, Egypt, <sup>4</sup>Department of Genetics, Cell Biology and Development, University of Minnesota, Minneapolis, MN, United States

Acute skeletal muscle injury is followed by satellite cell activation, proliferation, and differentiation to replace damaged fibers with newly regenerated muscle fibers, processes that involve satellite cell interactions with various niche signals. Here we show that satellite cell specific deletion of the chemokine receptor CXCR4, followed by suppression of recombination escapers, leads to defects in regeneration and satellite cell pool repopulation in both the transplantation and *in situ* injury contexts. Mechanistically, we show that endothelial cells and FAPs express the gene for the ligand, SDF1 $\alpha$ , and that CXCR4 is principally required for proper activation and for transit through the first cell division, and to a lesser extent the later cell divisions. In the absence of CXCR4, gene expression in quiescent satellite cells is not severely disrupted, but in activated satellite cells a subset of genes normally induced by activation fail to upregulate normally. These data demonstrate that CXCR4 signaling is essential to normal early activation, proliferation, and self-renewal of satellite cells.

## KEYWORDS

satellite cells, skeletal muscle, activation, regeneration, CXCR4

## Introduction

Skeletal muscle is a highly dynamic tissue with a remarkable capacity for rapid regeneration following injury. The essential precursors driving this regenerative process are the satellite cells, classified as a group of mononuclear, self-renewing, and tissue-resident stem cells accounting about 2%–5% of the mononuclear cells of skeletal muscle (Asakura et al., 2002; Bosnakovski et al., 2008; Shadrach and Wagers, 2011; Brack and Rando, 2012). During homeostasis, satellite cells are classically defined by their unique

location between the sarcolemma and basal lamina of multinucleated myofibers and by their expression of the paired homeobox protein PAX7 (Mauro 1961; Seale et al., 2000; Bosnakovski et al., 2008; Yin et al., 2013). The satellite cell pool is heterogenous, and has been described to express numerous surface markers including vascular cell adhesion molecule (VCAM-1), Integrin  $\alpha 7$  (ITGA7), neural cell adhesion molecule (NCAM1), hepatocyte growth factor receptor, also known as c-MET, and m-Cadherin (Cornelison et al., 2001; Fukada et al., 2004; Ieronimakis et al., 2010; Biressi et al., 2013; Liu et al., 2015). Various markers have been used either independently or in combination to isolate the satellite cell population, and among those frequently used is the chemokine receptor CXCR4 (Sherwood et al., 2004; Sacco et al., 2008; Conboy et al., 2010; Chapman et al., 2013; Yoshida et al., 2013; Stitelman et al., 2014; Gromova et al., 2015; Barruet et al., 2020). CXCR4 is present on most cells of the satellite cell pool, including more than 94% of Pax7-ZsGreen positive cells, which express a fluorescent reporter marking PAX7 expression that can be used to isolate fresh satellite cells from muscle digest (Maesner et al., 2016; Arpke et al., 2021). CXCR4 has also been documented on some satellite cell derived cell lines (Ratajczak et al., 2003; Vasyutina et al., 2005). Outside of skeletal muscle, CXCR4 is expressed in numerous types of blood cells, and in the central nervous system (Jazin et al., 1997; Moepps et al., 1997).

The CXCR4 receptor, when activated by its ligand CXCL12, also known as stromal cell-derived factor 1 (SDF-1), plays a crucial role in cell migration during inflammation and organogenesis (Cencioni et al., 2012; Zhao et al., 2014). It can mediate migration of resting leukocytes and hematopoietic progenitors (Janowski 2009; Monzel et al., 2018). Furthermore, CXCR4/SDF1 signaling is important for the migration of primordial germ cells, a function that is conserved in fish, birds, and mammals (Doitsidou et al., 2002; Knaut et al., 2003; Molyneaux et al., 2003; Stebler et al., 2004). CXCR4 or SDF1 mutations have been shown to affect the migration of cerebellar granule cells, hippocampal, and cortical neuronal progenitors (Lazarini et al., 2003). In addition to the regulation of various migration processes, CXCR4/SDF1 also controls growth and survival of various cell types (Molyneaux et al., 2003; Bianchi and Mezzapelle 2020).

During embryogenesis, the SDF1/CXCR4 axis has a major role in skeletal muscle development, particularly with regard to migration of myogenic progenitors. Population of the limb buds (Odemis et al., 2005; Yusuf et al., 2006), tongue, and facial muscles (Yahya et al., 2020) with myogenic progenitors have all been demonstrated to be dependent on CXCR4. SDF-1 is expressed in the mesenchyme of the limb and the first branchial arch, which represent targets of the migrating cells and the application of SDF-1 implants into the limb of chick embryos redirects the muscle progenitor cells toward the ectopic source of the factor and inhibits their differentiation (Vasyutina et al.,

2005). In addition, *Cxcr4* mutants mice show a significant increase in the number of apoptotic muscle progenitors, suggesting that *Cxcr4* signals provide not only attractive cues but also control survival (Chong et al., 2007; Bryson-Richardson and Currie 2008).

In adult skeletal muscle tissue the role of CXCR4 signaling in skeletal muscle physiology is less well defined. It has been shown that fibroblasts secrete SDF-1 influencing hematopoietic cells in muscle (Ratajczak et al., 2003), leading to the activation of signaling pathways which stimulate satellite cell migration to sites of inflammation or required regeneration (Ratajczak et al., 2003; Relaix et al., 2021). A recent study has suggested a role for CXCR4 in protecting the satellite cells against the inflammatory induced damage during muscle regeneration (Lahmann et al., 2021). While these studies suggest potential mechanisms by which CXCR4 signaling has an impact on muscle regeneration, well-defined mechanisms whereby CXCR4 regulates satellite cell function are yet to be determined. We therefore designed this study to address the *in vivo* necessity of CXCR4 in satellite cells. By investigating satellite cell maintenance, self-renewal, engraftment after transplantation, and muscle regeneration in the context of satellite cell-specific temporally-regulated genetic ablation of the CXCR4 receptor, we demonstrate a specific role for *Cxcr4* in the activation and early stages of proliferation of satellite cells.

## Materials and methods

### Mice

All animal experiments in this study were performed in accordance with protocols approved by the Institutional Animal Care and Use Committee at the University of Minnesota. We combined the *Cxcr4*<sup>fl</sup> (008,767 B6.129P2-*Cxcr4*<sup>tm2Yzo/J</sup> Jackson Laboratories), and *Pax7*-ZsGreen (Bosnakovski et al., 2008) alleles with either the *Pax7*-creERT2 (Keefe et al., 2015) (kindly provided by Gabrielle Kardon) or the *Ubc*-creERT2 (007,001 B6. Cg-<sup>Ndori1Tg(UBC-cre/ERT2)1Ejlb</sup>/1J Jackson Laboratories) alleles to generate both *Cxcr4*<sup>FL/FL</sup>; *Pax7*-creERT2; *Pax7*-ZsGreen mice and *Cxcr4*<sup>FL/FL</sup>; *Ubc*-creERT2; *Pax7*-ZsGreen mice. All experiments were conducted using adult mice 3–4 months of age. Transplant recipients were *NSG-mdx*<sup>4Cv</sup> mice (Arpke et al., 2013).

For *Cxcr4* conditional knockouts, all mice were treated for five consecutive days with 80 mg/kg IP tamoxifen (Sigma Aldrich) dissolved at a concentration of 85 mg per 1 ml 100% ethanol then mixed with sunflower oil (Sigma Aldrich) to reach a final concentration of 12.75 mg in 1 ml vehicle, after which mice were then maintained on tamoxifen diet (TD.140251 Envigo) for the remaining duration of each experiment. For the transplantation experiments, donor mice were not treated



with tamoxifen, however recipient mice were treated starting on the day of transplantation.

## Satellite cell harvest

Isolation of bulk satellite cells from hind limbs was performed as described previously (Arpke et al., 2013; Arpke and Kyba 2016). Briefly, hind limb muscles were carefully dissected and cut longitudinally with a razor blade parallel to the muscle fibers, using forceps each time pressing the blade to separate the fibers. The minced muscle was incubated shaking for 75 min in 0.2% collagenase type II (Gibco, Grand Island, NY) in high glucose Dulbecco's modified Eagle's medium (DMEM) containing 4 mM L-glutamine 4,500 mg/L glucose, and sodium pyruvate (HyClone, Logan, UT) supplemented with 1% Pen/Strep (Gibco) at 37°C. Samples were washed twice with Rinsing Solution (F-10+), Ham's/F-10 medium (HyClone) supplemented with 10% Horse Serum (HyClone), 1% 1 M HEPES buffer solution (Gibco), and 1% Pen/Strep. Samples were centrifuged at 500 G for 5 min. After aspiration of supernatant, the sample was resuspended in F-10 containing collagenase type II and dispase (Gibco), vortexed, and incubated shaking at 37°C for 30 min. Samples were vortexed again, drawn and released into a 10 ml syringe with a 16-gauge needle four times, then with a 18-gauge needle four times to release the cells from the muscle fibers prior to passing the cell suspension through a 40-µm cell strainer (Falcon, Hanover Park, IL, United States). The sample was drawn and released into a 10 ml syringe with the 18-gauge needle four additional times and passed through a new 40-µm cell strainer. Samples were centrifuged for 5 min 500 G at 4°C, and resuspended in Fluorescent-activated Cell Sorting (FACS) staining medium: Phosphate Buffered Saline (PBS, Corning, Manassas, VA, United States) containing 2% fetal bovine serum (HyClone) and 0.5 µg/ml propidium iodide, for FACS analysis and sorting on a FACS Aria II (BD Biosciences, San Diego, CA, United States).

Quantification of satellite cells from single injured or control TA muscles was performed similarly. Digested muscle samples were drawn and expelled into a 3 ml syringe four times with 18-gauge needle. The cell suspension was passed through a 40-µm cell strainer. 3 ml of F-10+ was added to each sample to prevent over-digestion; and samples were centrifuged, then resuspended in FACS staining medium. For transplanted TAs, the samples were stained using an antibody mixture of PE-Cy7 rat anti-mouse CD31, PE-Cy7 rat anti-mouse CD45, Biotin rat anti-mouse CD106 (VCAM) and PE Streptavidin from BD Biosciences; and ITGA7 647. Suppliers and clonal identifiers are provided in [Supplementary Table S1](#). The number of donor (ZsGreen<sup>+</sup>) satellite cells and total satellite cells (lineage negative; VCAM, ITGA7 double positive cells) was determined by running the entire volume through the FACS and recording all events. The TA samples were resuspended in 200 µl FACS staining

medium (PBS with 2% FBS and propidium iodide) then the total volume was run out on a BD FACS Aria II, with red (641 nm), blue (488 nm) and yellow-green (561 nm) lasers. Propidium iodide-negative (live) cells were gated into either PE (empty) vs. ZsGreen for unstained samples, or for stained samples: APC (ITGA7) vs. PE-Cy7 (Lin), gating Lin-neg cells into APC (ITGA7) vs. PE (VCAM), gating double-positive cells into SSC vs. ZsGreen and counting ZsGreen<sup>+</sup> cells. In order to detect the number of CXCR4<sup>+</sup> cells within the ZsGreen<sup>+</sup> population, the muscle digest was stained with Biotin rat anti-mouse CD184 (CXCR4) monoclonal antibody followed by Streptavidin-PE. In order to isolate the different niche cells we digested uninjured and 48 h post-CTX injury quadriceps muscles as previously described and stained the mononuclear cells with the following antibodies: FITC rat anti-mouse CD31, PE-Cy7 rat anti-mouse CD45, ITGA7 647 and PE rat anti-mouse CD140A (PDGFRα) (Bosnakovski et al., 2020).

## Colony forming cell assay

Satellite cells were identified by FACS and single cell-sorted into 96-well plates in mouse myogenic medium (MMM): DMEM/F12 medium without L-glutamine (Cell Gro, Manassas, VA; 15-090-CV) containing 20% FBS (HyClone), 10% horse serum (Gibco, 26050-088), 50 ng/µl human basic fibroblast growth factor (Peprotech, Rocky Hill, NJ; 100-18), 1% penicillin/streptomycin (Gibco, 15140-122), 1% Glutamax (Gibco, 35050-061), and 0.5% chick embryonic extract (US Biological, Swampscott, MA; C3999). Plates were maintained at 37°C at 5% CO<sub>2</sub>, 5% O<sub>2</sub>, 90% N<sub>2</sub> for 8 days. Colonies were identified and fixed with 4% paraformaldehyde for 20 min at room temperature, stained with MF20 myosin heavy chain antibody (Developmental Studies Hybridoma Bank, University of Iowa) and counterstained with DAPI and imaged on a Zeiss AxioObserver Z1 inverted microscope with an AxioCamMR3 camera (Thornwood, NY, United States) (Ippolito et al., 2012).

## TA injury and transplantation

Adult (3–4 months old) *Cxcr4*<sup>FL/FL</sup>; *Pax7*-ZsGreen mice carrying *Pax7*-creERT2 or not were anesthetized with ketamine and xylazine, both hind limbs shaved and sterilized using surgical betadine solution, the skin over the TA was opened with a scissor and both TA muscles were exposed. 25 µl cardiotoxin (10 µM in PBS, Sigma, Saint Louis, MO, United States) was injected with a Hamilton syringe and the skin was closed using nonabsorbable suture. For transplantation experiments, 48 h prior to transplantation of cells, 4 month-old NSG-mdx<sup>4Cv</sup> mice were anesthetized with ketamine and xylazine and both hind limbs were subjected to 1,200 cGy irradiation

using an RS 2000 Biological Research Irradiator (Rad Source Technologies, Inc., Suwanee, GA) with lead shields protecting the body and forelimbs. 24 h prior to transplant, cardiotoxin injury was performed as above. 24 h after this, 300 ZsGreen satellite cells were collected by FACS from donor mice and transplanted in a volume of 10  $\mu$ l PBS into each TA. 4 weeks after transplantation, one transplanted TA of each mouse was harvested and prepared for sectioning and staining as described previously (Arpke et al., 2013), while the other transplanted TA was prepared for FACS analysis as described above.

## Histology and immunohistochemistry for dystrophin and/or laminin

TA muscles were removed and placed in OCT Compound (Scigen Scientific, Gardena, CA, United States), frozen in liquid nitrogen-cooled 2-methylbutane (Sigma) and stored at  $-80^{\circ}\text{C}$ . 10  $\mu$ m cryosections were cut on a Leica CM3050 S cryostat (Leica Microsystems, Buffalo Grove, IL, United States). Cryosections were air dried then stained with H&E, Sirius Red/Fast Green (SR/FG) or processed for immunohistochemistry. Briefly, slides were fixed with 4% paraformaldehyde, washed 3 times with PBS, permeabilized with 0.3% Triton X-100 (sigma) and blocked for 1 h with 3% BSA in permeabilization solution. Slides were incubated overnight at  $4^{\circ}\text{C}$  with a rabbit polyclonal antibody to dystrophin and/or a mouse monoclonal antibody to laminin (antibody details in [Supplementary Table S1](#)), then sections were incubated for 90 min at RT with Alexa Fluor 555 goat anti-rabbit and/or Alexa Fluor 488 goat anti-mouse IgG antibodies (Life Technologies, Grand Island, NY, United States). Coverslips were mounted with Immu-Mount (Thermo Scientific, Kalamazoo, MI, United States). Slides were imaged with a Zeiss Axio Imager. M2 with an AxioCam MRm camera (Carl Zeiss Microscopy, LLC, Thornwood, NY, United States). Images from slides stained with laminin only were used to measure the fiber CSA, while in case of laminin and dystrophin co-staining the number of donor muscle fibers was determined by manually counting dystrophin+ fibers.

The percent fibrosis in the TA was quantified on SR/FG-stained TA sections using ImageJ software. The image was first converted to grayscale based on green, then the threshold was adjusted. The area-stained red was measured and normalized to cross-sectional area (CSA) (Bosnakovski et al., 2022).

## RNA extraction, cDNA synthesis, RTqPCR and transcriptional profiling

Satellite cells were sorted directly into the RNA lysis buffer and the RNA was extracted using the protocol provided with the RNeasy Mini Kit (Qiagen). cDNA was synthesized using High-Capacity cDNA Reverse Transcription Kit (Applied Biosystems). Efficiency of *Cxcr4* *in vivo* deletion was determined with

Mm01292123\_m1 *Cxcr4* TaqMan probe (ThermoFisher). To harvest the RNA from cultured myoblasts, medium was removed and RNA lysis buffer was applied directly over the adherent cell layer then. Lysate was processed as described by the manufacturer.

For RNA-seq, total RNA from freshly sorted and overnight cultured *Pax7*-ZsGreen<sup>+</sup> cells from both hind limbs of *Cxcr4* WT and *Cxcr4* KO mice was isolated as above. Total RNA samples were submitted to Genewiz (NJ, United States) for quality control analysis, library generation and sequencing using the Illumina HiSeq 2  $\times$  150 paired-end configuration. The raw sequencing data (FASTQ files) with approximately 20 million reads per sample were adapter trimmed (TrimGalore 0.6.0) and mapped to the GRCm38. p6/mm10 genome with STAR (2.7.2a). The number of reads mapping to GENCODE M25 gene annotations were quantified with Rsubread (2.2.6). Differential gene expression was determined using DESeq2 (1.34.0). Genes were ranked by the Wald test-statistic for gene set enrichment analysis (GSEA 4.1.0) using the top 500 up- and down-regulated genes upon satellite cell activation as previously defined in (Machado et al., 2017). Figures were prepared with ggplot2 (3.3.5). Sequence data is deposited in GEO (GSE205015).

## Measuring time to first division

*Pax7*-ZsGreen cells were isolated from *Cxcr4*<sup>FL/FL</sup>, *Ubc*-creERT2 wild type or mutant mice by FACS and plated for live-cell imaging into 0.1% gelatin-coated 24-well glass-bottom dishes (NC9988706; Mattek; Thermo Fisher Scientific; Waltham, MA, United States) (7,000 cells/well) containing myoblast growth medium, MGM: Ham's F10 medium with L-glutamine (HyClone) containing 20% FBS (HyClone) and 1% Glutamax (Gibco, 35050-061) 1% Pen/Strep (Gibco) and 10 ng/ml hb-FGF (PeproTech, Cranbury, NJ, United States). Cells from the two sources were treated with MGM containing 5 mM 4-hydroxy tamoxifen (4OHT) at the time of plating and provided fresh medium 18 h after plating. Time-lapse imaging was performed from 18 to 52 h after plating with a Nikon Eclipse Ti-inverted fluorescence microscope equipped with an automated stage (Prior) and a custom chamber to maintain a constant  $37^{\circ}\text{C}$  temperature, high humidity, and 5%  $\text{CO}_2$ . Multiple positions were analyzed per group with images acquired every 10 min using phase contrast. Images were collected using a 20X CFI Plan Apochromat Lambda (NA = 0.75) objective (Nikon). For each condition, at least 100 individual cells were tracked. Following imaging, data were exported as individual TIFFs for each position and time point. ImageJ was used to concatenate TIFF images from each location and time to first division was determined for each as previously described (Larson et al., 2022).

## In vitro EdU proliferation assay

*Pax7*-ZsGreen cells were isolated by FACS and plated into 0.1% gelatin-coated 96-well plates (1,000 cells/well) containing MGM. 4OHT (HelloBio) dissolved in DMSO was applied daily (5 mM final concentration). At day 7, we added EdU 10  $\mu$ M (Invitrogen) for 6 h, fixed cells with 4% PFA. Cells were stained with Click-iT EdU Cell Proliferation Kit for Imaging, Alexa FluorTM 555 dye (C10338; Invitrogen) according to manufacturer's instructions. The cells were then incubated in 4,6-diamidino-2-phenylindole (DAPI 1:1,000 dilution in PBS) for 20 min at room temperature. EdU+ nuclei were identified and imaged at 10X magnification on a Zeiss Observer. Z1 inverted microscope equipped with an AxioCam Mrm camera (Thornwood, NY, United States).

## ATP cell proliferation luciferase assay

*Pax7*-ZsGreen cells were isolated by FACS and plated into 0.1% gelatin-coated 96-well plates (1,000 cells/well) containing MGM with or without 5 mM 4OHT. At day 7 post-plating, medium was replaced with CellTiter-Glo (G7570; Promega, Madison, WI) reagent (1:3) in 100  $\mu$ l of PBS. Plates were allowed to equilibrate for 3 min, then read on a Cytation3 plate reader (BioTek, Winooski, VT, United States).

## Statistical analysis

All data were analyzed with two-tailed unpaired Student *t*-tests for determining significant differences between two groups or one-way ANOVA with Tukey's post hoc for determining significant differences between three or more groups; data was tested for normality using (Kolmogorov–Smirnov test). Significance was considered at *p* values of <0.05. Data are presented as mean  $\pm$  SEM unless otherwise indicated. All statistical testing was performed using GraphPad Prism 8.0 (GraphPad Software Inc., San Diego, CA, United States). Sample sizes are reported as the number of independent mice from which the cells were analyzed or isolated. All histology images were processed and analyzed in a blinded manner with samples being de-identified as to study or control.

## Results

### CXCR4 is necessary for repopulation of the satellite cell pool upon transplantation

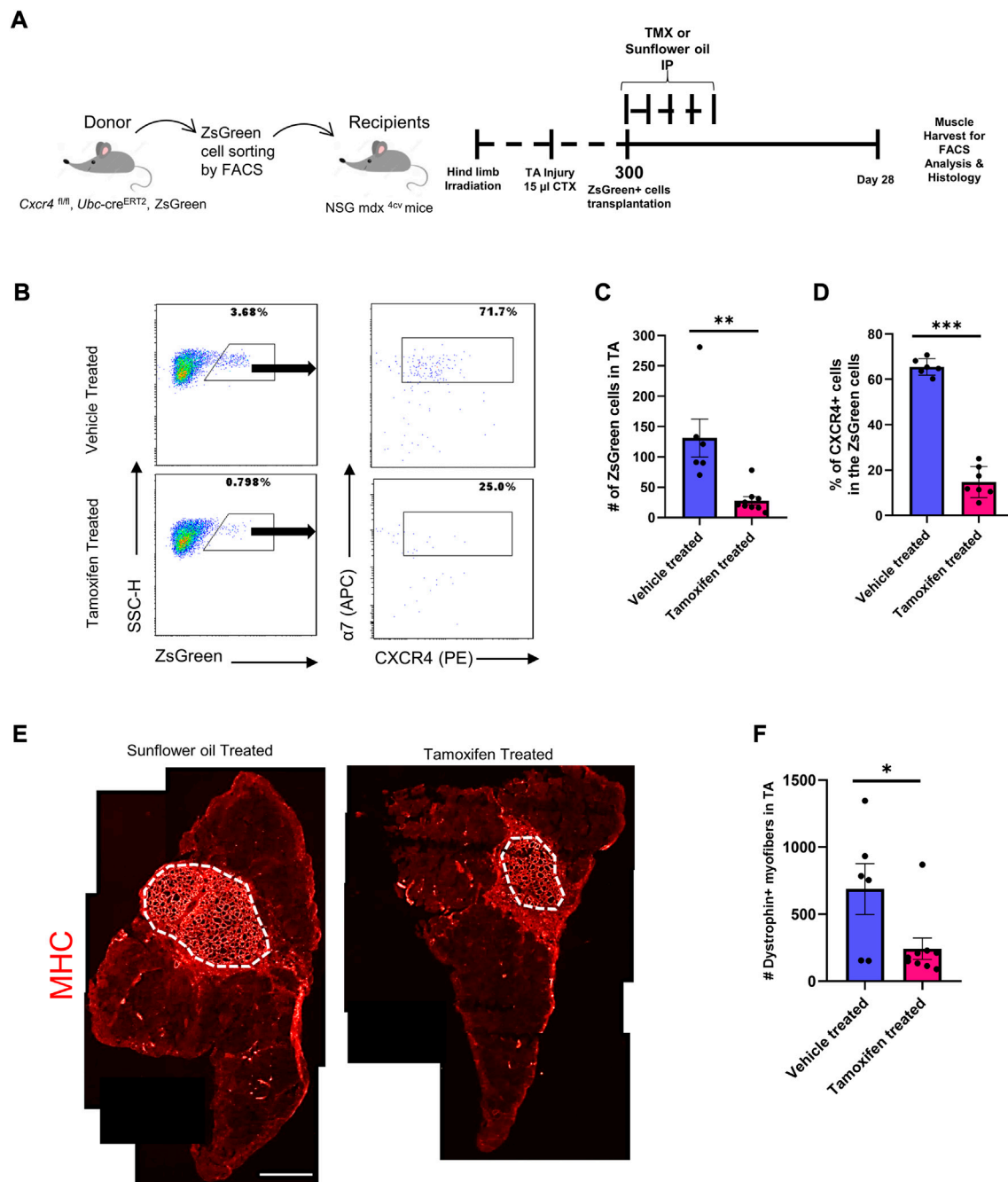
We previously developed a transplantation-based assay to monitor self-renewal and differentiation potential of satellite cells in which 300 *Pax7*-ZsGreen (Bosnakovski et al., 2008) cells are

transplanted bilaterally into injured, irradiated tibialis anterior muscles of NSG-mdx<sup>4Cv</sup> mice (Arpke et al., 2021). One month after transplant, one TA muscle is digested and run completely through a flow cytometer to quantify contribution to the satellite cell pool while the other TA muscle is used for dystrophin immunostaining to quantify contribution to the differentiated fiber population. We adapted this assay to test the role of CXCR4 in these processes by using donor *Pax7*-ZsGreen mice that also carried homozygous floxed *Cxcr4* alleles and the strong ubiquitously expressed *Ubc-creERT2*. Although *Ubc-creERT2* is expressed in every cell lineage enabling conditional knockout of *Cxcr4* in all cell types (Supplementary Figure S1B), because only satellite cells are transplanted, treatment of the recipient mice with tamoxifen deletes *Cxcr4* only in the donor cells. Half of the recipients received tamoxifen to delete *Cxcr4* while half received vehicle, starting on the day of transplant (Figure 1A). FACS analysis demonstrated that the *Cxcr4* knockout resulted in a tremendous inhibition of satellite cell self-renewal evident by a 3-fold drop in the number of *Pax7*-ZsGreen cells in the recipient TA muscles of the TMX-treated group (Figures 1B,C, Supplementary Figure S1A). To assess the *Cxcr4* deletion efficiency, we stained the TA muscle digest for cell surface receptors ITGA7 and CXCR4 and determined the frequency of CXCR4<sup>+</sup> cells among the ITGA7<sup>+</sup> ZsGreen<sup>+</sup> cells, which revealed a dramatic reduction of CXCR4<sup>+</sup> cells in the TMX-treated group, in those rare cells that populated the satellite cell compartment 1 month post-transplant (Figures 1B,D).

We then evaluated the differentiation efficiency of the *Cxcr4*-deleted satellite cells by counting dystrophin+ (donor-derived) fibers. This revealed a significant drop in the number of dystrophin+ fibers in the TA sections of the TMX-treated group compared to the vehicle treated (Figures 1E,F), indicating that absence of *Cxcr4* impaired both the repopulation of the satellite pool as well as the regeneration of new fibers.

We repeated these transplants using a design in which all mice were TMX-treated, but were transplanted with donor cells from mice either carrying or lacking *creERT2*. For these studies, we used the *Pax7-creERT2* allele (Keefe et al., 2015) which is satellite cell-specific but expresses at somewhat lower efficiency than *Ubc-creERT2*. To suppress revertants, after the course of TMX injections, recipients were kept on TMX chow. These conditions replicated results with *Ubc-creERT2* (Supplementary Figures S1C–E).

To evaluate the efficiency of *in vivo* deletion under steady state conditions prior to injury, we isolated hind limb satellite cells immediately after the course of five consecutive doses of TMX IP, and evaluated *Cxcr4* expression on *Pax7*-ZsGreen cells by FACS and RTqPCR spanning the deleted exon 2. While *Cxcr4* mRNA was reduced by 90%, protein expression levels on satellite cells were reduced more modestly (Supplementary Figures S2B–D), likely reflecting the fact that protein turnover is low in quiescent cells and suggesting that steady state changes might take longer timeframes to identify.

**FIGURE 1**

*Cxcr4* Knockout impairs engraftment and repopulation of the satellite cell pool upon transplantation. **(A)** Schematic for the transplantation assay. **(B)** Representative FACS plots from both the TMX- and vehicle-treated groups showing the number of the ZsGreen<sup>+</sup> cells in the TA muscle after transplantation and the percent of CXCR4<sup>+</sup> cells among the ZsGreen<sup>+</sup> ITGA7<sup>+</sup> cell fraction. **(C)** Total number of ZsGreen<sup>+</sup> cells in TA muscles of recipient NSG-mdx4cv mice. Vehicle treated ( $n = 6$ ). Tamoxifen treated ( $n = 9$ ). **(D)** Percentage of the CXCR4<sup>+</sup> population in the ZsGreen<sup>+</sup> cells in recipient TA muscles. **(E)** Representative immunofluorescence images for TA muscles stained by Dystrophin (Red). Scale bar = 100  $\mu$ m. **(F)** Total number of Dystrophin<sup>+</sup> fibers in the TA muscles of vehicle and tamoxifen treated recipient mice. Vehicle treated ( $n = 6$ ). Tamoxifen-treated ( $n = 9$ ). Data are presented as mean  $\pm$  SEM, \* $p < 0.05$ , \*\* $p < 0.01$  and \*\*\* $p < 0.001$  by  $t$ -test.



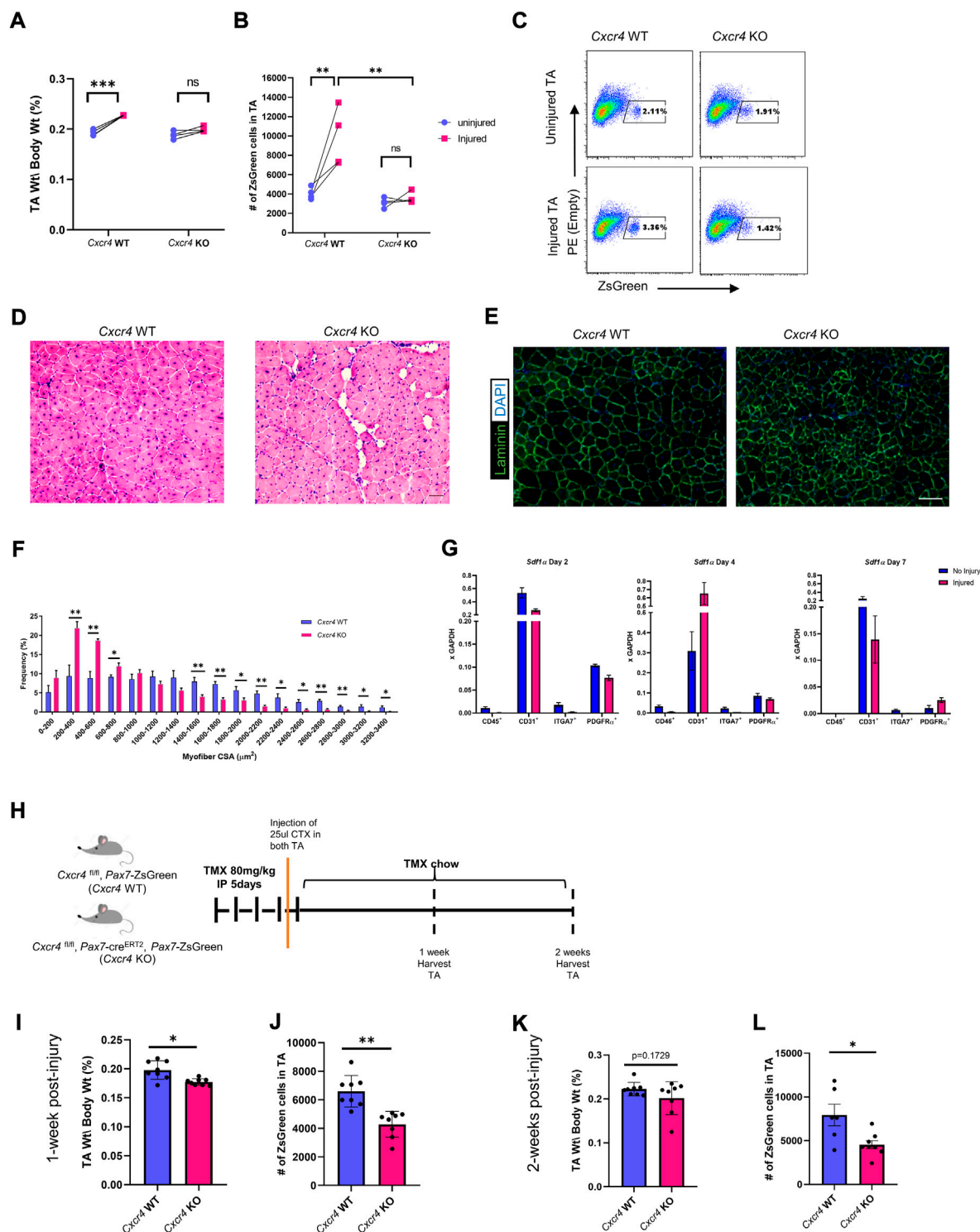


FIGURE 2

CXCR4 is necessary for proper skeletal muscle regeneration and expansion of the satellite cell pool after injury. **(A)** TA mass normalized to body weight in uninjured and injured, *Cxcr4* WT and KO, mice. **(B)** Total number of ZsGreen<sup>+</sup> cells in the TA muscle of uninjured and injured, *Cxcr4* WT ( $n = 4$ ) and KO ( $n = 4$ ), mice. **(C)** Representative FACS plots showing the total number of ZsGreen<sup>+</sup> cells in uninjured and injured, *Cxcr4* WT ( $n = 4$ ) and KO ( $n = 4$ ), mice. **(D)** Representative H&E staining of TA sections from *Cxcr4* WT and KO mice 4 weeks after the second injury. Scale bar = 50  $\mu$ m. **(E)** Representative IF staining for laminin (green) and DAPI (blue) in TA sections from *Cxcr4* WT and KO mice 4 weeks after the second injury. Scale bar = 100  $\mu$ m. **(F)** Myofiber cross sectional area distribution in TA muscles of *Cxcr4* WT ( $n = 5$ ) and KO ( $n = 5$ ), 4 weeks after the second injury. **(G)** RTqPCR (Continued)

**FIGURE 2 (Continued)**

for *Sdf1a* in hematopoietic (CD45<sup>+</sup>), endothelial (CD31<sup>+</sup>), myogenic (ITGA7<sup>+</sup>), and FAP cells (PDGFRα<sup>+</sup>) in uninjured and 2, 4, 7 days post-injury muscles ( $n = 4$ ) mice. (H) Schematic for the short-term (1 and 2 weeks) post-injury studies. (I) TA mass normalized to body weight in *Cxcr4* WT and KO mice 1 week post CTX injury. (J) Total number of ZsGreen<sup>+</sup> cells in the TA muscle of *Cxcr4* WT ( $n = 4$ ) and KO ( $n = 4$ ), mice 1 week post CTX injury. (K) TA mass normalized to body weight in *Cxcr4* WT and KO mice 2 weeks post CTX injury. (L) Total number of ZsGreen<sup>+</sup> cells in the TA muscle of *Cxcr4* WT ( $n = 4$ ) and KO ( $n = 4$ ), mice 2 weeks post CTX injury. Data are presented as mean  $\pm$  SEM, \* $p < 0.05$ , \*\* $p < 0.01$  and \*\*\* $p < 0.001$  by *t*-test and two-way ANOVA.

## CXCR4 enables expansion of the satellite cell pool after injury

Because post-transplant both self-renewal and differentiation were suppressed in the absence of CXCR4, we evaluated the early expansion of satellite cell-derived progenitors. We treated 3 month old female *Cxcr4*<sup>FL/FL</sup>; *Pax7*-creERT2; *Pax7*-ZsGreen mice with five daily doses of TMX IP and on day 4 performed unilateral CTX injury of the left TA muscle. CTX injury causes hypertrophy in WT mice and accordingly, 1 month later, TA muscles of *Cxcr4* WT mice had significantly increased in mass, while *Cxcr4* KO muscles were not significantly increased and were significantly smaller ( $p < 0.001$ ) than the injured WT (Figure 2A). We quantified the number of *Pax7*-ZsGreen cells by FACS in a subset of injured animals and found a significant failure of the satellite cells from *Cxcr4* KO to expand in response to injury, unlike the control which responded robustly to the injury by doubling the number of ZsGreen cells in the injured limb compared to the uninjured (Figures 2B,C).

## Histological abnormalities after double injury in *Cxcr4*-mutant muscle

Because previous work failed to detect histological damage after a single injury in the *Cxcr4* *Pax7*-cre-driven mutant (Lahmann et al., 2021), we treated mice with TMX IP for 5 days, placed on TMX chow to minimize escapers, and subjected TA muscles to two bouts of CTX injury, 3 weeks apart (Supplementary Figure S2E). 28 days after the second injury *Cxcr4*-KO<sup>PAX7</sup> muscle showed vacuolar degeneration together with smaller myofibers (Figures 2D–F). These data suggest that *Cxcr4* is necessary in satellite cells for optimal regenerative response, particularly to severe injury.

## Endothelial cells and fibroadipogenic progenitor are the primary sources of *Sdf1a* in skeletal muscle.

Activation is associated with early cytological changes in the inflammatory and fibroadipogenic progenitor (FAP) compartments of skeletal muscle (Joe et al., 2010). To determine what cell types are producing SDF1a, the ligand for

CXCR4, we sorted mononuclear cells from steady state and injured skeletal muscle into hematopoietic (CD45<sup>+</sup>), endothelial (CD31<sup>+</sup>), myogenic (ITGA7<sup>+</sup>) and FAP (PDGFRα<sup>+</sup>) components and investigated *Sdf1a* expression by RTqPCR (Supplementary Figure S3D). Almost all of the *Sdf1a* message was present in two cell types: endothelial cells and FAPs, and among these, more abundant in endothelial cells (Figure 2G). Interestingly, while in endothelial cells, *Sdf1a* expression fluctuated after injury (down at day 2, significantly elevated at day 4), it was fairly constant at these times in post-injury in FAPs.

## Satellite cell numbers decline early after injury.

We next investigated at what stage the difference in satellite cell numbers after injury could be detected. Using the same unilateral injury regimen, we analyzed muscles 1 and 2 weeks post-injury by FACS and histology (Figure 2H). Already 1 week post-injury, there was a significant reduction in the TA mass normalized to the body weight among the *Cxcr4* KO group together with a decline in the number of ZsGreen<sup>+</sup> cells in the TA. At 2 weeks post injury, although muscle mass caught up somewhat, the satellite cells failed to expand and were still significantly different between WT and KO (Figures 2I–L and Supplementary Figure S2G). Histology demonstrated poor regeneration, evident by widening of the interstitial space, vacuolar degeneration, myofiber necrosis and accumulation of interstitial cells (Supplementary Figure S2F) in the KO at both 1 and 2 weeks post-injury. Furthermore, Sirius Red Fast Green staining of the TA sections revealed a widening of the endomysium, with greater numbers of smaller fibers and a trend toward greater collagen/ECM deposition in the *Cxcr4* KO group (Supplementary Figures S2H,I).

## CXCR4 regulates satellite cell maintenance

The defective satellite cell expansion after injury in the absence of the CXCR4 led us to investigate whether CXCR4 plays any role in steady state muscle. We treated *Cxcr4*<sup>FL/FL</sup>; *Pax7*-creERT2; *Pax7*-ZsGreen mice with five doses of TMX IP then maintained them on TMX chow for 6 weeks

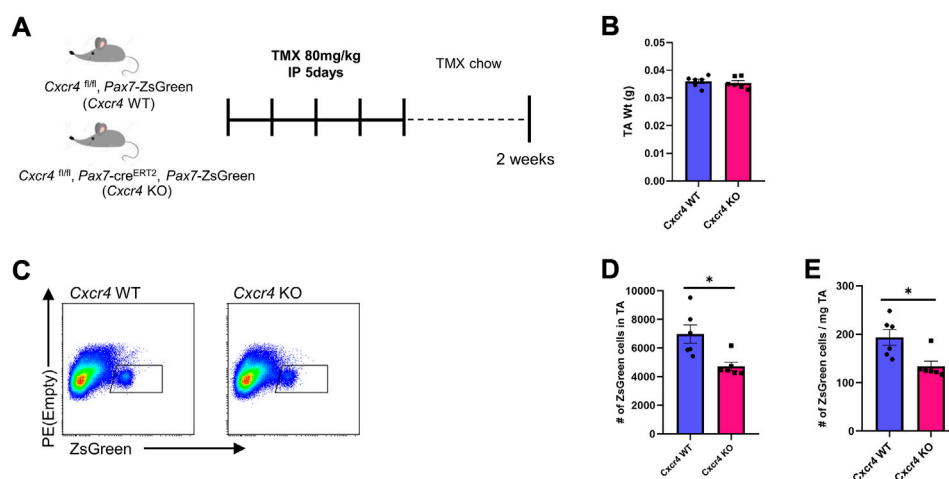


FIGURE 3

CXCR4 is necessary for satellite cell maintenance. (A) Schematic for Tamoxifen treatment and time of analysis. (B) TA mass normalized to body weight in *Cxcr4* WT and KO mice. (C) Representative FACS plots from *Cxcr4* WT and KO groups showing total number of ZsGreen<sup>+</sup> cells in the TA muscle. (D) Total number of ZsGreen<sup>+</sup> cells in the TA from CXCR4 WT ( $n = 3$ ) and KO ( $n = 3$ ) mice. (E) Total number of ZsGreen<sup>+</sup> cells per mg TA mass from *Cxcr4* WT and KO mice. Data are presented as mean  $\pm$  SEM, \* $p < 0.05$  by  $t$ -test.

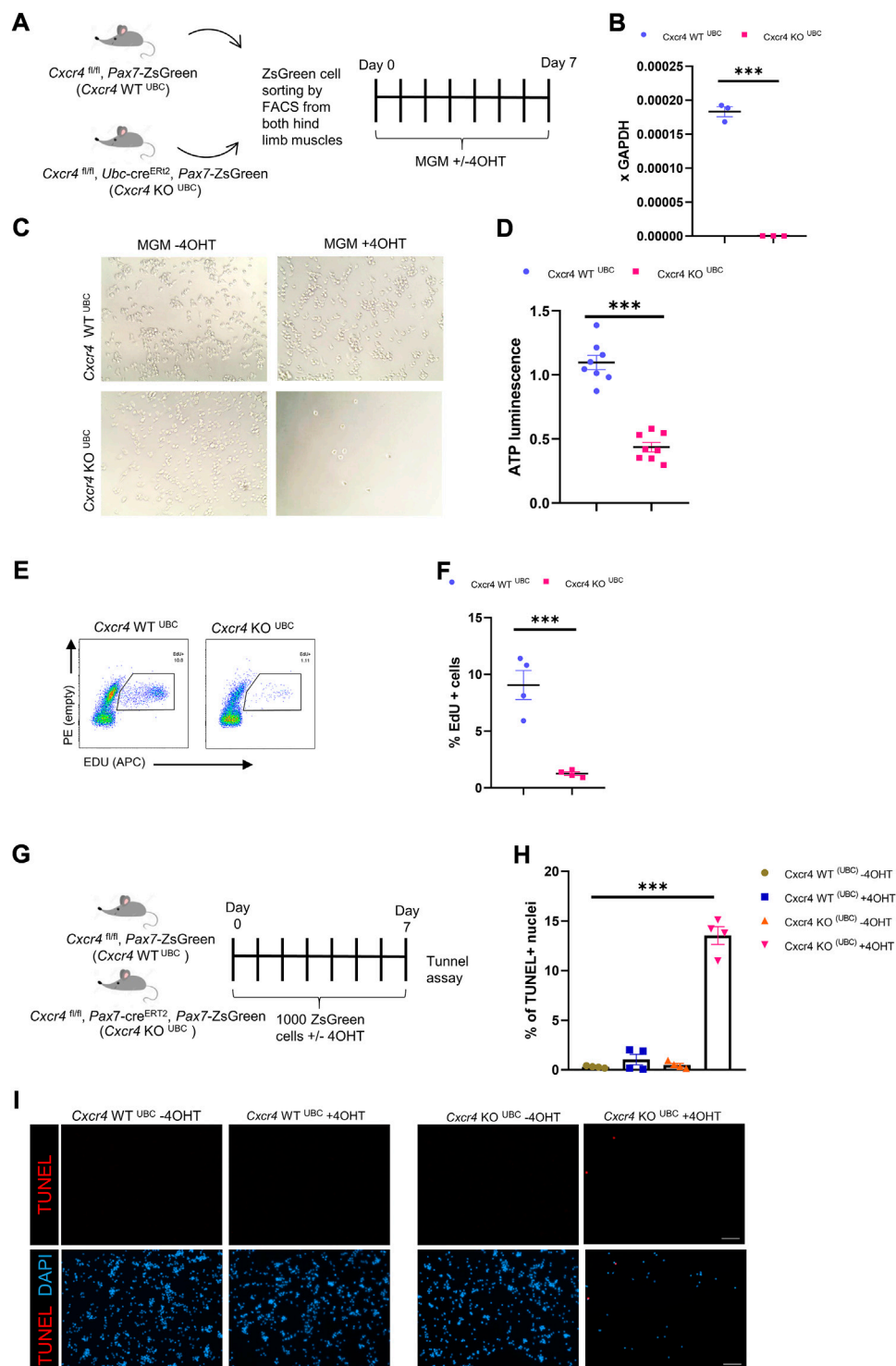
(Supplementary Figure S3A) and evaluated skeletal muscles from the hindlimbs, forelimbs and diaphragm. Muscle mass and histology was not significantly altered (Supplementary Figure S3B,C), with only modest and non-significant declines in the normalized diaphragm mass, and to an even lesser extent, the TA. In contrast to whole muscle, the satellite cell population showed a degree of dependence on *Cxcr4* even in the steady state, with *Pax7*-ZsGreen<sup>+</sup> cell numbers declining in the TA within 2 weeks of TMX treatment (Figure 3). As an additional control, we compared ZsGreen<sup>+</sup> cells in the hind limb muscles of the *Cxcr4*<sup>FL/FL</sup>; *Pax7*-ZsGreen; *Pax7*-creERT2 mice not treated with TMX to mice lacking the *Pax7*-creERT2 transgene, and found no difference in the frequency of satellite cells, demonstrating that the cre transgene has no effect in the absence of tamoxifen (Supplementary Figure S4D).

## CXCR4 regulates early satellite cell proliferation *in vitro*

To further characterize the satellite cell impairment, we studied the behavior of freshly isolated satellite cells in culture. *Cxcr4*<sup>FL/FL</sup>, *Pax7*-creERT2<sup>+/+</sup>, *Pax7*-ZsGreen mice and cre-neg controls were treated with tamoxifen (5 IP injections), and hind limb satellite cells plated into growth medium (Supplementary Figure S4A). Cells from mice lacking cre grew out much more efficiently (Supplementary Figure S4B); furthermore, adding 4OHT to the medium selectively suppressed outgrowth of cells from cre<sup>+</sup> mice, suggesting that escapers contributed to the residual growth of the FL/FL cells.

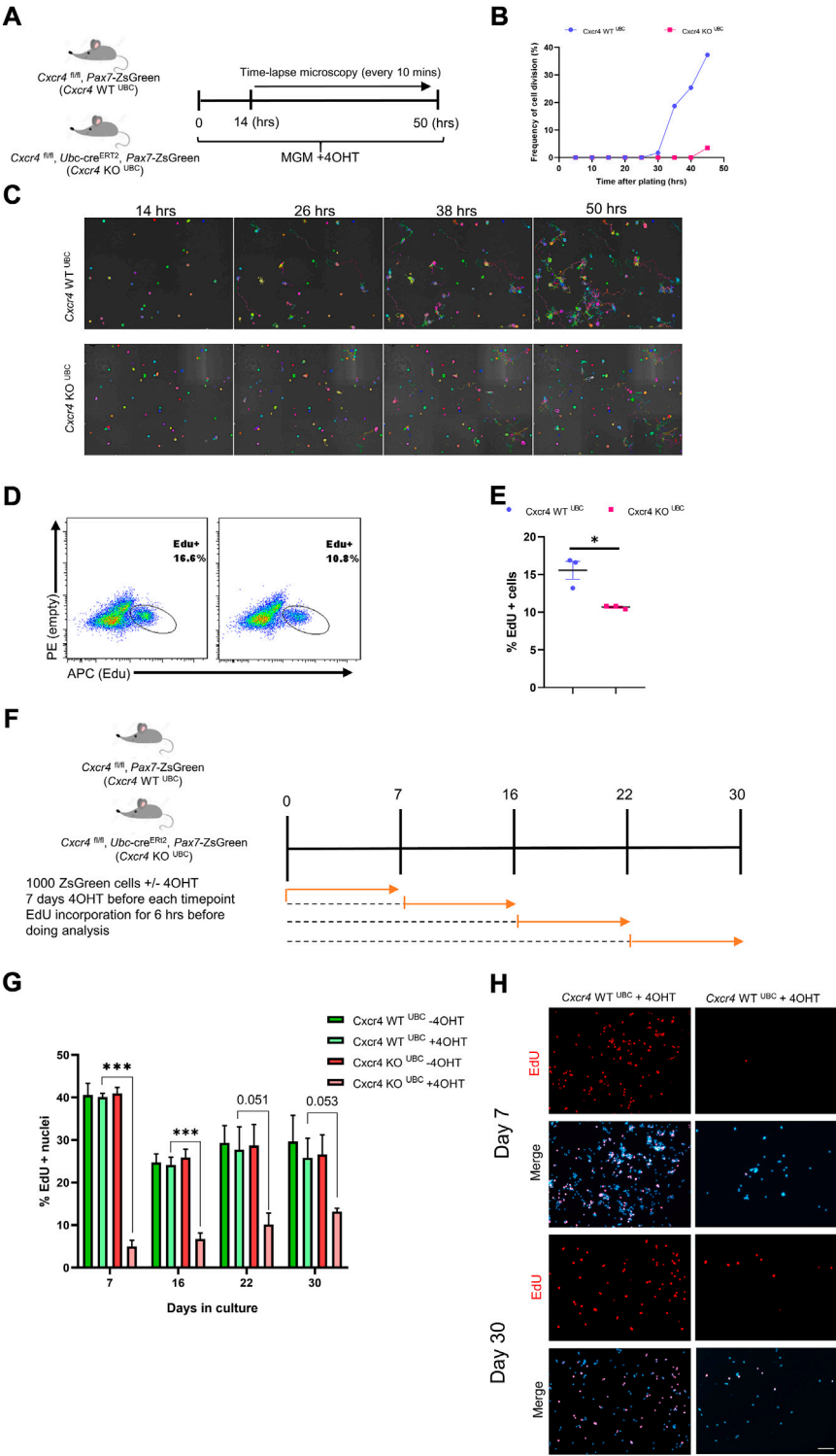
Because *Pax7* is downregulated upon activation, the *Pax7*-creERT2 allele is not expressed efficiently *in vitro*. To study deletion at later time points *in vitro*, we made use of the *Ubc*-cre allele. Short term cultures of satellite cells from *Cxcr4*<sup>FL/FL</sup>, *Ubc*-creERT2<sup>+/+</sup>, *Pax7*-ZsGreen mice exposed to 4OHT (4-hydroxy tamoxifen) *in vitro* efficiently lost *Cxcr4* expression (Figures 4A,B, Supplementary Figure S2B), and failed to proliferate, morphologically (Figure 4C), quantitatively by ATP assay (Figure 4D), and by EdU incorporation (Figures 4E,F). A large fraction of cells in the KO arm + 4OHT were undergoing apoptosis by the 7 day time point, as shown by TUNEL (Figures 4G–I). Time lapse imaging showed that the great majority of cells had not undertaken their first division by 50 h post-plating (Figures 5A,B), and furthermore showed greatly reduced cytomobility (Figure 5C, Supplementary Figure S4C, Supplementary Video S1).

We then tested whether CXCR4 was necessary for the proliferation of established myoblasts. When cultures obtained from *Cxcr4*<sup>FL/FL</sup>; *Ubc*-creERT2 satellite cells were passaged for 6 weeks as myoblasts and then exposed to 4OHT, cells continued to grow robustly, although they showed a modest but statistically significant decline in EdU incorporation suggesting a slightly longer cell cycle (Figures 5D,E). To dissect the temporal necessity of CXCR4, we set up a new experiment in which *Cxcr4* WT<sup>UBC</sup> and *Cxcr4* KO<sup>UBC</sup> cells were grown in myogenic growth medium and treated with 4OHT at various intervals (day 0, 7, 16 and 22), given 7 days of further growth to allow complete deletion of *Cxcr4*, treated with EdU for 6 h (Figure 5F). This revealed a much greater *Cxcr4*-dependence in the earliest cell divisions than in later divisions, with EdU incorporation in the absence of *Cxcr4*

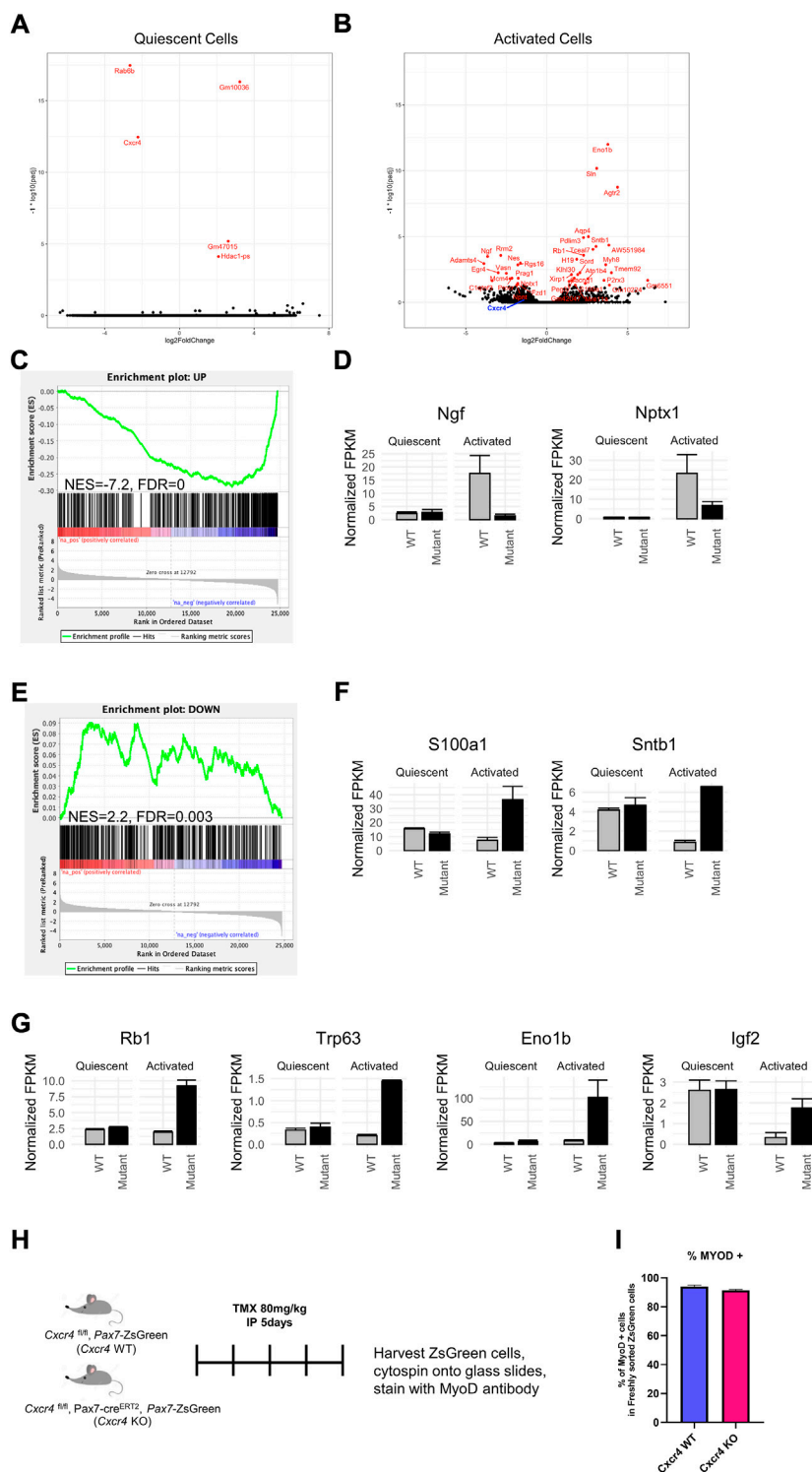
**FIGURE 4**

CXCR4 regulates early proliferation of satellite cells. **(A)** Schematic for Tamoxifen treatment and time of analysis. **(B)** RTqPCR for expression of *Cxcr4* in myoblasts from *Cxcr4*<sup>FL/FL</sup>; *Ubc-creERT2*; *Pax7-ZsGreen* mice (KO<sup>UBC</sup>) (n = 3) or *Cxcr4*<sup>FL/FL</sup>; *Ubc-creERT2*; *Pax7-ZsGreen* controls lacking cre (WT<sup>UBC</sup>) (n = 3), treated with 4OHT. **(C)** Representative bright field images for myoblasts from *Cxcr4*-KO<sup>UBC</sup> or WT<sup>UBC</sup> +/- 4OHT. **(D)** Cell growth assay measuring ATP luminescence in myoblasts from *Cxcr4*-KO<sup>UBC</sup> (n = 3) or WT<sup>UBC</sup> (n = 3) +/- 4OHT. Results are normalized to untreated. **(E)** Representative FACS plots for EdU staining of myoblasts 7 days in culture from *Cxcr4*-WT<sup>UBC</sup> +4OHT (n = 3) and *Cxcr4* KO<sup>UBC</sup> +4OHT (n = 3). **(F)** Frequency of EdU + cells for replicates of the cells shown in E. **(G)** Schematic for the in vitro analysis of apoptosis. **(H)** Frequency of TUNEL + nuclei in *Cxcr4*-WT<sup>UBC</sup> and KO<sup>UBC</sup> cultured satellite cells +/- 4OHT. **(I)** Representative immunofluorescence staining for TUNEL in *Cxcr4*-WT<sup>UBC</sup> and *Cxcr4*-KO<sup>UBC</sup> +/- 4OHT scale bar = 100  $\mu$ m. Note also the low cell number in KO<sup>UBC</sup> +4OHT. Data presented as mean  $\pm$  SEM, \*\*\*p < 0.001 by t-test and two-way ANOVA.





**FIGURE 5**  
Differential dependence of satellite cells vs. established myoblasts on CXCR4. **(A)** Schematic for time lapse experiment measuring time to first division. **(B)** Frequency of satellite cells having undertaken first division over time. **(C)** Representative images tracing satellite cell mobility during time lapse imaging. Colors were randomly assigned by the Nikon Element software for every Binary Particle in the Time lapse movie. **(D)** Representative FACS plots for Edu staining of established myoblasts (6 weeks in culture) from *Cxcr4*-KO<sup>UBC</sup> (*n* = 3) and *Cxcr4*-WT<sup>UBC</sup> (*n* = 3) mice. Established myoblasts were treated with 4OHT for 1 week, and treated with Edu for the last 6 h of the final day. **(E)** Quantification of Edu+ cells for the experiment shown in D. **(F)** Schematic for testing proliferation dependence on CXCR4 in cultured satellite cells over time. **(G)** Frequency of Edu+ nuclei in myoblasts tested after 4OHT addition at various times over 30 days in culture. Data are presented as mean ± SEM, \*\*\**p* < 0.001 by *t*-test. **(H)** Representative Edu incorporation at day 7 and day 30 in the experiment outlined in F. Scale bar = 100 μm.



**FIGURE 6** CXCR4 mediates the satellite cell early activation but not quiescence transcriptional profile. **(A)** Volcano plot showing differentially expressed genes in freshly isolated *Cxcr4*-KO <sup>PAX7</sup> or WT satellite cells from steady state muscle. The -log<sub>10</sub> p-value and log<sub>2</sub> fold changes of genes in *Cxcr4* knockout cells compared to controls are plotted such that genes that are more highly significant are higher on the y-axis. **(B)** Volcano plot showing differentially expressed genes in *Cxcr4*-KO <sup>PAX7</sup> or WT satellite cells undergoing activation (overnight culture in MGM). **(C)** Gene set enrichment analysis (GSEA) for changes between *Cxcr4*-KO <sup>PAX7</sup> and WT compared to wild type in the activated state, using a set of genes previously determined to be upregulated with activation (Machado et al., 2017). **(D)** Barplots of example genes that were within the activation-UP gene set with (Continued)

**FIGURE 6 (Continued)**

significant p-values (Benjamini–Hochberg adjusted p-value < 0.05). Note the lack of up-regulation in the mutant. (E) GSEA for *Cxcr4*-dependent transcriptional changes using the set of genes determined to be downregulated with activation by (Machado et al., 2017). Note the failure of down-regulation in the mutant. (F) Barplots of example genes that were within the activation-DOWN gene set with significant p-values (Benjamini–Hochberg adjusted p-value < 0.05). (G) Examples of genes dysregulated in the *Cxcr4* mutant that may be associated with cell cycle arrest. (H) Schematic of analysis of translation of MYOD1 transcript in freshly isolated cells of *Cxcr4* KO<sup>PAX7</sup> or WT<sup>PAX7</sup>. (I) Quantification of MYOD1 positive satellite cells immediately after muscle digestion and FACS isolation.

gradually increasing with age of culture (Figures 5G,H and Supplementary Figure S5A). Moreover, we assessed the colony-forming activity of satellite cells in the absence of CXCR4. Single satellite cells from *Cxcr4* -WT<sup>UBC</sup> and *Cxcr4*-KO<sup>UBC</sup> mice were plated in 96-well dishes + 4OHT and colonies were assessed 8 days later (Ippolito et al., 2012) (Supplementary Figure S5B). Both the ability of the cells to form colonies *in vitro* and the mean colony sizes were reduced in the *Ubc*-cre group compared to cre-negative controls (Supplementary Figures S5C,D).

## Transcriptional profile suggests defective activation in the absence of CXCR4.

To better understand the mechanism of *Cxcr4* activity in satellite cells, we performed transcriptional profiling. In the steady state, satellite cells lacking *Cxcr4* showed virtually no statistically significant differences in gene expression (Figure 6A). We next profiled activated satellite cells, by studying gene expression after isolation and overnight culture in growth medium. This revealed a large set of differentially expressed genes (Figure 6B), demonstrating that the primary activity of *Cxcr4* signaling as it relates to transcription is in activated as opposed to quiescent satellite cells (Supplementary Tables S2A,B). By inspection, we noted that many genes associated with early activation were diminished in expression levels in *Cxcr4* KO activated satellite cells, therefore we evaluated a set of previously-defined genes whose expression changes upon satellite cell activation (Machado et al., 2017). GSEA revealed a large subset of genes normally upregulated with activation to be showing defective upregulation in the *Cxcr4* KO (Figures 6C,D). Genes normally downregulated with activation also showed a statistically significant negative correlation, however the effect on these genes was much less pronounced than the effect on the upregulated set (Figures 6E,F). In addition to the misregulation of genes normally observed in activation, we also observed upregulation of the genes such as *Rb1* and *Trp63* that may block cell cycle progression and compromise satellite cell activation (Figure 6G). Paradoxically, we also noted upregulation of genes that can have growth-promoting effects, including the enolase paralog *Eno1b* and insulin

growth factor 2 (*Igf2*). Together these data demonstrate clearly that activation is impaired in the *Cxcr4* KO and suggest possible mechanisms that could be tested in future studies.

Activation doubtlessly involves multiple pathways, and is a multi-step process. One of the earliest events is the expression of certain proteins whose RNA is already present but not translated (Crist et al., 2012). One very clear example of this can be seen by immunostaining for MYOD1. In histological sections, satellite cells are negative for MYOD1 protein, however as soon as they are isolated, a process that involves enzyme incubation for at least an hour at 37°C, they become MYOD1 protein+. To evaluate this very early stage in activation, we sorted satellite cells from WT and Pax7-driven *Cxcr4* KO and spun them onto glass slides for immunostaining (Figure 6H). MYOD1 was present in almost all cells, in both the WT and KO arms (Figure 6I). This demonstrates that CXCR4 activity has no bearing on this earliest step in activation, and that its major activity is limited to a window of time between when cells become MYOD1+ and the first cell division.

## Discussion

CXCR4 is best known for its role in chemotaxis, and indeed its major role in embryonic myogenesis relates to migration of myogenic progenitors (Vasyutina et al., 2005; Yusuf et al., 2005; Yusuf et al., 2006; Rehimi et al., 2010). While satellite cells are not migratory between muscles (Schultz et al., 1986), they are motile along the fiber in response to activation (Gu et al., 2016), and they do occupy a stereotypical position in relation to the endothelial network (Verma et al., 2018), suggesting a requirement for chemotactic/sensing systems, and indeed our time lapse study demonstrated much reduced motility of *Cxcr4*-null satellite cells, suggesting a potential role for CXCR4 in satellite cell movement and orientation. Regarding roles in more regeneration-centric functions, such as activation, proliferation and differentiation, a recent study had shown that while *Cxcr4* mutation enhanced the regeneration phenotype of c-met mutation in satellite cells, deletion of *Cxcr4* alone had no discernable effect on the extent of regeneration after injury (Lahmann et al., 2021). We were therefore surprised at the extent of difference between *Cxcr4*-KO and -WT cells in our initial transplantation assay, an assay that is much more dependent on survival, proliferation,

and differentiation than on chemotaxis. CXCR4 was necessary both for the ability of satellite cells to repopulate the satellite cell pool, as well as for cells to be able to contribute efficiently to the population of new fibers. The likely reason this had not been appreciated previously is that the degree of regenerative demand on a per cell basis is much higher in a 300 cell transplant into an injured irradiated TA muscle than in a singly CTX-injured muscle. In addition, the tremendous potential of “escapers”, satellite cells that escape recombination, to suppress satellite cell specific deletion phenotypes has been recognized (Gunther et al., 2013; von Maltzahn et al., 2013), which motivated the addition of tamoxifen chow following the tamoxifen injections, and represents a difference in methodology compared to the Lahmann study. In the current study, we found that after a single CTX injury, which normally leads to substantial hypertrophy accompanied by a doubling of the satellite cell population, there was virtually no hypertrophy or expansion in the satellite cell pool if *Cxcr4* had been deleted in PAX7+ cells. Furthermore, in the more stringent double-CTX injury model, fiber size was significantly reduced in the regenerated muscles in which *Cxcr4* was deleted in PAX7+ cells.

Evaluating regenerating muscle at earlier time points revealed that the defect in regeneration was already manifest in *Cxcr4* mutants at the first week post-injury, both in terms of muscle mass and in the significant drop in numbers of the satellite cell pool. This suggested that CXCR4 signaling was most critical in the early stages of muscle regeneration, possibly for the cell divisions necessary to produce the large number of myoblasts that will differentiate into the mass of newly-generated muscle. To test this idea, we investigated the *Cxcr4*-dependence of proliferation by deleting *Cxcr4* in cells proliferating *in vitro*, comparing freshly isolated satellite cells, passaged satellite cells and established myoblasts. While cell division was impaired to some degree at all stages, demonstrating that CXCR4 signaling promotes cell cycle transit generally in myogenic progenitors, the impairment was more severe the younger the culture was. When *Cxcr4* was deleted prior to plating, most *Cxcr4*-deleted satellite cells failed to divide at all within the time frame of the study, in which almost all WT cells had undertaken their first division. Cell division represents the culmination of the activation process. To assess the earliest known event, translation of mRNAs sequestered in RNP granules, we assessed MYOD protein in freshly isolated *Cxcr4*-deleted satellite cells. This earliest step occurs during the enzyme digestion stage, and we found no difference in MYOD positivity between CXCR4 WT and KO satellite cells, with uniform staining in both populations.

To understand what specifically might be going awry slightly later in the activation process, we performed RNA-seq on freshly isolated satellite cells after a short period of culture, well prior to first division. In contrast to RNA-seq on Pax7-ZsGreen cells

immediately after FACS isolation, in which very few gene expression differences could be identified, RNA-seq on activated cells showed many differences, most particularly a highly significant enrichment for changes in genes normally upregulated by activation (Machado et al., 2017). While not all genes normally upregulated by activation were lower in the *Cxcr4* mutant, a clear subset of these genes was dependent on *Cxcr4* for their normal upregulation with activation. These data, together with the fact that most *Cxcr4* mutant satellite cells fail to divide, indicate that *Cxcr4* plays a key role in satellite cell activation. It is interesting to note that the alarmin HMGB1, which is known to promote signaling through CXCR4 (Schiraldi et al., 2012), was recently implicated as necessary for the G-alert state of several cell types, including satellite cells, in response to fracture injury (Lee et al., 2018). It would therefore be interesting to evaluate the degree to which entry into G-alert is affected in the *Cxcr4* KO.

The SDF1a/CXCR4 axis has also been implicated in cell survival in a number of studies (Jiang et al., 2018; Dalal et al., 2020; Aronovich et al., 2021; Lahmann et al., 2021). We observed an increase in TUNEL+ cells when *Cxcr4* was deleted in satellite cells cultured *in vitro*, suggesting a role for survival in addition to proliferation. However, given that the TUNEL staining was done 7 days after deletion, and in cells that were basically not dividing, the elevated apoptosis may represent a secondary effect.

To determine the source of the signal to which CXCR4 is responding, we sorted various subcomponents of the muscle mononuclear fraction and evaluated their expression of *Sdf1a*. While *Sdf1a* could be detected in all fractions, it was robustly expressed in two cell types: endothelial cells and FAPs. Although well expressed at all time points by endothelial cells, we found that the *Sdf1a* expression was reduced at 2 days post-injury, but significantly upregulated at 4 days post-injury. In FAPs, its expression did not change over these time points. Given the critical early necessity of *Cxcr4*, it was somewhat surprising to see *Sdf1a* expression trend downwards 2 days after injury in endothelial cells, thus since FAPs are known to promote proliferation of satellite cells (Joe et al., 2010), it may be through interaction with FAPs that this signal is primarily mediated in the earliest time points after injury. Notwithstanding, it would be interesting to determine the extent to which the SDF1a/CXCR4 axis affects the positioning of quiescent satellite cells in the vicinity of endothelial cells. The role of *Sdf1a* in endothelial cells and FAPs, both after injury or during steady state, will await cell type-specific deletion studies.

In summary, these studies demonstrate that maintained expression of *Cxcr4* from the fetal stage into the adult phase has functional consequences beyond chemotaxis. Using a protocol that involves following tamoxifen-mediated satellite cell-specific deletion with continued tamoxifen provision *via* food in order to suppress potential escapers, we find that *Cxcr4* is critically necessary for appropriate activation and for



early proliferation of satellite cells and their immediate progeny, and thereby necessary for normal skeletal muscle regeneration.

## Data availability statement

The sequence data presented in the study are deposited in the GEO repository, accession number GSE205015.

## Ethics statement

The animal study was reviewed and approved by the Institutional Animal Care and Use Committee of the University of Minnesota.

## Author contributions

AS, JW, BM, DO, and DB, investigation. AS, MG, and MK, analysis. MK, OM, and GH supervised the research. AS and MK prepared the manuscript.

## Funding

This work was supported by a grant from the National Institute on Aging (R01 AG062899) and by the Egyptian Cultural and Education Bureau Joint Supervision Program (JS 3732).

## References

- Aronovich, A., Moyal, L., Gorovitz, B., Amitay-Laish, I., Naveh, H. P., Forer, Y., et al. (2021). Cancer-associated fibroblasts in mycosis fungoides promote tumor cell migration and drug resistance through CXCL12/CXCR4. *J. Invest. Dermatol.* 141 (3), 619–627.e2. doi:10.1016/j.jid.2020.06.034
- Arpke, R. W., Darabi, R., Mader, T. L., Zhang, Y., Toyama, A., Lonetree, C. L., et al. (2013). A new immuno-, dystrophin-deficient model, the NSG-mdx4Cv mouse, provides evidence for functional improvement following allogeneic satellite cell transplantation. *Stem cells* 31 (8), 1611–1620. doi:10.1002/stem.1402
- Arpke, R. W., and Kyba, M. (2016). “Flow cytometry and transplantation-based quantitative assays for satellite cell self-renewal and differentiation,” in *Skeletal muscle regeneration in the mouse* (Berlin Germany: Springer), 163–179.
- Arpke, R. W., Shams, A. S., Collins, B. C., Larson, A. A., Lu, N., Lowe, D. A., et al. (2021). Preservation of satellite cell number and regenerative potential with age reveals locomotory muscle bias. *Skelet. Muscle* 11 (1), 22–12. doi:10.1186/s13395-021-00277-2
- Asakura, A., Seale, P., Girgis-Gabardo, A., and Rudnicki, M. A. (2002). Myogenic specification of side population cells in skeletal muscle. *J. Cell Biol.* 159 (1), 123–134. doi:10.1083/jcb.200202092
- Barruet, E., Garcia, S. M., Striedinger, K., Wu, J., Lee, S., Byrnes, L., et al. (2020). Functionally heterogeneous human satellite cells identified by single cell RNA sequencing. *Elife* 9, e51576. doi:10.7554/eLife.51576
- Bianchi, M. E., and Mezzapelle, R. (2020). The chemokine receptor CXCR4 in cell proliferation and tissue regeneration. *Front. Immunol.* 11, 2109. doi:10.3389/fimmu.2020.02109
- Biressi, S., Bjornson, C. R. R., Carlig, P. M. M., Nishijo, K., Keller, C., and Rando, T. A. (2013). Myf5 expression during fetal myogenesis defines the developmental progenitors of adult satellite cells. *Dev. Biol.* 379 (2), 195–207. doi:10.1016/j.ydbio.2013.04.021
- Bosnakovski, D., Oyler, D., Mitansoska, A., Douglas, M., Ener, E. T., Shams, A. S., et al. (2022). Persistent fibroadipogenic progenitor expansion following transient DUX4 expression provokes a profibrotic state in a mouse model for FSHD. *Int. J. Mol. Sci.* 23 (4), 1983. doi:10.3390/ijms23041983
- Bosnakovski, D., Shams, A. S., Yuan, C., da Silva, M. T., Ener, E. T., Baumann, C. W., et al. (2020). Transcriptional and cytopathological hallmarks of FSHD in chronic DUX4-expressing mice. *J. Clin. Invest.* 130 (5), 2465–2477. doi:10.1172/JCI133303
- Bosnakovski, D., Xu, Z., Li, W., Thet, S., Cleaver, O., Perlingeiro, R. C. R., et al. (2008). Prospective isolation of skeletal muscle stem cells with a Pax7 reporter. *Stem cells* 26 (12), 3194–3204. doi:10.1634/stemcells.2007-1017
- Brack, A. S., and Rando, T. A. (2012). Tissue-specific stem cells: Lessons from the skeletal muscle satellite cell. *Cell stem cell* 10 (5), 504–514. doi:10.1016/j.stem.2012.04.001
- Bryson-Richardson, R. J., and Currie, P. D. (2008). The genetics of vertebrate myogenesis. *Nat. Rev. Genet.* 9 (8), 632–646. doi:10.1038/nrg2369
- Cencioni, C., Capogrossi, M. C., and Napolitano, M. (2012). The SDF-1/CXCR4 axis in stem cell preconditioning. *Cardiovasc. Res.* 94 (3), 400–407. doi:10.1093/cvr/cvs132
- Chapman, M. R., Balakrishnan, K. R., Li, J., Conboy, M. J., Huang, H., Mohanty, S. K., et al. (2013). Sorting single satellite cells from individual myofibers reveals heterogeneity in cell-surface markers and myogenic capacity. *Integr. Biol.* 5 (4), 692–702. doi:10.1039/c3ib20290a
- Chong, S. W., Nguyet, L. M., Jiang, Y. J., and Korzh, V. (2007). The chemokine Sdf-1 and its receptor Cxcr4 are required for formation of muscle in zebrafish. *BMC Dev. Biol.* 7, 54. doi:10.1186/1471-213X-7-54

## Acknowledgments

We thank the University Imaging Center, Mark Sanders and Thomas Pengo for support with time lapse and other imaging.

## Conflict of interest

The authors declare that the research was conducted in the absence of any commercial or financial relationships that could be construed as a potential conflict of interest.

## Publisher's note

All claims expressed in this article are solely those of the authors and do not necessarily represent those of their affiliated organizations, or those of the publisher, the editors and the reviewers. Any product that may be evaluated in this article, or claim that may be made by its manufacturer, is not guaranteed or endorsed by the publisher.

## Supplementary material

The Supplementary Material for this article can be found online at: <https://www.frontiersin.org/articles/10.3389/fcell.2022.949532/full#supplementary-material>

- Conboy, M. J., Cerletti, M., Wagers, A. J., and Conboy, I. M. (2010). "Immunanalysis and FACS sorting of adult muscle fiber-associated stem/precursor cells," in *Protocols for adult stem cells* (Berlin, Germany: Springer), 165–173.
- Cornelison, D. D. W., Filla, M. S., Stanley, H. M., Rapraeger, A. C., and Olwin, B. B. (2001). Syndecan-3 and syndecan-4 specifically mark skeletal muscle satellite cells and are implicated in satellite cell maintenance and muscle regeneration. *Dev. Biol.* 239 (1), 79–94. doi:10.1006/dbio.2001.0416
- Crist, C. G., Montarras, D., and Buckingham, M. (2012). Muscle satellite cells are primed for myogenesis but maintain quiescence with sequestration of Myf5 mRNA targeted by microRNA-31 in mRNP granules. *Cell stem cell* 11 (1), 118–126. doi:10.1016/j.stem.2012.03.011
- Dalal, S., Daniels, C. R., Li, Y., Wright, G. L., Singh, M., and Singh, K. (2020). Exogenous ubiquitin attenuates hypoxia/reoxygenation-induced cardiac myocyte apoptosis via the involvement of CXCR4 and modulation of mitochondrial homeostasis. *Biochem. Cell Biol.* 98 (4), 492–501. doi:10.1139/bcb-2019-0339
- Doitsidou, M., Reichman-Fried, M., Stebler, J., Kopranner, M., Dorries, J., Meyer, D., et al. (2002). Guidance of primordial germ cell migration by the chemokine SDF-1. *Cell* 111 (5), 647–659. doi:10.1016/s0092-8674(02)01135-2
- Fukada, S., Higuchi, S., Segawa, M., Koda, K. i., Yamamoto, Y., Tsujikawa, K., et al. (2004). Purification and cell-surface marker characterization of quiescent satellite cells from murine skeletal muscle by a novel monoclonal antibody. *Exp. Cell Res.* 296 (2), 245–255. doi:10.1016/j.yexcr.2004.02.018
- Gromova, A., Tierney, M. T., and Sacco, A. (2015). FACS-based satellite cell isolation from mouse hind limb muscles. *Bio. Protoc.* 5 (16), e1558. doi:10.21769/bioprotoc.1558
- Gu, J. M., Wang, D. J., Peterson, J. M., Shintaku, J., Liyanarachchi, S., Coppola, V., et al. (2016). An NF- $\kappa$ B-EphrinA5-Dependent communication between NG2(+) interstitial cells and myoblasts promotes muscle growth in neonates. *Dev. Cell* 36 (2), 215–224. doi:10.1016/j.devcel.2015.12.018
- Gunther, S., Kim, J., Kostin, S., Lepper, C., Fan, C. M., and Braun, T. (2013). Myf5-positive satellite cells contribute to Pax7-dependent long-term maintenance of adult muscle stem cells. *Cell Stem Cell* 13 (5), 590–601. doi:10.1016/j.stem.2013.07.016
- Ieronimakis, N., Balasundaram, G., Rainey, S., Srirangam, K., Yablonka-Reuveni, Z., and Reyes, M. (2010). Absence of CD34 on murine skeletal muscle satellite cells marks a reversible state of activation during acute injury. *PLoS one* 5 (6), e10920. doi:10.1371/journal.pone.0010920
- Ippolito, J., Arpke, R. W., Haider, K. T., Zhang, J., and Kyba, M. (2012). Satellite cell heterogeneity revealed by G-Tool, an open algorithm to quantify myogenesis through colony-forming assays. *Skelet. Muscle* 2 (1), 13–12. doi:10.1186/2044-5040-2-13
- Janowski, M. (2009). Functional diversity of SDF-1 splicing variants. *Cell adh. Migr.* 3 (3), 243–249. doi:10.4161/cam.3.3.8260
- Jazin, E. E., Soderstrom, S., Ebendal, T., and Larhammar, D. (1997). Embryonic expression of the mRNA for the rat homologue of the fusin/CXCR-4 HIV-1 co-receptor. *J. Neuroimmunol.* 79 (2), 148–154. doi:10.1016/s0165-5728(97)00117-3
- Jiang, C., Ma, S., Hu, R., Wang, X., Li, M., Tian, F., et al. (2018). Effect of CXCR4 on apoptosis in osteosarcoma cells via the PI3K/Akt/NF- $\kappa$ B signaling pathway. *Cell. Physiol. biochem.* 46 (6), 2250–2260. doi:10.1159/000489593
- Joe, A. W. B., Yi, L., Natarajan, A., Le Grand, F., So, L., Wang, J., et al. (2010). Muscle injury activates resident fibro/adipogenic progenitors that facilitate myogenesis. *Nat. Cell Biol.* 12 (2), 153–163. doi:10.1038/ncb2015
- Keefe, A. C., Lawson, J. A., Flygare, S. D., Fox, Z. D., Colasanto, M. P., Mathew, S. J., et al. (2015). Muscle stem cells contribute to myofibers in sedentary adult mice. *Nat. Commun.* 6, 7087. doi:10.1038/ncomms8087
- Knaut, H., Werz, C., Geisler, R., and Nusslein-Volhard, C. (2003). A zebrafish homologue of the chemokine receptor Cxcr4 is a germ-cell guidance receptor. *Nature* 421 (6920), 279–282. doi:10.1038/nature01338
- Lahmann, I., Griger, J., Chen, J. S., Zhang, Y., Schuelke, M., and Birchmeier, C. (2021). Met and Cxcr4 cooperate to protect skeletal muscle stem cells against inflammation-induced damage during regeneration. *Elife* 10, e57356. doi:10.7554/eLife.57356
- Larson, A. A., Shams, A. S., McMillin, S. L., Sullivan, B. P., Vue, C., Roloff, Z. A., et al. (2022). Estradiol deficiency reduces the satellite cell pool by impairing cell cycle progression. *Am. J. Physiol. Cell Physiol.* 322, C1123–C1137. doi:10.1152/ajpcell.00429.2021
- Lazarini, F., Tham, T. N., Casanova, P., Arenzana-Seisdedos, F., and Dubois-Dalcq, M. (2003). Role of the  $\alpha$ -chemokine stromal cell-derived factor (SDF-1) in the developing and mature central nervous system. *Glia* 42 (2), 139–148. doi:10.1002/glia.10139
- Lee, G., Espirito Santo, A. I., Zwigenberger, S., Cai, L., Vogl, T., Feldmann, M., et al. (2018). Fully reduced HMGB1 accelerates the regeneration of multiple tissues by transitioning stem cells to GAlert. *Proc. Natl. Acad. Sci. U. S. A.* 115 (19), E4463–E4472. doi:10.1073/pnas.1802893115
- Liu, L., Cheung, T. H., Charville, G. W., and Rando, T. A. (2015). Isolation of skeletal muscle stem cells by fluorescence-activated cell sorting. *Nat. Protoc.* 10 (10), 1612–1624. doi:10.1038/nprot.2015.110
- Machado, L., Esteves de Lima, J., Fabre, O., Proux, C., Legendre, R., Szegedi, A., et al. (2017). *In situ* fixation redefines quiescence and early activation of skeletal muscle stem cells. *Cell Rep.* 21 (7), 1982–1993. doi:10.1016/j.celrep.2017.10.080
- Maesner, C. C., Almada, A. E., Wagersand Amy, J. (2016). Established cell surface markers efficiently isolate highly overlapping populations of skeletal muscle satellite cells by fluorescence-activated cell sorting. *Skelet. Muscle* 6 (1), 35. doi:10.1186/s13395-016-0106-6
- Mauro, A. (1961). Satellite cell of skeletal muscle fibers. *J. Biophys. Biochem. Cytol.* 9 (2), 493–495. doi:10.1083/jcb.9.2.493
- Moepps, B., FRodl, R., Rodewald, H. R., Baggiolini M. and Gierschik, P. (1997). Two murine homologues of the human chemokine receptor CXCR4 mediating stromal cell-derived factor 1 $\alpha$  activation of Gi2 are differentially expressed *in vivo*. *Eur. J. Immunol.* 27 (8), 2102–2112. doi:10.1002/eji.1830270839
- Molyneux, K. A., Kunwar, P. S., Schaible, K., Stebler, J., Sunshine, M. J., et al. (2003). The chemokine SDF1/CXCL12 and its receptor CXCR4 regulate mouse germ cell migration and survival. *Development* 130 (18), 4279–4286. doi:10.1242/dev.00640
- Monzel, C., Becker, A. S., Saffrich, R., Wuchter, P., Eckstein, V., Ho, A. D., et al. (2018). Dynamic cellular phenotyping defines specific mobilization mechanisms of human hematopoietic stem and progenitor cells induced by SDF1 $\alpha$  versus synthetic agents. *Sci. Rep.* 8 (1), 1841–1910. doi:10.1038/s41598-018-19557-x
- Odemis, V., Lamp, E., Pezeszki, G., Moepps, B., Schilling, K., Gierschik, P., et al. (2005). Mice deficient in the chemokine receptor CXCR4 exhibit impaired limb innervation and myogenesis. *Mol. Cell. Neurosci.* 30 (4), 494–505. doi:10.1016/j.mcn.2005.07.019
- Ratajczak, M. Z., Majka, M., Kucia, M., Drukala, J., Pietrzkowski, Z., Peiper, S., et al. (2003). Expression of functional CXCR4 by muscle satellite cells and secretion of SDF-1 by muscle-derived fibroblasts is associated with the presence of both muscle progenitors in bone marrow and hematopoietic stem/progenitor cells in muscles. *Stem cells* 21 (3), 363–371. doi:10.1634/stemcells.21-3-363
- Rehimi, R., Khalida, N., Yusuf, F., Morosan-Puopolo, G., and Brand-Saberi, B. (2010). A novel role of CXCR4 and SDF-1 during migration of cloacal muscle precursors. *Dev. Dyn.* 239 (6), 1622–1631. doi:10.1002/dvdy.22288
- Relaix, F., Bencze, M., Borok, M. J., Der Vartanian, A., Gattazzo, F., Mademtzoglou, D., et al. (2021). Perspectives on skeletal muscle stem cells. *Nat. Commun.* 12 (1), 692–711. doi:10.1038/s41467-020-20760-6
- Sacco, A., Doyonnas, R., Kraft, P., Vitorovic, S., and Blau, H. M. (2008). Self-renewal and expansion of single transplanted muscle stem cells. *Nature* 456 (7221), 502–506. doi:10.1038/nature07384
- Schiraldi, M., Raucci, A., Munoz, L. M., Livoti, E., Celona, B., Venereau, E., et al. (2012). HMGB1 promotes recruitment of inflammatory cells to damaged tissues by forming a complex with CXCL12 and signaling via CXCR4. *J. Exp. Med.* 209 (3), 551–563. doi:10.1084/jem.20111739
- Schultz, E., Jaryszak, D. L., Gibson, M. C., and Albright, D. J. (1986). Absence of exogenous satellite cell contribution to regeneration of frozen skeletal muscle. *J. Muscle Res. Cell Motil.* 7 (4), 361–367. doi:10.1007/BF01753657
- Seale, P., Sabourin, L. A., Gargis-GAardo, A., MAnsouri, A., Gruss, P., and Rudnicki, M. A. (2000). Pax7 is required for the specification of myogenic satellite cells. *Cell* 102 (6), 777–786. doi:10.1016/s0092-8674(00)00066-0
- Shadrach, J. L., and Wagers, A. J. (2011). Stem cells for skeletal muscle repair. *Philos. Trans. R. Soc. Lond. B Biol. Sci.* 366 (1575), 2297–2306. doi:10.1098/rstb.2011.0027
- Sherwood, R. I., Christensen, J. L., Conboy, I. M., Conboy, M. J., Rando, T. A., Weissman, I. L., et al. (2004). Isolation of adult mouse myogenic progenitors: Functional heterogeneity of cells within and engrafting skeletal muscle. *Cell* 119 (4), 543–554. doi:10.1016/j.cell.2004.10.021
- Stebler, J., Spieler, D., Slanchev, K., Molyneux, K. A., Richter, U., Cojocaru, V., et al. (2004). Primordial germ cell migration in the chick and mouse embryo: The role of the chemokine SDF-1/CXCL12. *Dev. Biol.* 272 (2), 351–361. doi:10.1016/j.ydbio.2004.05.009
- Stitelman, D. H., Brazelton, T., Bora, A., Traas, J., Merianos, D., Limberis, M., et al. (2014). Developmental stage determines efficiency of gene transfer to muscle satellite cells by *in utero* delivery of adeno-associated virus vector serotype 2/9. *Mol. Ther. Methods Clin. Dev.* 1, 14040. doi:10.1038/mtm.2014.40
- Vasyutina, E., Stebler, J., Brand-Saberi, B., Schulz, S., Raz, E., and Birchmeier, C. (2005). CXCR4 and Gab1 cooperate to control the development of migrating muscle progenitor cells. *Genes Dev.* 19 (18), 2187–2198. doi:10.1101/gad.346205
- Verma, M., Asakura, Y., Murakonda, B. S. R., Pengo, T., Latroche, C., Chazaud, B., et al. (2018). Muscle satellite cell cross-talk with a vascular niche maintains

quiescence via VEGF and notch signaling. *Cell Stem Cell* 23 (4), 530–543. doi:10.1016/j.stem.2018.09.007

von Maltzahn, J., Jones, A. E., Parks, R. J., and Rudnicki, M. A. (2013). Pax7 is critical for the normal function of satellite cells in adult skeletal muscle. *Proc. Natl. Acad. Sci. U. S. A.* 110 (41), 16474–16479. doi:10.1073/pnas.1307680110

Yahya, I., Boing, M., Pu, Q., Puchert, M., Oedemis, V., Engele, J., et al. (2020). Cxcr4 and Sdf-1 are critically involved in the formation of facial and non-somitic neck muscles. *Sci. Rep.* 10 (1), 5049. doi:10.1038/s41598-020-61960-w

Yin, H., Price, F., and Rudnicki, M. A. (2013). Satellite cells and the muscle stem cell niche. *Physiol. Rev.* 93 (1), 23–67. doi:10.1152/physrev.00043.2011

Yoshida, T., Galvez, S., Tiwari, S., Rezk, B. M., Semprun-Prieto, L., Higashi, Y., et al. (2013). Angiotensin II inhibits satellite cell proliferation and prevents skeletal

muscle regeneration. *J. Biol. Chem.* 288 (33), 23823–23832. doi:10.1074/jbc.M112.449074

Yusuf, F., Rehimi, R., Dai, F., and Brand-Saberi, B. (2005). Expression of chemokine receptor CXCR4 during chick embryo development. *Anat. Embryol.* 210 (1), 35–41. doi:10.1007/s00429-005-0013-9

Yusuf, F., Rehimi, R., Morosan-Puopolo, G., Dai, F., Zhang, X., and Brand-Saberi, B. (2006). Inhibitors of CXCR4 affect the migration and fate of CXCR4+ progenitors in the developing limb of chick embryos. *Dev. Dyn.* 235 (11), 3007–3015. doi:10.1002/dvdy.20951

Zhao, S., Wang, J., and Qin, C. (2014). Blockade of CXCL12/CXCR4 signaling inhibits intrahepatic cholangiocarcinoma progression and metastasis via inactivation of canonical Wnt pathway. *J. Exp. Clin. Cancer Res.* 33 (1), 103–112. doi:10.1186/s13046-014-0103-8

# Advantages of publishing in Frontiers



## OPEN ACCESS

Articles are free to read  
for greatest visibility  
and readership



## FAST PUBLICATION

Around 90 days  
from submission  
to decision



## HIGH QUALITY PEER-REVIEW

Rigorous, collaborative,  
and constructive  
peer-review



## TRANSPARENT PEER-REVIEW

Editors and reviewers  
acknowledged by name  
on published articles

## Frontiers

Avenue du Tribunal-Fédéral 34  
1005 Lausanne | Switzerland

Visit us: [www.frontiersin.org](http://www.frontiersin.org)

Contact us: [frontiersin.org/about/contact](http://frontiersin.org/about/contact)



## REPRODUCIBILITY OF RESEARCH

Support open data  
and methods to enhance  
research reproducibility



## DIGITAL PUBLISHING

Articles designed  
for optimal readership  
across devices



## FOLLOW US

@frontiersin



## IMPACT METRICS

Advanced article metrics  
track visibility across  
digital media



## EXTENSIVE PROMOTION

Marketing  
and promotion  
of impactful research



## LOOP RESEARCH NETWORK

Our network  
increases your  
article's readership